

# BIAXIAL CREEP AND PLASTIC FLOW OF ANISOTROPIC ALUMINIUM

by

DAVID WILLIAM ALAN REES, M.Sc., D.I.C., M.I.Mech.E.

A THESIS SUBMITTED TO THE COUNCIL OF  
NATIONAL ACADEMIC AWARDS FOR THE DOCTOR  
OF PHILOSOPHY DEGREE — December 1976

THE RESEARCH CONTAINED HEREIN WAS  
CONDUCTED IN THE SCHOOL OF MECHANICAL,  
AERONAUTICAL AND PRODUCTION ENGINEERING,  
KINGSTON POLYTECHNIC

Copy Number 2

THE LIBRARIAN,  
KINGSTON POLYTECHNIC,  
CANPURY PARK ROAD,  
KINGSTON UPON THAMES,  
SURREY



# CONTENTS

## LIST OF FIGURES, TABLES AND COMPUTER PROGRAMMES

	Page
ACKNOWLEDGEMENTS	xi
DECLARATION	xii
SUMMARY	xiii
LIST OF SYMBOLS	xv
INTRODUCTION	1
CHAPTER 1 LITERATURE REVIEW	
1.1 MULTIAXIAL STRESS CREEP	7
1.1.1 Equations on Isotropy	7
1.1.2 Equations on Anisotropy	11
1.2 CREEP OF PRESTRAINED MATERIAL	13
1.2.1 Amount of Prestrain	13
1.2.2 Temperature of Prestrain	15
1.2.3 Direction of Prestrain	16
1.2.4 Prestrain Rate	17
1.2.5 Time at which Prestrain is Introduced	18
1.2.6 Summary	19
CHAPTER 2 EXPERIMENTAL	
2.1 THE TEST RIG-MODIFICATIONS AND DESCRIPTION	21
2.1.1 Tension Loading System	22
2.1.2 Torsion Loading System	23
2.1.3 Combined Loading	24
2.1.4 Internal Pressure	25
2.2 TEST MATERIAL	25
2.3 TEST SPECIMENS	26
2.3.1 Tubular Specimens	27
2.3.2 Tension Creep Specimens	28
2.3.3 Isotropy, Hardness and Metallographic Examination	28
2.3.4 Cutting Plan	29
2.3.5 Material Preparation and Specimen Manufacture	30

	Page
2.4 DISPLACEMENT AND STRAIN MEASUREMENT	31
2.4.1 Extension and Twist Measurement	32
2.4.2 Diameter Measurement	32
2.4.3 Signal Conditioning and Recording	33
2.4.4 Strain Gauges	33
2.4.5 Calibrations	34
2.4.6 Accuracy	35
2.5 TEST PROCEDURE	36
2.5.1 Creep and Plastic Flow During Incremental Loading	36
2.5.2 Tension-Torsion Tests on Annealed Material	36
2.5.3 Tension-Torsion Tests on Extruded Material	36
2.5.4 Tension-Torsion Tests on Prestrained Material	36

### CHAPTER 3 THEORETICAL ANALYSIS

3.1 ANNEALED MATERIAL	63
3.1.1 Incremental Loading	63
3.1.2 Creep	67
3.1.3 Analysis of Anisotropy	63
3.2 EXTRUDED MATERIAL	69
3.3 PRESTRAINED MATERIAL	70
3.4 APPLICATION OF OTHER THEORIES	71
3.4.1 Bailey	71
3.4.2 Berman and Pai	72
3.4.3 Hu	73
3.5 GENERAL THEORIES OF ANISOTROPY	75
3.5.1 Edelman and Drucker	75
3.5.2 Yoshimura	78
3.5.3 Williams and Svensson	79

### CHAPTER 4 RESULTS FOR ANNEALED ALUMINIUM

4.1 ISOTROPY	81
4.2 CREEP AND PLASTIC FLOW DURING UNIAXIAL INCREMENTAL LOADING	82
4.3 CREEP AND PLASTIC FLOW DURING COMBINED LOADING	83
4.3.1 30 s Loading Strains	83
4.3.2 Short-Time Creep Strain	85
4.3.3 Long-Time Creep Strain	88

	Page
4.4 THEORETICAL PREDICTION OF ANISOTROPY	90
4.5 RECOVERY	91
CHAPTER 5 RESULTS FOR EXTRUDED ALUMINIUM	
5.1 ANISOTROPY	117
5.2 CREEP AND PLASTIC FLOW DURING COMBINED LOADING	118
5.2.1 Instantaneous and Transient Creep Strains	118
5.2.2 Transient Creep Time Exponents	119
5.3 CREEP	120
5.4 GENERAL COMMENTS ON FLOW IN EXTRUDED MATERIAL	121
5.5 THEORETICAL PREDICTIONS OF ANISOTROPY	121
5.5.1 Loading Strain	121
5.5.2 Creep	122
5.5.3 Axial Strain in Torsion	123
CHAPTER 6 RESULTS FOR PRESTRAINED ALUMINIUM	
6.1 STRAIN HISTORY PRIOR TO CREEP	137
6.2 CREEP	138
6.2.1 Prior Tension and Compression	138
6.2.2 Prior Positive and Negative Torsion	139
6.2.3 General Comments on the Creep of Prior Strained Material	140
6.3 SECONDARY CREEP RATES	140
6.4 INCREMENTAL LOADING CREEP	141
6.4.1 Prior Tension and Compression	141
6.4.2 Prior Positive and Negative Torsion	142
6.4.3 Creep Rates and Time Exponents	142
6.5 THE $k$ FACTOR	143
6.5.1 Instantaneous and Transient Creep Strains	143
6.5.2 Creep	144
6.6 THEORETICAL PREDICTIONS OF ANISOTROPY	145
6.6.1 Creep	145
6.6.2 Loading Strain	146
6.6.3 Anisotropic Theory for Creep	148

CHAPTER 7 DISCUSSION AND RECOMMENDATIONS  
FOR FUTURE WORK

7.1	PLASTIC FLOW	178
7.2	CREEP	179
7.3	DELAYED ELASTICITY	181
7.4	NET STRAIN	182
7.5	GENERAL COMMENTS	182
7.6	RECOMMENDATIONS FOR FUTURE WORK	183

CHAPTER 8 CONCLUSIONS

8.1	ANNEALED ALUMINIUM	187
8.2	EXTRUDED ALUMINIUM	188
8.3	PRESTRAINED ALUMINIUM	189

MAIN TEXT REFERENCES

191

APPENDIX I MULTIAXIAL CREEP AND  
PLASTIC FLOW

1	ISOTROPIC PLASTIC FLOW	2
1.1	Yield Criteria	3
1.2	Flow Rules	4
1.3	Equivalent Stress and Strain	6
1.4	The $\delta\lambda$ Term	8
2	MULTIAXIAL CREEP FOR AN ISOTROPIC MATERIAL	11
2.1	Relationships Between $\bar{\nu}$ and $\dot{\bar{\epsilon}}$	11
3	OTHER MULTIAXIAL CREEP RATE EQUATIONS	14
4	ANISOTROPIC PLASTIC FLOW	16
4.1	Forms of Anisotropy	16
4.2	The Deviatoric Plane	17
4.3	Effect of Plastic Flow on the Yield Surface	18
4.3.1	Isotropic Hardening	19
4.3.2	Minimum Surface	19
4.3.3	Rigid Translation	20
4.3.4	Combined Model	20
4.4	Anisotropic Plastic Flow Equations	20
5	MULTIAXIAL CREEP FOR AN ANISOTROPIC MATERIAL	21
5.1	Relationship Between $\bar{\nu}_a$ and $\dot{\bar{\epsilon}}_a$	22
	References	23

## APPENDIX II CALIBRATIONS

1	TENSILE CELLS - LEVER MAGNIFICATION	2
2	TORSION CELLS - PULLEY MAGNIFICATION	2
3	STRESS RATIO FOR COMBINED TENSION AND TORSION	3
4	AXIALITY OF LOADING	9
5	SPECIMEN GEOMETRY	10
	5.1 Well Thickness Variation	10
	5.2 Ovality	11
	5.3 Straightness Variation	11
6	CHOICE OF GAUGE LENGTH	11

## APPENDIX III CREEP AND PLASTIC FLOW OF ALUMINIUM DURING INCREMENTAL LOADING

1	SUMMARY	2
2	NOTATION	2
3	INTRODUCTION	3
4	ANALYSIS	5
5	EXPERIMENTAL	6
	5.1 Material and Specimens	6
	5.2 Apparatus	6
	5.3 Test Temperature	7
	5.4 Procedure	7
6	EXPERIMENTAL RESULTS	8
	6.1 Material Isotropy	8
	6.2 Transient Creep Analysis	8
	6.3 Parabolic Constants	9
	6.3.1 Effect on $m$	9
	6.3.2 Effect on $a$	10
	6.3.3 Effect on $\epsilon_0$	11
	6.4 Recovery	12
7	DISCUSSION	13
8	CONCLUSIONS	19
	References	21

## LIST OF FIGURES, TABLES AND COMPUTER PROGRAMMES

## CHAPTER 1

Fig.		Page
1.1	Effect of prestrain on creep in aluminium at 21°C	14

## CHAPTER 2

2.1	Complex stress machine	39
2.2	" " "	40
2.3	Tension loading system	41
2.4	Bridge and load cells	42
2.5	Combined loading system	43
2.6	Internal pressure set-up	44
2.7	Tubular creep specimen	45
2.8	Annealing blank	46
2.9	Tensile creep specimen	47
2.10	Tensile specimens	48
2.11	Cutting plan	49
2.12	Specimen positions in bar cross-section	50
2.13	Composite picture of creep specimen directions	51
2.14	Extension and twist measurement	52
2.15	Tensile creep extensometer	53
2.16A	Tensile prestrain set-up	54
2.16B	Tension and torsion prestrain adaptors	55
2.17A	Extension, twist and diameter measurement	56
2.17B	" " " " " "	57
2.18	Three channel transducer system	58
Table		
2.1	% Composition of ELA	59
2.2	V.P.N. annealing figures and photomicrograph	59
2.3	Tubular specimens-manufacturing operation sequence	60
2.4	Prestrain history	61

## CHAPTER 3

3.1	Axes of anisotropy	74
-----	--------------------	----

## CHAPTER 4

Fig.		Page
4.1	Tensile strength variation in annealed material	92
4.2	True stress-plastic strain logarithmic plot	92
4.3	$\epsilon_{\theta\theta}^p \vee \epsilon_{zz}^p$ of radial loading ( $\lambda = \text{constant}$ )	93
4.4	$\delta_{\theta z}^p \vee \epsilon_{zz}^p$ of radial loading ( $\lambda = \text{constant}$ )	93
4.5	Stress-plastic strain correlations for all tests	94
4.6	" " " predictions for $\lambda = 0.86$	95
4.7	Yield loci for Mises equivalent proof strains	96
4.8	" " " Tresca " " "	97
4.9	Transient $\epsilon_{zz}$ creep derivative plot for $\lambda = 0$ and $0.53$	93
4.10	Transient $\delta_{\theta z}$ " " " " $\lambda = \infty$ " "	99
4.11A	Primary $\epsilon_{zz}$ creep derivative plot for all stress ratios	100
4.11B	" $\delta_{\theta z}$ " " " " " " " "	101
4.12	$\delta_{\theta z} \vee \epsilon_{zz}$ creep for constant $\lambda$ tests	102
4.13	Constant $\lambda$ tubular specimens	103
 Table		
4.1	Variation in $m$ with $\lambda$ and stress increment	37
 Prog.		
4.1	Loading strains	104
4.2	Strain rates	108

## CHAPTER 5

5.1	Grain size variation in extruded material	125
5.2	Tensile strength variation in extruded material	126
5.3	Hardness variation in extruded material	126
5.4	$\epsilon_{\theta\theta} \vee \epsilon_{zz}, \delta_{\theta z} \vee \epsilon_{zz}$ of radial loading ( $\lambda = \text{constant}$ )	127
5.5	10 min $\epsilon_{zz}, \delta_{\theta z}$ transient creep derivative plot for $\lambda = 0.92$	128
5.6	$\epsilon_{zz} \vee \delta_{\theta z}$ total strains for constant $\lambda$ tests	129
 Prog.		
5.1	Strain rates	130

## CHAPTER 6

6.1	Tension and compression stress-strain path	150
6.2	+ve and -ve torsion stress-strain path	151
6.3A	$\epsilon_{zz}$ creep component for prior plastic axial strain ( $\int d\epsilon_{zz}^p$ )	152
6.3B	$\delta_{\theta z}$ " " " " " " " "	153
6.4A	$\delta_{\theta z}$ " " " " " shear " ( $\int d\delta_{\theta z}^p$ )	154
6.4B	$\epsilon_{zz}$ " " " " " " " "	155
6.5	Secondary creep rate correlation	156

Fig.		Page
6.6	Effect of prestrain on transient creep (10 min) shear strain at $\tau_{0z} = 14.25 \text{ N/mm}^2$	157
6.7	Effect of prestrain on transient creep (10 min) longitudinal strain at $\tau_{zz} = 15 \text{ N/mm}^2$	158
6.8	$\epsilon_{zz} \vee \delta_{0z}$ total strains for $\lambda = 0.95$ (nominal)	159
6.9	" " " " " " " " " "	160
Table		
6.1	Constants in the Bailey equation	145
6.2	$d\delta^p/d\epsilon^p$ comparison for 2% prior compression	147
Prog.		
6.1	Strain rates	161
6.2	Strain rates of Hu	175

#### A P P E N D I X I

Fig.		
1	Yield loci	25
2	Hardening models	26

#### A P P E N D I X II

Fig.		
1	Tension cell calibration (Denison)	13
2	" " " (Rig)	14
3	Torsion " " (Avery)	15
4	" " " (Rig)	16
5	Tension-torsion calibration	17

#### A P P E N D I X III

Fig.		
1	Logarithmic plot based on the law $\epsilon = \epsilon_0 + a \ln t$	23
2	Derivative analysis based on the parabolic law $\epsilon = \epsilon_0 + a t^m$ for the test of Fig. 1	24
3	Derivative analysis showing the effect of a 2% prior plastic prestrain on the parabolic time exponent $m$ .	25
4	Evaluation of parabolic constants $a$ and $\epsilon_0$ for the test in Fig. 2. Intercept is $\epsilon_0$ , slope is $a$ for the stress levels indicated.	26
5	Stress dependence of $a$ for $\Delta\sigma = 0.8 \text{ N/mm}^2$ at all test temperatures ( $a = k\sigma^p$ )	27
6	Stress dependence of $a$ for $\Delta\sigma = 2 \text{ N/mm}^2$ at all test temperatures ( $a = k\sigma^p$ )	28

Fig.

Page

7	Stress dependence of $a$ for $\Delta\sigma = 2.8 \text{ N/mm}^2$ at all test temperatures ( $a = k\sigma^p$ )	29
8	Temperature dependence of $k$ for $\Delta\sigma = 0.8, 2$ and $2.8 \text{ N/mm}^2$ ( $k = l \exp \frac{Q}{T}$ )	30
9	Stress increment dependence of $l$ ( $l = s \exp(r \cdot \Delta\sigma)$ )	31
10	Growth of $\epsilon_0$ with stress ( $\sigma$ ) for all tests	32
11	Mean curves showing relative amounts of total creep strain ( $\Sigma \epsilon^c$ ) and total instantaneous strain ( $\Sigma \epsilon_0$ ) with stress ( $\sigma$ ) and temperature ( $T$ )	33
12	Derivative analysis showing the effect on the constant $m$ when $\Delta\sigma$ is changed from $2.8$ to $0.8 \text{ N/mm}^2$ during test.	34
13	Photomicrograph showing grain boundary sliding	35
Table		
1	Variation of time exponent $m$ with stress level $\sigma$	35
2	" " " " " " temperature $T$ and stress increment value $\Delta\sigma$ .	35

## ACKNOWLEDGEMENTS

The author would like to express gratitude to:

The Director of Studies, Dr. S. B. Mathur for his continued help and interest in this research.

His advisers Mr. J. R. Heath-Smith and the late Mr. D. A. Berry of the Royal Aircraft Establishment, Farnborough, for their assistance given at the initiation of the research programme.

Mr. G. A. Woolvet for the use of the facilities in the School of Mechanical, Aeronautical and Production Engineering.

Messrs. R. Bax and J. Boyd for their skilful manufacture of the test specimens; and

Mrs. J. Lynn for her care in typing the thesis.



## **IMAGING SERVICES NORTH**

Boston Spa, Wetherby  
West Yorkshire, LS23 7BQ  
[www.bl.uk](http://www.bl.uk)

**DECLARATION PAGE NOT  
SCANNED**

## SUMMARY

Creep tests at room temperature under combined tension-torsion have been performed on thin walled tubes of commercially pure aluminium (ELA) in the annealed, extruded and prestrained conditions.

The required creep stresses were achieved by incremental loading along a constant stress ratio path (radial loading). Axial ( $\epsilon_{zz}$ ) and shear ( $\delta_{\theta z}$ ) strains were measured throughout deformation.

Strains produced by radial loading on annealed and extruded aluminium consisted of an instantaneous component and a short-time creep component. For all stress paths the latter component was of the form  $\epsilon \propto t^m$  where the time exponent  $m$  lay in the parabolic range  $0 < m < 1/2$ .

The plastic prestraining of annealed aluminium was either beneficial or detrimental to its combined tension-torsion creep resistance. Forward prestrains (in tension or positive torsion) or large reversed prestrains (in compression or negative torsion) were beneficial to creep resistance by hardening the aluminium in the direction of the stress path. The effect was to eliminate the short-time creep component of radial loading and to reduce the primary creep strains and secondary creep rates of ensuing long-time creep. Small amounts of reversed prestrain were detrimental to creep resistance by softening the aluminium in the direction of the stress path. The effect was to increase the parabolic creep component of radial loading ( $m$  lowered) and to increase the primary creep strains and secondary creep rates of ensuing long-time creep.

Experimental observations on flow behaviour were not in agreement with predictions from isotropic theory. The anisotropy in the three conditions of aluminium was examined in the instantaneous plastic strain increment vector of loading ( $d\delta_{\theta z}^p / d\epsilon_{zz}^p$ ) and in the strain rate vector of short and long-time creep ( $\dot{\delta}_{\theta z} / \dot{\epsilon}_{zz}$ ). For each stress path on annealed aluminium the colinearity in these vectors indicated an initially anisotropic material which hardened uniformly throughout deformation. Stress paths on extruded aluminium produced rotations in the initial instantaneous vectors of loading while stress paths on prestrained aluminium produced rotations in the instantaneous vectors of loading and in the strain rate vectors of long-time creep. With increasing stress of loading or with accumulating creep strain the vectors rotated into colinearity. The behaviour was typical of the nature of anisotropic hardening in material possessing a strain history.

Plastic strain increment ratios derived from the yield functions of Edelman and Drucker  $f = \frac{1}{2} C_{ijkl} (\sigma'_{ij} - m \epsilon'_{ij}) (\sigma'_{kl} - m \epsilon'_{kl})$  and Yoshimura  $f = \frac{1}{2} C_{ijkl} \sigma'_{ij} \sigma'_{kl} - m \epsilon'_{ij} \sigma'_{ij}$  were found to describe the plastic anisotropy in the three conditions of aluminium. Hill's yield function  $f = \frac{1}{2} C_{ijkl} \sigma'_{ij} \sigma'_{kl}$  was descriptive of the plastic anisotropy in uniform hardening. This led to an extension of each theory for creep. In general strain rate ratios derived from the extended theories were in good agreement with observations on creep anisotropy.

## LIST OF SYMBOLS

The following symbols have been employed to describe thin walled cylinder behaviour due to combined tension-torsion loading. (as in Appendix II).

a	Beam dimension.
A	Original specimen c.s.a.
A'	Current specimen c.s.a.
C	Combined load.
d	Specimen diameter.
$d_1, d_2$	Original outside and inside diameters.
$d'_1, d'_2$	Current outside and inside diameters.
h	Eccentricity of loading dimension.
$I_x$	Second moment of specimen area.
J	Polar moment of specimen area.
k	Diameter ratio ( $= d_1/d_2$ ).
$l_0$	Original specimen gauge length.
$l'$ or $l_1$	Current specimen gauge length.
$r, \theta, z$	Polar coordinates.
r	Specimen radius.
$r_m$	Mean radius.
t	Wall thickness.
T	Torsional load.
$T_1$	Applied specimen torque.
W	Tensile load.
$W_1$	Applied axial load.
$x, y, z$	Cartesian coordinates.

y	Linear dimension in bending theory.
z	Axial extension.
$e_{zz}$	Engineer's axial strain.
$\lambda, \lambda'$	Original and current stress ratio.
$\sigma_{zz}, \sigma'_{zz}$	Original and current axial stress.
$\tau_{xz}, \tau'_{xz}$	Original and current shear stress.

The following symbols have been used to describe the time independent plastic flow of Appendix I and Chapters 3-6.

$c, f, g$	Yield criteria functions.
$E, G, \nu$	Elastic constants.
$F, G, H, L, M, N$	Anisotropy constants.
$i, j, k$	Tensor suffices.
$J'_1, J'_2, J'_3$	Stress tensor invariants.
$k$	Shear yield stress.
$r$	Plastic strain increment ratio.
$Y$	Tensile yield stress.
$\beta_1, \beta_2, \beta_3$	Plastic strain increment ratio coefficients.
$e^e, e^p, e$	Elastic, plastic and total strains.
$de'_{ij}, de'_{ii}$	Plastic strain increment tensors.
$de'_1, de'_2, de'_3$	Principal plastic strain increments.
$de'_{rr}, de'_{\theta\theta}, de'_{zz}$	Normal plastic strain increments.
$d\delta^p_{e_z}$	Shear plastic strain increment.
$d\bar{e}^p$	Equivalent plastic strain increment.
$d\bar{e}^p_m, d\bar{e}^p_r$	von Mises and Tresca equivalent plastic strain increments.
$d\bar{e}^p_a$	Equivalent anisotropic plastic strain increment.
$d\delta^p$	Maximum plastic shear strain increment.
$dW^p$	Plastic work increment.
$\delta_{ij}$	Kronecker delta.
$\delta\lambda$	Flow rule parameter.
$\sigma_{ij}, \sigma_{ii}, \sigma_m$	Stress tensors.
$\sigma'_{ij}$	Deviatoric stress tensor.
$\sigma'_1, \sigma'_2, \sigma'_3$	Principal deviatoric stresses.
$\sigma_{zz}$	Axial stress.

$\tau_{02}$ 

Shear stress.

 $\tau$ 

Maximum shear stress.

 $\sigma$ 

Equivalent stress.

 $\sigma_M, \sigma_T$ 

von Mises and Tresca equivalent stresses.

 $\sigma_a, \sigma^*$ 

Equivalent anisotropic stresses.

 $\pi$ 

Deviatoric plane.

 $\alpha$ 

Rotation of the axes of anisotropy.

 $\theta$ 

Angle of twist.

The following symbols have been used to describe the creep behaviour of Appendix I and Chapters 3-6.

$a, b, B, B', B_1, B_2$	Constants in the transient creep equations.
$a', b'$	Long time creep constants.
$A, A', B, C, D, E, M, \sigma_0$	Experimental stress-strain rate constants.
$A_1, B_1$	Anisotropy coefficients.
$n, P, P_1, P_2$	Stress exponents.
$F$	Second invariant function.
$k, k'$	Flow rule constants.
$K, M, D$	Plastic potential functions.
$m, m_1, m_2$	Time exponents.
$q$	Stress difference exponent.
$t$	Time.
$T$	Absolute test temperature.
$T_m$	Absolute melt temperature.
$\epsilon_0$	Instantaneous elastic and plastic strains.
$\epsilon^c, \dot{\epsilon}^c$	Creep strain, creep strain rate.
$\dot{\epsilon}_{ij}$ or $\dot{\epsilon}'_{ij}$	Creep strain rate tensor.
$\dot{\epsilon}_1, \dot{\epsilon}_2, \dot{\epsilon}_3$	Principal creep strain rates.
$\dot{\epsilon}_{22}$ or $\dot{\epsilon}'_{22}$	Axial creep strain rate.
$\dot{\gamma}_{\theta 2}$ or $\dot{\gamma}'_{\theta 2}$	Shear creep strain rate.
$\dot{\epsilon}$ or $\dot{\epsilon}^c$	Equivalent creep strain rate.
$\dot{\epsilon}_M, \dot{\epsilon}_T$	von Mises and Tresca equivalent strain rates.
$\dot{\epsilon}_a, \dot{\epsilon}$	Anisotropic equivalent strain rates.
$\Delta\sigma_{22}$ or $d\sigma_{22}$	Axial stress increment.
$\Delta\tau_{\theta 2}$ or $d\tau_{\theta 2}$	Shear stress increment.
$\lambda$	Creep flow rule parameter.
$\phi$	Time function.

# INTRODUCTION

## INTRODUCTION

Most creep testing is performed by the application of one stress and the measurement of a corresponding strain. Tests of this kind on both ferrous and non-ferrous high temperature materials have been used to accumulate the great volume of creep and rupture data that is so useful to the designer (1)\*. Thus in recent years considerable advances have been made in the technology of components for high-temperature service; for example in gas turbines (2), chemical plant (3), supersonic aircraft (4) and space vehicles (5).

Although simple creep data may often be applied directly to such engineering problems there are many instances, however, where the imposed loading is complex in nature. An efficient and economical design must therefore account for multiaxial stress conditions. Consequently, over the past forty years the problem of creep due to combined loading has been the subject of investigation (6-17). Basically the nature of these investigations has been to confirm the use of theoretical equations that could be used with the conventional simple creep data to predict the measured creep rates of laboratory tests. The equations that have been verified in this way have then found great use in the design of components required to operate under creep conditions for any system of stress (18-25).

The multiaxial creep theory assumes a material that has the same flow properties in all directions irrespective of the direction of straining (isotropy). Its use therefore lies in its application to those ordinary polycrystalline metallic materials where the imposed strains occur over a great many randomly orientated crystal grains and exhibit a gross behaviour that is approximately isotropic. The assumption of isotropy does, however, present a serious limitation to the theory. It is well known that real materials exhibit a Bauschinger effect where, for example, a history of one directional straining is known to change the tensile and compressive strength of all other directions. A further restriction imposed on the theory is the assumptions that the initial condition of the material is perfectly homogenous and continuous. Thus both the crystal line structure and the initial condition of the crystal grains are ignored. Since rolled or drawn stock form the large part of engineering structures the flow properties would then vary depending upon the relative orientation of the applied stress system and the rolled direction. Most real engineering materials are, therefore, truly anisotropic.

\* Main text reference number

Anisotropic deformation is complex. To develop a theory which accounts for it in all possible stress systems would not seem an easy task. Nevertheless functions have been proposed for anisotropic yielding but their associated stress-plastic strain flow relations have not been verified experimentally. Stress-strain rate relations have been proposed for anisotropic creep deformation but their use has been restricted to instances where predictions based on isotropic theory have failed to agree with experimental observation. Neither the cause nor the effect of the anisotropy has been fully understood. The objective of the present work was to establish experimentally the creep behaviour in material of known initial anisotropy and to compare the results with available theoretical predictions. As a complement, the plastic flow generated by loading to the creep test stresses was to be compared with stress-plastic strain predictions derived from various anisotropic yield functions.

The experimental investigation entailed the measurement of the plastic strain and creep produced by a biaxial stress system in a commercial grade of pure aluminium (B.S. 1476 ELAM). In order to avoid the effects of structural instability due to high-temperature grain growth and recrystallisation in this material all experiments were conducted at a temperature of 21°C ( $T/T_m = 0.32$ ). The effect of each of the following types of initial anisotropy has been studied:

- (1) That due to the preferred grain orientation existing in a bar of extruded aluminium.
- (2) That due to a strain history in annealed aluminium. Various degrees of prior tension, compression, positive and negative torsion were chosen to provide a strain history.

The basis for comparison in each type was the plastic flow and creep behaviour of annealed aluminium in the near isotropic condition.

The biaxial stress system; that of combined tension-torsion, was applied to thin walled tubes of the test material in a rig designed specifically for this purpose. Loading was performed incrementally and in such a way that the ratio of shear to tensile stress was maintained constant ( $\lambda = \tau_{\theta z} / \sigma_{zz} = \text{constant}$ ). This has enabled the anisotropy of deformation to be examined in a plastic strain increment vector of loading ( $d\delta_{\theta z}^p / d\epsilon_{zz}^p$ ) and in a strain rate vector of ensuing creep ( $\dot{\delta}_{\theta z} / \dot{\epsilon}_{zz}$ ). A measurement of the degree of anisotropy in deformation for each initial condition of aluminium has been made in a 'k' factor of loading ( $\frac{d\delta_{\theta z}^p}{\lambda d\epsilon_{zz}^p}$ ) and creep ( $\frac{\dot{\delta}_{\theta z}}{\lambda \dot{\epsilon}_{zz}}$ ).

An examination of the directions of the strain vectors has enabled comparisons with theoretical predictions to be made. The most satisfactory predictions on anisotropic creep deformation were found from certain yield functions that had been adapted to the test conditions and then extended to creep.

The investigation on prestrained aluminium was additionally designed to establish the effect of prestrain on tension-torsion creep resistance. The results were interpreted from the hardening or softening effect that a prestrain had in the direction of an applied stress path. This led to understanding on the type of prestrain that would be most beneficial to creep resistance in any biaxial stress system.

# CHAPTER I

The first part of the book is devoted to a general survey of the subject. It is divided into three main sections: the first dealing with the history of the subject, the second with the principles of the subject, and the third with the practice of the subject. The first section is the most important, as it shows the development of the subject from its earliest beginnings to the present day. The second section is also very important, as it explains the principles which govern the subject. The third section is the least important, as it only deals with the practical details of the subject.

## CHAPTER 1

## LITERATURE REVIEW

The first laboratory tests on multiaxial stress creep were designed to check the validity of isotropic theory. In an attempt to obtain an initially isotropic test material a heat treatment was performed at a suitable stage in the manufacture of test specimens. In certain test programmes an isotropy check was made by a tensile strength examination on ancillary specimens cut from orthogonal directions in the material. The test specimens were then subjected to a multiaxial stress creep condition. Comparisons made between the creep strain rates measured in these tests and those calculated from isotropic theory enabled the theory to be verified experimentally. Some experimenters (8-11) report on poor agreement between measured strain rates and isotropic predictions. The discrepancy has been attributed (12) either to the failure in obtaining an initially isotropic material or to anisotropic creep deformation. Other experimenters (13-17) report on good agreement and so confirmed the theory.

The isotropic creep theory has successfully predicted the measured strain rates of some structures in multiaxial stress situations (18-23). However, for other structures a better agreement has been found with predictions obtained from variations to the theory (24,25). In general, the problem of initial anisotropy is more apparent in a structural material than in a carefully prepared test material. Structures fabricated from rolled or drawn stock are likely to be anisotropic by virtue of the preferred orientation of their grain structure or by an induced strain history. An investigation on the multiaxial stress creep in such initially anisotropic material does not appear in the literature.

In searching for improved creep resistance in engineering materials many experimenters have studied the effect of plastic prestrain on creep. Their published work (30-48) describes the way the basic creep curve of a material is modified by a prestraining operation and, generally, has been directed at finding the prestrain which yields maximum creep resistance. The creep curves and prestrains of this work were those produced by either a tension or a torsion stress system. The effect of prestrain on multiaxial stress creep resistance is not reported in the literature.

In reviewing the published work of relevance to the present investigation two surveys are presented; the first surveys the applicability of theoretical predictions to problems on multiaxial creep and the second surveys the effects of prior plastic strain on subsequent creep behaviour.

### 1.1 MULTIAXIAL STRESS CREEP

The theory describing strain rates in multiaxial stress creep is based on the assumption that creep deformation obeys the well established laws of plasticity. The development of the theory is given in Appendix I and the equations quoted here refer to this Appendix. Basically there are two sets of equation; the first set (equations (36) - (41)) describe isotropic creep deformation, while the second set (equations (43), (48) and (59)) describe anisotropic creep deformation. Experiments designed to test the validity of these equations have been of a biaxial stress type.

#### 1.1.1 Equations (36) - (41) on Isotropy

Equations of the form (36) were originally developed and used in engineering design by Soderberg (6) and Marin (7) with a von Mises definition of equivalent stress ( $\bar{\sigma} = \bar{\sigma}_M$ ). For a principal triaxial stress system ( $\sigma_1, \sigma_2, \sigma_3$ ) the principal secondary creep rates ( $\dot{\epsilon}_1, \dot{\epsilon}_2, \dot{\epsilon}_3$ ) are then,

$$\begin{aligned}\dot{\epsilon}_1 &= A \bar{\sigma}_M^{n-1} [\sigma_1 - \frac{1}{2}(\sigma_2 + \sigma_3)] \\ \dot{\epsilon}_2 &= A \bar{\sigma}_M^{n-1} [\sigma_2 - \frac{1}{2}(\sigma_1 + \sigma_3)] \\ \dot{\epsilon}_3 &= A \bar{\sigma}_M^{n-1} [\sigma_3 - \frac{1}{2}(\sigma_1 + \sigma_2)]\end{aligned}\tag{1.1}$$

where,

$$\bar{\sigma}_M = \frac{1}{\sqrt{2}} [(\sigma_1 - \sigma_2)^2 + (\sigma_2 - \sigma_3)^2 + (\sigma_1 - \sigma_3)^2]^{1/2}$$

and A and n are experimental constants.

The validity of the Marin-Soderberg equation (1.1) was first checked by Jamieson (8) with combined tension-torsion creep tests on lead tubes. This was followed with similar tests on steel tubes by Everett and Clark (9) and Tapsell and Johnson (10). Norton (11) checked equation (1.1) with internal pressure creep tests on closed ended steel tubes. In general some agreement was found between the measured creep rates of these early tests and the Marin-Soderberg isotropic predictions. Davis (12) later attributed the discrepancies either to a form of anisotropy which was initially present in the tubes or to a form of anisotropy which developed during the test.

Further work on internally pressurised 0.5% carbon-molybdenum steel tubes at 900 and 1050°F by Norton and Soderberg (13) confirmed equation (1.1) for the prediction of secondary circumferential creep rates. Likewise Marin, Faupel and Hu (14) have successfully applied the Marin-Soderberg equations to the prediction of axial and shear secondary creep rates in their combined tension-torsion ambient creep tests on commercially pure aluminium tubes. In general Marin et al found better agreement when the applied stresses were corrected for creep deformation.

Kennedy, Harms and Douglas (15) employed equation (36) for  $\bar{\sigma}$  written both as the von Mises and Tresca ( $\bar{\sigma}_T = \sigma_1 - \sigma_3$ ) definitions in their combined internal pressure-axial load tests on Inconel pipe at 1500°F. It was found that the von Mises equivalent stress gave the better correlation of axial secondary creep rates although the use of the Tresca equivalent stress in this equation was seen to be satisfactory in view of its simplicity in application and conservancy in prediction.

Stowell and Gregory (16) used a hyperbolic sinh function relationship between the von Mises equivalent stress and equivalent strain rate and thereby employed equations of the form (37) to the combined tension-torsion creep of an aluminium alloy at 400°F. For this stress system ( $\sigma_{zz}, \tau_{\theta z}$ ) and a von Mises definition of equivalent stress Stowell and Gregory used the following form of equation (37) for the prediction of axial and shear creep rates,

$$\dot{\epsilon}_{zz} = \frac{\sigma_{zz}}{(\sigma_{zz}^2 + 3\tau_{\theta z}^2)^{1/2}} \cdot M \frac{\sinh\left(\frac{\sigma_{zz}^2 + 3\tau_{\theta z}^2}{\sigma_0}\right)^{1/2}}{\sigma_0} \quad (1.2)$$

$$\dot{\gamma}_{\theta z} = \frac{3\tau_{\theta z}}{(\sigma_{zz}^2 + 3\tau_{\theta z}^2)^{1/2}} \cdot M \frac{\sinh\left(\frac{\sigma_{zz}^2 + 3\tau_{\theta z}^2}{\sigma_0}\right)^{1/2}}{\sigma_0}$$

where M and  $\sigma_0$  are experimental constants.

The authors found that equation (1.2) could be satisfactorily used to describe their experimental secondary creep rates. Furthermore in their examination of strain rate ratios in this work the authors indicated that equation (1.2) could probably be used, with the addition of a time function, for the prediction of primary creep rates. This indication was based on their observation that the ratio ( $\dot{\gamma}_{\theta z} / \dot{\epsilon}_{zz}$ ) was independent of primary creep time.

Johnson (17), in an outstanding contribution to this subject, demonstrated the general applicability of equation (41) to both primary and secondary creep. In his combined tension-torsion studies on many engineering materials at typical working temperatures Johnson showed, through the geometrical similarity of component creep curves, the

dependence of creep rate on stress and time to be separable functions during primary creep. This would confirm the aforementioned indication of Stowell and Gregory. For all materials Johnson showed the time dependence to be a simple power function with an exponent in the range of 0.44 - 0.77 whilst the stress dependence took on two separate forms at each temperature. The first form, associated with isotropic behaviour, was the simple power  $J_2'$  function written in equation (41) as  $F(J_2') = J_2'^p$  where  $J_2' = \bar{\sigma}_M/\sqrt{3}$  and  $p$  lay between 0 and 1 for all temperatures. This meant that for this stress range the Marin-Soderberg equations applied since equation (36) is then identical to equation (41) for the constants of equation (42) and with the addition of a time function  $\phi(t)$ . The second form, associated with an increase of anisotropy of deformation at higher stress levels, took on a complex power function. Over the whole range of stress Johnson employed a function of the type  $A'F(J_2') = A_1'(J_2')^{p_1} + A_2'(J_2')^{p_2}$  in equation (41) which deteriorated to  $A'J_2'^p$  for lower stress levels. In physical terms the anisotropy of these tests took the form of a redistribution of secondary ( $\dot{\epsilon}_2$ ) and minor ( $\dot{\epsilon}_3$ ) principal creep rates whilst the major principal creep rate ( $\dot{\epsilon}_1$ ) remained unaffected by stress level. Anisotropy constants  $A_1$  and  $B_1$  were accordingly introduced into equation (41) to account for this. The resulting equations, describing the principal creep rates at a primary creep time of 150 hours, were of the form,

$$\begin{aligned}\dot{\epsilon}_1 &= F(J_2') [A_1(\sigma_1 - \sigma_2) - B_1(\sigma_3 - \sigma_1)] \phi(t) \\ \dot{\epsilon}_2 &= F(J_2') [(\sigma_2 - \sigma_3) - A_1(\sigma_1 - \sigma_2)] \phi(t) \\ \dot{\epsilon}_3 &= F(J_2') [B_1(\sigma_3 - \sigma_1) - (\sigma_2 - \sigma_3)] \phi(t)\end{aligned}\tag{1.3}$$

noting that,  $J_2' = \bar{\sigma}_M/\sqrt{3}$  for  $\bar{\sigma}_M$  as defined in equation (1.1) and  $A_1(\sigma_1 - \sigma_2) - B_1(\sigma_3 - \sigma_1) = (\sigma_1 - \sigma_2) - (\sigma_3 - \sigma_1)$

The Marin-Soderberg equation (1.1) has found by far the greatest use in its application to structures. With it Johnson (18) developed the solutions to the creep of thick walled tubes subjected to combinations of applied axial load, bending moment and torque. Other practically significant structures that have been approached by equation (1.1) are the secondary creep in rotating discs (19), in loaded flat plates (20) and in shaft interference fits (21). More recently Ohnami and Motoie (22) have implied the use of this equation for secondary creep rate prediction in 0.12 - 0.15% carbon steel thick walled cylinders subjected to combined axial

load and internal pressure at 500°C. A satisfactory correlation with separate tension tests was observed, provided the equivalent stress and strain rate for the cylinder were defined at the inside or mean wall diameter. Clay (23) successfully applied the Marin-Soderberg equation to the secondary creep of circumferential ribbed stainless steel tubes at 785°C with both internal and external pressurisation. Corrections were made to the hoop stresses for the effects of rib reinforcements and wall thinning during straining. These tests were designed to simulate the environmental conditions of fuel cladding in advanced gas cooled reactors. The results showed the usefulness of the equation when applied to an important practical problem of this kind.

Not all experimenters have discovered satisfactory agreement between their measured creep rates and the predicted creep rates of the Marin-Soderberg equation however. Wahl (24), for example, preferred the Tresca criterion for use in equation (36) when describing the nature of creep in rotating discs and Venkatraman and Hodge (25) employed the Tresca criterion with its associated flow rule (equation 38) for their solution to creep in loaded plates. The Tresca flow rule with a von Mises equivalent stress (equation 39) has not appeared in the literature. Finnie (26), in an attempt to solve these inconsistencies, conducted tension, compression, torsion and internal pressure creep tests on aluminium and lead tubes at a homologous temperature ( $T/T_M$ ) of 0.56. The results of these tests showed that none of the available multiaxial creep rate equations were suitable for describing internal pressure creep when based on torsion creep data. Finnie observed, in his survey of the published data, that multiaxial creep tests performed below a homologous temperature of 0.5 correlated well on the basis of the Marin-Soderberg equation whilst those conducted above that temperature, in common with his, did not. He suggested that either the effect of hydrostatic stress on creep was no longer negligible at these temperatures or that the development of anisotropy was excessive.

In conclusion it would appear that equation (1.1) is suitable in its prediction of multiaxial creep rate components only to a limited range of stress and temperature. When this is so, the von Mises equivalent stress definition of  $\bar{\sigma}$  in this equation has been found more satisfactory than the Tresca definition. However, the latter definition has been occasionally employed with equation (1.1) for certain structures owing to its mathematical simplicity of application. At the higher stresses and temperatures where the equation has not been found satisfactory this has been attributed to some form of anisotropy and modification to the equation has then been made (equation 1.3).

### 1.1.2 Equations (43), (48) and (59) on Anisotropy

Bailey (27) proposed equation (43) as a general theory for the multiaxial creep in engineering components. For an isotropic material the following principal secondary creep rates were proposed,

$$\begin{aligned}\dot{\epsilon}_1 &= \frac{A \bar{\sigma}_m^{2m}}{2} \left[ (\sigma_1 - \sigma_2)^{n-2m} + (\sigma_1 - \sigma_3)^{n-2m} \right] \\ \dot{\epsilon}_2 &= \frac{A \bar{\sigma}_m^{2m}}{2} \left[ (\sigma_2 - \sigma_1)^{n-2m} + (\sigma_2 - \sigma_3)^{n-2m} \right] \\ \dot{\epsilon}_3 &= \frac{A \bar{\sigma}_m^{2m}}{2} \left[ (\sigma_3 - \sigma_1)^{n-2m} + (\sigma_3 - \sigma_2)^{n-2m} \right]\end{aligned}\quad (1.4)$$

where,

$$\bar{\sigma}_m = \frac{1}{\sqrt{2}} \left[ (\sigma_1 - \sigma_2)^2 + (\sigma_2 - \sigma_3)^2 + (\sigma_1 - \sigma_3)^2 \right]^{1/2} \quad \text{and}$$

A, m and n are experimental constants.

Bailey confirmed equation (1.4) with combined internal pressure -axial load ambient creep tests on annealed lead pipe. As discussed in Section 3 of Appendix I the Bailey equation (1.4) was used by Johnson as an alternative to his anisotropic equation containing the complex power function in  $J_2'$ . Equation (1.4) would, therefore, appear to represent anisotropy in a general way and indeed it contains the Marin-Soderberg isotropic theory as a special case (when  $n - 2m = 1$ ). It is interesting to note that Bailey proposed anisotropic equations by introducing constants into his equation (1.4) in a similar manner to that of equation (1.3). The resulting equations, however, have not appeared elsewhere in the literature.

Equation (48) was developed by Berman and Pai (28) in a theory based on a linear approximation to a general yield surface. Effectively the resulting creep rate equations are more general than the Marin-Soderberg type by virtue of the flexibility afforded to the definition of equivalent stress ( $\bar{\sigma}$ ). In correcting the errors between the measured creep rates of Stowell and Gregory and their isotropic calculations (equation 1.2) Berman and Pai used the following equations for the principal secondary creep rates,

$$\begin{aligned}\dot{\epsilon}_1 &= \frac{K(\bar{\sigma}_T)^n}{\bar{\sigma}_m} \left[ \sigma_1 - \frac{1}{2}(\sigma_2 + \sigma_3) \right] \\ \dot{\epsilon}_2 &= \frac{K(\bar{\sigma}_T)^n}{\bar{\sigma}_m} \left[ \sigma_2 - \frac{1}{2}(\sigma_1 + \sigma_3) \right] \\ \dot{\epsilon}_3 &= \frac{K(\bar{\sigma}_T)^n}{\bar{\sigma}_m} \left[ \sigma_3 - \frac{1}{2}(\sigma_1 + \sigma_2) \right]\end{aligned}\quad (1.5)$$

where,

$\bar{\sigma}_T$ , the Tresca equivalent stress, =  $\sigma_1 - \sigma_3$ ,

$\bar{\sigma}_M$  is the von Mises equivalent stress of equation (1.4) and K and n are experimental constants.

The Tresca definition of equivalent stress in equation (1.5) gave a better correlation with uniaxial tensile results (on which the prediction of multiaxial creep rates was based) than the von Mises definition did.

For a material exhibiting the type of anisotropy due to a preferred grain orientation equation (59) has been developed to describe this.

The creep strain rates are shown in Sections 4 and 5 of Appendix I to be an extension to Hill's theory of anisotropic plastic flow (29) with an associated definition of equivalent stress ( $\bar{\sigma}_a$ ) and strain rate ( $\dot{\epsilon}_a$ ).

For principal creep rates that is,

$$\begin{aligned}\dot{\epsilon}_1 &= \frac{\dot{\epsilon}_a}{2\bar{\sigma}_a} [F(\sigma_1 - \sigma_2) - H(\sigma_3 - \sigma_1)] \\ \dot{\epsilon}_2 &= \frac{\dot{\epsilon}_a}{2\bar{\sigma}_a} [G(\sigma_2 - \sigma_3) - F(\sigma_1 - \sigma_2)] \\ \dot{\epsilon}_3 &= \frac{\dot{\epsilon}_a}{2\bar{\sigma}_a} [H(\sigma_3 - \sigma_1) - G(\sigma_2 - \sigma_3)]\end{aligned}\quad (1.6)$$

where

$$\begin{aligned}\bar{\sigma}_a &= \frac{1}{\sqrt{2}} [F(\sigma_1 - \sigma_2)^2 + G(\sigma_2 - \sigma_3)^2 + H(\sigma_3 - \sigma_1)^2]^{1/2} \\ \dot{\epsilon}_a &= \frac{\sqrt{2}}{(GH + FG + HF)} [F(G\dot{\epsilon}_1 - H\dot{\epsilon}_2)^2 + H(G\dot{\epsilon}_1 - F\dot{\epsilon}_3)^2 + G(H\dot{\epsilon}_2 - F\dot{\epsilon}_3)^2]^{1/2}\end{aligned}$$

Equation (1.6) is sufficiently general to contain the Marin-Soderberg equation (1.1) as a special case (for  $F = G = H = 1$ ) but is probably more usefully applied to a material that retains its initial anisotropy during subsequent creep deformation since F, G and H are then assumed to be fixed constants. No published work exists, either to confirm or refute this assumption. Actually Johnson's equation (1.3) which is partly similar in form to equation (1.6) was used to describe the type of anisotropy that developed during test but then the 'constants' A, and B, of equation (1.3) were found to be complex functions of the applied stress system.

In conclusion it would appear that the Bailey equation (1.4) is the most general type of equation to describe anisotropic creep behaviour. Its one fault, however, lies in its inconsistency with the laws of plastic flow. As outlined in Section 3 of Appendix I the redefinition of an equivalent stress (equation (44)), necessary to correct this inconsistency, would unfortunately only add to the difficulty in applying the equation.

## 1.2 CREEP OF PRESTRAINED MATERIAL

It is well known that the introduction of certain types of prestrain may either improve creep resistance or impair it. A prestrain may be deliberately applied or it may be induced due to service loading. The latter being of an uncontrollable nature is of concern in engineering components that experience severe temperature gradients. Gas turbine blades and steam piping are examples of high-temperature components that can set up residual compressive plastic strains as a result of rapid heating and constrained expansion. At their steady working temperatures the effect of the loading is likely to cause creep in tension. For a full understanding of the performance of such components it is, therefore, necessary to study the extent to which creep is modified by prior plastic prestrain.

On the other hand, experiments have been carried out with a view to obtaining the nature of prestrain that would give the best creep resistance. The variables in the prestraining operation have been isolated and examined to this end. For a creep test of fixed stress and temperature, they are;

- (1) amount of prestrain
- (2) temperature of the prestraining operation
- (3) direction of prestrain with respect to subsequent creep direction
- (4) prestrain rate
- (5) time in the treatment of the metal or alloy at which prestrain is introduced.

The results of these investigations are reviewed in the paragraphs that follow. Except where otherwise stated the prestrains and subsequent creep strains are both of a simple tensile nature.

### 1.2.1 Amount of Prestrain

Tests of this kind involve the creep testing at fixed stress and temperature on material that has been prior strained by varying amounts. The simplest investigation is that for which the prestrain and creep temperatures are the same. An investigation of this kind was conducted by Hill (30) under the author's direction on specimens of commercially pure aluminium that had been prior strained by 5, 7, 9, 11 and 13%. The subsequent room-temperature creep curves (Fig. 1.1) show that creep resistance is enhanced by prior strain. The amount of primary creep and secondary creep rate are both reduced while the time to rupture is increased. These observations are in full agreement with those made by Andrade (31) in similar tests on lead.

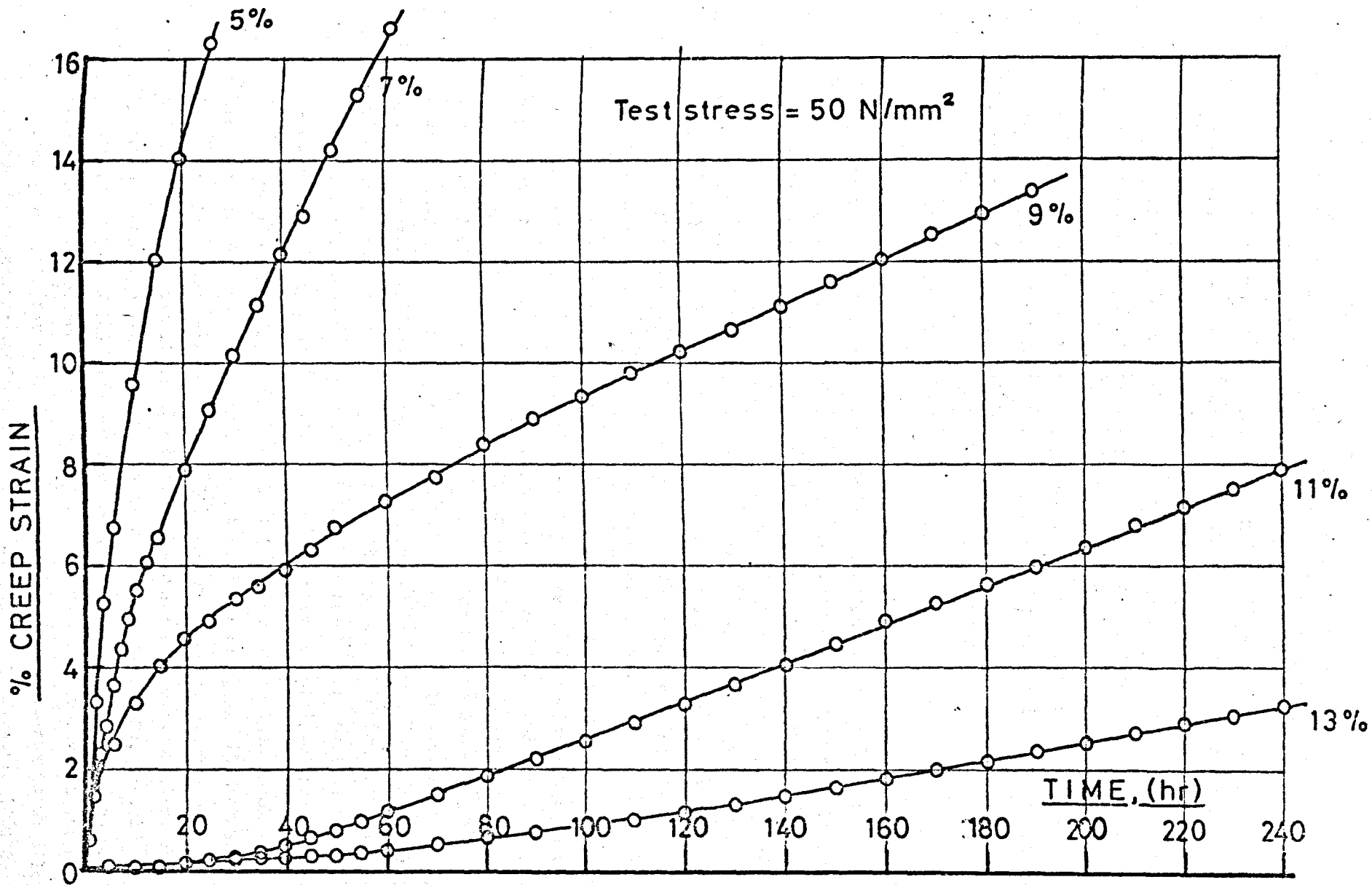


Fig.1 Effect of prestrain on creep in aluminium at 21°C (Hill(30))

Naturally it is of interest to know here if there is some value of prestrain that would have the maximum beneficial effect on creep properties. Zschokke and Niehus (32) discovered such optimum values in carbon steel that decreased with increasing creep temperature. Further evidence of this was found by Kozyrsky and Kononenko (33) in nickel alloys and Azhazha et al (34) in pure nickel. In these investigations the optimum prestrain was associated with a structure that exhibited its most resistant work hardened form. Prestrains in excess of the optimum value were then identified with either a nucleation of cracks at grain boundaries or softening from recrystallisation.

### 1.2.2 Temperature of Prestrain

The effect of introducing prestains at temperatures different from the creep test temperature have been studied in some detail but with apparently contradictory results. Similar beneficial effects to those described in paragraph 1.2.1 were observed by Wilms (35) on 99.99% pure aluminium prestrained by varying amounts at 20°C then tested for creep at 250 and 350°C. These observations were in agreement with those of Kennedy (36) who introduced prestains at different temperatures in lead wire and with those of Hazlett and Hansen (37) on prior prestrained/annealed pure nickel and solid solution nickel alloys.

Further investigations on the effect of a low-temperature prestrain have, in general, shown it to be more effective in improving subsequent creep properties than one applied at room-temperature. For the same degree of prestrain (3.5%) introduced in nickel at -269 and 27°C Azhazha et al (38) showed the lower temperature to be the more effective in improving the subsequent 700°C creep resistance. This is supported by Davies et al (39) who prestrained a dilute nickel alloy by 15 and 25% at -196, 20 and 500°C and reported that the low-temperature treatment was equivalent in its beneficial effect on the subsequent creep and fracture properties at 500°C to increasing the prestrain value in their higher temperature treatments.

On the other hand Martinod et al (40) who prestrained an aluminium alloy (equivalent to RR58) at 20°C and tested for creep at 175°C observed increases in primary creep strain and secondary creep rate and generally a decrease in rupture life. The comparison, made with an unprestrained specimen tested for creep at the same stress and temperature, showed prestrain to have a deleterious effect on creep resistance. Mention should also be made of the work of Grant et al (41) who in their investigation on creep rupture life for high purity aluminium and aluminium-magnesium alloy introduced prestains above and below the creep test temperature (260°C) to show no significant improvement in creep life.

An explanation of these contradictions may lie in the relative magnitudes of the creep test stress and the chosen prestrain values. In the programme of testing employed by Hill care was taken in choosing a creep test stress that lay in the mid range of stresses used originally to reach the levels of prestrain. Thus in some instances (5 and 7%) the test stress exceeded the prestress whilst in others (11 and 13%) the prestress exceeded the test stress. The greatest benefit, attained for 13% prestrain, meant that the prestress exceeded the test stress by the maximum amount. Had the creep test been at a higher temperature than the prestraining temperature then in view of the reduction in flow stress with increased temperature, this improvement would possibly have been lessened. It is feasible therefore that for certain combinations of stress and temperature no benefit in creep properties would be observed by a prestraining operation. Davies et al add support to this in concluding that an improvement in creep resistance and rupture life was only obtained for the condition where the prestrain exceeded the instantaneous loading strain of annealed metal. The tests of Kozyrskiy and Kononenco add further support. Investigating the effect of prestrain at 20°C on the secondary creep rate at 700°C in a 1.8% aluminium-nickel alloy these authors showed the magnitude of the creep stress to have a significant effect on subsequent creep properties. At a stress of 2.5 kg/mm<sup>2</sup> a maximum beneficial effect was seen for a prestrain approaching 5% but in raising the creep stress to 5 kg/mm<sup>2</sup>, in otherwise identical test conditions, no improvement was observed over the whole range of prestrain.

On the other hand Wilson (42), investigating the effect of a constant 3% prestrain on the creep properties of RR58 at 150°C for various stress levels, agreed with Martinod et al for each of his chosen stress levels. It is likely, however, that a prestrain results in the formation of cavities at grain boundaries for this particular alloy. This is discussed in more detail in paragraphs 1.2.3 and 1.2.5.

### 1.2.3 Direction of Prestrain

The few experiments in which the directions of the prestrain and subsequent creep strain have been reversed are of a torsional nature. Initial plastic compression followed by creep in tension does not appear in the literature probably because of the difficulties inherent in such tests. The problems of axiality of loading, prevention of instability and changing cross sectional areas associated with tension and compression are avoided to some extent in torsion tests.

Whatever the method of strain reversal, however, the reduction in the value of yield stress that accompanies it (Bauschinger effect) might be expected to impair the creep properties of that direction just as the increased yield stress of a prestrained direction has, in general, been seen to improve the subsequent creep properties of that direction.

The observations of Biscaya (43) on thin walled tubes of RR58 were shown to be in complete contrast to this expected trend. Applying a plastic shear strain of 1% at room-temperature (20°C) in both the same and opposite directions to the subsequent creep direction at 150°C, Biscaya showed, for a creep shear stress of 29.7 N/mm<sup>2</sup>, prestrain in the same direction to be detrimental and reversed straining to be beneficial. The comparison was made with a creep curve obtained from an unprestrained specimen tested at the same creep stress and temperature. Huston (44) in extending the work of Biscaya eliminated the ageing effects likely to occur in heating from prestrain to creep temperatures in this alloy by introducing prestrain at the same temperature. For a common temperature of 150°C Huston also showed a prestrain in the same direction as the subsequent creep direction to be detrimental. A reversed prestrain, however, was only shown to be beneficial in lowering the secondary creep rate. The effect of the increased prestrain temperature was shown to be equivalent in its effect on subsequent creep to reducing the amount of prestrain at room-temperature.

Since these trends are consistent with those of Wilson and Martinod et al for the same alloy Huston concluded that the detrimental effect in this alloy was likely to be the formation of voids at grain boundaries due to the prestrain—that are enlarged by the creep strain in the same direction.

The effect of reversed straining on the creep of pure metals and solid solutions is not well understood although some experimental work (45, 46) on repeated stress reversals indicate that the creep process is accelerated by reversed straining.

#### 1.2.4 Prestrain Rate

There is some published evidence that the rate of straining employed for the prestrain can markedly affect the subsequent creep properties. In general, prestraining at fast strain rates improves creep strength. Wilms and Rea (47) employed two strain rates,  $6 \times 10^{-3}$  and  $6 \times 10^{-4}$  in/min, in applying a 2% prestrain at 1065°C to a chromium alloy. The faster strain rate was seen to be the more beneficial in improving the subsequent creep properties at 1065°C. Further support on this is provided by Hodgson (48) who showed improvements in secondary creep rate resistance for fast prestraining in a ferrite-pearlite structure of an alloy steel.

### 1.2.5 Time at which Prestrain is Introduced

In order to study the changes in dislocation density and distribution of precipitates and their effect on subsequent creep properties Wilson and Martinod et al applied their tensile prestrains before the ageing treatment in an RR58 alloy. The resulting detrimental effect that occurred in creep of the same direction was attributed to an increase in the number of dislocations available for slip. Biscaya and Huston who both showed this detrimental effect for a torsional prestrain introduced after ageing concluded that void formation was the likely cause. The conclusion was based on the fact that reversed prestrain would introduce the same dislocation density as a forward prestrain of the same amount and, therefore, the same number of available slip mechanisms. This implies that a prestrain of either direction in this alloy would have the same detrimental effect on subsequent creep properties. Since a reversed prestrain was in fact shown to be beneficial to creep properties then void formation was thought to be a particular feature of this alloy.

In pure metals and solid solutions it is known (49) that inhomogeneous deformation within individual grains and across grain boundaries has the effect of fragmenting individual grains into a large number of closely spaced subgrains. In order to stabilise such a structure Hazlett and Hansen carried out a recovery anneal following their prestraining of nickel and nickel alloys. The effect of varying degrees of stable subgrain structure on the subsequent creep properties then formed the basis of this investigation. The resulting trend would appear to be little different from that for a subgrain structure produced by prestrain alone (Fig. 1.1). The effect of a recovery anneal is to relieve lattice distortion and perfect the subgrains. Since Wilms identified these two effects with the first stage in the creep curve for prestrained pure aluminium then this might explain the similar behaviour. Furthermore, in either condition both Wilms and Hazlett and Hansen observed that the final stage in the subsequent creep curve appeared to be the attainment of a creep rate comparable to that of the annealed metal. This Wilms associated with a marked growth in the initial substructure that finally reached the equilibrium size of annealed metal. However, in contrast, Davies et al in a more detailed study on the effect of a recovery anneal concluded that over a wide stress range the subsequent creep and fracture resistance were more improved by a prestrain-recovery treatment than by a prestrain treatment alone.

### 1.2.6 Summary

In view of the considerable diversity in experimental procedures it is not possible to arrive at any specific conclusions from the published data. In some instances recovery anneals were given after prestraining. The degrees of prestrain vary widely as do the straining and testing temperatures. Over the whole range of tests no attempt seems to have been made in standardising the levels of prestrain or in choosing the straining and testing temperatures as fixed fractions of the melting point. Some of the higher temperature studies may further have been complicated by recrystallisation and grain growth occurring during creep, or recovery and ageing effects occurring during the heating from prestrain to creep temperatures. However the following trends were made evident by this work:

- (1) The effect of prestrain on subsequent creep properties depends upon the amount, direction and rate of the prestrain and the temperature of application. It further depends upon the creep test stress and temperature, the structure and chemical composition of the test material.
- (2) In general, for pure metals and solid solutions creep resistance is enhanced by a prior plastic prestrain. The maximum benefit is approached at some optimum prestrain level that is best introduced at lower temperatures. The effect of prestrain on alloys is less well defined and depends upon whether the structure is resistant to void formation. In either case if benefit is observed then it is because the creep stress and temperature do not upset the stability of the structure.

# CHAPTER 2

## CHAPTER 2

## EXPERIMENTAL

The test rig used in these tests was essentially a modified version of a machine originally designed by Mathur and Alexander (50) to subject tubular specimens to combinations of tension, torsion and internal pressure at room or elevated temperatures.

In this chapter an outline of these modifications is given along with subsequent machine calibrations. Further details are given on the choice of specimen sizes, the test material, heat treatment and machining procedure. A description of the instrumentation used in the measurement of specimen displacements is also explained and lastly, the test procedure is outlined.

### 2.1 THE TEST RIG - MODIFICATIONS AND DESCRIPTION

Originally the machine had been designed to have a load capacity of 110 kN in tension and 500 Nm in torsion. For the present series of tests the following modifications were made:

- (1) The loads were applied by weights thus eliminating the water piping, reservoir and pump of the previous system. (Loads were applied here by controlling the water flow to tension and torsion buckets).
- (2) The load capacity was reduced to 40 kN in tension and 150 Nm in torsion. The selection of these figures was based on two factors,
  - (a) pure aluminium has approximately one twelfth the yield stress of the previous test material (RR58);
  - (b) it was favourable to select figures that did not involve a radical redesign of the machine.
- (3) The existing Duralumin tension load cells were replaced by ones of reduced cross-sectional area. Thus the smallest tensile load that could be accurately recorded was 5 N. The existing torsion load cells were found to be satisfactory in recording loads of the same order.
- (4) A beam was added that made possible the application of combined tension and torsion loads of any desired ratio.

The resulting modified machine is that shown photographed in Fig. 2.1.\* A detailed description of the more important component parts is now given.

### 2.1.1 Tension Loading System (Figs. 2.2, 2.3, 2.4)

Tension was produced by applying weights (1) to a five-to-one lever (2). This then acted at a connecting rod carrier and was transmitted to the test specimen (3) through a cross member (4) containing the two tension load cells (5), and a torsion cell (6). The transmission was made, in the first instance, by in-line running pulleys (7) then connecting rod links and knife edges (8) and (9) and finally through eight bolt flanges (10) screwed to the specimen ends. Further crossed knife edges (Fig. 2.4) in the tensile linkage rested on hardened steel plates and provided axially of loading. All knife edges had  $90^\circ$  included angles in contact with  $120^\circ$  plates which therefore permitted a  $\pm 15^\circ$  rotation from the vertical position. Alignment of the torque cells and specimen was ensured by the machined dowels (Fig. 2.4) linking them — the torque was transmitted by square and registers between these components and the flange block.

In the original design of the machine a facility existed to maintain a constant tension lever ratio automatically throughout the straining process (Fig. 2.3). This amounted to a microswitch control on the height of fulcrum (11) that would compensate for a 7.5 mm extension on the specimen and linkages. To achieve this the fulcrum was rigidly fixed to a cross beam (12) and this whole assembly was supported by two moveable hardened steel wedges (13). The wedges were driven inwards by a slow speed (0.5 rev/min) electric motor (14) through a compound gear train (15) and a screwed shaft (16) to give a lift rate of  $65 \times 10^{-3}$  mm/min for the cross beam. On the basis of some preliminary testing the automatic wedge control was seen to be tantamount to increasing the load on the specimen during test. This facility was therefore not used in the programme of testing reported here. All the creep tests of this thesis are that of a "constant load" type but with some error due to a changing lever ratio. Actually the tests approximate to that of the "constant stress" type since the reduction in load due to a decreasing magnification ratio is matched by a reduction in cross-sectional area.

To measure the tensile load two Duralumin load cells (5) (Fig. 2.4) were connected in parallel and as close to the test specimen as was possible. The 32 mm shank diameter was machined to 12.7 mm over a length of 100 mm. The  $252 \text{ mm}^2$  area over this length was calculated to give a

\* All figures are given at the end of this Chapter.

maximum load measuring capacity of 37.5 kN at a limiting elastic stress of  $150 \text{ N/mm}^2$ . This easily accommodated an ultimate tensile load of 8 kN on a tubular test specimen of area  $127 \text{ mm}^2$ . Four electrical resistance strain gauges were attached to each cell, two longitudinally and two laterally. The four gauges of each cell (abcd) formed a separate Wheatstone's bridge circuit (Fig. 2.4) that compensated for bending effects by measuring only axial loads. The two circuits were each energised from a common 6V stabilized power supply. Loads were then calculated from the out of balance voltage of each bridge measured from a d.c. potentiometer by switching in each circuit separately. The load-out of balance voltage characteristic for each cell had previously been obtained from a calibration on a Denison tension machine (see Appendix II).

### 2.1.2. Torsion Loading System (Figs. 2.2, 2.4, 2.5)

A torque was produced by applying weights to load hanger (17) which was transmitted to the test specimen by a cross beam (18), cables and pulleys (19). A central load applied to the hanger of this cross beam was supported and split four ways by the lower two outer pulleys (Fig. 2.2). Each load component was then directed through four further pulleys so that the whole arrangement served to apply equal and opposite tangential loads at diametrically opposite points on in-line horizontal pulleys (20). Each pulley was 254 mm in diameter with  $90^\circ$  peripheral cable grooves. The two inner pulleys were attached to the machine by rigid fork arm uprights (21) clamped to an adjustable table (22). When locked this table formed a rigid anchorage for one end of the specimen assembly. The two outer pulleys were mounted on horizontal fork arms (23) and clamped to adjustable cross bars (24). Both the table and the cross bars were bolted to the main columns of the machine by half shell Tufnol bearings (25). Experiment showed that their resistance to sliding was of the order 0.16 MN per column which therefore eliminated any possibility of slip during test.

To record the specimen torque two solid Duralumin cells, 29.2 mm diameter (6) were connected in series with the test specimen and on either side of it. Each cell was capable of measuring a maximum torque of 425 Nm at a limiting elastic shear stress of  $85 \text{ N/mm}^2$  - which easily accommodated an ultimate specimen torque of 65 Nm. Each cell was bonded with two-paired element torque strain gauges. The four gauges of each cell were arranged in the bridge circuit of Fig. 2.4 in such a way as to record torsion only. Thus for a superimposed tensile load the bridge circuit produced a net cancellation in the axial component of strain in each gauge. Like the tension circuit the gauges of each torsion cell

formed a separate circuit (efgh) and were energised from the same 6 V stabilised supply. The outputs from the two torsion circuits were measured separately by switching in each circuit to the common d.c. potentiometer. The torque-out of balance voltage characteristic for each cell had previously been obtained from a calibration on an Avery reversed torsion machine (see Appendix II).

### 2.1.3 Combined Loading (Fig. 2.5)

Tension and torsion combined loading could be produced in one of two ways:

- (1) By applying weights to the loading ends (1) and (17) of the tension and torsion levers respectively;
- (2) By applying weights at some intermediate beam position (26).

The latter method was the more useful since it allowed combined loading to be applied in any desired proportion. This was achieved simply by applying weights at the appropriate position on the beam (27) that connected the tension lever (2) and torsion cross beam (18) (Fig. 2.2). Moreover this proportion was maintained when loading incrementally - a feature important in certain plasticity studies, known as radial loading. This meant that the ratio of shear to tensile stress was maintained at a constant positive value when loading in this manner. A negative ratio was also possible by applying the combined load to a cantilever extension at either end of the beam. In this way one of the loads would be increased whilst the other decreased proportionately. Obviously for such a negative ratio a load would have to be in existence at either the tension or torsion support in the first instance.

The beam, made from an aluminium alloy, was 50 mm deep, 18 mm wide and 1525 mm long. It was symmetrically supported on a length of 545 mm by two close fitting spindles (28) that passed through the beam and weight hanger brackets (29). The weight hangers were therefore free to rotate about the spindles and a further spindle (30) on the tension bracket allowed for the attachment of the tension cable. The torsional weight hanger (17) was centralised on its cross beam (18) by two locknuts (31) and weights applied at the intermediate position (26) were transmitted to the beam by a 90° knife edge. To reduce its weight the beam was drilled at intervals along the length and tapered for 430 mm beyond the "supports". Beam cross-sectional dimensions were chosen to accommodate a maximum bending stress of 20 N/mm<sup>2</sup> under combined loading.

In the original design of the machine combined loading was achieved by a method similar to (1). In the present design method (2) was used exclusively for combined loading. Calibrations made at eighth and third positions between the supports of the beam are given in Appendix II. This involved finding an experimental stress ratio  $\lambda = \tau_{0z} / \tau_{zz}$  for each position and then comparing it with the theoretical value calculated from beam equilibrium. Fig. 5 of Appendix II showed good agreement between each experimental and theoretical  $\lambda$  value. Theoretical considerations on the change in  $\lambda$  during plastic deformation showed it to increase by  $\frac{1}{2}\%$  for each 1% of plastic axial strain. For an expected total axial strain of order 5% (plastic strain + creep strain) in the present tests a  $2\frac{1}{2}\%$  increase in  $\lambda$  was not of serious concern.

#### 2.1.4. Internal Pressure

In thin walled cylinder testing the introduction of an internal bore pressure in addition to axial tension and/or torsion would provide alternative loading systems. For the purpose of future work (Section 7.6 paragraph (7)) the internal pressure arrangement of Fig. 2.6 is suggested for use with this rig.

A nitrogen bottle with regulator valve and pressure gauge would serve to supply nitrogen at the required test pressure through the top flange block and alignment dowel. Provided leakage was not excessive the test pressure should be maintained for the duration of the creep test by the reservoir of nitrogen in the bottle. To reduce and to seal the volume enclosed by the specimen bore each alignment dowel could be made with a core-bar extension and O-ring recesses as shown. A flexible inlet pipe and sprung loaded extensometer probes (Fig. 2.14) would allow the specimen to deform without restriction during test.

## 2.2 TEST MATERIAL

The main test programme entailed the experimental investigation of flow behaviour in a structurally anisotropic material and in a prestrained material. For simplicity it was decided to manufacture test specimens from the following three forms of a common material.

- (1) In solid extruded bar form. The material was expected to be highly anisotropic due to a preferred grain structure.
- (2) In prestrained form. Known prestrains were to be applied to material in a near isotropic condition.

(3) In near isotropic form.\* This was to provide a basis in the investigation.

Consistency in (1) demanded that the entire stock be from the same melt while (2) and (3) required that the extruded structure should be heat treatable into an approximately isotropic condition. To meet these requirements a pure metal was chosen as the test material.

In a review of published data made by Graham (51) it was concluded that the behaviour of pure metals in engineering environments followed the same creep laws as complex alloy steels and dispersion hardened alloys. It would therefore not seem to matter whether a pure metal or an alloy was chosen in which to investigate anisotropy. However the test temperature can render a material with an anisotropy in deformation which is peculiar to the test conditions (see Section 7.5). In a pure metal this is typified by high temperature grain growth and recrystallisation. To avoid this in the present work a test temperature well below the recrystallisation temperature was chosen (21°C).

Copper and aluminium of commercial purity were each considered as a test material. Ultimately the choice was limited by cost and consequently aluminium was chosen. A 9.10 m length of bar was purchased from High Duty Alloys Ltd to the following specification:

"A semi-continuous casting of one 220 lb Hiduminium 1A melt, analysed-machined and extruded under production conditions to  $1\frac{3}{4}$  in. diameter bar".

Hiduminium 1A, as extruded, is made approximately to the same composition as B.S. 1476-ELAM (Table 2.1)†.

### 2.3 TEST SPECIMENS

Test specimens were machined for the following three investigations:

- (1) Combined stress studies in the main test programme. Tubular specimens were chosen for the reasons outlined in paragraph 2.3.1.
- (2) A study on the plastic flow and creep produced by incremental tensile loading.
- (3) 'Hounsfield' studies on the tensile isotropy of the annealed aluminium.

\* Allowing for a small degree of anisotropy.

† All Tables are given at the end of this Chapter.

### 2.3.1 Tubular Specimens

A biaxial stress system is most closely represented by stressing a tube in one of the following three ways:

- (1) combined tension-torsion.
- (2) combined torsion-internal pressure.
- (3) combined tension-internal pressure.

A tubular specimen is suitable for this provided the wall thickness is of such a thickness that,

- (1) the variation in shear stress across the wall, due to an applied torque, is negligible.
- (2) the radial stress through the wall, due to an internal pressure, is small enough to be neglected and that the circumferential stress is kept to a minimum.
- (3) buckling does not occur.

The effect of these on the choice of specimen sizes may conveniently be investigated in terms of a mean diameter thickness ratio ( $d/t$ ). To meet the first stipulation (1) the wall thickness ( $t$ ) should be made as small as possible, thus ( $d/t$ ) should be high. This is also the requirement for stipulation (2). The buckling condition (3) however requires that ( $d/t$ ) be made small from the following considerations.

Plastic buckling involving torsion is likely when one principal stress is negative, as in the case of pure torsion ( $\sigma_1 = \tau$ ,  $\sigma_2 = -\tau$ ,  $\sigma_3 = 0$ ). Here Finnie (52) has shown that for a tube of gauge length  $l$  satisfying dimensionally,

$$25 (t/d) < (l/d)^2 < 5/4 (d/t) \quad (2.1)$$

that the maximum shear strain which can be attained before buckling is given by,

$$\gamma = 4.67 (d/l)^{1/2} / (d/t)^{5/4} \quad (2.2)$$

Thus to accommodate large shear strains ( $d/t$ ) should be kept to a minimum. This is more clearly seen if  $d$  is written as,

$$d = k + t$$

where  $k$ , the tube inside diameter, is a fixed constant here. Hence equation (2.2) can then be written as,

$$\gamma = 4.67 \left( \frac{k+t}{l} \right)^{1/2} / (k/t + 1)^{5/4} \quad (2.3)$$

which demands that  $t$  be kept to a maximum if large shear strains are required.

A  $(d/t)$  ratio of 18 was chosen as a final compromise. This would mean an elastic circumferential stress variation for a pressurised cylinder (53) of  $\pm 6\%$  on the mean value, and from equation (2.2), a 10% shear strain before the onset of buckling.\*

Two further factors were considered in the selection of this ratio. Firstly, the accuracy of strain measurement increases as the specimen sizes increase and secondly, the difficulty in manufacturing tubes with the necessary uniformity in wall thickness increases with decreasing thickness.

The specimens were manufactured to the sizes shown in Fig. 2.7. A wall thickness of 1.5 mm was chosen on a 25.4 mm bore with a gauge length of 50 mm. The choice of this gauge length is discussed in Appendix II. To suit existing machine parts the ends were screwed  $1\frac{3}{4}$ " x 20 t.p.i. and 1" alignment dowels governed the bore size. Two 0.8 mm ridges at the gauge length extremities allowed an extensometer to be mounted. Mathur and Alexander showed a ridge of this size not to affect significantly the gauge length stress distribution in combined tension-torsion.

### 2.3.2 Tension Creep Specimens (Fig. 2.9)

These were machined to B.S.3500 1969, Part 3. The ends were machined with  $3/16$ " diameter reamed holes to suit the pull rods of existing creep machines. A pair of 0.9 mm ridges defined the gauge length and allowed an extensometer to be mounted. These specimens were used to examine incremental loading strains (Appendix III).

### 2.3.3 Isotropy, Hardness and Metallographic Examination

A series of Hounsfield tensile specimens (Fig. 2.10(a)) were manufactured from longitudinal, transverse and oblique directions. The specimens were used to assess the isotropy of the test material. This investigation was supplemented by metallographic observations on discs of test material taken from the bar at positions immediately adjacent to the Hounsfield positions.

A further series of tensile specimens was manufactured to B.S. 18, 1962 (Fig. 2.10(b)). Their ends were threaded to  $5/16$ " B.S.F. to suit the jaws of an Instron machine. These specimens were used to establish tensile data for the test material.

---

\* The consideration given to circumferential and radial stress variation has been made in anticipation of future work that involves internal pressure (see paragraph 2.1.4).

### 2.3.4 Cutting Plan (Fig. 2.11)

The specimens described in paragraphs 2.3.1 - 2.3.3 were cut from the bar in the following way:

The 9.10 m of bar was supplied in four lengths A, B, C and D. The numbers and letters in the cutting plan refer to,

- O - 5 tension creep specimens
- X - hardness and metallography discs
- Y - 3 transverse Hounsfield specimens
- Z - 8 longitudinal Hounsfield specimens
- S - 6 longitudinal tension specimens
- E - used for experimental machining

and every number (1 - 47) represented one tubular specimen. Numbers made to identify position in the length are shown above each bar.

A longitudinal scribed line served to identify the cross-sectional positions of specimens taken from pieces O, Y and Z. With the exception of specimens whose axes coincided with the bar axis all other longitudinal specimens were machined from these pieces so that their axes coincided with the mid-wall diameter of a tubular specimen (26.9 mm). The transverse specimens of piece Y were machined with their axes lying tangential to this diameter.

Fig. 2.12(a) shows the angular positions of the Hounsfield longitudinal (L) and transverse (T) specimens with respect to the scribed line ( $0^\circ$ ). Fig. 2.12(b) shows the positions of some oblique Hounsfield specimens machined in tandem with oblique creep specimens.

The 66 mm overall length of a tension creep specimen made it impossible to machine it in the transverse direction. Various oblique directions were therefore chosen and specimens were machined in such a way that their central portions contained what would have been the wall of a tubular specimen had it been machined there. Of the five specimens machined from each bar piece (O) in Fig. 2.12(b), two were oblique (O) and three were longitudinal (L). The longitudinal specimens were suitably identified in the cross-section in terms of an angle made to the scribed line ( $0^\circ$ ) and Fig. 2.13(a) shows a composite picture of all longitudinal creep specimen directions.

To identify the cross-sectional positions of oblique specimens a rectangular coordinate system was used that identified '1' with the longitudinal direction. Thus the oblique specimen shown in Fig. 2.13(a) could be completely defined by a plane (1-2) and an angle ( $180^\circ$ ). Fig. 2.13(b) shows the composite picture made by the axes of all such oblique

specimens and the angles  $\beta$  and  $\gamma$  between them. The angle between each oblique axis and the longitudinal direction ( $\alpha$ ) was  $21.8^\circ$ .

All angular positions in the cross-section were measured in a clockwise direction from the scribed line as a datum when viewed in the cutting plan from right to left.

### 2.3.5 Material Preparation and Specimen Manufacture

Two types of anisotropy are likely in a machined specimen. The first, associated with the extrusion process, is a preferred grain orientation and the second, associated with machining, is a strain hardening effect. In order to study the effect of anisotropy due only to a prestrain history it was necessary to perform the prestraining operation on initially isotropic material. An anneal was therefore necessary to recrystallise and stress relieve the grain structure. To avoid possible distortion in the finished specimen sizes the anneal was carried out at a blank stage (Figs. 2.8 and 2.9(a)) prior to finished machining. The machining of the specimen to final dimensions was then completed by taking successive cuts each not greater than 0.25 mm.

The best combination of time and temperature to be used in the anneal was found in the following way:

A disc of bar material, 8 mm thick, was split into segments each identified by a letter (A - O). Five temperatures, 300, 350, 400, 450 and  $500^\circ\text{C}$ , were chosen and three times,  $\frac{1}{2}$ ,  $1\frac{1}{2}$  and  $2\frac{1}{2}$  hours, so that each segment was annealed at one of the fifteen time-temperature combinations for a rapid rate of heating. Having cooled in the furnace, a Vickers pyramid hardness test was carried out on each segment and all those which showed a (V.P.N.)<sub>5</sub> of less than 19 were prepared for metallographic examination. Segments were mounted, polished and etched in the usual way. From the microscopic examination the best combination of time and temperature was thought to be:  $2\frac{1}{2}$  hours at  $450^\circ\text{C}$ . The judgement was based on that segment which exhibited a uniform recrystallised structure of equiaxed fine grains. The average grain size of this structure measured by the intercept method, was found to be 0.22 mm, which would give seven grains across the wall of a tubular specimen. Table 2.2 gives the hardness figures for each segment along with a Vickers photomicrograph of the chosen structure.

The tests on 'as extruded' material were performed on tubes that had been given a light stress relieve anneal ( $150^\circ\text{C}$  for 2 hours) at the blank stage (Fig. 2.8) of manufacture.

The gauge length profile of each specimen in Figs. 2.7 - 2.10 was produced from a respective template used in conjunction with a Mimik copy attachment, a Harrison 12" swing centre lathe and a single point cutting tool.

Table 2.3 shows the operation sequence employed in the manufacture of a tubular specimen (Fig. 2.7). This was designed to ensure concentricity of tube diameters, square end registers and threaded ends. In order to avoid residual surface stresses in the gauge length no polishing, grinding or reaming operations were permitted after annealing. Light finish machining was performed by the sequence of four operations in 'B'. The wall thickness and bore diameter of each finished tube were measured on 90° diameters for each of five gauge length positions. A Solex air gauge recorded a maximum variation of  $\begin{matrix} +.013 \\ -.010 \end{matrix}$  mm on an average bore diameter of 25.402 mm and a micrometer recorded a maximum variation of  $\begin{matrix} +.003 \\ -.007 \end{matrix}$  mm on an average wall thickness of 1.503 mm. A Societe Genevoise measurement of gauge length showed this to be repeatable at 50 mm. In Appendix II the variations in tube geometry are shown to be less significant than load eccentricity in their effects on applied stress.

Micrometer measurements on the diameter of each finished tension creep specimen (Fig. 2.9) showed a maximum variation of  $\begin{matrix} +.006 \\ -.008 \end{matrix}$  mm on an average diameter of 5.644 mm. A repeatable gauge length of 28.233 mm was to be used in subsequent strain calculation as the 'original length'.

#### 2.4. DISPLACEMENT AND STRAIN MEASUREMENT

Ideally, combined tension-torsion deformation in a thin walled cylinder would be studied from simultaneous measurements of current extension, diameter, thickness and twist. However, the arrangement of transducers necessary to record these from the gauge length would be complicated and might well restrict the deformation. The comparisons between experimental creep rates and isotropic calculations in Section 1.1 have been made possible simply from measurements made of extension and twist. In the present work anisotropic theories were to be applied to experimental results in a  $\frac{d\delta_{\theta 2}}{d\epsilon_{zz}^p}$  ratio of radial loading and in a  $\frac{\delta_{\theta 2}}{\epsilon_{zz}}$  ratio of ensuing creep. A  $\frac{d\epsilon_{\theta\theta}^p}{d\epsilon_{zz}^p}$  of loading was also to be measured. For this purpose an extensometer was designed that was capable of continuously measuring extension, twist and diameter of a deforming tube. A description of this follows.

#### 2.4.1 Extension and Twist Measurement

These displacements were measured from two linear variable differential transformer (l.v.d.t) transducers mounted in the extensometer of Fig. 2.14. The extensometer consisted of two steel clamping rings that each matched three portions of the specimen gauge length ridges. The location was made only by inverted ridges in the rings. To accommodate changes in diameter of the specimen during test one portion of each ring was made as a sprung loaded insert. 'Duralumin' brackets were made to house both transducers and were attached to the rings in such a way that the one measuring extensions lay vertically at 75 mm from the specimen centre line whilst the torsional displacements were measured by a transducer lying horizontally at 50 mm radius. A brass disc served as a datum for each transducer and for setting purposes these were made adjustable. Various sizes of transducer could be mounted in this extensometer by exchanging sleeves in each bracket. Generally, a  $\pm 2.5$  mm high precision type was employed in the measurement of these displacements. Both transducers were calibrated in a universal measuring machine (see paragraph 2.4.5).

In the measurement of extensions for the tension creep specimens of Fig. 2.9 two inductance transducers were attached in parallel with and on each side of the specimen. The attachment was made by two sprung loaded rings in the extensometer of Fig. 2.15. A dogleg between each ring and transducer bracket allowed each transducer to be sited well clear of a furnace bottom.

The extensometry used in the application of prestrain was basically the same as that described above for extension and twist measurements. Here, however, the extensometer rings were attached to the "blank" specimen by three pointed screws (Fig. 2.16A). The whole arrangement was then adapted to fit either the alignment spigots of a 250 kN 'Instron' machine or the end registers of a 15000 Kg cm 'Avery' reversed torsion machine (Fig. 2.16B). The sizes of a prestrain blank are shown in Fig. 2.16A.

#### 2.4.2 Diameter Measurement

Diametrical changes were measured by three sprung steel cantilevers which made  $120^\circ$  contact with the gauge length centre. The cantilevers were made for attachment to the lower machine flange and to pass through clearance holes in the lower clamping ring. Figs. 2.17A and B then shows the set up for the measurement of extension, twist and diametrical changes.

Each cantilever had two 5 mm strain gauges stuck on its tensile and compressive faces and near the fixed end where the bending moment was a

maximum. All six gauges were connected in series and formed the active arm of a Wheatstone bridge measuring circuit. The diameter gauge was calibrated on a stepped shaft (see paragraph 2.4.5).

### 2.4.3 Signal Conditioning and Recording

The three displacements were measured by means of the three channel transducer system shown diagrammatically in Fig. 2.18.

The system including the two l.v.d.t transducers was supplied by Sangamo Controls Ltd., Brighton. The l.v.d.t transducer consists of a single primary winding, two secondary windings and a moveable ferromagnetic core. The movement of this core increases the voltage in one secondary winding and decreases it in the other to produce a proportional voltage output. A four arm inductive bridge circuit was used here to measure this output. Thus the primary windings were energised by a common 5 kHz carrier oscillator supply and the voltage output for each transducer was conditioned at its respective module by a range, gain and sensitivity setting. Thereafter the signal was amplified, demodulated, filtered and then read on an indicator. In a similar way the resistive output from the strain gauged cantilevers, proportional to changes in specimen diameter, was measured in the half bridge circuit of Fig. 2.18.

For a continuous recording of transducer displacements an output jack served to by-pass the indicator unit for display on a potentiometric recorder. A three pen 'Rikadenki' chart recorder was employed for this purpose. Various combinations of module range settings and recorder voltage settings allowed the chart to be calibrated for a range of displacements from 0.05 - 5 mm.

For the measurement of tensile creep displacements the extensometer of Fig. 2.15 was used with two matched inductive transducers. The output signals here were electrically averaged, conditioned in a 'C.N.S' transducer meter, and recorded by one channel of a two channel 'T.O.A' polyrecorder. Combinations of the six meter sensitivities and recorder voltage settings allowed the chart to be calibrated for a range of displacements from 0.01 - 2.5 mm.

### 2.4.4 Strain Gauges

A number of tests were performed using strain gauges affixed to the outer diameters of tubular specimens. Two arrangements were used:

- (a) measurement of axial or circumferential strain using 'TML', YL10 gauges;

(b) measurement of axial, circumferential and  $45^\circ$  strains using 'TML', YRS5 rosettes.

In both cases three gauges were placed  $120^\circ$  apart around the tube — each gauge connected in series with the other two of the same direction. Direct strain readings were obtained from each direction by using a 'Tinsley' strain measuring bridge and selector switch. Where a continuous recording was required the resistive output was conditioned and amplified and recorded in an identical manner to the diameter gauge of paragraph 2.4.3. The gauges were either of a post yield type that measured up to 10% strain or the small strain ( $< 2\%$ ) elastic type.

#### 2.4.5 Calibrations

Both l.v.d.t transducers of the extensometer described in paragraph 2.4.1 were calibrated in terms of chart widths for the available meter range settings. To do this a displacement was applied directly to the transducer probes firstly in a 'Societe Genevoise' Universal Measuring machine for a master calibration and, secondly, in a bench micrometer to provide checks at the start and finish of a test. The torsional transducer was further calibrated in a 'Watts' 10" circular division tester. For this the extensometer rings of Fig. 2.14 were attached to a split mandrel in the same way as they would have been to a tubular test specimen. Two two halves of the mandrel could be moved apart or rotated at the centre of its 50 mm gauge length to simulate an axial displacement or an angular rotation. Through the latter the rotary table yielded a calibration figure of  $1.116^\circ/\text{mm}$  over all ranges including the maximum displacement (5 mm). Displacements greater than this were calibrated for a  $\pm 12.5$  mm transducer. It was found that the same calibration figure held provided the displacement did not exceed 9 mm either side of the horizontal centre line A-A of Fig. 2.14. Thereafter the change in the radius of rotation was seen as a departure from linearity in the calibration. Operating within this range allowed rotations of up to  $16^\circ$  to be measured without adjustment to the torsional micrometer. Since this corresponds to a shear strain of 7.5% the extensometer was considered suitable for the measurement of all tubular shear strain prior to buckling (see paragraph 2.3.1).

In order to avoid spurious signals from a non flat tensile platform or a non vertical torsional rest the 'Duralumin' mounting brackets were adjusted for the extensometer in position on the split mandrel so that,

- (1) no "tensile displacement" was recorded for a twist.
- (2) no "torsional displacement" was recorded for an extension.

The diameter gauge described in paragraph 2.4.2 was calibrated with a stepped shaft of diameters 28.5, 26.5, 24.5, 22.5 and 21.5 mm. This was lowered vertically into the gauge to allow the cantilevers to make contact with each diameter in turn. Thus the chart width was then understood in terms of specimen diametrical changes.

A further check on the angle of twist ( $\theta$ )<sup>o</sup> for small torsional displacements ( $\delta$  mm) was made from the tangent of this angle and the radius of rotation ( $r_m$  mm) of the transducer probe. Thus

$$\theta = \tan^{-1}(\delta/r_m) = \tan^{-1}(\delta/50.8) \quad (2.4)$$

which for 1 mm displacement yields

$$\theta = 1.125^\circ/\text{mm}.$$

#### 2.4.6 Accuracy

From the master calibrations the overall accuracy of displacement measurement was assessed as  $\pm 1.0\%$  on full scale chart deflection. Included in this are the individual performances of each component of the system. These were stated by the manufacturers as follows:

transducers  $\pm 0.1\%$  linearity,  $\pm 0.0002\%$  repeatability,  
 meter  $\pm 0.1\%$  linearity,  $\pm 0.5\%$  100 hour stability,  
 recorder  $\pm 0.15\%$  linearity,  $\pm 0.07\%$  resolution.

The calibration further showed that the smallest displacement measurable with this system without interference from noise was of the order of 0.0005 mm. The system therefore was suitable for measuring the small displacements associated with elastic loading, larger elastic plus plastic displacements and long-time creep displacements.

The investigation may conveniently be divided into four separate studies. These are described in the following paragraphs and run in the order in which each study was executed.

### 2.5.1 Creep and Plastic Flow During Incremental Loading

Since loading in the rig was incremental in nature an initial study was made of the nature of strain associated with short-time incremental loading. This study was made for simple tensile loading on annealed material.

The specimens of Fig. 2.9 were mounted in the extensometer of Fig. 2.15 and placed in an 'EMEC' creep machine with a three zone furnace and temperature controller. An examination was made of the effect of load increment value and test temperature on the strains that occurred between successive increments of load. A more detailed description of this procedure is given in Section 5 of Appendix III.

### 2.5.2. Tension-Torsion Tests on Annealed Material

By radial loading in the test rig eight cylinders of Fig. 2.7 were each tested for a constant ratio ( $\lambda$ ) of shear to tensile stress. All cylinders were loaded in 50 N increments to a load level for which the von Mises equivalent stress (see equation (3.1)) was approximately constant at  $37.5 \text{ N/mm}^2$ . Thereafter the cylinders were left to creep for 100 hours and for the duration of the creep test continuous measurements of the shear and axial strains were made. For each 50 N load increment the associated instantaneous shear, axial and diametrical strains were recorded. Fifteen minutes were then allowed to record the transient creep strains before the next 50 N increment was applied. During this interval the load cell outputs were measured. These outputs were used in equation (12) of Appendix II to calculate stress ratios of 0, 0.12, 0.53, 0.86, 1.81 and  $\infty$  for these tests. Two tests (0 and 0.53) were repeated.

### 2.5.3 Tension-Torsion Tests on Extruded Material

Six cylinders were tested in a procedure identical to that described in paragraph 2.5.2 for annealed material but with creep tests of 300-400 hours duration.

### 2.5.4 Tension-Torsion Tests on Prestrained Material

The cylinders of Fig. 2.7 were creep tested for a constant stress ratio ( $\lambda = \tau_{\theta z} / \sigma_{zz}$ ) of 0.95 but with a varying prestrain history. Each

cylinder was loaded in the test rig to 800 N in 50 N increments and then left to creep for a period of 300-400 hours. A 800 N load applied at a stress ratio of 0.95 corresponded to a tensile stress ( $\sigma_{zz}$ ) of  $16 \text{ N/mm}^2$  (equation (13) Appendix II) and a shear stress ( $\tau_{\theta z}$ ) of  $15.2 \text{ N/mm}^2$ .

The prestrain history of each specimen is given in Table 2.4. Tensile and compressive prestrains were applied in a 250 kN Instron machine at a displacement rate of 0.5 mm/min. Forward and reversed shear prestrains were applied in a 15000 kg cm Avery reversed torsion machine at a twist rate of  $3\frac{1}{3}^\circ/\text{min}$ . On a 50 mm gauge length these corresponded to an axial strain rate of  $\dot{\epsilon}_{zz} = 1.67 \times 10^{-4} \text{ s}^{-1}$  and a shear strain rate of  $\dot{\gamma}_{\theta z} = 2.75 \times 10^{-4} \text{ s}^{-1}$ .

For the larger tensile and torsional prestrains of Table 2.4 the extruded bar was machined to the blanks of Fig. 2.8 annealed and then prestrained in the adaptors of Fig. 2.16B before light machining to the test cylinder dimensions. Smaller prestrains were applied directly to finished cylinders. The same torsional adaptors of Fig. 2.16B were used to apply shear prestrains to specimens of finished dimensions but screwed flanges were used with the tension adaptors in applying tensile prestrain.

All compressive prestrains were applied to annealed cylinders (of dimensions: i.d. = 24 mm, o.d. = 44.4 mm and length = 165 mm) in the flat plattens of the Instron machine with 'Molyclip' as a lubricant. They were then light machined into the test cylinders of Fig. 2.7.

The tensile and compressive prestrain values ( $\epsilon_{zz}^p$ ) of Table 2.4 were calculated from the measured displacements ( $z$ ) of two circumferentially scribed lines originally 50 mm apart ( $l$ ) in the set up of Fig. 2.16A.

Then,

$$\epsilon_{zz}^p = \frac{z}{l} \times 100\% \quad (2.5)$$

The shear prestrain values ( $\gamma_{\theta z}^p$ ) of Table 2.4 were calculated from the measured angular rotation ( $\theta$  rads) of an original longitudinal line over the 50 mm length ( $l$ ) in a set up similar to Fig. 2.16A. Then,

$$\gamma_{\theta z}^p = \frac{r_m \theta}{l} \times 100\% \quad (2.6)$$

where  $r_m$  is the mean wall cylinder radius.

The shear prestrain values were chosen to give the same von Mises equivalent strain ( $\bar{\epsilon}_m^p$ ) as for tension and compression. Then from equation (3.9), for tension or compression  $\bar{\epsilon}_m^p = \epsilon_{zz}^p$  and for torsion  $\bar{\epsilon}_m^p = \gamma_{\theta z}^p / \sqrt{3}$ .

On completion of all the creep tests of paragraphs 2.5.1 - 2.5.4 the cylinders were unloaded and tested for recovery by allowing 15 minutes of recording time between successive load decrements. When completely unloaded the cylinders were further tested for recovery over a period of approximately 20 hours using a sensitive chart range. Such a period was always found to be adequate for measuring total strain recovery in the three conditions of material.

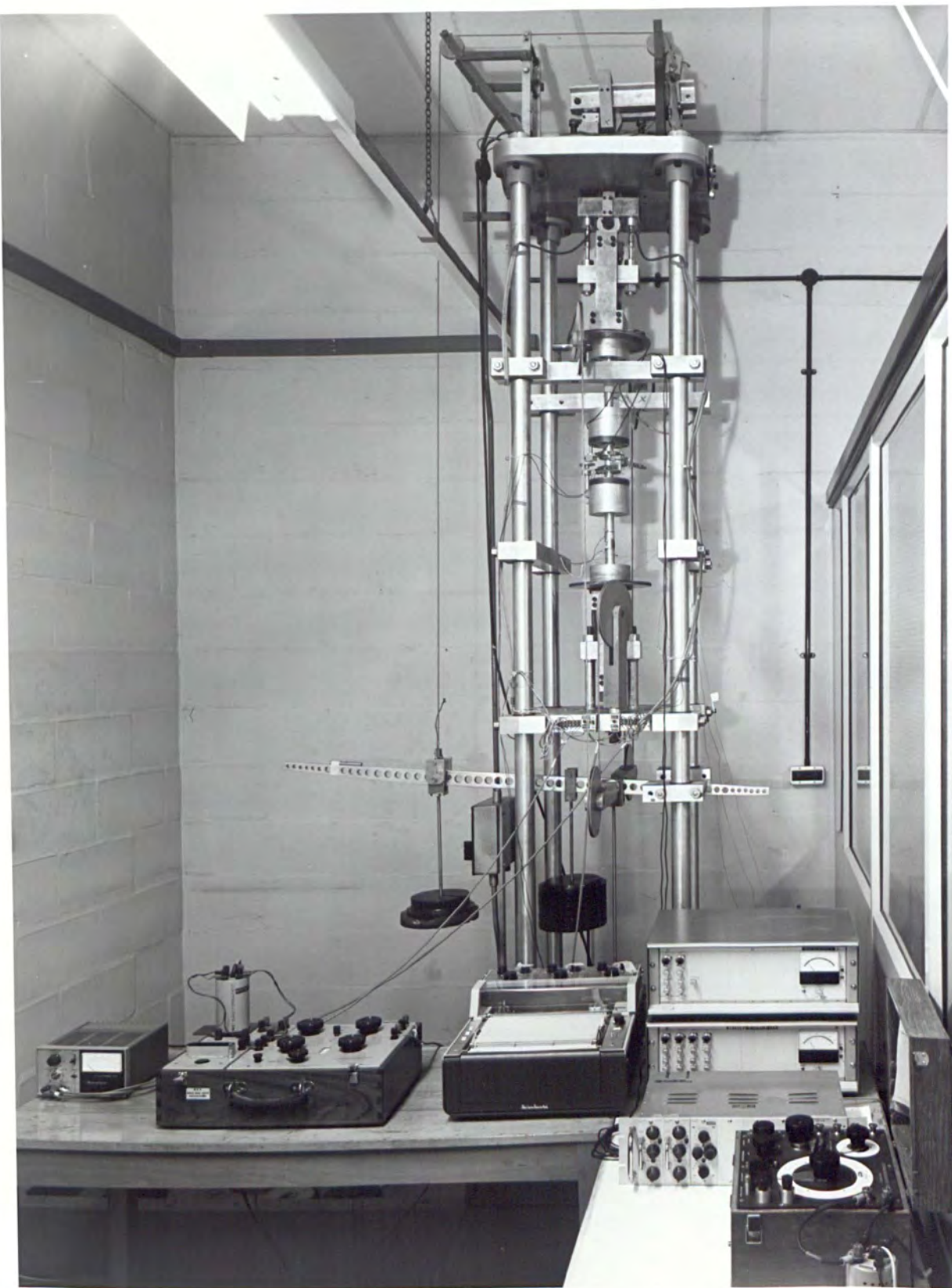


**Fig. 2.1 Complex Stress Machine**

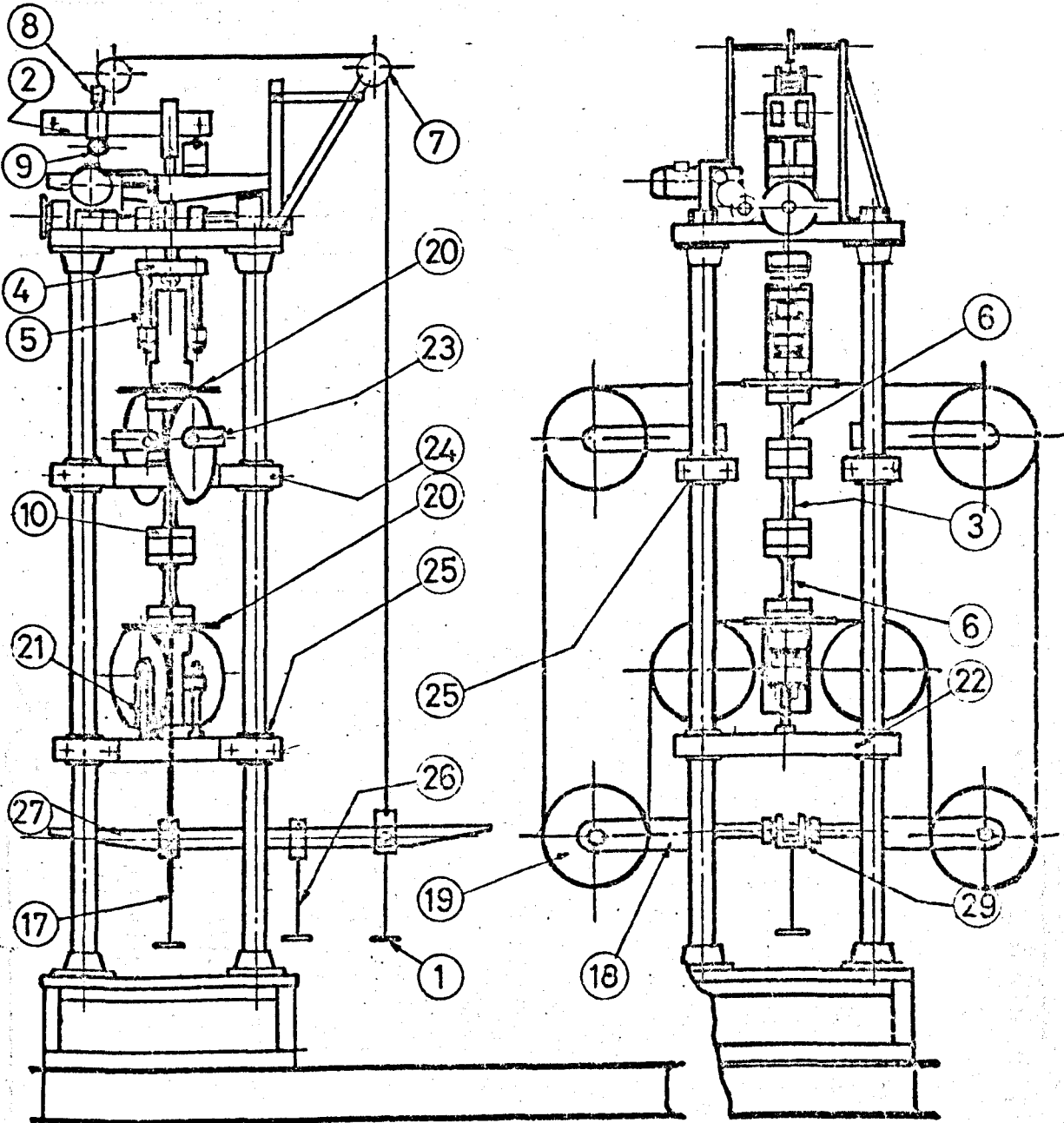
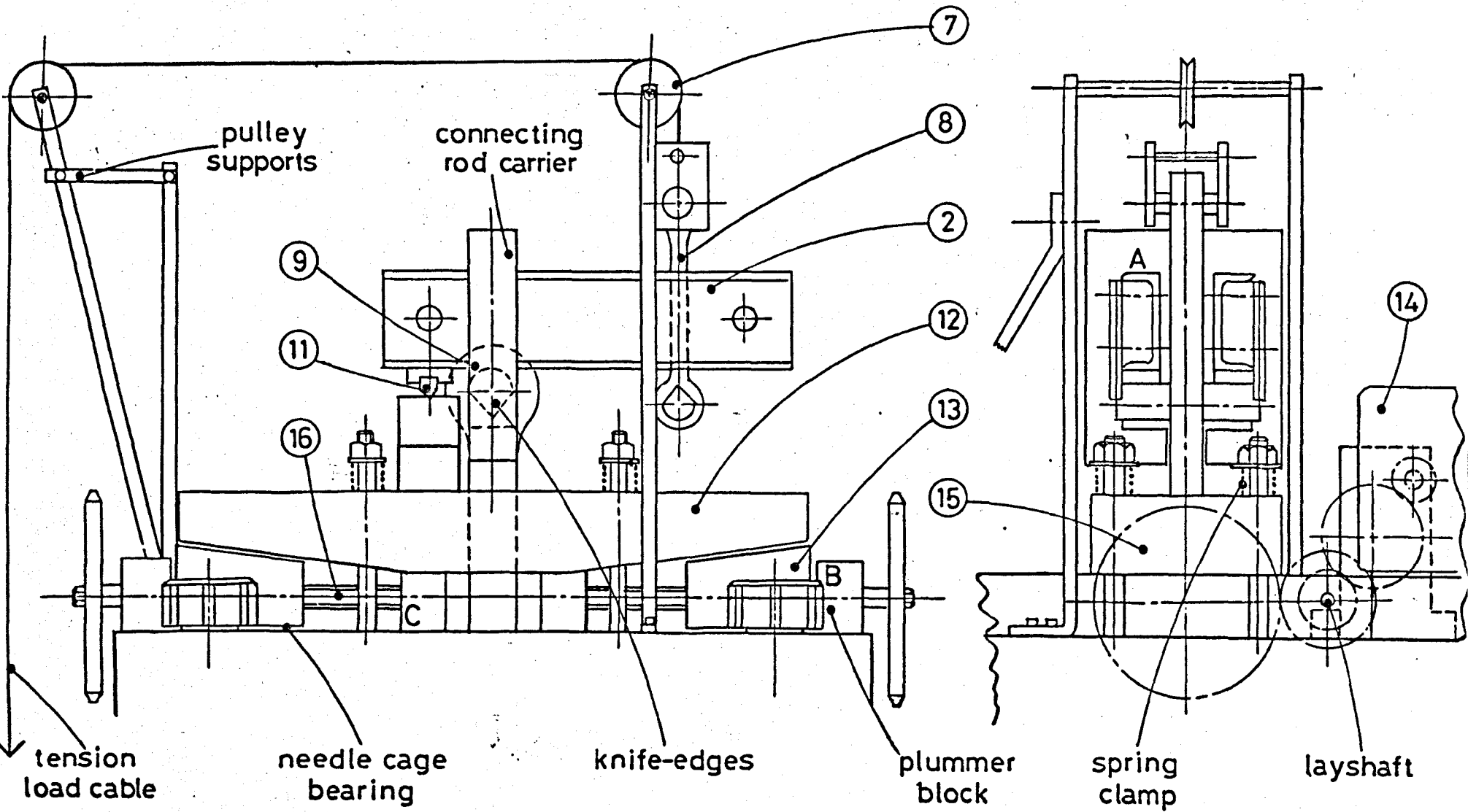
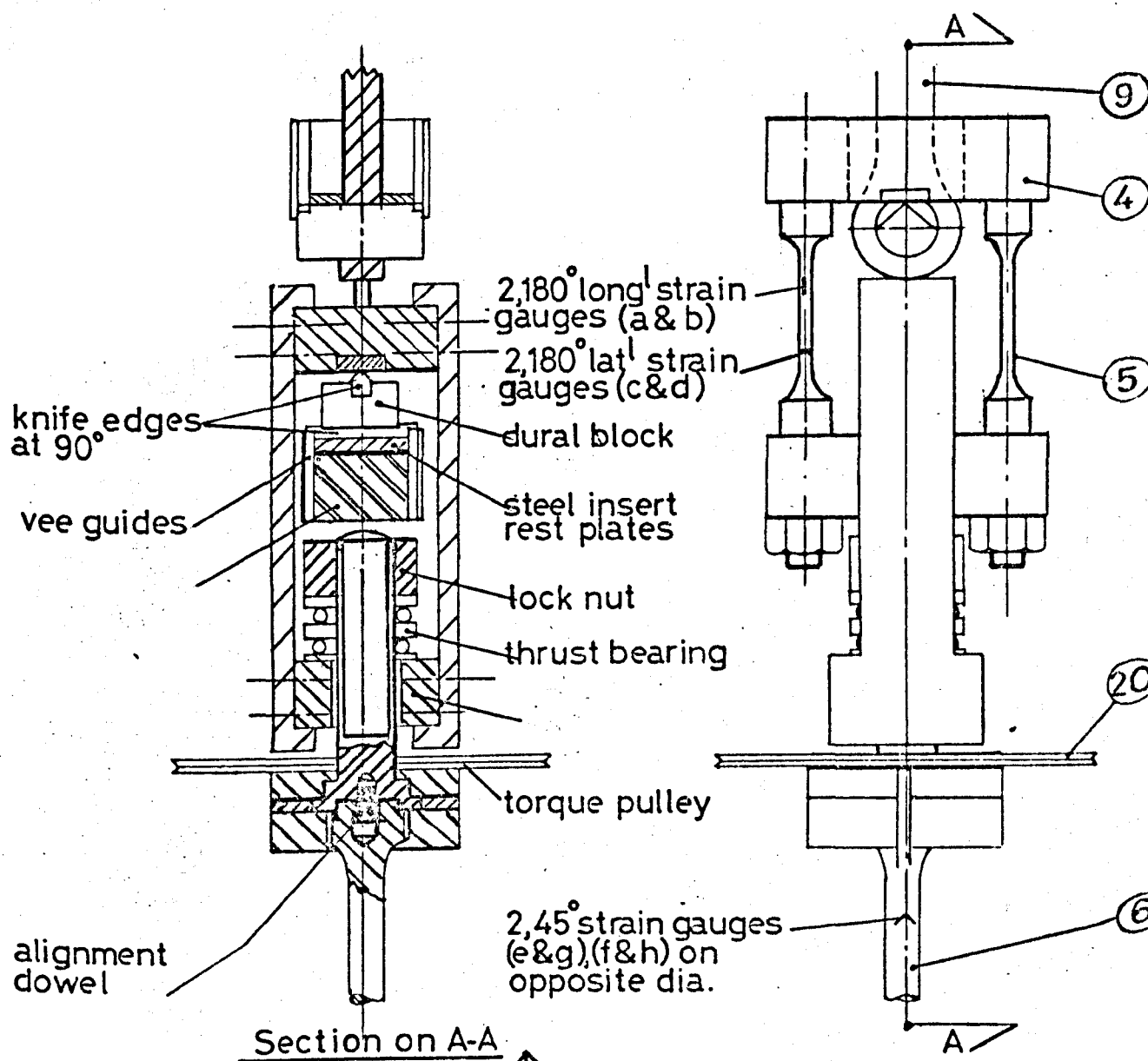


Fig. 2.2. Complex Stress Machine



**Fig 2.3 Tension Loading System**



alignment dowel

Section on A-A

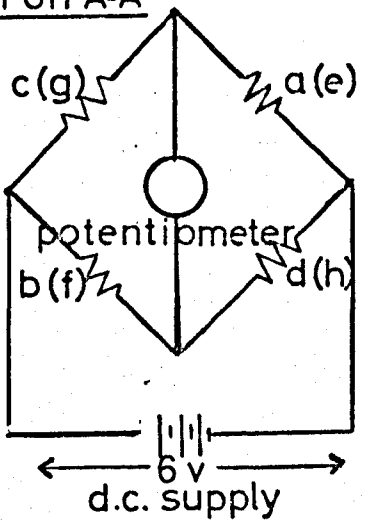
2,180° long<sup>l</sup> strain gauges (a & b)  
2,180° lat<sup>l</sup> strain gauges (c & d)

dural block  
steel insert rest plates

lock nut  
thrust bearing

torque pulley

2,45° strain gauges (e & g), (f & h) on opposite dia.



Tension (abcd) & Torsion (efgh) strain gauge bridge circuit

Fig. 2.4. Bridge & Load Cells

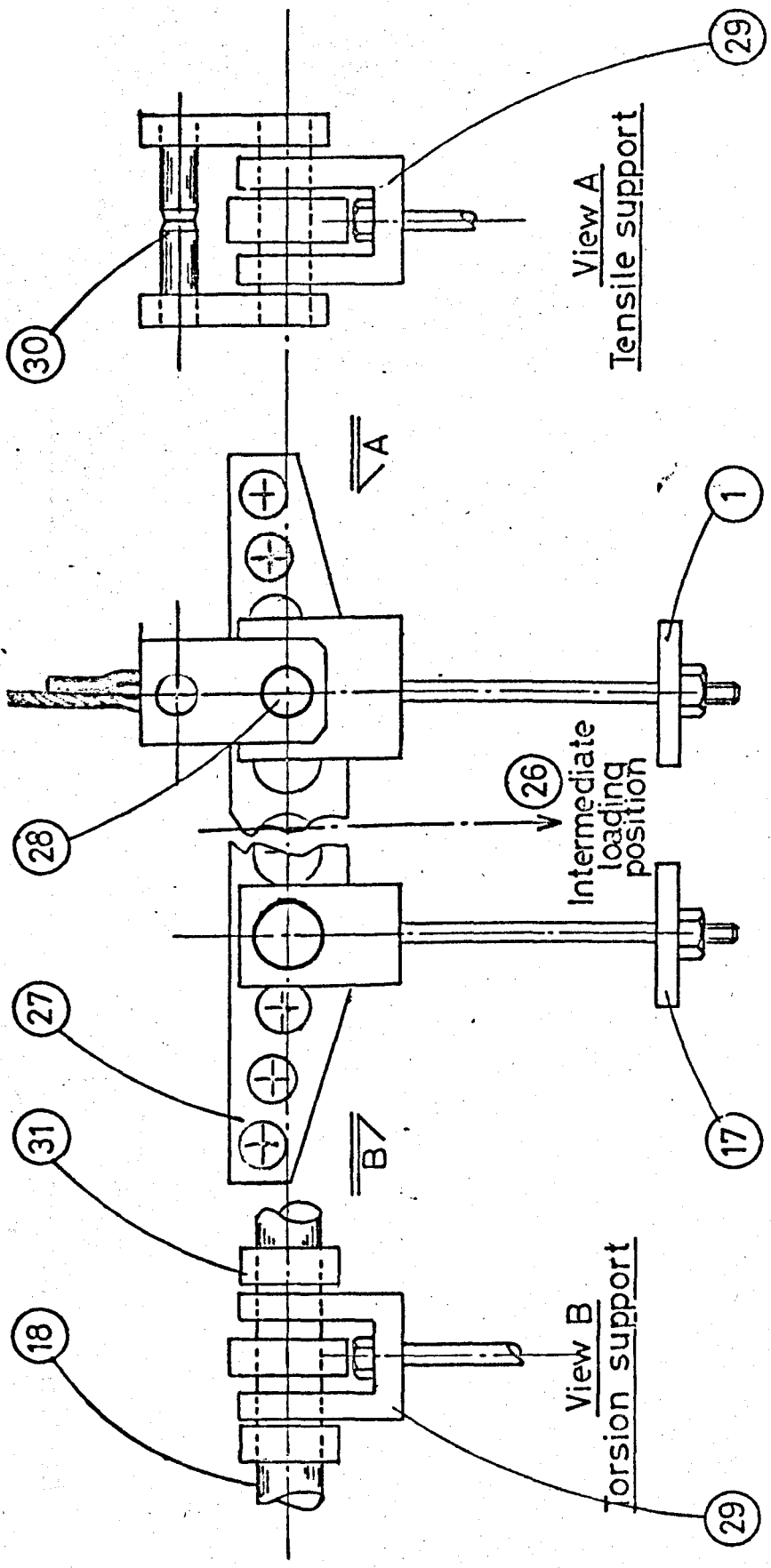


Fig. 2.5. Combined Loading System

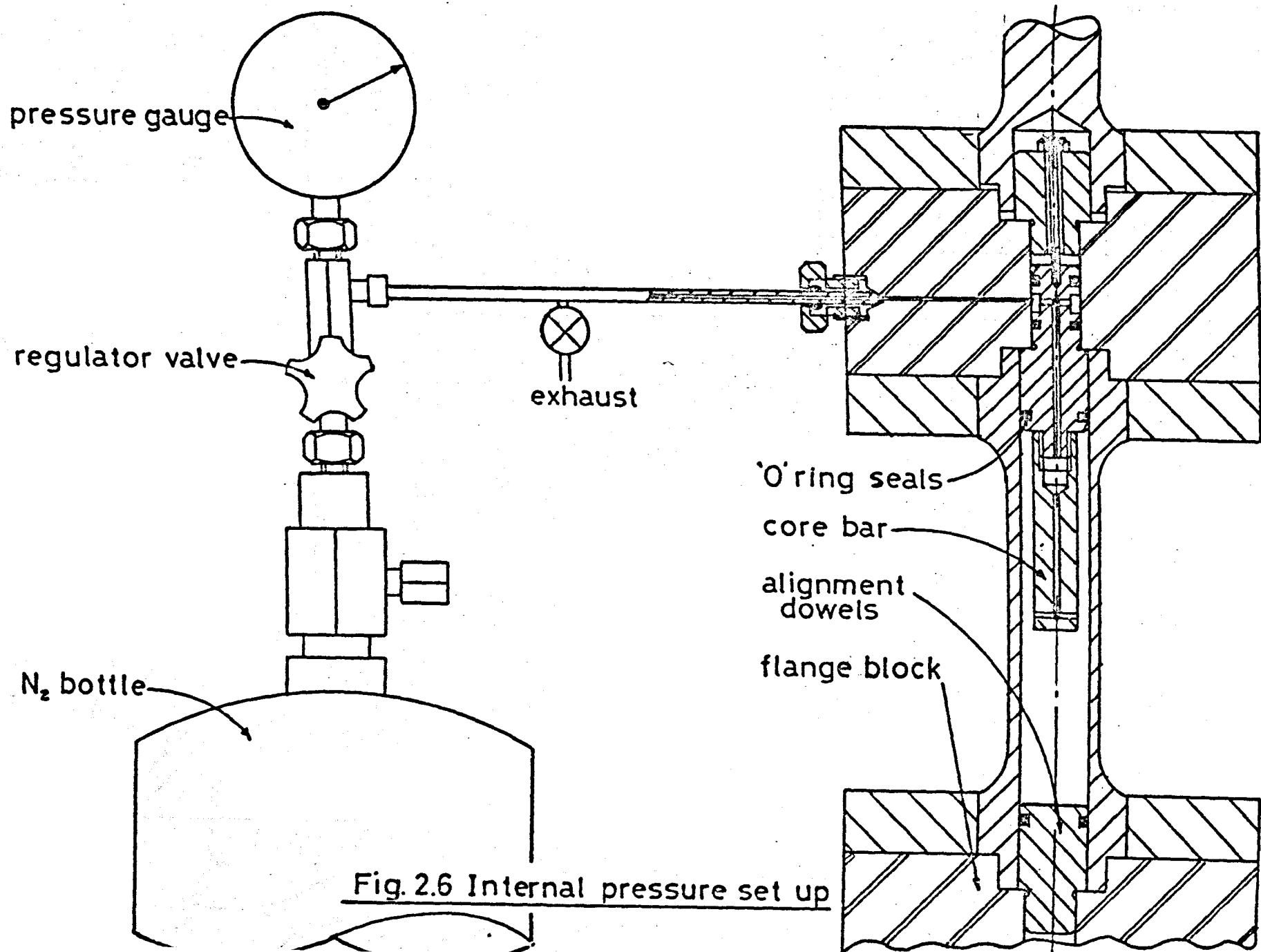


Fig. 2.6 Internal pressure set up

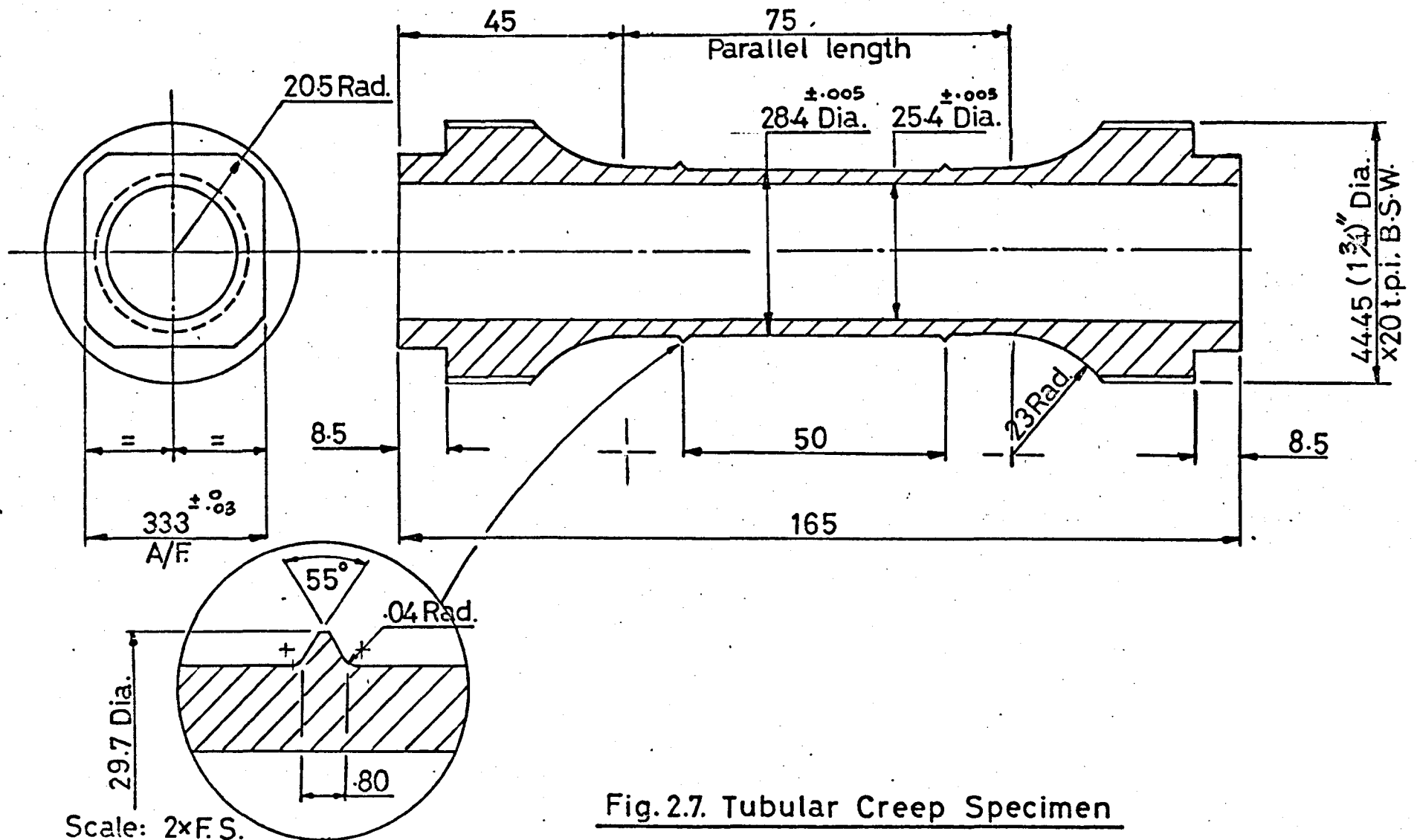


Fig. 2.7. Tubular Creep Specimen

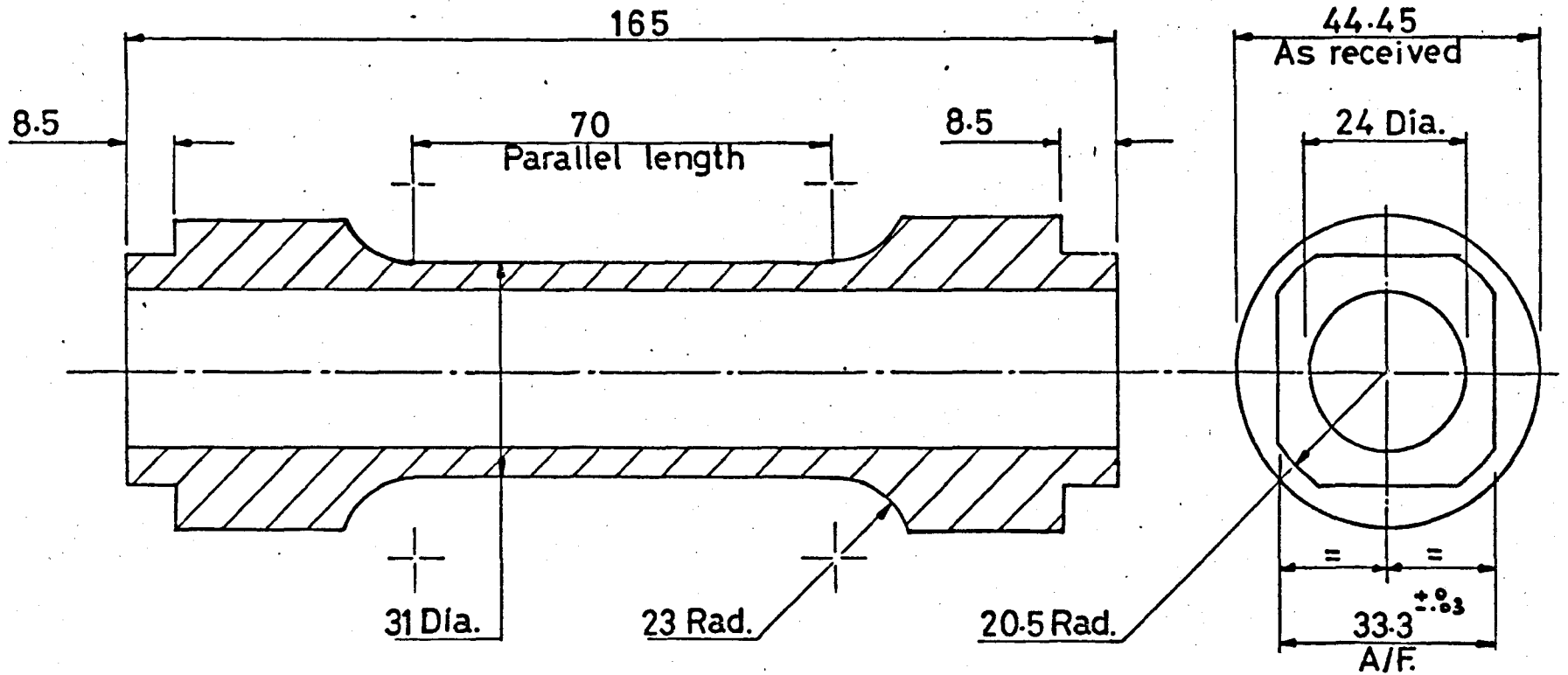


Fig.2.8. Annealing Blank

(a) Annealing Blank

(b) Finished Sizes

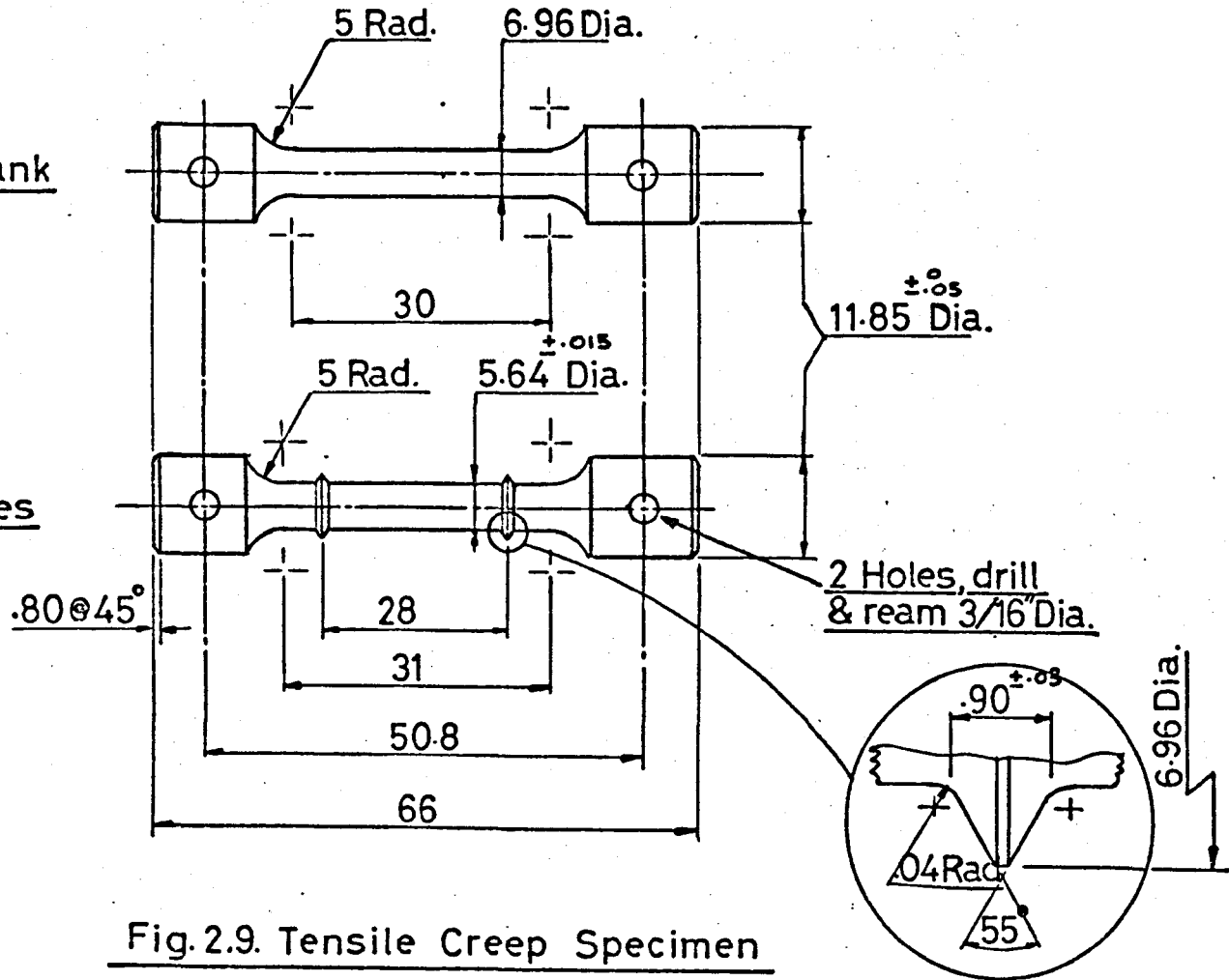
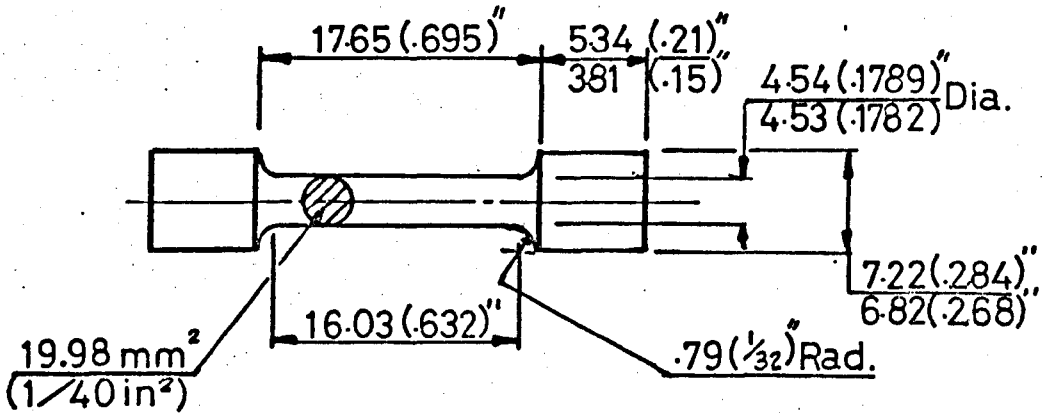
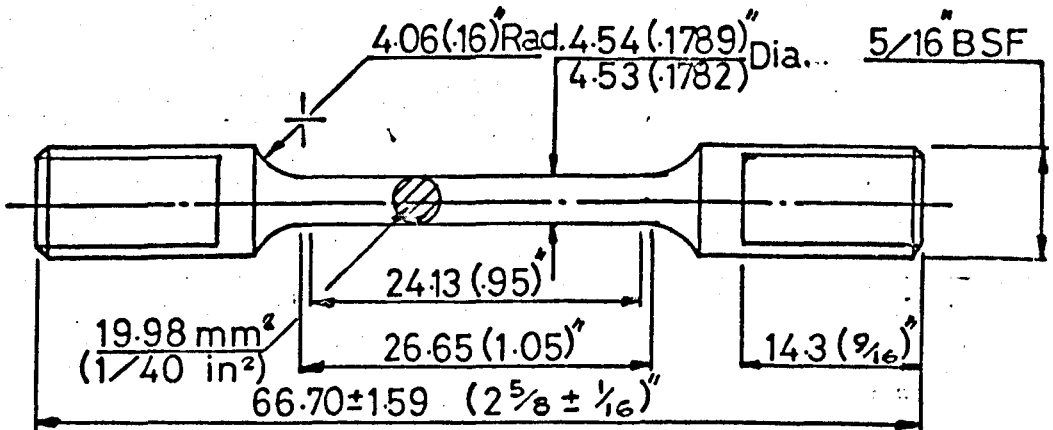


Fig. 2.9. Tensile Creep Specimen



(a) Hounsfield Type



(b) Instron Type

Fig. 2.10. Tensile Specimens

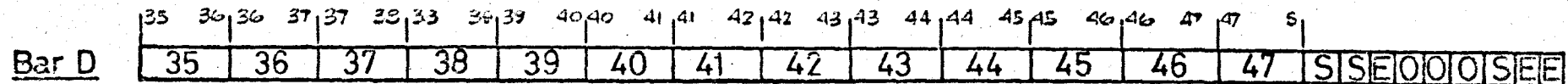
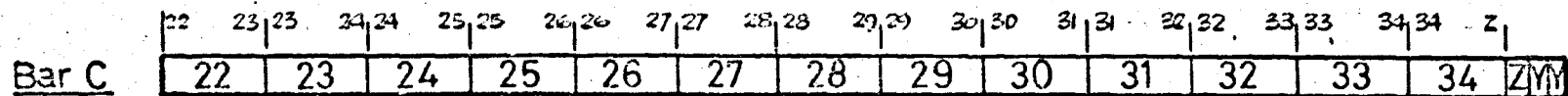
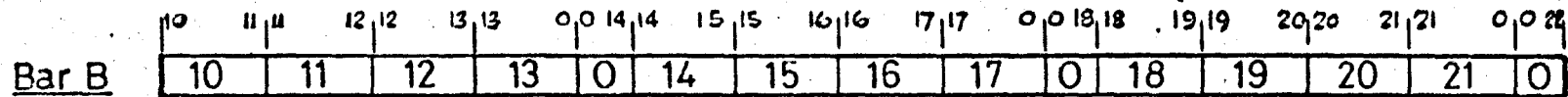
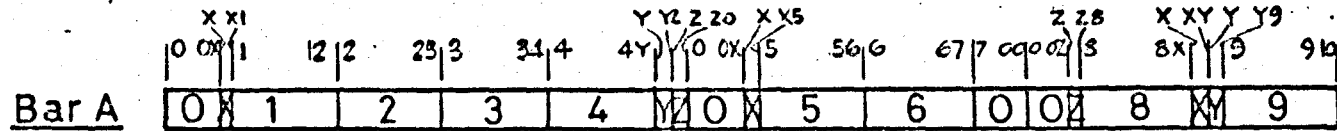
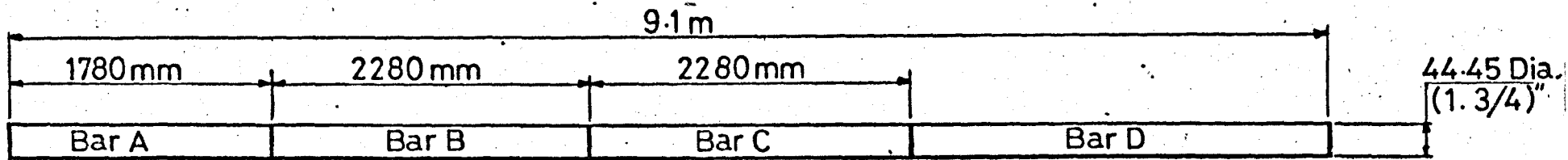
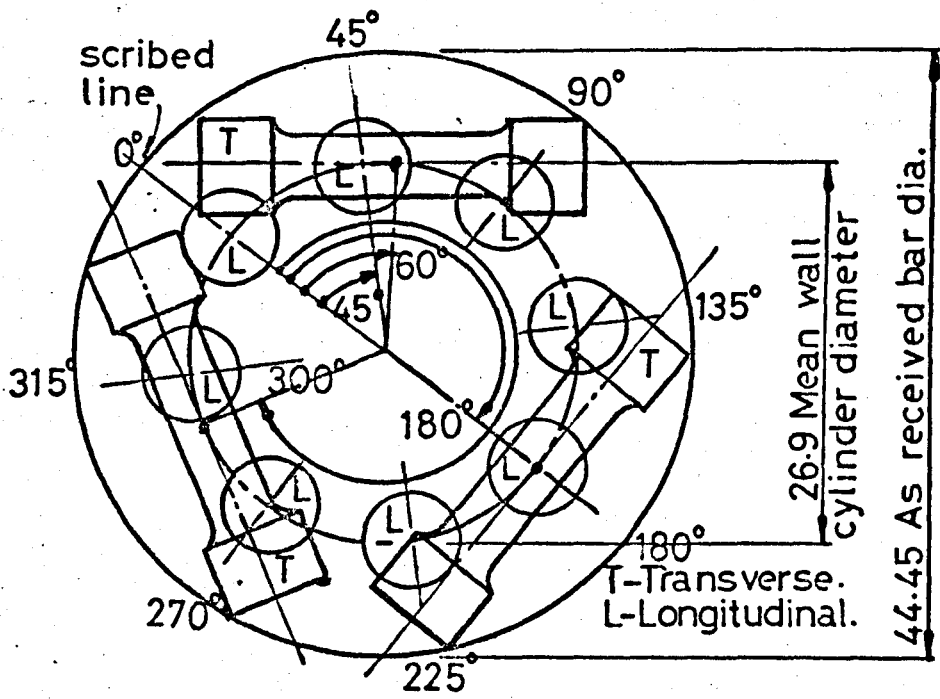
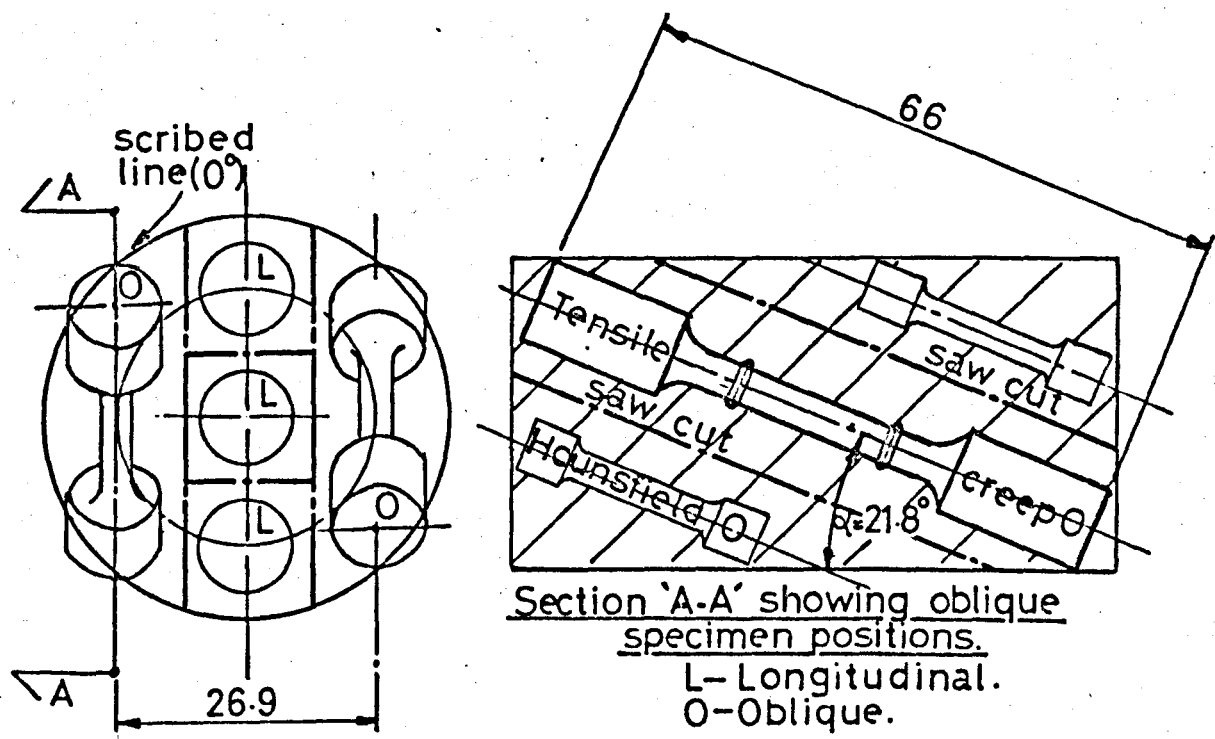


Fig. 2.11. Cutting Plan



(a) Hounsfield Positions (Pieces 'Y' & 'Z')



(b) Creep Specimen Positions (Piece 'O')

Fig.2.12. Specimen Positions In Bar Cross Section

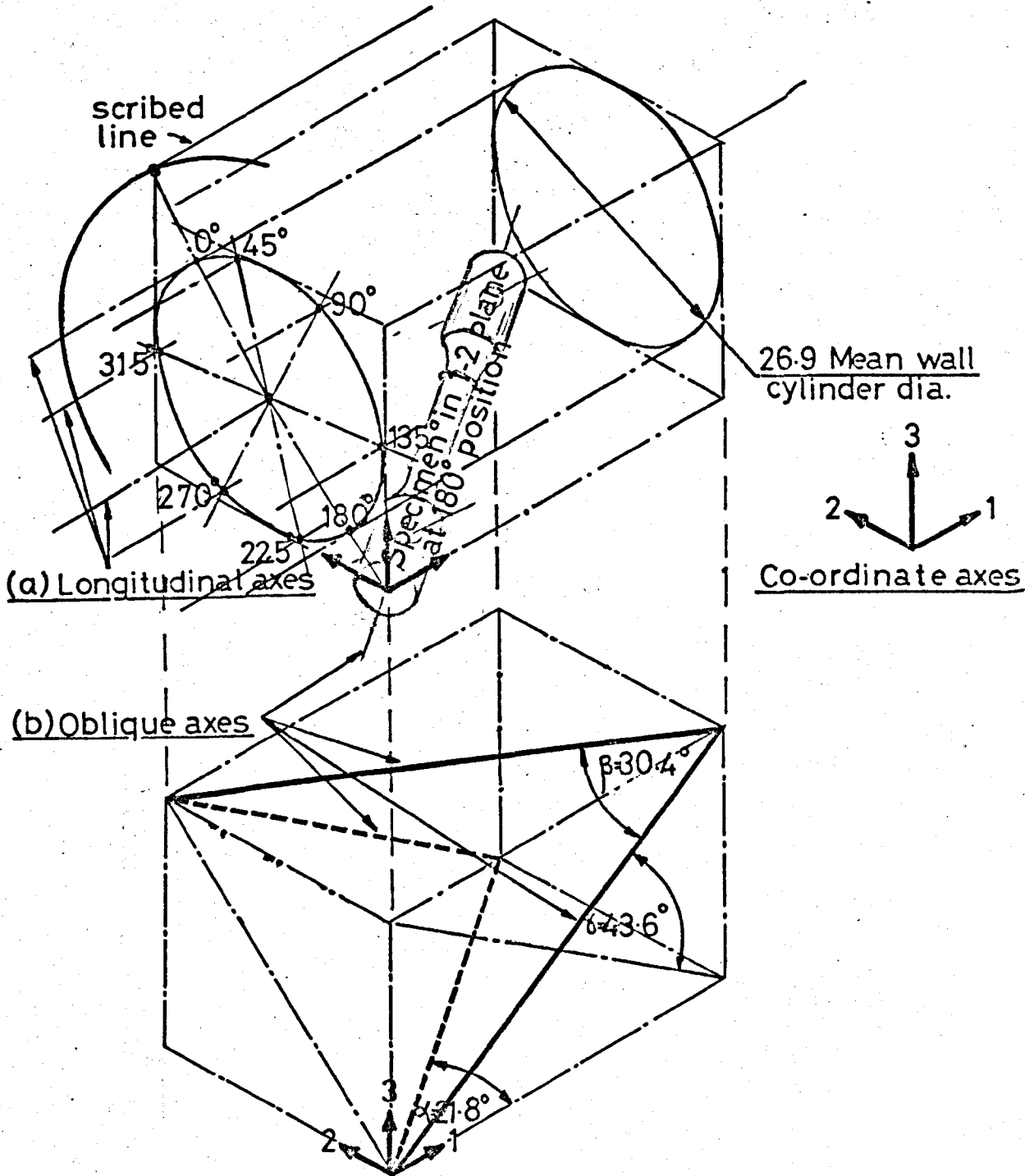


Fig.2.13. Composite Pictures Of Creep Specimen Directions

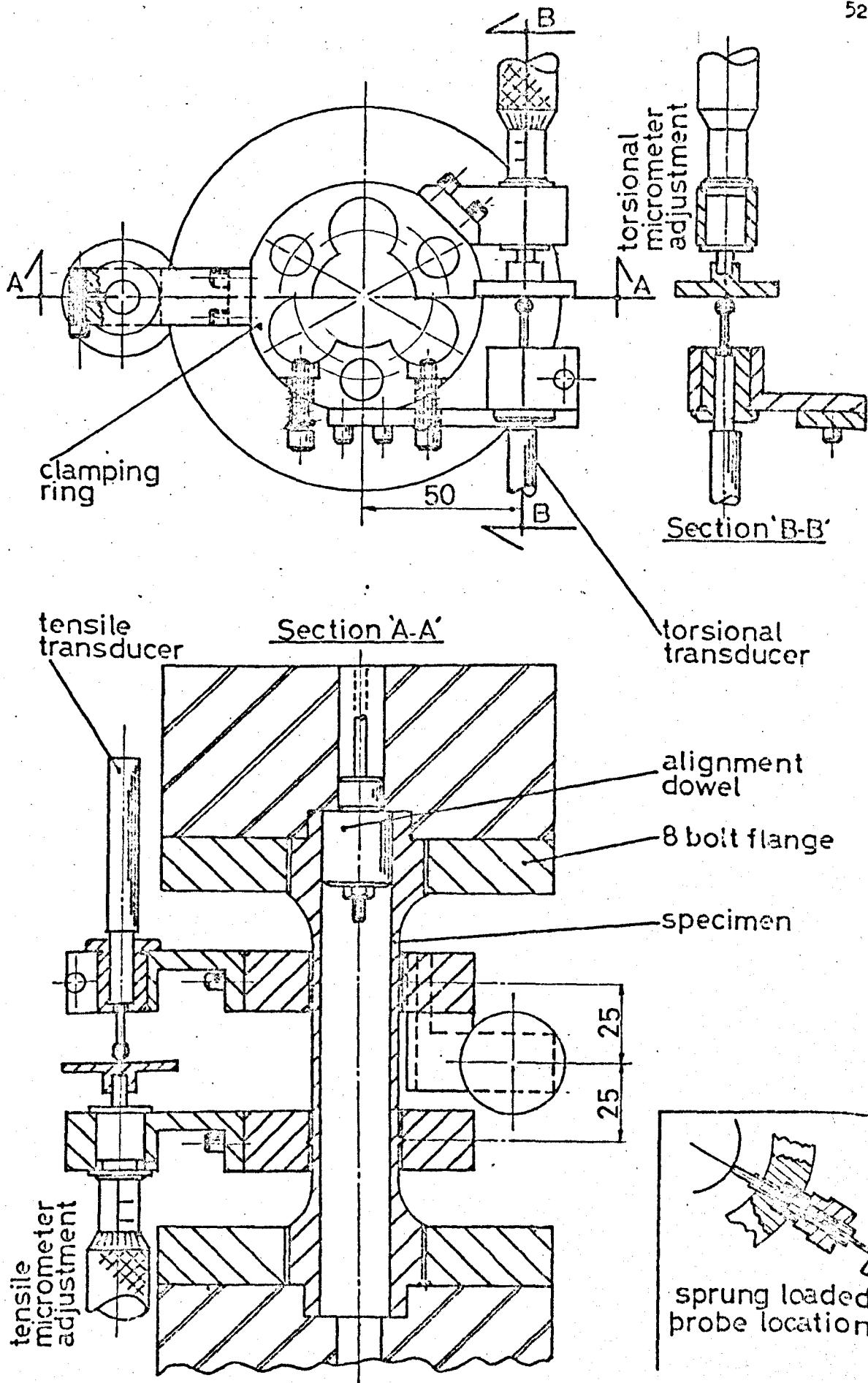


Fig.2.14. Extension & Twist Measurement

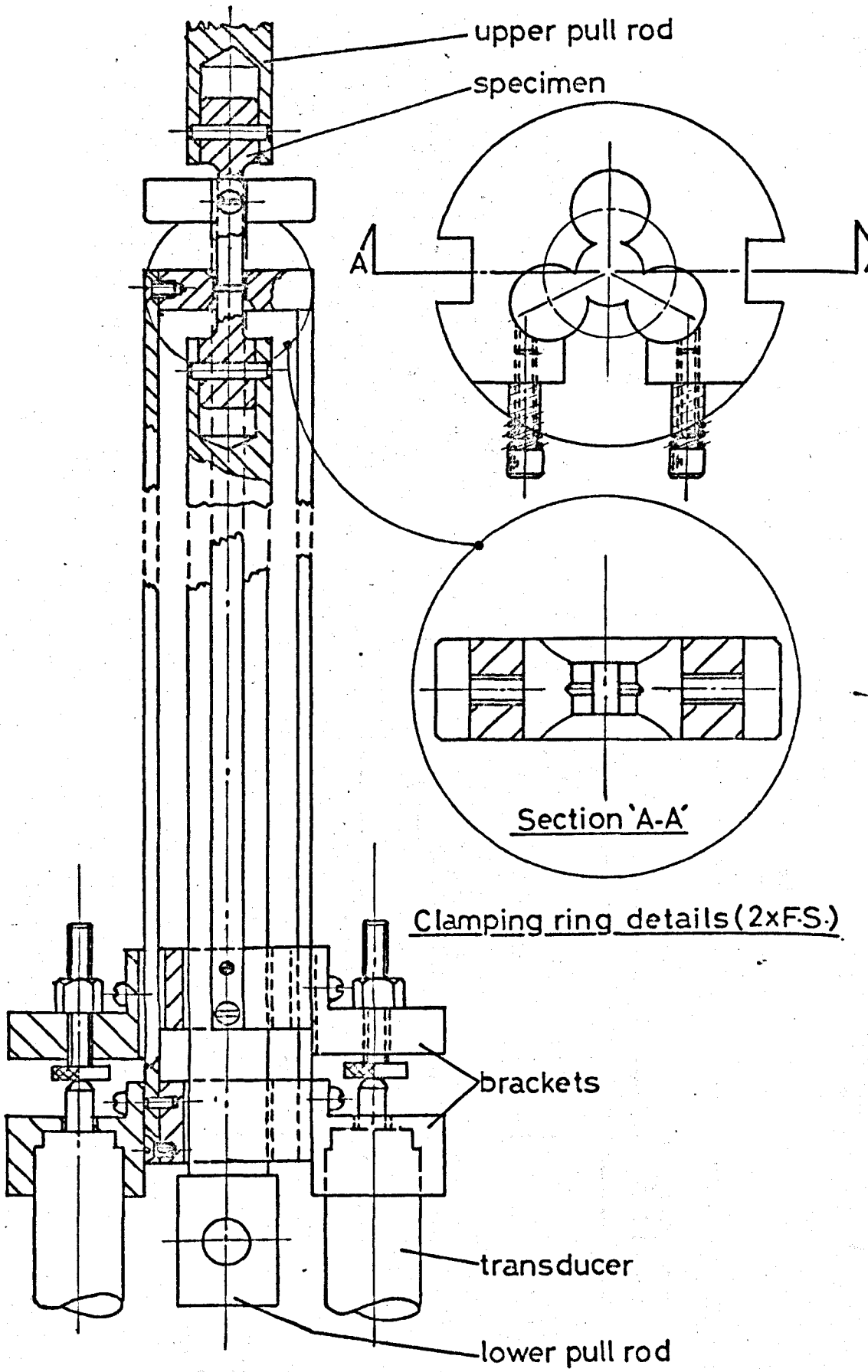


Fig. 2.15. Tensile Creep Extensometer

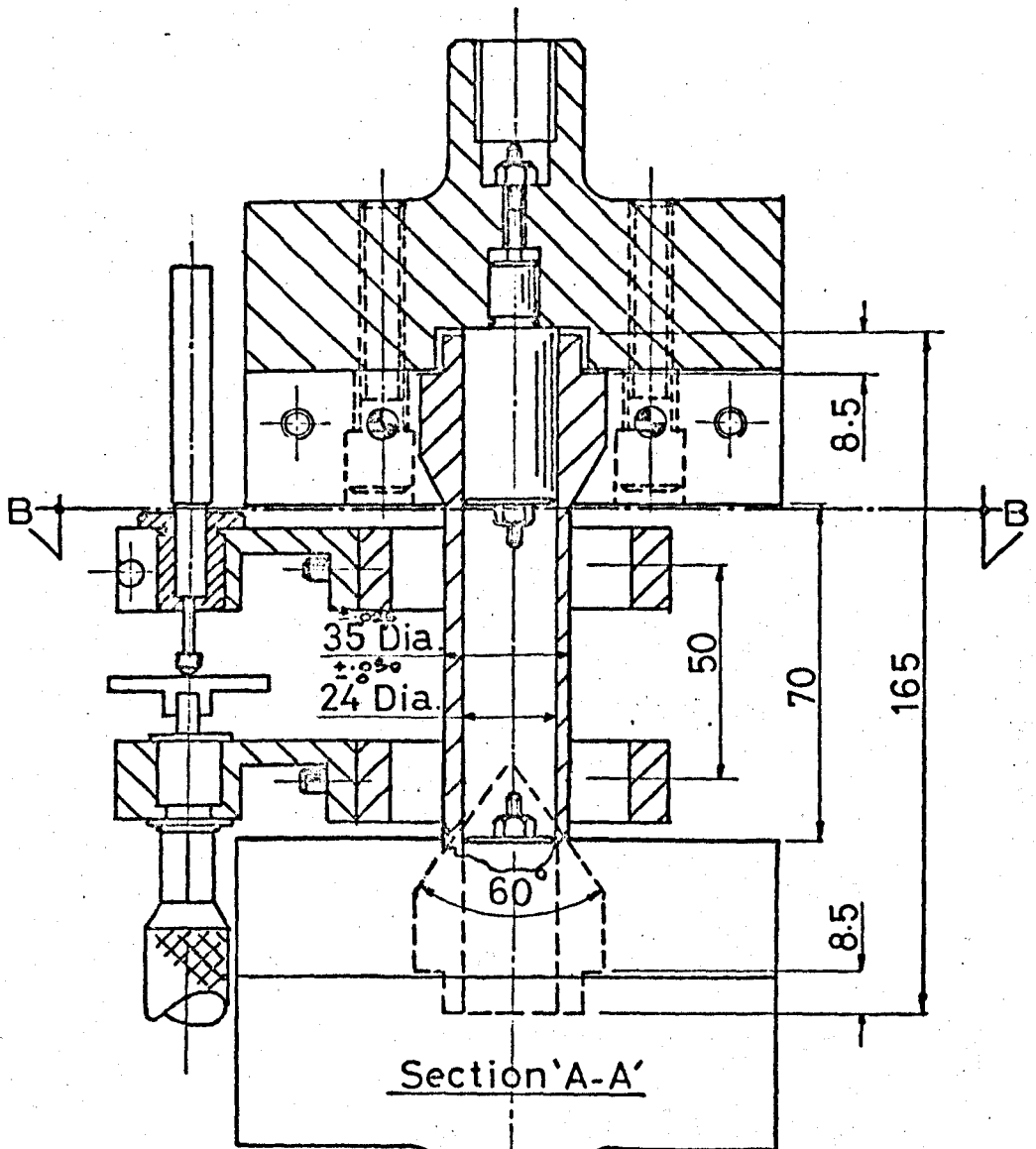
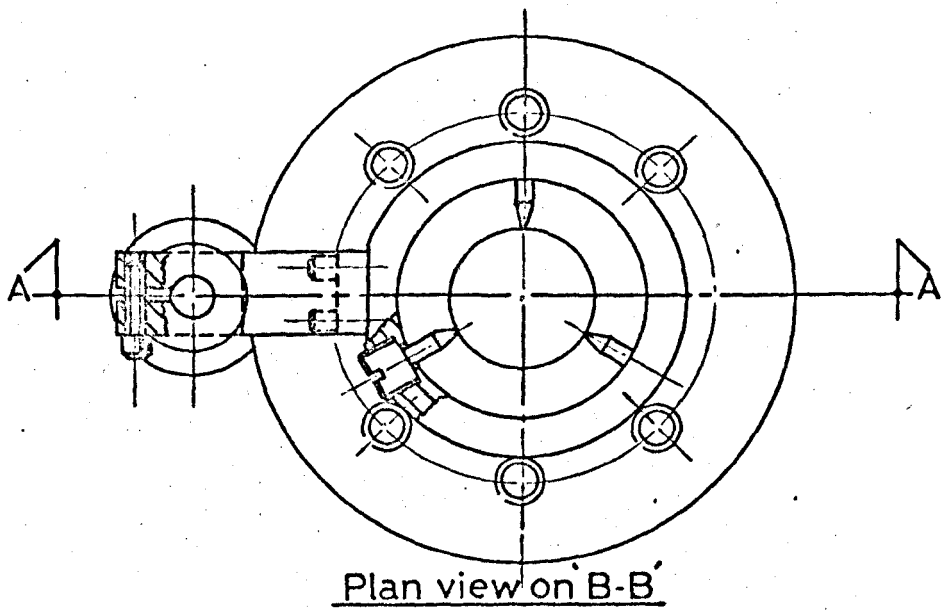


Fig. 2.16A Tensile Prestrain Set-up



Fig.2.16B Tension & Torsion Prestrain Adaptors

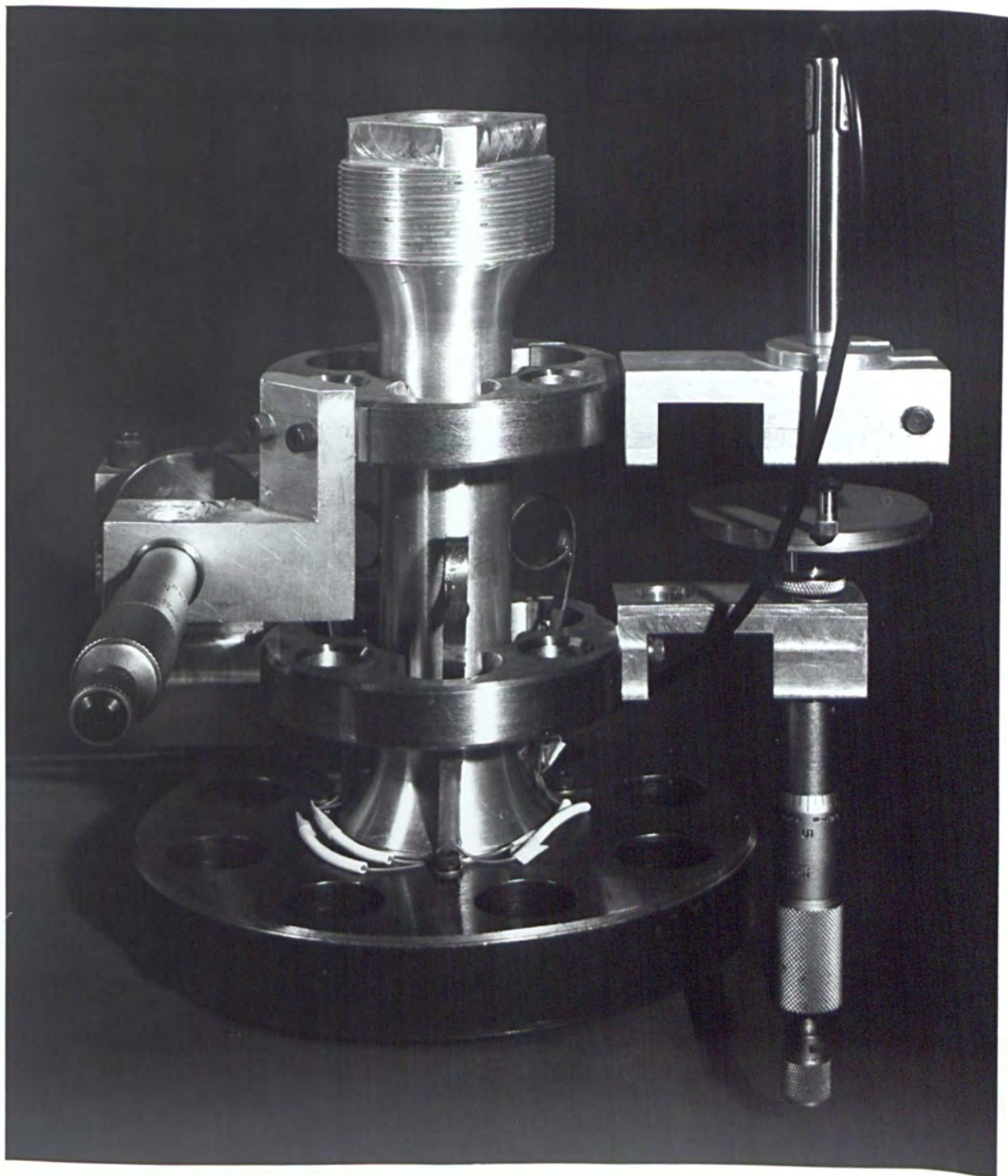


Fig.2.17A. Extension, Twist & Diameter Measurement

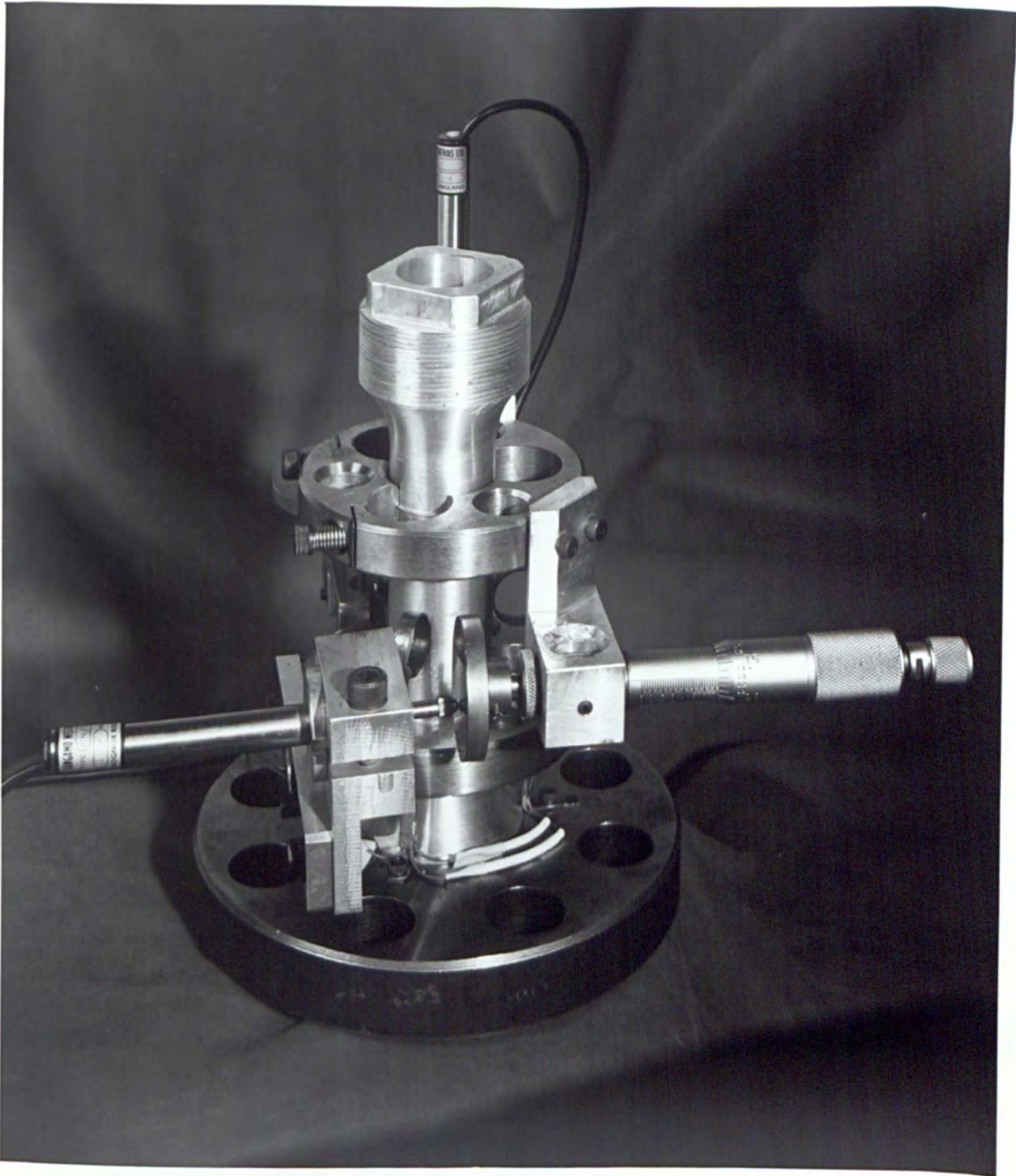


Fig.2.17B Extension, Twist & Diameter Measurement

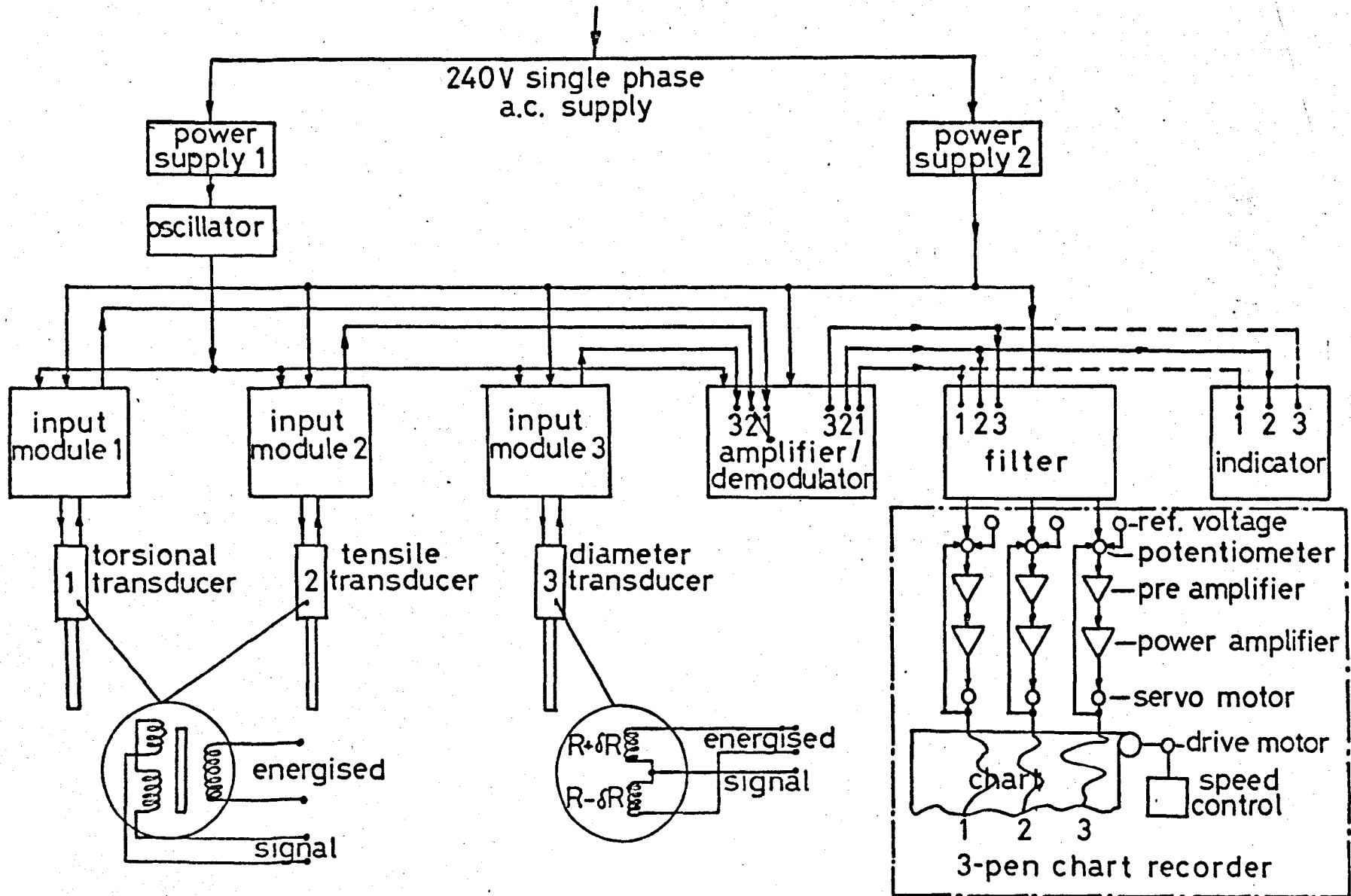


Fig.2.18. Three Channel Transducer System

TABLE 2.1 % Composition

Element	Mg	Cu	Si	Fe	Mn	Zn	Ni	Ti	A
'Hid 1A'	< 0.005	< 0.005	< 0.04	0.04	< 0.01	0.02	< 0.015	< 0.015	Bal
BS 1476-EIAM	-	0.02	0.15	0.15	-	-	-	-	99.8 Min.

TABLE 2.2 V.P.N. Figures (5 Kg load, 2/3 objective lens)

Temp (°C) \ Time (hr)	300	350	400	450	500
$\frac{1}{2}$	A 21	B 18	C 17.4	D 15.7	E 14.9
$1\frac{1}{2}$	F 20	G 17.9	H 16.4	I 15.6	J 14.8
$2\frac{1}{2}$	K 18.9	L 17.5	M 16.3	N 15.7	O 14.7

N.B. Each figure is the average of three impressions made per segment.

Segment N -  $2\frac{1}{2}$  hr at  $450^{\circ}\text{C}$ 

(x 50)

Etchant: HF - 42%, HCl - 16%, H<sub>2</sub>O - 42%  
(percentages by volume)

TABLE 2.3 Tubular Specimens - Operation Sequence

Op	Machine Procedure
<u>A.</u>	<u>Blank (Fig. 2.8)</u>
1	Mark off bar in billet lengths and number both ends of each billet on lateral identification line.
2	Power-saw billets to length (6.625")
3	Face ends and centre-drill, keeping length .010" over-size. Transfer numbers to ends of billet and in line with identification line.
4	Between centres, turn O/D to 1.748" to suit cradle and face both ends to length, without removing numbers. Length should now be 165 mm. Turn 41 mm dia. x 8.5 mm each end.
5	In 3 jaw chuck bore .875" dia roughing hole.
6	Using .875" mandrel in dividing head, mill 33.3 mm A/F x 8.5 mm long. Flats at each end to be in line. Identification numbers must not be machined out.
7	Still using .875" mandrel, set up roughing pattern for Mimik unit and machine waist O/D to 31 mm.
8	Set up cradle on cross slide concentric with lathe spindle, using hollow 1.748" O/D test bar and 12" x 1" dia. arm to carry clock gauge. Bore I/D to 24 mm.
9	Anneal at 450°C for 2½ hours. Cool in furnace.
<u>B.</u>	<u>Finish (Fig. 2.7)</u>
1	Bore to 25.4 mm + .005/- .000 in radial cuts of .175, .175, .125, .125, .05, .05 mm. Check with air plug gauge.
2	Set up finishing pattern for Mimik unit and, using 25.4 mm mandrel <u>between centres</u> , turn waist diameter to 29 mm in 4 radial cuts of .25 mm.
3	Screw-cut (Whitworth Form) 1¼" x 20 T.P.I. using sulphur and cutting oil and at not more than 156 r.p.m.
4	Finalise 28.4 mm + .005/- .000 diameter using Mimik unit.

TABLE 2.4 Prestrain History (%)

TENSION AND COMPRESSION ( $\dot{\epsilon}_{zz} = 1.67 \times 10^{-4} \text{ s}^{-1}$ )		FORWARD AND REVERSED TORSION ( $\dot{\gamma}_{\theta z} = 2.75 \times 10^{-4} \text{ s}^{-1}$ )		
Nom. $\epsilon_{zz}^P$	Act. (Equiv) $\epsilon_{zz}^P = \bar{\epsilon}_M^P$	Nom. $\gamma_{\theta z}^P$	Act. $\gamma_{\theta z}^P$	Equiv. $\bar{\epsilon}_M^P = \gamma_{\theta z}^P / \sqrt{3}$
-4	-4.28	-6.93	-7.00	-4.04
-3	-3.28	-5.20	-5.25	-3.03
-2	-1.87	-3.46	-3.45	-1.99
0	0	0	0	0
2	1.98	3.46	3.52	2.03
3	2.96	5.20	5.18	2.99
4	3.92			

Two additional prestrains were examined, one in tension at 6.7% and one in reversed torsion at an equivalent strain of -2.7%

All specimens were tested for creep at a stress ratio ( $\frac{\tau_{\theta z}}{\sigma_{zz}}$ ) of 0.95. That is a tensile stress ( $\sigma_{zz}$ ) of 16 N/mm<sup>2</sup> and a shear stress ( $\tau_{\theta z}$ ) of 15.2 N/mm<sup>2</sup>.

CHAPTER 3

The analysis of the stress-strain curves and results of analysis for various loading conditions and materials are similar. The location of the yield point is determined by the intersection of the stress-strain curve with the yield stress  $\sigma_y$  and  $\epsilon_y$  respectively. The plastic work done in the region of a plastic strain increment  $d\epsilon$  is given by the equation (3.1) and the yield function is given in equation (3.2).

3.1.1. YIELDING

The analysis of stress-strain curves was performed on annealed material. The analysis was performed by dividing into paragraphs on loading, creep and unloading.

# CHAPTER 3

The following equations were used in the calculation of stress and strain of radial loading:

A von Mises equivalent stress for an applied  $(\sigma_{11}, \sigma_{22})$  stress level is given from equation (3.5) as,

$$\sigma_e = \sqrt{\frac{1}{2}(\sigma_{11} - \sigma_{22})^2 + 3\tau_{12}^2} \quad (3.1)$$

and the cross-sectional strain is given from equation (3.6) as,

$$\epsilon = \frac{1}{E} \left[ \frac{1}{2}(\sigma_{11} + \sigma_{22}) + 3\tau_{12}^2 \right] \quad (3.2)$$

where it should be noted that the principal stresses  $(\sigma_1, \sigma_2, \sigma_3)$  in equations (3.1) and (3.2) are,

$$\begin{aligned} \sigma_1 &= \frac{1}{2}(\sigma_{11} + \sigma_{22}) + \sqrt{\frac{1}{4}(\sigma_{11} - \sigma_{22})^2 + 3\tau_{12}^2} \\ \sigma_2 &= \frac{1}{2}(\sigma_{11} + \sigma_{22}) - \sqrt{\frac{1}{4}(\sigma_{11} - \sigma_{22})^2 + 3\tau_{12}^2} \\ \sigma_3 &= 0 \end{aligned} \quad (3.3)$$

The plastic work done in a plastic strain increment is given as,

$$dW = \sigma_e d\epsilon \quad (3.4)$$

## THEORETICAL ANALYSIS

In this Chapter the relevant equations and methods of analysis for annealed, extruded and prestrained aluminium are outlined. The theories of Appendix I are applied to a combined tension-torsion stress system by replacing suffices 1, 2 and 3 by  $z$ ,  $\theta$  and  $r$  respectively. For prestrained aluminium the derivation of a plastic strain increment ratio ( $d\delta^p/d\epsilon^p$ ) from three anisotropic yield functions is given in Section 3.5.

3.1 ANNEALED MATERIAL (Chapter 4)

For constant stress ratio tests performed on annealed material the analysis may conveniently be divided into paragraphs on loading, creep and anisotropy.

## 3.1.1 Incremental Loading

The following equations were used in the calculation of stress and strain of radial loading;

A von Mises equivalent stress for an applied ( $\sigma_{zz}, \tau_{\theta z}$ ) stress level is given from equation (15)\* as,

$$\bar{\sigma}_M = \sqrt{\sigma_{zz}^2 + 3\tau_{\theta z}^2} \quad (3.1)$$

and the Tresca equivalent stress is given from equation (16) as,

$$\bar{\sigma}_T = \sqrt{\sigma_{zz}^2 + 4\tau_{\theta z}^2} \quad (3.2)$$

where it should be noted that the principal stresses ( $\sigma_1, \sigma_2, \sigma_3$ ) in equations (15) and (16) are,

$$\begin{aligned} \sigma_1 &= \sigma_{zz}/2 + \frac{1}{2} \sqrt{\sigma_{zz}^2 + 4\tau_{\theta z}^2} \\ \sigma_2 &= \sigma_{zz}/2 - \frac{1}{2} \sqrt{\sigma_{zz}^2 + 4\tau_{\theta z}^2} \\ \sigma_3 &= 0 \end{aligned} \quad (3.3)$$

The maximum shear stress in combined tension torsion is given as,

$$\tau = \frac{1}{2} (\sigma_1 - \sigma_2)$$

which, from equation (3.3), may be written as,

$$\tau = \frac{1}{2} \sqrt{\sigma_{zz}^2 + 4\tau_{\theta z}^2} \quad (3.4)$$

\* Single equation numbers refer to Appendix I.

The total strain (elastic + plastic) components associated with an increment of combined load are given by,

$$\begin{aligned} d\epsilon_{zz} &= \frac{dl}{l} \\ d\epsilon_{\theta\theta} &= \frac{dr}{r} \\ d\gamma_{\theta z} &= r \frac{d\theta}{l} \end{aligned} \quad (3.5)$$

where  $dl$ ,  $dr$  and  $d\theta$  are the length, radial and twist changes respectively on an original length  $l$  ( $= 50$  mm) and a mean radius  $r$  ( $= 13.45$  mm).

If  $d\sigma_{zz}$  and  $d\tau_{\theta z}$  are the axial and shear stress increments associated with the increment of combined load then the plastic strain components are,

$$\begin{aligned} d\epsilon_{zz}^p &= \frac{dl}{l} - \frac{d\sigma_{zz}}{E} \\ d\epsilon_{\theta\theta}^p &= \frac{dr}{r} - \nu \frac{d\sigma_{zz}}{E} \\ d\gamma_{\theta z}^p &= r \frac{d\theta}{l} - \frac{d\tau_{\theta z}}{G} \end{aligned} \quad (3.6)$$

where  $E$ ,  $G$  and  $\nu$  are elastic constants.

The total plastic strain components associated with an applied  $\sigma_{zz}, \tau_{\theta z}$  stress level are then,

$$\begin{aligned} \epsilon_{zz}^p &= \int d\epsilon_{zz}^p = \int \left( \frac{dl}{l} - \frac{d\sigma_{zz}}{E} \right) \\ \epsilon_{\theta\theta}^p &= \int d\epsilon_{\theta\theta}^p = \int \left( \frac{dr}{r} - \nu \frac{d\sigma_{zz}}{E} \right) \\ \gamma_{\theta z}^p &= \int d\gamma_{\theta z}^p = \int \left( r \frac{d\theta}{l} - \frac{d\tau_{\theta z}}{G} \right) \end{aligned} \quad (3.7)$$

The equivalent plastic strain increment based on the von Mises yield criterion may be written from equation (19) as,

$$d\bar{\epsilon}_M^p = \sqrt{(d\epsilon_{zz}^p)^2 + (d\gamma_{\theta z}^p)^2} / \sqrt{3} \quad (3.8)$$

for any one increment, and

$$\bar{\epsilon}_M^p = \int d\bar{\epsilon}_M^p = \int \sqrt{(d\epsilon_{zz}^p)^2 + (d\gamma_{\theta z}^p)^2} / \sqrt{3} \quad (3.9)$$

as the total equivalent Mises plastic strain, provided  $d\epsilon_{\theta\theta}^p = -\frac{d\epsilon_{zz}^p}{2}$  from equation (7).

For this system the Tresca equivalent plastic strain is normally written (see (54))<sup>\*</sup> from the work hardening hypothesis as,

$$d\bar{\epsilon}_T^p = \sqrt{(d\epsilon_{zz}^p)^2 + (d\gamma_{\theta z}^p)^2} / 4 \quad (3.10)$$

for any one increment, and

$$\bar{\epsilon}_T^p = \int d\bar{\epsilon}_T^p = \int \sqrt{(d\epsilon_{zz}^p)^2 + (d\gamma_{\theta z}^p)^2} / 4 \quad (3.11)$$

as the total equivalent Tresca plastic strain.

Lastly the maximum plastic shear strain is given by,

$$\gamma^p = \int d\gamma^p = \int (d\epsilon_1^p - d\epsilon_2^p)$$

which, for principal strain increments of,

$$\frac{d\epsilon_1^p}{d\epsilon_2^p} = \frac{d\epsilon_{zz}^p}{4} \pm \frac{1}{2} \sqrt{\left(\frac{3}{2}d\epsilon_{zz}^p\right)^2 + (d\gamma_{\theta z}^p)^2}$$

may be written as,

$$\gamma^p = \int d\gamma^p = \frac{3}{2} \int \sqrt{(d\epsilon_{zz}^p)^2 + (d\gamma_{\theta z}^p)^2} / 2.25 \quad (3.12)$$

The stress plastic strain increment relationships for a tension-torsion system are given from the Levy-Mises flow rule (equation (9))

as,

$$d\epsilon_{zz}^p = \delta\lambda \cdot \tau_{zz}' = \delta\lambda \left( \tau_{zz} - \frac{1}{3} \tau_{zz} \right) = \frac{2}{3} \delta\lambda \cdot \tau_{zz}$$

$$d\gamma_{\theta z}^p = 2 \cdot d\epsilon_{\theta z}^p = 2 \cdot \delta\lambda \cdot \tau_{\theta z}$$

\* Main text reference

Hence the ratio of shear to axial plastic strain components is,

$$r = \frac{d\gamma_{\theta z}^p}{d\epsilon_{zz}^p} = 3 \frac{\tau_{\theta z}}{\sigma_{zz}} \quad (3.13)$$

which, for radial loading ( $\lambda = \tau_{\theta z} / \sigma_{zz}$ ), may be written as,

$$r = 3\lambda \quad (3.14)$$

A computer programme was written to evaluate the quantities in equations(3.1)-(3.12). The total strains of equation(3.5) were based on chart displacements which occurred 30 s after the application of a load increment. That is,

$$dl = (30 \text{ s chart displacement for tension transducer} \times \text{scale}) \text{ mm}$$

$$dr = (30 \text{ s chart displacement for diameter gauge} \times \text{scale}) \text{ mm}$$

$$d\theta = (30 \text{ s chart displacement for torsion transducer} \times \text{scale}) \text{ mm} \times 1.116 \frac{\circ}{\text{mm}} \times \frac{180}{\pi}$$

The tensile stress increment  $d\sigma_{zz}$  of equation(3.6), corresponding to an increment (dC) of combined load, was evaluated from equation(13) of Appendix II. That is:

$$d\sigma_{zz} = \frac{dC}{126.76} \left[ 11.72 \left( \frac{l_1}{C} \right) + 12.05 \left( \frac{l_2}{C} \right) \right]$$

The corresponding shear stress increment in equation(3.6) was evaluated from,

$$d\tau_{\theta z} = \lambda d\sigma_{zz}$$

where the stress ratio  $\lambda$  of this equation and equation(3.14) was evaluated from equation(12) of Appendix II. That is,

$$\lambda = \frac{18.88 \times (2l_1/l_1)}{11.72 + 12.05 (l_2/l_1)}$$

The transient creep strains which occurred between increments of combined load were analysed in an identical manner to that of uniaxial loading. This procedure is outlined in Section 4 of Appendix III. Then in finite difference form the tensile and shear creep rates for the  $i$ th point are given by,

$$\dot{\epsilon}_{zz,i}^c = \frac{\epsilon_{zz,i+1}^c - \epsilon_{zz,i-1}^c}{t_{i+1} - t_{i-1}} \quad (3.15)$$

$$\dot{\gamma}_{\theta z,i}^c = \frac{\gamma_{\theta z,i+1}^c - \gamma_{\theta z,i-1}^c}{t_{i+1} - t_{i-1}}$$

### 3.1.2 Creep

The longitudinal creep strain is given by,

$$\epsilon_{zz} = \int_{l_0}^{l_1} \frac{dl}{l} = \ln\left(\frac{l_1}{l_0}\right)$$

where  $l_1$  and  $l_0$  are the current and original gauge lengths respectively of creep deformation. For an extension  $Z$  on an original length  $l_0$  this equation may be written as,

$$\epsilon_{zz} = \ln\left(1 + \frac{Z}{l_0}\right) \quad (3.16)$$

which, for small extensions, approximates to,

$$\epsilon_{zz} \approx Z/l_0$$

The shear creep strain is given by,

$$\gamma_{\theta z} = \tan\left(\frac{r\theta}{l_0}\right) \quad (3.17)$$

where  $\theta$  is the angle of twist (in degrees) on a mean radius  $r$  and over a length  $l_0$ . For small angles of twist equation (3.17) approximates to,

$$\gamma_{\theta z} \approx \frac{r\theta}{l_0}$$

with  $\theta$  in radians.

For any time  $t_1$  on the creep curves the strain rates  $\dot{\epsilon}_{zz}$  and  $\dot{\gamma}_{\theta z}$  were evaluated by the 3, 5 and 7 point central difference formulae (55)\*. Thus for an equally divided creep curve of time interval  $h$  these are,

$$\begin{aligned} \text{3 point} \quad \dot{\epsilon}_{zz_i} &= \frac{1}{2h} [\epsilon_{zz_{i+1}} - \epsilon_{zz_{i-1}}] \\ \text{5 point} \quad \dot{\epsilon}_{zz_i} &= \frac{1}{12h} [-\epsilon_{zz_{i+2}} + 8\epsilon_{zz_{i+1}} - 8\epsilon_{zz_{i-1}} + \epsilon_{zz_{i-2}}] \\ \text{7 point} \quad \dot{\epsilon}_{zz_i} &= \frac{1}{60h} [\epsilon_{zz_{i+3}} - 9\epsilon_{zz_{i+2}} + 45\epsilon_{zz_{i+1}} - 45\epsilon_{zz_{i-1}} + 9\epsilon_{zz_{i-2}} - \epsilon_{zz_{i-3}}] \end{aligned} \quad (3.18)$$

for axial strain rates with a similar set of equations for shear strain rates.

The stress-creep rate relationships are given from the Levy-Mises flow rule of equations(9) and (31) as,

$$\dot{\epsilon}_{zz} = \dot{\lambda} \tau'_{zz} \phi(t) = \frac{2}{3} \dot{\lambda} \tau_{zz} \phi(t) \tag{3.19}$$

$$\dot{\gamma}_{\theta z} = 2 \dot{\epsilon}_{\theta z} = 2 \dot{\lambda} \tau_{\theta z} \phi(t)$$

and assuming that  $\phi(t)$  is the same function for both creep strain components we then have an isotropic ratio of shear to axial creep rates of,

$$\frac{\dot{\gamma}_{\theta z}}{\dot{\epsilon}_{zz}} = 3 \lambda \tag{3.20}$$

This equation was the basis for studies on creep anisotropy.

### 3.1.3 Analysis of Anisotropy

If a constant  $k$  is introduced into equation (3.20) such that

$$k = \frac{\dot{\gamma}_{\theta z} / \dot{\epsilon}_{zz}}{\lambda} \tag{3.21}$$

then an experimentally observed  $k$  value of 3 would confirm the flow rule of equation (3.20) for annealed material. An examination of the  $k$  values in creep was made in a computer programme that evaluated the strain rates of equation (3.18) at time intervals throughout the creep period. In this programme the extension ( $z$ ), angle of twist ( $\theta$ ) and stress ratio ( $\lambda$ ) of equations (3.16), (3.17) and (3.21) respectively were calculated from chart and load cell readings in an identical manner to that described in paragraph 3.1.1 for incremental loading.

A  $k$  value ( $= \tau/\lambda$ ) may be similarly defined from equation (3.14) for the plastic strain increment components of loading. Here  $k$  was simply obtained from the slope of the total plastic strain plot of loading, i.e.  $\int d\gamma_{\theta z}^p$  v  $\int d\epsilon_{zz}^p$  of equation (3.7).

Values of  $k$  in loading and in creep that do not equal 3 may be explained in terms of the anisotropic theory of Hill (29). Equation (54) of Appendix I is then applied by identifying the anisotropic axes 1, 2 and 3 of this theory with the  $z, \theta$  and  $r$  directions respectively. For combined tension-torsion ( $\tau_{zz}, \tau_{\theta z}$ ) the theoretical plastic strain increment ratios are then,

$$\frac{d\epsilon_{\theta\theta}^p}{d\epsilon_{zz}^p} = \frac{-F}{F+H} \tag{3.22}$$

$$\frac{d\epsilon_{rr}^p}{d\epsilon_{zz}^p} = \frac{-H}{F+H} \tag{3.23}$$

$$\frac{d\gamma_{\theta z}^p}{d\epsilon_{zz}^p} = \frac{2d\epsilon_{\theta z}^p}{d\epsilon_{zz}^p} = \left( \frac{6L}{F+H} \right) \frac{\tau_{\theta z}}{\sigma_{zz}} \tag{3.24}$$

The constants F, H and L can then be obtained from the solutions to these equations in using the corresponding plastic strain increment ratios of the experimental tests.

Hill's theory may be applied to creep simply by writing the plastic strain increments as creep strain rates (see Section 2 of Appendix I). Then equations (3.22) - (3.24) become,

$$\frac{\dot{\epsilon}_{\theta\theta}}{\dot{\epsilon}_{zz}} = \frac{-F}{F+H} \tag{3.25}$$

$$\frac{\dot{\epsilon}_{rr}}{\dot{\epsilon}_{zz}} = \frac{-H}{F+H} \tag{3.26}$$

$$\frac{\dot{\gamma}_{\theta z}}{\dot{\epsilon}_{zz}} = \left( \frac{6L}{F+H} \right) \frac{\tau_{\theta z}}{\sigma_{zz}} \tag{3.27}$$

In its simplest form the theory would assume the same constants F, H and L in both plastic flow and creep and a theoretical k value which is independent of stress ratio (  $\lambda = \tau_{\theta z} / \sigma_{zz}$  ). That is, from equations (3.24) and (3.27),

$$k = \frac{6L}{(F+H)} \tag{3.28}$$

Thus if the same k value is observed throughout plastic flow and creep in tests of different  $\lambda$  values then this would confirm the simplest application of Hill's theory.

### 3.2 EXTRUDED MATERIAL (Chapter 5)

For constant stress ratio tests performed on extruded material the loading strains, creep strains and stress ratios were evaluated in an identical manner to that described for annealed material in paragraphs 3.1.1 and 3.1.2.

The experimental k values of plastic flow and creep were found by the previously described methods (paragraph 3.1.3). These were compared with the theoretical prediction of Hill (equation (3.28)) and the predictions from the anisotropic theories of Sections 3.4 and 3.5.

For example, the theory of Bailey (27) has been applied to combined tension-torsion ( $\sigma_{zz}, \tau_{\theta z}$ ) in Section 3.4. Then for a constant stress ratio type test ( $\lambda = \tau_{\theta z} / \sigma_{zz}$ ) equation (3.36) would predict a k value in creep of,

$$k = \frac{\dot{\gamma}_{\theta z} / \dot{\epsilon}_{zz}}{\lambda} = 3(\lambda)^{n-2m-1} \quad (3.29)$$

where n and m are constants which could be made to account for an experimentally observed k value.

If the experimental flow behaviour indicates an extruded material possessing a residual strain history then a theoretical k value for this situation may be obtained from the general anisotropy theories of Section 3.5. Assuming that the residual strain is compressive ( $-\epsilon_{ii}^p$ ) the theory of Edelman and Drucker (58) would then predict, from equation (3.46), a k value in loading of,

$$k = \frac{\frac{A}{\lambda} \left( 1 + \frac{3m\epsilon_{ii}^p}{2\sigma_{ii}} \right) + B}{\frac{C}{\lambda} \left( 1 + \frac{3m\epsilon_{ii}^p}{2\sigma_{ii}} \right) + A} \quad (3.30)$$

where  $\sigma_{ii}^*$  is the tensile stress of loading, A, B, C are experimental constants of anisotropy and m is a Bauschinger parameter.

### 3.3 PRESTRAINED MATERIAL (Chapter 6)

The axial and shear prestrains of Table 2.4 were evaluated from equations (2.5) and (2.6) respectively.

For a constant stress ratio test ( $\lambda = 0.95$ ) performed on prestrained material the loading strain and creep strain components were evaluated from equations (3.5), (3.16) and (3.17).

To assist in the understanding of the creep of prior strained material the strain history of all specimens prior to creep will be presented in the form of composite stress-strain curves. All axial and shear prestrains will be shown on the one plot together with the like strain component of combined loading.

The subsequent creep curves will be plotted together in a similar way. Thus for all prior axial strain the like component

\* In tensor notation

$$\begin{aligned} \sigma_{zz} &= \sigma_{ii} \\ \epsilon_{zz}^p &= \epsilon_{ii}^p \end{aligned}$$

creep curves ( $\epsilon_{zz}$  vs  $t$  and  $\delta_{\theta z}$  vs  $t$ ) of each subsequent creep test ( $\lambda = 0.95$ ) will be presented together in the one strain-time plot. To aid comparison the results for annealed material at this stress ratio will also be shown. A similar presentation will be made for the chosen forward and reverse shear prestrains.

An analysis of the  $k$  values of equation (3.21) was again made for each test by employing the previously described method (paragraph 3.1.3). Comparisons with the predictions of Sections 3.4 and 3.5 were made.

### 3.4 APPLICATION OF OTHER THEORIES

In applying other theories to the combined tension-torsion studies of these tests then this is most conveniently done by comparing the predicted and experimentally measured ratios of shear to axial strain rate ( $\dot{\delta}_{\theta z} / \dot{\epsilon}_{zz}$ ).

#### 3.4.1 Bailey (27)\*

The ratio ( $\dot{\delta}_{\theta z} / \dot{\epsilon}_{zz}$ ) is best obtained from this theory by using the appropriate equivalent stress definition ( $\bar{\sigma}$ ) as a plastic potential in equation (4.5). Thus for a general stress system in polar coordinates equation (4.4) takes the form,

$$\bar{\sigma}^q = \left(\frac{1}{2}\right)^{1/q} \left\{ (\sigma_{zz} - \sigma_{\theta\theta})^q + (\sigma_{\theta\theta} - \sigma_{rr})^q + (\sigma_{rr} - \sigma_{zz})^q + 3[(\tau_{\theta z}^q + \tau_{z\theta}^q) + (\tau_{\theta r}^q + \tau_{r\theta}^q) + (\tau_{zr}^q + \tau_{rz}^q)] \right\}^{1/q} \quad (3.31)$$

where  $q = n - 2m + 1$

which, for combined tension-torsion, reduces to,

$$\bar{\sigma}^q = \left\{ \frac{\sigma_{zz}^q + (-\sigma_{zz})^q + 3(\tau_{\theta z}^q + \tau_{z\theta}^q)}{2} \right\}^{1/q} \quad (3.32)$$

Then  $\dot{\epsilon}_{zz}$  from equation (4.5) is given by,

$$\dot{\epsilon}_{zz} = \frac{\partial \bar{\sigma}^q}{\partial \sigma_{zz}} \dot{\bar{\sigma}} = \frac{1}{q} (\bar{\sigma})^{\frac{1-q}{q}} \cdot \frac{q}{2} \left\{ (\sigma_{zz})^{q-1} + (-\sigma_{zz})^{q-1} \right\} \dot{\bar{\sigma}}$$

It follows that if  $\dot{\epsilon}_{zz}$  is to have a value then  $q - 1$  must be even.

Then,

$$\dot{\epsilon}_{zz} = (\bar{\sigma})^{\frac{1-q}{q}} \dot{\bar{\sigma}} \sigma_{zz}^{q-1} \quad (3.33)$$

Now,

$$\begin{aligned}\dot{\epsilon}_{\theta z} &= \frac{\partial \dot{\sigma}}{\partial \tau_{\theta z}} \dot{\epsilon} = \frac{1}{q} \left(\frac{\dot{\sigma}}{\sigma}\right)^{\frac{1-q}{q}} \cdot \frac{3}{2} q \tau_{\theta z}^{q-1} \dot{\epsilon} \\ &= \left(\frac{\dot{\sigma}}{\sigma}\right)^{\frac{1-q}{q}} \dot{\epsilon} \cdot \frac{3}{2} (\tau_{\theta z})^{q-1}\end{aligned}$$

Similarly,

$$\begin{aligned}\dot{\epsilon}_{z\theta} &= \frac{\partial \dot{\sigma}}{\partial \tau_{z\theta}} \dot{\epsilon} \\ &= \left(\frac{\dot{\sigma}}{\sigma}\right)^{\frac{1-q}{q}} \dot{\epsilon} \cdot \frac{3}{2} (\tau_{z\theta})^{q-1}\end{aligned}$$

So that,

$$\dot{\gamma}_{\theta z} = \dot{\epsilon}_{\theta z} + \dot{\epsilon}_{z\theta} = \left(\frac{\dot{\sigma}}{\sigma}\right)^{\frac{1-q}{q}} \dot{\epsilon} \cdot 3 (\tau_{\theta z})^{q-1} \quad (3.34)$$

Then dividing equation (3.34) by (3.33) we have,

$$\frac{\dot{\gamma}_{\theta z}}{\dot{\epsilon}_{zz}} = 3 \left(\frac{\tau_{\theta z}}{\sigma_{zz}}\right)^{q-1} = 3 \left(\frac{\tau_{\theta z}}{\sigma_{zz}}\right)^{n-2m} \quad (3.35)$$

For radial loading where  $\lambda = \tau_{\theta z} / \sigma_{zz} = \text{constant}$ ,

$$\frac{\dot{\gamma}_{\theta z}}{\dot{\epsilon}_{zz}} = 3(\lambda)^{n-2m} \quad (3.36)$$

Equation (3.36) would therefore be suitable to describe that type of behaviour where  $\dot{\gamma}_{\theta z} / \dot{\epsilon}_{zz}$  takes on a different value for each stress ratio ( $\lambda$ ) such that a parabolic relationship exists between them.

#### 3.4.2 Berman and Pai (28)

Equation (4.9) may be used to find the  $\dot{\gamma}_{\theta z} / \dot{\epsilon}_{zz}$  ratio. If  $\bar{\sigma}_m$  is written as the equivalent stress for combined tension-torsion (equation 3.1). Then,

$$\begin{aligned}\dot{\epsilon}_{zz} &= k (\bar{\sigma}_T)^n \frac{\partial (\sigma_{zz}^2 + 3\tau_{\theta z}^2)^{1/2}}{\partial \sigma_{zz}} \\ &= k \left(\frac{\bar{\sigma}_T}{\bar{\sigma}_m}\right)^n \sigma_{zz}\end{aligned}$$

and,

$$\begin{aligned}\dot{\gamma}_{\theta z} &= k (\bar{\sigma}_T)^n \frac{\partial (\sigma_{zz}^2 + 3\tau_{\theta z}^2)^{1/2}}{\partial \tau_{\theta z}} \\ &= k \left(\frac{\bar{\sigma}_T}{\bar{\sigma}_m}\right)^n 3\tau_{\theta z}\end{aligned}$$

so that,

$$\frac{\dot{\gamma}_{\theta z}}{\dot{\epsilon}_{zz}} = 3 \left( \frac{\tau_{\theta z}}{\sigma_{zz}} \right) \quad (3.37)$$

which is the same as that predicted by the Levy-Mises flow rule (see equation (3.20)).

Equation (51) may be used to predict a  $\dot{\gamma}_{\theta z} / \dot{\epsilon}_{zz}$  ratio where the Tresca equivalent stress ( $\bar{\sigma}_T$ ) is used as a plastic potential. For combined tension-torsion this is given by equation (3.2) and,

$$\begin{aligned} \dot{\epsilon}_{zz} &= k (\bar{\sigma}_M)^n \frac{\partial (\sigma_{zz}^2 + 4\tau_{\theta z}^2)^{1/2}}{\partial \sigma_{zz}} \\ &= k \left( \frac{\bar{\sigma}_M}{\bar{\sigma}_T} \right)^n \sigma_{zz} \end{aligned}$$

$$\begin{aligned} \dot{\gamma}_{\theta z} &= k (\bar{\sigma}_M)^n \frac{\partial (\sigma_{zz}^2 + 4\tau_{\theta z}^2)^{1/2}}{\partial \tau_{\theta z}} \\ &= k \left( \frac{\bar{\sigma}_M}{\bar{\sigma}_T} \right)^n 4\tau_{\theta z} \end{aligned}$$

so that,

$$\frac{\dot{\gamma}_{\theta z}}{\dot{\epsilon}_{zz}} = 4 \left( \frac{\tau_{\theta z}}{\sigma_{zz}} \right) \quad (3.38)$$

which is the same as that predicted by the Tresca flow rule.

The theory of Berman and Pai is therefore only made different from the established flow rules of Levy-Mises and Tresca by virtue of the flexibility given to the definition of  $\bar{\sigma}$  in the correlation of multi-axial and uniaxial data.

### 3.4.3 Hu (56)

Hu extended Hill's theory for anisotropic plastic flow to account for a rotation of the principal axes of anisotropy. In this theory it is assumed that the principal axes (1, 2) of anisotropy and the cylindrical coordinates ( $r, \theta$ ) are initially coincident. Then for a thin walled tube with an imposed tension-torsion loading system the resulting axial extension and angle of twist ( $\theta$ ) are assumed to cause a rotation ( $\alpha$ ) of the axes of anisotropy (Fig. 3.1).

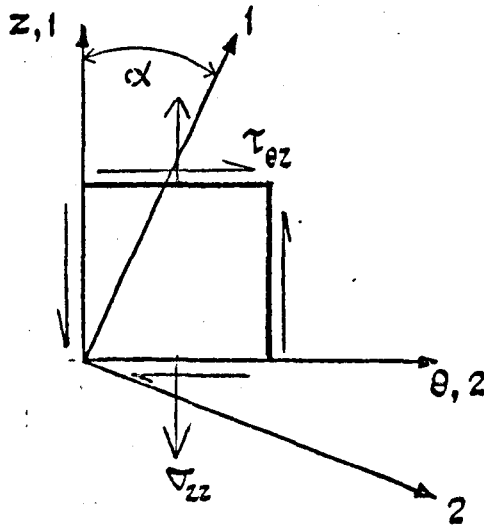


Fig. 3.1 Axes of anisotropy

By transforming the  $\sigma_{zz}, \tau_{\theta z}$  stress components along the rotated axes of anisotropy the plastic strain increment components may then be found from equation (54). These components may in turn be transformed to the  $Z, \theta$  loading axes to give, for the terminology used here, a ratio of plastic shear strain to axial strain increment of,

$$\frac{d\delta_{\theta z}^p}{d\epsilon_{zz}^p} = \frac{\beta_2 \sigma_{zz} + \beta_3 \tau_{\theta z}}{\beta_1 \sigma_{zz} + \beta_2 \tau_{\theta z}} = \frac{\beta_2 + \lambda \beta_3}{\beta_1 + \lambda \beta_2} \quad (3.39)$$

where,

$$\beta_1 = (F+H)\cos^4\alpha + (F+G)\sin^4\alpha - 2F\sin^2\alpha\cos^2\alpha + \frac{3L}{2}\sin^2 2\alpha$$

$$\beta_2 = (F+H)\cos^2\alpha\sin 2\alpha - (2F+G)\sin^2\alpha\sin 2\alpha + F\cos^2\alpha\sin 2\alpha - 3L\cos 2\alpha\sin 2\alpha$$

$$\beta_3 = (4F+H+G)\sin^2 2\alpha + 6L\cos^2 2\alpha$$

Thus as Hu points out the ratio of the strain increments as given by equation (3.39) will not remain constant if the angle of rotation of the axes of anisotropy  $\alpha$  changes with the angle of twist  $\theta$  of the tube during plastic deformation. The nature of the change may only be defined if the relationship between  $\alpha$  and  $\theta$  is specified.

For creep deformation  $\theta$  and hence  $\alpha$  are functions of time. The same ratio of equation (3.39) applies for strain rates because,

$$\frac{\dot{\delta}_{\theta z}^p}{\dot{\epsilon}_{zz}^p} = \frac{\frac{d\delta_{\theta z}^p}{d\alpha} \times \frac{d\alpha}{dt}}{\frac{d\epsilon_{zz}^p}{d\alpha} \times \frac{d\alpha}{dt}} = \frac{d\delta_{\theta z}^p}{d\epsilon_{zz}^p} \quad (3.40)$$

The dependence of the angle of twist on time is known in creep since this is proportional to the shape of the shear creep curve ( $\delta_{\theta z}$  vs  $t$ ) when  $\delta_{\theta z} \approx r\theta/l$  but in order to evaluate the strain rate ratio the relationship between  $\alpha$  and  $\theta$  has to be specified as before.

Note that for isotropy all the constants are unity and equation (3.39) reduces to equation (3.13).

### 3.5 GENERAL THEORIES OF ANISOTROPY

A general theory is one that accounts for initial material anisotropy, a prior plastic strain and a Bauschinger effect. In allowing for these the following theories are essentially modifications to the Von Mises yield criterion  $f(\sigma_{ij}) = \frac{1}{2}(\sigma'_{ij})^2$ . A brief review of their form is given by Shahabi and Shelton (57).

#### 3.5.1 Edelman and Drucker (58)

Proposed the yield criterion,

$$f(\sigma_{ij}) = \frac{1}{2} C_{ijkl} (\sigma'_{ij} - m \epsilon_{ij}^p) (\sigma'_{kl} - m \epsilon_{kl}^p) = k^2 \quad (3.41)$$

where,

$C_{ijkl}$  is an anisotropy parameter

$m$  is a Bauschinger parameter

$\epsilon_{ij}^p$  are the prior strains.

The stress-strain relations and more particularly here, the  $\frac{d\gamma^p}{d\epsilon^p}$  ratio for plastic deformation may then be obtained from equation (8)

in the following way,

Expanding (3.41) for  $i = 1, 2, 3$

$$f = \frac{1}{2} C_{11kl} (\sigma'_{1j} - m \epsilon_{1j}^p) (\sigma'_{kl} - m \epsilon_{kl}^p) + \frac{1}{2} C_{21kl} (\sigma'_{2j} - m \epsilon_{2j}^p) (\sigma'_{kl} - m \epsilon_{kl}^p) + \frac{1}{2} C_{31kl} (\sigma'_{3j} - m \epsilon_{3j}^p) (\sigma'_{kl} - m \epsilon_{kl}^p)$$

and for  $j = 1, 2, 3$

$$f = \frac{1}{2} C_{11kl} (\sigma'_{11} - m \epsilon_{11}^p) (\sigma'_{kl} - m \epsilon_{kl}^p) + \frac{1}{2} C_{21kl} (\sigma'_{21} - m \epsilon_{21}^p) (\sigma'_{kl} - m \epsilon_{kl}^p) + \frac{1}{2} C_{31kl} (\sigma'_{31} - m \epsilon_{31}^p) (\sigma'_{kl} - m \epsilon_{kl}^p) \\ + \frac{1}{2} C_{12kl} (\sigma'_{12} - m \epsilon_{12}^p) (\sigma'_{kl} - m \epsilon_{kl}^p) + \frac{1}{2} C_{22kl} (\sigma'_{22} - m \epsilon_{22}^p) (\sigma'_{kl} - m \epsilon_{kl}^p) + \frac{1}{2} C_{32kl} (\sigma'_{32} - m \epsilon_{32}^p) (\sigma'_{kl} - m \epsilon_{kl}^p) \\ + \frac{1}{2} C_{13kl} (\sigma'_{13} - m \epsilon_{13}^p) (\sigma'_{kl} - m \epsilon_{kl}^p) + \frac{1}{2} C_{23kl} (\sigma'_{23} - m \epsilon_{23}^p) (\sigma'_{kl} - m \epsilon_{kl}^p) + \frac{1}{2} C_{33kl} (\sigma'_{33} - m \epsilon_{33}^p) (\sigma'_{kl} - m \epsilon_{kl}^p)$$

and for  $k = 1, 2, 3$ ,

$$\begin{aligned}
 f = & \frac{1}{2} C_{111l} (\sigma_{11}' - m \epsilon_{11}^p) (\sigma_{1l}' - m \epsilon_{1l}^p) + \frac{1}{2} C_{211l} (\sigma_{21}' - m \epsilon_{21}^p) (\sigma_{1l}' - m \epsilon_{1l}^p) + \frac{1}{2} C_{311l} (\sigma_{31}' - m \epsilon_{31}^p) (\sigma_{1l}' - m \epsilon_{1l}^p) \\
 & + \frac{1}{2} C_{121l} (\sigma_{12}' - m \epsilon_{12}^p) (\sigma_{1l}' - m \epsilon_{1l}^p) + \frac{1}{2} C_{221l} (\sigma_{22}' - m \epsilon_{22}^p) (\sigma_{1l}' - m \epsilon_{1l}^p) + \frac{1}{2} C_{321l} (\sigma_{32}' - m \epsilon_{32}^p) (\sigma_{1l}' - m \epsilon_{1l}^p) \\
 & + \frac{1}{2} C_{131l} (\sigma_{13}' - m \epsilon_{13}^p) (\sigma_{1l}' - m \epsilon_{1l}^p) + \frac{1}{2} C_{231l} (\sigma_{23}' - m \epsilon_{23}^p) (\sigma_{1l}' - m \epsilon_{1l}^p) + \frac{1}{2} C_{331l} (\sigma_{33}' - m \epsilon_{33}^p) (\sigma_{1l}' - m \epsilon_{1l}^p) \\
 & + \frac{1}{2} C_{112l} (\sigma_{11}' - m \epsilon_{11}^p) (\sigma_{2l}' - m \epsilon_{2l}^p) + \frac{1}{2} C_{212l} (\sigma_{21}' - m \epsilon_{21}^p) (\sigma_{2l}' - m \epsilon_{2l}^p) + \frac{1}{2} C_{312l} (\sigma_{31}' - m \epsilon_{31}^p) (\sigma_{2l}' - m \epsilon_{2l}^p) \\
 & + \frac{1}{2} C_{122l} (\sigma_{12}' - m \epsilon_{12}^p) (\sigma_{2l}' - m \epsilon_{2l}^p) + \frac{1}{2} C_{222l} (\sigma_{22}' - m \epsilon_{22}^p) (\sigma_{2l}' - m \epsilon_{2l}^p) + \frac{1}{2} C_{322l} (\sigma_{32}' - m \epsilon_{32}^p) (\sigma_{2l}' - m \epsilon_{2l}^p) \quad (3.42) \\
 & + \frac{1}{2} C_{132l} (\sigma_{13}' - m \epsilon_{13}^p) (\sigma_{2l}' - m \epsilon_{2l}^p) + \frac{1}{2} C_{232l} (\sigma_{23}' - m \epsilon_{23}^p) (\sigma_{2l}' - m \epsilon_{2l}^p) + \frac{1}{2} C_{332l} (\sigma_{33}' - m \epsilon_{33}^p) (\sigma_{2l}' - m \epsilon_{2l}^p) \\
 & + \frac{1}{2} C_{113l} (\sigma_{11}' - m \epsilon_{11}^p) (\sigma_{3l}' - m \epsilon_{3l}^p) + \frac{1}{2} C_{213l} (\sigma_{21}' - m \epsilon_{21}^p) (\sigma_{3l}' - m \epsilon_{3l}^p) + \frac{1}{2} C_{313l} (\sigma_{31}' - m \epsilon_{31}^p) (\sigma_{3l}' - m \epsilon_{3l}^p) \\
 & + \frac{1}{2} C_{123l} (\sigma_{12}' - m \epsilon_{12}^p) (\sigma_{3l}' - m \epsilon_{3l}^p) + \frac{1}{2} C_{223l} (\sigma_{22}' - m \epsilon_{22}^p) (\sigma_{3l}' - m \epsilon_{3l}^p) + \frac{1}{2} C_{323l} (\sigma_{32}' - m \epsilon_{32}^p) (\sigma_{3l}' - m \epsilon_{3l}^p) \\
 & + \frac{1}{2} C_{133l} (\sigma_{13}' - m \epsilon_{13}^p) (\sigma_{3l}' - m \epsilon_{3l}^p) + \frac{1}{2} C_{233l} (\sigma_{23}' - m \epsilon_{23}^p) (\sigma_{3l}' - m \epsilon_{3l}^p) + \frac{1}{2} C_{333l} (\sigma_{33}' - m \epsilon_{33}^p) (\sigma_{3l}' - m \epsilon_{3l}^p)
 \end{aligned}$$

### (1) Prior Tension and Compression

Identifying 1,2,3 with the axial, circumferential and radial directions respectively, then for prior tensile or compressive strain  $(\epsilon_{11}^p, \epsilon_{22}^p, \epsilon_{33}^p)$  with subsequent combined tension-torsion deviatoric stress  $(\sigma_{11}', \sigma_{22}', \sigma_{33}', \sigma_{12}', \sigma_{21}')$ , we have the following function from the expansion ( $l=1,2,3$ ) of equation (3.42),

$$\begin{aligned}
 f = & \frac{1}{2} C_{1111} (\sigma_{11}' - m \epsilon_{11}^p)^2 + \frac{1}{2} C_{2111} \sigma_{21}' (\sigma_{11}' - m \epsilon_{11}^p) + \frac{1}{2} C_{1211} \sigma_{12}' (\sigma_{11}' - m \epsilon_{11}^p) + \frac{1}{2} C_{2211} (\sigma_{22}' - m \epsilon_{22}^p) (\sigma_{11}' - m \epsilon_{11}^p) \\
 & + \frac{1}{2} C_{3311} (\sigma_{33}' - m \epsilon_{33}^p) (\sigma_{11}' - m \epsilon_{11}^p) + \frac{1}{2} C_{1121} \sigma_{21}' (\sigma_{11}' - m \epsilon_{11}^p) + \frac{1}{2} C_{2121} (\sigma_{21}')^2 + \frac{1}{2} C_{1221} (\sigma_{12}' \sigma_{21}') \\
 & + \frac{1}{2} C_{2221} \sigma_{21}' (\sigma_{22}' - m \epsilon_{22}^p) + \frac{1}{2} C_{3321} \sigma_{21}' (\sigma_{33}' - m \epsilon_{33}^p) + \frac{1}{2} C_{1122} \sigma_{12}' (\sigma_{11}' - m \epsilon_{11}^p) + \frac{1}{2} C_{2122} \sigma_{21}' \sigma_{12}' + \frac{1}{2} C_{1222} (\sigma_{12}')^2 \\
 & + \frac{1}{2} C_{2222} \sigma_{12}' (\sigma_{22}' - m \epsilon_{22}^p) + \frac{1}{2} C_{3322} \sigma_{12}' (\sigma_{33}' - m \epsilon_{33}^p) + \frac{1}{2} C_{1122} (\sigma_{11}' - m \epsilon_{11}^p) (\sigma_{22}' - m \epsilon_{22}^p) + \frac{1}{2} C_{2122} \sigma_{21}' (\sigma_{22}' - m \epsilon_{22}^p) \\
 & + \frac{1}{2} C_{1222} \sigma_{12}' (\sigma_{22}' - m \epsilon_{22}^p) + \frac{1}{2} C_{2222} (\sigma_{22}' - m \epsilon_{22}^p)^2 + \frac{1}{2} C_{3322} (\sigma_{33}' - m \epsilon_{33}^p) (\sigma_{22}' - m \epsilon_{22}^p) + \frac{1}{2} C_{1133} (\sigma_{11}' - m \epsilon_{11}^p) (\sigma_{33}' - m \epsilon_{33}^p) \\
 & + \frac{1}{2} C_{2333} \sigma_{21}' (\sigma_{33}' - m \epsilon_{33}^p) + \frac{1}{2} C_{1233} \sigma_{12}' (\sigma_{33}' - m \epsilon_{33}^p) + \frac{1}{2} C_{2233} (\sigma_{22}' - m \epsilon_{22}^p) (\sigma_{33}' - m \epsilon_{33}^p) + \frac{1}{2} C_{3333} (\sigma_{33}' - m \epsilon_{33}^p)^2 \quad (3.43)
 \end{aligned}$$

Converting from deviatoric to absolute stress from equation (1),

$$\sigma_{11}' = \frac{2}{3} \sigma_{11}, \quad \sigma_{22}' = -\frac{1}{3} \sigma_{11}, \quad \sigma_{33}' = -\frac{1}{3} \sigma_{11}, \quad \sigma_{12}' = \sigma_{12}, \quad \sigma_{21}' = \sigma_{21}$$

we then have the following plastic strain increments with 'f' of

equation (3.43) as the plastic potential in equation (8),

$$\begin{aligned}
 d\epsilon_{11}^p = \frac{\partial f}{\partial \sigma_{11}} \delta \lambda = & \left\{ \frac{4}{9} (C_{1111} - \frac{C_{1122}}{2} - \frac{C_{1133}}{2} - \frac{C_{2211}}{2} - \frac{C_{3311}}{2} + \frac{C_{2222}}{4} + \frac{C_{2233}}{4} + \frac{C_{3322}}{4} + \frac{C_{3333}}{4}) \sigma_{11} \right. \\
 & + \frac{1}{3} (C_{1211} + C_{1122} - \frac{C_{2212}}{2} - \frac{C_{3312}}{2} - \frac{C_{1222}}{2} - \frac{C_{1233}}{2}) \sigma_{12} + \frac{1}{3} (C_{2111} + C_{1121} - \frac{C_{2221}}{2} \\
 & - \frac{C_{3321}}{2} - \frac{C_{2212}}{2} - \frac{C_{2133}}{2}) \sigma_{21} - \frac{2m}{3} \left[ (C_{1111} - \frac{C_{1122}}{4} - \frac{C_{1133}}{4} - \frac{C_{2211}}{4} - \frac{C_{3311}}{4}) \epsilon_{11}^p \right. \\
 & + (C_{1122} + \frac{C_{2211}}{2} - \frac{C_{2222}}{2} - \frac{C_{2233}}{4} - \frac{C_{3322}}{4}) \epsilon_{22}^p + (C_{1133} + \frac{C_{3311}}{2} - \frac{C_{3333}}{2} \\
 & \left. \left. - \frac{C_{2233}}{4} - \frac{C_{3322}}{4}) \epsilon_{33}^p \right] \right\} \delta \lambda.
 \end{aligned}$$

$$d\epsilon_{12}^P = \frac{\partial f}{\partial \sigma_{12}} \cdot \delta\lambda = \left\{ \frac{1}{3}(C_{1211} + C_{1112} - \frac{C_{2212}}{2} - \frac{C_{3312}}{2} - \frac{C_{1222}}{2} - \frac{C_{1233}}{2}) \sigma_{11} + \frac{1}{2}(C_{1221} + C_{2112}) \sigma_{21} \right. \\ \left. + C_{1212} \sigma_{12} - \frac{m}{2} \left[ (C_{1211} + C_{1112}) \epsilon_{11}^P + (C_{2212} + C_{1222}) \epsilon_{22}^P + (C_{3312} + C_{1233}) \epsilon_{33}^P \right] \right\} \delta\lambda. \quad (3.44)$$

$$d\epsilon_{21}^P = \frac{\partial f}{\partial \sigma_{21}} \cdot \delta\lambda = \left\{ \frac{1}{3}(C_{2111} + C_{1121} - \frac{C_{2221}}{2} - \frac{C_{3321}}{2} - \frac{C_{2122}}{2} - \frac{C_{2133}}{2}) \sigma_{11} + \frac{1}{2}(C_{1221} + C_{2112}) \sigma_{12} \right. \\ \left. + C_{2121} \sigma_{21} - \frac{m}{2} \left[ (C_{2111} + C_{1121}) \epsilon_{11}^P + (C_{2221} + C_{2122}) \epsilon_{22}^P + (C_{3321} + C_{2133}) \epsilon_{33}^P \right] \right\} \delta\lambda.$$

Now,

$$\frac{d\delta^P}{d\epsilon^P} = \frac{d\epsilon_{12}^P + d\epsilon_{21}^P}{d\epsilon_{11}^P} \quad (3.45)$$

Putting  $\sigma_{12} = \sigma_{21}$  and  $\epsilon_{22}^P = \epsilon_{33}^P = -\frac{\epsilon_{11}^P}{2}$  \* we have from equations (3.44) and (3.45),

$$\frac{d\delta^P}{d\epsilon^P} = \frac{A(\sigma_{11} - \frac{3m}{2}\epsilon_{11}^P) + B\sigma_{12}}{C(\sigma_{11} - \frac{3m}{2}\epsilon_{11}^P) + A\sigma_{12}} \quad (3.46)$$

where,

$$A = \frac{1}{3}(C_{1112} + C_{1121} + C_{1211} + C_{2111} - \frac{C_{2212}}{2} - \frac{C_{2221}}{2} - \frac{C_{3312}}{2} - \frac{C_{3321}}{2} - \frac{C_{1222}}{2} - \frac{C_{1233}}{2} - \frac{C_{2122}}{2} - \frac{C_{2133}}{2})$$

$$B = C_{1212} + C_{1221} + C_{2112} + C_{2121}$$

$$C = \frac{4}{9}(C_{1111} - \frac{C_{1122}}{2} - \frac{C_{1133}}{2} - \frac{C_{2211}}{2} - \frac{C_{3311}}{2} + \frac{C_{2222}}{4} + \frac{C_{2233}}{4} + \frac{C_{3322}}{4} + \frac{C_{3333}}{4})$$

## (2) Prior Forward and Reversed Torsion

For prior shear strain ( $\epsilon_{12}^P, \epsilon_{21}^P$ ) with subsequent combined tension-torsion deviatoric stress ( $\sigma_{11}', \sigma_{22}', \sigma_{33}', \sigma_{12}', \sigma_{21}'$ ) we have the following function from the expansion ( $l=1,2,3$ ) of equation (3.42),

$$f = \frac{1}{2}C_{1111} \sigma_{11}'^2 + \frac{1}{2}C_{2111} \sigma_{11}'(\sigma_{21}' - m\epsilon_{21}^P) + \frac{1}{2}C_{1211} \sigma_{11}'(\sigma_{12}' - m\epsilon_{12}^P) + \frac{1}{2}C_{2211} \sigma_{22}' \sigma_{11}' + \frac{1}{2}C_{3311} \sigma_{33}' \sigma_{11}' \\ + \frac{1}{2}C_{1121} \sigma_{11}'(\sigma_{21}' - m\epsilon_{21}^P) + \frac{1}{2}C_{2121} (\sigma_{21}' - m\epsilon_{21}^P)^2 + \frac{1}{2}C_{1221} (\sigma_{12}' - m\epsilon_{12}^P)(\sigma_{21}' - m\epsilon_{21}^P) + \frac{1}{2}C_{2221} \sigma_{22}' (\sigma_{21}' - m\epsilon_{21}^P) \\ + \frac{1}{2}C_{3321} \sigma_{33}' (\sigma_{21}' - m\epsilon_{21}^P) + \frac{1}{2}C_{1112} \sigma_{11}'(\sigma_{12}' - m\epsilon_{12}^P) + \frac{1}{2}C_{2112} (\sigma_{21}' - m\epsilon_{21}^P)(\sigma_{12}' - m\epsilon_{12}^P) + \frac{1}{2}C_{1212} (\sigma_{12}' - m\epsilon_{12}^P)^2 \\ + \frac{1}{2}C_{2212} \sigma_{22}' (\sigma_{12}' - m\epsilon_{12}^P) + \frac{1}{2}C_{3312} \sigma_{33}' (\sigma_{12}' - m\epsilon_{12}^P) + \frac{1}{2}C_{1122} \sigma_{11}' \sigma_{22}' + \frac{1}{2}C_{2122} \sigma_{22}' (\sigma_{21}' - m\epsilon_{21}^P) \\ + \frac{1}{2}C_{1222} \sigma_{22}' (\sigma_{12}' - m\epsilon_{12}^P) + \frac{1}{2}C_{2222} \sigma_{22}'^2 + \frac{1}{2}C_{3322} \sigma_{33}' \sigma_{22}' + \frac{1}{2}C_{1133} \sigma_{11}' \sigma_{33}' + \frac{1}{2}C_{2133} \sigma_{33}' (\sigma_{21}' - m\epsilon_{21}^P) \\ + \frac{1}{2}C_{1233} \sigma_{33}' (\sigma_{12}' - m\epsilon_{12}^P) + \frac{1}{2}C_{2233} \sigma_{22}' \sigma_{33}' + \frac{1}{2}C_{3333} \sigma_{33}'^2$$

Then from equation (8) the plastic strain increments are,

$$d\epsilon_{11}^P = \left\{ \frac{4}{9}(C_{1111} - \frac{C_{1122}}{2} - \frac{C_{1133}}{2} - \frac{C_{2211}}{2} - \frac{C_{3311}}{2} + \frac{C_{2222}}{4} + \frac{C_{2233}}{4} + \frac{C_{3322}}{4} + \frac{C_{3333}}{4}) \sigma_{11} + \frac{1}{3}(C_{1211} + C_{1112} \right. \\ \left. - \frac{C_{2212}}{2} - \frac{C_{3312}}{2} - \frac{C_{1222}}{2} - \frac{C_{1233}}{2}) (\sigma_{12}' - m\epsilon_{12}^P) + \frac{1}{3}(C_{2111} + C_{1121} - \frac{C_{2221}}{2} - \frac{C_{3321}}{2} - \frac{C_{2122}}{2} - \frac{C_{2133}}{2}) (\sigma_{21}' - m\epsilon_{21}^P) \right\} \delta\lambda.$$

$$d\epsilon_{12}^P = \left\{ \frac{1}{3}(C_{1211} + C_{1112} - \frac{C_{2212}}{2} - \frac{C_{3312}}{2} - \frac{C_{1222}}{2} - \frac{C_{1233}}{2}) \sigma_{11} + \frac{1}{2}(C_{1221} + C_{2112}) (\sigma_{21}' - m\epsilon_{21}^P) + C_{1212} (\sigma_{12}' - m\epsilon_{12}^P) \right\} \delta\lambda.$$

$$d\epsilon_{21}^P = \left\{ \frac{1}{3}(C_{2111} + C_{1121} - \frac{C_{2221}}{2} - \frac{C_{3321}}{2} - \frac{C_{2122}}{2} - \frac{C_{2133}}{2}) \sigma_{11} + \frac{1}{2}(C_{1221} + C_{2112}) (\sigma_{12}' - m\epsilon_{12}^P) + C_{2121} (\sigma_{21}' - m\epsilon_{21}^P) \right\} \delta\lambda.$$

\* For tensile straining on annealed material Fig.4.3 confirms  $\epsilon_{00}^P = -\frac{\epsilon_{xx}^P}{2}$  (or  $\epsilon_{22}^P = -\frac{\epsilon_{11}^P}{2}$ ). Then  $\epsilon_{33}^P = -\frac{\epsilon_{11}^P}{2}$  from constancy of volume ( $\epsilon_{11}^P + \epsilon_{22}^P + \epsilon_{33}^P = 0$ ).

and from equation (3.45),

$$\frac{d\delta^P}{d\epsilon^P} = \frac{A\sigma_{11} + B(\sigma_{12} - \frac{m\delta_0^P}{2})}{C\sigma_{11} + A(\sigma_{12} - \frac{m\delta_0^P}{2})} \quad (3.47)$$

for  $\sigma_{12} = \sigma_{21}$ ,  $\epsilon_{12}^P = \epsilon_{21}^P = \frac{\delta_0^P}{2}$  \* and the constants A, B, C of equation (3.46).

### 3.5.2 Yoshimura (59)

Rationalized the Edelman and Drucker theory with the yield criterion,

$$f = \frac{1}{2} C'_{ijkl} \sigma'_{ij} \sigma'_{kl} - m' \epsilon'_{ij} \sigma'_{ij} \quad (3.48)$$

where,

$C'_{ijkl}$  is an anisotropy parameter,

$m'$  is a Bauschinger coefficient,

$\epsilon'_{ij}$  are the prior strains.

#### (1) Prior Tension and Compression

The function corresponding to equation (3.43) in this theory is,

$$\begin{aligned} f = & (C'_{1111} \sigma'_{11} + C'_{2111} \sigma'_{21} \sigma'_{11} + C'_{1211} \sigma'_{12} \sigma'_{11} + C'_{2211} \sigma'_{22} \sigma'_{11} + C'_{3311} \sigma'_{33} \sigma'_{11} + C'_{1121} \sigma'_{11} \sigma'_{21} + C'_{2121} \sigma'_{21} \sigma'_{21} \\ & + C'_{1221} \sigma'_{12} \sigma'_{21} + C'_{2221} \sigma'_{22} \sigma'_{21} + C'_{3321} \sigma'_{33} \sigma'_{21} + C'_{1112} \sigma'_{11} \sigma'_{12} + C'_{2112} \sigma'_{21} \sigma'_{12} + C'_{1212} \sigma'_{12} \sigma'_{12} \\ & + C'_{2212} \sigma'_{22} \sigma'_{12} + C'_{3312} \sigma'_{33} \sigma'_{12} + C'_{1122} \sigma'_{11} \sigma'_{22} + C'_{2122} \sigma'_{21} \sigma'_{22} + C'_{1222} \sigma'_{12} \sigma'_{22} + C'_{2222} \sigma'_{22} \sigma'_{22} \\ & + C'_{3322} \sigma'_{33} \sigma'_{22} + C'_{1133} \sigma'_{11} \sigma'_{33} + C'_{2133} \sigma'_{21} \sigma'_{33} + C'_{1233} \sigma'_{12} \sigma'_{33} + C'_{2233} \sigma'_{22} \sigma'_{33} + C'_{3333} \sigma'_{33} \sigma'_{33}) \\ & - 9m(\epsilon'_{11} \sigma'_{11} + \epsilon'_{22} \sigma'_{22} + \epsilon'_{33} \sigma'_{33}). \end{aligned} \quad (3.49)$$

Then from equations (8) and (3.49),

$$d\epsilon'_{11} = \left\{ \frac{4}{9} (C'_{1111} - \frac{C'_{1122}}{2} - \frac{C'_{1133}}{2} - \frac{C'_{2211}}{2} - \frac{C'_{3311}}{2} + \frac{C'_{2222}}{4} + \frac{C'_{2233}}{4} + \frac{C'_{3322}}{4} + \frac{C'_{3333}}{4}) \sigma'_{11} + \frac{1}{3} (C'_{1211} + C'_{1112} - \frac{C'_{2212}}{2} - \frac{C'_{3312}}{2} - \frac{C'_{1222}}{2} - \frac{C'_{1233}}{2}) \sigma'_{12} + \frac{1}{3} (C'_{2111} + C'_{1121} - \frac{C'_{2221}}{2} - \frac{C'_{3321}}{2} - \frac{C'_{2122}}{2} - \frac{C'_{2133}}{2}) \sigma'_{21} - 3m' (2\epsilon'_{11} - \epsilon'_{22} - \epsilon'_{33}) \right\} \delta\lambda.$$

$$d\epsilon'_{12} = \left\{ \frac{1}{3} (C'_{1211} + C'_{1112} - \frac{C'_{2212}}{2} - \frac{C'_{3312}}{2} - \frac{C'_{1222}}{2} - \frac{C'_{1233}}{2}) \sigma'_{11} + \frac{1}{2} (C'_{1221} + C'_{2112}) \sigma'_{21} + C'_{2121} \sigma'_{12} \right\} \delta\lambda.$$

$$d\epsilon'_{21} = \left\{ \frac{1}{3} (C'_{2111} + C'_{1121} - \frac{C'_{2221}}{2} - \frac{C'_{3321}}{2} - \frac{C'_{2122}}{2} - \frac{C'_{2133}}{2}) \sigma'_{11} + \frac{1}{2} (C'_{1221} + C'_{2112}) \sigma'_{12} + C'_{2121} \sigma'_{21} \right\} \delta\lambda.$$

and from equation (3.45),

$$\frac{d\delta^P}{d\epsilon^P} = \frac{A'\sigma_{11} + B'\sigma_{12}}{C'\sigma_{11} + A'\sigma_{12} - 9m'\epsilon_{11}^P} \quad (3.50)$$

for  $\sigma_{12} = \sigma_{21}$ ,  $\epsilon_{22}^P = \epsilon_{33}^P = -\frac{\epsilon_{11}^P}{2}$  and,

$$A' = \frac{1}{3} (C'_{1112} + C'_{1121} + C'_{1211} + C'_{2111} - \frac{C'_{2212}}{2} - \frac{C'_{2221}}{2} - \frac{C'_{3312}}{2} - \frac{C'_{3321}}{2} - \frac{C'_{1222}}{2} - \frac{C'_{1233}}{2} - \frac{C'_{2122}}{2} - \frac{C'_{2133}}{2})$$

$$B' = C'_{1212} + C'_{1221} + C'_{2112} + C'_{2121}$$

$$C' = \frac{4}{9} (C'_{1111} - \frac{C'_{1122}}{2} - \frac{C'_{1133}}{2} - \frac{C'_{2211}}{2} - \frac{C'_{3311}}{2} + \frac{C'_{2222}}{4} + \frac{C'_{2233}}{4} + \frac{C'_{3322}}{4} + \frac{C'_{3333}}{4})$$

\* The 'engineering' shear strain is twice the 'tensor' shear strain.

## (2) Prior Forward and Reversed Torsion

The plastic strain increments are,

$$d\epsilon_{11}^P = \left\{ \frac{4}{9} (C'_{1111} - \frac{C'_{1122}}{2} - \frac{C'_{1133}}{2} - \frac{C'_{2211}}{2} - \frac{C'_{3311}}{2} + \frac{C'_{2222}}{4} + \frac{C'_{2233}}{4} + \frac{C'_{3322}}{4} + \frac{C'_{3333}}{4}) \sigma_{11} + \frac{1}{3} (C'_{1211} + C'_{1112} - \frac{C'_{2212}}{2} - \frac{C'_{3312}}{2} - \frac{C'_{2222}}{2} - \frac{C'_{1233}}{2}) \sigma_{12} + \frac{1}{3} (C'_{2111} + C'_{1121} - \frac{C'_{2221}}{2} - \frac{C'_{3321}}{2} - \frac{C'_{2122}}{2} - \frac{C'_{2133}}{2}) \sigma_{21} \right\} \delta\lambda.$$

$$d\epsilon_{12}^P = \left\{ \frac{1}{3} (C'_{1211} + C'_{1112} - \frac{C'_{2212}}{2} - \frac{C'_{3312}}{2} - \frac{C'_{2222}}{2} - \frac{C'_{1233}}{2}) \sigma_{11} + \frac{1}{2} (C'_{1221} + C'_{2112}) \sigma_{21} + C'_{1212} \sigma_{12} - 9m' \epsilon_{12}^P \right\} \delta\lambda.$$

$$d\epsilon_{21}^P = \left\{ \frac{1}{3} (C'_{2111} + C'_{1121} - \frac{C'_{2221}}{2} - \frac{C'_{3321}}{2} - \frac{C'_{2122}}{2} - \frac{C'_{2133}}{2}) \sigma_{11} + \frac{1}{2} (C'_{1221} + C'_{2112}) \sigma_{12} + C'_{2121} \sigma_{21} - 9m' \epsilon_{21}^P \right\} \delta\lambda.$$

Then from equation (3.45),

$$\frac{d\delta^P}{d\epsilon^P} = \frac{A' \sigma_{11} + B' \sigma_{12} - 9m' \delta_0^P}{C' \sigma_{11} + A' \sigma_{12}} \quad (3.51)$$

for  $\sigma_{12} = \sigma_{21}$ ,  $\delta_0^P = (\epsilon_{12}^P + \epsilon_{21}^P)$  and the constants A', B', C' of equation (3.50).

## 3.5.3 Williams and Svensson (60,61)

Extended the Yoshimura theory with the yield criterion,

$$f = (I_{ijkl} + A_0 \epsilon_{ij}^P \epsilon_{kl}^P) (\sigma_{ij} + \alpha_{ij}) (\sigma_{kl} + \alpha_{kl}) = k^2 \quad (3.52)$$

where,

$$I_{ijkl} = \delta_{ik} \delta_{jl} - \frac{1}{3} \delta_{ij} \delta_{kl}$$

$$\alpha_{ij} = \epsilon_{ij}^P (L_{pqrs} \sigma_{pq} \sigma_{rs} - m)$$

and,

$A_0$  is an anisotropy parameter,

$m$  is a Bauschinger effect parameter,

$L_{pqrs}$  is a distortion parameter,

$\epsilon_{ij}^P$  are the prior strains.

For prior tension ( $\epsilon_0^P$ ) and subsequent combined tension-torsion ( $\sigma_{11}, \sigma_{12}$ )

these authors quote (60),

$$\frac{d\delta^P}{d\epsilon^P} = \frac{6\sigma_{12} + 6 \left[ 1 + \frac{3A_0(\epsilon_0^P)^2}{2} \right] \left[ \sigma_{11} + \frac{3\epsilon_0^P}{2} (L_{3333} \sigma_{11}^2 + 2L_{2323} \sigma_{12}^2 - m) \right] (2\epsilon_0^P L_{2323} \sigma_{12})}{2 \left[ 1 + \frac{3A_0(\epsilon_0^P)^2}{2} \right] \left[ \sigma_{11} + \frac{3\epsilon_0^P}{2} (L_{3333} \sigma_{11}^2 + 2L_{2323} \sigma_{12}^2 - m) \right] (1 + 3\epsilon_0^P L_{3333} \sigma_{11})} \quad (3.53)$$

For prior torsion ( $\delta_0^P$ ) and subsequent combined tension-torsion ( $\sigma_{11}, \sigma_{12}$ )

these authors quote (61),

$$\frac{d\delta^P}{d\epsilon^P} = \frac{3 \left[ 1 + \frac{A_0(\delta_0^P)^2}{2} \right] \left[ \sigma_{12} + \frac{\delta_0^P}{2} (L_{3333} \sigma_{11}^2 + 2L_{2323} \sigma_{12}^2 - m) \right] (2 + 4\delta_0^P L_{2323} \sigma_{12})}{2\sigma_{11} + 6 \left[ 1 + \frac{A_0(\delta_0^P)^2}{2} \right] \left[ \sigma_{12} + \frac{\delta_0^P}{2} (L_{3333} \sigma_{11}^2 + 2L_{2323} \sigma_{12}^2 - m) \right] (\delta_0^P L_{3333} \sigma_{11})} \quad (3.54)$$

A comparison of the  $\frac{d\delta^P}{d\epsilon^P}$  ratio of each theory and the measured ratio of prior strained material is made in Chapters 5 and 6. Their extension as anisotropic theories for creep is also discussed.

CHAPTER 4

RESULTS FOR SPECIFIC TESTS

In this chapter the results are covered in three sections. Firstly, an isotropy study of extruded, annealed, and drawn sheets associated with tensile tests is presented. Secondly, the combined tests are analyzed.

4.1 ISOTROPY

The results for the longitudinal (L), transverse (T) and oblique (O) 'Barnhart's' tensile tests in the direction of Fig. 2.1(d) are given in Fig. 4.1. The oblique tests were drawn and the material exhibited tensile elongation in the order of an engineering strain (e) of 15%. The average values for the L, T and O are shown in

# CHAPTER 4

The combined stress study in section 4.1 however showed anisotropy to be a real effect and was attributed to the greater strength of the extruded direction. The material was, therefore, left slightly anisotropic after drawing.

The results of 'Barnhart's' tensile tests on the longitudinally and transversely of Fig. 2.1(d) are shown in Fig. 4.1. Tensile tests were performed at a constant strain rate of  $10^{-3}$  in./in.<sup>2</sup> and the results showed anisotropy to be a real effect and was attributed to the greater strength of the extruded direction.

$$\sigma = \frac{E \epsilon}{1 + \nu} \quad (4.1)$$

Further study will show that anisotropy in the range of  $10^{-3}$  to  $10^{-2}$  in./in.<sup>2</sup> should be noted as a rate effect and the results of the combined tests will be used for strain rate in

## CHAPTER 4

## RESULTS FOR ANNEALED ALUMINIUM

In this chapter the results are covered in three sections. Firstly, an isotropy study is presented, secondly the nature of strain associated with incremental loading is summarised and finally the combined tests are analysed.

4.1 ISOTROPY

The results for the longitudinal (L), transverse (T) and oblique (O) 'Hounsfield' tensile tests on the specimens of Fig. 2.10(a) are given in Fig. 4.1\*. Basically this figure shows that the material exhibited tensile isotropy to the order of an engineering nominal strain ( $\epsilon$ ) of 15%. The average curve of each (L), (T) and (O) set shown in this figure would indicate a slightly greater strength in the (L) direction but this difference appears to be no more than the inter-specimen variability for any one set.

The combined stress study of Section 4.3 however showed anisotropy to be a real effect which was attributed to the greater strength of the extruded direction. The material was, therefore, left slightly anisotropic after annealing.

The results of three 'Instron' tensile tests on the longitudinally cut specimens of Fig. 2.10(b) are given in Fig. 4.2. These tests were performed at a nominal strain rate of  $\dot{\epsilon} = 3.33 \times 10^{-3} \text{ s}^{-1}$  and when plotted logarithmically here show a true stress-plastic strain law of the form,

$$\sigma = 111(\epsilon^p)^{0.27}$$

$$\text{or } \epsilon^p = \sigma^{3.7} / 37.61 \times 10^6 \quad (4.1)$$

Further tests (not shown) at strain rates in the range of  $3.33 \times 10^{-1} - 3.33 \times 10^{-5} \text{ s}^{-1}$  showed no marked strain rate effect and the law of equation (4.1) was therefore seen to be valid for strain rates in this range.

\* Figures are given at the end of this Chapter.

#### 4.2 CREEP AND PLASTIC FLOW DURING UNIAXIAL INCREMENTAL LOADING

The results of these tests, performed on the specimens of Fig. 2.9, are presented in Appendix III. In summary, these tests showed that the forward strain which occurred between increments of load comprised of two components,

- (1) Instantaneous strain ( $\epsilon_o$ )
- (2) Creep strain ( $\epsilon^c$ )

Over a wide range of stress and temperature ( $0.3 < T/T_m < 0.6$ ) the creep strain component was shown to be describable by a simple parabolic law,  $\epsilon^c = at^m$  such that the total strain,

$$\epsilon = \epsilon_o + at^m \quad (4.2)$$

In general the time exponent  $m$  in this equation increased with increasing test temperature and decreasing load increment. The parameter  $a$  in equation (4.2) was shown to be dependent upon applied stress level ( $\sigma$ ), temperature ( $T$ ) and stress increment ( $\Delta\sigma$ ) in the form,

$$a = s \exp(\Delta\sigma) \exp(q/T) \sigma^p \quad (4.3)$$

where  $s$ ,  $q$  and  $p$  were constants such that,

$$\dot{\epsilon}^c = 177.8 \times 10^{-8} m \exp(\Delta\sigma) \exp\left(\frac{-5950}{T}\right) \sigma^{6.2} t^{m-1} \quad (4.4)$$

The instantaneous strain component ( $\epsilon_o$ ) comprised a plastic component ( $\epsilon^p$ ) and a very much smaller recoverable elastic component ( $\epsilon^e = \sigma/E$ ) such that,

$$\epsilon_o = \epsilon^e + \epsilon^p \quad (4.5)$$

and the growth of instantaneous strain ( $\sum \epsilon_o$ ) was found to depend upon stress level and temperature in the way that is understood for tensile behaviour. That is, the stress dependence was typically described in form by equation (4.1) to account for work hardening, whilst the effect of an increasing temperature was to lower the stress to reach a specified strain.

The almost complete absence of a recoverable component of creep strain (anelastic strain) in these tests was attributed to grain boundary sliding being the predominant mechanism in the deformation. Tensile creep isotropy was observed from specimens cut with their axes in longitudinal and oblique directions (Fig. 2.13).

### 4.3 CREEP AND PLASTIC FLOW DURING COMBINED LOADING

This is analysed in three paragraphs. The first relates to the nature of the 30 s plastic loading strain components (  $d\epsilon_{zz}^p$ ,  $d\gamma_{\theta z}^p$  ) in terms of the applied stresses (  $\tau_{zz}$ ,  $\tau_{\theta z}$  ) from plasticity theory. The second paragraph deals with the short-time (30 s - 15 min) creep strain components that occurred between successive increments of load and the third paragraph contains an analysis of the long-time creep strains at the chosen stress ratios.

#### 4.3.1 30 s Loading Strains

These were analysed in the manner outlined in Chapter 3. For the three tests where diametral changes were measured the plastic strain components were computed from equation (3.6) to show from Fig. 4.3 that,

$$\frac{d\epsilon_{\theta\theta}^p}{d\epsilon_{zz}^p} = -\frac{1}{2} \quad (4.6)$$

which, from the constancy of volume condition (  $d\epsilon_{ii}^p = 0$  ), is in accordance with classical plasticity theory. Thus, apparently, equations (3.9) and (3.11) are justified in formulating equivalent strains.

Programme 4.1\* was written for this purpose where equations (3.5), (3.6), (3.8) and (3.10) were firstly evaluated for each load increment and then were successively summed to form the total strains of equations (3.7), (3.9) and (3.11) at each equivalent stress level (equations (3.1) and (3.2)). The elastic constants E, G and  $\nu$  were rather difficult to obtain from this series of tests since the stress-strain loading plots showed little or no linear portion. The unloading curves for the prestrain test series (see Chapter 6) were always linear however and the slopes of these were used to determine

$E = 68,300 \text{ N/mm}^2$ ,  $G = 24,200 \text{ N/mm}^2$ , and  $\nu = 0.32$  for use in Programme 4.1.

Fig. 4.4 was constructed from the third and fourth output columns of this programme and shows the relationship between shear strain (  $\gamma_{\theta z}^p$  ) and longitudinal strain (  $\epsilon_{zz}^p$  ) plastic components for each stress ratio (  $\lambda = \tau_{\theta z} / \tau_{zz}$  ). With the exception of one test (  $\lambda = 0.12$  ), which was associated with a changing stress ratio, the  $\gamma_{\theta z}^p$  vs  $\epsilon_{zz}^p$  plots were all linear. The slopes of each plot, taken as r from equation (3.14), and the constant k, taken as  $r/\lambda$  are shown in the table of this figure. The Levy-Mises equation (3.14) predicts k as 3. For this material an average k is nearer 2.6 than 3 and we therefore have,

$$\frac{d\gamma_{\theta z}^p}{d\epsilon_{zz}^p} = 2.6 \left( \frac{\tau_{\theta z}}{\tau_{zz}} \right) \quad (4.7)$$

\* Programmes are given at the end of this Chapter.

The absolute magnitude of the strain components may be derived in terms of the applied stresses provided some equivalent stress-strain correlation exists for all tests. The last four columns of Programme 4.1 output gives the Mises and Tresca values as defined by equations (3.1), (3.9), (3.2) and (3.11) respectively. These are shown plotted logarithmically in Fig. 4.5 together with a further correlation as made on the basis of maximum shear stress vs maximum shear strain (equations (3.4) and (3.12)). The law of equation (4.1) is also shown in the Mises and Tresca correlations. Comparison of the three plots shows the Tresca equivalent stress definition ( $\bar{\sigma}_T$ ) and its associated equivalent strain ( $\int d\bar{\epsilon}_T^p$ ) to give the best correlation. Assuming linearity on this plot we therefore have an equivalent stress-strain law of the form,

$$\int d\bar{\epsilon}_T^p = A(\bar{\sigma}_T)^n \quad (4.8)$$

or, from equations (3.2) and (3.11), that,

$$\int [(\lambda d\epsilon_{zz}^p)^2 + (d\gamma_{\theta z}^p)^2/4]^{1/2} = A[\tau_{zz}^2 + 4\tau_{\theta z}^2]^{n/2} \quad (4.9)$$

Then solving equations (4.9) and (4.7) the total strain components are,

$$\begin{aligned} \int d\epsilon_{zz}^p &= \frac{2A\tau_{zz}^n(1+4\lambda^2)^{n/2}}{[4+(2.6\lambda)^2]^{1/2}} \\ \int d\gamma_{\theta z}^p &= \frac{5.2A\tau_{\theta z}^n(1+4\lambda^2)^{n/2}}{\lambda^{n-1}[4+(2.6\lambda)^2]^{1/2}} \end{aligned} \quad (4.10)$$

Obviously A and n can be calculated from the Tresca correlation so that equation (4.10) accurately fits the experimental data. It is more usual however to base the correlations of Fig. 4.5 on a simple tension test. Thus taking A and n from equation (4.1) as  $1/(37.61 \times 10^6)$  and 3.7 respectively for use in equation (4.10) its predictions for the  $\lambda = 0.86$  test are given in Fig. 4.6. This shows that the equivalent stress-strain law of equation (4.8) is approximate only in describing real behaviour when based on a separate tension test. A further prediction is shown in Fig. 4.6 for the Levy-Mises law of equation (3.13) and equation (4.1) with Mises definitions of equivalent stress and strain. That is,

$$\begin{aligned} \int d\epsilon_{zz}^p &= \tau_{zz}^n A(1+3\lambda^2)^{\frac{n-1}{2}} \\ \int d\gamma_{\theta z}^p &= 3\tau_{\theta z}^n A\left(\frac{1+3\lambda^2}{\lambda^2}\right)^{\frac{n-1}{2}} \end{aligned} \quad (4.11)$$

Clearly this is seen to be unsatisfactory for this purpose.

Programme 4.1 also allows for the construction of yield loci. Since stress-strain linearity was not a feature of loading the loci of Figs. 4.7A and 4.8A were constructed for constant values of equivalent strain ( $\int d\bar{\epsilon}^p$ ). The loci then show the combined stress condition for equivalent strains of 0.002, 0.005, 0.010, 0.015 and 0.020. Thus in Fig. 4.7A the Mises equivalent strain ( $\int d\bar{\epsilon}_m^p$ ) loci were constructed from plots typical of Fig. 4.7B for  $\lambda = 0.86$ . A superimposed Mises locus shows the stress values to be underestimated on the tensile axis. A similar construction for the Tresca equivalent strain ( $\int d\bar{\epsilon}_T^p$ ) in Fig. 4.8A shows the Tresca locus to represent more closely the combined stress state for a specified  $\int d\bar{\epsilon}_T^p$  value which further confirms the  $\bar{\sigma}_T$  vs  $\int d\bar{\epsilon}_T^p$  correlation of Fig. 4.5. The loci were constructed from the plotted points and the strain increment vectors of Fig. 4.4 shown on each stress path. The loci were then drawn to pass through each point on the stress path and in a direction normal to the strain increment vector at that point. This normality rule implies that for an ellipse  $\sigma_{22}^2 + k \tau_{\theta z}^2 = \gamma^2$  joining the experimental points and whose normal direction is  $k \tau_{\theta z} / \sigma_{22}$  then  $k$  from equation (4.7) is 2.6. Actually a locus of this  $k$  value would underestimate the increased strength of the extruded direction and to include this a locus of  $k = 4$  represents more closely the overall behaviour.\* The fact that the strain increment ratio vector remained constant in direction for any radial stress path further implies that the locus retains its initial shape as plastic flow progresses. The net result as seen in Fig. 4.7A and 4.8A is a series of inflated loci.

#### 4.3.2 Short-Time Creep Strain

The transient creep strain that occurred between increments of combined load were analysed by computing the axial and shear strain rates for intervals of time up to the application of the next increment. Thus at the points marked by the bracketed symbols in Fig. 4.4 the ensuing creep rates as computed from equation (3.15) are shown plotted below in Fig. 4.4A.

---

\* A locus of  $k=4$  would not predict the correct plastic strain increment directions of each stress path. The difficulty lies in knowing the correct equivalent proof strain to define yield for the material. The loci of Figs 4.7A and 4.8A indicate that neither the von Mises nor the Tresca equivalent proof strain is the correct definition. The problem can be overcome by employing a backward extrapolation method to define yield but for the present material the well rounded  $\nabla_{\sigma, \tau} \epsilon^p$  characteristic left the method open to error.

For annealed En 25 steel a correct equivalent strain has been found by an empirical method(54) which includes the angle between the stress and plastic strain increment vectors of each radial loading path.

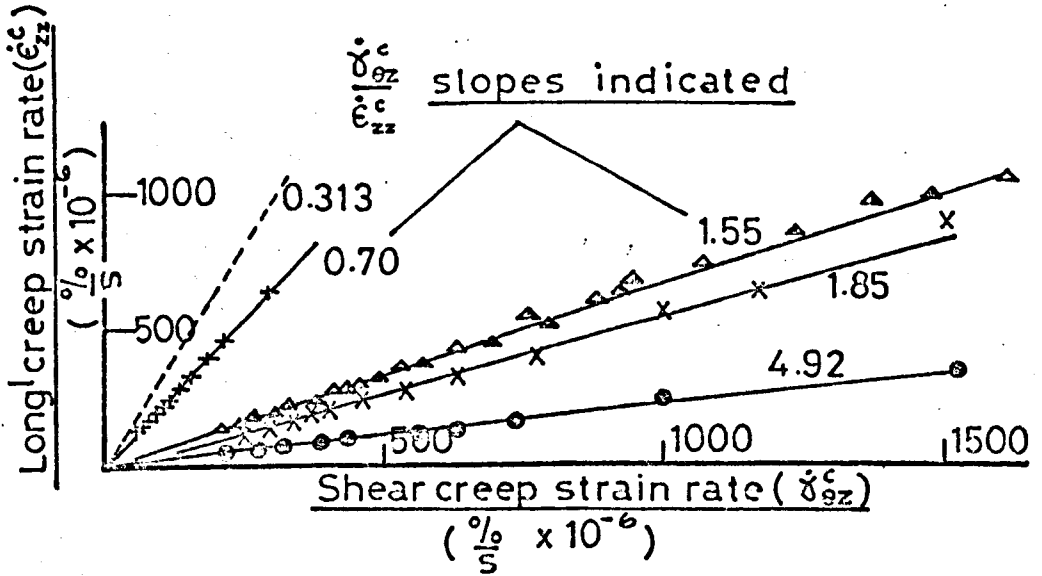


Fig. 4.4A  $\dot{\gamma}_{\theta z}^c$  vs  $\dot{\epsilon}_{zz}^c$  of radial loading ( $\lambda = \text{constant}$ )

This figure shows that for all times in the creep interval the ratio of shear to axial creep rate is the same as the instantaneous strain increment ratio ( $r$  in Fig. 4.4) for each stress path. Equation (4.7) may therefore be extended to short-time creep strain. That is,

$$\frac{d\delta_{\theta z}^c}{d\epsilon_{zz}^c} = \frac{\dot{\gamma}_{\theta z}^c}{\dot{\epsilon}_{zz}^c} = 2.6 \left( \frac{\gamma_{\theta z}}{\epsilon_{zz}} \right) \quad (4.12)$$

The strain rate computations are shown plotted against time for  $\lambda = 0, 0.53$  and  $\infty$  in Figs. 4.9 and 4.10 for the stress levels indicated. Linearity on these logarithmic plots means that the creep strain components in this interval are describable by the parabolic time laws

$$\begin{aligned} \epsilon_{zz}^c &= at^{m_1} \\ \gamma_{\theta z}^c &= bt^{m_2} \end{aligned} \quad (4.13)$$

$m_1$  and  $m_2$  are used here since for any one test (defined by  $\lambda$ ) the time exponents of the strain components were not strictly equal. Thus  $m_1$  for  $\lambda = 0.53$  in Fig. 4.9 is 0.266 while  $m_2$  for the same test in Fig. 4.10 is 0.308. Considering only the longitudinal strain components the time exponent  $m_1$  in Fig. 4.9 is seen to be independent of applied stress level for any one test but from test to test  $m_1$  did vary. The variation is seen to be consistent with the observations made on the uniaxial tests of Section 4.2 where  $m$  increased with decreasing load increment. Thus for the tension test ( $\lambda = 0$ ) of Fig. 4.9  $m_1 = 0.215$  with  $\Delta \sigma_{zz} = 1.94 \text{ N/mm}^2$

while the test for  $\lambda = 0.53$  shows  $m_1 = 0.266$  with  $\Delta \sigma_{22} = 1.2 \text{ N/mm}^2$ . A similar observation is made for  $m_2$  with the shear strain components in the table of Fig. 4.10. Table 4.1 below shows that these trends are consistent through all the tests.

Table 4.1 Variation in  $m$  with  $\lambda$  and stress increment

$\lambda = \tau_{\theta z} / \sigma_{zz}$	$\Delta \sigma_{zz}$ N/mm <sup>2</sup>	$\Delta \tau_{\theta z}$ N/mm <sup>2</sup>	$m_1$	$m_2$
0	1.938	-	0.215	-
0.12	1.808	0.217	0.226	0.325
0.53	1.215	0.644	0.266	0.308
0.86	0.998	0.858	0.309	0.283
1.81	0.661	1.196	0.326	0.249
	-	1.800	-	0.188

It is of interest to compare the  $m_1 = 0.215$  value here with that for a test in Appendix III (Table 2) where for approximately the same stress increment ( $\Delta \sigma = 2 \text{ N/mm}^2$ )  $m = 0.345$ . This difference may be attributed to specimen size effect where the cylinder of this test has five times the number of grains in the cross-section.

In Appendix III the stress dependence of  $\dot{\epsilon}^c$  in the equation  $\dot{\epsilon}^c = m \sigma^p$  was found to be of the form  $\dot{\epsilon}^c = B \sigma^p$  such that,

$$\dot{\epsilon}^c = m B \sigma^p t^{m-1} \quad (4.14)$$

It was found that a similar stress dependence also existed for the strain components here. That is,

$$\begin{aligned} \dot{\epsilon}_{zz}^c &= m_1 B_1 \sigma_1^{p_1} t^{m_1-1} \\ \dot{\gamma}_{\theta z}^c &= m_2 B_2 \sigma_2^{p_2} t^{m_2-1} \end{aligned} \quad (4.15)$$

Only if  $m_1 = m_2$  and  $p_1 = p_2$  is it possible to formulate the multi-axial counterpart of equation (4.14). If this were the case then, guided by the incremental plastic strain correlation of equation (4.9) and the strain increment ratio of equation (4.7) it is likely that for strain rates,

$$\dot{\bar{\epsilon}}^c = m B \bar{\sigma}^p t^{m-1} \quad (4.16)$$

where

$$\dot{\bar{\epsilon}}^c = \left[ (\dot{\epsilon}_{zz}^c)^2 + (\dot{\gamma}_{\theta z}^c)^2 / 4 \right]^{1/2} \quad (4.17)$$

and

$$\bar{\sigma} = \left[ \sigma_{zz}^2 + 4 \tau_{\theta z}^2 \right]^{1/2}$$

to give component creep strain predictions similar to that for the plastic strains of equation (4.10). That is,

$$\begin{aligned} \epsilon_{22}^c &= \frac{2B' \tau_{22}^p (1+4\lambda^2)^{p/2}}{[4+(2.6\lambda)^2]^{1/2}} t^m \\ \gamma_{\theta_2}^c &= \frac{5.2B' \tau_{\theta_2}^p (1+4\lambda^2)^{p/2}}{\lambda^{n-1} [4+(2.6\lambda)^2]^{1/2}} t^m \end{aligned} \quad (4.18)$$

Although equation (4.18) is not strictly applicable to these tests it is possible that for certain materials and radial loading they would apply.

#### 4.3.3 Long-Time Creep Strain

The long-time axial and shear creep strains and strain rates were evaluated by equations (3.16), (3.17) and (3.18) in Programme 4.2 for time intervals up to 100 hours. The longitudinal and shear creep strain rates are shown plotted against time in the logarithmic axes of Figs. 4.11A and 4.11B respectively. These figures show that for long-time constant stress primary creep the time exponent  $m$  that describes it is the same for both longitudinal and shear creep strain components and independent of stress ratio. Thus for all tests,

$$\begin{aligned} \epsilon_{22}^c &= a' t^{0.21} \\ \gamma_{\theta_2}^c &= b' t^{0.21} \end{aligned} \quad (4.19)$$

The final two columns of Programme 4.2 output examines the  $k$  value of equation (3.21) for the selected time intervals. It is seen that in almost all tests and for most times  $k$  approximates to the value of 3 as predicted from the Levy-Mises flow rule of equation (3.20). The effect of a stress ratio that changes with the development of plastic strain is contained in the last column of  $k'$  values. Then from equation (21) Appendix II

$$\dot{\gamma}_{\theta_2} / \dot{\epsilon}_{22} = k' \lambda' = k' \lambda (1 + e_{22})^{1/2}$$

so that

$$k' = \frac{\dot{\gamma}_{\theta_2} / \dot{\epsilon}_{22}}{\lambda (1 + e_{22})^{1/2}} = \frac{k}{(1 + e_{22})^{1/2}} \quad (4.20)$$

which means that  $k$  varies by  $\frac{1}{2}\%$  for each 1% of nominal longitudinal strain. Since  $e_{22}$  was never greater than 3% in the combined tests then this variation is seen not to be an important effect here. The variation in  $k$  is attributed to the difficulties of accurately measuring strain

rates with the three point formula of equation (3.18). The same order of variation was apparent when the strain rate computation was based on the five and seven point formulae of equation (3.18). The  $k$  values in creep are more clearly seen in Fig. 4.12 where the shear creep strain ( $\delta_{\theta z}$ ) and the longitudinal creep strain ( $\epsilon_{zz}$ ) of Programme 4.2 are plotted for the times indicated. For each of the chosen stress ratios ( $\lambda$ ) Fig. 4.12 shows that  $\delta_{\theta z}$  plots linearly with  $\epsilon_{zz}$  throughout the time of creep. The slope of each plot has then been used to calculate the  $k$  values in the table of Fig. 4.12. Since these compare with the  $k$  values of Fig. 4.4 this implies that the plastic strain increments ratio ( $d\delta_{\theta z}^p/d\epsilon_{zz}^p$ ) of loading remains fixed in direction, but grows in magnitude, throughout creep. This, of course, is consistent with the observations made on the short-time creep strain in paragraph 4.3.2. Equation (4.12) therefore applies to both short and long-time creep strains for constant stress ratio tests on this material.

Combining equations (4.12) and (4.19) we have, for the first 100 hours of primary creep,

$$\frac{\dot{\delta}_{\theta z}}{\dot{\epsilon}_{zz}} = 2.6 \frac{\tau_{\theta z}}{\sigma_{zz}} = \frac{b'}{a'} \quad (4.21)$$

The sudden change in the  $k$  value for the  $\lambda = 1.81$  test at 25 hours (Fig. 4.12) was identified with the onset of buckling in this specimen (see Fig. 4.13). Since the corresponding shear strain was 4.5% then Finnie's prediction of a 10% creep buckling strain (equation 2.2) is rather conservative here. Over the whole of the 150 hour creep period, however, no other specimens were observed to buckle and for the pure torsion test ( $\lambda = \infty$ ) a shear strain of 5.3% was achieved.

The  $k$  values of the  $\lambda = 0.122$  test in Programme 4.2 are incorrect since this was not the stress ratio at the start of creep. A value of 0.27 was calculated from the strain increment vector of Fig. 4.4 ( $d\delta_{\theta z}^p/d\epsilon_{zz}^p = 0.7$ ) as being a more realistic figure. The  $k$  value based on this  $\lambda$  value is seen to be consistent with the other tests in the table of Fig. 4.12.

It is probable that equation (4.21) would have also applied to secondary creep had the test been conducted for longer times. Indeed the work on extruded material in the following chapter shows a linear  $\delta_{\theta z} \propto \epsilon_{zz}$  plot for up to 500 hours of creep. The slope of such a plot is thus only likely to change its direction in annealed material if instability sets in.

A Marin-Soderberg (6) isotropic prediction on the absolute magnitudes of the creep rate components may be obtained from equation (3.19) with  $\dot{\lambda}$  written as  $3\dot{\bar{\epsilon}}/2\bar{\sigma}$  (equation (32) Appendix I). For all creep times a  $\dot{\bar{\epsilon}}, \bar{\sigma}$  correlation of the form  $\dot{\bar{\epsilon}} = A\bar{\sigma}^n$  is assumed so that,

$$\begin{aligned}\dot{\epsilon}_{zz} &= \frac{\dot{\bar{\epsilon}}}{\bar{\sigma}} \tau_{zz} \phi(t) = A\bar{\sigma}^{n-1} \tau_{zz} \phi(t) \\ \dot{\delta}_{\theta z} &= \frac{3\dot{\bar{\epsilon}}}{\bar{\sigma}} \tau_{\theta z} \phi(t) = 3A\bar{\sigma}^{n-1} \tau_{\theta z} \phi(t)\end{aligned}\quad (4.22)$$

where  $\phi(t) = t^{-0.79}$  for primary creep (Fig. 4.11) and  $\phi(t) = 1$  for secondary creep. A and n are constants obtained from uniaxial creep tests.

It is obvious from a consideration of the  $\dot{\delta}_{\theta z}/\dot{\epsilon}_{zz}$  ratio of equation (4.22) that the isotropic prediction ( $\dot{\delta}_{\theta z}/\dot{\epsilon}_{zz} = 3\tau_{\theta z}/\tau_{zz}$ ) would not be in agreement with experimental observation (equation (4.21)).

#### 4.4 THEORETICAL PREDICTION OF ANISOTROPY

The plastic flow and creep produced by radial loading on annealed aluminium may be described by Hill's theory (see paragraph 3.1.3). Comparing equations (3.22) and (3.24) with equations (4.6) and (4.7) respectively we have for plastic flow,

$$\begin{aligned}\frac{d\epsilon_{\theta\theta}^p}{d\epsilon_{zz}^p} &= \frac{-F}{(F+H)} = -\frac{1}{2} \\ \frac{d\delta_{\theta z}^p}{d\epsilon_{zz}^p} &= \frac{6L}{(F+H)} \frac{\tau_{\theta z}}{\tau_{zz}} = 2.6 \frac{\tau_{\theta z}}{\tau_{zz}}\end{aligned}\quad (4.23)$$

The constants are independent of stress ratio. Thus if  $F = H = 1$  then  $L = 5.2/6.0$ . Furthermore a comparison of equation (3.27) with equations (4.12) and (4.21) shows that the same constants apply to creep rates during both short and long-time creep deformation. Hill's theory is therefore suitable to describe an initial anisotropy which is preserved throughout subsequent deformation. The anisotropy is not severe since for an isotropic von Mises material  $F = H = L = 1$ .

#### 4.5 RECOVERY

Unloading from the test stresses, following 100 hours of creep, recovered strain components that were mostly elastic in nature. An extremely small time dependent recovered strain (anelastic strain) was evident in each specimen at lower stresses but this was only a small fraction of the overall recovered strain. The same observation was made for the uniaxial tests in Appendix III. The nature of the instantaneous 'delayed elastic strain' is discussed in Chapter 7 (Section 7.3).

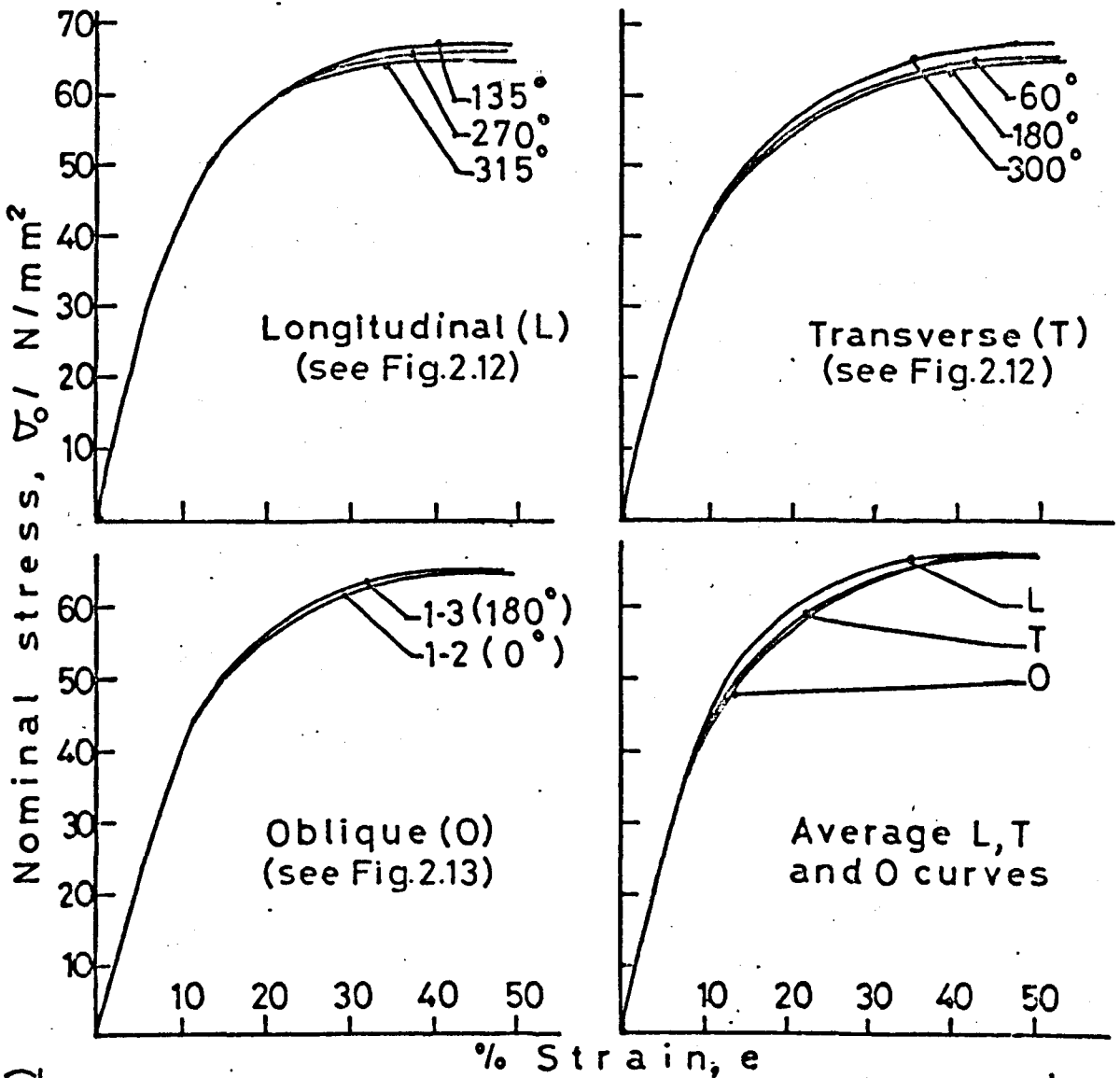


Fig.4.1 Tensile strength variation in annealed mat<sup>1</sup>

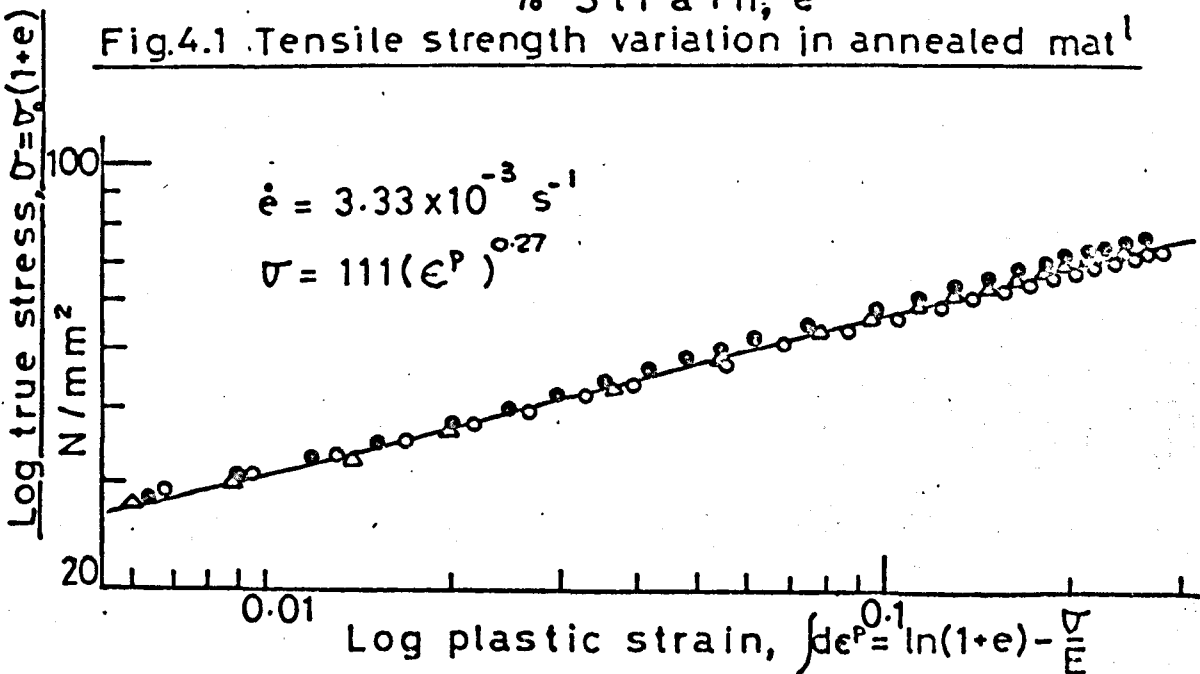


Fig.4.2 True stress-plastic strain logarithmic plot

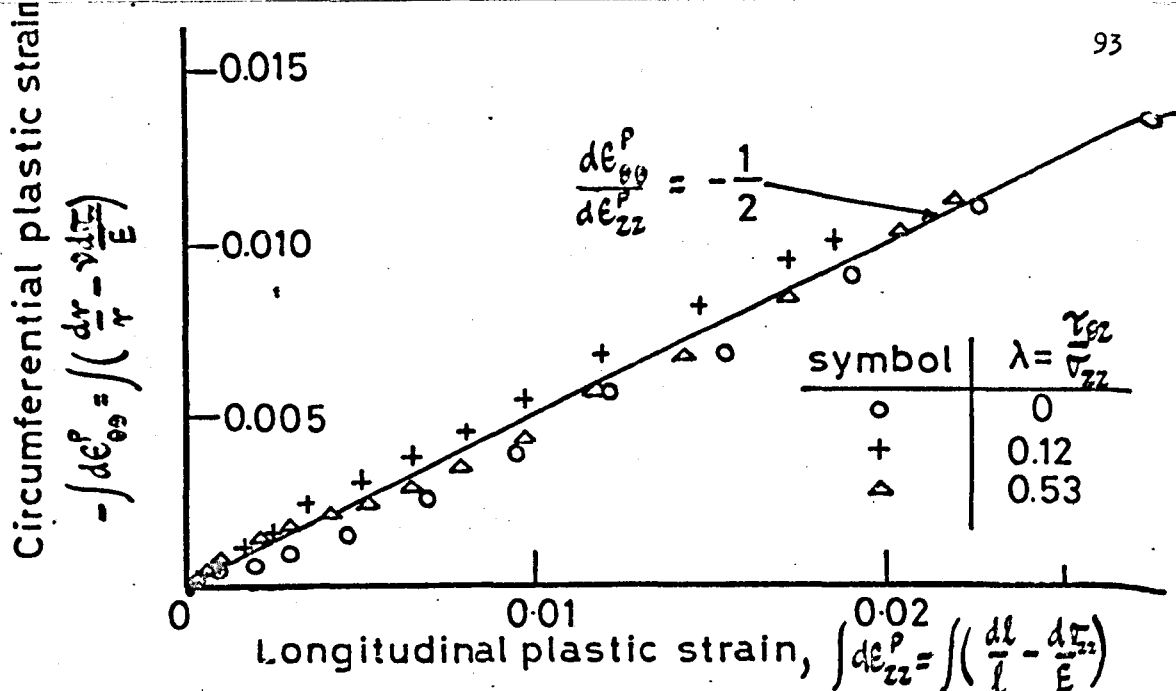


Fig.4.3  $\epsilon_{\theta\theta}^P \nu \epsilon_{zz}^P$  for radial loading ( $\lambda = \text{constant}$ )

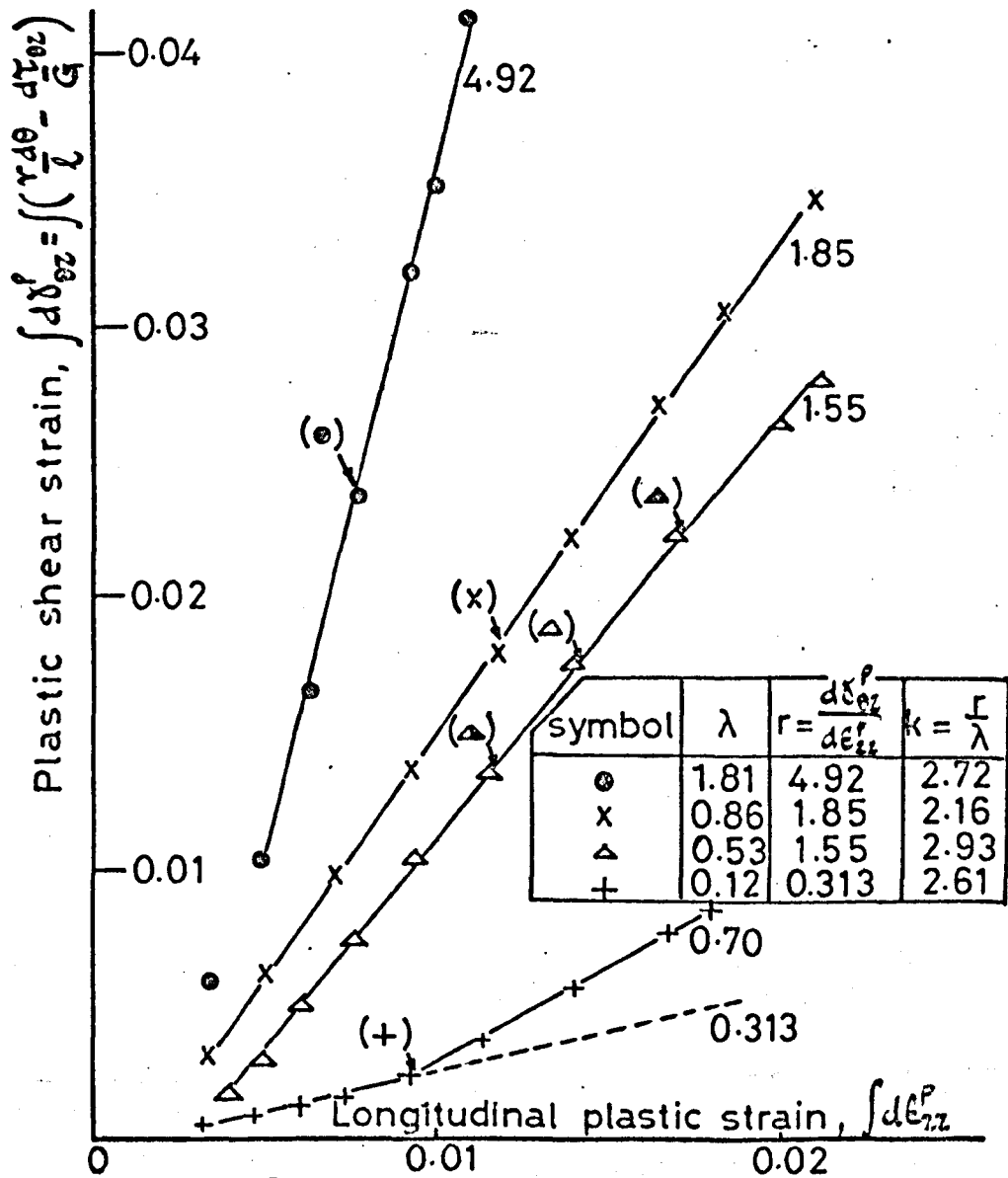


Fig.4.4  $\delta_{\theta z}^P \nu \epsilon_{zz}^P$  for radial loading ( $\lambda = \text{constant}$ )

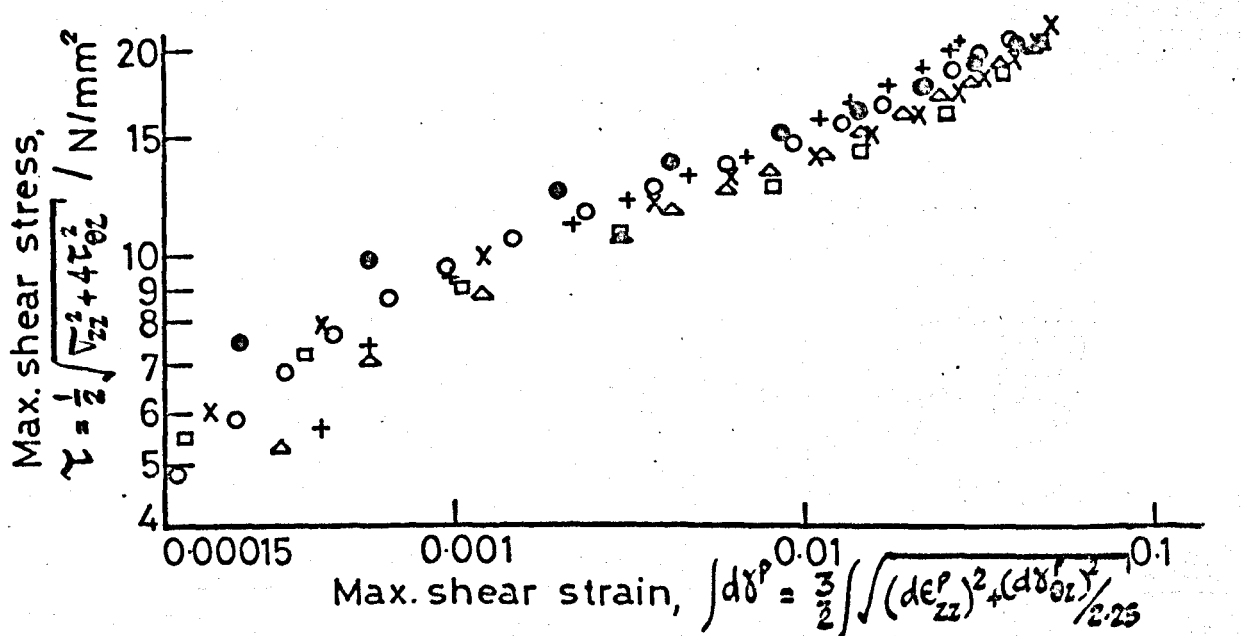
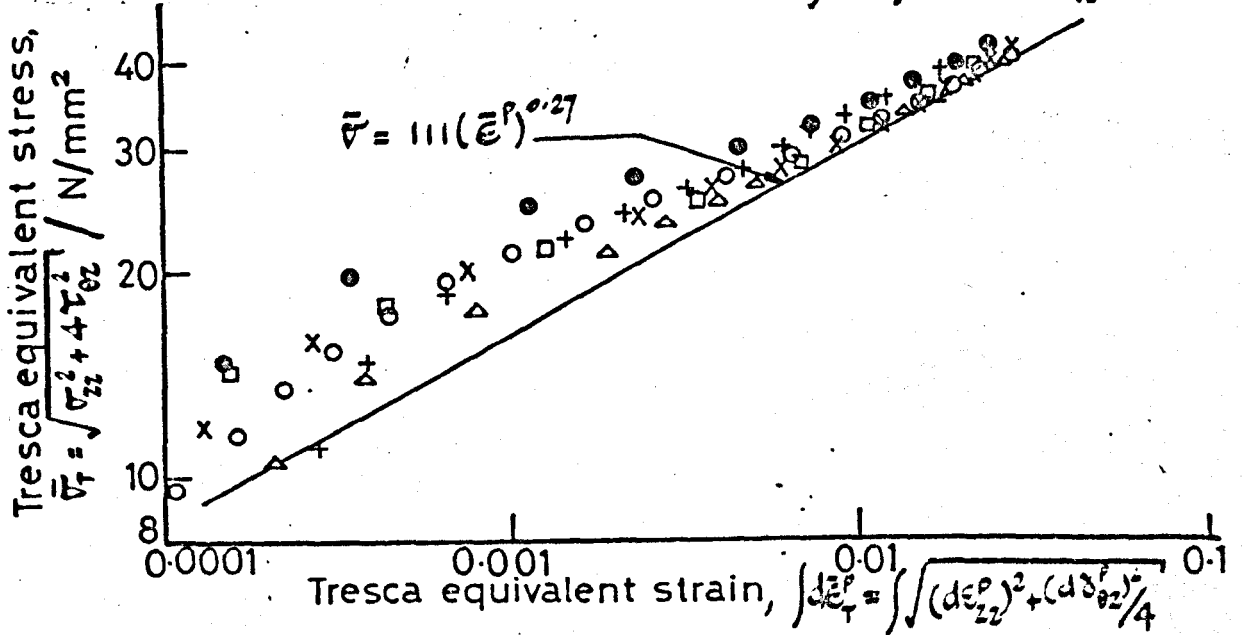
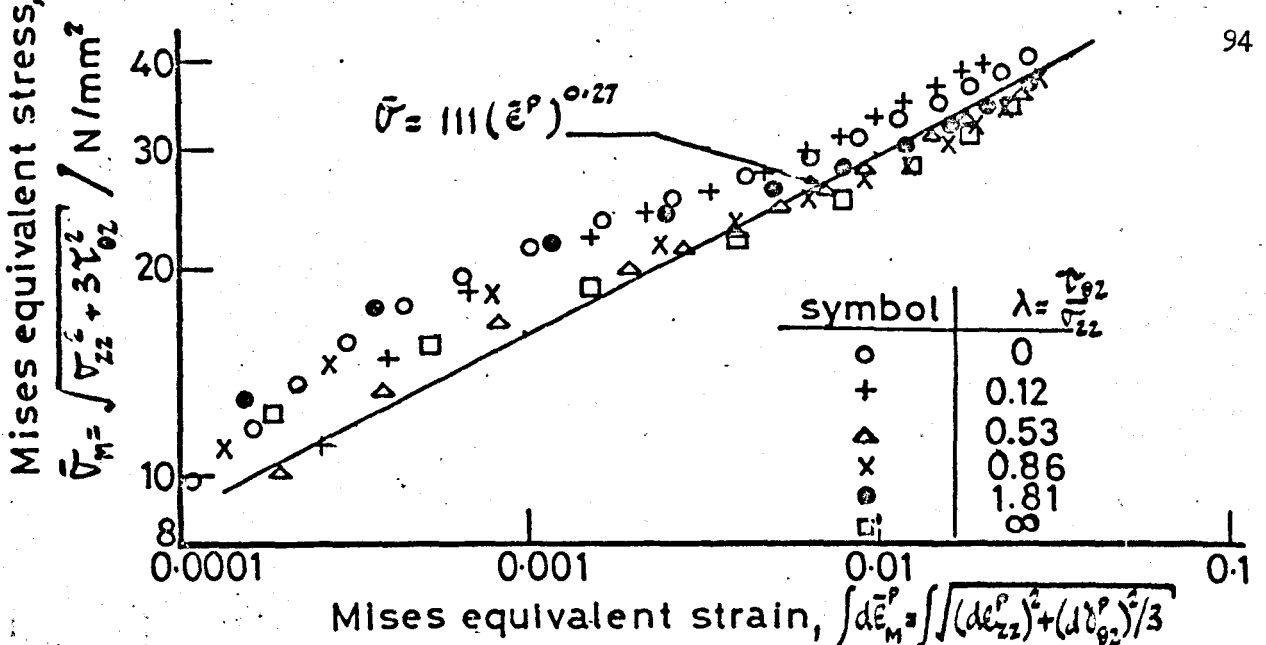


Fig.4.5 Stress-plastic strain correlations for all tests

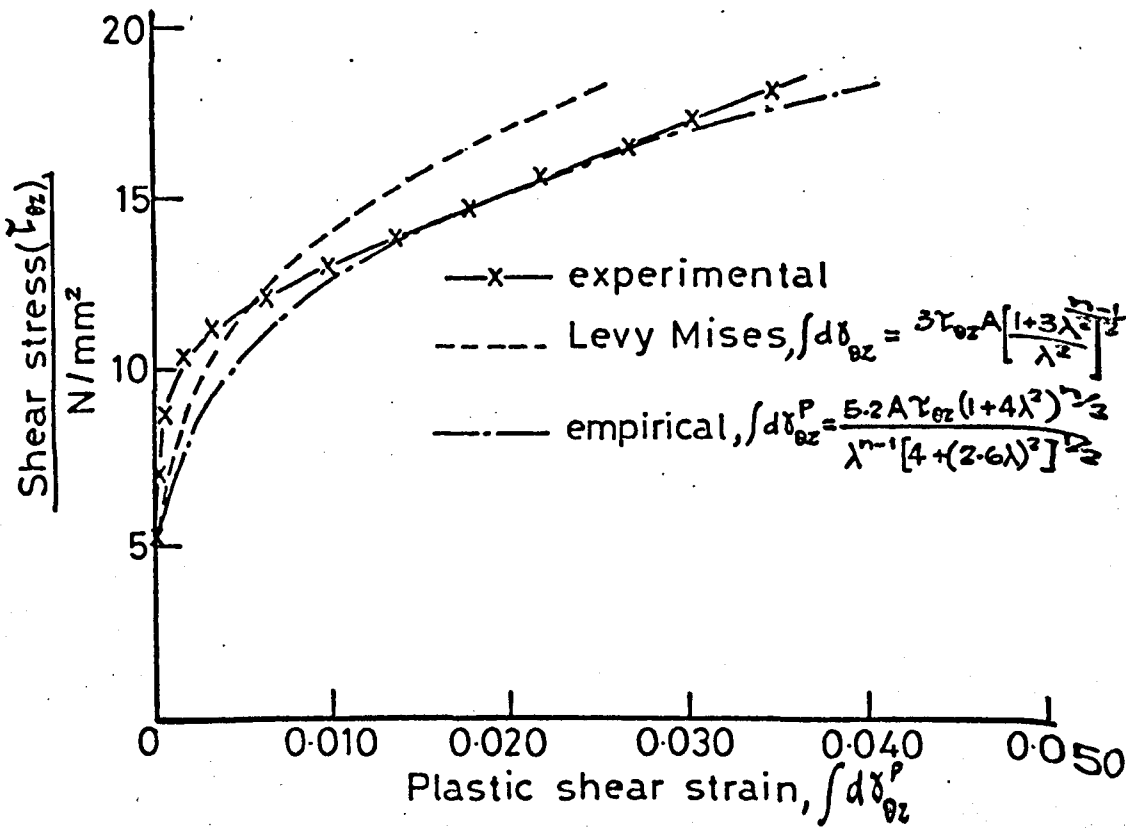
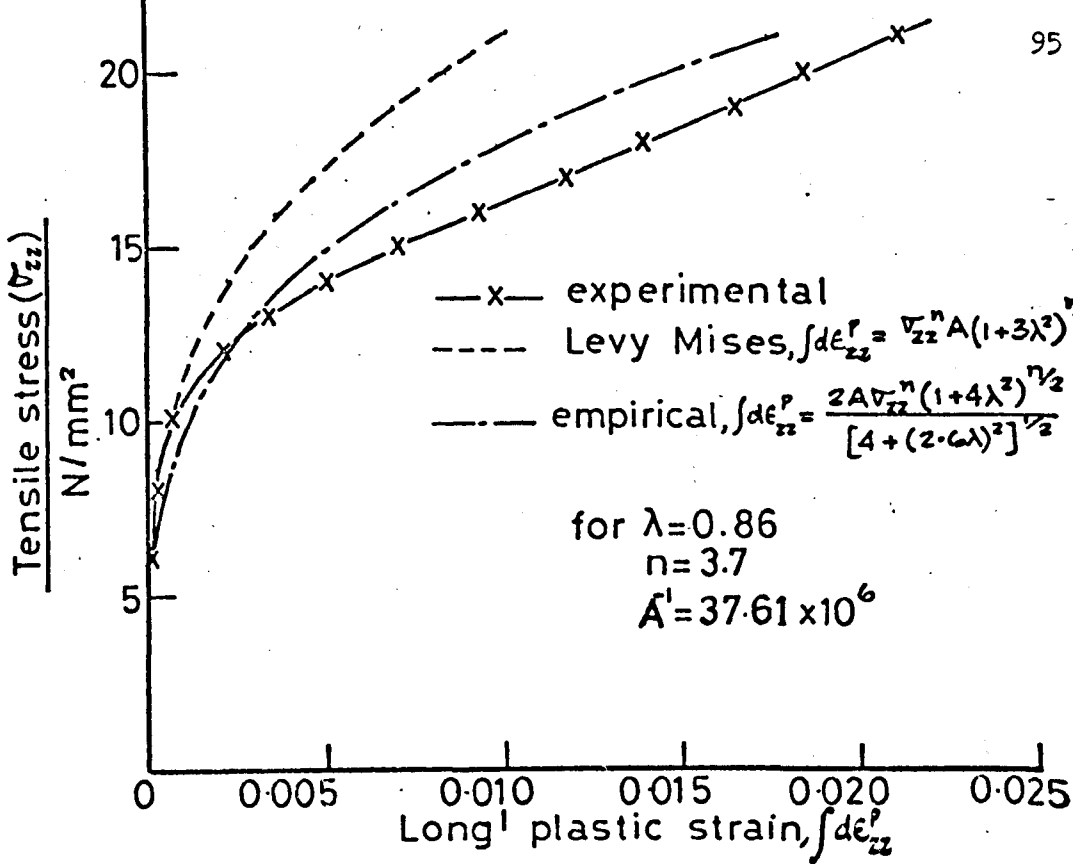


Fig.4.6 Stress-plastic strain predictions for  $\lambda=0.86$

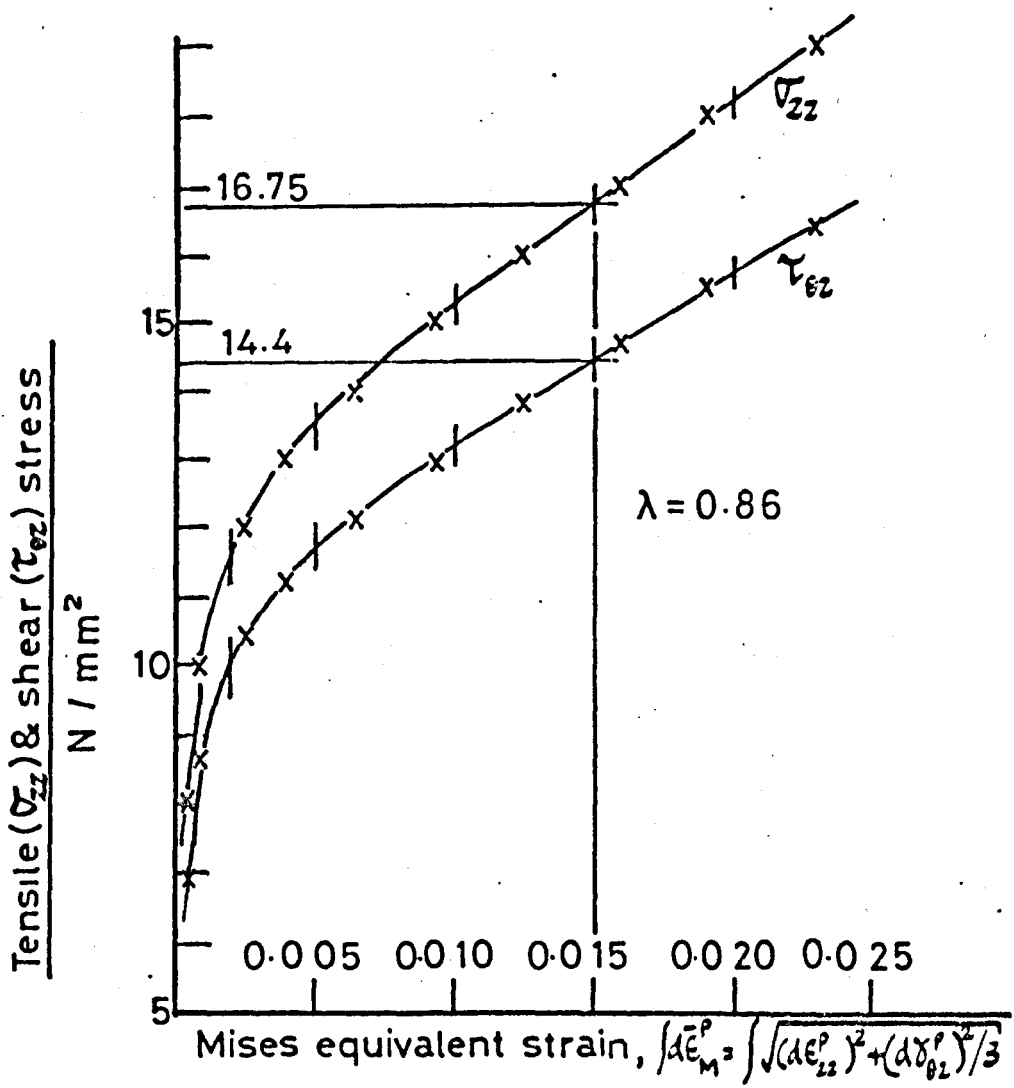
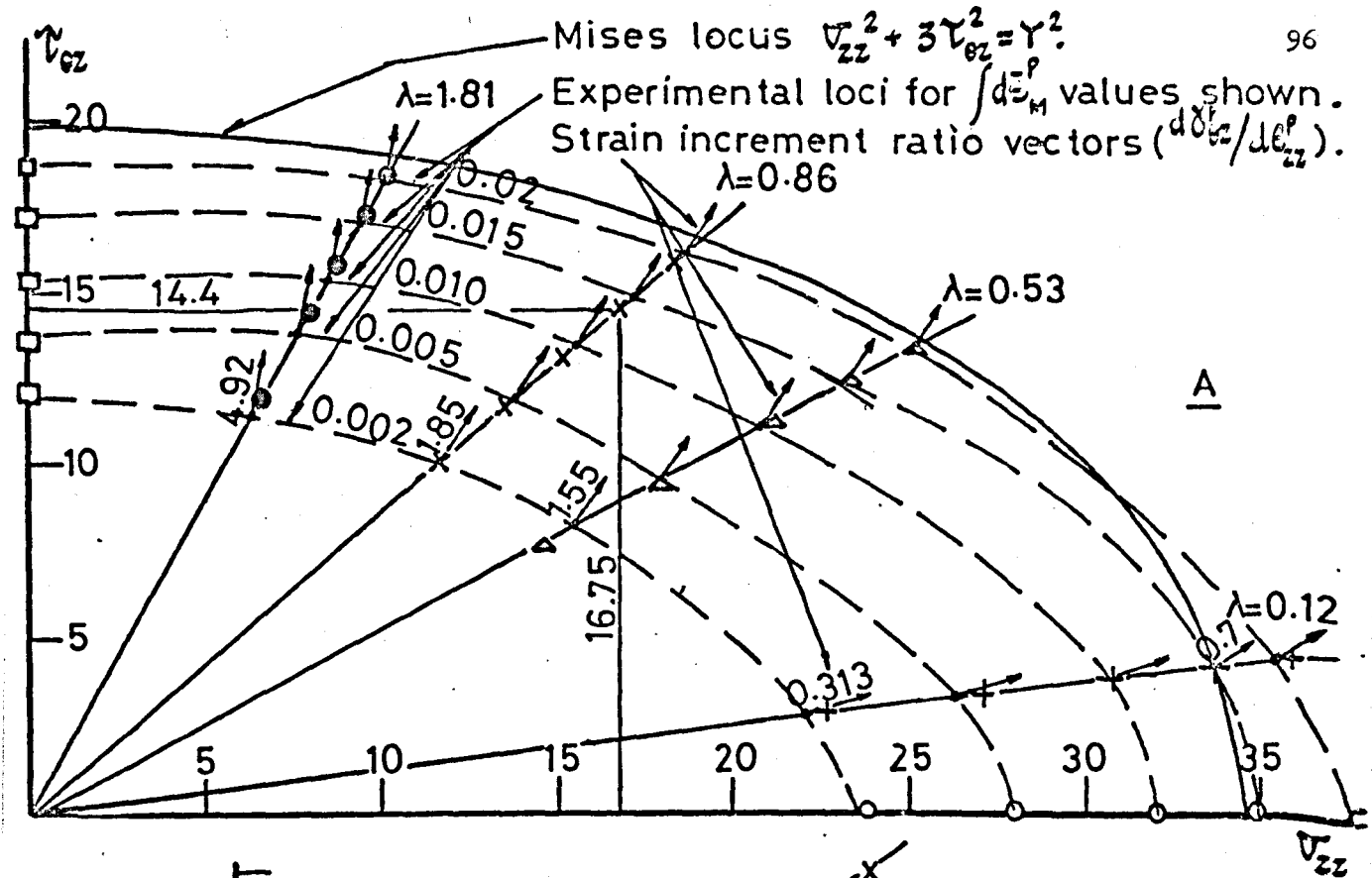


Fig.4.7 Yield loci for Mises equivalent proof strains

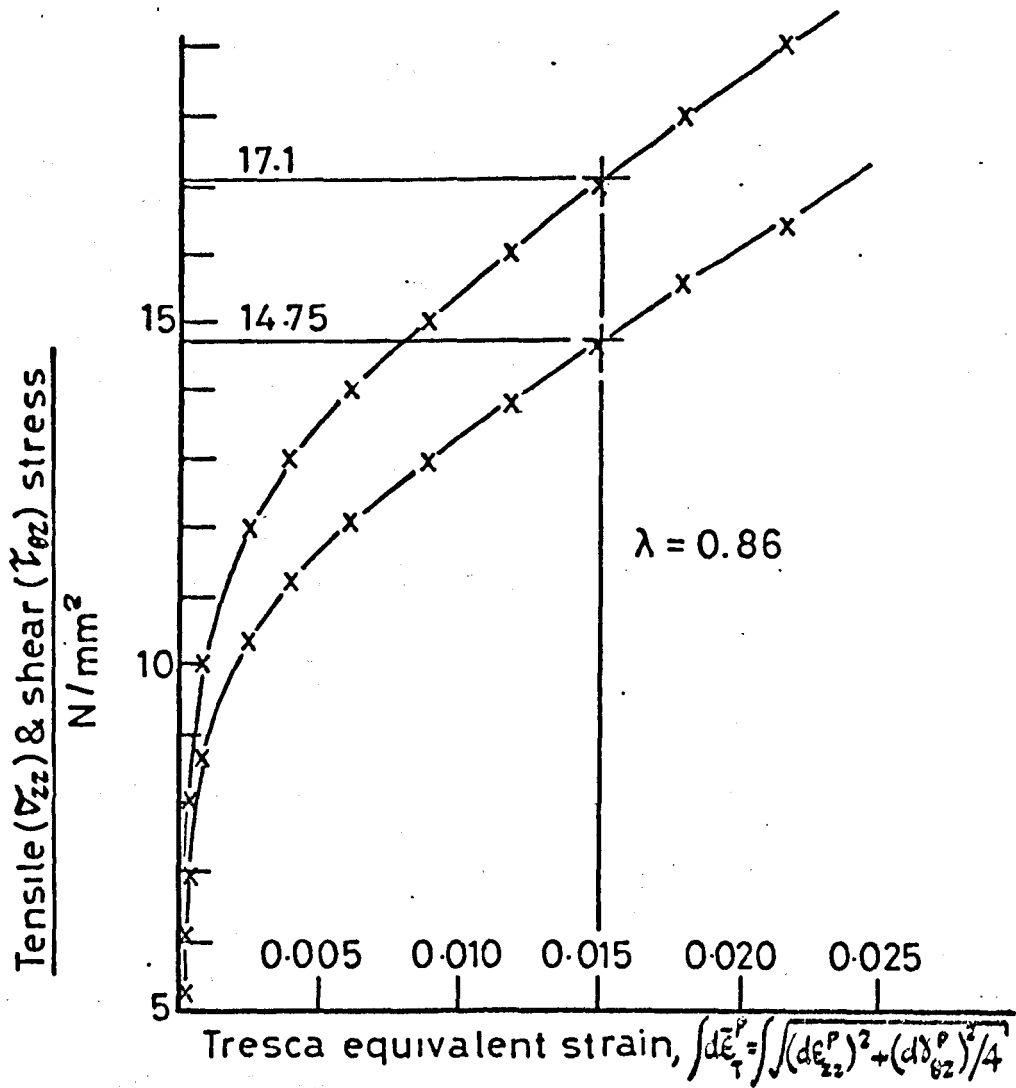
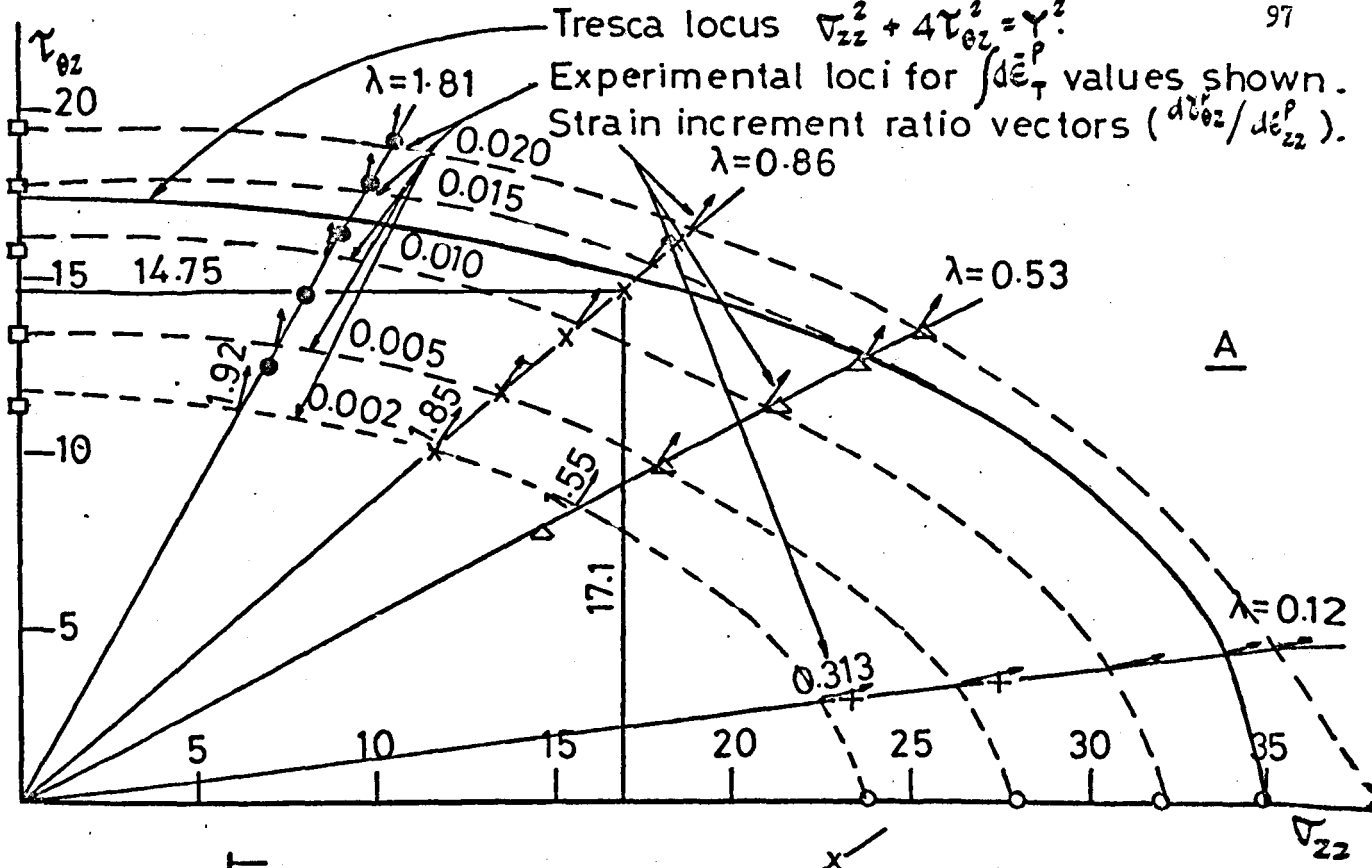


Fig. 4.8 Yield loci for Tresca equivalent proof strains

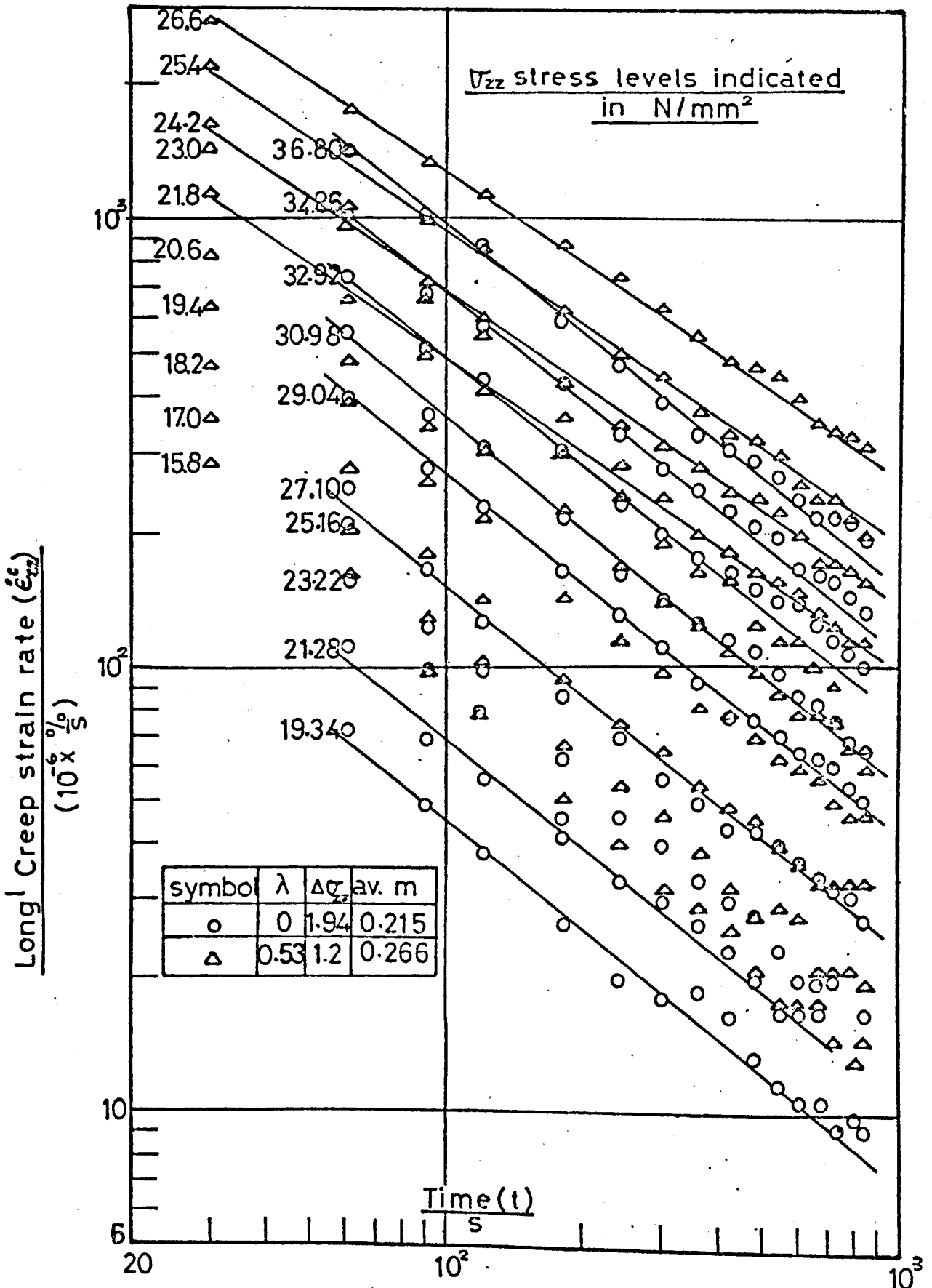


Fig.4.9 Transient  $\epsilon_{zz}$  creep derivative plot for  $\lambda=0$  &  $0.53$

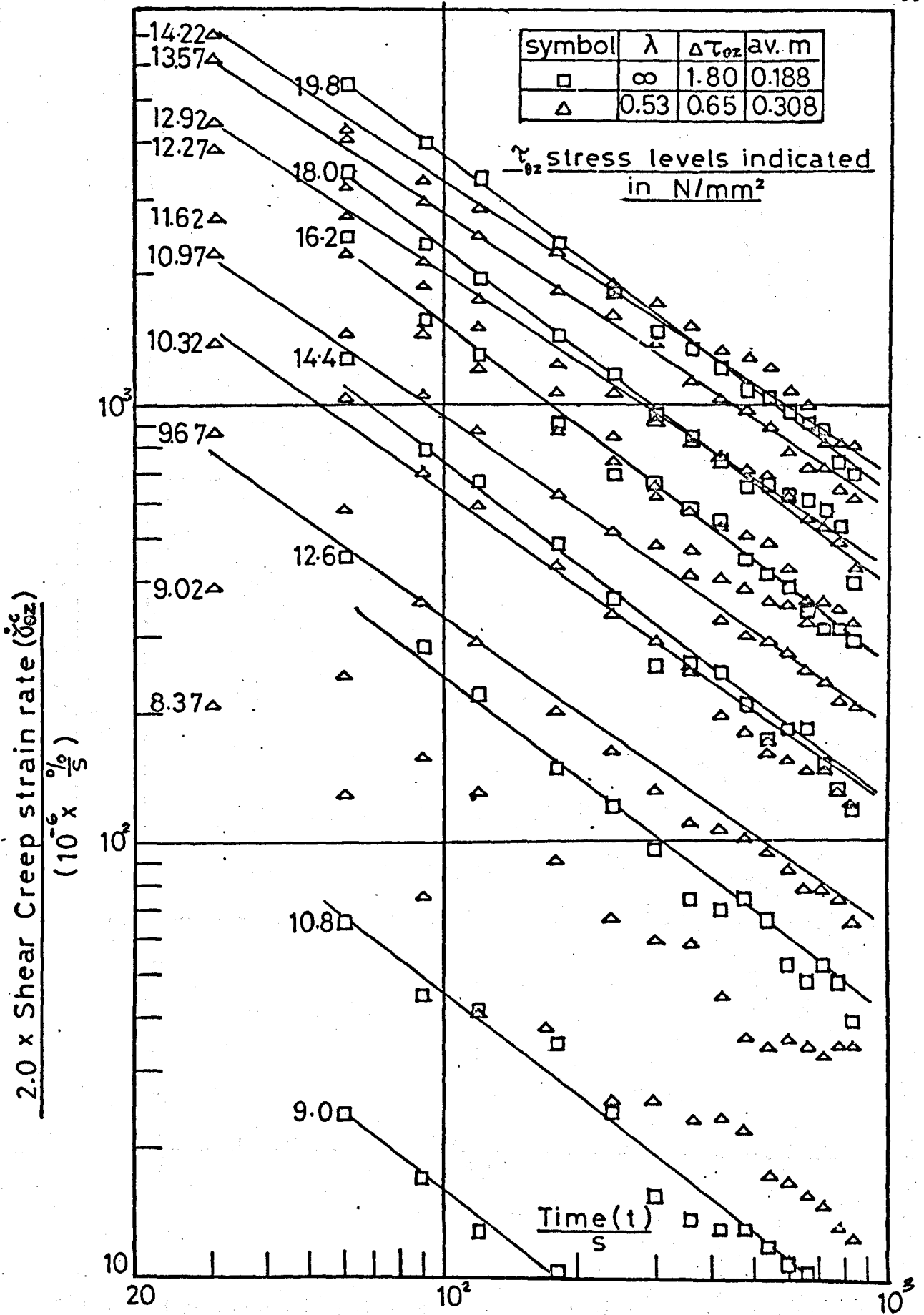


Fig.4.10 Transient  $\gamma_{0z}$  creep derivative plot for  $\lambda = \infty$  & 0.53

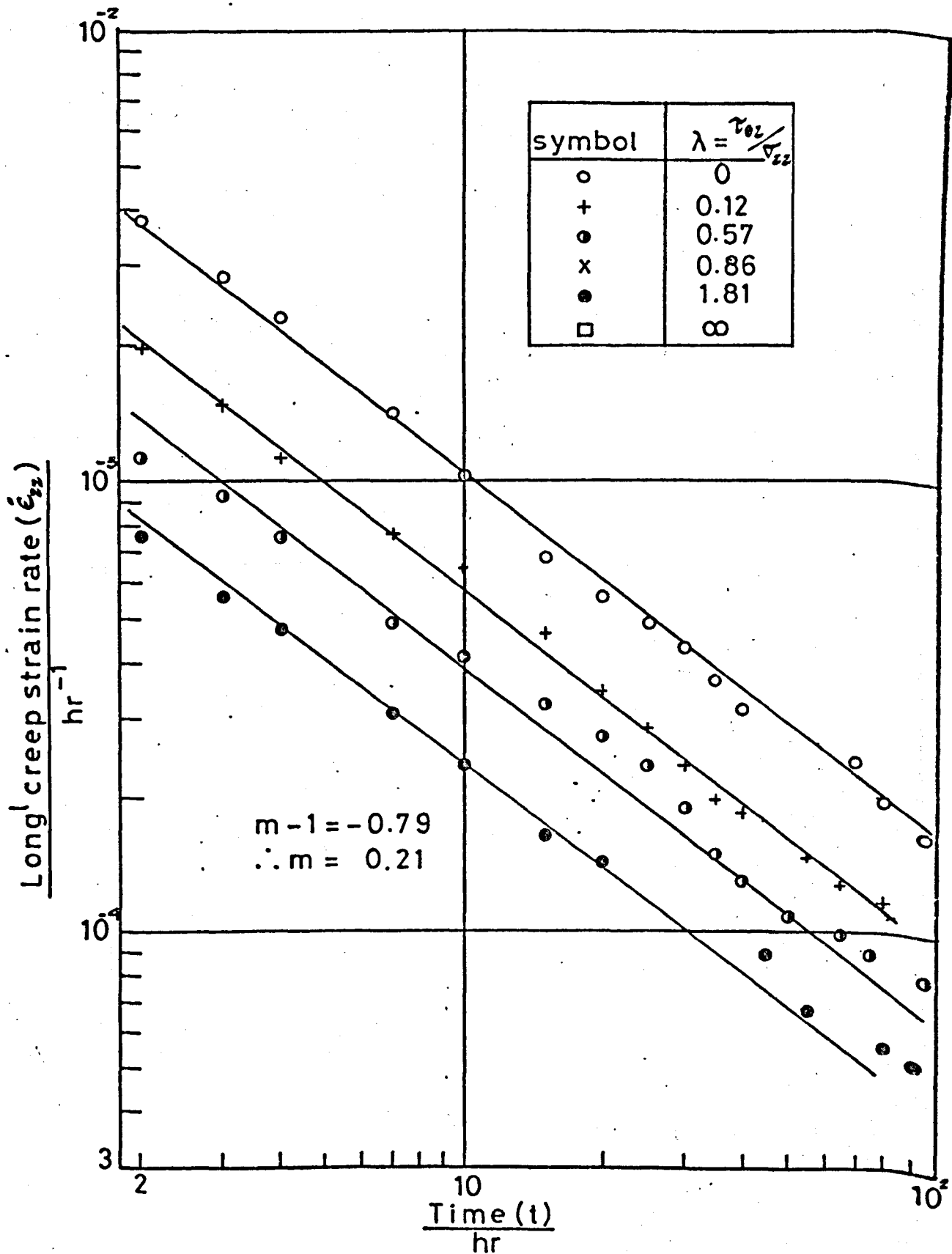


Fig. 4.11A Primary  $\epsilon_{zz}$  creep derivative plot for all stress ratios

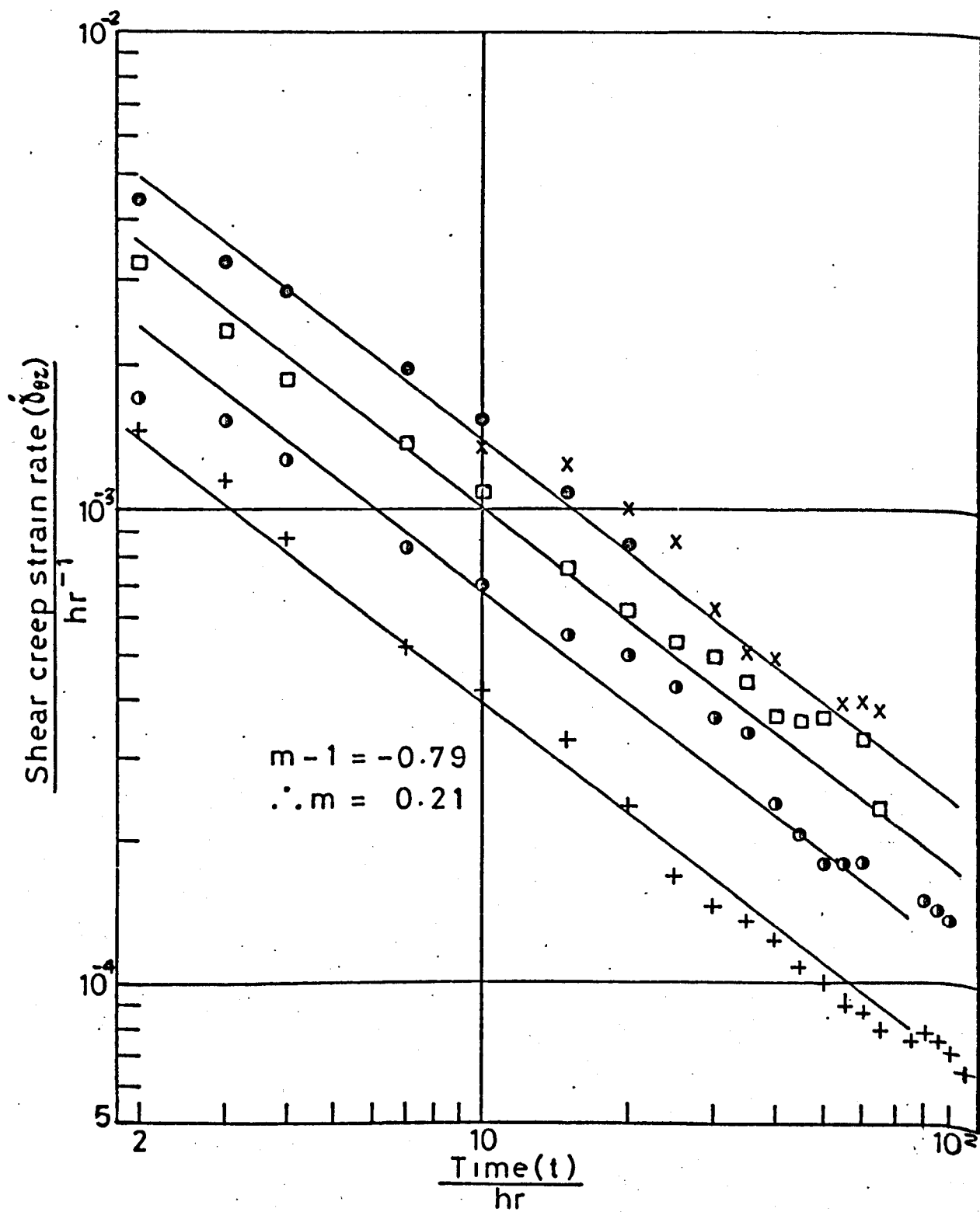


Fig.4.11B Primary  $\dot{\gamma}_{\theta z}$  creep derivative plot for all stress ratios

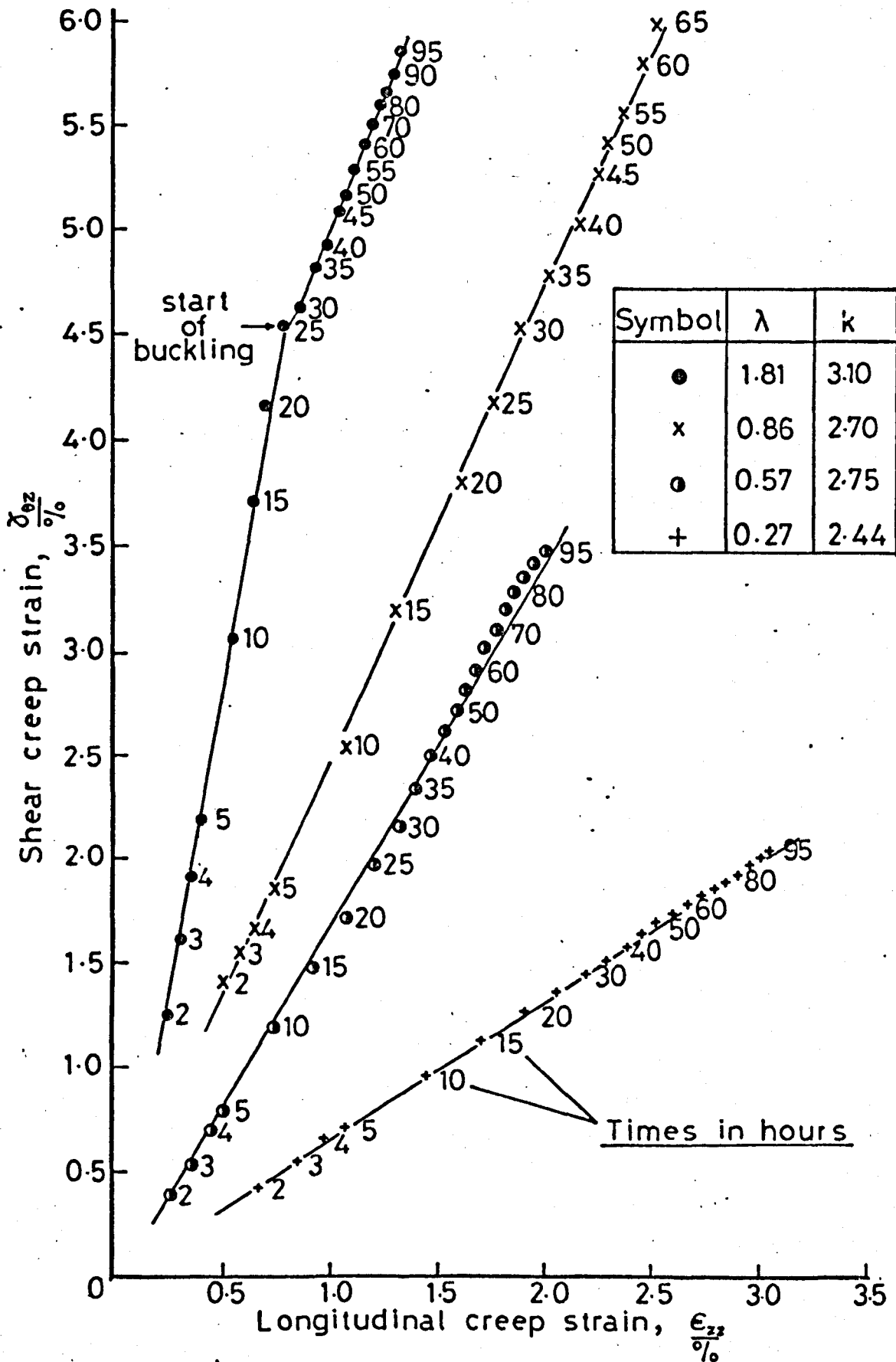


Fig.4.12  $\delta_{ez} v \epsilon_{zz}$  creep for constant  $\lambda$  tests



Fig. 4.13 Constant  $\lambda$  tubular specimens

\*\* KINGSTON POLYTECHNIC 4120 \*\*

&JOB; MAPE/R008/DR; LOADING STRAINS;

&OPTIONS;MOTHY;

&FORTRAN; D;

```

0* C
1* C
2*   DIMENSION DELS(50),DELT(50),DELC(50)

3*   READ(3,50) GL
4*   READ(3,50) RADM
5*   READ(3,50) RADN
6*   READ(3,50) E
7*   READ(3,50) G
8*   READ(3,51) M
9*   K=0
10*  1 READ(3,50) CON
11*  READ(3,50) XLAM
12*  READ(3,51) N
13*  WRITE(2,100) XLAM
14*  SZZ=0.0
15*  SSZ=0.0
16*  DESZT=0.0
17*  DEZZT=0.0
18*  DEBPM=0.0
19*  DEBPT=0.0
20*  READ(3,52) (DELC(I),DELT(I),DELS(I), I=1,N)
21*  DO 2 I=1,N
22*  IF(XLAM.NE.9.0) GO TO 4
23*  DELSZ=CON*DELC(I)
24*  DELTZ=0.0
25*  GO TO 3
26*  4 DELTZ=CON*DELC(I)
27*  DELSZ=XLAM*DELTZ
28*  3 DEZZ=DELT(I)/GL
29*  DEZZP=DEZZ-DELTZ/E
30*  THETA=DELS(I)*1.116*22.0/1260.0
31*  GAMMA=(RADN*THETA)/GL
32*  DESZP=(GAMMA-DELSZ/G)/2.0
33*  DEBPV=SQRT((DEZZP*DEZZP)+(4.0*DESZP*DESZP)/3.0)
34*  DEBPR=SQRT((DEZZP*DEZZP)+(DESZP*DESZP))
35*  SZZ=SZZ+DELTZ
36*  SSZ=SSZ+DELSZ
37*  SIGBM=SQRT((SZZ*SZZ)+(3.0*SSZ*SSZ))
38*  SIGBT=SQRT((SZZ*SZZ)+(4.0*SSZ*SSZ))
39*  DEZZT=DEZZT+DEZZP
40*  DESZT=DESZT+(2.0*DESZP)
41*  DEBPM=DEBPM+DEBPV
42*  DEBPT=DEBPT+DEBPR
43*  WRITE(2,101) SZZ,SSZ,DEZZT,DESZT,SIGBM,DEBPM,SIGBT,DEBPT
44*  STOP
45*
46*  50 FORMAT(6X,F0.0)
47*  51 FORMAT(10)
48*  52 FORMAT(2X,F0.0,F0.0,F0.0)
49*  100 FORMAT(1H1,25X,37HMISES AND TRESCA STRESS - STRAINS FOR,
50*  122H RADIAL LOADING      = ,F5.3///)
51*  101 FORMAT(5X,8E13.5)
52*
53*  END
54*

```

MISES AND TRESCA STRESS - STRAINS FOR RADIAL LOADING  $\lambda = 0.000$

$\sigma_{zz}$	$\tau_{\theta z}$	$\int d\epsilon_{zz}^p$	$\int d\gamma_{\theta z}^p$	$\bar{\sigma}_m$	$\int d\epsilon_m^p$	$\bar{\sigma}_T$	$\int d\epsilon_T^p$
0.19375E+01	0.00000E+00	-0.15967E-04	0.00000E+00	0.19375E+01	0.15967E-04	0.19375E+01	0.15967E-04
0.38750E+01	0.00000E+00	-0.37350E-05	0.00000E+00	0.38750E+01	0.28200E-04	0.38750E+01	0.28200E-04
0.58125E+01	0.00000E+00	0.11698E-04	0.00000E+00	0.58125E+01	0.43633E-04	0.58125E+01	0.43633E-04
0.77500E+01	0.00000E+00	0.39930E-04	0.00000E+00	0.77500E+01	0.71865E-04	0.77500E+01	0.71865E-04
0.96875E+01	0.00000E+00	0.77763E-04	0.00000E+00	0.96875E+01	0.10970E-03	0.96875E+01	0.10970E-03
0.11625E+02	0.00000E+00	0.13120E-03	0.00000E+00	0.11625E+02	0.16313E-03	0.11625E+02	0.16313E-03
0.13562E+02	0.00000E+00	0.18923E-03	0.00000E+00	0.13562E+02	0.22116E-03	0.13562E+02	0.22116E-03
0.15500E+02	0.00000E+00	0.28146E-03	0.00000E+00	0.15500E+02	0.31340E-03	0.15500E+02	0.31340E-03
0.17437E+02	0.00000E+00	0.41669E-03	0.00000E+00	0.17437E+02	0.44863E-03	0.17437E+02	0.44863E-03
0.19375E+02	0.00000E+00	0.62573E-03	0.00000E+00	0.19375E+02	0.65766E-03	0.19375E+02	0.65766E-03
0.21312E+02	0.00000E+00	0.98736E-03	0.00000E+00	0.21312E+02	0.10193E-02	0.21312E+02	0.10193E-02
0.23250E+02	0.00000E+00	0.16010E-02	0.00000E+00	0.23250E+02	0.16329E-02	0.23250E+02	0.16329E-02
0.25187E+02	0.00000E+00	0.25826E-02	0.00000E+00	0.25187E+02	0.26146E-02	0.25187E+02	0.26146E-02
0.27125E+02	0.00000E+00	0.41743E-02	0.00000E+00	0.27125E+02	0.42062E-02	0.27125E+02	0.42062E-02
0.29062E+02	0.00000E+00	0.64419E-02	0.00000E+00	0.29062E+02	0.64738E-02	0.29062E+02	0.64738E-02
0.31000E+02	0.00000E+00	0.89255E-02	0.00000E+00	0.31000E+02	0.89575E-02	0.31000E+02	0.89575E-02
0.32937E+02	0.00000E+00	0.11607E-01	0.00000E+00	0.32937E+02	0.11639E-01	0.32937E+02	0.11639E-01
0.34875E+02	0.00000E+00	0.14915E-01	0.00000E+00	0.34875E+02	0.14947E-01	0.34875E+02	0.14947E-01
0.36812E+02	0.00000E+00	0.18466E-01	0.00000E+00	0.36812E+02	0.18498E-01	0.36812E+02	0.18498E-01
0.38750E+02	0.00000E+00	0.22098E-01	0.00000E+00	0.38750E+02	0.22130E-01	0.38750E+02	0.22130E-01
0.40687E+02	0.00000E+00	0.26670E-01	0.00000E+00	0.40687E+02	0.26702E-01	0.40687E+02	0.26702E-01

MISES AND TRESCA STRESS - STRAINS FOR RADIAL LOADING  $\lambda = 0.122$

$\sigma_{zz}$	$\tau_{\theta z}$	$\int d\epsilon_{zz}^p$	$\int d\gamma_{\theta z}^p$	$\bar{\sigma}_m$	$\int d\epsilon_m^p$	$\bar{\sigma}_T$	$\int d\epsilon_T^p$
0.36150E+01	0.44103E+00	0.13707E+03	0.14318E-05	0.36948E+01	0.13707E-03	0.37211E+01	0.13707E-03
0.72300E+01	0.88206E+00	0.19414E-03	0.12089E-04	0.73897E+01	0.19448E-03	0.74421E+01	0.19439E-03
0.10845E+02	0.13231E+01	0.27822E-03	0.24057E-04	0.11084E+02	0.27883E-03	0.11163E+02	0.27868E-03
0.14460E+02	0.17641E+01	0.39529E-03	0.38593E-04	0.14779E+02	0.39620E-03	0.14884E+02	0.39598E-03
0.18075E+02	0.22052E+01	0.65836E-03	0.72156E-04	0.18474E+02	0.65999E-03	0.18605E+02	0.65958E-03
0.21690E+02	0.26462E+01	0.14754E-02	0.21118E-03	0.22169E+02	0.14810E-02	0.22326E+02	0.14796E-02
0.23498E+02	0.28667E+01	0.20930E-02	0.32787E-03	0.24016E+02	0.21022E-02	0.24187E+02	0.20999E-02
0.25305E+02	0.30872E+01	0.31785E-02	0.54153E-03	0.25864E+02	0.31947E-02	0.26047E+02	0.31907E-02
0.27113E+02	0.33077E+01	0.45880E-02	0.77615E-03	0.27711E+02	0.46107E-02	0.27908E+02	0.46051E-02
0.28920E+02	0.35282E+01	0.60736E-02	0.10501E-02	0.29559E+02	0.61047E-02	0.29768E+02	0.60969E-02
0.30728E+02	0.37488E+01	0.75591E-02	0.14661E-02	0.31406E+02	0.76095E-02	0.31629E+02	0.75969E-02
0.32535E+02	0.39693E+01	0.91606E-02	0.24770E-02	0.33253E+02	0.93141E-02	0.33490E+02	0.92763E-02
0.34343E+02	0.41898E+01	0.11404E-01	0.37102E-02	0.35101E+02	0.11668E-01	0.35350E+02	0.11603E-01
0.36150E+02	0.44103E+01	0.13992E-01	0.56824E-02	0.36948E+02	0.14495E-01	0.37211E+02	0.14372E-01
0.37958E+02	0.46308E+01	0.16681E-01	0.76625E-02	0.38796E+02	0.17417E-01	0.39071E+02	0.17238E-01
0.38861E+02	0.47411E+01	0.17936E-01	0.85338E-02	0.39719E+02	0.18769E-01	0.40001E+02	0.18565E-01

MISES AND TRESCA STRESS - STRAINS FOR RADIAL LOADING  $\lambda = 0.532$

$\sigma_{zz}$	$\tau_{\theta z}$	$\int d\epsilon_{zz}^p$	$\int d\alpha_{\theta z}^p$	$\bar{\sigma}_M$	$\int d\bar{\epsilon}_M^p$	$\bar{\sigma}_T$	$\int d\bar{\epsilon}_T^p$
0.24300E+01	0.12928E+01	0.56422E-04	-0.13702E-05	0.33043E+01	0.56427E-04	0.35482E+01	0.56426E-04
0.48600E+01	0.25855E+01	0.10284E-03	0.11517E-04	0.66087E+01	0.10344E-03	0.70964E+01	0.10329E-03
0.72900E+01	0.38783E+01	0.21327E-03	0.29646E-04	0.99130E+01	0.21436E-03	0.10645E+02	0.21409E-03
0.97200E+01	0.51710E+01	0.38769E-03	0.71729E-04	0.13217E+02	0.39046E-03	0.14193E+02	0.38977E-03
0.12150E+02	0.64638E+01	0.82011E-03	0.19705E-03	0.16522E+02	0.82890E-03	0.17741E+02	0.82671E-03
0.14580E+02	0.77566E+01	0.19545E-02	0.54986E-03	0.19826E+02	0.19815E-02	0.21289E+02	0.19748E-02
0.15795E+02	0.84029E+01	0.27627E-02	0.91156E-03	0.21478E+02	0.28162E-02	0.23063E+02	0.28030E-02
0.17010E+02	0.90493E+01	0.38590E-02	0.15558E-02	0.23130E+02	0.39738E-02	0.24837E+02	0.39455E-02
0.18225E+02	0.96957E+01	0.49332E-02	0.28762E-02	0.24782E+02	0.52910E-02	0.26612E+02	0.52064E-02
0.19440E+02	0.10342E+02	0.62034E-02	0.49854E-02	0.26435E+02	0.70507E-02	0.28386E+02	0.68574E-02
0.20655E+02	0.10988E+02	0.75896E-02	0.74564E-02	0.28087E+02	0.90399E-02	0.30160E+02	0.87142E-02
0.21870E+02	0.11635E+02	0.93718E-02	0.10480E-01	0.29739E+02	0.11535E-01	0.31934E+02	0.11051E-01
0.23085E+02	0.12281E+02	0.11504E-01	0.13630E-01	0.31391E+02	0.14337E-01	0.33708E+02	0.13702E-01
0.24300E+02	0.12928E+02	0.14036E-01	0.17577E-01	0.33043E+02	0.17743E-01	0.35482E+02	0.16912E-01
0.25515E+02	0.13574E+02	0.16838E-01	0.22231E-01	0.34695E+02	0.21626E-01	0.37256E+02	0.20555E-01
0.26730E+02	0.14220E+02	0.19981E-01	0.26271E-01	0.36348E+02	0.25539E-01	0.39030E+02	0.24291E-01
0.27277E+02	0.14511E+02	0.21333E-01	0.27806E-01	0.37091E+02	0.27156E-01	0.39829E+02	0.25845E-01

MISES AND TRESCA STRESS - STRAINS FOR RADIAL LOADING  $\lambda = 0.863$

$\sigma_{zz}$	$\tau_{\theta z}$	$\int d\epsilon_{zz}^p$	$\int d\alpha_{\theta z}^p$	$\bar{\sigma}_M$	$\int d\bar{\epsilon}_M^p$	$\bar{\sigma}_T$	$\int d\bar{\epsilon}_T^p$
0.19950E+01	0.17217E+01	-0.92094E-05	0.32875E-05	0.35878E+01	0.94029E-05	0.39796E+01	0.93549E-05
0.39900E+01	0.34434E+01	0.15581E-04	0.12865E-04	0.71757E+01	0.34803E-04	0.79591E+01	0.34604E-04
0.59850E+01	0.51651E+01	0.11377E-03	0.46554E-04	0.10764E+02	0.13490E-03	0.11939E+02	0.13423E-03
0.79800E+01	0.68867E+01	0.24136E-03	0.14838E-03	0.14351E+02	0.27539E-03	0.15918E+02	0.27160E-03
0.99750E+01	0.86084E+01	0.69215E-03	0.50968E-03	0.17939E+02	0.77210E-03	0.19898E+02	0.75724E-03
0.11970E+02	0.10330E+02	0.21829E-02	0.16179E-02	0.21527E+02	0.23944E-02	0.23877E+02	0.23477E-02
0.12967E+02	0.11191E+02	0.34083E-02	0.30883E-02	0.23321E+02	0.38851E-02	0.25867E+02	0.37767E-02
0.13965E+02	0.12052E+02	0.50397E-02	0.61453E-02	0.25115E+02	0.62886E-02	0.27857E+02	0.60123E-02
0.14962E+02	0.12913E+02	0.70491E-02	0.98627E-02	0.26909E+02	0.92287E-02	0.29847E+02	0.87495E-02
0.15960E+02	0.13773E+02	0.93565E-02	0.13664E-01	0.28703E+02	0.12413E-01	0.31836E+02	0.11739E-01
0.16957E+02	0.14634E+02	0.11832E-01	0.17806E-01	0.30497E+02	0.15855E-01	0.33826E+02	0.14966E-01
0.17955E+02	0.15495E+02	0.13921E-01	0.21948E-01	0.32291E+02	0.19031E-01	0.35816E+02	0.17908E-01
0.18952E+02	0.16356E+02	0.16593E-01	0.26976E-01	0.34085E+02	0.22976E-01	0.37806E+02	0.21577E-01
0.19950E+02	0.17217E+02	0.18378E-01	0.30541E-01	0.35878E+02	0.25700E-01	0.39796E+02	0.24100E-01
0.20947E+02	0.18078E+02	0.21004E-01	0.34940E-01	0.37672E+02	0.29353E-01	0.41785E+02	0.27525E-01

MISES AND TRESCA STRESS - STRAINS FOR RADIAL LOADING  $\lambda = 1.807$

$\sigma_{zz}$	$\tau_{\theta z}$	$\int d\epsilon_{zz}^p$	$\int d\alpha_{\theta z}^p$	$\bar{\sigma}_M$	$\int d\epsilon_M^p$	$\bar{\sigma}_T$	$\int d\epsilon_T^p$
0.13210E+01	0.23870E+01	0.32659E-04	-0.95301E-05	0.43404E+01	0.33119E-04	0.49535E+01	0.33005E-04
0.26420E+01	0.47741E+01	0.63318E-04	-0.19030E-06	0.86808E+01	0.64249E-04	0.99070E+01	0.64017E-04
0.39630E+01	0.71611E+01	0.14698E-03	0.52655E-04	0.13021E+02	0.15330E-03	0.14860E+02	0.15175E-03
0.52840E+01	0.95482E+01	0.32284E-03	0.21086E-03	0.17362E+02	0.35146E-03	0.19814E+02	0.34458E-03
0.66050E+01	0.11935E+02	0.10135E-02	0.10452E-02	0.21702E+02	0.11935E-02	0.24767E+02	0.11515E-02
0.72655E+01	0.13129E+02	0.19458E-02	0.24531E-02	0.23872E+02	0.24304E-02	0.27244E+02	0.23197E-02
0.79260E+01	0.14322E+02	0.35362E-02	0.57322E-02	0.26042E+02	0.49030E-02	0.29721E+02	0.46038E-02
0.85865E+01	0.15516E+02	0.49565E-02	0.10343E-01	0.28213E+02	0.79201E-02	0.32198E+02	0.73115E-02
0.92470E+01	0.16709E+02	0.63908E-02	0.16573E-01	0.30383E+02	0.11792E-01	0.34674E+02	0.10741E-01
0.99075E+01	0.17903E+02	0.78731E-02	0.23537E-01	0.32553E+02	0.16078E-01	0.37151E+02	0.14525E-01
0.10568E+02	0.19096E+02	0.93675E-02	0.31953E-01	0.34723E+02	0.21161E-01	0.39628E+02	0.18991E-01
0.11228E+02	0.20290E+02	0.11034E-01	0.41234E-01	0.36893E+02	0.26773E-01	0.42105E+02	0.23921E-01

MISES AND TRESCA STRESS - STRAINS FOR RADIAL LOADING  $\lambda = \infty$

$\sigma_{zz}$	$\tau_{\theta z}$	$\int d\epsilon_{zz}^p$	$\int d\alpha_{\theta z}^p$	$\bar{\sigma}_M$	$\int d\epsilon_M^p$	$\bar{\sigma}_T$	$\int d\epsilon_T^p$
0.00000E+00	0.18000E+01	0.00000E+00	-0.41420E-05	0.31177E+01	0.23914E-05	0.36000E+01	0.20710E-05
0.00000E+00	0.36000E+01	0.00000E+00	-0.61873E-05	0.62354E+01	0.35722E-05	0.72000E+01	0.30936E-05
0.00000E+00	0.36000E+01	0.00000E+00	0.84284E-04	0.62354E+01	0.55806E-04	0.72000E+01	0.48329E-04
0.00000E+00	0.54000E+01	0.00000E+00	0.12941E-03	0.93531E+01	0.81861E-04	0.10800E+02	0.70894E-04
0.00000E+00	0.72000E+01	0.00000E+00	0.29929E-03	0.12471E+02	0.17994E-03	0.14400E+02	0.15583E-03
0.00000E+00	0.90000E+01	0.00000E+00	0.87750E-03	0.15588E+02	0.51377E-03	0.18000E+02	0.44494E-03
0.00000E+00	0.10800E+02	0.00000E+00	0.25355E-02	0.18706E+02	0.14710E-02	0.21600E+02	0.12739E-02
0.00000E+00	0.12600E+02	0.00000E+00	0.68955E-02	0.21824E+02	0.39883E-02	0.25200E+02	0.34540E-02
0.00000E+00	0.14400E+02	0.00000E+00	0.13441E-01	0.24942E+02	0.77675E-02	0.28800E+02	0.67269E-02
0.00000E+00	0.16200E+02	0.00000E+00	0.21439E-01	0.28059E+02	0.12385E-01	0.32400E+02	0.10726E-01
0.00000E+00	0.18000E+02	0.00000E+00	0.31691E-01	0.31177E+02	0.18304E-01	0.36000E+02	0.15852E-01
0.00000E+00	0.19800E+02	0.00000E+00	0.42152E-01	0.34295E+02	0.24344E-01	0.39600E+02	0.21082E-01

END

\*\* KINGSTON POLYTECHNIC 4120 \*\*

&JOB: MAPE/R008/DR; STRAIN RATES;

&OPTIONS;MOTHY;

&FORTRAN; D;

```

0* C
1* C
2*      DIMENSION T(100), DEZZ(100), DGAMMA(100), EZZ(100), GAMMA(100)

3*      READ(3,50) GL
4*      READ(3,50) RADN
5*      READ(3,51) M
6*      K=0
7*      1 READ(3,50) SZZ
8*      READ(3,50) XLAM
9*      READ(3,50) C1
10*     READ(3,50) C2
11*     READ(3,51) N
12*     IF(XLAM.NE.9.0) GO TO 6
13*     SSZ=SZZ
14*     SZZ=0.0
15*     GO TO 7
16*     6 SSZ=XLAM*SZZ
17*     7 WRITE(2,100) XLAM,SZZ,SSZ
18*     READ(3,52) (T(I),DEZZ(I),DGAMMA(I), I=1,N)
19*     DO 2 I = 1,N
20*     Z=C1*DEZZ(I)
21*     BR=1.0+Z/GL
22*     EZZ(I)=ALOG(BR)
23*     X=C2*DGAMMA(I)
24*     PHI=(RADN*1.116*X*3.14159)/(180.0*GL)
25*     GAMMA(I)=SIN(PHI)/COS(PHI)
26*     L=I-1
27*     IF(L.LT.2) GO TO 2
28*     REZZ=(EZZ(L+1)-EZZ(L-1))/(T(L+1)-T(L-1))
29*     RGAMMA=(GAMMA(L+1)-GAMMA(L-1))/(T(L+1)-T(L-1))
30*     IF(XLAM.NE.9.0.AND.XLAM.NE.0.0) GO TO 4
31*     A=0.0
32*     B=0.0
33*     GO TO 5
34*     4 A=RGAMMA/(REZZ*XLAM)
35*     XLAMC=XLAM*SQRT(BR)
36*     B=RGAMMA/(REZZ*XLAMC)
37*     5 WRITE(2,101) T(L),EZZ(L),GAMMA(L),REZZ, RGAMMA, A, B
38*     2 CONTINUE
39*     K=K+1
40*     IF(K.LT.M) GO TO 1
41*     STOP
42*     50 FORMAT(6X,F0.0)
43*     51 FORMAT(I0)
44*     52 FORMAT(2X,F0.0,F0.0,F0.0)
45*     100 FORMAT(1H1,30X,30HCREEP STRAINS AND STRAIN RATES,
46*     126H FOR RADIAL LOADING      = ,F5.3//
47*     240X,12HWHERE      = ,F6.2,1X,15HN/MM AND      = ,F6.2,
48*     31X,4HN/MM///)
49*     101 FORMAT(19X,F5.1,6E13.5)
50*     END

```

CREEP STRAINS AND STRAIN RATES FOR RADIAL LOADING  $\lambda = 0.000$

WHERE  $\sigma_{22} = 40.70 \text{ N/MM}^2$  AND  $\tau_{\theta z} = 0.00 \text{ N/MM}^2$

$t$	$\epsilon_{22}$	$\gamma_{\theta z}$	$\dot{\epsilon}_{22}$	$\dot{\gamma}_{\theta z}$	$k$	$k'$
2.0	0.11712E-01	0.00000E+00	0.37024E-02	0.00000E+00	0.00000E+00	0.00000E+00
3.0	0.14865E-01	0.00000E+00	0.28044E-02	0.00000E+00	0.00000E+00	0.00000E+00
4.0	0.17321E-01	0.00000E+00	0.22818E-02	0.00000E+00	0.00000E+00	0.00000E+00
5.0	0.19429E-01	0.00000E+00	0.14006E-02	0.00000E+00	0.00000E+00	0.00000E+00
10.0	0.25725E-01	0.00000E+00	0.10181E-02	0.00000E+00	0.00000E+00	0.00000E+00
15.0	0.29609E-01	0.00000E+00	0.66916E-03	0.00000E+00	0.00000E+00	0.00000E+00
20.0	0.32416E-01	0.00000E+00	0.54614E-03	0.00000E+00	0.00000E+00	0.00000E+00
25.0	0.35071E-01	0.00000E+00	0.48211E-03	0.00000E+00	0.00000E+00	0.00000E+00
30.0	0.37237E-01	0.00000E+00	0.42326E-03	0.00000E+00	0.00000E+00	0.00000E+00
35.0	0.39303E-01	0.00000E+00	0.36007E-03	0.00000E+00	0.00000E+00	0.00000E+00
40.0	0.40838E-01	0.00000E+00	0.30670E-03	0.00000E+00	0.00000E+00	0.00000E+00
45.0	0.42370E-01	0.00000E+00	0.39697E-03	0.00000E+00	0.00000E+00	0.00000E+00
50.0	0.44808E-01	0.00000E+00	0.46306E-03	0.00000E+00	0.00000E+00	0.00000E+00
55.0	0.47001E-01	0.00000E+00	0.38589E-03	0.00000E+00	0.00000E+00	0.00000E+00
60.0	0.48666E-01	0.00000E+00	0.32335E-03	0.00000E+00	0.00000E+00	0.00000E+00
65.0	0.50234E-01	0.00000E+00	0.28014E-03	0.00000E+00	0.00000E+00	0.00000E+00
70.0	0.51468E-01	0.00000E+00	0.23709E-03	0.00000E+00	0.00000E+00	0.00000E+00
75.0	0.52605E-01	0.00000E+00	0.21787E-03	0.00000E+00	0.00000E+00	0.00000E+00
80.0	0.53647E-01	0.00000E+00	0.19400E-03	0.00000E+00	0.00000E+00	0.00000E+00
85.0	0.54545E-01	0.00000E+00	0.17963E-03	0.00000E+00	0.00000E+00	0.00000E+00
90.0	0.55443E-01	0.00000E+00	0.16531E-03	0.00000E+00	0.00000E+00	0.00000E+00
95.0	0.56198E-01	0.00000E+00	0.16045E-03	0.00000E+00	0.00000E+00	0.00000E+00

CREEP STRAINS AND STRAIN RATES FOR RADIAL LOADING  $\lambda = 0.122$

WHERE  $\bar{V}_{22} = 38.85 \text{ N/MM}^2$  AND  $\bar{\gamma}_{\theta z} = 4.74 \text{ N/MM}^2$

t	$\epsilon_{22}$	$\gamma_{\theta z}$	$\dot{\epsilon}_{22}$	$\dot{\gamma}_{\theta z}$	k	k'
2.0	0.67568E-02	0.40539E-02	0.19958E-02	0.14594E-02	0.59938E+01	0.59684E+01
3.0	0.85012E-02	0.53511E-02	0.14942E-02	0.11351E-02	0.62268E+01	0.61965E+01
4.0	0.97453E-02	0.63241E-02	0.11191E-02	0.86485E-03	0.63343E+01	0.63004E+01
5.0	0.10739E-01	0.70808E-02	0.78558E-03	0.51352E-03	0.53580E+01	0.53194E+01
10.0	0.14459E-01	0.94052E-02	0.63394E-03	0.41353E-03	0.53469E+01	0.53014E+01
15.0	0.17079E-01	0.11216E-01	0.45929E-03	0.32435E-03	0.57885E+01	0.57336E+01
20.0	0.19052E-01	0.12649E-01	0.34499E-03	0.23516E-03	0.55872E+01	0.55301E+01
25.0	0.20529E-01	0.13568E-01	0.28046E-03	0.16759E-03	0.48980E+01	0.48447E+01
30.0	0.21856E-01	0.14325E-01	0.23097E-03	0.14326E-03	0.50842E+01	0.50265E+01
35.0	0.22838E-01	0.15000E-01	0.19634E-03	0.13516E-03	0.56424E+01	0.55756E+01
40.0	0.23820E-01	0.15676E-01	0.18145E-03	0.12164E-03	0.54950E+01	0.54277E+01
45.0	0.24653E-01	0.16217E-01	0.14701E-03	0.10813E-03	0.60291E+01	0.59534E+01
50.0	0.25290E-01	0.16757E-01	0.14199E-03	0.10002E-03	0.57740E+01	0.56992E+01
55.0	0.26073E-01	0.17217E-01	0.14679E-03	0.89211E-04	0.49815E+01	0.49153E+01
60.0	0.26758E-01	0.17650E-01	0.12713E-03	0.86509E-04	0.55776E+01	0.55019E+01
65.0	0.27344E-01	0.18082E-01	0.12704E-03	0.72993E-04	0.47094E+01	0.46439E+01
70.0	0.28028E-01	0.18379E-01	0.11721E-03	0.64883E-04	0.45375E+01	0.44732E+01
75.0	0.28516E-01	0.18731E-01	0.10737E-03	0.75698E-04	0.57787E+01	0.56952E+01
80.0	0.29102E-01	0.19136E-01	0.11707E-03	0.78403E-04	0.54894E+01	0.54085E+01
85.0	0.29687E-01	0.19515E-01	0.10726E-03	0.75700E-04	0.57851E+01	0.56985E+01
90.0	0.30174E-01	0.19893E-01	0.87713E-04	0.70294E-04	0.65689E+01	0.64693E+01
95.0	0.30564E-01	0.20218E-01	0.73064E-04	0.64888E-04	0.72795E+01	0.71678E+01

CREEP STRAINS AND STRAIN RATES FOR RADIAL LOADING  $\lambda = 0.532$

WHERE  $\bar{\nu}_{zz} = 27.30 \text{ N/MM}^2$  AND  $\bar{\tau}_{\theta z} = 14.52 \text{ N/MM}^2$

t	$\epsilon_{zz}$	$\gamma_{\theta z}$	$\dot{\epsilon}_{zz}$	$\dot{\gamma}_{\theta z}$	k	k'
2.0	0.59487E-02	0.57389E-02	0.20273E-02	0.19768E-02	0.18328E+01	0.18259E+01
3.0	0.75290E-02	0.76520E-02	0.14806E-02	0.16580E-02	0.21050E+01	0.20956E+01
4.0	0.89098E-02	0.90549E-02	0.12568E-02	0.13711E-02	0.20506E+01	0.20404E+01
5.0	0.10043E-01	0.10394E-01	0.10888E-02	0.12330E-02	0.21287E+01	0.21123E+01
10.0	0.15443E-01	0.16453E-01	0.83331E-03	0.98860E-03	0.22300E+01	0.22096E+01
15.0	0.18376E-01	0.20280E-01	0.55170E-03	0.73998E-03	0.25212E+01	0.24949E+01
20.0	0.20960E-01	0.23853E-01	0.49667E-03	0.68906E-03	0.26078E+01	0.25775E+01
25.0	0.23342E-01	0.27171E-01	0.45663E-03	0.65727E-03	0.27056E+01	0.26713E+01
30.0	0.25526E-01	0.30425E-01	0.38783E-03	0.57441E-03	0.27840E+01	0.27463E+01
35.0	0.27221E-01	0.32915E-01	0.29038E-03	0.40214E-03	0.26032E+01	0.25664E+01
40.0	0.28430E-01	0.34447E-01	0.21267E-03	0.30644E-03	0.27085E+01	0.26690E+01
45.0	0.29347E-01	0.35979E-01	0.20759E-03	0.36394E-03	0.32955E+01	0.32456E+01
50.0	0.30505E-01	0.38086E-01	0.27001E-03	0.41507E-03	0.28895E+01	0.28436E+01
55.0	0.32048E-01	0.40130E-01	0.28413E-03	0.37682E-03	0.24929E+01	0.24517E+01
60.0	0.33347E-01	0.41854E-01	0.23567E-03	0.33216E-03	0.26493E+01	0.26041E+01
65.0	0.34404E-01	0.43451E-01	0.21137E-03	0.31304E-03	0.27838E+01	0.27349E+01
70.0	0.35460E-01	0.44985E-01	0.22553E-03	0.31308E-03	0.26095E+01	0.25621E+01
75.0	0.36659E-01	0.46582E-01	0.20613E-03	0.29395E-03	0.26805E+01	0.26307E+01
80.0	0.37522E-01	0.47924E-01	0.13890E-03	0.23008E-03	0.31136E+01	0.30549E+01
85.0	0.38048E-01	0.48883E-01	0.10052E-03	0.15979E-03	0.29882E+01	0.29312E+01
90.0	0.38527E-01	0.49522E-01	0.90900E-04	0.10867E-03	0.22471E+01	0.22037E+01
95.0	0.38957E-01	0.49970E-01	0.76516E-04	0.89494E-04	0.21985E+01	0.21558E+01

CREEP STRAINS AND STRAIN RATES FOR RADIAL LOADING  $\lambda = 0.565$

WHERE  $\tau_{22} = 25.50 \text{ N/MM}^2$  AND  $\tau_{\theta 2} = 14.41 \text{ N/MM}^2$

t	$\epsilon_{22}$	$\gamma_{\theta 2}$	$\dot{\epsilon}_{22}$	$\dot{\gamma}_{\theta 2}$	k	k'
2.0	0.29835E-02	0.37489E-02	0.11422E-02	0.16976E-02	0.26307E+01	0.26255E+01
3.0	0.39761E-02	0.52344E-02	0.91771E-03	0.15208E-02	0.29331E+01	0.29260E+01
4.0	0.48190E-02	0.67906E-02	0.74348E-03	0.12733E-02	0.30311E+01	0.30228E+01
5.0	0.54631E-02	0.77809E-02	0.48663E-03	0.82530E-03	0.30017E+01	0.29901E+01
10.0	0.77388E-02	0.11742E-01	0.40038E-03	0.69328E-03	0.30647E+01	0.30502E+01
15.0	0.94668E-02	0.14714E-01	0.32069E-03	0.54477E-03	0.30066E+01	0.29902E+01
20.0	0.10946E-01	0.17190E-01	0.27095E-03	0.49528E-03	0.32353E+01	0.32157E+01
25.0	0.12176E-01	0.19667E-01	0.23124E-03	0.42456E-03	0.32495E+01	0.32281E+01
30.0	0.13258E-01	0.21436E-01	0.18678E-03	0.36091E-03	0.34200E+01	0.33961E+01
35.0	0.14044E-01	0.23276E-01	0.14732E-03	0.33970E-03	0.40811E+01	0.40512E+01
40.0	0.14731E-01	0.24833E-01	0.12759E-03	0.28311E-03	0.39271E+01	0.38972E+01
45.0	0.15320E-01	0.26197E-01	0.11280E-03	0.23358E-03	0.36650E+01	0.36360E+01
50.0	0.15859E-01	0.27168E-01	0.98038E-04	0.20528E-03	0.37060E+01	0.36759E+01
55.0	0.16300E-01	0.28160E-01	0.93088E-04	0.17697E-03	0.33649E+01	0.33367E+01
60.0	0.16790E-01	0.28938E-01	0.97942E-04	0.17698E-03	0.31983E+01	0.31708E+01
65.0	0.17280E-01	0.29929E-01	0.97894E-04	0.18407E-03	0.33280E+01	0.32986E+01
70.0	0.17769E-01	0.30779E-01	0.97846E-04	0.19116E-03	0.34579E+01	0.34265E+01
75.0	0.18258E-01	0.31841E-01	0.88022E-04	0.19117E-03	0.38440E+01	0.38083E+01
80.0	0.18649E-01	0.32691E-01	0.83094E-04	0.14870E-03	0.31673E+01	0.31372E+01
85.0	0.19089E-01	0.33328E-01	0.92829E-04	0.14163E-03	0.27003E+01	0.26740E+01
90.0	0.19578E-01	0.34107E-01	0.92788E-04	0.13455E-03	0.25665E+01	0.25410E+01
95.0	0.20017E-01	0.34673E-01	0.78105E-04	0.11331E-03	0.25677E+01	0.25417E+01

CREEP STRAINS AND STRAIN RATES FOR RADIAL LOADING  $\lambda = 0.863$

WHERE  $\sigma_{zz} = 20.95 \text{ N/MM}^2$  AND  $\tau_{\theta z} = 18.08 \text{ N/MM}^2$

t	$\epsilon_{zz}$	$\gamma_{\theta z}$	$\dot{\epsilon}_{zz}$	$\dot{\gamma}_{\theta z}$	k	k'
2.0	0.47885E-02	0.13905E-01	0.74623E-03	0.24861E-02	0.38604E+01	0.38492E+01
3.0	0.57832E-02	0.15459E-01	0.84522E-03	0.15539E-02	0.21303E+01	0.21234E+01
4.0	0.64790E-02	0.17013E-01	0.74512E-03	0.14763E-02	0.22958E+01	0.22874E+01
5.0	0.72735E-02	0.18411E-01	0.75998E-03	0.13729E-02	0.20933E+01	0.20818E+01
10.0	0.11039E-01	0.25250E-01	0.57415E-03	0.13369E-02	0.26981E+01	0.26806E+01
15.0	0.13015E-01	0.31780E-01	0.55232E-03	0.12441E-02	0.26100E+01	0.25885E+01
20.0	0.16562E-01	0.37691E-01	0.48250E-03	0.98005E-03	0.23536E+01	0.23327E+01
25.0	0.17840E-01	0.41581E-01	0.16707E-03	0.74697E-03	0.51809E+01	0.51338E+01
30.0	0.18233E-01	0.45161E-01	0.24528E-03	0.60708E-03	0.28680E+01	0.28390E+01
35.0	0.20293E-01	0.47652E-01	0.38222E-03	0.49826E-03	0.15105E+01	0.14940E+01
40.0	0.22055E-01	0.50143E-01	0.23490E-03	0.48280E-03	0.23816E+01	0.23548E+01
45.0	0.22642E-01	0.52480E-01	0.97771E-04	0.38944E-03	0.46155E+01	0.45626E+01
50.0	0.23033E-01	0.54037E-01	0.10748E-03	0.34278E-03	0.36955E+01	0.36520E+01
55.0	0.23717E-01	0.55907E-01	0.10744E-03	0.38960E-03	0.42019E+01	0.41516E+01
60.0	0.24107E-01	0.57933E-01	0.97609E-04	0.39748E-03	0.47186E+01	0.46607E+01
65.0	0.24693E-01	0.59882E-01	0.10732E-03	0.37418E-03	0.40400E+01	0.39894E+01

CREEP STRAINS AND STRAIN RATES FOR RADIAL LOADING  $\lambda = 1.807$

WHERE  $\sigma_{zz} = 11.20 \text{ N/MM}^2$  AND  $\tau_{\theta z} = 20.24 \text{ N/MM}^2$

t	$\epsilon_{zz}$	$\gamma_{\theta z}$	$\dot{\epsilon}_{zz}$	$\dot{\gamma}_{\theta z}$	k	k'
2.0	0.25257E-02	0.12481E-01	0.75098E-03	0.43847E-02	0.32311E+01	0.32261E+01
3.0	0.31242E-02	0.16130E-01	0.55425E-03	0.32329E-02	0.32279E+01	0.32221E+01
4.0	0.36342E-02	0.18947E-01	0.47553E-03	0.28171E-02	0.32784E+01	0.32717E+01
5.0	0.40753E-02	0.21764E-01	0.30529E-03	0.19426E-02	0.35214E+01	0.35118E+01
10.0	0.54659E-02	0.30602E-01	0.23297E-03	0.15246E-02	0.36215E+01	0.36100E+01
15.0	0.64050E-02	0.37009E-01	0.16134E-03	0.10830E-02	0.37147E+01	0.37016E+01
20.0	0.70794E-02	0.41432E-01	0.14362E-03	0.83343E-03	0.32114E+01	0.31988E+01
25.0	0.78412E-02	0.45344E-01	0.16401E-03	0.46810E-03	0.15795E+01	0.15726E+01
30.0	0.87195E-02	0.46113E-01	0.15316E-03	0.25656E-03	0.92699E+00	0.92266E+00
35.0	0.93728E-02	0.47909E-01	0.12283E-03	0.30790E-03	0.13872E+01	0.13803E+01
40.0	0.99478E-02	0.49192E-01	0.10425E-03	0.28871E-03	0.15326E+01	0.15246E+01
45.0	0.10415E-01	0.50796E-01	0.88618E-04	0.24382E-03	0.15226E+01	0.15144E+01
50.0	0.10834E-01	0.51631E-01	0.76901E-04	0.19252E-03	0.13854E+01	0.13777E+01
55.0	0.11184E-01	0.52722E-01	0.64224E-04	0.20537E-03	0.17696E+01	0.17595E+01
60.0	0.11476E-01	0.53684E-01	0.55449E-04	0.13479E-03	0.13452E+01	0.13373E+01
65.0	0.11739E-01	0.54069E-01	0.46682E-04	0.14122E-03	0.16741E+01	0.16641E+01
70.0	0.11943E-01	0.55097E-01	0.41809E-04	0.12197E-03	0.16144E+01	0.16046E+01
75.0	0.12157E-01	0.55289E-01	0.47632E-04	0.10272E-03	0.11934E+01	0.11860E+01
80.0	0.12419E-01	0.56124E-01	0.55395E-04	0.13482E-03	0.13469E+01	0.13384E+01
85.0	0.12711E-01	0.56637E-01	0.52466E-04	0.13484E-03	0.14222E+01	0.14130E+01
90.0	0.12944E-01	0.57472E-01	0.51480E-04	0.18622E-03	0.20018E+01	0.19886E+01
95.0	0.13226E-01	0.58500E-01	0.66030E-04	0.22477E-03	0.18839E+01	0.18711E+01

CREEP STRAINS AND STRAIN RATES FOR RADIAL LOADING  $\lambda = \infty$

WHERE  $\nu_{22} = 0.00 \text{ N/MM}^2$  AND  $\tau_{\theta 2} = 21.60 \text{ N/MM}^2$

t	$\epsilon_{22}$	$\delta_{\theta 2}$	$\dot{\epsilon}_{22}$	$\dot{\delta}_{\theta 2}$	k	k'
2.0	0.00000E+00	0.10113E-01	0.00000E+00	0.32004E-02	0.00000E+00	0.00000E+00
3.0	0.00000E+00	0.12801E-01	0.00000E+00	0.23684E-02	0.00000E+00	0.00000E+00
4.0	0.00000E+00	0.14849E-01	0.00000E+00	0.18564E-02	0.00000E+00	0.00000E+00
5.0	0.00000E+00	0.16514E-01	0.00000E+00	0.13659E-02	0.00000E+00	0.00000E+00
10.0	0.00000E+00	0.23044E-01	0.00000E+00	0.10821E-02	0.00000E+00	0.00000E+00
15.0	0.00000E+00	0.27335E-01	0.00000E+00	0.75576E-03	0.00000E+00	0.00000E+00
20.0	0.00000E+00	0.30602E-01	0.00000E+00	0.61498E-03	0.00000E+00	0.00000E+00
25.0	0.00000E+00	0.33485E-01	0.00000E+00	0.52539E-03	0.00000E+00	0.00000E+00
30.0	0.00000E+00	0.35856E-01	0.00000E+00	0.49345E-03	0.00000E+00	0.00000E+00
35.0	0.00000E+00	0.38420E-01	0.00000E+00	0.43584E-03	0.00000E+00	0.00000E+00
40.0	0.00000E+00	0.40214E-01	0.00000E+00	0.36540E-03	0.00000E+00	0.00000E+00
45.0	0.00000E+00	0.42073E-01	0.00000E+00	0.35263E-03	0.00000E+00	0.00000E+00
50.0	0.00000E+00	0.43741E-01	0.00000E+00	0.36551E-03	0.00000E+00	0.00000E+00
55.0	0.00000E+00	0.45729E-01	0.00000E+00	0.38481E-03	0.00000E+00	0.00000E+00
60.0	0.00000E+00	0.47589E-01	0.00000E+00	0.32714E-03	0.00000E+00	0.00000E+00
65.0	0.00000E+00	0.49000E-01	0.00000E+00	0.23095E-03	0.00000E+00	0.00000E+00
70.0	0.00000E+00	0.49898E-01	0.00000E+00	0.16682E-03	0.00000E+00	0.00000E+00
75.0	0.00000E+00	0.50668E-01	0.00000E+00	0.15400E-03	0.00000E+00	0.00000E+00
80.0	0.00000E+00	0.51438E-01	0.00000E+00	0.14117E-03	0.00000E+00	0.00000E+00
85.0	0.00000E+00	0.52080E-01	0.00000E+00	0.11551E-03	0.00000E+00	0.00000E+00
90.0	0.00000E+00	0.52593E-01	0.00000E+00	0.10910E-03	0.00000E+00	0.00000E+00
95.0	0.00000E+00	0.53171E-01	0.00000E+00	0.96272E-04	0.00000E+00	0.00000E+00

EXPERIMENT FOR ANISOTROPIC ALUMINUM

In this Chapter the creep and plastic flow behavior of an extruded material is analyzed. A study of anisotropic procedures are analyzed.

5.1. ANISOTROPY

Metallographic studies to sections of extruded bar revealed the extruded material to possess a preferred grain orientation that was neither uniform in cross-section nor in length. Fig. 5.1 shows the grain size variation in three mutually perpendicular directions for a disc of extruded bar. The longitudinal 'bar' section in Fig. 5.2 displays the grain texture as revealed by the etching process. The figures show

# CHAPTER 5

bar reeling. The concentration of heat at the bar centre has caused partial recrystallization and the grains there are larger and more rounded than those at the bar edge. The transverse 'bar' study in Fig. 5.3 shows the large order of variation in grain size between edge and centre.

The results of longitudinal (L), transverse (T) and oblique (O) 'Hounsfield' tensile tests on specimens of Fig. 5.1 (see also Fig. 5.2). The figure shows the wide variation in tensile strength for the (L), (T) and (O) directions and the steady wide variation in tensile strength between specimens having the same orientation. The variation is particularly noticeable in specimens cut longitudinally from the bar and since they were cut on a cross-sectional diameter that would correspond to the max. wall diameter of a tubular specimen it is thus known that tubular specimens cut from extruded material are composed of anisotropic material.

The variation of hardness for three mutually perpendicular directions is shown in Fig. 5.4. Figure 5.5 shows the hardness 0 and 90° (0.015") figures are also in step between 0 and 90° about an average figure of 11. Figure 5.6 shows the average length (longitudinal) and (transverse) figures are also in step about an average figure of 11. The order of the hardness figures is not possible

## RESULTS FOR EXTRUDED ALUMINIUM

In this Chapter the creep and plastic flow behaviour of as-extruded material is analysed. A study of material anisotropy precedes the analysis.

5.1 ANISOTROPY

Metallographic studies on sections of extruded bar revealed the extruded material to possess a preferred grain orientation that was neither uniform in cross-section nor in length. Fig. 5.1\* shows the grain size variation in three mutually perpendicular directions for a disc of extruded bar. The longitudinal 'macro' studies in Fig. 5.1 display the grain texture as produced by the extrusion process. These studies also show the variation in grain size from the outside to the centre of the bar resulting from the obviously severe temperature gradient of this extrusion. The concentration of heat at the bar centre has caused partial recrystallisation and the grains there are larger and more equiaxed than those at the bar edge. The transverse 'micro' study in Fig. 5.1 shows the large order of variation in grain size between edge and centre.

The results of longitudinal (L), transverse (T) and oblique (O) 'Hounsfield' tensile tests on specimens of Fig. 2.10(a) are shown in Fig. 5.2. The figure shows the wide variation in tensile strengths for the (L), (T) and (O) directions and the similarly wide variation in tensile strength between specimens from any one direction. The variation is particularly noticeable in specimens cut longitudinally from the bar and since these were cut on a cross-sectional diameter that would correspond to the mean wall diameter of a tubular specimen it is thus known that tubular specimens cut from extruded material are composed of anisotropic material.

The variation of hardness for three mutually perpendicular directions is shown in Fig. 5.3. Along a diameter the transverse  $0^\circ$  and  $90^\circ$  (V.P.N.) figures are seen to vary between 22 and 24.5 about an average figure of 23. Along a diametrical distance in the length the longitudinal (V.P.N.) figures varied between 20.3 and 21.5 about an average figure of 20.7. In view of the inconsistency in tensile strengths it is not possible

\* Figures are given at the end of this Chapter.

to arrive at a correlation between strength and hardness in Figs. 5.2 and 5.3. However, hardness tests performed on the Hounsfield specimens prior to testing showed greatest tensile strength to be associated with greatest hardness in this material.

## 5.2 CREEP AND PLASTIC FLOW DURING COMBINED LOADING

From the preceding study it was recognised that each cylinder was composed of anisotropic material. Furthermore from the grain size and strength variation this was not an anisotropy that could be said to be the same in each cylinder. Thus in performing constant stress ratio loading tests on cylinders of extruded material no attempt was made to construct a yield locus or to correlate the loading stresses with plastic strains in the manner of annealed material analysis (Chapter 4). The plastic anisotropy of extruded material was studied simply from a component strain plot.

### 5.2.1 Instantaneous and Transient Creep Strains

For each of the chosen stress ratios the loading strains are shown in the total strain  $\delta_{\theta z} \vee \epsilon_{zz}$  and  $\epsilon_{\theta\theta} \vee \epsilon_{zz}$  plots of Fig. 5.4. The region between successive symbols in this figure represent the total strains associated with an increment of combined loading. This is shown as consisting of two components, an instantaneous strain (30 s) and a transient creep strain (30 s - 10 min). In common with equation (4.12) for annealed material both components are seen to follow the same direction in Fig. 5.4. Thus for extruded material we have for any increment of combined loading,

$$\frac{d\epsilon_{\theta\theta}^p}{d\epsilon_{zz}^p} = \frac{\dot{\epsilon}_{\theta\theta}^c}{\dot{\epsilon}_{zz}^c} \quad (5.1)$$

$$\frac{d\delta_{\theta z}^p}{d\epsilon_{zz}^p} = \frac{\dot{\delta}_{\theta z}^c}{\dot{\epsilon}_{zz}^c}$$

where  $d\epsilon_{ij}^p = d\epsilon_{ij} - d\epsilon_{ij}^c$  and the elastic components ( $d\epsilon_{ij}^c$ ) are subtracted from the instantaneous strains ( $d\epsilon_{ij}$ ) in equation (3.6).

One difference between the loading strain plots on extruded material (Fig. 5.4) and those of annealed material (Fig. 4.4) is the rotation in the  $d\delta/d\epsilon$  vector of extruded material. Thus while the linearity in  $\delta_{\theta z}^p \vee \epsilon_{zz}^p$  in Fig. 4.4 indicates a  $d\delta_{\theta z}^p / d\epsilon_{zz}^p$  vector that is independent of stress level the rotation of the vector in Fig. 5.5 indicates a dependence on stress level. The tests on prestrained material in Chapter 6 show that a rotation in the  $\delta_{\theta z} \vee \epsilon_{zz}$  plot is

typical of a material with a prior plastic strain history, and furthermore a rotation of the Fig. 5.4 type is typical of prior compressive strain. It is likely therefore that the extrusion left the material with a residual compressive strain history and that the stress relieving treatment given to each cylinder during machining did not remove it.

With increasing stress the  $d\delta/d\epsilon$  vector of Fig. 5.4 approaches a constant direction as the accumulating plastic strain nullifies the effect of the residual strain. For the last combined stress increment the corresponding vector has been used to calculate the indicated  $k$  value ( $= \frac{d\delta/d\epsilon}{\lambda}$ ) in Fig. 5.4. A  $k$  value that is independent of stress ratio ( $\lambda$ ) would imply a material that either behaves isotropically ( $k = 3$ ) or one that behaves in a simple anisotropic manner (e.g.  $k \approx 2.6$  for annealed material). The fact that  $k$  is not independent of stress ratio in Fig. 5.4 would therefore indicate a material which is anisotropically complex. A cylinder made from such material therefore possesses an anisotropy which is peculiar to the grain texture and strength variation existing in its gauge length.

The behaviour of extruded material is further different from the behaviour of annealed material in the  $\epsilon_{\theta\theta} \vee \epsilon_{zz}$  plot of Fig. 5.4. For annealed material equation (4.6) applied for all stress ratios but clearly  $d\epsilon_{\theta\theta}^p/d\epsilon_{zz}^p \neq -1/2$  in Fig. 5.4.

One interesting observation made during purely torsional loading ( $\lambda = \infty$ ) was a noticeable extension in a tube manufactured from extruded material. This would violate any theoretical assumption made on zero length changes in torsion. Fig. 5.4 shows the  $\delta_{\theta z} \vee \epsilon_{zz}$  plot for  $\lambda = \infty$  and again equation (5.1) is seen to apply.

A theoretical solution to these observations is discussed in Section 5.5.

### 5.2.2 Transient Creep Time Exponents

A study of the  $\epsilon_{zz}, \delta_{\theta z}$  transient loading creep is made in the derivative plots of Fig. 5.5 for  $\lambda = 0.92$ . For any particular time in the 10 min creep period the respective  $\dot{\epsilon}_{zz}^c, \dot{\delta}_{\theta z}^c$  creep rates occurred simultaneously. For simplicity the component creep rates are shown on a displaced time axis.

Linearity on this plot implies parabolic creep of the form,

$$\begin{aligned}\dot{\epsilon}_{zz}^c &= at^{m_1} \\ \dot{\delta}_{\theta z}^c &= bt^{m_2}\end{aligned}\tag{5.2}$$

and parallelism implies that  $m_1$  and  $m_2$  are independent of tensile and shear stress respectively. In common with the behaviour of annealed material the time exponents  $m_1$  and  $m_2$  of extruded material were not strictly equal for the two strain components and Fig. 5.5 shows that  $m_1 = 0.175$ ,  $m_2 = 0.237$  for  $\lambda = 0.92$ . The same observations were made for all other stress paths on extruded material and the overall variation in the  $m$  values was of a similar order to that of annealed material. (see Table 4.1).

### 5.3 CREEP

For each of the chosen stress ratios Programme 5.1\* shows the  $k$  value of equation (3.21) at initially 1 then 5 and finally 10 hourly intervals for 300-400 hours of creep. In common with the long-time creep strains of annealed material (paragraph 4.3.3) there is again evidence of a constant  $k$  value in the creep of extruded material. This is more clearly seen in the total strain  $\delta_{\theta z} \vee \epsilon_{zz}$  plot of Fig. 5.6 where the loading strains of Fig. 5.4 are shown up to the point 'X' with the creep strains of Programme 5.1 thereafter added for the hourly times indicated.

Fig. 5.6 shows that for each stress ratio the  $d\delta/d\epsilon$  vector of the 'X' stress level remains fixed in direction and grows in magnitude as the creep strain accumulates. Thus equation (5.1) would also apply to long-time creep strain throughout both its primary and secondary stages. (In all tests the primary creep stage was complete by a time of 200 hours).

The  $\delta_{\theta z} \vee \epsilon_{zz}$  plot for pure torsion in Fig. 5.6 ( $\lambda = \infty$ ) indicates that the cylinder lengthens during torsional loading and continues to lengthen during creep. There is no evidence of a rotation in the  $d\delta/d\epsilon$  vector and a constant  $d\delta/d\epsilon$  value of 4.54 applied throughout the whole of flow for this test.

\* Given at the end of this Chapter.

#### 5.4 GENERAL COMMENTS ON FLOW IN EXTRUDED MATERIAL

The point to be made regarding these tests is the danger in applying theories of plastic flow and creep in designs involving material of extruded stock. For example, if the Marin-Soderberg type equation ( $k = 3$ ) were applied in this work for a prediction of secondary creep rates it should be appreciated, from the  $k$  values of Fig. 5.6, that this would only approximate to the real behaviour. The theoretical study in the following section shows that only if the initial anisotropy is understood and only if the prestrain history is known would it then be possible to arrive at a more accurate prediction.

#### 5.5 THEORETICAL PREDICTIONS OF ANISOTROPY

The observed behaviour in Fig. 5.6 may be theoretically described from the general anisotropy theories of Section 3.5 in Chapter 3. The length changes in torsion are also considered in terms of these theories and Hu's theory (paragraph 3.4.3.)

In applying theory it is assumed that a residual compressive strain exists in the material following the extrusion. The resulting  $d\delta^p/d\epsilon^p$  ratios of loading and the  $\delta/\epsilon$  ratios of creep are qualitative only.

##### 5.5.1 Loading Strain

For a compressive prestrain history the theories of Edelman and Drucker, Yoshimura and Williams and Svensson predict  $d\delta^p/d\epsilon^p$  ratios as given by equations (3.46), (3.50) and (3.53) respectively. The latter theory is rejected here on the grounds that it describes only the anisotropy of a prestrain on an initially von Mises material since for  $\epsilon_0^p = 0$ ,  $d\delta^p/d\epsilon^p = 3\lambda$  in equation (3.53). The anisotropy of a grain texture cannot therefore be described by the Williams and Svensson theory (see p.147).

For radial loading ( $\lambda = \sigma_{12}/\sigma_{11} = \text{constant}$ ) the Edelman and Drucker theory of equation (3.46) can be written for a compressive prestrain ( $-\epsilon_{11}^p$ ) as,

$$\frac{d\delta^p}{d\epsilon^p} = \frac{A \left(1 + \frac{3m\epsilon_{11}^p}{2\sigma_{11}}\right) + B\lambda}{C \left(1 + \frac{3m\epsilon_{11}^p}{2\sigma_{11}}\right) + A\lambda} \quad (5.3)$$

and the Yoshimura theory of equation (3.50) can be written as,

$$\frac{d\delta^p}{d\epsilon^p} = \frac{A' + B'\lambda}{C' + A'\lambda + \frac{9m'\epsilon_{11}^p}{\sigma_{11}}} \quad (5.4)$$

where the constants  $A, B, C, m, A', B', C'$  and  $m'$  in equations (5.3) and (5.4) describe the anisotropy of a grain texture and a prior plastic strain.

Both equations would predict a rotation in the  $d\delta^p/d\epsilon^p$  vector of loading (defined by  $\sigma_{11}$ )\* that would approach a constant value with increasing  $\sigma_{11}$ . This is consistent with experimental observation in Fig. 5.4. Furthermore with  $A, B, C$  etc. as positive constants in equations (5.3) and (5.4) then both theories predict the rotations of the correct type (increasing  $d\delta^p/d\epsilon^p$  with increasing  $\sigma_{11}$ ).

### 5.5.2 Creep

Writing the plastic strain increment ratios of equations (5.3) and (5.4) as creep strain rate ratios ( $\dot{\delta}/\dot{\epsilon}$ ) for creep (see Section 2 Appendix I) implies that the direction of the  $d\delta/d\epsilon$  loading vector remains fixed in direction during creep since  $\sigma_{11}$  is then a constant. This is clearly consistent with Fig. 5.6 for the observations made on transient creep and long-time creep. The theories of Edelman and Drucker and Yoshimura are therefore suitable to qualitatively describe the overall plastic flow and creep behaviour in extruded material. Since the anisotropy of the grain texture was different with each test cylinder then the constants  $A, B, C$  etc. in equations (5.3) and (5.4) would need to be separately defined in describing the  $k$  values ( $= \frac{\dot{\delta}/\dot{\epsilon}}{\lambda}$ ) of creep in Fig. 5.6.

Hill's theory of equation (3.28) could be made to account for the creep  $k$  values of Fig. 5.6 in the constants  $F, H$  and  $L$ . That is,

$$k = \frac{\dot{\delta}/\dot{\epsilon}}{\lambda} = \frac{6L}{F+H} \quad (5.5)$$

This theory would not however predict the rotation in the  $d\delta^p/d\epsilon^p$  vector of loading for the same constants in equation (3.24).

Bailey's theory of equation (3.36) could also describe the creep  $k$  values of Fig. 5.6 in the constants  $n$  and  $m$ . Then from equation (3.36),

$$k = \frac{\dot{\delta}/\dot{\epsilon}}{\lambda} = 3(\lambda)^{n-2m-1} \quad (5.6)$$

The theory was only proposed for creep but if  $\dot{\delta}/\dot{\epsilon}$  were written as  $d\delta^p/d\epsilon^p$  in equation (3.36) it is clear that for the same constants the theory would not predict a rotation in the  $d\delta/d\epsilon$  vector of loading.

\* In tensor notation  $\sigma_{22} = \sigma_{11}$

Obviously the theory of Berman and Pai would be unsuitable to describe the creep of extruded material since these predict  $k$  values of 3 and 4 respectively from equations (3.37) and (3.38).

Hu's theory of equation (3.39) would account for a rotation in the  $d\delta/d\epsilon$  vector of loading when the axis of anisotropy  $\alpha$  (Fig. 3.1) changes with the angle of twist  $\theta$ . However in applying equation (3.39) to creep by equation (3.40) it is difficult to see how the constant  $k$  values of Fig. 5.6 could be accounted for in this theory.

### 5.5.3 Axial Strain in Torsion

The presence of axial strain for  $\lambda = \infty$  in Figs. 5.4 and 5.6 can again be qualitatively studied from a consideration of the  $d\delta^p/d\epsilon^p$  vector of loading and the  $\dot{\delta}/\dot{\epsilon}$  ratio of creep. Then assuming an anisotropic material with residual compressive strain ( $-\epsilon_{11}^p$ ) we have from equation (3.46) with  $\sigma_{11} = 0$  in torsion an Edelman and Drucker prediction of,

$$\frac{d\delta^p}{d\epsilon^p} = \frac{B + \frac{3Am\epsilon_{11}^p}{2\sigma_{12}}}{A + \frac{3Cm\epsilon_{11}^p}{2\sigma_{12}}} \quad (5.7)$$

and from equation (3.50) a Yoshimura prediction of,

$$\frac{d\delta^p}{d\epsilon^p} = \frac{B'}{A' + \frac{9m'\epsilon_{11}^p}{\sigma_{12}}} \quad (5.8)$$

With  $A, B, C$  etc as fixed positive constants in equations (5.7) and (5.8) both theories predict a rotating  $d\delta^p/d\epsilon^p$  vector of increasing magnitude for increasing shear stress ( $\sigma_{12}$ )\*. Since this was not the observed behaviour in Fig. 5.4 it is probable that no residual strain was present in the gauge length of the cylinder used for this test. Then for  $\epsilon_{11}^p = 0$  the right-hand sides of equations (5.7) and (5.8) become  $B/A$  and  $B'/A'$  respectively. Both theories can then be made to satisfactorily describe the constant ratio of 4.54 throughout loading and throughout creep in Fig. 5.6 since,

$$\frac{d\delta^p}{d\epsilon^p} = \frac{\dot{\delta}}{\dot{\epsilon}} = \frac{B}{A} = \frac{B'}{A'} = 4.54 \quad (5.9)$$

\* In tensor notation  $\tau_{\theta z} = \sigma_{12}$

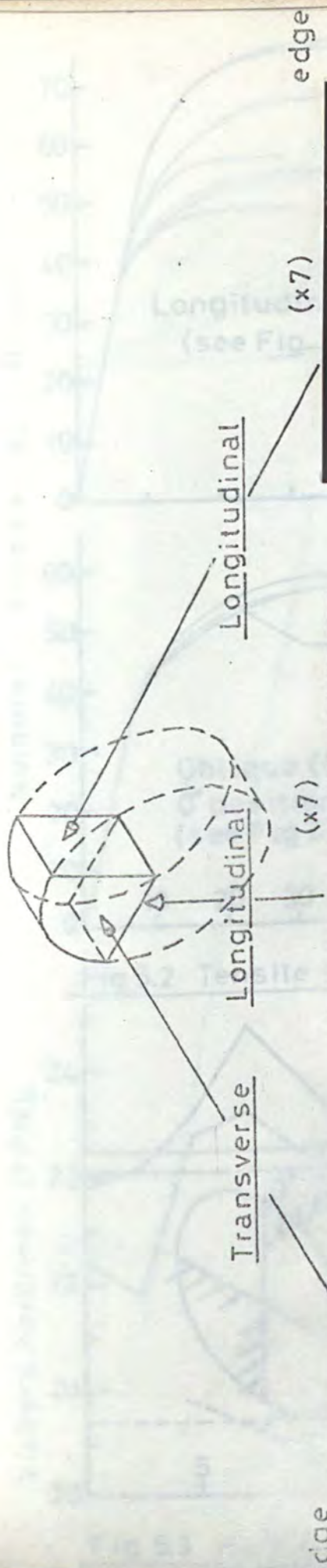
Hu's theory of equation (3.39) would be written for torsion as,

$$\frac{d\delta^p}{d\epsilon^p} = \frac{\beta_3}{\beta_2} \quad (5.10)$$

This problem has also been considered by Hill (see reference (1) Appendix I) who shows that  $\beta_3 = 1/\gamma^2$ . Hence equation (5.10) becomes

$$\frac{d\delta^p}{d\epsilon^p} = \frac{1}{\gamma^2 \beta_2} \quad (5.11)$$

Hill makes the assumption that the axes of anisotropy (1 and 2 in Fig. 3.1) always coincide with the axes of major and minor principal strain. Then the angle  $\alpha$  in Fig. 3.1 would vary between  $45^\circ$  and  $90^\circ$  during torsion. With F, G, H and L as constants describing plastic anisotropy equation (5.11) would predict a rotating  $d\delta^p/d\epsilon^p$  vector of torsional loading and from equation (3.40) a rotating  $\dot{\delta}/\dot{\epsilon}$  vector of creep. The theory is therefore not consistent with the experimentally observed constant value of 4.54 in creep.



edge

(x7)

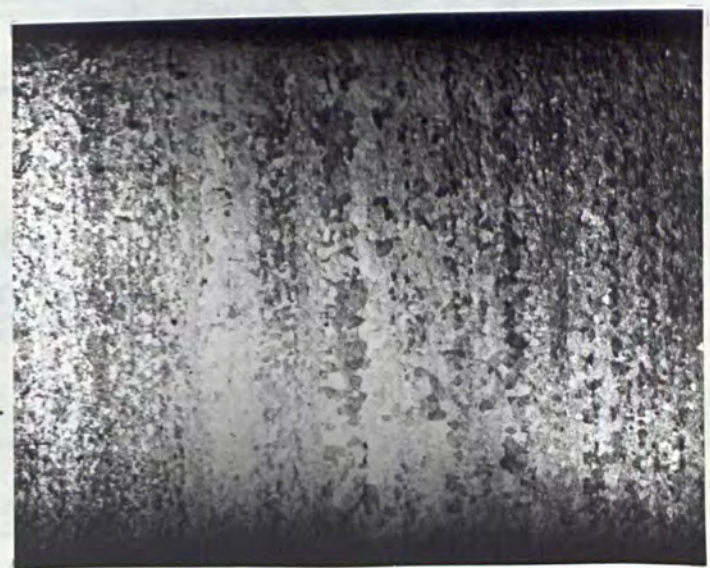
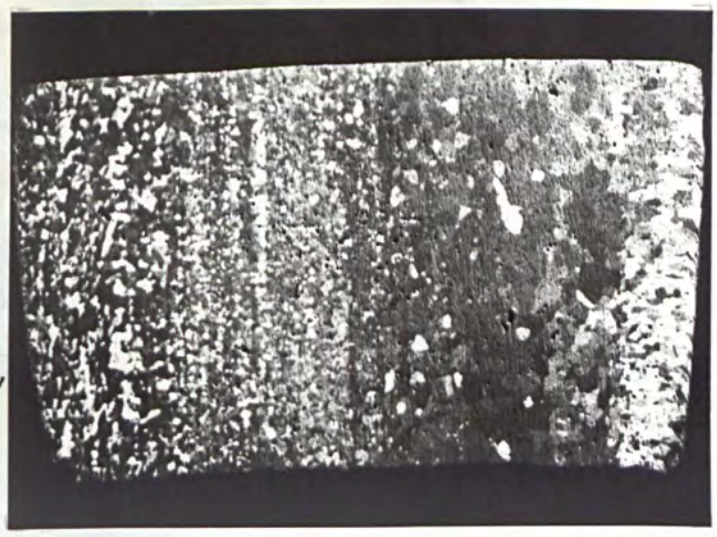
Longitudinal

Longitudinal

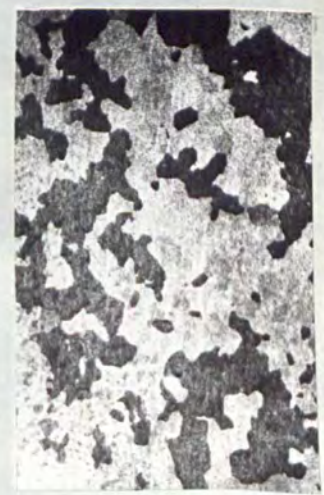
(x7)

Transverse

edge



(x100)



centre

centre

Fig.5.1 Grain size variation in extruded material

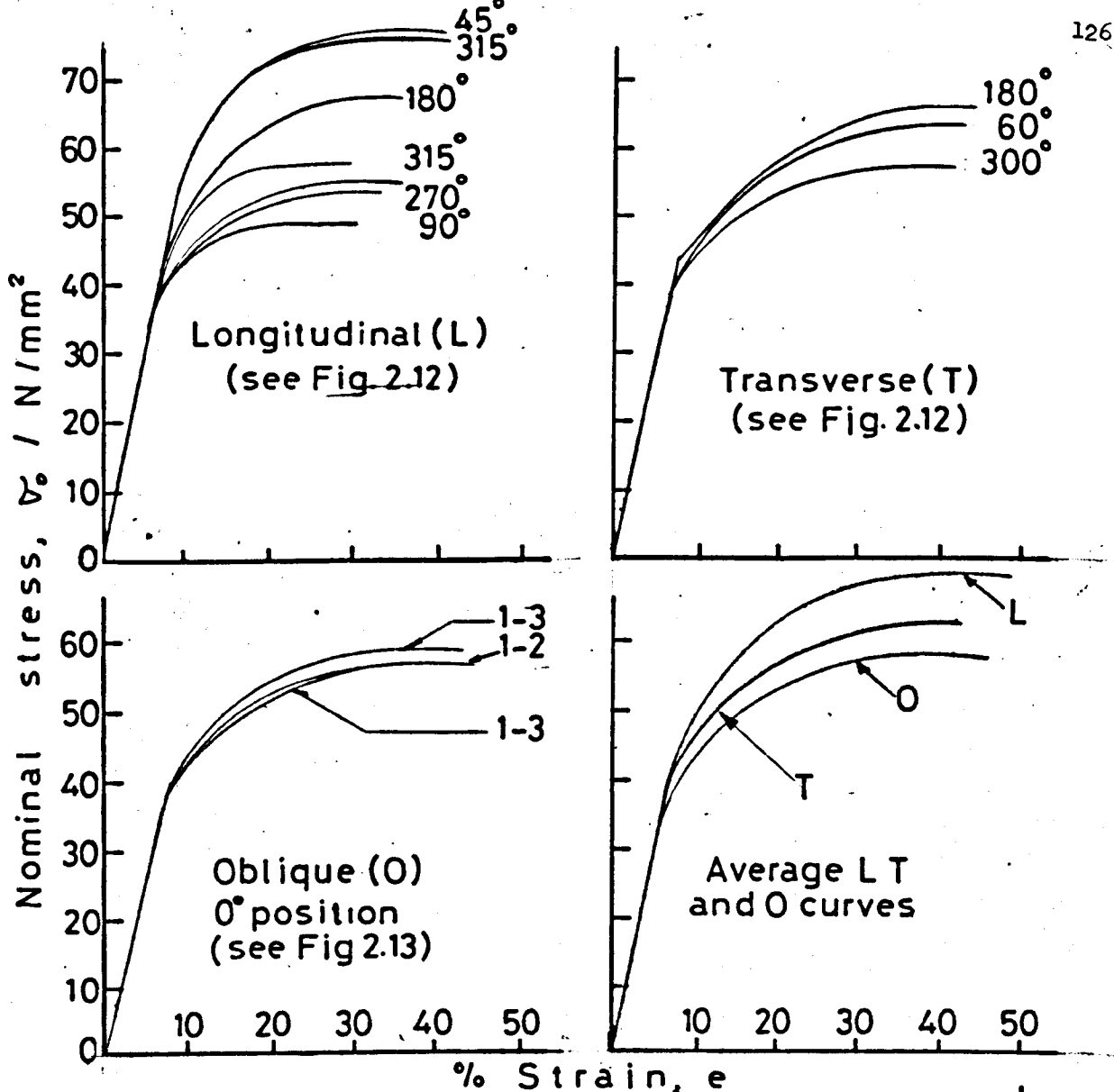


Fig 5.2 Tensile strength variation of extruded mat<sup>l</sup>

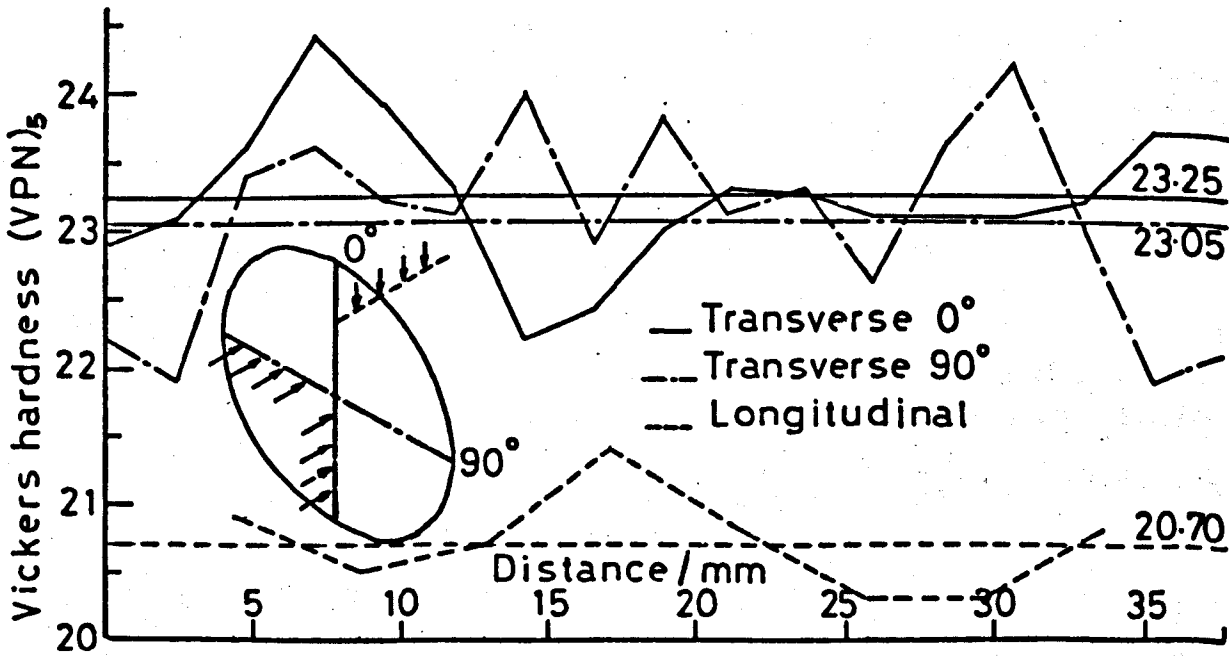


Fig 5.3 Hardness variation in extruded material

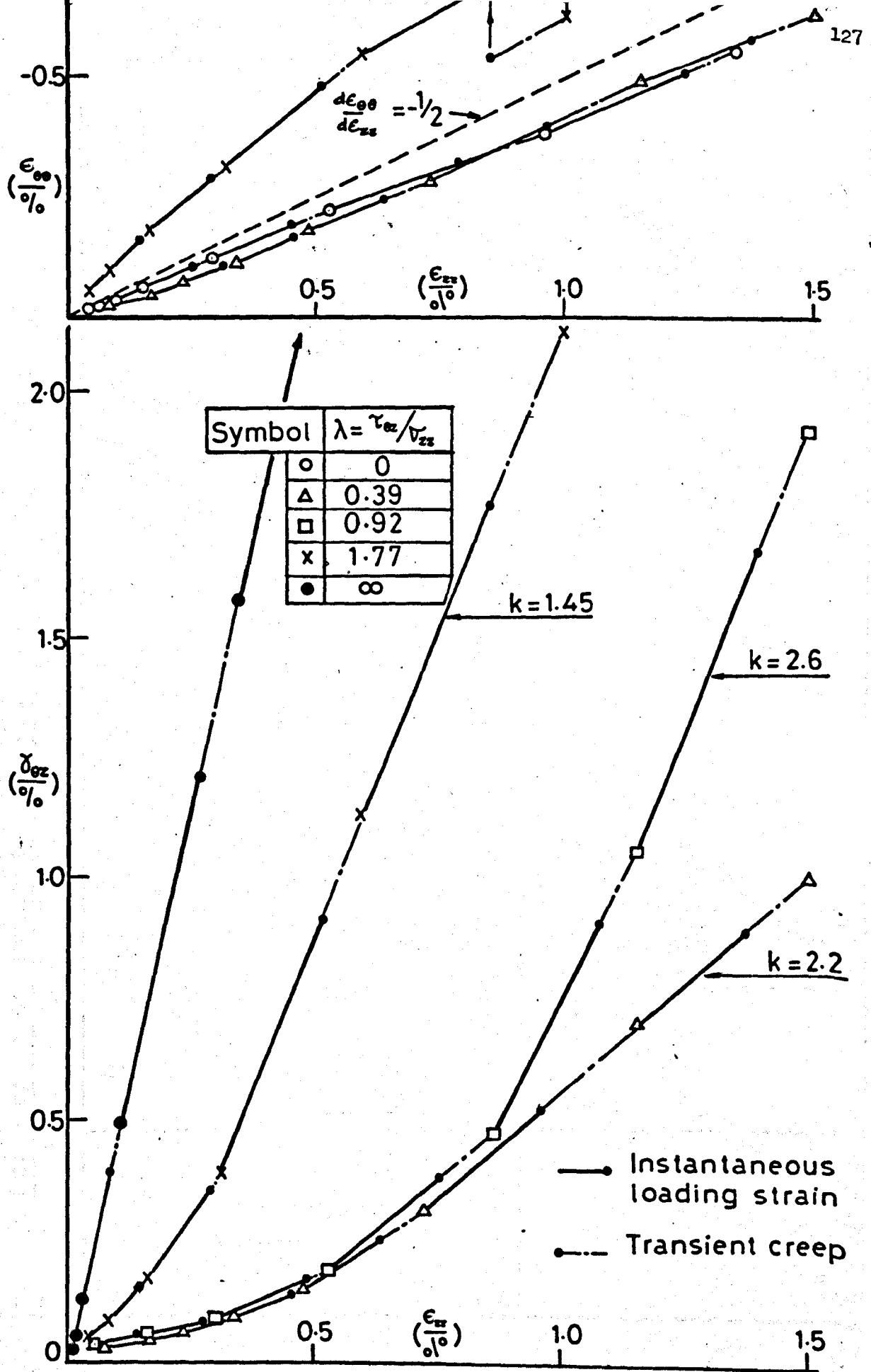


Fig.5.4  $\epsilon_{\theta} \nu \epsilon_z$ ,  $\delta_{gz} \nu \epsilon_z$  of radial loading ( $\lambda = \text{constant}$ )

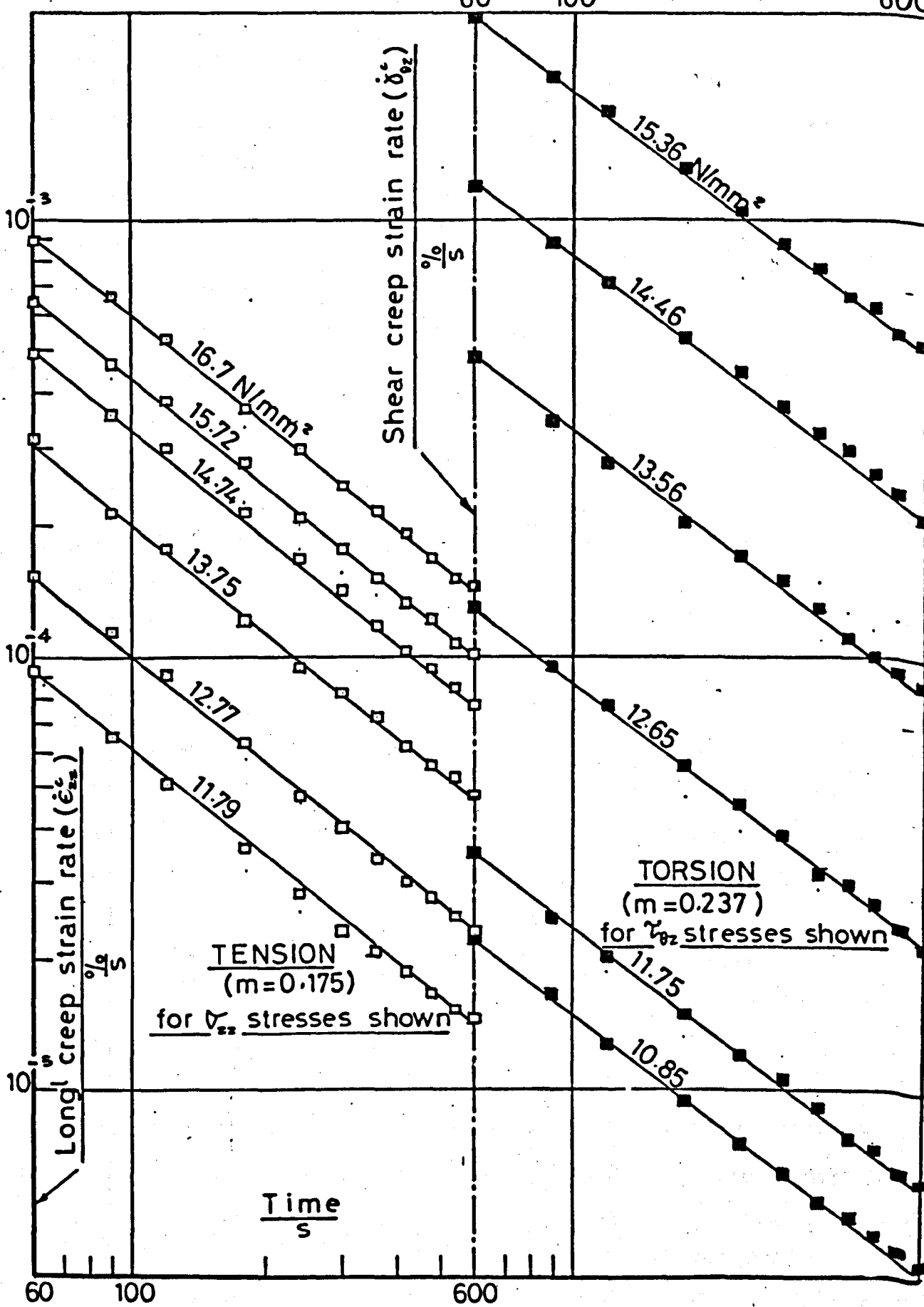


Fig 5.5 10 min  $\epsilon_{zz}, \gamma_{zz}$  transient creep derivative plot for  $\lambda=0.92$

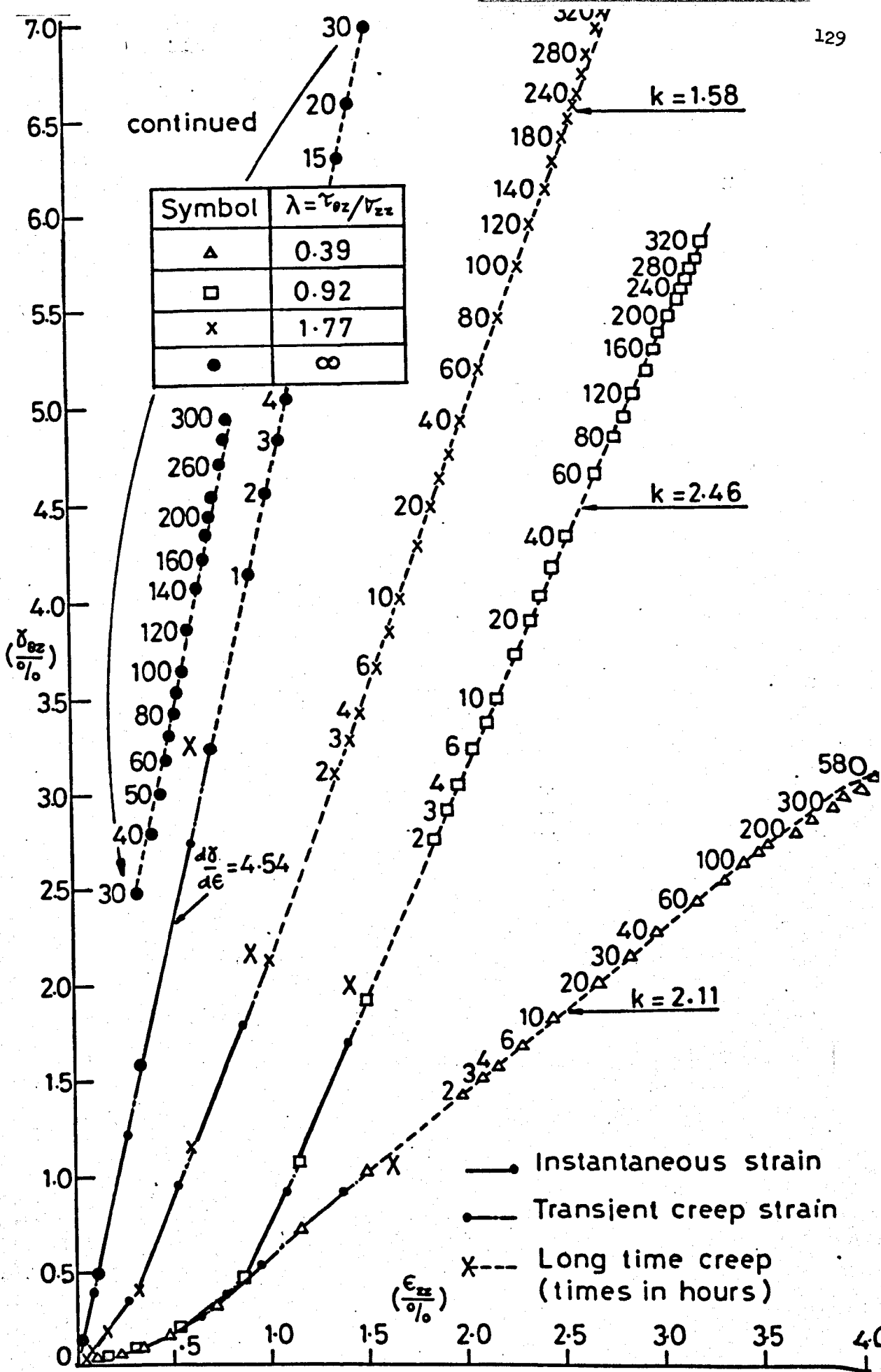


Fig 5.6  $\epsilon_{zz}, \gamma_{\theta z}$  Total strains for constant  $\lambda$  tests.

\*\* KINGSTON POLYTECHNIC 4120 \*\*

&JOB; MAPE/R008/DR; STRAIN RATES;

&OPTIONS;MOTHY;

&FORTRAN; D;

0\* C  
1\* C  
2\*

DIMENSION T(100), DEZZ(100), DGAMMA(100), EZZ(100), GAMMA(100)

```

3*   READ(3,50) GL
4*   READ(3,50) RADN
5*   READ(3,51) M
6*   K=0
7*   1 READ(3,50) SZZ
8*   READ(3,50) XLAM
9*   READ(3,50) C1
10*  READ(3,50) C2
11*  READ(3,51) N
12*  IF(XLAM.NE.9.0) GO TO 6
13*  SSZ=SZZ
14*  SZZ=0.0
15*  GO TO 7
16*  6 SSZ=XLAM*SZZ
17*  7 WRITE(2,100) XLAM,SZZ,SSZ
18*  READ(3,52) (T(I),DEZZ(I),DGAMMA(I), I=1,N)
19*  DO 2 I = 1,N
20*  Z=C1*DEZZ(I)
21*  EZZ(I)=Z/GL
22*  X=C2*DGAMMA(I)
23*  PHI=(RADN*1.116*X*3.14159)/(180.0*GL)
24*  GAMMA(I)=SIN(PHI)/COS(PHI)
25*  L=I-1
26*  IF(L.LT.2) GO TO 2
27*  REZZ=(EZZ(L+1)-EZZ(L-1))/(T(L+1)-T(L-1))
28*  RGAMMA=(GAMMA(L+1)-GAMMA(L-1))/(T(L+1)-T(L-1))
29*  IF(XLAM.NE.9.0,AND,XLAM.NE.0.0) GO TO 4
30*  A=0.0
31*  GO TO 5
32*  4 A=RGAMMA/(REZZ*XLAM)
33*  5 WRITE(2,101) T(L),EZZ(L),GAMMA(L),REZZ,RGAMMA,A
34*  2 CONTINUE
35*  K=K+1
36*  IF(K.LT.M) GO TO 1
37*  STOP
38*  50 FORMAT(6X,F0.0)
39*  51 FORMAT(I0)
40*  52 FORMAT(2X,F0.0,F0.0,F0.0)
41*  100 FORMAT(1H1,30X,30HCREEP STRAINS AND STRAIN RATES,
42*  126H FOR RADIAL LOADING      = ,F5.3//
43*  240X,12HWHERE      = ,F6.2,1X,15HN/MM AND      = ,F6.2,
44*  31X,4HN/MM///)
45*  101 FORMAT(25X,F5.1,5E13.5)
46*  END

```

CREEP STRAINS AND STRAIN RATES FOR RADIAL LOADING  $\lambda = 0.000$ WHERE  $\sigma_{zz} = 36.90 \text{ N/MM}^2$  AND  $\tau_{\theta z} = 0.00 \text{ N/MM}^2$ 

t	$\epsilon_{zz}$	$\delta_{\theta z}$	$\dot{\epsilon}_{zz}$	$\dot{\delta}_{\theta z}$	k
2.0	0.49153E-02	0.00000E+00	0.12836E-02	0.00000E+00	0.00000E+00
3.0	0.60098E-02	0.00000E+00	0.96515E-03	0.00000E+00	0.00000E+00
4.0	0.68456E-02	0.00000E+00	0.73630E-03	0.00000E+00	0.00000E+00
5.0	0.74824E-02	0.00000E+00	0.59700E-03	0.00000E+00	0.00000E+00
6.0	0.80396E-02	0.00000E+00	0.53730E-03	0.00000E+00	0.00000E+00
7.0	0.85570E-02	0.00000E+00	0.48755E-03	0.00000E+00	0.00000E+00
8.0	0.90147E-02	0.00000E+00	0.45770E-03	0.00000E+00	0.00000E+00
9.0	0.94724E-02	0.00000E+00	0.41790E-03	0.00000E+00	0.00000E+00
10.0	0.98505E-02	0.00000E+00	0.30845E-03	0.00000E+00	0.00000E+00
15.0	0.11323E-01	0.00000E+00	0.24278E-03	0.00000E+00	0.00000E+00
20.0	0.12278E-01	0.00000E+00	0.18507E-03	0.00000E+00	0.00000E+00
25.0	0.13174E-01	0.00000E+00	0.19303E-03	0.00000E+00	0.00000E+00
30.0	0.14209E-01	0.00000E+00	0.19502E-03	0.00000E+00	0.00000E+00
35.0	0.15124E-01	0.00000E+00	0.17114E-03	0.00000E+00	0.00000E+00
40.0	0.15920E-01	0.00000E+00	0.14726E-03	0.00000E+00	0.00000E+00
45.0	0.16597E-01	0.00000E+00	0.13333E-03	0.00000E+00	0.00000E+00
50.0	0.17253E-01	0.00000E+00	0.11144E-03	0.00000E+00	0.00000E+00
55.0	0.17711E-01	0.00000E+00	0.91540E-04	0.00000E+00	0.00000E+00
60.0	0.18169E-01	0.00000E+00	0.83580E-04	0.00000E+00	0.00000E+00
65.0	0.18547E-01	0.00000E+00	0.69650E-04	0.00000E+00	0.00000E+00
70.0	0.18865E-01	0.00000E+00	0.57710E-04	0.00000E+00	0.00000E+00
75.0	0.19124E-01	0.00000E+00	0.49750E-04	0.00000E+00	0.00000E+00
80.0	0.19363E-01	0.00000E+00	0.45770E-04	0.00000E+00	0.00000E+00
85.0	0.19582E-01	0.00000E+00	0.41790E-04	0.00000E+00	0.00000E+00
90.0	0.19781E-01	0.00000E+00	0.39800E-04	0.00000E+00	0.00000E+00
95.0	0.19980E-01	0.00000E+00	0.39800E-04	0.00000E+00	0.00000E+00
100.0	0.20179E-01	0.00000E+00	0.35820E-04	0.00000E+00	0.00000E+00
105.0	0.20338E-01	0.00000E+00	0.31840E-04	0.00000E+00	0.00000E+00
110.0	0.20497E-01	0.00000E+00	0.31840E-04	0.00000E+00	0.00000E+00
115.0	0.20656E-01	0.00000E+00	0.39800E-04	0.00000E+00	0.00000E+00
120.0	0.20895E-01	0.00000E+00	0.43780E-04	0.00000E+00	0.00000E+00
125.0	0.21094E-01	0.00000E+00	0.51740E-04	0.00000E+00	0.00000E+00
130.0	0.21412E-01	0.00000E+00	0.59700E-04	0.00000E+00	0.00000E+00
135.0	0.21691E-01	0.00000E+00	0.49750E-04	0.00000E+00	0.00000E+00
140.0	0.21910E-01	0.00000E+00	0.43780E-04	0.00000E+00	0.00000E+00
145.0	0.22129E-01	0.00000E+00	0.47760E-04	0.00000E+00	0.00000E+00
150.0	0.22387E-01	0.00000E+00	0.54393E-04	0.00000E+00	0.00000E+00
160.0	0.22945E-01	0.00000E+00	0.48755E-04	0.00000E+00	0.00000E+00
170.0	0.23363E-01	0.00000E+00	0.48755E-04	0.00000E+00	0.00000E+00
180.0	0.23920E-01	0.00000E+00	0.50745E-04	0.00000E+00	0.00000E+00
190.0	0.24378E-01	0.00000E+00	0.45770E-04	0.00000E+00	0.00000E+00
200.0	0.24835E-01	0.00000E+00	0.51740E-04	0.00000E+00	0.00000E+00
210.0	0.25412E-01	0.00000E+00	0.50745E-04	0.00000E+00	0.00000E+00
220.0	0.25850E-01	0.00000E+00	0.48755E-04	0.00000E+00	0.00000E+00
230.0	0.26387E-01	0.00000E+00	0.48755E-04	0.00000E+00	0.00000E+00
240.0	0.26825E-01	0.00000E+00	0.40795E-04	0.00000E+00	0.00000E+00
250.0	0.27203E-01	0.00000E+00	0.39800E-04	0.00000E+00	0.00000E+00
260.0	0.27621E-01	0.00000E+00	0.36815E-04	0.00000E+00	0.00000E+00
270.0	0.27940E-01	0.00000E+00	0.30845E-04	0.00000E+00	0.00000E+00
280.0	0.28238E-01	0.00000E+00	0.29850E-04	0.00000E+00	0.00000E+00
290.0	0.28537E-01	0.00000E+00	0.28855E-04	0.00000E+00	0.00000E+00
300.0	0.28815E-01	0.00000E+00	0.29850E-04	0.00000E+00	0.00000E+00
310.0	0.29134E-01	0.00000E+00	0.25870E-04	0.00000E+00	0.00000E+00
320.0	0.29333E-01	0.00000E+00	0.22885E-04	0.00000E+00	0.00000E+00

WHERE  $\sigma_{zz} = 25.65 \text{ N/MM}^2$  AND  $\tau_{\theta z} = 9.95 \text{ N/MM}^2$

t	$\epsilon_{zz}$	$\delta_{\theta z}$	$\dot{\epsilon}_{zz}$	$\dot{\delta}_{\theta z}$	k
2.0	0.50745E-02	0.41055E-02	0.12835E-02	0.10597E-02	0.21289E+01
3.0	0.60894E-02	0.50519E-02	0.89550E-03	0.75979E-03	0.21879E+01
4.0	0.68655E-02	0.56251E-02	0.68655E-03	0.57985E-03	0.21779E+01
5.0	0.74625E-02	0.62116E-02	0.59700E-03	0.53986E-03	0.23318E+01
6.0	0.80595E-02	0.67048E-02	0.54725E-03	0.42656E-03	0.20100E+01
7.0	0.85570E-02	0.70647E-02	0.44775E-03	0.35991E-03	0.20728E+01
8.0	0.89550E-02	0.74246E-02	0.37810E-03	0.33325E-03	0.22728E+01
9.0	0.93132E-02	0.77312E-02	0.32830E-03	0.30659E-03	0.23370E+01
10.0	0.96316E-02	0.80378E-02	0.28192E-03	0.23550E-03	0.21541E+01
15.0	0.11005E-01	0.91442E-02	0.23482E-03	0.18929E-03	0.20787E+01
20.0	0.11980E-01	0.99307E-02	0.17910E-03	0.14530E-03	0.20921E+01
25.0	0.12796E-01	0.10597E-01	0.16517E-03	0.13997E-03	0.21853E+01
30.0	0.13631E-01	0.11330E-01	0.15522E-03	0.13998E-03	0.23254E+01
35.0	0.14348E-01	0.11997E-01	0.12935E-03	0.11732E-03	0.23387E+01
40.0	0.14925E-01	0.12504E-01	0.10746E-03	0.89321E-04	0.21434E+01
45.0	0.15422E-01	0.12890E-01	0.10348E-03	0.79990E-04	0.19933E+01
50.0	0.15960E-01	0.13304E-01	0.10945E-03	0.83990E-04	0.19788E+01
55.0	0.16517E-01	0.13730E-01	0.10149E-03	0.77325E-04	0.19647E+01
60.0	0.16975E-01	0.14077E-01	0.81590E-04	0.66660E-04	0.21068E+01
65.0	0.17333E-01	0.14397E-01	0.73630E-04	0.47996E-04	0.16809E+01
70.0	0.17711E-01	0.14557E-01	0.79600E-04	0.45330E-04	0.14685E+01
75.0	0.18129E-01	0.14850E-01	0.67660E-04	0.59996E-04	0.22865E+01
80.0	0.18388E-01	0.15157E-01	0.53730E-04	0.51997E-04	0.24955E+01
85.0	0.18666E-01	0.15370E-01	0.51740E-04	0.43997E-04	0.21928E+01
90.0	0.18905E-01	0.15597E-01	0.49750E-04	0.43998E-04	0.22805E+01
95.0	0.19164E-01	0.15810E-01	0.55720E-04	0.42665E-04	0.19745E+01
100.0	0.19462E-01	0.16023E-01	0.51740E-04	0.38665E-04	0.19270E+01
105.0	0.19681E-01	0.16197E-01	0.41790E-04	0.30666E-04	0.18922E+01
110.0	0.19880E-01	0.16330E-01	0.37810E-04	0.26666E-04	0.18186E+01
115.0	0.20059E-01	0.16463E-01	0.29850E-04	0.22666E-04	0.19581E+01
120.0	0.20179E-01	0.16557E-01	0.21890E-04	0.17333E-04	0.20418E+01
125.0	0.20278E-01	0.16637E-01	0.17910E-04	0.16000E-04	0.23036E+01
130.0	0.20358E-01	0.16717E-01	0.17910E-04	0.12000E-04	0.17277E+01
135.0	0.20457E-01	0.16757E-01	0.15920E-04	0.13333E-04	0.21596E+01
140.0	0.20517E-01	0.16850E-01	0.15920E-04	0.16000E-04	0.25916E+01
145.0	0.20616E-01	0.16917E-01	0.15920E-04	0.12000E-04	0.19437E+01
150.0	0.20676E-01	0.16970E-01	0.17247E-04	0.12444E-04	0.18606E+01
160.0	0.20875E-01	0.17103E-01	0.17910E-04	0.14000E-04	0.20157E+01
170.0	0.21034E-01	0.17250E-01	0.24875E-04	0.19333E-04	0.20042E+01
180.0	0.21373E-01	0.17490E-01	0.30845E-04	0.18667E-04	0.15606E+01
190.0	0.21651E-01	0.17623E-01	0.28855E-04	0.10000E-04	0.89367E+00
200.0	0.21950E-01	0.17690E-01	0.25870E-04	0.13334E-04	0.13291E+00
210.0	0.22169E-01	0.17890E-01	0.21890E-04	0.16667E-04	0.19634E+00
220.0	0.22387E-01	0.18023E-01	0.22385E-04	0.15334E-04	0.17278E+00
230.0	0.22626E-01	0.18197E-01	0.23880E-04	0.14667E-04	0.15838E+00
240.0	0.22865E-01	0.18317E-01	0.16915E-04	0.73336E-05	0.11180E+00
250.0	0.22965E-01	0.18343E-01	0.14925E-04	0.66670E-05	0.11519E+00
260.0	0.23164E-01	0.18450E-01	0.19900E-04	0.13334E-04	0.17278E+00
270.0	0.23363E-01	0.18610E-01	0.22885E-04	0.18668E-04	0.21034E+00
280.0	0.23621E-01	0.18823E-01	0.19900E-04	0.20668E-04	0.26782E+00
290.0	0.23761E-01	0.19023E-01	0.13930E-04	0.16001E-04	0.29620E+00
300.0	0.23900E-01	0.19143E-01	0.13930E-04	0.10667E-04	0.19747E+00
310.0	0.24039E-01	0.19237E-01	0.99500E-05	0.80006E-05	0.20734E+00
320.0	0.24099E-01	0.19303E-01	0.59700E-05	0.60005E-05	0.25918E+00
330.0	0.24159E-01	0.19357E-01	0.79600E-05	0.46670E-05	0.15119E+00
340.0	0.24258E-01	0.19397E-01	0.99500E-05	0.33336E-05	0.86394E+00
350.0	0.24358E-01	0.19423E-01	0.99500E-05	0.60005E-05	0.15551E+00
360.0	0.24457E-01	0.19517E-01	0.89550E-05	0.10001E-04	0.28798E+00
370.0	0.24537E-01	0.19623E-01	0.99500E-05	0.12001E-04	0.31102E+00
380.0	0.24656E-01	0.19757E-01	0.99500E-05	0.10001E-04	0.25919E+00
390.0	0.24736E-01	0.19823E-01	0.89550E-05	0.66673E-05	0.19199E+00
400.0	0.24835E-01	0.19890E-01	0.86233E-05	0.35559E-05	0.10633E+00
420.0	0.24994E-01	0.19930E-01	0.79600E-05	0.26669E-05	0.86396E+00

CREEP STRAINS AND STRAIN RATES FOR RADIAL LOADING  $\lambda = 0.922$ WHERE  $\sigma_{zz} = 16.70 \text{ N/MM}^2$  AND  $\tau_{\theta z} = 15.40 \text{ N/MM}^2$ 

t	$\epsilon_{zz}$	$\delta_{\theta z}$	$\dot{\epsilon}_{zz}$	$\dot{\delta}_{\theta z}$	k
2.0	0.35798E-02	0.84191E-02	0.89496E-03	0.20374E-02	0.24691E+00
3.0	0.42759E-02	0.99573E-02	0.59664E-03	0.14303E-02	0.26000E+00
4.0	0.47731E-02	0.11280E-01	0.47234E-03	0.11335E-02	0.26027E+00
5.0	0.52206E-02	0.12224E-01	0.42262E-03	0.94457E-03	0.24241E+00
6.0	0.56184E-02	0.13169E-01	0.42262E-03	0.90411E-03	0.23203E+00
7.0	0.60658E-02	0.14032E-01	0.32318E-03	0.72870E-03	0.24455E+00
8.0	0.62647E-02	0.14626E-01	0.24860E-03	0.60726E-03	0.26494E+00
9.0	0.65630E-02	0.15247E-01	0.27346E-03	0.58028E-03	0.23015E+00
10.0	0.68116E-02	0.15787E-01	0.21545E-03	0.47235E-03	0.23778E+00
15.0	0.78558E-02	0.18081E-01	0.17899E-03	0.39409E-03	0.23880E+00
20.0	0.86016E-02	0.19728E-01	0.12927E-03	0.30503E-03	0.25592E+00
25.0	0.91485E-02	0.21131E-01	0.11436E-03	0.26726E-03	0.25348E+00
30.0	0.97451E-02	0.22400E-01	0.94468E-04	0.22678E-03	0.26036E+00
35.0	0.10093E-01	0.23399E-01	0.84524E-04	0.17819E-03	0.22865E+00
40.0	0.10590E-01	0.24182E-01	0.84524E-04	0.15660E-03	0.20094E+00
45.0	0.10938E-01	0.24965E-01	0.74580E-04	0.14850E-03	0.21596E+00
50.0	0.11336E-01	0.25667E-01	0.69608E-04	0.15661E-03	0.24402E+00
55.0	0.11634E-01	0.26531E-01	0.64636E-04	0.15391E-03	0.25827E+00
60.0	0.11983E-01	0.27206E-01	0.59664E-04	0.13502E-03	0.24544E+00
65.0	0.12231E-01	0.27881E-01	0.54692E-04	0.11882E-03	0.23563E+00
70.0	0.12529E-01	0.28394E-01	0.44748E-04	0.89118E-04	0.21600E+00
75.0	0.12679E-01	0.28773E-01	0.39776E-04	0.81018E-04	0.22092E+00
80.0	0.12927E-01	0.29205E-01	0.34804E-04	0.75618E-04	0.23565E+00
85.0	0.13027E-01	0.29529E-01	0.19888E-04	0.62116E-04	0.33875E+00
90.0	0.13126E-01	0.29826E-01	0.24860E-04	0.54015E-04	0.23566E+00
95.0	0.13275E-01	0.30069E-01	0.29832E-04	0.45914E-04	0.16693E+00
100.0	0.13424E-01	0.30285E-01	0.19888E-04	0.40513E-04	0.22094E+00
105.0	0.13474E-01	0.30474E-01	0.14916E-04	0.54018E-04	0.39278E+00
110.0	0.13574E-01	0.30825E-01	0.19888E-04	0.59420E-04	0.32405E+00
115.0	0.13673E-01	0.31068E-01	0.24860E-04	0.48617E-04	0.21211E+00
120.0	0.13822E-01	0.31311E-01	0.39776E-04	0.59422E-04	0.16203E+00
125.0	0.14071E-01	0.31662E-01	0.49720E-04	0.72929E-04	0.15909E+00
130.0	0.14319E-01	0.32041E-01	0.34804E-04	0.81034E-04	0.25253E+00
135.0	0.14419E-01	0.32473E-01	0.19888E-04	0.64829E-04	0.35354E+00
140.0	0.14518E-01	0.32689E-01	0.19888E-04	0.48623E-04	0.26516E+00
145.0	0.14618E-01	0.32959E-01	0.19888E-04	0.54026E-04	0.29463E+00
150.0	0.14717E-01	0.33229E-01	0.19888E-04	0.50425E-04	0.27500E+00
160.0	0.14916E-01	0.33715E-01	0.17402E-04	0.44574E-04	0.27781E+00
170.0	0.15065E-01	0.34121E-01	0.14916E-04	0.47277E-04	0.34377E+00
180.0	0.15214E-01	0.34661E-01	0.14916E-04	0.44576E-04	0.32413E+00
190.0	0.15363E-01	0.35012E-01	0.17402E-04	0.43227E-04	0.26942E+00
200.0	0.15562E-01	0.35525E-01	0.22374E-04	0.47281E-04	0.22920E+00
210.0	0.15811E-01	0.35958E-01	0.22374E-04	0.40528E-04	0.19646E+00
220.0	0.16010E-01	0.36336E-01	0.14916E-04	0.40529E-04	0.29470E+00
230.0	0.16109E-01	0.36768E-01	0.14916E-04	0.35126E-04	0.25541E+00
240.0	0.16308E-01	0.37038E-01	0.14916E-04	0.25670E-04	0.18665E+00
250.0	0.16408E-01	0.37282E-01	0.99440E-05	0.22968E-04	0.25051E+00
260.0	0.16507E-01	0.37498E-01	0.99440E-05	0.18915E-04	0.20631E+00
270.0	0.16606E-01	0.37660E-01	0.99440E-05	0.14862E-04	0.16210E+00
280.0	0.16706E-01	0.37795E-01	0.14916E-04	0.18916E-04	0.13754E+00
290.0	0.16905E-01	0.38038E-01	0.14916E-04	0.29725E-04	0.21614E+00
300.0	0.17004E-01	0.38390E-01	0.12430E-04	0.36482E-04	0.31833E+00
310.0	0.17153E-01	0.38768E-01	0.14916E-04	0.47293E-04	0.34388E+00
320.0	0.17303E-01	0.39335E-01	0.19888E-04	0.56753E-04	0.30951E+00

CREEP STRAINS AND STRAIN RATES FOR RADIAL LOADING  $\lambda = 1.772$ WHERE  $\sigma_{zz} = 9.15 \text{ N/MM}^2$  AND  $\tau_{\theta z} = 16.21 \text{ N/MM}^2$ 

t	$\epsilon_{zz}$	$\delta_{\theta z}$	$\dot{\epsilon}_{zz}$	$\dot{\delta}_{\theta z}$	k
2.0	0.34566E-02	0.93096E-02	0.93290E-03	0.26716E-02	0.16161E+00
3.0	0.42717E-02	0.11550E-01	0.68740E-03	0.18216E-02	0.14955E+00
4.0	0.48314E-02	0.12953E-01	0.51555E-03	0.13089E-02	0.14328E+00
5.0	0.53028E-02	0.14167E-01	0.44190E-03	0.11200E-02	0.14304E+00
6.0	0.57152E-02	0.15193E-01	0.37807E-03	0.10256E-02	0.15309E+00
7.0	0.60589E-02	0.16219E-01	0.33388E-03	0.98516E-03	0.16651E+00
8.0	0.63830E-02	0.17163E-01	0.30442E-03	0.90422E-03	0.16762E+00
9.0	0.66678E-02	0.18027E-01	0.27496E-03	0.82327E-03	0.16897E+00
10.0	0.69329E-02	0.18810E-01	0.20458E-03	0.58038E-03	0.16009E+00
15.0	0.78953E-02	0.21509E-01	0.16105E-03	0.46703E-03	0.16365E+00
20.0	0.85434E-02	0.23480E-01	0.11391E-03	0.34558E-03	0.17120E+00
25.0	0.90344E-02	0.24965E-01	0.90344E-04	0.26730E-03	0.16697E+00
30.0	0.94468E-02	0.26153E-01	0.74632E-04	0.22142E-03	0.16743E+00
35.0	0.97807E-02	0.27179E-01	0.61866E-04	0.18092E-03	0.16504E+00
40.0	0.10066E-01	0.27962E-01	0.52046E-04	0.14853E-03	0.16105E+00
45.0	0.10301E-01	0.28664E-01	0.45172E-04	0.12153E-03	0.15182E+00
50.0	0.10517E-01	0.29178E-01	0.40262E-04	0.11883E-03	0.16656E+00
55.0	0.10704E-01	0.29853E-01	0.44190E-04	0.14584E-03	0.18625E+00
60.0	0.10959E-01	0.30636E-01	0.48118E-04	0.14585E-03	0.17105E+00
65.0	0.11185E-01	0.31311E-01	0.40262E-04	0.12425E-03	0.17415E+00
70.0	0.11362E-01	0.31878E-01	0.49100E-04	0.12695E-03	0.14591E+00
75.0	0.11676E-01	0.32581E-01	0.60884E-04	0.14317E-03	0.13270E+00
80.0	0.11971E-01	0.33310E-01	0.58920E-04	0.15668E-03	0.15007E+00
85.0	0.12265E-01	0.34148E-01	0.54010E-04	0.14588E-03	0.15243E+00
90.0	0.12511E-01	0.34769E-01	0.44190E-04	0.12427E-03	0.15871E+00
95.0	0.12707E-01	0.35390E-01	0.43208E-04	0.12968E-03	0.16938E+00
100.0	0.12943E-01	0.36066E-01	0.48118E-04	0.13509E-03	0.15844E+00
105.0	0.13188E-01	0.36741E-01	0.44190E-04	0.12159E-03	0.15528E+00
110.0	0.13385E-01	0.37282E-01	0.36334E-04	0.10268E-03	0.15948E+00
115.0	0.13552E-01	0.37768E-01	0.30442E-04	0.99982E-04	0.18535E+00
120.0	0.13689E-01	0.38282E-01	0.31424E-04	0.10269E-03	0.18441E+00
125.0	0.13866E-01	0.38795E-01	0.34370E-04	0.10539E-03	0.17305E+00
130.0	0.14033E-01	0.39335E-01	0.31424E-04	0.91886E-04	0.16501E+00
135.0	0.14180E-01	0.39714E-01	0.27496E-04	0.72971E-04	0.14977E+00
140.0	0.14308E-01	0.40065E-01	0.22586E-04	0.75676E-04	0.18908E+00
145.0	0.14406E-01	0.40471E-01	0.21604E-04	0.72975E-04	0.19062E+00
150.0	0.14524E-01	0.40795E-01	0.23568E-04	0.72077E-04	0.17259E+00
160.0	0.14759E-01	0.41552E-01	0.22586E-04	0.67575E-04	0.16884E+00
170.0	0.14976E-01	0.42146E-01	0.22586E-04	0.64876E-04	0.16210E+00
180.0	0.15211E-01	0.42849E-01	0.21604E-04	0.62176E-04	0.16241E+00
190.0	0.15408E-01	0.43390E-01	0.18558E-04	0.45958E-04	0.13901E+00
200.0	0.15584E-01	0.43768E-01	0.15221E-04	0.36498E-04	0.13532E+00
210.0	0.15712E-01	0.44120E-01	0.10902E-04	0.32443E-04	0.16950E+00
220.0	0.15800E-01	0.44417E-01	0.10311E-04	0.28389E-04	0.15537E+00
230.0	0.15918E-01	0.44688E-01	0.10311E-04	0.32445E-04	0.17758E+00
240.0	0.16007E-01	0.45066E-01	0.13257E-04	0.45966E-04	0.19567E+00
250.0	0.16183E-01	0.45607E-01	0.16203E-04	0.52728E-04	0.18364E+00
260.0	0.16331E-01	0.46121E-01	0.15221E-04	0.48674E-04	0.18046E+00
270.0	0.16488E-01	0.46580E-01	0.18167E-04	0.52733E-04	0.16381E+00
280.0	0.16694E-01	0.47175E-01	0.20131E-04	0.56792E-04	0.15920E+00
290.0	0.16890E-01	0.47716E-01	0.19149E-04	0.59500E-04	0.17535E+00
300.0	0.17077E-01	0.48365E-01	0.19149E-04	0.56798E-04	0.16739E+00
310.0	0.17273E-01	0.48852E-01	0.15712E-04	0.47334E-04	0.17001E+00
320.0	0.17391E-01	0.49312E-01	0.14239E-04	0.47336E-04	0.18761E+00

CREEP STRAINS AND STRAIN RATES FOR RADIAL LOADING  $\lambda = \infty$

WHERE  $\sigma_{zz} = 0.00 \text{ N/MM}^2$  AND  $\tau_{\theta z} = 19.60 \text{ N/MM}^2$

t	$\epsilon_{zz}$	$\delta_{\theta z}$	$\dot{\epsilon}_{zz}$	$\dot{\delta}_{\theta z}$	k
1.0	0.21408E-02	0.87728E-02	0.10540E-02	0.54402E-02	0.00000E+00
2.0	0.30049E-02	0.12943E-01	0.77087E-03	0.34894E-02	0.00000E+00
3.0	0.36825E-02	0.15758E-01	0.57447E-03	0.24907E-02	0.00000E+00
4.0	0.41539E-02	0.17925E-01	0.45172E-03	0.19702E-02	0.00000E+00
5.0	0.45859E-02	0.19698E-01	0.38789E-03	0.16607E-02	0.00000E+00
6.0	0.49296E-02	0.21246E-01	0.33388E-03	0.15341E-02	0.00000E+00
7.0	0.52537E-02	0.22766E-01	0.29951E-03	0.13794E-02	0.00000E+00
8.0	0.55287E-02	0.24005E-01	0.25041E-03	0.61934E-03	0.00000E+00
9.0	0.57545E-02	0.24005E-01	0.21604E-03	0.10839E-02	0.00000E+00
10.0	0.59607E-02	0.26173E-01	0.18658E-03	0.10700E-02	0.00000E+00
15.0	0.68740E-02	0.30425E-01	0.14534E-03	0.70403E-03	0.00000E+00
20.0	0.74141E-02	0.33213E-01	0.98200E-04	0.50701E-03	0.00000E+00
25.0	0.78560E-02	0.35495E-01	0.80524E-04	0.41694E-03	0.00000E+00
30.0	0.82193E-02	0.37382E-01	0.89362E-04	0.36628E-03	0.00000E+00
35.0	0.87496E-02	0.39158E-01	0.81506E-04	0.30715E-03	0.00000E+00
40.0	0.90344E-02	0.40454E-01	0.54010E-04	0.24237E-03	0.00000E+00
45.0	0.92897E-02	0.41581E-01	0.45172E-04	0.21421E-03	0.00000E+00
50.0	0.94861E-02	0.42596E-01	0.37316E-04	0.18322E-03	0.00000E+00
55.0	0.96629E-02	0.43413E-01	0.33388E-04	0.16350E-03	0.00000E+00
60.0	0.98200E-02	0.44231E-01	0.29460E-04	0.15505E-03	0.00000E+00
65.0	0.99575E-02	0.44964E-01	0.27496E-04	0.13251E-03	0.00000E+00
70.0	0.10095E-01	0.45556E-01	0.25532E-04	0.11842E-03	0.00000E+00
75.0	0.10213E-01	0.46148E-01	0.21604E-04	0.11278E-03	0.00000E+00
80.0	0.10311E-01	0.46684E-01	0.19640E-04	0.10997E-03	0.00000E+00
85.0	0.10409E-01	0.47248E-01	0.19640E-04	0.10716E-03	0.00000E+00
90.0	0.10507E-01	0.47756E-01	0.19640E-04	0.10152E-03	0.00000E+00
95.0	0.10606E-01	0.48263E-01	0.22586E-04	0.10717E-03	0.00000E+00
100.0	0.10733E-01	0.48827E-01	0.21604E-04	0.11563E-03	0.00000E+00
105.0	0.10822E-01	0.49419E-01	0.20622E-04	0.12128E-03	0.00000E+00
110.0	0.10939E-01	0.50040E-01	0.23568E-04	0.11565E-03	0.00000E+00
115.0	0.11057E-01	0.50576E-01	0.21604E-04	0.98729E-04	0.00000E+00
120.0	0.11156E-01	0.51027E-01	0.18658E-04	0.10156E-03	0.00000E+00
125.0	0.11244E-01	0.51591E-01	0.19640E-04	0.11284E-03	0.00000E+00
130.0	0.11352E-01	0.52156E-01	0.22586E-04	0.10721E-03	0.00000E+00
135.0	0.11470E-01	0.52664E-01	0.19640E-04	0.95929E-04	0.00000E+00
140.0	0.11548E-01	0.53115E-01	0.19640E-04	0.90290E-04	0.00000E+00
145.0	0.11666E-01	0.53566E-01	0.21604E-04	0.87473E-04	0.00000E+00
150.0	0.11764E-01	0.53990E-01	0.12439E-04	0.71487E-04	0.00000E+00
160.0	0.11853E-01	0.54639E-01	0.98200E-05	0.63496E-04	0.00000E+00
170.0	0.11961E-01	0.55260E-01	0.10311E-04	0.59267E-04	0.00000E+00
180.0	0.12059E-01	0.55824E-01	0.93290E-05	0.55037E-04	0.00000E+00
190.0	0.12147E-01	0.56360E-01	0.10802E-04	0.52218E-04	0.00000E+00
200.0	0.12275E-01	0.56868E-01	0.11293E-04	0.50809E-04	0.00000E+00
210.0	0.12373E-01	0.57377E-01	0.88380E-05	0.49401E-04	0.00000E+00
220.0	0.12452E-01	0.57856E-01	0.83470E-05	0.47992E-04	0.00000E+00
230.0	0.12540E-01	0.58336E-01	0.83470E-05	0.45171E-04	0.00000E+00
240.0	0.12619E-01	0.58760E-01	0.78560E-05	0.42350E-04	0.00000E+00
250.0	0.12697E-01	0.59183E-01	0.83470E-05	0.43764E-04	0.00000E+00
260.0	0.12786E-01	0.59635E-01	0.88380E-05	0.50826E-04	0.00000E+00
270.0	0.12874E-01	0.60200E-01	0.10311E-04	0.59301E-04	0.00000E+00
280.0	0.12992E-01	0.60821E-01	0.10311E-04	0.55068E-04	0.00000E+00
290.0	0.13080E-01	0.61301E-01	0.93290E-05	0.52248E-04	0.00000E+00
300.0	0.13178E-01	0.61866E-01	0.88380E-05	0.48014E-04	0.00000E+00

# CHAPTER 6

## CHAPTER 6

## RESULTS FOR PRESTRAINED ALUMINIUM

In this Chapter the biaxial creep behaviour of prior strained material is presented. The effect of prestrain on the subsequent loading strains of the chosen stress path ( $\lambda = 0.95$ ) complement the study.

6.1 STRAIN HISTORY PRIOR TO CREEP

The stress-strain paths for the chosen prestrains of Table 2.4 are shown in Figs. 6.1 and 6.2.\* The figures also include the subsequent loading strains for the  $\lambda = 0.95$  stress path. Thus for the tension (OCA) and compression (ODA) stress paths of Fig. 6.1(a) the corresponding stress-strain path plus the tensile stress - 10 min strain component of incremental reloading (AB) are shown in Fig. 6.1(b). The latter components are shown in two composite figures to an enlarged scale, one for prior compression and one for prior tension. The associated shear stress - 10 min strain components for the path AB are shown in Fig. 6.1(c).

The forward (OCA) and reversed (ODA) torsion stress paths of Fig. 6.2(a) are similarly presented in the shear stress-strain paths of Fig. 6.2(b). In this case the shear stress - 10 min strain components of subsequent incremental loading (stress path AB) are added to Fig. 6.2(b) and the associated tensile stress - 10 min. strain components are shown separately in Fig. 6.2(c).

The most obvious effect in Figures 6.1 and 6.2 is the reduction in tensile and shear yield stress as caused by the application of a combined stress system. For example, following a 2% tensile prestrain (Fig. 6.1(b)) the yield stress in tension is  $33 \text{ N/mm}^2$ . The application of the combined stresses of path AB reduces this to below  $16 \text{ N/mm}^2$ . This, of course, is consistent with the concept of a yield locus as indeed are the observed cross-effects in these figures where, for example, increasing amounts of prior tension (OCA in Fig. 6.1(a)) are seen in Fig. 6.1(c) to increase the shear yield stress as well as the tensile yield stress for the stress path AB. A similar cross-effect is seen in Fig. 6.2(c) where increasing amounts of prior positive torsion

\* Figures are given at the end of this Chapter.

(OCA in Fig. 6.2(a)) increase the subsequent tensile yield stress as well as the shear yield stress of path AB. The effect was such that high 'forward' prestrain resulted in subsequent deformation of the same direction that was mostly elastic. Here elastic moduli figures were obtained. A check on these figures was further made from the unloading paths from the prestrains. The differences were attributable to the hysteresis effect between loading and unloading in this material (see Fig. 6.2). The moduli were taken as,

$$E = 68.3 \text{ kN/mm}^2, \quad G = 24.2 \text{ kN/mm}^2.$$

A similar cross-effect was observed in the torsion of path AB following prior compression (Fig. 6.1(c)) and in the tension of path AB following prior negative torsion (Fig. 6.2(c)). However the other stress-strain component of path AB was then in a direction opposite to that of the prestrain and a marked Bauschinger effect was evident. The subsequent deformation then exhibited little or no elastic behaviour and it was thus not possible to obtain elastic moduli. This was particularly noticeable on material of low compressive prestrain during the subsequent tension of AB (Fig. 6.1(b)) and on material of low negative shear strain during the subsequent positive torsion of AB (Fig. 6.2(b)).

Fig. 6.1(c) shows that the shear modulus remains unaffected by prior tension and compression. Similarly Fig. 6.2(c) shows that the tensile modulus remains unaffected by prior positive and negative torsion.

## 6.2 CREEP

The tensile ( $\epsilon_{zz}$ ) and shear ( $\delta_{\theta z}$ ) creep curves of the stresses  $\tau_{zz} = 16 \text{ N/mm}^2$  and  $\tau_{\theta z} = 15.2 \text{ N/mm}^2$  and for the prior strain histories of Figs. 6.1 and 6.2 are shown plotted in Figs. 6.3 and 6.4 from the first three columns of Programme 6.1.\*

### 6.2.1 Prior Tension and Compression

Figs. 6.3A and 6.3B show similar trends on the effect of prior plastic strain on creep strength as was its effect on the yield strength of Fig. 6.1. For a creep time of 250 hours (Fig. 6.3A) the tensile creep resistance is increasingly improved by increasing amounts of tensile and compressive prestrain. For a fixed prestrain value, however,

\* Programmes are given at the end of this Chapter.

the material exhibited more tensile creep after compressive prestraining than after tensile prestraining. The Bauschinger effect is therefore evident in creep and in Fig. 6.3B, for a creep time of 250 hours the cross-effect is also evident. That is, the shear creep resistance is increasingly improved by increasing amounts of tensile and compressive prestrain. For a fixed prestrain value however the material exhibited more shear creep after compressive prestraining than after tensile prestraining.

In comparing the creep curves of annealed and prestrained material in Figs. 6.3A and 6.3B a low prestrain is seen to have little or no effect in improving creep resistance. Indeed a small compressive prestrain yields more  $\epsilon_{22}$  and  $\delta_{\theta 2}$  primary creep strain than for the annealed metal. The secondary creep rates are however little different for the two materials.

Where an improvement in creep resistance is observed (i.e. for prestrains  $\gt \pm 2\%$ ) both the amount of primary creep strain and the secondary creep rate are reduced. For prestrains  $\gt \pm 4\%$  little or no primary creep is evident with secondary creep forming the larger part of the subsequent deformation.

### 6.2.2 Prior Positive and Negative Torsion

The  $\delta_{\theta 2}, \epsilon_{22}$  creep curves following prestrains of this type are shown in Figs. 6.4A and 6.4B respectively and the trends are similar to those for prior tension and compression.

The Bauschinger effect is again evident in Fig. 6.4A where a prior plastic shear strain of opposite direction to the subsequent creep shear strain is less effective in reducing the amount of  $\delta_{\theta 2}$  creep strain than is a prior plastic strain of the same direction. Fig. 6.4B shows the effect of prior plastic shear strain on the axial  $\epsilon_{22}$  creep component. Typically after 250 hours of creep a cross-effect is evident where increasing amounts of forward and reversed shear prestrain are seen to increasingly improve the tensile creep resistance. For a fixed prestrain value a forward prestrain is more effective in this respect.

In comparing the creep curves of prior strained material with those for annealed material little, if any, reduction in both the amount of primary creep strain and secondary creep rate is seen for prior equivalent strains of  $\pm 2\%$  in Fig. 6.4A and for  $-2\%$  in Fig. 6.4B. Prestrains greater than these amounts are seen to reduce both the amount of primary creep strain and the secondary creep rate.

### 6.2.3 General Comments on the Creep of Prior Strained Material

The creep behaviour of Figs. 6.3 and 6.4 can be simply understood from the prior strain histories of Figs. 6.1 and 6.2 respectively. In general, if a prestrain serves to eliminate both the tensile and shear plastic strain components of subsequent combined loading then correspondingly there will be little ensuing creep strain. In tests of this type the prestrain that is most effective in providing biaxial creep resistance is the one that avoids a Bauschinger effect and fully exploits a beneficial cross-effect. A positive prestrain (either tension or positive torsion) does this when the creep stress system is combined tension and positive torsion.

### 6.3 SECONDARY CREEP RATES

Fig. 6.5 correlates the secondary creep rates of prior strained material with the amount of prior strain. In Fig. 6.5(a) the secondary shear creep rates ( $\dot{\gamma}_{\theta z}$ ) of Figs. 6.3B and 6.4A are plotted logarithmically to a base of prior equivalent plastic strain (for tension and compression  $\int d\bar{\epsilon}_M^p = \int d\epsilon_{zz}^p$  and for forward and reversed torsion  $\int d\bar{\epsilon}_M^p = \int d\gamma_{\theta z}^p/\sqrt{3}$ ). Fig. 6.5(b) is a similar plot for the secondary axial creep rates ( $\dot{\epsilon}_{zz}$ ) of Figs. 6.3A and 6.4B. The ordinates of Figs. 6.5(a) and 6.5(b) are combined in Fig. 6.5(c) with an equivalent secondary creep rate defined from equation (3.9) as

$$\dot{\bar{\epsilon}}_M = \sqrt{(\dot{\epsilon}_{zz})^2 + (\dot{\gamma}_{\theta z})^2/3} \quad (6.1)$$

This provides a satisfactory correlation for the secondary creep rates of material prior strained in tension, compression, positive and negative torsion. The usefulness of Fig. 6.5(c) would lie in its ability to correlate the secondary creep rates of material with a complex prior strain history.

The horizontal lines attached to the symbols in Fig. 6.5(c) indicate the extent of the shift in each point when the prior equivalent plastic strain contains both the amount of prestrain and the subsequent loading strain. It is interesting to note that the curve is then approximately symmetrical about the  $\dot{\bar{\epsilon}}_M$  axis. A test performed for a tensile prestrain of 6.7% indicates the shape of the curve for higher prior strains.

It should be noted firstly that a correlation of this type

assumes a von Mises material and secondly that the tensile and shear prestrains were performed at slightly different strain rates (Table 2.4).

#### 6.4 INCREMENTAL LOADING CREEP

In common with loading on annealed and extruded material loading to the creep test stresses ( $\tau_{\theta z} = 15.2$ ,  $\tau_{zz} = 16 \text{ N/mm}^2$ ) on prestrained material was again performed incrementally with a time of 10 min allowed between successive increments. The question of whether creep occurred during this period follows directly from the observations made in Section 6.1 regarding the modes of deformation following a prestrain. Then, whenever the instantaneous strain contained a plastic strain component creep deformation immediately followed. If on the other hand the instantaneous strain was entirely elastic then no creep was evident.

Where it occurred the following observations were made regarding the nature of this creep strain. The basis of the observation is the fact that annealed material displayed parabolic  $\epsilon_{zz}$  and  $\gamma_{\theta z}$  creep throughout combined loading (Chapter 4).

##### 6.4.1 Prior Tension and Compression

For a low tensile prestrain (2%) both  $\epsilon_{zz}$  and  $\gamma_{\theta z}$  creep components were eliminated at the initial stages of loading. With increased load a sudden change from instantaneous strain to creep strain was evident in both  $\epsilon_{zz}$  and  $\gamma_{\theta z}$  and this change became more gradual (as for annealed material) as the loading reached completion. With increasing tensile prestrain (3- 6.7%) no subsequent  $\epsilon_{zz}$  creep was evident and only for shear stresses greater than  $11 \text{ N/mm}^2$  was any  $\gamma_{\theta z}$  creep noticeable. This again showed the sudden change between strain components and a linear dependence of  $\gamma_{\theta z}$  creep with time ( $\gamma = \gamma_0 + bt$ ).

For a low compressive prestrain (-2%) the subsequent  $\epsilon_{zz}$  creep was always evident in parabolic form. The  $\gamma_{\theta z}$  creep was first observed in linear form, for  $\tau_{\theta z} > 7 \text{ N/mm}^2$ . With increasing compressive prestrain (-3, -4%) the  $\epsilon_{zz}$  creep was initially linear and for  $\tau_{zz} > 10 \text{ N/mm}^2$  it became parabolic and  $\gamma_{\theta z}$  first became evident in linear form. With increased stress the  $\gamma_{\theta z}$  creep also became parabolic.

#### 6.4.2 Prior Positive and Negative Torsion

Low positive shear prestrained material ( $\int d\epsilon_M^p = 2\%$ ) showed a subsequent incremental creep behaviour similar to that for a material of low tensile prestrain. Initially both  $\epsilon_{zz}$  and  $\delta_{\theta z}$  creep components were eliminated. Then for  $6 < \tau_{\theta z} < 12 \text{ N/mm}^2$  the creep components displayed a linear dependence on time and thereafter a parabolic dependence. For higher positive shear prestrain ( $\int d\epsilon_M^p = 3, 4\%$ ) no subsequent  $\delta_{\theta z}$  creep was evident and only for  $\tau_{zz} > 13 \text{ N/mm}^2$  did a linear  $\epsilon_{zz}$  component appear.

Low negative shear prestrains ( $\int d\epsilon_M^p < -2.7\%$ ) displayed subsequent  $\epsilon_{zz}, \delta_{\theta z}$  parabolic creep throughout loading. With increasing negative shear prestrain ( $\int d\epsilon_M^p = -3, -4\%$ )  $\delta_{\theta z}$  creep was initially linear and finally parabolic during loading.  $\epsilon_{zz}$  creep appeared in the same way but none was evident for  $\tau_{zz} < 11 \text{ N/mm}^2$ .

#### 6.4.3 Creep Rates and Time Exponents

A study of the parabolic type creep observed at higher stresses in material of low initial prestrain is made in the derivative plots of Figs. 6.6 and 6.7. It should be noted that the shear ( $\dot{\delta}_{\theta z}^c$ ) and longitudinal ( $\dot{\epsilon}_{zz}^c$ ) creep rates of like symbols in these figures occurred simultaneously throughout the creep period.

Fig. 6.6 shows the effect of prior strain on  $\dot{\delta}_{\theta z}^c$  for a constant shear stress of  $14.25 \text{ N/mm}^2$ . To aid comparison various degrees of prior tension and compression are shown together with the plot for annealed material. Similarly prior forward and reversed torsion are shown together but on a displaced time axis. For any given time Fig. 6.6 shows that increasing amounts of prior compression, positive and negative torsion are increasingly effective in reducing the  $\dot{\delta}_{\theta z}^c$  of annealed material. However, in general for a given prior equivalent strain tension and positive torsion are more effective than compression and negative torsion in this respect.

The effect of prior strain on the  $\dot{\delta}_{\theta z}^c$  time exponent ( $m$ ) is shown in the tables of Fig. 6.6. The most obvious effect is the considerable lowering of the  $m$  value as caused by prior torsion. Reversed torsion is seen to reduce  $m$  to a negative value. The  $m$  value for prior tension and compression is little different from the  $m$  value of annealed material.

Fig. 6.7 shows the effect of prior strain on  $\dot{\epsilon}_{zz}^c$  for a constant tensile stress of  $15 \text{ N/mm}^2$ . For any given time the figure shows that increasing prior compression and positive torsion are increasingly effective in reducing  $\dot{\epsilon}_{zz}^c$ . However, for any given prior equivalent strain tension and positive torsion are more effective than compression and negative torsion in this respect. All prior tension, compression and positive torsion reduce the  $\dot{\epsilon}_{zz}^c$  of annealed material.

The effect of prior strain on the  $\epsilon_{zz}^c$  time exponent ( $m$ ) is shown in the tables of Fig. 6.7. All prior strain is seen to reduce the  $m$  value of annealed material. Prior torsion is the more effective in reducing  $m$  to a negative value.

## 6.5 THE $k$ FACTOR

For each of the chosen prestrains the last column of Programme 6.1 shows the  $k$  value of equation (3.21) at initially 1 then 5 and finally 10 hourly intervals for 300-400 hours of creep. In addition to the annealed material ( $\int d\epsilon_M^p = 0$ ) there is also evidence of a constant  $k$  value for the creep of lower prestrained material. This is more clearly seen in the total strain  $\delta_{\theta z}$  vs  $\epsilon_{zz}$  plots of Figs. 6.8 and 6.9. In Fig. 6.8 the instantaneous loading strains and their associated transient creep strains are shown up to point 'X'. Where the scale of this figure permits, the ensuing 'long time' creep strains of columns 1 and 2 in Programme 6.1 are added to point 'X' for the times indicated. To allow the creep strains to be added in this way for all tests Fig. 6.9 shows the same plot but to a condensed scale.

### 6.5.1 Instantaneous and Transient Creep Strains

In common with the tests on annealed material (Fig. 4.4 Chapter 4) Fig. 6.8 displays a  $d\delta/d\epsilon$  vector whose direction is independent of stress level when  $\int d\epsilon_M^p = 0$ . For prestrained material however where significant plastic strain occurred upon reloading, there is a considerable departure from this direction. Furthermore the direction of the vector is seen to be stress dependent for a prestrained material and a common feature is that with increasing stress the vector rotates toward the vector direction of annealed material. For any particular stress increment, i.e. the region between successive symbols in Fig. 6.8, the associated instantaneous and transient creep strain components are seen to follow the same direction.

For prior tension the  $\frac{d\delta}{d\epsilon}$  value is seen to be initially higher than that for annealed material (2.33). On the other hand prior compressed material displays a lower value. This is undoubtedly due to the axial strengthening and weakening of the material as caused by prior tension and compression respectively.

For prior positive and negative torsion the trends are not so clearly defined, with the  $\frac{d\delta}{d\epsilon}$  values being generally less than the "annealed" value. Such behaviour can be explained in terms of a complex interaction between either weakening and strengthening in shear and an associated cross-effect in tension. Thus for a prior reversed torsion the subsequent weakening in both positive torsion and tension (see Fig. 6.2(c)) resulted in a low  $\frac{d\delta}{d\epsilon}$  value.

### 6.5.2 Creep

Fig. 6.9 shows that the  $\frac{d\delta}{d\epsilon}$  vector of the 'X' stress level need not remain fixed in direction with accumulating creep strain. Only for annealed and highly prestrained material did the vector remain fixed in direction. A rotation of this direction is seen to occur during creep in lower prestrained material. Where such a rotation appears Fig. 6.9 shows that it may occur relatively quickly, e.g. during the first 5 hours for 2% compression or it may take longer, e.g. during the first 250 hours for 3% reversed torsion (Fig. 6.8). There thus appears to be no relationship between the time of such a rotation and the primary and secondary creep stages of Figs. 6.3 and 6.4.

The question of whether or not a rotation occurs would seem to depend upon the relative magnitudes of the loading strain, the creep strain and the prestrain. For lower prestrains the subsequent loading strains of Figs. 6.1 and 6.2 are seen to be high and a rotation is evident in the  $\frac{d\delta}{d\epsilon}$  vectors of Fig. 6.8. This is seen to continue during creep in Fig. 6.9. On the other hand for larger prestrains, where the subsequent loading strains are mostly elastic, no such rotation was evident. It is likely of course that insufficient time was allowed during the creep of highly prior strained material for enough creep strain to accumulate and so begin to nullify the prestrain effect. It is probably at this point that a rotation starts.

After the rotations in Fig. 6.9 the  $\frac{\delta}{\epsilon}$  vector is then seen to settle at a constant value which approximates to that of the annealed material. In comparing the indicated k values there is some evidence that these depend upon the magnitude and nature of the prior strain. In this respect a prestrain has a lasting effect in creep.

## 6.6 THEORETICAL PREDICTIONS OF ANISOTROPY

To describe theoretically the observations on prestrained material as outlined in this Chapter is no easy matter. Considering the strain ratio ( $\frac{d\delta}{d\epsilon}$  or  $\frac{\delta}{\epsilon}$ ) on material where rotations occurred, a theory is required that could, for a fixed stress ratio, predict the  $\frac{d\delta}{d\epsilon}$  rotation of Fig. 6.8, its continuation and final constant  $\frac{\delta}{\epsilon}$  ratio during creep in Fig. 6.9.

### 6.6.1 Creep

In considering the theoretical  $\frac{\delta_{02}}{\epsilon_{22}}$  ratios in Section 3.4 of Chapter 3 it is clear that none of these anisotropic theories in their existing form is readily amenable to this requirement for creep.

Bailey's theory of equation (3.36) would not be suitable in its intended form. While the theory could account for any steady  $\frac{\delta_{02}}{\epsilon_{22}}$  ratio with  $n$  and  $m$  as fixed constants, a  $\frac{\delta_{02}}{\epsilon_{22}}$  rotation could only be described from this theory if  $n$  and  $m$  were made functions of the prior strain history and subsequent creep strain. The theory would be best made to describe the steady  $k$  values of Fig. 6.9 with the  $n-2m$  constants of Table 6.1.

TABLE 6.1 Constants in the Bailey Equation (3.36)

Prior Strain	$\int d\bar{\epsilon}_m^p, \%$	$n - 2m$
± Tension	+ 2	5.480
	- 2	0.172
Annealed	0	2.680
± Torsion	- 2	-4.936
	- 2.7	3.435
	+ 2	-0.207

Berman and Pai's theory of equations (3.37) and (3.38) predict a  $k$  value of 3 and 4 respectively for all stress ratios. The theory therefore assumes either a von Mises ( $k = 3$ ) or Tresca ( $k = 4$ ) material and while some of the  $k$  values in Fig. 6.9 approximate to  $k = 3$  the theory cannot account for the overall creep behaviour of prestrained material.

Hu's theory of equation (3.39) has been applied to the test for 2% prior compression in Programme 6.2. The constants F, G, H and L have been taken as those for annealed material (see Section 4.4 Chapter 4) and the 1 axis of anisotropy has been assumed to rotate in phase with the angle of twist during creep ( $\alpha = \phi = \frac{\theta}{I}$ ). A comparison of the experimentally measured k values with those predicted by Hu's theory for the creep times shown clearly indicates that

- (1) neither the rotation or the steady k value of 3.36 is predicted by the theory for the  $\alpha = \phi$  assumption.
- (2) little variation in the k value occurs with the chosen constants for large  $\alpha$ .

The theory is therefore clearly unsuitable when applied in this way to a prestrained material.

#### 6.6.2 Loading Strain

A theoretical solution to the  $\frac{d\delta_{12}}{d\epsilon_{22}}$  vector behaviour of Fig. 6.9 can be attempted from the general anisotropy theories of Section 3.5 in Chapter 3. For the prior strain histories of interest here the subsequent plastic flow vectors  $\frac{d\delta_{12}^p}{d\epsilon_{22}^p}$  of combined loading may be theoretically predicted in the following way:

- (1) Edelman and Drucker

For zero prestrain both equations (3.46) and (3.47) reduce to

$$\frac{d\delta^p}{d\epsilon^p} = \frac{A\sigma_{11} + B\sigma_{12}}{C\sigma_{11} + A\sigma_{12}} = \frac{A + B\lambda}{C + A\lambda} \quad (6.2)$$

This equation should describe the plastic flow in annealed material—thus comparing equations (6.2) and (4.7) it must follow that  $A = 0$  and  $B/C = 2.6$ . Then for an annealed material with prior tension or compression equation (3.46) becomes

$$\frac{d\delta^p}{d\epsilon^p} = \frac{2.6\lambda}{1 - \frac{3m\epsilon_{11}^p}{2C\sigma_{11}}} \quad (6.3)$$

and for prior positive or negative torsion equation (3.47) becomes

$$\frac{d\delta^p}{d\epsilon^p} = 2.6\lambda - \frac{m\gamma_0^p}{2C\sigma_{11}} \quad (6.4)$$

## (2) Yoshimura

Following the same reasoning as for the previous theory we have here that  $A' = 0$ , and  $B'/C' = 2.6$ . Then for prior tension or compression equation (3.50) becomes

$$\frac{d\delta^p}{d\epsilon^p} = \frac{2.6\lambda}{1 - \frac{9m'\epsilon_{II}^p}{C'\sigma_{II}}} \quad (6.5)$$

and for prior positive or negative torsion equation (3.51) becomes,

$$\frac{d\delta^p}{d\epsilon^p} = 2.6\lambda - \frac{9m'\gamma_0^p}{C'\sigma_{II}} \quad (6.6)$$

## (3) Williams and Svensson

A point to note in equations (3.53) and (3.54) is that for zero prestrain both equations reduce to  $\frac{d\delta^p}{d\epsilon^p} = 3\lambda$ . The theory therefore describes the anisotropy of deformation due to a prior strain on an initially von Mises material. It would seem a limitation of the theory that initial material anisotropy cannot be described and it thus remains uncertain how the constants  $A_0$ ,  $L_{2323}$ ,  $L_{3333}$  and  $m$  are defined for a prior strain on a  $\frac{d\delta^p}{d\epsilon^p} = 2.6\lambda$  material.

For the same type of prestrain both sets of equations (6.3), (6.5) and (6.4), (6.6) in the Edelman and Drucker and Yoshimura theories are seen to be of the same form. A comparison between the theoretical predictions of equations (6.3) and (6.5) and the experimentally measured  $\frac{d\delta^p}{d\epsilon^p}$  values of Fig. 6.8 for 2% prior compression is made in Table 6.2 for the stress levels indicated. Both theories have been made to fit the first experimental  $\frac{d\delta^p}{d\epsilon^p}$  value and therefore reduce to the same equation for the given  $\lambda$  and  $\epsilon_{II}^p$  of this test. That is,

$$\frac{d\delta^p}{d\epsilon^p} = \frac{2.262}{1 + \left(\frac{126.3}{\sigma_{II}}\right)} \quad (6.7)$$

Table 6.2  $\frac{d\delta^p}{d\epsilon^p}$  Comparison for 2% Prior Compression

$\sigma_{II}$ , N/mm <sup>2</sup>	12.09	13.10	14.10	15.11	16.12
$\frac{d\delta^p}{d\epsilon^p}$ , (Fig. 6.8)	0.198	0.252	0.305	0.513	0.588
$\frac{d\delta^p}{d\epsilon^p}$ , Eqn (6.7)	0.198	0.213	0.227	0.242	0.256

The Table shows that the theories at least give a qualitative representation of a rotating,  $d\delta^p/de^p$  vector for a prior compressed material. The  $d\delta^p/de^p$  behaviour of a material with 2% prior tension in Fig. 6.8 would be similarly described by equations (6.3) and (6.5).

The theories would appear to fail for prior reversed torsion since neither equation (6.4) nor (6.6) could describe the experimental  $d\delta^p/de^p$  values in Fig. 6.8 for a prior -2% equivalent shear strain ( $\delta_0^p = 3.45\%$ ). With  $m$  and  $m'$  as positive constants then  $d\delta^p/de^p > 2.6\lambda$  from each theory. The experimental trend, however, was such that  $d\delta^p/de^p < 2.6\lambda$  for all stress levels. With  $m$  and  $m'$  as negative constants the observed behaviour would be satisfactorily described, but it is doubtful for either theory and with  $m$  positive when describing prior compression that it should then be taken as negative in order to describe prior reversed torsion. It is an interesting point however that the Bauschinger term in each theory can be made to account for the observed cross-effects in this material merely by changing its sign.

If for a fixed prestrain value it were assumed that  $m/C$  in the Edelman and Drucker theory equalled  $m'/C'$  in the Yoshimura theory then for the prestrains described by equations (6.3) - (6.6) the former theory would always predict  $d\delta^p/de^p$  values closest to the  $2.6\lambda$  value for each stress level. The rotation is therefore less severe in the Edelman and Drucker theory.

### 6.6.3 Anisotropic Theory for Creep

Following Section (2) of Appendix I the anisotropic theories of time independent plastic flow may be extended to creep simply by rewriting the plastic strain increments as creep strain rates. A suitable time function  $\phi(t)$  should also be included. Then, for example, equation (3.46) would become,\*

$$\frac{\dot{\gamma}_{02}}{\dot{\epsilon}_{22}} = \frac{\left\{ A(\sigma_{11} - \frac{3m\epsilon_{11}^p}{2}) + B\sigma_{12} \right\} \phi(t)}{\left\{ C(\sigma_{11} - \frac{3m\epsilon_{11}^p}{2}) + A\sigma_{12} \right\} \phi(t)} \quad (6.8)$$

---

\* or from  $\dot{\epsilon}_{ij} = \frac{\partial f}{\partial \sigma_{ij}} \dot{\lambda} \phi(t)$

where  $f = \frac{1}{2} C_{ijkl} (\sigma'_{ij} - m\epsilon'_{ij}) (\sigma'_{kl} - m\epsilon'_{kl}) \phi(t)$

It is normally assumed that  $\phi(t)$  is the same function for each component creep curve of a multiaxial stress system. The creep rate ratios and the corresponding plastic strain increment ratio would then be identical expressions.

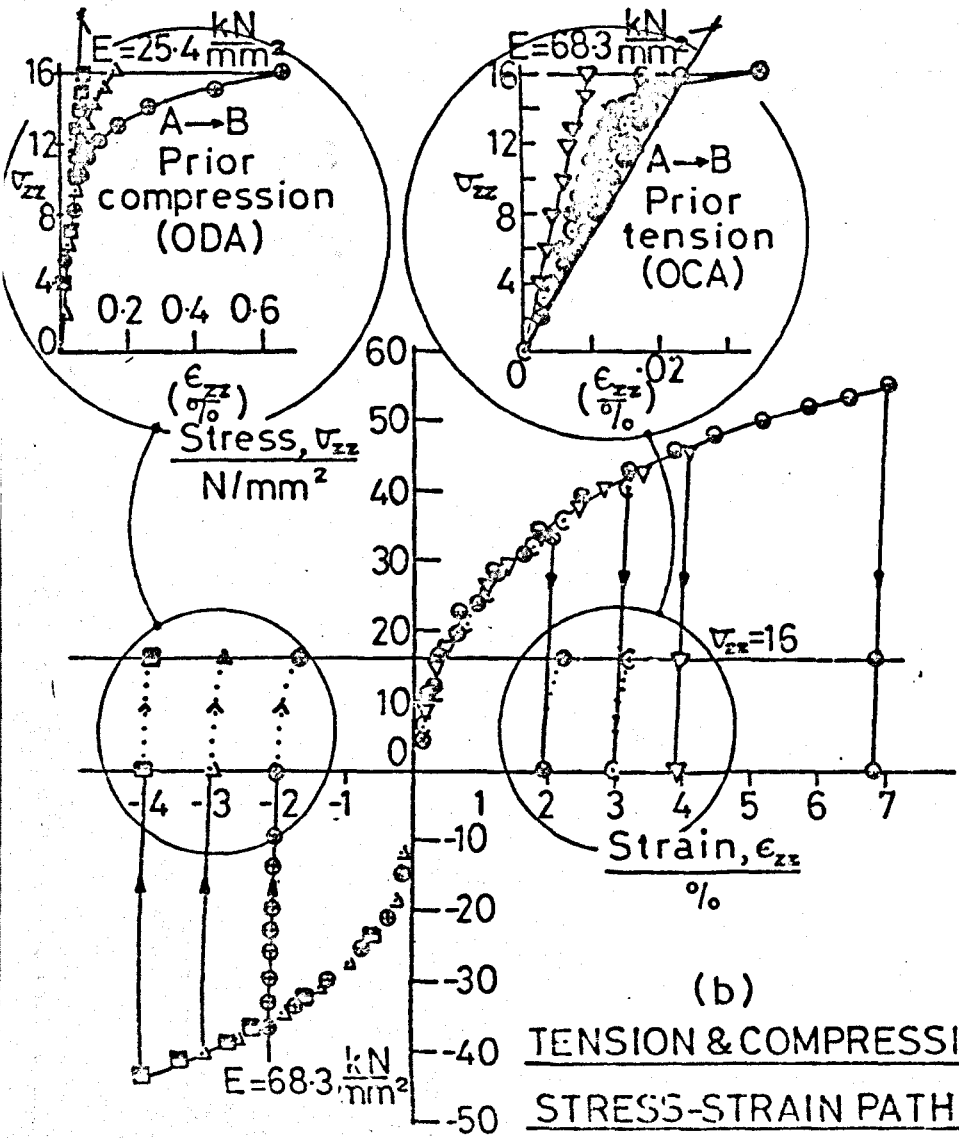
In this work with  $\int d\epsilon_m^p = -2\%$  prior torsion and compression a logarithmic plot of  $\dot{\gamma}_{\theta 2}$  vs  $t$  and  $\dot{\epsilon}_{22}$  vs  $t$  from Programme 6.1 showed  $\phi(t) = t^{-0.765}$  for primary creep ( $\phi(t) = 1$  for secondary creep).

Since it has been shown in Chapter 4 that  $\frac{d\dot{\gamma}_{\theta 2}^p}{d\epsilon_{22}^p} = \frac{\dot{\gamma}_{\theta 2}}{\dot{\epsilon}_{22}} = 2.6\lambda$

for annealed material we can apply the reasoning of paragraph 6.6.2 to creep and arrive at the same expressions (6.3) - (6.6) for the  $\dot{\gamma}_{\theta 2}/\dot{\epsilon}_{22}$  ratio of prestrained material. For example equation (6.3) would become

$$\frac{\dot{\gamma}_{\theta 2}}{\dot{\epsilon}_{22}} = \frac{2.6\lambda}{1 - \frac{3\mu_1 \epsilon_{22}^p}{2C V_{22}}} \quad (6.9)$$

While these equations describe the steady  $\dot{\gamma}/\dot{\epsilon}$  values of Fig. 6.9 (with  $m$  a negative constant) it is difficult to see how the rotations are accounted for with  $V_{22}$  a constant in creep. If the stress ratio  $\lambda$  and stress  $V_{22}$  were corrected for current creep deformation from equations (20) and (21) of Appendix II then this would explain some change in the  $\dot{\gamma}/\dot{\epsilon}$  ratio during creep.



(c) SHEAR STRESS-STRAIN PATH FOR A → B ( $\lambda = 0.95$ )

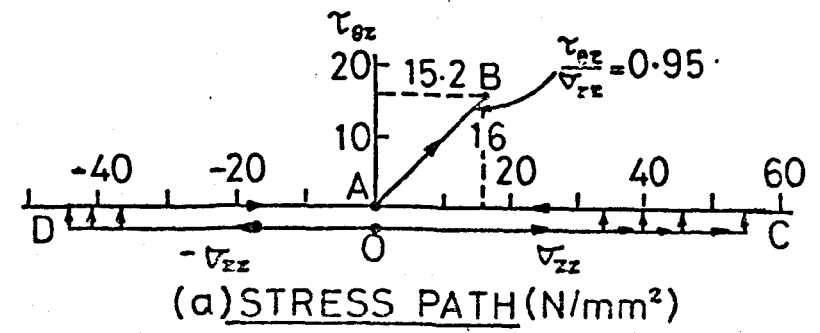
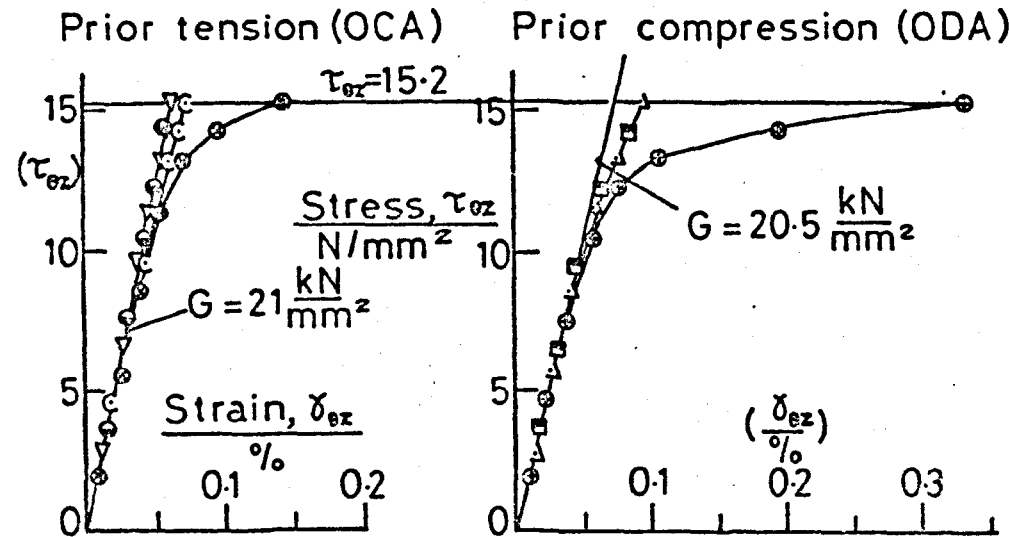


Fig. 6.1

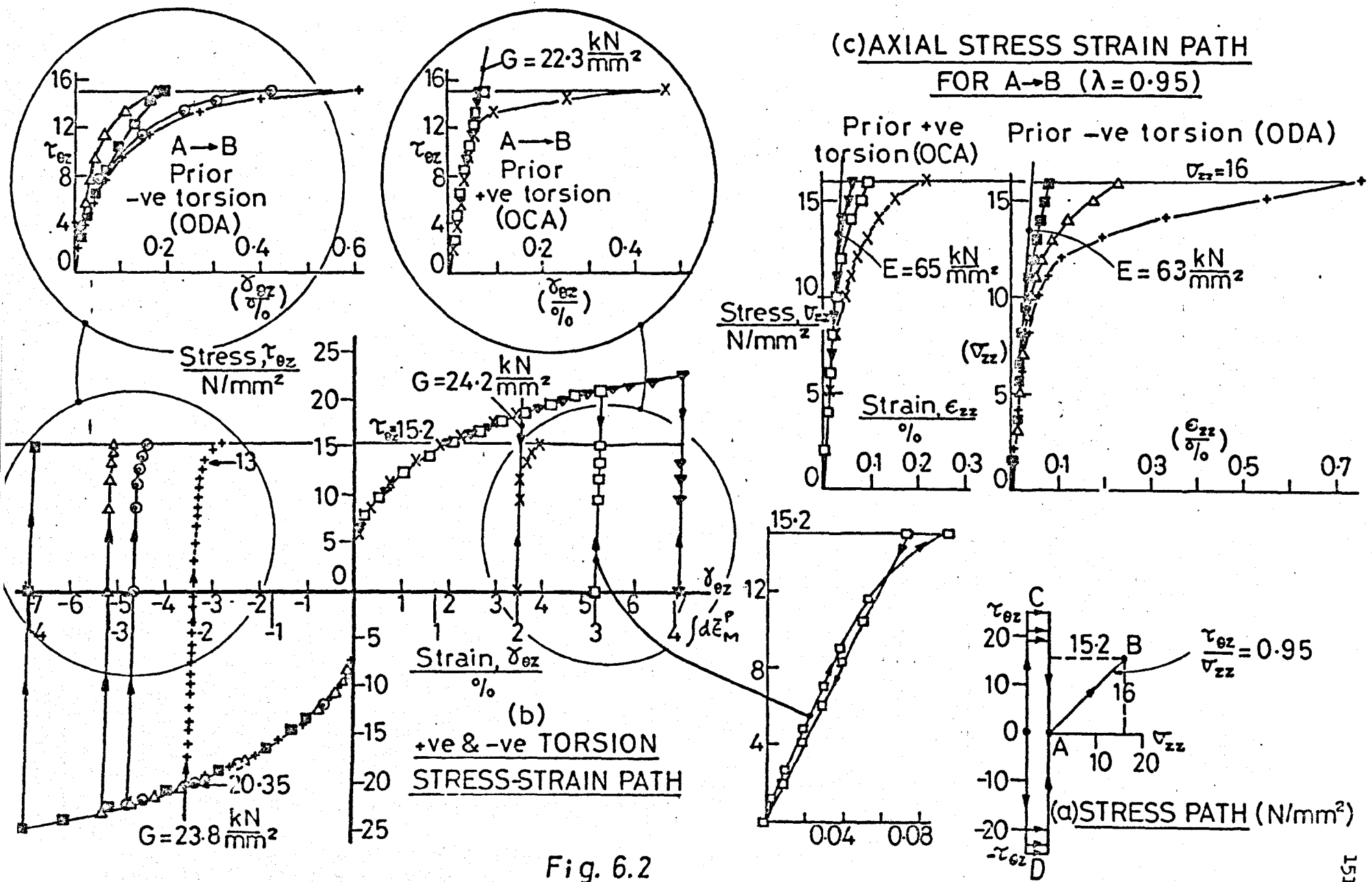


Fig. 6.2

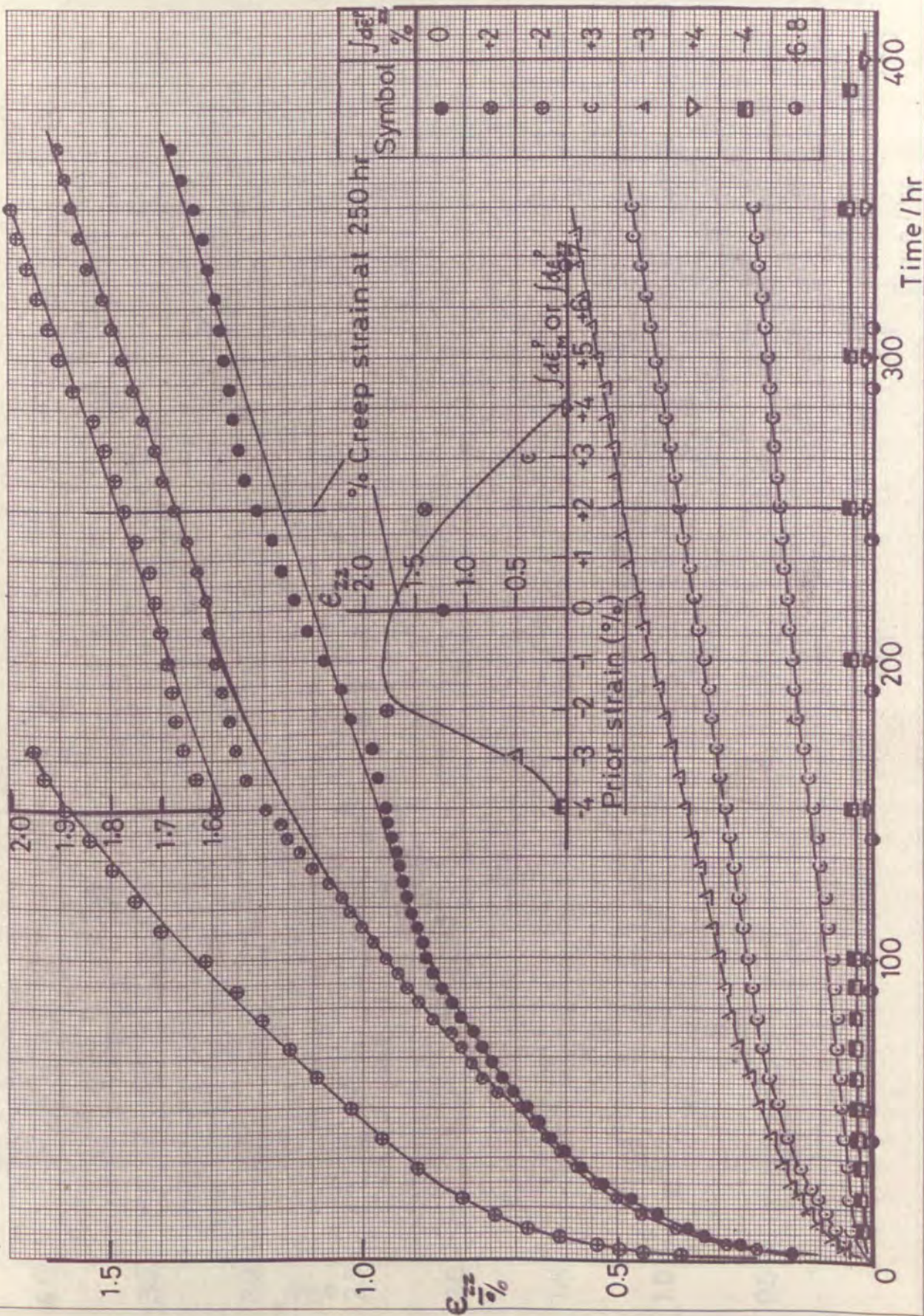


Fig. 6.3A  $\epsilon_{zz}$  Creep component for prior plastic axial strain ( $J_{def}$ )

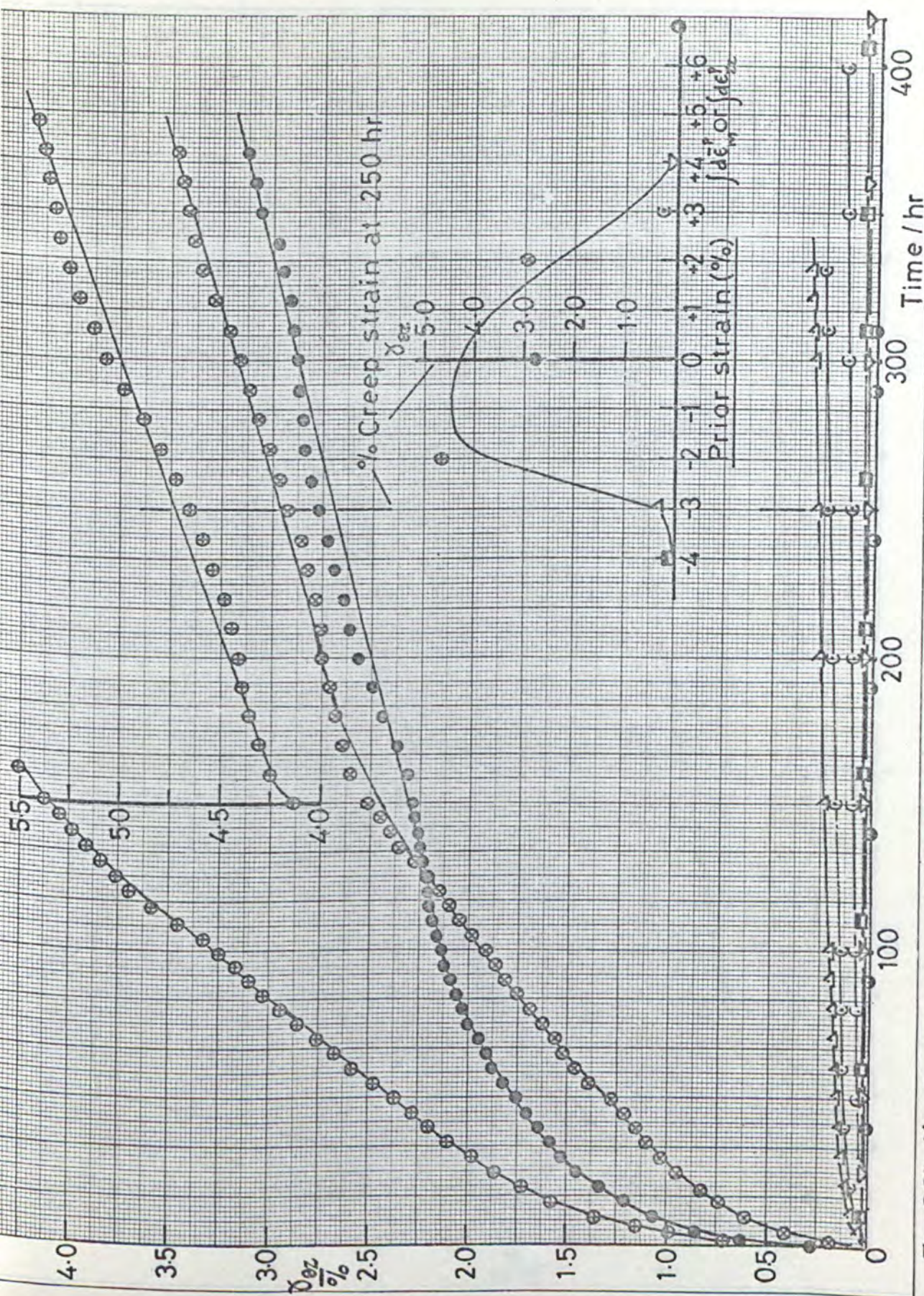


Fig. 6.3B  $\delta_{\epsilon_{zz}}$  Creep component for prior plastic axial strain ( $\delta\epsilon_{zz}^p$ )

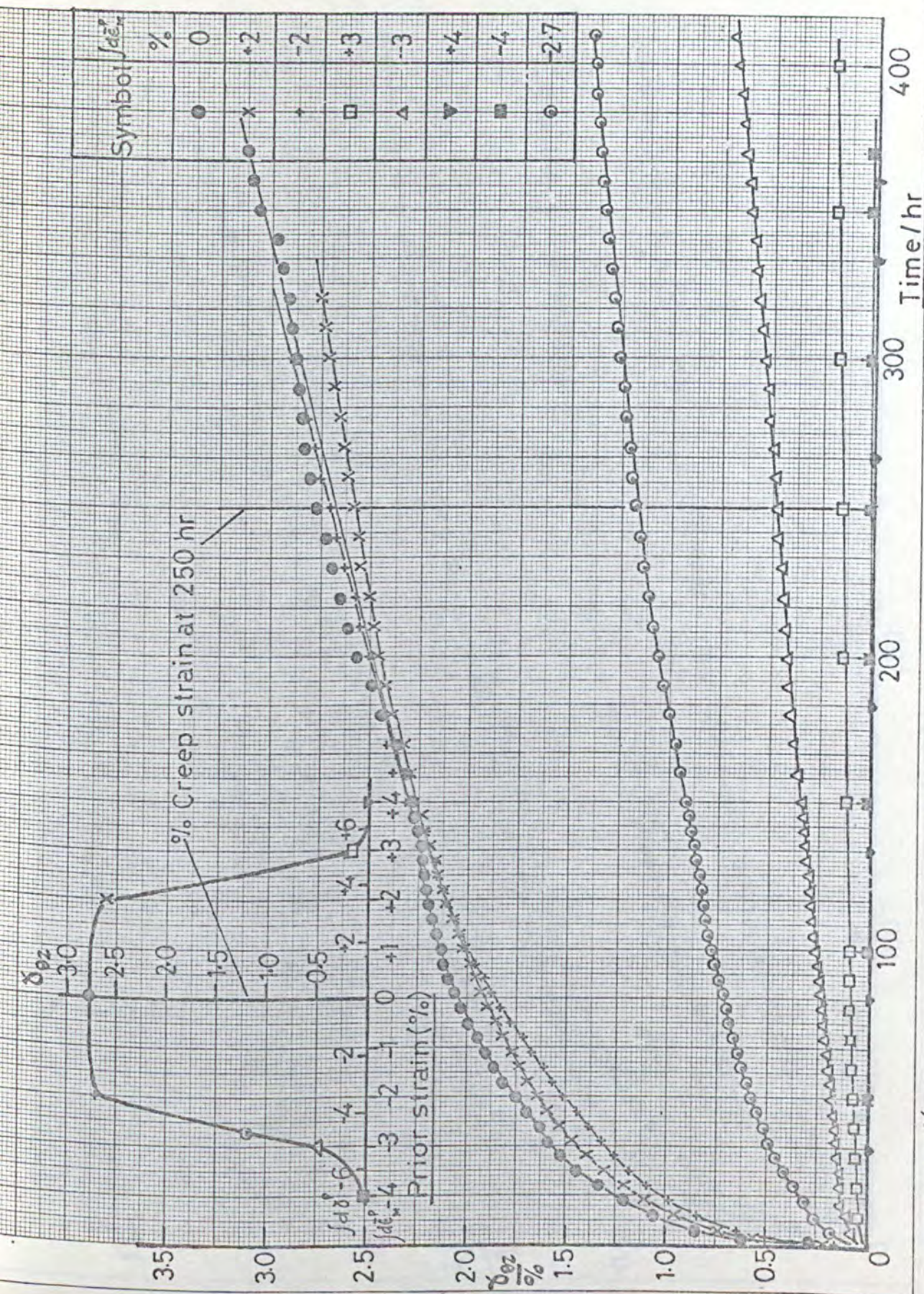


Fig. 6.4A  $\int d\epsilon_{xz}^p$  Creep component for prior plastic shear strain ( $\int d\epsilon_{xz}^p$ )

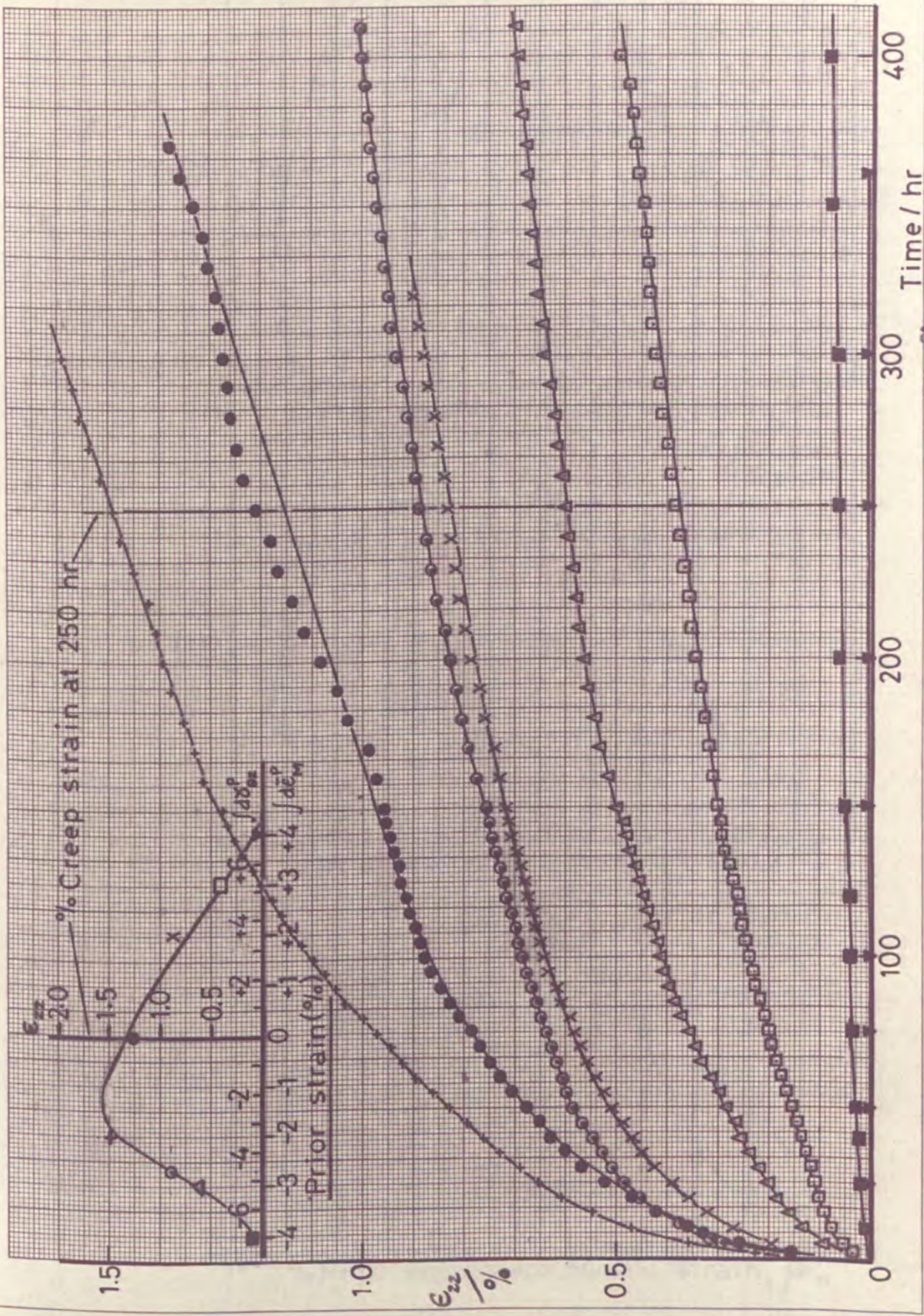


Fig. 6.4B  $E_{zz}$  Creep component for prior plastic shear strain ( $\int d\delta_{yz}^p$ )

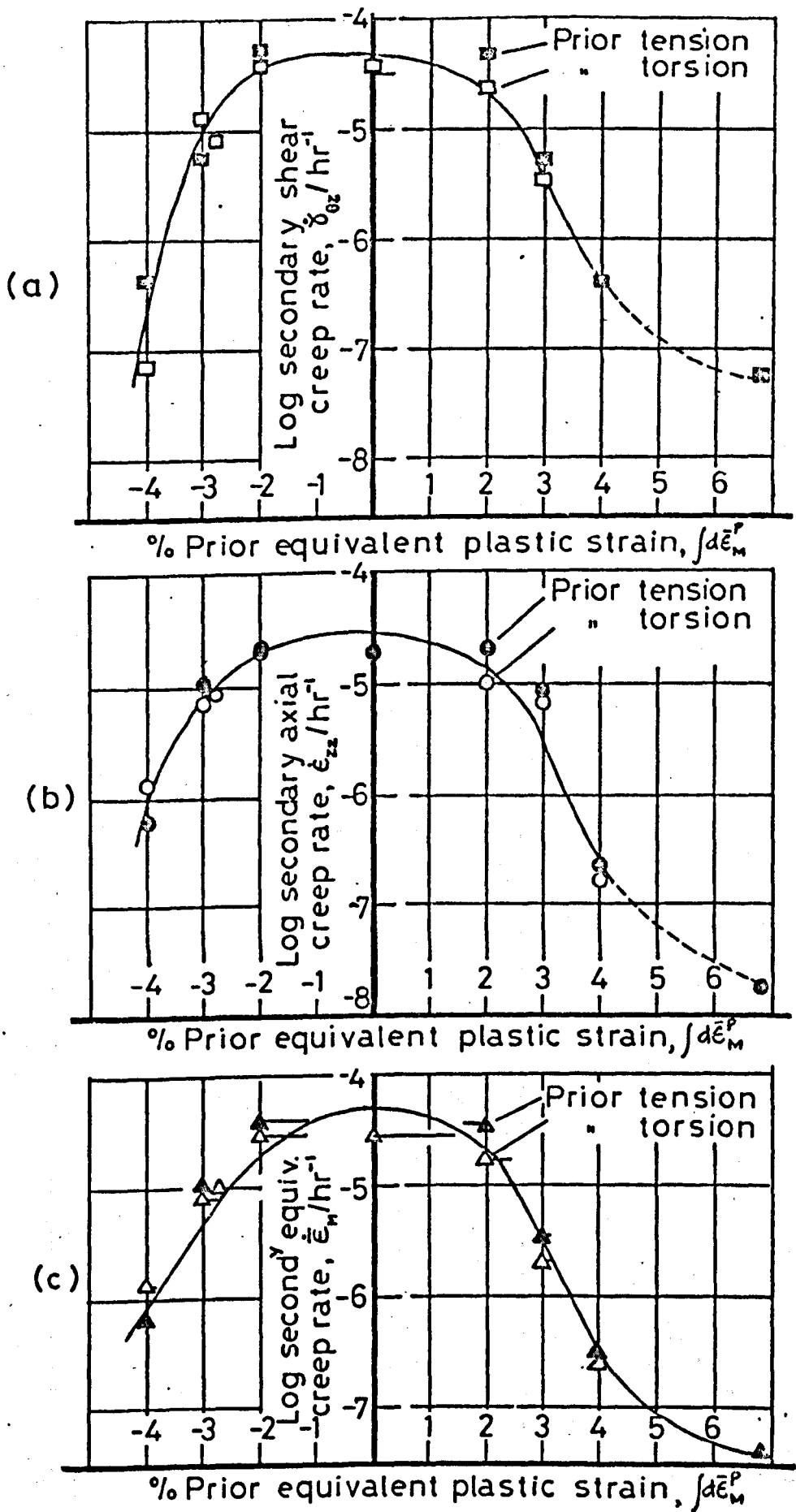


Fig.6.5 Secondary creep rate correlation

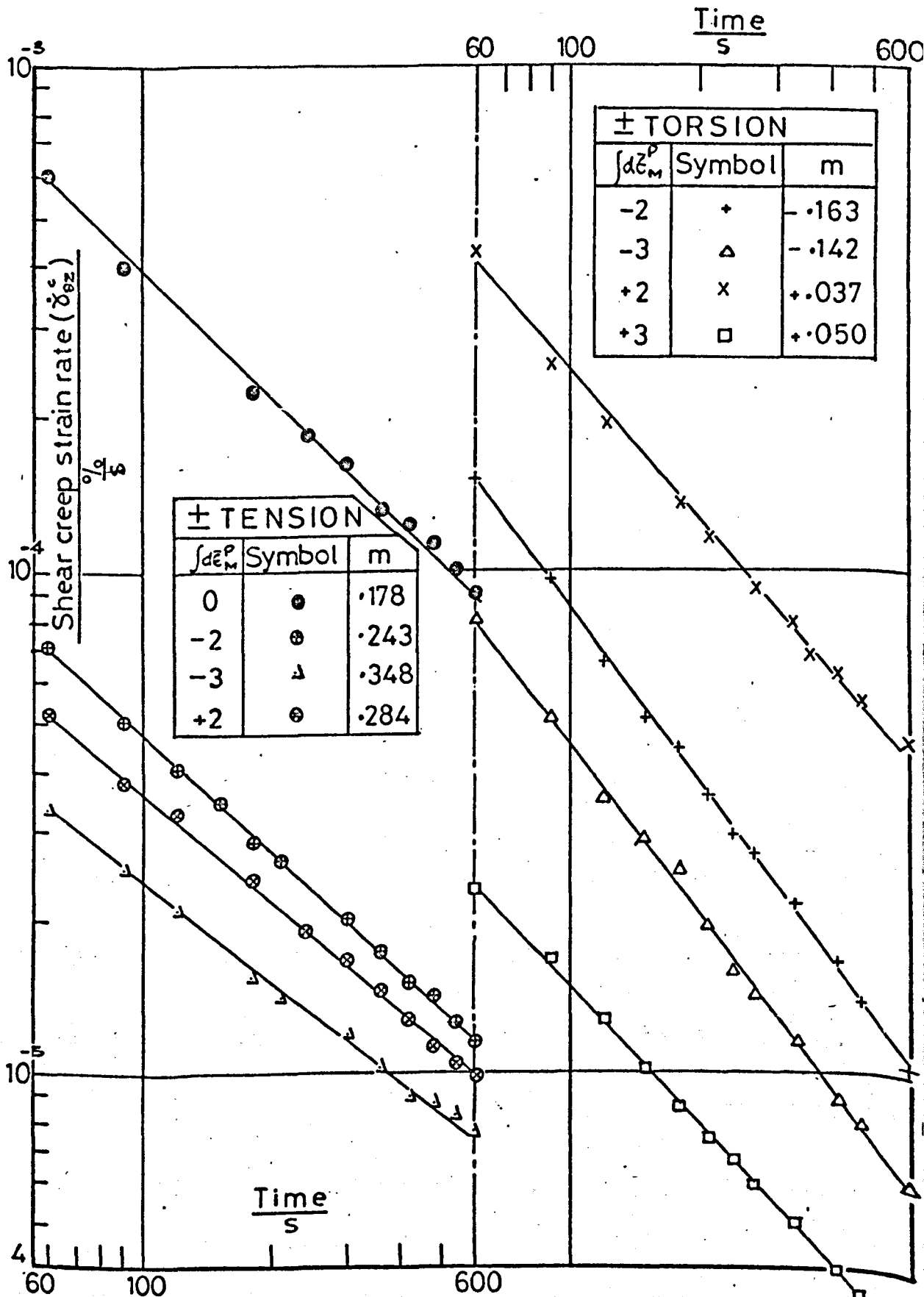


Fig. 6.6 Effect of prestrain on transient creep (10 min) shear strain at  $\tau_{\theta z} = 14.25 \text{ N/mm}^2$ .

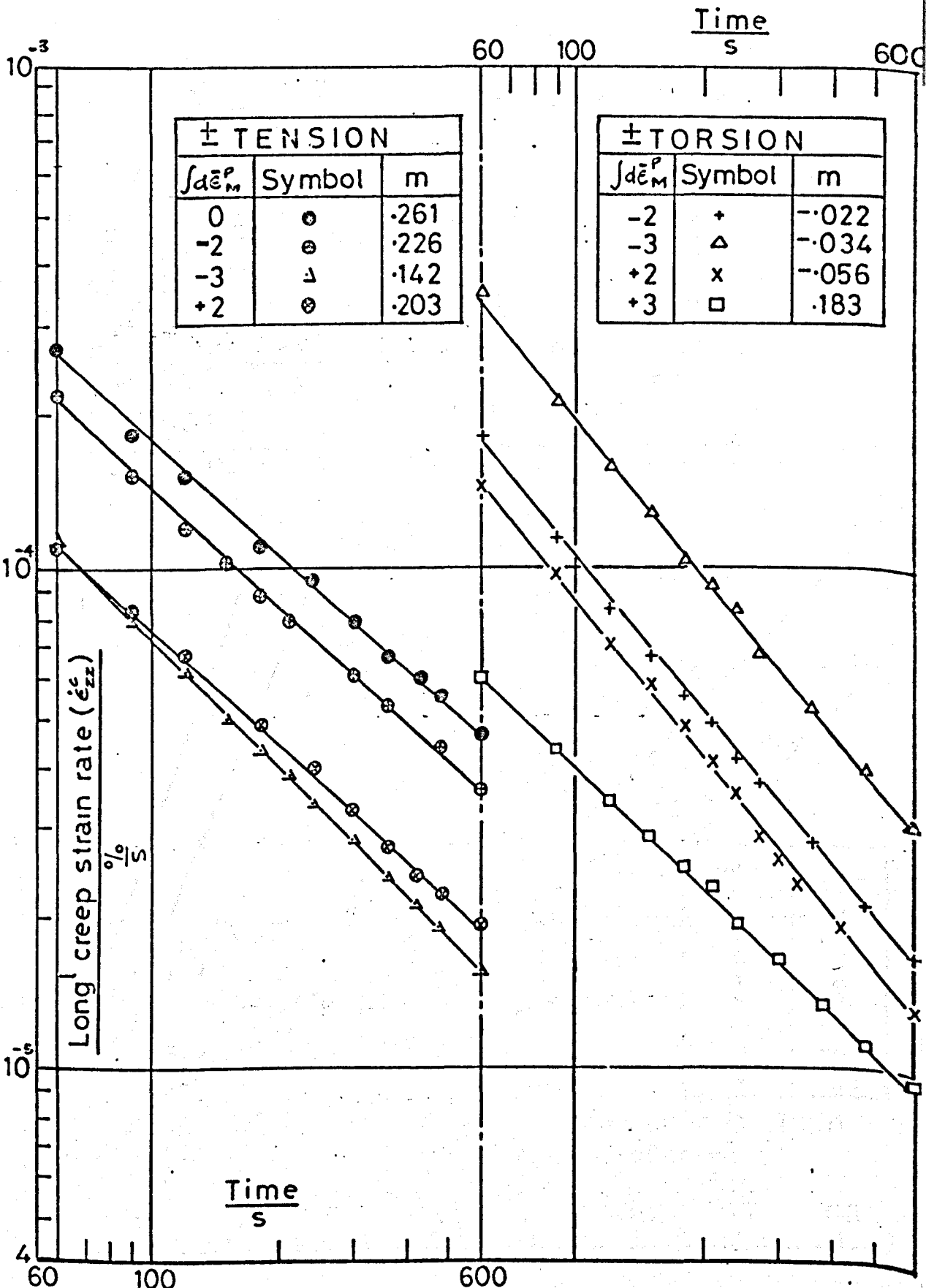


Fig. 6.7 Effect of prestrain on transient creep  
(10 min) long strain at  $\sigma_{zz} = 15 \text{ N/mm}^2$

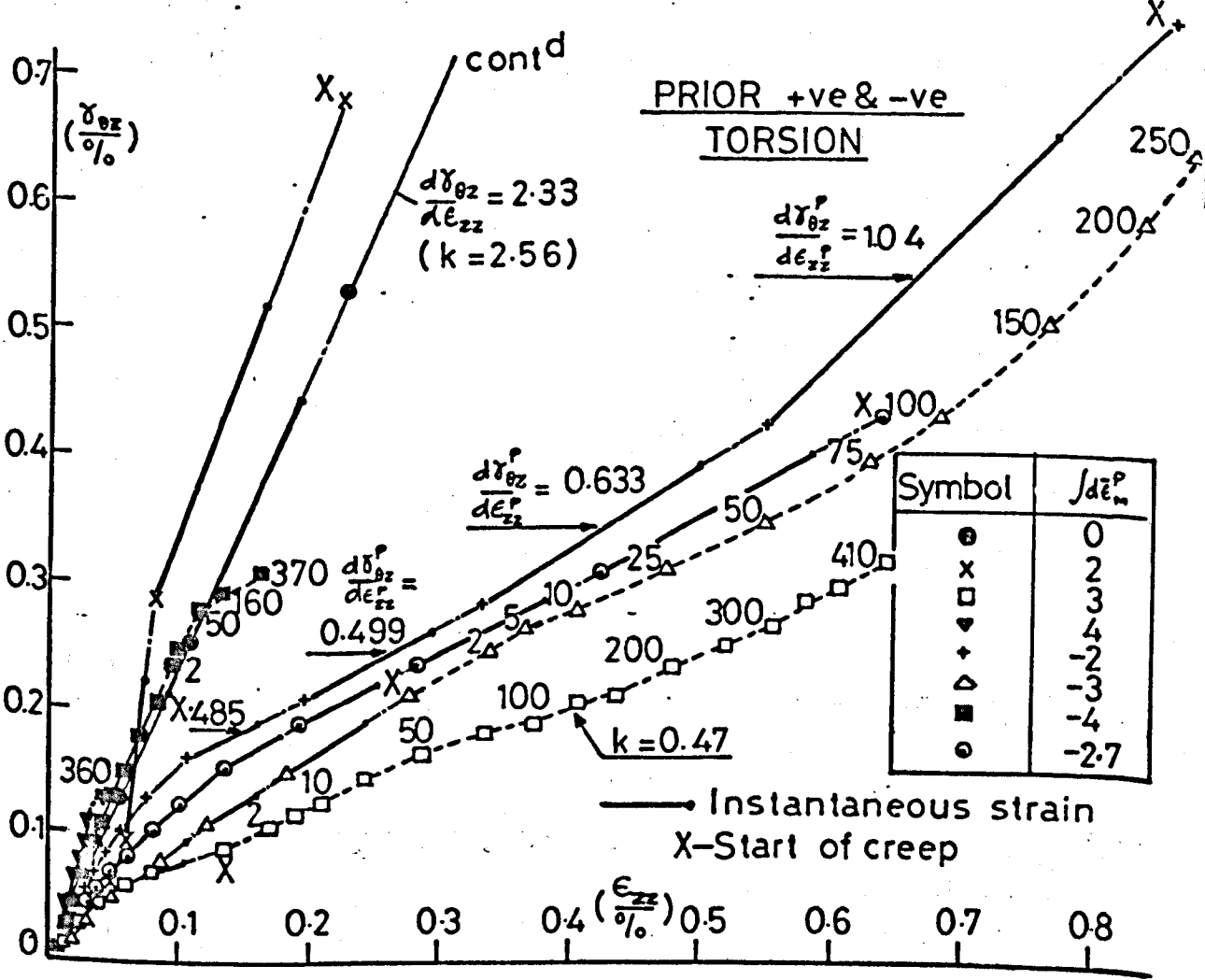
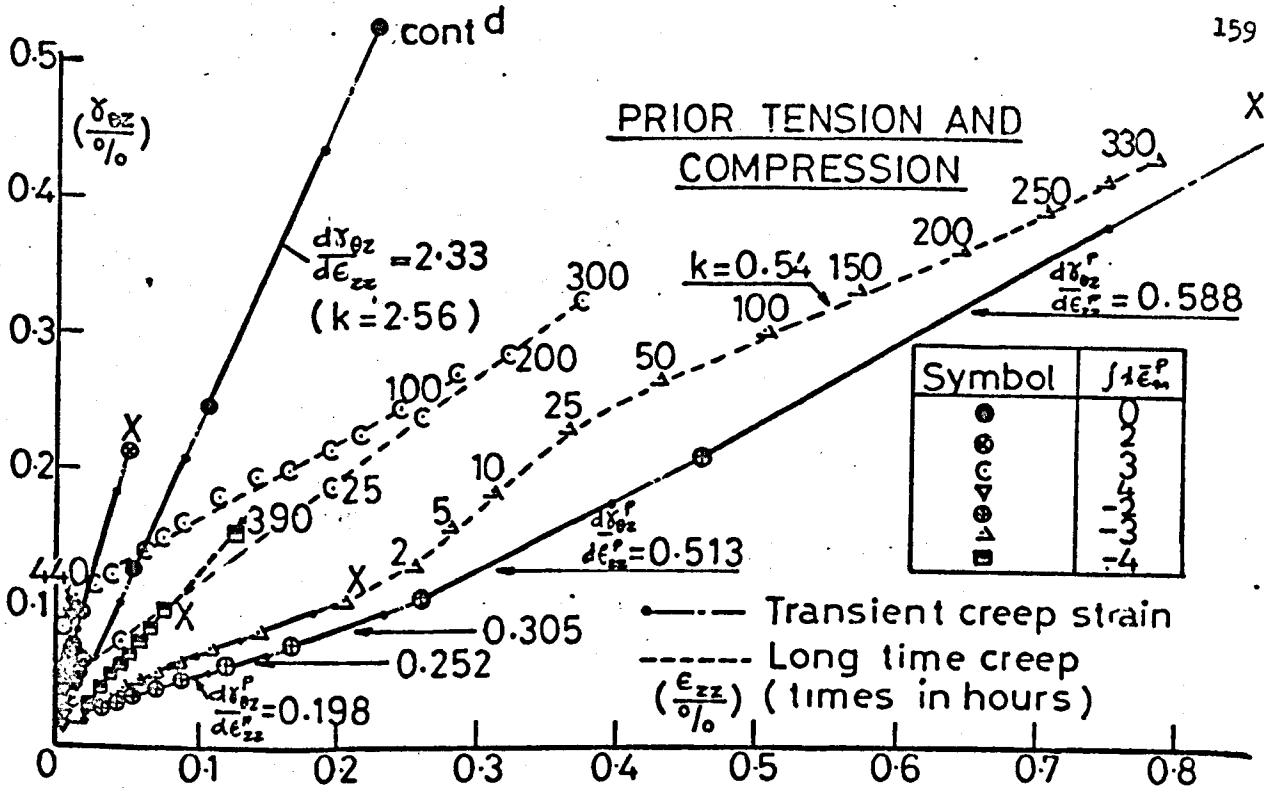


Fig.6.8  $\varepsilon_{zz}, \gamma_{\theta z}$  Total strains for  $\lambda = 0.95$  (noml)

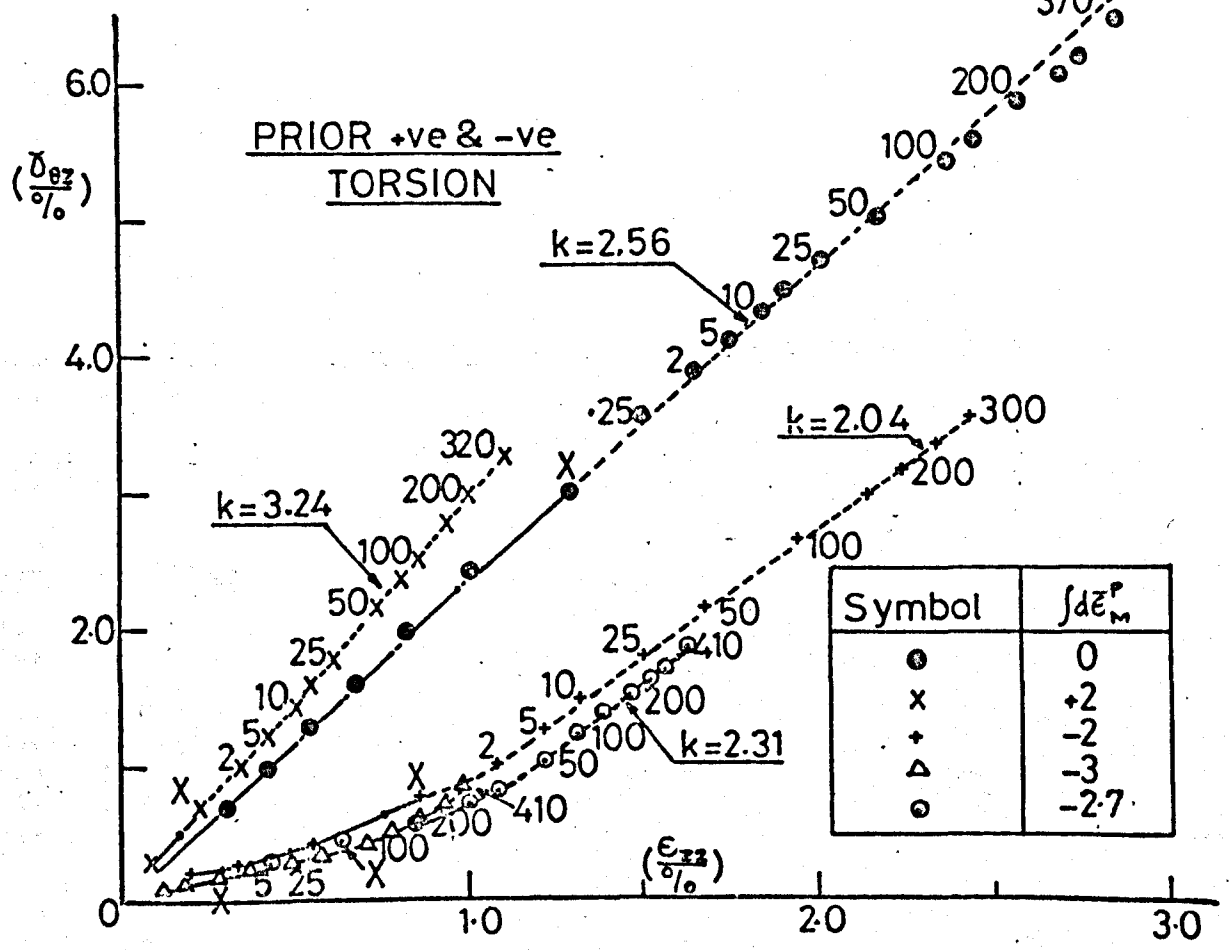
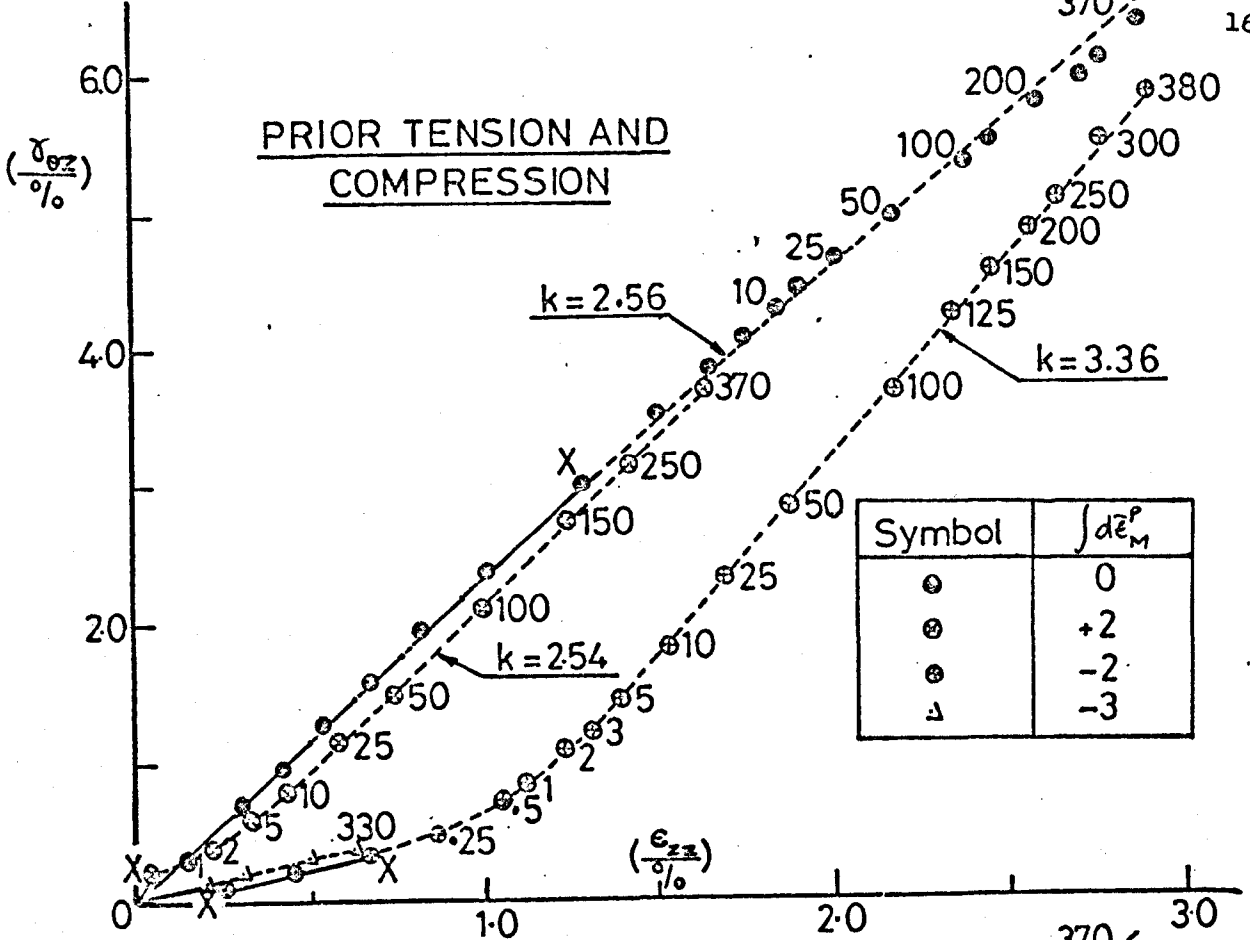


Fig.6.9  $\epsilon_{zz}, \gamma_{\theta z}$  Total strains for  $\lambda = 0.95$  (nom<sup>l</sup>)

\*\* KINGSTON POLYTECHNIC 4120 \*\*

&JOB; MAPE/R008/DR; STRAIN RATES;

&OPTIONS;MOTHY;

&FORTRAN; D:

```

0* C
1* C
2*     DIMENSION T(100), DEZZ(100), DGAMMA(100), EZZ(100), GAMMA(100)

3*     READ(3,50) GL
4*     READ(3,50) RADN
5*     READ(3,51) M
6*     K=0
7*     1 READ(3,50) DEBPM
8*     READ(3,50) XLAM
9*     READ(3,50) C1
10*    READ(3,50) C2
11*    READ(3,51) N
12*    WRITE(2,100) DEBPM
13*    READ(3,52) (T(I),DEZZ(I),DGAMMA(I), I=1,N)
14*    B=0.0
15*    DO 2 I = 1,N
16*    Z=C1*DEZZ(I)
17*    BR=1.0+Z/GL
18*    EZZ(I)=ALOG(BR)
19*    X=C2*DGAMMA(I)
20*    PHI=(RADN*1.116*X*3.14159)/(180.0*GL)
21*    GAMMA(I)=SIN(PHI)/COS(PHI)
22*    L=I-1
23*    IF(L.LT.2) GO TO 2
24*    REZZ=(EZZ(L+1)-EZZ(L-1))/(T(L+1)-T(L-1))
25*    RGAMMA=(GAMMA(L+1)-GAMMA(L-1))/(T(L+1)-T(L-1))
26*    A=RGAMMA/(REZZ*XLAM)
27*    B=B+A
28*    WRITE(2,101) T(L),EZZ(L),GAMMA(L),REZZ,RGAMMA,A
29*    2 CONTINUE
30*    AV=B/FLOAT(L-1)
31*    WRITE(2,102) AV
32*    K=K+1
33*    IF(K.LT.M) GO TO 1
34*    STOP
35*    50 FORMAT(6X,F0.0)
36*    51 FORMAT(I0)
37*    52 FORMAT(2X,F0.0,F0.0,F0.0)
38*    100 FORMAT(////16X,30H CREEP DATA FOR A PRIOR STRAIN,
39*    115H HISTORY      = ,F5.2,1X,17H% TENSION/TORSION////)
40*    101 FORMAT(20X,F4.0,5E12.4)
41*    102 FORMAT(/54X,18H AVERAGE K VALUE = ,E12.4)
42*    END

```

t	$\epsilon_{zz}$	$\delta_{\theta z}$	$\dot{\epsilon}_{zz}$	$\dot{\delta}_{\theta z}$	k
2.	0.1518E-02	0.3330E-02	0.3180E-03	0.7111E-03	0.2457E+01
3.	0.1934E-02	0.4214E-02	0.3790E-03	0.8065E-03	0.2338E+01
4.	0.2276E-02	0.4943E-02	0.3056E-03	0.7154E-03	0.2573E+01
5.	0.2545E-02	0.5645E-02	0.2444E-03	0.5853E-03	0.2632E+01
6.	0.2765E-02	0.6113E-02	0.2321E-03	0.4813E-03	0.2279E+01
7.	0.3009E-02	0.6608E-02	0.2198E-03	0.4553E-03	0.2276E+01
8.	0.3204E-02	0.7024E-02	0.1954E-03	0.3902E-03	0.2195E+01
9.	0.3400E-02	0.7388E-02	0.1709E-03	0.3642E-03	0.2342E+01
10.	0.3546E-02	0.7752E-02	0.1261E-03	0.3122E-03	0.2720E+01
15.	0.4156E-02	0.9261E-02	0.1122E-03	0.2706E-03	0.2649E+01
20.	0.4669E-02	0.1046E-01	0.1024E-03	0.2290E-03	0.2456E+01
25.	0.5181E-02	0.1155E-01	0.9750E-04	0.1977E-03	0.2229E+01
30.	0.5644E-02	0.1244E-01	0.8040E-04	0.1561E-03	0.2134E+01
35.	0.5985E-02	0.1311E-01	0.6089E-04	0.1145E-03	0.2066E+01
40.	0.6252E-02	0.1358E-01	0.4870E-04	0.9887E-04	0.2231E+01
45.	0.6472E-02	0.1410E-01	0.4868E-04	0.1119E-03	0.2526E+01
50.	0.6739E-02	0.1470E-01	0.5840E-04	0.1249E-03	0.2350E+01
55.	0.7056E-02	0.1535E-01	0.5352E-04	0.1119E-03	0.2297E+01
60.	0.7274E-02	0.1582E-01	0.4378E-04	0.8587E-04	0.2155E+01
65.	0.7493E-02	0.1621E-01	0.3405E-04	0.7546E-04	0.2436E+01
70.	0.7615E-02	0.1657E-01	0.3404E-04	0.8587E-04	0.2772E+01
75.	0.7834E-02	0.1707E-01	0.4862E-04	0.9368E-04	0.2117E+01
80.	0.8101E-02	0.1751E-01	0.4618E-04	0.7807E-04	0.1858E+01
85.	0.8295E-02	0.1785E-01	0.3645E-04	0.6245E-04	0.1883E+01
90.	0.8466E-02	0.1813E-01	0.3158E-04	0.4944E-04	0.1720E+01
95.	0.8611E-02	0.1834E-01	0.3158E-04	0.3903E-04	0.1358E+01
100.	0.8781E-02	0.1852E-01	0.2429E-04	0.4164E-04	0.1884E+01
105.	0.8854E-02	0.1876E-01	0.1700E-04	0.4424E-04	0.2850E+01
110.	0.8951E-02	0.1897E-01	0.1700E-04	0.3123E-04	0.2019E+01
115.	0.9024E-02	0.1907E-01	0.1700E-04	0.2602E-04	0.1633E+01
120.	0.9121E-02	0.1923E-01	0.1942E-04	0.2863E-04	0.1620E+01
125.	0.9218E-02	0.1936E-01	0.1699E-04	0.2602E-04	0.1683E+01
130.	0.9291E-02	0.1949E-01	0.1456E-04	0.2863E-04	0.2150E+01
135.	0.9364E-02	0.1964E-01	0.1699E-04	0.2863E-04	0.1852E+01
140.	0.9461E-02	0.1977E-01	0.1456E-04	0.2863E-04	0.2160E+01
145.	0.9510E-02	0.1993E-01	0.9707E-05	0.2602E-04	0.2946E+01
150.	0.9558E-02	0.2003E-01	0.1294E-04	0.2429E-04	0.2062E+01
160.	0.9704E-02	0.2029E-01	0.1335E-04	0.3644E-04	0.3000E+01
170.	0.9825E-02	0.2076E-01	0.2911E-04	0.6506E-04	0.2456E+01
180.	0.1029E-01	0.2160E-01	0.3274E-04	0.6246E-04	0.2096E+01
190.	0.1048E-01	0.2201E-01	0.2788E-04	0.5856E-04	0.2308E+01
200.	0.1084E-01	0.2277E-01	0.3272E-04	0.6116E-04	0.2054E+01
210.	0.1113E-01	0.2323E-01	0.2544E-04	0.4555E-04	0.1957E+01
220.	0.1135E-01	0.2368E-01	0.2422E-04	0.4034E-04	0.1830E+01
230.	0.1162E-01	0.2404E-01	0.2180E-04	0.3384E-04	0.1706E+01
240.	0.1179E-01	0.2435E-01	0.2300E-04	0.4035E-04	0.1928E+01
250.	0.1208E-01	0.2485E-01	0.2663E-04	0.4555E-04	0.1880E+01
260.	0.1232E-01	0.2527E-01	0.1936E-04	0.3124E-04	0.1773E+01
270.	0.1247E-01	0.2547E-01	0.1331E-04	0.1952E-04	0.1612E+01
280.	0.1259E-01	0.2566E-01	0.9678E-05	0.1432E-04	0.1626E+01
290.	0.1266E-01	0.2576E-01	0.7258E-05	0.1302E-04	0.1971E+01
300.	0.1273E-01	0.2592E-01	0.7257E-05	0.1692E-04	0.2562E+01
310.	0.1280E-01	0.2610E-01	0.8466E-05	0.1822E-04	0.2365E+01
320.	0.1290E-01	0.2628E-01	0.1209E-04	0.2213E-04	0.2011E+01
330.	0.1305E-01	0.2654E-01	0.1209E-04	0.2343E-04	0.2129E+01
340.	0.1314E-01	0.2675E-01	0.1692E-04	0.5988E-04	0.3888E+01
350.	0.1339E-01	0.2774E-01	0.2055E-04	0.6899E-04	0.3689E+01
360.	0.1355E-01	0.2813E-01	0.1813E-04	0.3515E-04	0.2131E+01
370.	0.1375E-01	0.2844E-01	0.1812E-04	0.2864E-04	0.1736E+01

ADD 0.2805E-02

AVERAGE K VALUE = 0.2215E+01

CREEP DATA FOR A PRIOR STRAIN HISTORY  $\int d\epsilon_M^P = 4.00 \% \text{ TENSION/}$

t	$\epsilon_{zz}$	$\gamma_{\theta z}$	$\dot{\epsilon}_{zz}$	$\dot{\gamma}_{\theta z}$	k
2.	0.9800E-05	0.6563E-04	0.3920E-05	0.1050E-04	0.2823E+01
3.	0.1274E-04	0.7350E-04	0.2450E-05	0.9188E-05	0.3952E+01
4.	0.1470E-04	0.8400E-04	0.3430E-05	0.9188E-05	0.2823E+01
5.	0.1960E-04	0.9188E-04	0.4410E-05	0.9188E-05	0.2195E+01
6.	0.2352E-04	0.1024E-03	0.2450E-05	0.6563E-05	0.2823E+01
7.	0.2450E-04	0.1050E-03	0.4900E-06	0.1313E-05	0.2823E+01
8.	0.2450E-04	0.1050E-03	0.1470E-05	0.2625E-05	0.1682E+01
9.	0.2744E-04	0.1103E-03	0.2450E-05	0.5250E-05	0.2258E+01
10.	0.2940E-04	0.1155E-03	0.2123E-05	0.3938E-05	0.1954E+01
15.	0.4018E-04	0.1339E-03	0.1176E-05	0.3150E-05	0.2823E+01
20.	0.4116E-04	0.1470E-03	0.5880E-06	0.1838E-05	0.3293E+01
25.	0.3430E-04	0.1523E-03	0.3920E-06	0.1050E-05	0.2823E+01
30.	0.3724E-04	0.1575E-03	0.4900E-06	0.1575E-05	0.3387E+01
35.	0.3920E-04	0.1680E-03	0.6860E-06	0.2100E-05	0.3226E+01
40.	0.4410E-04	0.1785E-03	0.9800E-06	0.1313E-05	0.1411E+01
45.	0.4900E-04	0.1811E-03	0.1960E-06	0.1313E-05	0.7057E+01
50.	0.4214E-04	0.1916E-03	0.3920E-06	0.1575E-05	0.4234E+01
55.	0.4508E-04	0.1969E-03	0.4900E-06	0.5250E-06	0.1129E+01
60.	0.4704E-04	0.1969E-03	0.5880E-06	0.7875E-06	0.1411E+01
65.	0.5096E-04	0.2048E-03	0.5880E-06	0.1313E-05	0.2352E+01
70.	0.5292E-04	0.2100E-03	0.1960E-06	0.7875E-06	0.4234E+01
75.	0.5292E-04	0.2126E-03	0.1960E-06	0.5250E-06	0.2823E+01
80.	0.5488E-04	0.2153E-03	0.4900E-06	0.5250E-06	0.1129E+01
85.	0.5782E-04	0.2179E-03	0.8819E-06	0.7875E-06	0.9409E+00
90.	0.6370E-04	0.2231E-03	0.7840E-06	0.1050E-05	0.1411E+01
95.	0.6566E-04	0.2284E-03	0.2940E-06	0.5250E-06	0.1682E+01
100.	0.6664E-04	0.2284E-03	0.1960E-06	0.2625E-06	0.1411E+01
105.	0.6762E-04	0.2310E-03	0.1960E-06	0.2625E-06	0.1411E+01
110.	0.6860E-04	0.2310E-03	0.1960E-06	0.2625E-06	0.1411E+01
115.	0.6958E-04	0.2336E-03	0.1960E-06	0.5250E-06	0.2823E+01
120.	0.7056E-04	0.2363E-03	0.1960E-06	0.2625E-06	0.1411E+01
125.	0.7154E-04	0.2363E-03	0.2940E-06	0.2625E-06	0.9409E+00
130.	0.7350E-04	0.2389E-03	0.4900E-06	0.5250E-06	0.1129E+01
135.	0.7644E-04	0.2415E-03	0.3920E-06	0.7875E-06	0.2117E+01
140.	0.7742E-04	0.2468E-03	0.1960E-06	0.7875E-06	0.4234E+01
145.	0.7840E-04	0.2494E-03	0.2940E-06	0.1050E-05	0.3764E+01
150.	0.8036E-04	0.2573E-03	0.2613E-06	0.5250E-06	0.2117E+01
160.	0.8232E-04	0.2573E-03	0.1960E-06	0.1313E-06	0.7057E+00
170.	0.8428E-04	0.2599E-03	0.1960E-06	0.2625E-06	0.1411E+01
180.	0.8624E-04	0.2625E-03	0.1960E-06	0.3938E-06	0.2117E+01
190.	0.8820E-04	0.2678E-03	0.3430E-06	0.3938E-06	0.1210E+01
200.	0.9310E-04	0.2704E-03	0.4900E-06	0.5250E-06	0.1129E+01
210.	0.9800E-04	0.2783E-03	0.4410E-06	0.6563E-06	0.1568E+01
220.	0.1019E-03	0.2835E-03	0.3430E-06	0.2625E-06	0.8065E+00
230.	0.1049E-03	0.2835E-03	0.1960E-06	0.2625E-06	0.1411E+01
240.	0.1058E-03	0.2888E-03	0.9799E-07	0.2625E-06	0.2823E+01
250.	0.1068E-03	0.2888E-03	0.9799E-07	0.1313E-06	0.1411E+01
260.	0.1078E-03	0.2914E-03	0.9799E-07	0.1313E-06	0.1411E+01
270.	0.1088E-03	0.2914E-03	0.9799E-07	0.1313E-06	0.1411E+01
280.	0.1098E-03	0.2940E-03	0.9799E-07	0.2625E-06	0.2823E+01
290.	0.1107E-03	0.2966E-03	0.9799E-07	0.6563E-06	0.7057E+01
300.	0.1117E-03	0.3071E-03	0.9799E-07	0.6563E-06	0.7057E+01
310.	0.1127E-03	0.3098E-03	0.9799E-07	0.1313E-06	0.1411E+01
320.	0.1137E-03	0.3098E-03	0.9799E-07	0.2625E-06	0.2823E+01
330.	0.1147E-03	0.3150E-03	0.9799E-07	0.3938E-06	0.4234E+01
340.	0.1156E-03	0.3176E-03	0.1470E-06	0.1313E-06	0.9410E+00
350.	0.1176E-03	0.3176E-03	0.1470E-06	0.1313E-06	0.9410E+00
360.	0.1186E-03	0.3203E-03	0.1960E-06	0.2625E-06	0.1411E+01
370.	0.1215E-03	0.3229E-03	0.2450E-06	0.1313E-06	0.5646E+00
380.	0.1235E-03	0.3229E-03	0.1960E-06	0.1313E-06	0.7057E+00
390.	0.1254E-03	0.3255E-03	0.2940E-06	0.2625E-06	0.9410E+00
400.	0.1294E-03	0.3281E-03	0.4899E-06	0.2625E-06	0.5646E+00
410.	0.1352E-03	0.3308E-03	0.3919E-06	0.2625E-06	0.7057E+00

AVERAGE K VALUE = 0.1650E+01

t	$\epsilon_{zz}$	$\delta\sigma_z$	$\dot{\epsilon}_{zz}$	$\dot{\delta}\sigma_z$	k
2.	0.1230E-03	0.9127E-04	0.3364E-04	0.2282E-04	0.7248E+00
3.	0.1531E-03	0.1158E-03	0.2552E-04	0.2387E-04	0.9995E+00
4.	0.1740E-03	0.1390E-03	0.2088E-04	0.1790E-04	0.9162E+00
5.	0.1949E-03	0.1517E-03	0.1856E-04	0.1053E-04	0.6063E+00
6.	0.2111E-03	0.1601E-03	0.1856E-04	0.6670E-05	0.3840E+00
7.	0.2320E-03	0.1650E-03	0.1624E-04	0.8425E-05	0.5544E+00
8.	0.2436E-03	0.1769E-03	0.1044E-04	0.9478E-05	0.9702E+00
9.	0.2528E-03	0.1839E-03	0.1044E-04	0.7372E-05	0.7546E+00
10.	0.2644E-03	0.1917E-03	0.1005E-04	0.7957E-05	0.8458E+00
15.	0.3132E-03	0.2317E-03	0.8349E-05	0.6108E-05	0.7816E+00
20.	0.3479E-03	0.2528E-03	0.6494E-05	0.5055E-05	0.8317E+00
25.	0.3781E-03	0.2822E-03	0.6030E-05	0.5617E-05	0.9952E+00
30.	0.4082E-03	0.3089E-03	0.6261E-05	0.4774E-05	0.8146E+00
35.	0.4407E-03	0.3300E-03	0.6029E-05	0.3862E-05	0.6842E+00
40.	0.4685E-03	0.3475E-03	0.4638E-05	0.2808E-05	0.6469E+00
45.	0.4871E-03	0.3581E-03	0.4406E-05	0.3019E-05	0.7321E+00
50.	0.5126E-03	0.3777E-03	0.5333E-05	0.4774E-05	0.9564E+00
55.	0.5404E-03	0.4058E-03	0.6261E-05	0.4915E-05	0.8387E+00
60.	0.5752E-03	0.4269E-03	0.6029E-05	0.3300E-05	0.5848E+00
65.	0.6007E-03	0.4388E-03	0.4637E-05	0.1825E-05	0.4206E+00
70.	0.6216E-03	0.4451E-03	0.3246E-05	0.1755E-05	0.5777E+00
75.	0.6332E-03	0.4564E-03	0.2782E-05	0.2387E-05	0.9167E+00
80.	0.6494E-03	0.4690E-03	0.4173E-05	0.2457E-05	0.6291E+00
85.	0.6749E-03	0.4809E-03	0.4637E-05	0.2387E-05	0.5500E+00
90.	0.6958E-03	0.4929E-03	0.4173E-05	0.2668E-05	0.6830E+00
95.	0.7166E-03	0.5076E-03	0.3941E-05	0.3089E-05	0.8374E+00
100.	0.7352E-03	0.5238E-03	0.3709E-05	0.3300E-05	0.9505E+00
105.	0.7537E-03	0.5406E-03	0.4636E-05	0.3300E-05	0.7604E+00
110.	0.7815E-03	0.5568E-03	0.5332E-05	0.3159E-05	0.6331E+00
115.	0.8070E-03	0.5722E-03	0.4866E-05	0.4704E-05	0.1032E+01
120.	0.8302E-03	0.6038E-03	0.7418E-05	0.8425E-05	0.1213E+01
125.	0.8812E-03	0.6565E-03	0.9735E-05	0.8215E-05	0.9015E+00
130.	0.9276E-03	0.6860E-03	0.8800E-05	0.5336E-05	0.6472E+00
135.	0.9693E-03	0.7098E-03	0.6953E-05	0.4915E-05	0.7551E+00
140.	0.9971E-03	0.7351E-03	0.5099E-05	0.5055E-05	0.1059E+01
145.	0.1020E-02	0.7604E-03	0.9270E-05	0.5125E-05	0.5907E+00
150.	0.1090E-02	0.7864E-03	0.1174E-04	0.5008E-05	0.4557E+00
160.	0.1196E-02	0.8355E-03	0.9269E-05	0.4739E-05	0.5463E+00
170.	0.1275E-02	0.8811E-03	0.1156E-04	0.3791E-05	0.3496E+00
180.	0.1428E-02	0.9113E-03	0.1156E-04	0.2984E-05	0.2752E+00
190.	0.1507E-02	0.9408E-03	0.6255E-05	0.3475E-05	0.5936E+00
200.	0.1553E-02	0.9808E-03	0.5791E-05	0.3019E-05	0.5570E+00
210.	0.1623E-02	0.1001E-02	0.5791E-05	0.2703E-05	0.4987E+00
220.	0.1669E-02	0.1035E-02	0.5327E-05	0.2598E-05	0.5210E+00
230.	0.1729E-02	0.1053E-02	0.5327E-05	0.1825E-05	0.3661E+00
240.	0.1776E-02	0.1071E-02	0.4053E-05	0.1966E-05	0.5182E+00
250.	0.1810E-02	0.1092E-02	0.3937E-05	0.2106E-05	0.5716E+00
260.	0.1854E-02	0.1114E-02	0.4168E-05	0.2106E-05	0.5399E+00
270.	0.1894E-02	0.1135E-02	0.4284E-05	0.2036E-05	0.5078E+00
280.	0.1940E-02	0.1154E-02	0.4515E-05	0.3089E-05	0.7310E+00
290.	0.1984E-02	0.1196E-02	0.5441E-05	0.4915E-05	0.9650E+00
300.	0.2049E-02	0.1253E-02	0.6251E-05	0.3862E-05	0.6600E+00
310.	0.2109E-02	0.1274E-02	0.6251E-05	0.3511E-05	0.6000E+00
320.	0.2174E-02	0.1323E-02	0.6019E-05	0.4107E-05	0.7291E+00
330.	0.2229E-02	0.1356E-02	0.5671E-05	0.3370E-05	0.6349E+00
340.	0.2287E-02	0.1390E-02	0.3588E-05	0.2352E-05	0.7004E+00
350.	0.2301E-02	0.1403E-02	0.2893E-05	0.1264E-05	0.4667E+00
360.	0.2345E-02	0.1415E-02	0.3935E-05	0.1966E-05	0.5338E+00
370.	0.2380E-02	0.1442E-02	0.3472E-05	0.2212E-05	0.6806E+00
380.	0.2415E-02	0.1460E-02	0.3587E-05	0.3054E-05	0.9096E+00
390.	0.2452E-02	0.1503E-02	0.4050E-05	0.3686E-05	0.9724E+00
400.	0.2496E-02	0.1533E-02	0.3703E-05	0.2036E-05	0.5875E+00
410.	0.2526E-02	0.1544E-02	0.3008E-05	0.1018E-05	0.3615E+00

AVERAGE K VALUE = 0.6853E+00

CREEP DATA FOR A PRIOR STRAIN HISTORY  $\int d\epsilon_M^P = 2.00$  % TENSION/TORSION

t	$\epsilon_{zz}$	$\gamma_{\theta z}$	$\dot{\epsilon}_{zz}$	$\dot{\gamma}_{\theta z}$	k
2.	0.1782E-02	0.1896E-02	0.5283E-03	0.8720E-03	0.1714E+01
3.	0.2207E-02	0.2717E-02	0.3911E-03	0.7425E-03	0.1971E+01
4.	0.2564E-02	0.3381E-02	0.3250E-03	0.6161E-03	0.1968E+01
5.	0.2858E-02	0.3949E-02	0.2663E-03	0.5340E-03	0.2082E+01
6.	0.3097E-02	0.4449E-02	0.2247E-03	0.4676E-03	0.2161E+01
7.	0.3307E-02	0.4885E-02	0.2002E-03	0.4139E-03	0.2146E+01
8.	0.3497E-02	0.5276E-02	0.1880E-03	0.3855E-03	0.2129E+01
9.	0.3683E-02	0.5655E-02	0.1758E-03	0.3570E-03	0.2109E+01
10.	0.3849E-02	0.5990E-02	0.1399E-03	0.2738E-03	0.2033E+01
15.	0.4522E-02	0.7298E-02	0.1151E-03	0.2161E-03	0.1949E+01
20.	0.5000E-02	0.8152E-02	0.8923E-04	0.2092E-03	0.2434E+01
25.	0.5415E-02	0.9390E-02	0.7749E-04	0.2073E-03	0.2778E+01
30.	0.5775E-02	0.1022E-01	0.6626E-04	0.1498E-03	0.2347E+01
35.	0.6077E-02	0.1089E-01	0.5796E-04	0.1258E-03	0.2253E+01
40.	0.6355E-02	0.1148E-01	0.5210E-04	0.1119E-03	0.2230E+01
45.	0.6598E-02	0.1201E-01	0.5354E-04	0.1175E-03	0.2280E+01
50.	0.6890E-02	0.1266E-01	0.7591E-04	0.1864E-03	0.2550E+01
55.	0.7357E-02	0.1387E-01	0.7686E-04	0.1909E-03	0.2579E+01
60.	0.7659E-02	0.1457E-01	0.5203E-04	0.1201E-03	0.2397E+01
65.	0.7877E-02	0.1507E-01	0.3987E-04	0.9480E-04	0.2469E+01
70.	0.8057E-02	0.1551E-01	0.4131E-04	0.1011E-03	0.2542E+01
75.	0.8291E-02	0.1608E-01	0.5734E-04	0.1327E-03	0.2404E+01
80.	0.8631E-02	0.1684E-01	0.6364E-04	0.1391E-03	0.2269E+01
85.	0.8927E-02	0.1747E-01	0.5099E-04	0.1138E-03	0.2317E+01
90.	0.9141E-02	0.1798E-01	0.3836E-04	0.9481E-04	0.2567E+01
95.	0.9311E-02	0.1842E-01	0.4223E-04	0.1037E-03	0.2549E+01
100.	0.9563E-02	0.1902E-01	0.5242E-04	0.1435E-03	0.2843E+01
105.	0.9835E-02	0.1986E-01	0.5240E-04	0.1429E-03	0.2831E+01
110.	0.1009E-01	0.2044E-01	0.4463E-04	0.1049E-03	0.2442E+01
115.	0.1028E-01	0.2091E-01	0.3492E-04	0.8977E-04	0.2669E+01
120.	0.1044E-01	0.2134E-01	0.4412E-04	0.1163E-03	0.2738E+01
125.	0.1072E-01	0.2207E-01	0.6060E-04	0.1454E-03	0.2492E+01
130.	0.1104E-01	0.2280E-01	0.5670E-04	0.1328E-03	0.2431E+01
135.	0.1129E-01	0.2340E-01	0.4700E-04	0.1075E-03	0.2375E+01
140.	0.1151E-01	0.2387E-01	0.3730E-04	0.1012E-03	0.2816E+01
145.	0.1166E-01	0.2441E-01	0.4262E-04	0.1201E-03	0.2927E+01
150.	0.1194E-01	0.2507E-01	0.4390E-04	0.1024E-03	0.2423E+01
160.	0.1232E-01	0.2594E-01	0.2977E-04	0.6639E-04	0.2316E+01
170.	0.1253E-01	0.2640E-01	0.1790E-04	0.3857E-04	0.2237E+01
180.	0.1268E-01	0.2672E-01	0.1379E-04	0.3004E-04	0.2262E+01
190.	0.1281E-01	0.2700E-01	0.1185E-04	0.2687E-04	0.2355E+01
200.	0.1292E-01	0.2725E-01	0.1040E-04	0.2276E-04	0.2273E+01
210.	0.1302E-01	0.2746E-01	0.8948E-05	0.2213E-04	0.2569E+01
220.	0.1309E-01	0.2770E-01	0.1378E-04	0.3415E-04	0.2573E+01
230.	0.1329E-01	0.2814E-01	0.1886E-04	0.4047E-04	0.2229E+01
240.	0.1347E-01	0.2851E-01	0.2200E-04	0.5059E-04	0.2388E+01
250.	0.1373E-01	0.2915E-01	0.2368E-04	0.5439E-04	0.2385E+01
260.	0.1395E-01	0.2959E-01	0.1860E-04	0.4807E-04	0.2683E+01
270.	0.1411E-01	0.3011E-01	0.2126E-04	0.5313E-04	0.2595E+01
280.	0.1437E-01	0.3066E-01	0.2053E-04	0.4617E-04	0.2335E+01
290.	0.1452E-01	0.3104E-01	0.2004E-04	0.5123E-04	0.2655E+01
300.	0.1477E-01	0.3168E-01	0.2221E-04	0.5440E-04	0.2543E+01
310.	0.1496E-01	0.3212E-01	0.1955E-04	0.5630E-04	0.2990E+01
320.	0.1516E-01	0.3281E-01	0.2437E-04	0.6642E-04	0.2830E+01
330.	0.1545E-01	0.3345E-01	0.2292E-04	0.5219E-04	0.2365E+01
340.	0.1562E-01	0.3385E-01	0.1520E-04	0.3606E-04	0.2464E+01
350.	0.1575E-01	0.3417E-01	0.1254E-04	0.2878E-04	0.2383E+01
360.	0.1587E-01	0.3443E-01	0.1037E-04	0.2404E-04	0.2407E+01
370.	0.1596E-01	0.3465E-01	0.8921E-05	0.2341E-04	0.2725E+01

AVERAGE K VALUE = 0.2420E+01

CREEP DATA FOR A PRIOR STRAIN HISTORY  $\int d\epsilon_M^p = -2.00$  % TENSION/TORSION

t	$\epsilon_{zz}$	$\gamma_{\theta z}$	$\dot{\epsilon}_{zz}$	$\dot{\gamma}_{\theta z}$	k
2.	0.3720E-02	0.6466E-02	0.8918E-03	0.1807E-02	0.2329E+01
3.	0.4477E-02	0.7553E-02	0.6469E-03	0.1155E-02	0.2051E+01
4.	0.5014E-02	0.8775E-02	0.4514E-03	0.1155E-02	0.2940E+01
5.	0.5380E-02	0.9862E-02	0.3658E-03	0.1019E-02	0.3201E+01
6.	0.5746E-02	0.1081E-01	0.3291E-03	0.8830E-03	0.3084E+01
7.	0.6038E-02	0.1163E-01	0.2681E-03	0.8015E-03	0.3436E+01
8.	0.6282E-02	0.1242E-01	0.2437E-03	0.6793E-03	0.3204E+01
9.	0.6526E-02	0.1299E-01	0.2314E-03	0.5706E-03	0.2834E+01
10.	0.6745E-02	0.1356E-01	0.1664E-03	0.4529E-03	0.3129E+01
15.	0.7524E-02	0.1570E-01	0.1290E-03	0.3723E-03	0.3317E+01
20.	0.8035E-02	0.1728E-01	0.9973E-04	0.2935E-03	0.3383E+01
25.	0.8521E-02	0.1864E-01	0.8753E-04	0.2500E-03	0.3283E+01
30.	0.8910E-02	0.1978E-01	0.7777E-04	0.2364E-03	0.3495E+01
35.	0.9299E-02	0.2100E-01	0.7045E-04	0.2201E-03	0.3592E+01
40.	0.9615E-02	0.2198E-01	0.5829E-04	0.1767E-03	0.3484E+01
45.	0.9882E-02	0.2277E-01	0.5827E-04	0.1712E-03	0.3378E+01
50.	0.1020E-01	0.2369E-01	0.7281E-04	0.1957E-03	0.3090E+01
55.	0.1061E-01	0.2473E-01	0.7036E-04	0.2148E-03	0.3508E+01
60.	0.1090E-01	0.2584E-01	0.5579E-04	0.2012E-03	0.4145E+01
65.	0.1117E-01	0.2674E-01	0.5334E-04	0.1631E-03	0.3515E+01
70.	0.1143E-01	0.2747E-01	0.5333E-04	0.1794E-03	0.3867E+01
75.	0.1170E-01	0.2853E-01	0.5574E-04	0.1903E-03	0.3925E+01
80.	0.1199E-01	0.2938E-01	0.6057E-04	0.1740E-03	0.3302E+01
85.	0.1231E-01	0.3027E-01	0.5813E-04	0.1577E-03	0.3119E+01
90.	0.1257E-01	0.3095E-01	0.4843E-04	0.1414E-03	0.3356E+01
95.	0.1279E-01	0.3169E-01	0.5326E-04	0.1414E-03	0.3052E+01
100.	0.1311E-01	0.3237E-01	0.5566E-04	0.1577E-03	0.3257E+01
105.	0.1335E-01	0.3326E-01	0.5806E-04	0.2067E-03	0.4092E+01
110.	0.1369E-01	0.3443E-01	0.7739E-04	0.2557E-03	0.3797E+01
115.	0.1412E-01	0.3582E-01	0.7737E-04	0.2475E-03	0.3678E+01
120.	0.1446E-01	0.3691E-01	0.6284E-04	0.1904E-03	0.3483E+01
125.	0.1475E-01	0.3773E-01	0.5316E-04	0.1469E-03	0.3177E+01
130.	0.1499E-01	0.3838E-01	0.5073E-04	0.1415E-03	0.3206E+01
135.	0.1526E-01	0.3914E-01	0.4588E-04	0.1388E-03	0.3476E+01
140.	0.1545E-01	0.3977E-01	0.3622E-04	0.1306E-03	0.4145E+01
145.	0.1562E-01	0.4045E-01	0.4828E-04	0.1497E-03	0.3563E+01
150.	0.1593E-01	0.4126E-01	0.4505E-04	0.1379E-03	0.3518E+01
160.	0.1629E-01	0.4251E-01	0.3016E-04	0.9389E-04	0.3579E+01
170.	0.1654E-01	0.4314E-01	0.2050E-04	0.5716E-04	0.3205E+01
180.	0.1670E-01	0.4366E-01	0.1326E-04	0.4083E-04	0.3538E+01
190.	0.1680E-01	0.4396E-01	0.3439E-05	0.2586E-04	0.3522E+01
200.	0.1687E-01	0.4418E-01	0.9644E-05	0.2042E-04	0.2433E+01
210.	0.1699E-01	0.4437E-01	0.9643E-05	0.2858E-04	0.3407E+01
220.	0.1707E-01	0.4475E-01	0.1326E-04	0.5172E-04	0.4484E+01
230.	0.1726E-01	0.4540E-01	0.2049E-04	0.5989E-04	0.3360E+01
240.	0.1748E-01	0.4594E-01	0.2169E-04	0.6126E-04	0.3247E+01
250.	0.1769E-01	0.4663E-01	0.2048E-04	0.6262E-04	0.3515E+01
260.	0.1789E-01	0.4720E-01	0.2168E-04	0.6399E-04	0.3393E+01
270.	0.1813E-01	0.4790E-01	0.2288E-04	0.8033E-04	0.4036E+01
280.	0.1834E-01	0.4880E-01	0.2768E-04	0.9667E-04	0.4014E+01
290.	0.1868E-01	0.4984E-01	0.3129E-04	0.9532E-04	0.3502E+01
300.	0.1897E-01	0.5071E-01	0.2526E-04	0.7218E-04	0.3284E+01
310.	0.1919E-01	0.5128E-01	0.2285E-04	0.6537E-04	0.3288E+01
320.	0.1943E-01	0.5202E-01	0.2405E-04	0.6538E-04	0.3125E+01
330.	0.1967E-01	0.5259E-01	0.2044E-04	0.4904E-04	0.2758E+01
340.	0.1983E-01	0.5300E-01	0.1202E-04	0.3405E-04	0.3256E+01
350.	0.1991E-01	0.5327E-01	0.9614E-05	0.2724E-04	0.3257E+01
360.	0.2003E-01	0.5354E-01	0.9614E-05	0.2588E-04	0.3095E+01
370.	0.2010E-01	0.5379E-01	0.6008E-05	0.2452E-04	0.4691E+01
380.	0.2015E-01	0.5403E-01	0.4806E-05	0.2725E-04	0.6516E+01

AVERAGE K VALUE = 0.3449E+01

CREEP DATA FOR A PRIOR STRAIN HISTORY  $\int d\epsilon_m^p = -3.00$  % TENSION/TORSION

t	$\epsilon_{zz}$	$\delta_{\theta z}$	$\dot{\epsilon}_{zz}$	$\dot{\delta}_{\theta z}$	k
2.	0.5203E-03	0.2628E-03	0.1227E-03	0.1117E-03	0.1029E+01
3.	0.6381E-03	0.3877E-03	0.9323E-04	0.1051E-03	0.1275E+01
4.	0.7068E-03	0.4731E-03	0.7360E-04	0.8542E-04	0.1312E+01
5.	0.7853E-03	0.5585E-03	0.6869E-04	0.7556E-04	0.1244E+01
6.	0.8442E-03	0.6242E-03	0.6378E-04	0.5585E-04	0.9902E+00
7.	0.9128E-03	0.6702E-03	0.5887E-04	0.4928E-04	0.9465E+00
8.	0.9619E-03	0.7227E-03	0.5886E-04	0.4928E-04	0.9466E+00
9.	0.1031E-02	0.7687E-03	0.5886E-04	0.4599E-04	0.8835E+00
10.	0.1080E-02	0.8147E-03	0.4087E-04	0.4709E-04	0.1303E+01
15.	0.1276E-02	0.1051E-02	0.3531E-04	0.3811E-04	0.1220E+01
20.	0.1433E-02	0.1196E-02	0.2942E-04	0.2234E-04	0.8586E+00
25.	0.1570E-02	0.1275E-02	0.3039E-04	0.1774E-04	0.6600E+00
30.	0.1737E-02	0.1373E-02	0.2941E-04	0.1708E-04	0.6568E+00
35.	0.1864E-02	0.1445E-02	0.2548E-04	0.1643E-04	0.7288E+00
40.	0.1991E-02	0.1537E-02	0.2352E-04	0.1708E-04	0.8212E+00
45.	0.2099E-02	0.1616E-02	0.2450E-04	0.1183E-04	0.5459E+00
50.	0.2236E-02	0.1656E-02	0.2548E-04	0.1051E-04	0.4666E+00
55.	0.2354E-02	0.1721E-02	0.2155E-04	0.1183E-04	0.6204E+00
60.	0.2452E-02	0.1774E-02	0.1959E-04	0.1183E-04	0.6826E+00
65.	0.2550E-02	0.1840E-02	0.1959E-04	0.1117E-04	0.6447E+00
70.	0.2648E-02	0.1886E-02	0.1763E-04	0.6570E-05	0.4214E+00
75.	0.2726E-02	0.1905E-02	0.1469E-04	0.5913E-05	0.4552E+00
80.	0.2795E-02	0.1945E-02	0.1371E-04	0.7227E-05	0.5961E+00
85.	0.2863E-02	0.1978E-02	0.1175E-04	0.6570E-05	0.6323E+00
90.	0.2912E-02	0.2011E-02	0.9791E-05	0.6570E-05	0.7587E+00
95.	0.2961E-02	0.2043E-02	0.1077E-04	0.5913E-05	0.6208E+00
100.	0.3020E-02	0.2070E-02	0.9790E-05	0.3285E-05	0.3794E+00
105.	0.3059E-02	0.2076E-02	0.1077E-04	0.4599E-05	0.4829E+00
110.	0.3128E-02	0.2116E-02	0.1077E-04	0.5256E-05	0.5519E+00
115.	0.3167E-02	0.2129E-02	0.1468E-04	0.5256E-05	0.4048E+00
120.	0.3275E-02	0.2168E-02	0.1272E-04	0.4599E-05	0.4087E+00
125.	0.3294E-02	0.2175E-02	0.9787E-05	0.3285E-05	0.3795E+00
130.	0.3372E-02	0.2201E-02	0.1566E-04	0.7227E-05	0.5219E+00
135.	0.3451E-02	0.2247E-02	0.1566E-04	0.7227E-05	0.5219E+00
140.	0.3529E-02	0.2273E-02	0.1370E-04	0.6570E-05	0.5423E+00
145.	0.3588E-02	0.2313E-02	0.1468E-04	0.5913E-05	0.4556E+00
150.	0.3676E-02	0.2332E-02	0.1370E-04	0.7446E-05	0.6147E+00
160.	0.3793E-02	0.2424E-02	0.1272E-04	0.6570E-05	0.5842E+00
170.	0.3930E-02	0.2464E-02	0.1467E-04	0.5256E-05	0.4051E+00
180.	0.4087E-02	0.2530E-02	0.1418E-04	0.7227E-05	0.5763E+00
190.	0.4214E-02	0.2608E-02	0.1467E-04	0.5256E-05	0.4052E+00
200.	0.4380E-02	0.2635E-02	0.1467E-04	0.5256E-05	0.4053E+00
210.	0.4507E-02	0.2714E-02	0.1222E-04	0.6242E-05	0.5776E+00
220.	0.4624E-02	0.2760E-02	0.1466E-04	0.6242E-05	0.4814E+00
230.	0.4800E-02	0.2838E-02	0.1466E-04	0.6570E-05	0.5068E+00
240.	0.4918E-02	0.2891E-02	0.9772E-05	0.4271E-05	0.4942E+00
250.	0.4996E-02	0.2924E-02	0.7817E-05	0.4928E-05	0.7128E+00
260.	0.5074E-02	0.2990E-02	0.5862E-05	0.4928E-05	0.9505E+00
270.	0.5113E-02	0.3022E-02	0.5862E-05	0.2957E-05	0.5703E+00
280.	0.5191E-02	0.3049E-02	0.7815E-05	0.4928E-05	0.7130E+00
290.	0.5269E-02	0.3121E-02	0.1074E-04	0.4928E-05	0.5186E+00
300.	0.5406E-02	0.3147E-02	0.1270E-04	0.4928E-05	0.4388E+00
310.	0.5523E-02	0.3220E-02	0.1416E-04	0.6242E-05	0.4984E+00
320.	0.5689E-02	0.3272E-02	0.1269E-04	0.5256E-05	0.4682E+00
330.	0.5777E-02	0.3325E-02	0.9763E-05	0.6242E-05	0.7229E+00

AVERAGE K VALUE = 0.6657E+00

CREEP DATA FOR A PRIOR STRAIN HISTORY  $\int d\epsilon_M^p = -4.00$  % TENSION/TORSION

t	$\epsilon_{22}$	$\gamma_{\theta 2}$	$\dot{\epsilon}_{22}$	$\dot{\gamma}_{\theta 2}$	k
2.	0.9348E-04	0.1493E-03	0.2214E-04	0.2489E-04	0.1158E+01
3.	0.1058E-03	0.1624E-03	0.1599E-04	0.1048E-04	0.6750E+00
4.	0.1255E-03	0.1703E-03	0.1599E-04	0.9169E-05	0.5906E+00
5.	0.1378E-03	0.1808E-03	0.8609E-05	0.9169E-05	0.1097E+01
6.	0.1427E-03	0.1886E-03	0.4919E-05	0.6549E-05	0.1371E+01
7.	0.1476E-03	0.1939E-03	0.6149E-05	0.7859E-05	0.1316E+01
8.	0.1550E-03	0.2043E-03	0.8609E-05	0.1048E-04	0.1254E+01
9.	0.1648E-03	0.2148E-03	0.8609E-05	0.1048E-04	0.1254E+01
10.	0.1722E-03	0.2253E-03	0.6149E-05	0.6986E-05	0.1170E+01
15.	0.2017E-03	0.2567E-03	0.3935E-05	0.4192E-05	0.1097E+01
20.	0.2115E-03	0.2672E-03	0.1230E-05	0.3144E-05	0.2633E+01
25.	0.2140E-03	0.2882E-03	0.1476E-05	0.2882E-05	0.2011E+01
30.	0.2263E-03	0.2960E-03	0.3443E-05	0.1834E-05	0.5485E+00
35.	0.2484E-03	0.3065E-03	0.3689E-05	0.2358E-05	0.6582E+00
40.	0.2632E-03	0.3196E-03	0.1722E-05	0.1834E-05	0.1097E+01
45.	0.2656E-03	0.3249E-03	0.7378E-06	0.1310E-05	0.1828E+01
50.	0.2706E-03	0.3327E-03	0.9837E-06	0.1834E-05	0.1920E+01
55.	0.2755E-03	0.3432E-03	0.1722E-05	0.1572E-05	0.9403E+00
60.	0.2878E-03	0.3484E-03	0.1967E-05	0.7859E-06	0.4114E+00
65.	0.2952E-03	0.3510E-03	0.9837E-06	0.1310E-05	0.1371E+01
70.	0.2976E-03	0.3615E-03	0.4919E-06	0.1310E-05	0.2743E+01
75.	0.3001E-03	0.3641E-03	0.4919E-06	0.1834E-05	0.3840E+01
80.	0.3025E-03	0.3799E-03	0.1230E-05	0.1834E-05	0.1536E+01
85.	0.3124E-03	0.3825E-03	0.1476E-05	0.7859E-06	0.5485E+00
90.	0.3173E-03	0.3877E-03	0.7378E-06	0.1048E-05	0.1463E+01
95.	0.3197E-03	0.3930E-03	0.4918E-06	0.7859E-06	0.1646E+01
100.	0.3222E-03	0.3956E-03	0.4918E-06	0.5240E-06	0.1097E+01
105.	0.3247E-03	0.3982E-03	0.1230E-05	0.1048E-05	0.8777E+00
110.	0.3345E-03	0.4061E-03	0.1967E-05	0.1572E-05	0.8228E+00
115.	0.3443E-03	0.4139E-03	0.1475E-05	0.1310E-05	0.9143E+00
120.	0.3493E-03	0.4192E-03	0.1230E-05	0.7859E-06	0.6583E+00
125.	0.3566E-03	0.4218E-03	0.1230E-05	0.5240E-06	0.4389E+00
130.	0.3616E-03	0.4244E-03	0.1967E-05	0.5240E-06	0.2743E+00
135.	0.3763E-03	0.4270E-03	0.1721E-05	0.1048E-05	0.6269E+00
140.	0.3788E-03	0.4349E-03	0.9836E-06	0.1310E-05	0.1371E+01
145.	0.3861E-03	0.4401E-03	0.9836E-06	0.5240E-06	0.5486E+00
150.	0.3886E-03	0.4401E-03	0.3279E-06	0.1747E-06	0.5486E+00
160.	0.3911E-03	0.4427E-03	0.2459E-06	0.1310E-06	0.5486E+00
170.	0.3935E-03	0.4427E-03	0.1230E-06	0.3930E-06	0.3292E+01
180.	0.3935E-03	0.4506E-03	0.1230E-06	0.6549E-06	0.5486E+01
190.	0.3960E-03	0.4558E-03	0.1230E-06	0.5240E-06	0.4389E+01
200.	0.3960E-03	0.4611E-03	0.1230E-06	0.1048E-05	0.8778E+01
210.	0.3984E-03	0.4768E-03	0.2459E-06	0.9169E-06	0.3840E+01
220.	0.4009E-03	0.4794E-03	0.2459E-06	0.3930E-06	0.1646E+01
230.	0.4034E-03	0.4847E-03	0.2459E-06	0.5240E-06	0.2194E+01
240.	0.4058E-03	0.4899E-03	0.1230E-06	0.3930E-06	0.3292E+01
250.	0.4058E-03	0.4925E-03	0.1230E-06	0.2620E-06	0.2194E+01
260.	0.4083E-03	0.4951E-03	0.2459E-06	0.2620E-06	0.1097E+01
270.	0.4107E-03	0.4978E-03	0.1229E-06	0.5240E-06	0.4389E+00
280.	0.4329E-03	0.5056E-03	0.2213E-05	0.3930E-06	0.1829E+00
290.	0.4550E-03	0.5056E-03	0.2090E-05	0.2620E-06	0.1291E+00
300.	0.4747E-03	0.5109E-03	0.1229E-05	0.5240E-06	0.4389E+00
310.	0.4796E-03	0.5161E-03	0.4918E-06	0.5240E-06	0.1097E+01
320.	0.4845E-03	0.5213E-03	0.3688E-06	0.3930E-06	0.1097E+01
330.	0.4870E-03	0.5240E-03	0.2459E-06	0.1310E-06	0.5486E+00
340.	0.4894E-03	0.5240E-03	0.1229E-06	0.1310E-06	0.1097E+01
350.	0.4894E-03	0.5266E-03	0.1229E-06	0.2620E-06	0.2195E+01
360.	0.4919E-03	0.5292E-03	0.2459E-06	0.3930E-06	0.1646E+01
370.	0.4943E-03	0.5344E-03	0.2459E-06	0.5240E-06	0.2195E+01
380.	0.4968E-03	0.5397E-03	0.1229E-06	0.3930E-06	0.3292E+01
390.	0.4968E-03	0.5423E-03	0.1229E-06	0.2620E-06	0.2195E+01

AVERAGE K VALUE = 0.1601E+01

t	$\epsilon_{zz}$	$\gamma_{\theta z}$	$\dot{\epsilon}_{zz}$	$\dot{\gamma}_{\theta z}$	k
2.	0.3655E-03	0.1827E-03	0.9136E-04	0.4566E-04	0.5374E+00
3.	0.4396E-03	0.2114E-03	0.7160E-04	0.2870E-04	0.4310E+00
4.	0.5087E-03	0.2401E-03	0.5925E-04	0.2609E-04	0.4735E+00
5.	0.5581E-03	0.2635E-03	0.4690E-04	0.2218E-04	0.5085E+00
6.	0.6025E-03	0.2844E-03	0.4196E-04	0.1957E-04	0.5014E+00
7.	0.6420E-03	0.3027E-03	0.4196E-04	0.1696E-04	0.4346E+00
8.	0.6864E-03	0.3183E-03	0.3949E-04	0.1957E-04	0.5328E+00
9.	0.7210E-03	0.3418E-03	0.3209E-04	0.1827E-04	0.6121E+00
10.	0.7506E-03	0.3549E-03	0.2879E-04	0.1696E-04	0.6334E+00
15.	0.8937E-03	0.4436E-03	0.2567E-04	0.1487E-04	0.6231E+00
20.	0.1007E-02	0.5036E-03	0.2122E-04	0.1122E-04	0.5685E+00
25.	0.1106E-02	0.5558E-03	0.1875E-04	0.9133E-05	0.5237E+00
30.	0.1195E-02	0.5949E-03	0.1776E-04	0.8611E-05	0.5212E+00
35.	0.1284E-02	0.6419E-03	0.1776E-04	0.8872E-05	0.5371E+00
40.	0.1372E-02	0.6836E-03	0.1628E-04	0.5480E-05	0.3619E+00
45.	0.1446E-02	0.6967E-03	0.1529E-04	0.4697E-05	0.3303E+00
50.	0.1525E-02	0.7306E-03	0.1924E-04	0.7567E-05	0.4230E+00
55.	0.1639E-02	0.7724E-03	0.2219E-04	0.6784E-05	0.3287E+00
60.	0.1747E-02	0.7984E-03	0.2022E-04	0.5740E-05	0.3053E+00
65.	0.1841E-02	0.8298E-03	0.1775E-04	0.7045E-05	0.4267E+00
70.	0.1925E-02	0.8689E-03	0.1528E-04	0.6523E-05	0.4589E+00
75.	0.1994E-02	0.8950E-03	0.1627E-04	0.3653E-05	0.2414E+00
80.	0.2087E-02	0.9054E-03	0.1775E-04	0.4436E-05	0.2688E+00
85.	0.2171E-02	0.9393E-03	0.1676E-04	0.5740E-05	0.3683E+00
90.	0.2255E-02	0.9628E-03	0.1232E-04	0.3914E-05	0.3415E+00
95.	0.2294E-02	0.9785E-03	0.1232E-04	0.2870E-05	0.2505E+00
100.	0.2378E-02	0.9915E-03	0.1626E-04	0.4436E-05	0.2933E+00
105.	0.2457E-02	0.1023E-02	0.1380E-04	0.4697E-05	0.3660E+00
110.	0.2516E-02	0.1038E-02	0.1232E-04	0.4697E-05	0.4100E+00
115.	0.2580E-02	0.1070E-02	0.1035E-04	0.6262E-05	0.6508E+00
120.	0.2620E-02	0.1101E-02	0.1133E-04	0.4436E-05	0.4209E+00
125.	0.2694E-02	0.1114E-02	0.1429E-04	0.1305E-05	0.9819E-01
130.	0.2763E-02	0.1114E-02	0.1429E-04	0.2348E-05	0.1767E+00
135.	0.2836E-02	0.1138E-02	0.1379E-04	0.4436E-05	0.3458E+00
140.	0.2901E-02	0.1159E-02	0.1133E-04	0.3653E-05	0.3467E+00
145.	0.2950E-02	0.1174E-02	0.7881E-05	0.2870E-05	0.3916E+00
150.	0.2979E-02	0.1187E-02	0.8865E-05	0.4697E-05	0.5697E+00
160.	0.3083E-02	0.1245E-02	0.9603E-05	0.5219E-05	0.5843E+00
170.	0.3171E-02	0.1292E-02	0.8618E-05	0.3653E-05	0.4558E+00
180.	0.3255E-02	0.1318E-02	0.8617E-05	0.3392E-05	0.4233E+00
190.	0.3344E-02	0.1359E-02	0.8616E-05	0.4044E-05	0.5047E+00
200.	0.3427E-02	0.1399E-02	0.7877E-05	0.3783E-05	0.5165E+00
210.	0.3501E-02	0.1435E-02	0.6400E-05	0.3131E-05	0.5261E+00
220.	0.3555E-02	0.1461E-02	0.7630E-05	0.3262E-05	0.4597E+00
230.	0.3654E-02	0.1500E-02	0.9598E-05	0.4175E-05	0.4677E+00
240.	0.3747E-02	0.1545E-02	0.9105E-05	0.4044E-05	0.4776E+00
250.	0.3836E-02	0.1581E-02	0.8612E-05	0.3262E-05	0.4072E+00
260.	0.3920E-02	0.1610E-02	0.7627E-05	0.3131E-05	0.4414E+00
270.	0.3988E-02	0.1644E-02	0.7626E-05	0.3262E-05	0.4599E+00
280.	0.4072E-02	0.1675E-02	0.7134E-05	0.3653E-05	0.5506E+00
290.	0.4131E-02	0.1717E-02	0.6641E-05	0.3392E-05	0.5492E+00
300.	0.4205E-02	0.1743E-02	0.7379E-05	0.3131E-05	0.4563E+00
310.	0.4279E-02	0.1780E-02	0.5657E-05	0.3914E-05	0.7440E+00
320.	0.4318E-02	0.1821E-02	0.4919E-05	0.3914E-05	0.8556E+00
330.	0.4377E-02	0.1858E-02	0.5410E-05	0.3523E-05	0.7001E+00
340.	0.4426E-02	0.1892E-02	0.4918E-05	0.3262E-05	0.7131E+00
350.	0.4475E-02	0.1923E-02	0.5901E-05	0.3001E-05	0.5467E+00
360.	0.4544E-02	0.1952E-02	0.6393E-05	0.2740E-05	0.4608E+00
370.	0.4603E-02	0.1978E-02	0.7376E-05	0.4175E-05	0.6086E+00
380.	0.4692E-02	0.2035E-02	0.8605E-05	0.4827E-05	0.6032E+00
390.	0.4775E-02	0.2074E-02	0.1131E-04	0.5480E-05	0.5211E+00
400.	0.4918E-02	0.2145E-02	0.1376E-04	0.9133E-05	0.7134E+00
410.	0.5051E-02	0.2257E-02	0.1376E-04	0.1096E-04	0.8563E+00

AVERAGE K VALUE = 0.5154E+00

CREEP DATA FOR A PRIOR STRAIN HISTORY  $\int d\epsilon_p = 2.00\%$  TENSION/TORSION

t	$\epsilon_{11}$	$\delta\epsilon_2$	$\dot{\epsilon}_{11}$	$\dot{\delta}\epsilon_2$	K
2.	0.1224E-02	0.2992E-02	0.3426E-03	0.1041E-02	0.3238E+01
3.	0.1518E-02	0.3850E-02	0.2691E-03	0.7804E-03	0.3092E+01
4.	0.1762E-02	0.4553E-02	0.2201E-03	0.6764E-03	0.3276E+01
5.	0.1958E-02	0.5203E-02	0.1834E-03	0.5853E-03	0.3403E+01
6.	0.2129E-02	0.5723E-02	0.1711E-03	0.4943E-03	0.3079E+01
7.	0.2300E-02	0.6191E-02	0.1589E-03	0.4293E-03	0.2880E+01
8.	0.2447E-02	0.6582E-02	0.1466E-03	0.3902E-03	0.2837E+01
9.	0.2594E-02	0.6972E-02	0.1222E-03	0.3772E-03	0.3291E+01
10.	0.2691E-02	0.7336E-02	0.9772E-04	0.3122E-03	0.3406E+01
15.	0.3180E-02	0.8845E-02	0.8548E-04	0.2492E-03	0.3115E+01
20.	0.3546E-02	0.9834E-02	0.6836E-04	0.2003E-03	0.3124E+01
25.	0.3864E-02	0.1085E-01	0.6589E-04	0.1899E-03	0.3073E+01
30.	0.4205E-02	0.1173E-01	0.6100E-04	0.1639E-03	0.2865E+01
35.	0.4473E-02	0.1249E-01	0.4634E-04	0.1431E-03	0.3292E+01
40.	0.4669E-02	0.1316E-01	0.3658E-04	0.1249E-03	0.3640E+01
45.	0.4839E-02	0.1374E-01	0.3657E-04	0.1093E-03	0.3186E+01
50.	0.5034E-02	0.1426E-01	0.3657E-04	0.1015E-03	0.2959E+01
55.	0.5205E-02	0.1475E-01	0.3412E-04	0.8847E-04	0.2764E+01
60.	0.5376E-02	0.1514E-01	0.3168E-04	0.8847E-04	0.2977E+01
65.	0.5522E-02	0.1564E-01	0.2924E-04	0.8847E-04	0.3226E+01
70.	0.5668E-02	0.1603E-01	0.2680E-04	0.7546E-04	0.3002E+01
75.	0.5790E-02	0.1639E-01	0.2192E-04	0.7026E-04	0.3417E+01
80.	0.5887E-02	0.1673E-01	0.2192E-04	0.7286E-04	0.3544E+01
85.	0.6009E-02	0.1712E-01	0.2192E-04	0.6245E-04	0.3038E+01
90.	0.6106E-02	0.1735E-01	0.2922E-04	0.5465E-04	0.1994E+01
95.	0.6301E-02	0.1767E-01	0.2922E-04	0.7026E-04	0.2564E+01
100.	0.6398E-02	0.1806E-01	0.1461E-04	0.6245E-04	0.4558E+01
105.	0.6447E-02	0.1829E-01	0.1461E-04	0.5725E-04	0.4179E+01
110.	0.6545E-02	0.1863E-01	0.1460E-04	0.5985E-04	0.4369E+01
115.	0.6593E-02	0.1889E-01	0.1704E-04	0.4944E-04	0.3094E+01
120.	0.6715E-02	0.1912E-01	0.1704E-04	0.4164E-04	0.2606E+01
125.	0.6764E-02	0.1931E-01	0.1217E-04	0.4424E-04	0.3876E+01
130.	0.6837E-02	0.1957E-01	0.1703E-04	0.5205E-04	0.3258E+01
135.	0.6934E-02	0.1983E-01	0.2190E-04	0.4684E-04	0.2281E+01
140.	0.7056E-02	0.2003E-01	0.1460E-04	0.3904E-04	0.2851E+01
145.	0.7080E-02	0.2022E-01	0.7298E-05	0.4945E-04	0.7223E+01
150.	0.7129E-02	0.2053E-01	0.1297E-04	0.4164E-04	0.3422E+01
160.	0.7274E-02	0.2084E-01	0.1338E-04	0.3513E-04	0.2800E+01
170.	0.7396E-02	0.2123E-01	0.1459E-04	0.4424E-04	0.3233E+01
180.	0.7566E-02	0.2173E-01	0.1459E-04	0.4425E-04	0.3233E+01
190.	0.7688E-02	0.2212E-01	0.1337E-04	0.4034E-04	0.3216E+01
200.	0.7834E-02	0.2253E-01	0.1337E-04	0.3774E-04	0.3009E+01
210.	0.7955E-02	0.2287E-01	0.1215E-04	0.2863E-04	0.2512E+01
220.	0.8077E-02	0.2310E-01	0.9721E-05	0.2733E-04	0.2997E+01
230.	0.8150E-02	0.2342E-01	0.7290E-05	0.2473E-04	0.3616E+01
240.	0.8223E-02	0.2360E-01	0.7290E-05	0.1692E-04	0.2474E+01
250.	0.8295E-02	0.2376E-01	0.7289E-05	0.2343E-04	0.3426E+01
260.	0.8368E-02	0.2407E-01	0.9718E-05	0.2343E-04	0.2570E+01
270.	0.8490E-02	0.2422E-01	0.8503E-05	0.1952E-04	0.2448E+01
280.	0.8538E-02	0.2446E-01	0.9716E-05	0.2993E-04	0.3285E+01
290.	0.8684E-02	0.2482E-01	0.1214E-04	0.2603E-04	0.2285E+01
300.	0.8781E-02	0.2498E-01	0.8500E-05	0.2082E-04	0.2612E+01
310.	0.8854E-02	0.2524E-01	0.7285E-05	0.1952E-04	0.2857E+01
320.	0.8927E-02	0.2537E-01	0.6071E-05	0.1952E-04	0.3429E+01

ADD 0.2113E-02

AVERAGE K VALUE = 0.3185E+01

CREEP DATA FOR A PRIOR STRAIN HISTORY  $\int d\epsilon_M^P = -2.00 \% \text{ TENSION/TORSION}$

t	$\epsilon_{22}$	$\gamma_{\theta z}$	$\dot{\epsilon}_{22}$	$\dot{\gamma}_{\theta z}$	K
2.	0.2236E-02	0.2371E-02	0.6382E-03	0.1120E-02	0.1935E+01
3.	0.2751E-02	0.3492E-02	0.5029E-03	0.8468E-03	0.1856E+01
4.	0.3242E-02	0.4065E-02	0.4169E-03	0.6254E-03	0.1654E+01
5.	0.3585E-02	0.4742E-02	0.3064E-03	0.5993E-03	0.2156E+01
6.	0.3855E-02	0.5263E-02	0.2573E-03	0.4690E-03	0.2010E+01
7.	0.4100E-02	0.5680E-02	0.2327E-03	0.4039E-03	0.1913E+01
8.	0.4320E-02	0.6071E-02	0.1960E-03	0.3778E-03	0.2126E+01
9.	0.4492E-02	0.6436E-02	0.1714E-03	0.3778E-03	0.2430E+01
10.	0.4663E-02	0.6827E-02	0.1591E-03	0.2910E-03	0.2016E+01
15.	0.5446E-02	0.8182E-02	0.1370E-03	0.2476E-03	0.1992E+01
20.	0.6033E-02	0.9302E-02	0.1076E-03	0.1980E-03	0.2029E+01
25.	0.6522E-02	0.1016E-01	0.8555E-04	0.1642E-03	0.2116E+01
30.	0.6889E-02	0.1094E-01	0.7085E-04	0.1459E-03	0.2271E+01
35.	0.7231E-02	0.1162E-01	0.7083E-04	0.1251E-03	0.1947E+01
40.	0.7597E-02	0.1219E-01	0.6836E-04	0.1095E-03	0.1765E+01
45.	0.7914E-02	0.1272E-01	0.6346E-04	0.1225E-03	0.2128E+01
50.	0.8232E-02	0.1342E-01	0.6831E-04	0.1303E-03	0.2103E+01
55.	0.8598E-02	0.1402E-01	0.7073E-04	0.1173E-03	0.1828E+01
60.	0.8939E-02	0.1459E-01	0.5852E-04	0.1095E-03	0.2062E+01
65.	0.9183E-02	0.1511E-01	0.4875E-04	0.9904E-04	0.2240E+01
70.	0.9426E-02	0.1558E-01	0.5117E-04	0.1043E-03	0.2246E+01
75.	0.9694E-02	0.1616E-01	0.5603E-04	0.1147E-03	0.2256E+01
80.	0.9987E-02	0.1673E-01	0.6089E-04	0.1121E-03	0.2029E+01
85.	0.1030E-01	0.1728E-01	0.5357E-04	0.9383E-04	0.1931E+01
90.	0.1052E-01	0.1767E-01	0.4138E-04	0.7559E-04	0.2014E+01
95.	0.1072E-01	0.1803E-01	0.3894E-04	0.7819E-04	0.2214E+01
100.	0.1091E-01	0.1845E-01	0.4866E-04	0.9905E-04	0.2244E+01
105.	0.1120E-01	0.1902E-01	0.5109E-04	0.9123E-04	0.1969E+01
110.	0.1142E-01	0.1936E-01	0.3891E-04	0.6517E-04	0.1846E+01
115.	0.1159E-01	0.1968E-01	0.3161E-04	0.5735E-04	0.2000E+01
120.	0.1174E-01	0.1994E-01	0.3647E-04	0.5995E-04	0.1813E+01
125.	0.1196E-01	0.2027E-01	0.4375E-04	0.7559E-04	0.1905E+01
130.	0.1218E-01	0.2069E-01	0.3888E-04	0.6778E-04	0.1922E+01
135.	0.1235E-01	0.2095E-01	0.3402E-04	0.4171E-04	0.1352E+01
140.	0.1252E-01	0.2111E-01	0.3158E-04	0.4171E-04	0.1456E+01
145.	0.1266E-01	0.2137E-01	0.2429E-04	0.5214E-04	0.2366E+01
150.	0.1276E-01	0.2163E-01	0.3076E-04	0.5909E-04	0.2118E+01
160.	0.1312E-01	0.2226E-01	0.2792E-04	0.4562E-04	0.1801E+01
170.	0.1332E-01	0.2254E-01	0.1942E-04	0.3519E-04	0.1998E+01
180.	0.1351E-01	0.2296E-01	0.2063E-04	0.3519E-04	0.1881E+01
190.	0.1373E-01	0.2325E-01	0.1941E-04	0.2737E-04	0.1555E+01
200.	0.1390E-01	0.2351E-01	0.1577E-04	0.3259E-04	0.2278E+01
210.	0.1405E-01	0.2390E-01	0.1334E-04	0.3780E-04	0.3124E+01
220.	0.1417E-01	0.2426E-01	0.2183E-04	0.4563E-04	0.2305E+01
230.	0.1448E-01	0.2481E-01	0.2910E-04	0.4302E-04	0.1630E+01
240.	0.1475E-01	0.2512E-01	0.2061E-04	0.3650E-04	0.1953E+01
250.	0.1489E-01	0.2554E-01	0.1939E-04	0.3911E-04	0.2224E+01
260.	0.1514E-01	0.2591E-01	0.2181E-04	0.3129E-04	0.1582E+01
270.	0.1533E-01	0.2617E-01	0.2059E-04	0.3650E-04	0.1955E+01
280.	0.1555E-01	0.2664E-01	0.1574E-04	0.3650E-04	0.2556E+01
290.	0.1565E-01	0.2690E-01	0.1695E-04	0.3390E-04	0.2205E+01
300.	0.1589E-01	0.2731E-01	0.2058E-04	0.3520E-04	0.1886E+01

ADD 0.1328E-02

AVERAGE K VALUE = 0.2023E+01

CREEP DATA FOR A PRIOR STRAIN HISTORY  $\int d\epsilon_M = -2.70\%$  TENSION/TORSION

t	$\epsilon_{zz}$	$\delta\epsilon_z$	$\dot{\epsilon}_{zz}$	$\dot{\delta}\epsilon_z$	k
2.	0.2109E-02	0.1041E-02	0.4572E-03	0.3336E-03	0.8125E+00
3.	0.2467E-02	0.1335E-02	0.3179E-03	0.2669E-03	0.9348E+00
4.	0.2745E-02	0.1575E-02	0.2384E-03	0.2135E-03	0.9974E+00
5.	0.2944E-02	0.1762E-02	0.1887E-03	0.2002E-03	0.1181E+01
6.	0.3123E-02	0.1975E-02	0.1390E-03	0.2202E-03	0.1764E+01
7.	0.3222E-02	0.2202E-02	0.1489E-03	0.1668E-03	0.1247E+01
8.	0.3420E-02	0.2309E-02	0.1787E-03	0.1201E-03	0.7486E+00
9.	0.3579E-02	0.2442E-02	0.1290E-03	0.1268E-03	0.1094E+01
10.	0.3678E-02	0.2562E-02	0.9591E-04	0.1223E-03	0.1420E+01
15.	0.4155E-02	0.3176E-02	0.8332E-04	0.1094E-03	0.1463E+01
20.	0.4512E-02	0.3657E-02	0.6544E-04	0.9342E-04	0.1590E+01
25.	0.4809E-02	0.4110E-02	0.5353E-04	0.8541E-04	0.1777E+01
30.	0.5047E-02	0.4511E-02	0.4559E-04	0.7340E-04	0.1793E+01
35.	0.5265E-02	0.4844E-02	0.3963E-04	0.6673E-04	0.1875E+01
40.	0.5443E-02	0.5178E-02	0.3368E-04	0.6272E-04	0.2074E+01
45.	0.5602E-02	0.5472E-02	0.3764E-04	0.5472E-04	0.1619E+01
50.	0.5820E-02	0.5725E-02	0.3169E-04	0.5071E-04	0.1782E+01
55.	0.5919E-02	0.5979E-02	0.1980E-04	0.5071E-04	0.2852E+01
60.	0.6018E-02	0.6232E-02	0.2376E-04	0.4538E-04	0.2127E+01
65.	0.6156E-02	0.6432E-02	0.2376E-04	0.4004E-04	0.1877E+01
70.	0.6255E-02	0.6633E-02	0.1980E-04	0.3737E-04	0.2102E+01
75.	0.6354E-02	0.6806E-02	0.1979E-04	0.3603E-04	0.2027E+01
80.	0.6453E-02	0.6993E-02	0.1781E-04	0.3737E-04	0.2336E+01
85.	0.6532E-02	0.7180E-02	0.1781E-04	0.3470E-04	0.2169E+01
90.	0.6631E-02	0.7340E-02	0.1979E-04	0.3470E-04	0.1953E+01
95.	0.6730E-02	0.7527E-02	0.1781E-04	0.3203E-04	0.2003E+01
100.	0.6809E-02	0.7660E-02	0.1781E-04	0.3070E-04	0.1920E+01
105.	0.6908E-02	0.7834E-02	0.1583E-04	0.3203E-04	0.2254E+01
110.	0.6968E-02	0.7981E-02	0.1385E-04	0.2803E-04	0.2254E+01
115.	0.7047E-02	0.8114E-02	0.1780E-04	0.2669E-04	0.1670E+01
120.	0.7146E-02	0.8247E-02	0.1582E-04	0.2536E-04	0.1785E+01
125.	0.7205E-02	0.8368E-02	0.1384E-04	0.2936E-04	0.2362E+01
130.	0.7284E-02	0.8541E-02	0.1187E-04	0.2803E-04	0.2630E+01
135.	0.7324E-02	0.8648E-02	0.1186E-04	0.2536E-04	0.2380E+01
140.	0.7403E-02	0.8795E-02	0.1582E-04	0.2936E-04	0.2067E+01
145.	0.7482E-02	0.8941E-02	0.1384E-04	0.2803E-04	0.2255E+01
150.	0.7541E-02	0.9075E-02	0.1450E-04	0.2847E-04	0.2187E+01
160.	0.7699E-02	0.9369E-02	0.1680E-04	0.3003E-04	0.1990E+01
170.	0.7877E-02	0.9676E-02	0.1384E-04	0.3003E-04	0.2417E+01
180.	0.7976E-02	0.9969E-02	0.1284E-04	0.2936E-04	0.2546E+01
190.	0.8134E-02	0.1026E-01	0.1482E-04	0.3003E-04	0.2257E+01
200.	0.8272E-02	0.1057E-01	0.1185E-04	0.2870E-04	0.2696E+01
210.	0.8371E-02	0.1084E-01	0.1284E-04	0.2603E-04	0.2257E+01
220.	0.8529E-02	0.1109E-01	0.1284E-04	0.2669E-04	0.2315E+01
230.	0.8628E-02	0.1137E-01	0.9874E-05	0.2402E-04	0.2709E+01
240.	0.8727E-02	0.1157E-01	0.9873E-05	0.2069E-04	0.2333E+01
250.	0.8825E-02	0.1178E-01	0.9872E-05	0.1935E-04	0.2183E+01
260.	0.8924E-02	0.1196E-01	0.7897E-05	0.1735E-04	0.2447E+01
270.	0.8983E-02	0.1213E-01	0.7897E-05	0.1735E-04	0.2447E+01
280.	0.9082E-02	0.1230E-01	0.9870E-05	0.1602E-04	0.1807E+01
290.	0.9181E-02	0.1245E-01	0.9869E-05	0.1535E-04	0.1732E+01
300.	0.9279E-02	0.1261E-01	0.1283E-04	0.1535E-04	0.1332E+01
310.	0.9437E-02	0.1276E-01	0.7894E-05	0.1602E-04	0.2260E+01
320.	0.9437E-02	0.1293E-01	0.3946E-05	0.1735E-04	0.4896E+01
330.	0.9516E-02	0.1311E-01	0.6906E-05	0.1668E-04	0.2690E+01
340.	0.9575E-02	0.1327E-01	0.5919E-05	0.1468E-04	0.2762E+01
350.	0.9635E-02	0.1340E-01	0.5919E-05	0.1401E-04	0.2637E+01
360.	0.9694E-02	0.1355E-01	0.6905E-05	0.1401E-04	0.2260E+01
370.	0.9773E-02	0.1368E-01	0.5918E-05	0.1268E-04	0.2386E+01
380.	0.9812E-02	0.1380E-01	0.4931E-05	0.1201E-04	0.2713E+01
390.	0.9871E-02	0.1392E-01	0.4931E-05	0.1268E-04	0.2864E+01
400.	0.9911E-02	0.1405E-01	0.4931E-05	0.1201E-04	0.2713E+01
410.	0.9970E-02	0.1416E-01	0.4931E-05	0.1001E-04	0.2261E+01

AVERAGE K VALUE = 0.2108E+01

CREEP DATA FOR A PRIOR STRAIN HISTORY  $\int d\epsilon_M^P = -3.00 \% \text{ TENSION/TORSION}$

t	$\epsilon_{zz}$	$\delta\epsilon_z$	$\dot{\epsilon}_{zz}$	$\dot{\delta}\epsilon_z$	k
2.	0.6398E-03	0.3589E-03	0.1499E-03	0.6646E-04	0.4757E+00
3.	0.7397E-03	0.4254E-03	0.1099E-03	0.5317E-04	0.5190E+00
4.	0.8596E-03	0.4652E-03	0.8993E-04	0.3988E-04	0.4758E+00
5.	0.9196E-03	0.5051E-03	0.6993E-04	0.3988E-04	0.6118E+00
6.	0.9995E-03	0.5450E-03	0.8991E-04	0.3988E-04	0.4759E+00
7.	0.1099E-02	0.5849E-03	0.7991E-04	0.3323E-04	0.4462E+00
8.	0.1159E-02	0.6115E-03	0.6992E-04	0.3988E-04	0.6120E+00
9.	0.1239E-02	0.6646E-03	0.6991E-04	0.3988E-04	0.6120E+00
10.	0.1299E-02	0.6912E-03	0.5659E-04	0.2659E-04	0.5041E+00
15.	0.1579E-02	0.8241E-03	0.5392E-04	0.2526E-04	0.5026E+00
20.	0.1838E-02	0.9438E-03	0.4192E-04	0.1861E-04	0.4763E+00
25.	0.1998E-02	0.1010E-02	0.3194E-04	0.1595E-04	0.5359E+00
30.	0.2158E-02	0.1103E-02	0.3592E-04	0.1462E-04	0.4368E+00
35.	0.2357E-02	0.1156E-02	0.3392E-04	0.1329E-04	0.4205E+00
40.	0.2497E-02	0.1236E-02	0.2793E-04	0.1462E-04	0.5617E+00
45.	0.2637E-02	0.1303E-02	0.2793E-04	0.1329E-04	0.5107E+00
50.	0.2776E-02	0.1369E-02	0.3191E-04	0.1595E-04	0.5363E+00
55.	0.2956E-02	0.1462E-02	0.3789E-04	0.1994E-04	0.5647E+00
60.	0.3155E-02	0.1569E-02	0.3589E-04	0.1861E-04	0.5564E+00
65.	0.3315E-02	0.1648E-02	0.2791E-04	0.2127E-04	0.8177E+00
70.	0.3434E-02	0.1781E-02	0.2392E-04	0.1861E-04	0.8348E+00
75.	0.3554E-02	0.1834E-02	0.2591E-04	0.1196E-04	0.4955E+00
80.	0.3693E-02	0.1901E-02	0.2590E-04	0.1595E-04	0.6607E+00
85.	0.3813E-02	0.1994E-02	0.2391E-04	0.1994E-04	0.8948E+00
90.	0.3932E-02	0.2100E-02	0.2191E-04	0.1462E-04	0.7159E+00
95.	0.4032E-02	0.2140E-02	0.1594E-04	0.1063E-04	0.7160E+00
100.	0.4092E-02	0.2207E-02	0.1593E-04	0.1462E-04	0.9846E+00
105.	0.4191E-02	0.2286E-02	0.1792E-04	0.1462E-04	0.8753E+00
110.	0.4271E-02	0.2353E-02	0.1991E-04	0.1329E-04	0.7162E+00
115.	0.4390E-02	0.2419E-02	0.1792E-04	0.1329E-04	0.7958E+00
120.	0.4450E-02	0.2486E-02	0.1394E-04	0.1063E-04	0.8187E+00
125.	0.4530E-02	0.2526E-02	0.1394E-04	0.1329E-04	0.1023E+01
130.	0.4589E-02	0.2619E-02	0.1792E-04	0.1861E-04	0.1114E+01
135.	0.4709E-02	0.2712E-02	0.1991E-04	0.1728E-04	0.9314E+00
140.	0.4789E-02	0.2791E-02	0.1194E-04	0.1728E-04	0.1553E+01
145.	0.4828E-02	0.2885E-02	0.1393E-04	0.1595E-04	0.1228E+01
150.	0.4928E-02	0.2951E-02	0.2123E-04	0.2038E-04	0.1030E+01
160.	0.5147E-02	0.3190E-02	0.1890E-04	0.2260E-04	0.1283E+01
170.	0.5306E-02	0.3403E-02	0.1194E-04	0.1795E-04	0.1613E+01
180.	0.5385E-02	0.3549E-02	0.1094E-04	0.1462E-04	0.1434E+01
190.	0.5525E-02	0.3695E-02	0.1094E-04	0.1130E-04	0.1108E+01
200.	0.5604E-02	0.3775E-02	0.8950E-05	0.1063E-04	0.1275E+01
210.	0.5704E-02	0.3908E-02	0.7955E-05	0.1130E-04	0.1524E+01
220.	0.5763E-02	0.4001E-02	0.6960E-05	0.1063E-04	0.1639E+01
230.	0.5843E-02	0.4121E-02	0.7953E-05	0.1130E-04	0.1524E+01
240.	0.5922E-02	0.4227E-02	0.6959E-05	0.1063E-04	0.1640E+01
250.	0.5982E-02	0.4333E-02	0.4970E-05	0.1263E-04	0.2726E+01
260.	0.6022E-02	0.4480E-02	0.7952E-05	0.1329E-04	0.1794E+01
270.	0.6141E-02	0.4599E-02	0.7951E-05	0.1329E-04	0.1794E+01
280.	0.6181E-02	0.4746E-02	0.6957E-05	0.1462E-04	0.2255E+01
290.	0.6280E-02	0.4892E-02	0.9937E-05	0.1529E-04	0.1651E+01
300.	0.6380E-02	0.5051E-02	0.6956E-05	0.1595E-04	0.2461E+01
310.	0.6419E-02	0.5211E-02	0.7948E-05	0.1462E-04	0.1974E+01
320.	0.6539E-02	0.5344E-02	0.7948E-05	0.1329E-04	0.1794E+01
330.	0.6578E-02	0.5477E-02	0.3974E-05	0.1462E-04	0.3948E+01
340.	0.6618E-02	0.5636E-02	0.3974E-05	0.1396E-04	0.3769E+01
350.	0.6658E-02	0.5756E-02	0.4967E-05	0.1196E-04	0.2585E+01
360.	0.6717E-02	0.5875E-02	0.4967E-05	0.1196E-04	0.2585E+01
370.	0.6757E-02	0.5995E-02	0.4966E-05	0.1196E-04	0.2585E+01
380.	0.6817E-02	0.6115E-02	0.3973E-05	0.1130E-04	0.3052E+01
390.	0.6837E-02	0.6221E-02	0.3973E-05	0.1196E-04	0.3231E+01
400.	0.6896E-02	0.6354E-02	0.6952E-05	0.1329E-04	0.2052E+01
410.	0.6976E-02	0.6487E-02	0.6951E-05	0.1329E-04	0.2052E+01

ADD 0.03718E-02

AVERAGE K VALUE = 0.1304E+01

CREEP DATA FOR A PRIOR STRAIN HISTORY  $\int d\epsilon_M^P = -4.00 \% \text{ TENSILE/TORSION}$

t	$\epsilon_{22}$	$\gamma_{02}$	$\dot{\epsilon}_{22}$	$\dot{\gamma}_{02}$	k
2.	0.9102E-04	0.3425E-04	0.2091E-04	0.7574E-05	0.3813E+00
3.	0.1058E-03	0.3952E-04	0.1722E-04	0.6257E-05	0.3825E+00
4.	0.1255E-03	0.4676E-04	0.1476E-04	0.3952E-05	0.2819E+00
5.	0.1353E-03	0.4742E-04	0.1107E-04	0.6586E-06	0.6263E-01
6.	0.1476E-03	0.4808E-04	0.7379E-05	0.9879E-06	0.1409E+00
7.	0.1500E-03	0.4940E-04	0.6149E-05	0.1647E-05	0.2819E+00
8.	0.1599E-03	0.5137E-04	0.6149E-05	0.1317E-05	0.2255E+00
9.	0.1623E-03	0.5203E-04	0.4919E-05	0.6586E-06	0.1409E+00
10.	0.1697E-03	0.5269E-04	0.4919E-05	0.1207E-05	0.2584E+00
15.	0.1919E-03	0.5927E-04	0.4427E-05	0.7903E-06	0.1879E+00
20.	0.2140E-03	0.6059E-04	0.2951E-05	0.5269E-06	0.1879E+00
25.	0.2214E-03	0.6454E-04	0.3197E-05	0.6586E-06	0.2168E+00
30.	0.2460E-03	0.6718E-04	0.3935E-05	0.5269E-06	0.1409E+00
35.	0.2607E-03	0.6981E-04	0.3689E-05	0.7903E-06	0.2255E+00
40.	0.2829E-03	0.7508E-04	0.3935E-05	0.6586E-06	0.1762E+00
45.	0.3001E-03	0.7640E-04	0.3689E-05	0.1976E-06	0.5638E-01
50.	0.3197E-03	0.7706E-04	0.2951E-05	0.2634E-06	0.9397E-01
55.	0.3296E-03	0.7903E-04	0.1721E-05	0.1317E-06	0.8055E-01
60.	0.3370E-03	0.7837E-04	0.1967E-05	0.0000E+00	0.0000E+00
65.	0.3493E-03	0.7903E-04	0.2951E-05	0.1976E-06	0.7048E-01
70.	0.3665E-03	0.8035E-04	0.1967E-05	0.1317E-06	0.7048E-01
75.	0.3689E-03	0.8035E-04	0.4918E-06	0.6586E-07	0.1410E+00
80.	0.3714E-03	0.8101E-04	0.1475E-05	0.1976E-06	0.1410E+00
85.	0.3837E-03	0.8233E-04	0.2213E-05	0.1976E-06	0.9398E-01
90.	0.3935E-03	0.8298E-04	0.1230E-05	0.1317E-06	0.1128E+00
95.	0.3960E-03	0.8364E-04	0.2459E-06	0.1317E-06	0.5639E+00
100.	0.3960E-03	0.8430E-04	0.2459E-06	0.1317E-06	0.5639E+00
105.	0.3984E-03	0.8496E-04	0.1721E-05	0.1317E-06	0.8055E-01
110.	0.4132E-03	0.8562E-04	0.2705E-05	0.1317E-06	0.5126E-01
115.	0.4255E-03	0.8628E-04	0.1475E-05	0.1317E-06	0.9398E-01
120.	0.4279E-03	0.8694E-04	0.7377E-06	0.6586E-07	0.9398E-01
125.	0.4329E-03	0.8694E-04	0.1475E-05	0.6586E-07	0.4699E-01
130.	0.4427E-03	0.8760E-04	0.2459E-05	0.6586E-07	0.2819E-01
135.	0.4575E-03	0.8760E-04	0.2213E-05	0.6586E-07	0.3133E-01
140.	0.4648E-03	0.8825E-04	0.9835E-06	0.6586E-07	0.7049E-01
145.	0.4673E-03	0.8825E-04	0.1475E-05	0.6586E-07	0.4699E-01
150.	0.4796E-03	0.8891E-04	0.2623E-05	0.2634E-06	0.1057E+00
160.	0.5066E-03	0.9221E-04	0.2090E-05	0.1647E-06	0.8293E-01
170.	0.5214E-03	0.9221E-04	0.2090E-05	0.6586E-07	0.3317E-01
180.	0.5484E-03	0.9352E-04	0.2213E-05	0.9879E-07	0.4700E-01
190.	0.5656E-03	0.9418E-04	0.1844E-05	0.6586E-07	0.3760E-01
200.	0.5853E-03	0.9484E-04	0.1844E-05	0.1317E-06	0.7520E-01
210.	0.6025E-03	0.9682E-04	0.1721E-05	0.1317E-06	0.8057E-01
220.	0.6197E-03	0.9747E-04	0.1598E-05	0.3293E-07	0.2169E-01
230.	0.6345E-03	0.9747E-04	0.1475E-05	0.3293E-07	0.2350E-01
240.	0.6492E-03	0.9813E-04	0.8604E-06	0.3293E-07	0.4029E-01
250.	0.6517E-03	0.9813E-04	0.6146E-06	0.3293E-07	0.5640E-01
260.	0.6615E-03	0.9879E-04	0.6146E-06	0.6586E-07	0.1128E+00
270.	0.6640E-03	0.9945E-04	0.7375E-06	0.3293E-07	0.4700E-01
280.	0.6763E-03	0.9945E-04	0.6146E-06	0.3293E-07	0.5640E-01
290.	0.6763E-03	0.1001E-03	0.7375E-06	0.3293E-07	0.4700E-01
300.	0.6910E-03	0.1001E-03	0.1352E-05	0.6586E-07	0.5128E-01
310.	0.7033E-03	0.1014E-03	0.1106E-05	0.6586E-07	0.6267E-01
320.	0.7131E-03	0.1014E-03	0.1475E-05	0.3293E-07	0.2350E-01
330.	0.7328E-03	0.1021E-03	0.9833E-06	0.6586E-07	0.7051E-01
340.	0.7328E-03	0.1027E-03	0.8604E-06	0.6586E-07	0.8058E-01
350.	0.7500E-03	0.1034E-03	0.1229E-05	0.6586E-07	0.5641E-01
360.	0.7574E-03	0.1041E-03	0.1229E-05	0.6586E-07	0.5641E-01
370.	0.7746E-03	0.1047E-03	0.1598E-05	0.6586E-07	0.4339E-01

(x10)

(x10)

(x10)

AVERAGE K VALUE = 0.1209E+00

# Programme 6.2

175

\*\* KINGSTON POLYTECHNIC 4120 \*\*

&JOB; MAPE/R008/DR; STRAIN RATES;

&OPTIONS;MOTHY;

&FORTRAN; D;

```
0* C
1* C
2*   DIMENSION T(100), DEZZ(100), DGAMMA(100), EZZ(100), GAMMA(100)
3*   READ(3,49) F,G,H,EL
4*   READ(3,50) GL
5*   READ(3,50) RADN
6*   READ(3,51) M
7*   K=0
8*   1 READ(3,50) DEBPM
9*   READ(3,50) XLAM
10*  READ(3,50) C1
11*  READ(3,50) C2
12*  READ(3,51) N
13*  WRITE(2,100) DEBPM
14*  READ(3,52) (T(I),DEZZ(I),DGAMMA(I), I=1,N)
15*  DO 2 I =1,N
16*  Z=C1*DEZZ(I)
17*  BR=1.0+Z/GL
18*  EZZ(I)=ALOG(BR)
19*  X=C2*DGAMMA(I)
20*  AA=(RADN*1.116*X*3.14159)/(180.0*GL)
21*  GAMMA(I)=SIN(AA)/COS(AA)
22*  L=I-1
23*  IF(L.LT.2) GO TO 2
24*  REZZ=(EZZ(L+1)-EZZ(L-1))/(T(L+1)-T(L-1))
25*  RGAMMA=(GAMMA(L+1)-GAMMA(L-1))/(T(L+1)-T(L-1))
26*  A=RGAMMA/(REZZ*XLAM)
27*  U=COS(AA)**4
28*  V=SIN(AA)**4
29*  W=SIN(2.0*AA)**2
30*  XX=COS(AA)*COS(AA)*SIN(2.0*AA)
31*  Y=SIN(AA)*SIN(AA)*SIN(2.0*AA)
32*  ZZ=SIN(4.0*AA)
33*  BET1=(F+H)*U+(F+G)*V-F*W/2.0+(1.5*W*EL)
34*  BET2=(2.0*F+H)*XX-(2.0*F+H)*Y-(1.5*EL*ZZ)
35*  BET3=(4.0*F+H+G-6.0*EL)*W+(6.0*EL)
36*  RGTZ=BET2+(XLAM*BET3)
37*  REZ=BET1+(XLAM*BET2)
38*  AT=RGTZ/(REZ*XLAM)
39*  WRITE(2,101) T(L),A,AT
40*  2 CONTINUE
41*  K=K+1
42*  IF(K.LT.M) GO TO 1
43*  STOP
44*  49 FORMAT(2X,4F0.0)
45*  50 FORMAT(6X,F0.0)
46*  51 FORMAT(I0)
47*  52 FORMAT(2X,3F0.0)
48*  100 FORMAT(////17X,46HCOMPARISON OF ( X ) VALUES FOR A PR
49*  117X,21HSTRAIN HISTORY =,F5.2,1X,17H% TENSION/TORSION///
50*  217X,41HTIME (HRS) EXPERIMENTAL HU'S VALUE//)
51*  101 FORMAT(20X,F4.0,2E18.6)
52*  END
```

TIME (HRS)      EXPERIMENTAL      HU'S VALUE

2.	0.232864E+01	0.259779E+01
3.	0.205148E+01	0.259730E+01
4.	0.294031E+01	0.259687E+01
5.	0.320126E+01	0.259650E+01
6.	0.308377E+01	0.259618E+01
7.	0.343639E+01	0.259588E+01
8.	0.320432E+01	0.259567E+01
9.	0.283400E+01	0.259545E+01
10.	0.312867E+01	0.259466E+01
15.	0.331711E+01	0.259410E+01
20.	0.338263E+01	0.259362E+01
25.	0.328335E+01	0.259323E+01
30.	0.349472E+01	0.259281E+01
35.	0.359171E+01	0.259249E+01
40.	0.348400E+01	0.259223E+01
45.	0.337801E+01	0.259193E+01
50.	0.308964E+01	0.259160E+01
55.	0.350816E+01	0.259125E+01
60.	0.414498E+01	0.259097E+01
65.	0.351471E+01	0.259075E+01
70.	0.386742E+01	0.259043E+01
75.	0.392474E+01	0.259019E+01
80.	0.330241E+01	0.258993E+01
85.	0.311802E+01	0.258973E+01
90.	0.335616E+01	0.258953E+01
95.	0.305207E+01	0.258934E+01
100.	0.325714E+01	0.258909E+01
105.	0.409173E+01	0.258878E+01
110.	0.379720E+01	0.258841E+01
115.	0.367755E+01	0.258813E+01
120.	0.348324E+01	0.258793E+01
125.	0.317676E+01	0.258777E+01
130.	0.320585E+01	0.258758E+01
135.	0.347610E+01	0.258743E+01
140.	0.414519E+01	0.258727E+01
145.	0.356338E+01	0.258708E+01
150.	0.351832E+01	0.258680E+01
160.	0.357878E+01	0.258666E+01
170.	0.320460E+01	0.258654E+01
180.	0.353829E+01	0.258648E+01
190.	0.352198E+01	0.258643E+01
200.	0.243326E+01	0.258639E+01
210.	0.340690E+01	0.258631E+01
220.	0.448441E+01	0.258617E+01
230.	0.336046E+01	0.258606E+01
240.	0.324677E+01	0.258592E+01
250.	0.351505E+01	0.258580E+01
260.	0.339293E+01	0.258566E+01
270.	0.403615E+01	0.258549E+01
280.	0.401386E+01	0.258529E+01
290.	0.350190E+01	0.258513E+01
300.	0.328390E+01	0.258503E+01
310.	0.328830E+01	0.258490E+01
320.	0.312479E+01	0.258480E+01
330.	0.275789E+01	0.258473E+01
340.	0.325650E+01	0.258468E+01
350.	0.325709E+01	0.258464E+01
360.	0.309454E+01	0.258460E+01
370.	0.469119E+01	0.258456E+01
380.	0.651613E+01	0.258451E+01

Constant value (k=3.36 in Fig 6.9)

# CHAPTER 7

## CHAPTER 7

## DISCUSSION AND RECOMMENDATIONS FOR FUTURE WORK

In this Chapter the overall flow behaviour of annealed, extruded and prestrained aluminium is discussed. Particular comments are made regarding the test conditions and finally, suggestions for future work are outlined.

7.1 PLASTIC FLOW

Radial loading on annealed aluminium (Chapter 4) produced plastic strain increment vectors for each stress path that remained fixed in direction. In applying the normality rule to the directions of these vectors it was shown that the locus describing initial yielding in this material inflated uniformly as strain hardening proceeded. In general, when uniform hardening is evident, the locus could be a von Mises or Tresca type or some other locus which is descriptive of initial anisotropy in the material. On the deviatoric plane a succession of concentric circles and hexagons would describe uniform hardening in von Mises and Tresca materials respectively (see Section 4.2\*). The present work confirms the use of Hill's theory (29) for describing uniform hardening in an initially anisotropic material. Mehan (20)\* has similarly used the theory in accounting for the plastic flow produced by radial loading on anisotropic zirconium-tin alloy. In general Hill's theory is suitable to describe an initial anisotropy which is preserved throughout radial loading. The initial anisotropy referred to here is a structural property. It can exist in non severe form in an annealed structure or in severe form in a textured structure.

Radial loading on extruded (Chapter 5) and prestrained aluminium (Chapter 6) produced rotations in the plastic strain increment vectors for each stress path. The normality rule would then indicate a changing shape of locus within the vicinity of the stress path. A similar behaviour was observed by Rogan and Shelton (54) and Shahabi and Shelton (57) in a yield loci study of radial loading on prestrained En24 and En 25 steel. Thus for a material possessing a strain history, due to a change in direction of the stress path or in the presence of residual strain, the assumption of uniform strain hardening during radial loading would be invalid. Furthermore, where the direction of the stress path is reversed (paragraph 4.3.1)\*, the uniform hardening theory would fail to display a

\* Appendix I.

positive Bauschinger effect. Clearly any other hardening concept which ignores the Bauschinger effect, e.g. the minimum surface model (paragraph 4.3.2\*), is also invalid. A Bauschinger effect is evident in the kinematic hardening model (paragraph 4.3.3\*) where the yield locus is carried by the stress path. A further requirement of an anisotropic hardening model is that it should describe the observed cross-effects associated with subsequent stress paths. Depending upon the relative directions of the prestrain path and the subsequent stress path a cross-effect may be evident by either softening or hardening of the material (see Figs. 6.1 and 6.2). The kinematic model in displaying no cross-effects is therefore not wholly descriptive of anisotropic hardening. However a model which combines uniform and kinematic hardening (paragraph 4.3.4\*) displays both Bauschinger and cross-effects and thereby describes anisotropic hardening more closely. The theories of Edelman and Drucker (58) and Yoshimura (59) are consistent with the combined model in allowing for a Bauschinger effect, a cross-effect and initial material anisotropy. In the present work plastic strain increment directions derived from the yield function of each theory were descriptive of the observed rotations in the plastic strain increment vectors. The theory of Williams and Svensson (60, 61) is also consistent with the combined hardening model and further allows for distortion in subsequent yield loci. However it has been shown in Chapters 5 and 6 that in assuming a virgin material of the von Mises type this theory does not allow for initial anisotropy. The former theories allow for this in a yield function which reduces to the Hill type (  $\frac{1}{2} C_{ijkl} \sigma'_{ij} \sigma'_{kl}$  ) for zero strain history (  $\epsilon'_{ij} = 0$  ). Thus of all the yield criteria written as some function of the second invariant of the deviatoric stress tensor (  $J'_2$  ) only those containing a coefficient  $C_{ijkl}$  of  $J'_2$  (  $= \frac{1}{2} \sigma'_{ij} \sigma'_{kl}$  ) will describe plastic flow in an initially anisotropic material.

## 7.2 CREEP

At a test temperature of  $T/T_m = 0.32$  the mechanics of plastic deformation in aluminium (f.c.c.) involves the production, movement, interaction and multiplication of dislocations by the processes of cross slip and climb. In general for the same test conditions creep arises through the operation of the same processes together with a possible contribution due to viscous grain boundary deformation (62). The latter component

predominates with increasing temperature (Appendix III). In the present work where creep has been shown to be time dependent plasticity the modes of time independent and time dependent deformation are then equivalent. Macroscopically this creep has been described in replacing plastic strain increments by strain rates of creep. It follows from Section 7.1 that the initial condition of the material must govern the correct choice of plasticity theory for creep. The Levy-Mises flow rule ( $d\epsilon_{ij}^p = \lambda \sigma_{ij}'$ ) when so applied to creep ( $\dot{\epsilon}_{ij} = \lambda \sigma_{ij}'$ ) assumes isotropic creep strain hardening and can therefore only describe the creep rates of radial loading in an isotropic material. In Chapter 4 it was shown that creep rate ratios derived from the yield function of Hill were consistent with the observed colinearity in the plastic strain increment vectors and creep rate vectors for all stress paths on annealed aluminium. This indicates the general use of Hill's theory to describe creep produced by radial loading on initially anisotropic material. However creep produced by radial loading on material possessing a strain history can only be described by a theory that accounts for a Bauschinger effect, a cross-effect and initial material anisotropy. Thus for aluminium in the extruded and prestrained conditions it was shown in Chapters 5 and 6 that the theories of Edelman and Drucker and Yoshimura could be made consistent with plastic strain increment vectors which rotated with increasing stress of radial loading and which grew in a constant direction during short-time creep (10 min). The theories were also consistent with a linear growth in the plastic strain increment vector for long-time creep ( $\approx 300$  hr) in extruded material (Chapter 5). They could not however be made to account for strain rate vectors which rotated in the long-time creep of prestrained material (Chapter 6).

By prestraining annealed aluminium with either tensile or positive shear strain then its resistance to combined tension-torsion creep was improved (Chapter 6). Prestrains of this type hardened the material in the direction of the combined stress path ( $\lambda = 0.95$ ). Low compressive and negative shear prestrains softened the material in the  $\lambda = 0.95$  stress direction and were thereby detrimental to creep resistance. The implication of the overall behaviour is that the biaxial stress creep resistance of a material can be improved by a prestraining operation that hardens the material in those directions where creep stresses are to be applied. It is possible however that a prestrain which hardens the material on one stress path softens it to another (57). To establish where a prestrain can be used to advantage it is therefore necessary to know the creep behaviour of a prestrained material for all combined stress paths (see paragraph (3) Section 7.6).

### 7.3 DELAYED ELASTICITY

Following the creep period, for the three conditions of aluminium, there was an instantaneous recovery of elastic strain associated with unloading from the stressed state. Further measurement of time dependent recovery showed this component never to exceed 5% of the total recovered strain. The elastic strain was thus the dominant component in the recovery of aluminium at the chosen test conditions. Gittus (62) attributes this "delayed elastic strain" to a return of displaced atoms to their equilibrium positions following the removal of external perturbing stresses. He further defines delayed elastic moduli  $E'$ ,  $G'$  and  $\nu'$  in relating stress to delayed strain. In the present work measurements of the moduli  $E'$  and  $G'$  from specimens that were not too severely deformed showed that these were no different from  $E$  and  $G$  of elasticity in Chapter 6. Thus for a decrement of unloading the measured delayed elastic strain increment components can be expressed as,

$$\begin{aligned} d\epsilon_{zz}^e &= \frac{d\tau_{zz}}{E'} \\ d\delta_{\theta z}^e &= \frac{d\tau_{\theta z}}{G'} \end{aligned} \quad (7.1)$$

The total elastic strain recovered from the creep stresses  $\tau_{zz}, \tau_{\theta z}$  comprises the following components,

$$\begin{aligned} \epsilon_{zz}^e &= \frac{\tau_{zz}}{E'} \\ \epsilon_{\theta\theta}^e &= \epsilon_{rr}^e = -\frac{\nu'\tau_{zz}}{E'} \\ \delta_{\theta z}^e &= \frac{\tau_{\theta z}}{G'} \end{aligned} \quad (7.2)$$

In general the delayed elastic strains may be written as the sum of a deviatoric and a dilatational component (if  $\nu' \neq 1/2$ ). That is,

$$d\epsilon_{ij}^e = \frac{d\sigma_{ij}'}{2G} + \frac{(1-2\nu')}{3E'} \delta_{ij} d\sigma_{ii}' \quad (7.3)$$

which yields stress-delayed strain equations similar to those of conventional elasticity. That is,

$$\begin{aligned} d\epsilon_{11}^e &= \frac{1}{E'} [d\sigma_{11}' - \nu'(d\sigma_{22}' + d\sigma_{33}')] \text{ etc.} \\ d\epsilon_{12}^e &= \frac{d\delta_{12}^e}{2} = \frac{d\sigma_{12}'}{2G'} \text{ etc.} \end{aligned} \quad (7.4)$$

## 7.4 NET STRAIN

In general the net strain ( $\epsilon_{ij}^N$ ) in the fully unloaded cylinders of these tests is given by,

$$\epsilon_{ij}^N = \text{prestrain} + \text{loading strain} + \text{creep strain} - \text{delayed elastic strain} \quad (7.5)$$

A theoretical prediction of the net strain is possible provided that the strain history is known and noting from Section 7.3 that,

$$\text{delayed elastic strain} = \text{elastic loading strain} \quad (7.6)$$

Then equation (7.5) becomes,

$$\epsilon_{ij}^N = \text{prestrain} + \text{plastic loading strain} + \text{creep strain} \\ (\epsilon_{ij}^{op}) \quad \left( \int d\epsilon_{ij}^p \right) \quad \left( \int \dot{\epsilon}_{ij}^c dt \right) \quad (7.7)$$

For a yield function 'f' that defines the anisotropy in the cylinder equation (7.7) may be written as,

$$\epsilon_{ij}^N = \epsilon_{ij}^{op} + \int_e \frac{\partial f}{\partial \sigma_{ij}} d\lambda + \int_t \frac{\partial f}{\partial \dot{\sigma}_{ij}} \dot{\lambda} \phi(t) dt \quad (7.8)$$

Before the integration of equation (7.8) can be performed  $\delta\lambda$ , for loading, should contain a correlation between the equivalent stress and equivalent plastic strain increment (see paragraph (2) Section 7.6). Similarly  $\dot{\lambda}$ , for creep, should contain a correlation between the equivalent stress and equivalent strain rate. The function  $\phi(t)$  should define the creep rate-time dependence e.g. for annealed aluminium in the primary range  $\phi(t) = t^{-0.79}$  (Chapter 4).

## 7.5 GENERAL COMMENTS

It must be emphasised that the observations made throughout the present work apply to cylinders of commercially pure anisotropic aluminium tested in combined tension-torsion at 21°C. ( $T/T_m = 0.32$ ). It is probable that combined tension-torsion tests performed on other anisotropic pure metals would reveal similar trends on plastic flow and creep at test temperatures where the mechanics of deformation are the same. However

it would be necessary to conduct further experiments to establish flow behaviour for any departure from these test conditions. For example the problem of thermal instability has arisen in the tensile creep of pure metals and solid solutions when higher test temperatures assist grain growth and recrystallisation (39). A further factor to be considered at higher test temperatures is the contribution made to creep deformation in viscous grain boundary sliding (62). In tensile creep tests on alloys an increased test temperature has caused recovery and ageing effects (42) while the introduction of prestrain has resulted in the formation of undesirable cavities at grain boundaries (44). It is for these reasons that discrepancies have arisen in published uniaxial creep data (see paragraph 1.2.6 Chapter 1). For the same reasons discrepancies are likely to arise in biaxial creep data. For example the particular type of strain induced anisotropy observed by Johnson (17) in his combined tension-torsion tests on engineering alloys was not evident in the present tests on a ductile pure metal.

Furthermore the observations of the present work are particular characteristics of radial loading paths. By maintaining a constant ratio between the stresses this provides the simplest possible method for experimental verification of the theory of plasticity. For example the Levy-Mises flow rule for isotropic material predicts a constant ratio between plastic strain increments. Anisotropic theories for prestrained material predict a rotation in the plastic strain increment vector. Such predictions have been readily checked in the present experimental work. The theories have then been extended to predict the creep deformation associated with radial loading. Before the flow behaviour can be predicted for any other stress path, e.g. a stepped or zig-zag type, it would be necessary to consider the loading strain history of that path.

## 7.6 RECOMMENDATIONS FOR FUTURE WORK

The following suggestions would usefully extend studies on creep and plastic flow in anisotropic material.

- (1) The rotations in the  $\dot{\gamma}_{e_z}/\dot{\epsilon}_{z_z}$  vector of creep in Fig. 6.9 occurred within the creep period ( $\approx$  400 hours) only for cylinders prestrained by relatively small amounts. It would be important to establish if a rotation occurs for a creep period  $>$  400 hours in cylinders prestrained by larger amounts.

There is also a need to develop a theory which can account for such a rotation.

(2) In the present work plastic strain increment directions derived from the yield functions of Edelman and Drucker and Yoshimura were descriptive of rotations in the plastic strain increment vectors produced by radial loading on prior strained material. In order to establish which theory is the more accurate in its prediction on the plastic strain increment magnitudes it would be necessary to conduct further experiments. The measured plastic strain increment magnitudes from radial loading tests performed on specimens prestrained by the same amount would make for the simplest comparison with theoretical prediction. Theoretical magnitudes of the plastic strain increment components ( $d\epsilon_{ij}^p$ ) would be given from  $d\epsilon_{ij}^p = \frac{\partial f}{\partial \sigma_{ij}} \delta\lambda$  with  $f$  written as the anisotropic yield function and  $\delta\lambda$  replaced by an equivalent stress and an equivalent plastic strain increment of the respective theory. (In Appendix I this method was used to obtain the plastic strain increments of equation (56) from Hill's theory. Here  $\delta\lambda$ , the equivalent stress and equivalent plastic strain increment were defined by equations (55), (57) and (58) respectively). Before the theoretical plastic strain increment components could be calculated it would be necessary to find the correlation between equivalent stress and equivalent plastic strain increment for all radial loading paths on prestrained material.

(3) In Chapter 6 an improvement in the creep resistance of annealed aluminium was observed for prestrains that raised the yield stresses in this material (hardening). Since a yield locus relates the yield stresses of all combined stress paths it should be possible to predict overall creep behaviour from a yield loci comparison of the annealed and prestrained materials. Then for all stress paths applied in the region where the prestrain hardens the material an improvement in creep resistance should be expected. For all stress paths applied in the region where the prestrain softens the material then no improvement in creep resistance should be expected. The validity of this postulation should be checked experimentally.

(4) The prestrain-secondary creep rate correlations of Fig. 6.5 were constructed from a combined stress creep test ( $\lambda = 0.95$ ) performed on specimens with either an axial or a shear prestrain history. It would be a useful exercise to check the correlations with the creep rates from specimens of known complex prestrain history. In the present test rig this could be most simply achieved by prestraining along any  $\lambda$  stress path prior to the  $\lambda = 0.95$  creep test.

(5) In the one test where torsional creep buckling occurred (Fig. 4.12) Finnie's prediction of equation (2.2) considerably overestimated the critical shear strain at buckling. One possible reason is that a purely torsional theory has been applied to a combined tension-torsion test. It would therefore seem necessary to modify the theory for combined stress systems involving torsion. An empirical type modification should be possible from a test programme which serves to correlate creep buckling strains with stress ratio and stress level.

(6) For an anisotropy of the Hill type (paragraph 3.1.3) it would be interesting to know how the constants F, G, H, etc. relate to the initial structure. For example it is not known what effect grain size and degree of crystallographic orientation have on the constants.

(7) An examination of anisotropic flow in biaxial stress systems other than combined tension-torsion would complement the present work. For example in thin walled cylinder testing this could be achieved by combining tension with internal pressure (paragraph 2.1.4). Then for a stress ratio  $\beta = \sigma_{\theta\theta} / \sigma_{zz}$  an examination of the  $d\epsilon_{\theta\theta}^p / d\epsilon_{zz}^p$  of loading and the  $\dot{\epsilon}_{\theta\theta} / \dot{\epsilon}_{zz}$  of creep would reveal trends in anisotropic flow behaviour.



## CHAPTER 8

## CONCLUSIONS

These conclusions apply to room temperature (21°C) combined tension-torsion deformation in each of the following three conditions of anisotropic EIA aluminium.

8.1 ANNEALED ALUMINIUM

(1) Incremental loading generated axial ( $\epsilon_{zz}$ ) and shear strains ( $\delta_{\theta z}$ ) which consisted of instantaneous and short-time (15 min.) creep components. The latter component was of the  $t^m$  form throughout loading. For each stress path the time exponent  $m$  was independent of stress level and for all stress paths  $m$  lay in the parabolic range  $0 < m < \frac{1}{2}$ . A power function in time for primary creep (up to 100 hr) was followed by these strains.

(2) Radial type loading produced instantaneous plastic strain increment vectors ( $d\delta_{\theta z}^p/d\epsilon_{zz}^p$ ) and short-time creep rate vectors ( $\delta_{\theta z}/\dot{\epsilon}_{zz}$ ) for each stress path that were colinear. In the absence of torsional buckling the strain rate vectors of ensuing long-time creep were also colinear. Such behaviour was indicative of an initially anisotropic material which hardened uniformly throughout subsequent deformation.

(3) Plastic strain increment ratios derived from the yield function of Hill  $f = \frac{1}{2} C_{ijkl} \nu_{ij}' \nu_{kl}'$  were descriptive of the observed plastic anisotropy. The theory could be made to describe creep anisotropy in replacing the derived plastic strain increments with strain rates (e.g.  $\dot{\epsilon}_{zz} = d\epsilon_{zz}^p/dt$ ). It is concluded that Hill's theory is suitable to describe an initial, structural anisotropy which is preserved during deformation by radial loading.

(4) Isotropic theory of plastic flow (Levy-Mises) and creep (Marin-Soderberg) were valid only to a first approximation in their predictions on the experimental observations.

## 8.2 EXTRUDED ALUMINIUM

(1) In common with annealed aluminium a short time  $t^m$  creep component was evident in both the measured axial and shear strains throughout incremental loading. For each stress path  $m$  was independent of stress level and for all stress paths  $m$  lay in the range  $0 < m < 1/2$ .

(2) Radial type loading produced instantaneous plastic strain increment vectors and short-time creep rate vectors for each combined stress path which were not wholly colinear. The plastic strain increment vectors of initial loading rotated with increasing stress and grew in constant direction during short-time creep. The vectors of final loading and ensuing long-time creep ( $\approx 400$  hr) were colinear for each stress path. A torsion test produced significant axial strain ( $\approx 2\%$  total) and colinearity in the vectors of plastic flow and creep throughout deformation.

The overall flow behaviour was indicative of an anisotropy which was a particular function of the non uniform grain structure and residual compressive strain history that existed in the gauge length of each test cylinder.

(3) Plastic strain increment ratios derived from the yield functions of Edelman and Drucker  $f = \frac{1}{2} C_{ijkl} (\sigma_{ij} - m e_{ij}^p) (\sigma_{kl} - m e_{kl}^p)$  and Yoshimura  $f = \frac{1}{2} C_{ijkl} \sigma_{ij} \sigma_{kl} - m e_{ij}^p \sigma_{ij}$  closely described the observed anisotropic plastic flow behaviour in each test cylinder. Anisotropic creep deformation was described by extending these theories as Hill's theory was extended for annealed aluminium. Quantitative predictions to the flow in cylinders of extruded aluminium were seen to be possible only if the anisotropic nature of their grain texture and residual strain history were known.

(4) The anisotropic theories of Hill, Bailey and Hu, while accounting for initial structural anisotropy in plastic flow and creep, did not allow for the effect of the residual strain history (i.e. a cross-effect and Bauschinger effect). The theories of Williams and Svensson and Berman and Pai are based on the assumption of initial material isotropy and therefore did not allow for the anisotropy in the non uniform grain structure.

### 8.3 PRESTRAINED ALUMINIUM

(1) Plastically prestraining annealed aluminium with forward strains (in tension or positive torsion) or with large reversed strains ( $> 2\%$  in compression or negative torsion) was beneficial to creep resistance by hardening the aluminium in the direction of the stress path ( $\lambda = 0.95$ ). The effect was to eliminate the short-time creep component of radial loading and to reduce the primary creep strains and secondary creep rates of ensuing long-time creep.

For forward and reversed prestrains  $\leq 3\%$  a short-time creep component was first observed during loading in linear form ( $m = 1$ ). With continued loading the creep component reverted to parabolic form ( $t^m$ ).

Increasing forward prestrains were more beneficial than increasing reversed prestrains in successively reducing the primary creep strains and secondary creep rates of long-time creep. ( $\approx 400$  hr).

(2) Plastically prestraining annealed aluminium with small reversed strain ( $\leq 2\%$ ) was detrimental to creep resistance by softening the aluminium in the direction of the stress path (Bauschinger effect). The effect was to increase the parabolic creep component of loading ( $m$  was small or negative) and to increase the primary creep strains and secondary creep rates of ensuing long-time creep.

(3) Subsequent flow behaviour depended upon the relative magnitudes of the prestrain and the total accumulated strain. Prestrains  $\leq \pm 3\%$  destroyed colinearity in the instantaneous plastic strain increment vectors and creep rate vectors of radial loading. In common with extruded aluminium the plastic strain increment vectors rotated with increasing stress and grew in constant direction during short-time creep. The rotation further continued in the long-time strain rate vectors of primary and secondary creep and finally ceased when the total accumulated strain nullified the prestrain effect. Colinear vector behaviour, approximating to the direction of the as-annealed vector, was evident thereafter. Prestrains  $\geq 4\%$  resulted in only elastic strain during radial loading with no rotation in the strain rate vector for up to 400 hours of ensuing creep.

The overall flow behaviour was indicative of an anisotropy which was a function of both the annealed structure and the prestrain history.

(4) Plastic strain increment ratios and creep rate ratios derived from the yield functions of Edelman and Drucker and Yoshimura closely described the observed anisotropic plastic flow and short-time creep behaviour for radial loading. These theories could not be made to describe the rotation in the strain rate vector for long-time creep when extended by the usual method (i.e.  $\dot{\epsilon}_{ij} = d\epsilon_{ij}^p/dt$ ).

(5) For the reasons outlined in paragraph (4) of Section 8.2 the anisotropic theories of Bailey, Berman and Pai, Hu and Williams and Svendsen were inadequate in their predictions on the experimental observations.

## ADVERTISE

## MAIN TEXT REFERENCES

- (1) Materials Properties Handbook. Published for the Aeronautics and Materials Panel of AASSTO, 1942.
- (2) EDWARDS, J.L. 'By the Application of Power'. *Aeronautical Jnl.* Feb. 1975, 59-61.
- (3) KOELMANU, G. (ed). 'Materials Technology in Space Manufacturing Process'. 1956 (Pergamon Press).
- (4) BRATH-SMITH J.R. and HUNTER, F.B. 'Effects of heat on fatigue in aircraft structures'. *Proc. Inst. 1952* and 'Problems with Fatigue in Aircraft'. *June 1975*, 891.
- (5) THOMPSON, V.T. and GIBSON, R.W. (ed) 'Materials in Space

# REFERENCES

- (6) SO...  
*Trans. ASEE 1941*, 49, 113-115.
- (7) HARRIS, J. 'Design of structures subjected to creep at high temperatures'. *J. Appl. Mech.* 1957, 24, 65-68.
- (8) JAMESON, J. 'The temperature-relaxing of the plastic flow of lead'. *Ph.D. Thesis, University of Michigan 1953*.
- (9) EYENETI, F.A. and CLINE, A.D. 'Effects on corrosion creep tests for comparison with tensile creep tests on a carbon-manganese steel'. *Trans. ASEE 1942*, 50, 211.
- (10) HANSEL, E.J. and JOHNSON, A.E. 'Creep under combined tension and torsion'. *Engineering 1940*, 150, 14, 61, 104, 134, 164.
- (11) HUNTER, F.B. 'Progress report on creep creep tests'. *Trans. ASEE, 1941*, 49, 113.
- (12) DAVIS, G.A. 'Classification of creep creep tests for various types of high temperature creep creep tests'. *Proc. Joint Research Committee*. *Trans. ASEE 1941*, 49, 113.

## APPENDIX

## MAIN TEXT REFERENCES

- (1) Materials Properties Handbook. Published for the Structures and Materials Panel of AGARD, 1962.
- (2) EDWARDS, J.L. 'By the Application of Power'. Aeronautical Jnl. Feb. 1975, 59-84.
- (3) EDELEANU, C. (ed) 'Materials Technology in Steam Reforming Process'. 1966 (Pergamon Press).
- (4) HEATH-SMITH J.R. and KIDDLE, F.E. 'Effects of heat on fatigue in aircraft structure'. Proc. 8th ICAF sym. 'Problems with Fatigue in Aircraft'. June 1975, 801.
- (5) THOMPSON, V.E. and GATLAND, K.W. (ed) 'Materials in Space Technology'. 1963 (Iliffe Books Ltd.)
- (6) SODERBERG, C.R. 'Plasticity and Creep in Machine Design'. Trans. ASME 1936, 58(8), 733-743.
- (7) MARIN, J. 'Design of members subject to creep at high temperatures'. J. Appl. Mech. 1937, 4(2), 55-58.
- (8) JAMIESON, J. 'An investigation relating to the plastic flow of lead'. Ph.D. Thesis, University of Michigan 1933.
- (9) EVERETT, F.L. and CLARK, C.L. 'Report on torsion creep tests for comparison with tension creep tests on a carbon-molybdenum steel'. Proc. ASTM 1939, 39, 215.
- (10) TAPSELL, H.J. and JOHNSON, A.E. 'Creep under combined tension and torsion'. Engineering 1940, 150, 24, 61, 104, 134, 164.
- (11) NORTON, F.H. 'Progress report on tubular creep tests'. Trans. ASME, 1941, 63, 735.
- (12) DAVIES, E.A. 'Correlation of test results for various types of high temperature tests carried out for the Joint Research Committee'. Proc. ASTM 1939, 39, 234.

- (13) NORTON, F. H. and SODERBERG, C.R. 'Report on tubular creep tests of 0.5% Mo-C steel'. Trans. ASME 1942, 64(8), 768-777.
- (14) MARIN, J., FAUPEL, J. H. and HU, L. W. 'Combined tension-torsion creep-time relations for aluminium alloy 2S-0'. Proc. ASTM 1950, 50, 1054-1072.
- (15) KENNEDY, C. R., HARMS, W. O. and DOUGLAS, D. A. 'Multiaxial creep studies on Inconel at 1500<sup>o</sup>F. J. Basic Eng., Trans. ASME 1959, 81, 599-609.
- (16) STOWELL, E. Z. and GREGORY, R. K. 'Steady-state biaxial creep'. J. Appl. Mech., Paper No. 64-WA/APM-19.
- (17) JOHNSON, A. E. 'Complex stress creep relaxation and fracture of metallic alloys'. Edinburgh, HMSO, 1962.
- (18) JOHNSON, A. E., HENDERSON, J. and KHAN, B. 'Multiaxial creep-strain/complex-stress/time relations for metallic alloys with some application to structures'. Proc. Jnt. Int. Conf. on creep (I.Mech.E.) 1963, 2-27.
- (19) POPOV, E. P. 'Stresses in turbine discs at high temperatures'. J. Franklin Inst. 1947, 243, 365.
- (20) KACHANOV, L. N. 'Certain problems in the theory of creep'(in Russian).. Gosudarst. Izdat. Tekhn-Teor. Lit., Leningrad, 1949.
- (21) ODQVIST, F. K. G. 'Theory of creep under combined stresses with application to high temperature machinery'. Roy. Swed. Acad. Eng. Res. Proc. 1936, 141, 31.
- (22) OHNAMI, M. and MOTOIE, K. 'Creep and creep rupture of a cylindrical tube specimen subjected to combined axial load and internal pressure at elevated temperatures'. Proc. 9th Jap. Cong. Test. Mat. 1966, 39-43.
- (23) CLAY, B.D. 'The biaxial creep measurement of thin walled tubes'. J. Mat. Sci. 1974, 9, 1275-1278.

- (24) WAHL, A. M. 'Creep tests of rotating discs at elevated temperatures and comparison with experiment'. Mech. Engng. 1954, 76(1), 50-51.
- (25) VENKATRAMAN, B. and HODGE, P. G. 'Creep behaviour of circular plates'. J. Mech. Phys. Solids 1958, 6(2), 163-176.
- (26) FINNIE, I. 'An experimental study of multiaxial creep in tubes'. Proc. Jnt. Int. Conf. on creep (I.Mech.E.) 1963, 2-21.
- (27) BAILEY, R. W. 'The utilization of creep test data in engineering design'. Proc. Instn. Mech. Engrs. 1935, 131(11), 131-349.
- (28) BERMAN, I. and PAI, D. H. 'A theory of anisotropic steady-state creep'. Int. J. Mech. Sci. 1966, 8, 341-352.
- (29) HILL, R. 'A theory of yielding and plastic flow of anisotropic metals'. Proc. Roy. Soc. Lond. 1948, 193A, 281.
- (30) HILL, G. 'Effect of prestrain on the tensile creep in aluminium'. B.Sc. project rpt, Kingston Poly. 1975.
- (31) ANDRADE, A. N. DA. C. 'The viscous flow in metals and allied phenomena'. Proc. Royl Soc. 1914, 90A, 329.
- (32) ZSCHOKKE, H. R. and NIEHUS, K. H. 'Requirements of steel for gas turbines'. J. Iron and Steel Inst. 1947, 156, 271.
- (33) KOZYRSKIY, G. YA. and KONONENKO, V. A. 'An investigation on the creep of preliminary deformed nickel polycrystals (in Russian)'. Phy. Metals and Metallography 1966, 22(1), 105.
- (34) AZHAZHA, V. M., GINDIN, I. A. and STARODUBOV, YA. D. 'A comparison of the influence of preliminary deformation at 300°K on the creep characteristics of nickel polycrystals at 700°C (in Russian)'. Phy. Metals and Metallography 1963, 15(1), 119.
- (35) WILMS, G. R. 'Some observations on the creep of prestrained aluminium'. J. Inst. Metals 1954-55, 83, 427-432.

- (36) KENNEDY, A. J. 'The effects of instantaneous prestrain on the characteristics of creep in lead polycrystals'. Proc. Phys. Soc., London 1949, 628, 501.
- (37) HAZLETT, T. H. and HANSEN, R. D. 'Influence of substructure on the shape of the creep curve'. Trans. ASM 1955, 47, 508-519.
- (38) AZHAZHA, V. M., GINDIN, I. A. and STARODUBOV, YA. D. 'The effect of stress and temperature on the creep behaviour of nickel polycrystals preliminary deformed at 12°K (in Russian)'. Phy. Metals and Metallography 1964, 18(4), 511.
- (39) DAVIES, P. W., RICHARDS, J. D. and WILSHIRE, B. 'The effect of some variations in prestrain treatment on the creep and fracture properties of pure nickel and a dilute nickel alloy'. Metallurgia 1963, 68, 259-263.
- (40) MARTINOD, H., RENON, Mme C. and CALVET, J. 'The effect of strain hardening on the mechanical properties and creep resistance of aluminium alloys used in aeronautics, (in French)'. Revue de Metallurgie 1966, 815.
- (41) GRANT, N. J., CHAUDHURI, A. R., SILVER, I.R. and GANOW, D. C. 'Effect of prestrain on the creep-rupture properties of high-purity aluminium and an Al-2% Mg Alloy'. Trans. Metallurgical Soc. AIME 1959, 215, 540.
- (42) WILSON, R. N. 'The influence of 3% prestrain on the creep strength of Al-2.5%, Cu-1.2% Mg Alloys at 150°C'. J. Inst. Metals 1973, 101, 188-196.
- (43) BISCAYA, J. M. DE. A. 'The influence of plastic prestrain on the creep properties of an Aluminium - 2.5%, Copper - 1.25% Magnesium Alloy'. M.Sc. Thesis, University of London 1971.
- (44) HUSTON, R. J. 'The influence of plastic prestrain on the creep properties of an Aluminium - 2.5%, Copper - 1.25% Magnesium alloy'. M.Sc. Thesis, University of London 1972.
- (45) MORROW, J. and HALFORD, G. R. 'Creep under repeated stress reversals'. Proc. Jnt. Int. Conf. on Creep (I.Mech.E.) 1963, 3-43.

- (46) HUGHES, A. N. 'Creep of a 20% Cr and a 25% Nb steel under reversed creep conditions'. UKAEA, TRG Rpt. No. 1018(6), 1965.
- (47) WILMS, G.R. and REA, T.W. 'Tensile creep on extruded Cr alloys'. J. Less-Common Metals 1964, 7, 296-315.
- (48) HODGSON, B. J.R. 'Dependence of creep rate on pre-strain rate in a conventional low alloy steel'. Nature 1969, 223, 392.
- (49) WOOD, W. A. and WILMS, G.R. 'Mechanism of creep in metals'. J. Inst. Metals 1949, 75, 693.
- (50) MATHUR, S. B. and ALEXANDER, J. M. 'A complex creep testing machine'. Jt. conf. on test machines and mat. testing. I.Mech.E./Soc. Env. Eng. 1965, 275-283.
- (51) GRAHAM, A. 'Materials properties in complex stress theory'. Advances in Creep Design, 1971. Applied Science Ltd.
- (52) FINNIE, I. 'Creep buckling of tubes in torsion'. J.Aeronaut. Sc. 1958, 25, 66.
- (53) PUGH, H. Ll. D., MAIR, W.M. and RAPIER, A.C. 'The plastic yielding of metals under combined stress'. NEL Rpt. No. 43, 1962, East Kilbride, Glasgow.
- (54) ROGAN, J. and SHELTON, A. 'Yield and subsequent flow behaviour of some annealed steels under combined stress'. J. Strain Analysis 1969. 4, 127.
- (55) DORN, W. S. and McCracken, D. D. Numerical Methods with Fortran IV Case Studies 1972, Wiley.
- (56) HU, L. W. 'Studies on plastic flow of anisotropic metals'. Trans. A.S.M.E. 1955, 55-A-79, 1-7.
- (57) SHAHABI, S. N. and SHELTON, A. 'The anisotropic yield, flow and creep behaviour of pre-strained En 24 steel'. J.Mech. Engng. Sci. 1975, 17(2), 93-104.

- (58) EDELMAN, F. and DRUCKER, D. C. 'Some extensions to elementary plasticity theory'. J. Franklin Inst. 1951, 251, 581.
- (59) YOSHIKURA, Y. 'Hypothetical theory of anisotropy and the Bauschinger effect due to a plastic strain history'. Aero. Res. Inst. Univ. of Tokyo, Rep. No. 349, 1959.
- (60) WILLIAMS, J. F. and SVENSSON, N. L. 'Effect of tensile prestrain on the yield locus of 1100-F aluminium'. J. Strain Analysis 1970, 5(2), 128-139.
- (61) WILLIAMS, J. F. and SVENSSON, N. L. 'Effect of torsional prestrain on the yield locus of 1100-F aluminium'. J. Strain Analysis 1971, 6(4), 263-272.
- (62) GITTUS, J. 'Creep, Viscoelasticity and Creep Fracture in Solids'. 1975 (Applied Science Publishers), Chapter 14.

# APPENDIX I

$$\begin{aligned} V_1 &= V_0 + V_1 + V_2 \\ V_1 A_1^2 &= V_0 A_0^2 + V_1 A_1^2 + V_2 A_2^2 \\ &+ V_3 A_3^2 + V_4 A_4^2 + V_5 A_5^2 \\ &+ V_6 A_6^2 + V_7 A_7^2 + V_8 A_8^2 \end{aligned}$$

In addition, suffixes  $n = 1, 2, 3, \dots$  are used to denote lower  
expansion to correctly represent all components of a particular  
quantity. Thus,

## APPENDIX I

## MULTIAXIAL CREEP AND PLASTIC FLOW

Basically the equations describing multi-axial creep rates have been developed by introducing a time derivative to the laws of time independent plastic flow. In following such a development this appendix outlines the important equations of time independent plastic flow and their application to the creep of isotropic and anisotropic material.

1. ISOTROPIC PLASTIC FLOW

Where applicable nine component cartesian tensor notation is used throughout for brevity. Thus a general stress and corresponding plastic strain increment tensor is represented by  $\sigma_{ij}$  and  $d\epsilon_{ij}^p$  respectively where  $i = j = 1, 2, 3$ . The stress tensor is symmetrical since  $\sigma_{ij} = \sigma_{ji}$  which means that each shear stress has a complement ( $\sigma_{12} = \sigma_{21}$ ,  $\sigma_{23} = \sigma_{32}$ ,  $\sigma_{13} = \sigma_{31}$ ). Thus both the stress and plastic strain increment tensors have six independent components only. That is,

$$\begin{aligned}\sigma_{ij} &\equiv \sigma_{11}, \sigma_{22}, \sigma_{33}, \sigma_{12}, \sigma_{23}, \sigma_{13} \\ d\epsilon_{ij}^p &\equiv d\epsilon_{11}^p, d\epsilon_{22}^p, d\epsilon_{33}^p, d\epsilon_{12}^p, d\epsilon_{23}^p, d\epsilon_{13}^p\end{aligned}$$

Where a repeated suffix appears in a tensor or in any tensor expression a summation convention is implied. Thus,

$$\begin{aligned}\sigma_{ii} &= \sigma_{11} + \sigma_{22} + \sigma_{33} \\ \sigma_{ij} d\epsilon_{ij}^p &= \sigma_{11} d\epsilon_{11}^p + \sigma_{12} d\epsilon_{12}^p + \sigma_{13} d\epsilon_{13}^p \\ &\quad + \sigma_{21} d\epsilon_{21}^p + \sigma_{22} d\epsilon_{22}^p + \sigma_{23} d\epsilon_{23}^p \\ &\quad + \sigma_{31} d\epsilon_{31}^p + \sigma_{32} d\epsilon_{32}^p + \sigma_{33} d\epsilon_{33}^p\end{aligned}$$

An additional suffix  $k = 1, 2, 3$  is introduced to certain tensor expressions to correctly represent all the components of a particular quantity. Thus,

$$\begin{aligned}
 \sigma_{ij} \sigma_{jk} \sigma_{ki} &= \sigma_{1j} \sigma_{jk} \sigma_{k1} + \sigma_{2j} \sigma_{jk} \sigma_{k2} + \sigma_{3j} \sigma_{jk} \sigma_{k3} && (\text{for } i = 1, 2, 3) \\
 &= \sigma_{11} \sigma_{1k} \sigma_{k1} + \sigma_{12} \sigma_{2k} \sigma_{k1} + \sigma_{13} \sigma_{3k} \sigma_{k1} \\
 &\quad + \sigma_{21} \sigma_{1k} \sigma_{k2} + \sigma_{22} \sigma_{2k} \sigma_{k2} + \sigma_{23} \sigma_{3k} \sigma_{k2} \\
 &\quad + \sigma_{31} \sigma_{1k} \sigma_{k3} + \sigma_{32} \sigma_{2k} \sigma_{k3} + \sigma_{33} \sigma_{3k} \sigma_{k3} && (\text{for } i=j=1, 2, 3)
 \end{aligned}$$

The 27 terms then obtained from the expansion of this expression for  $k = 1, 2, 3$  yield an expression for one of the three independent invariants of the stress tensor ( $\sigma_{ij}$ ).

Lastly it is necessary to introduce the Kronecker delta ( $\delta_{ij}$ ) when dealing with deviatoric stress components. The latter is the component of stress remaining after the hydrostatic stress state ( $\sigma_m$ ) has been removed from the stress tensor ( $\sigma_{ij}$ ). Since this applies only to normal and not shear components of applied stress the Kronecker delta ( $\delta_{ij}$ ) is introduced to form the deviatoric stress tensor ( $\sigma'_{ij}$ ) thus

$$\sigma'_{ij} = \sigma_{ij} - \delta_{ij} \sigma_m$$

where  $\sigma_m = \frac{1}{3} \sigma_{ii}$  (1)

and  $\delta_{ij} = 1$  for  $i = j$  and 0 for  $i \neq j$

### 1.1 Yield Criteria

Any yield criterion for an isotropic material with an imposed plastic stress tensor ( $\sigma'_{ij}$ ) is formulated from the invariants of that tensor. Furthermore since it is a basic assumption in plasticity theory that a hydrostatic tension or compression ( $\sigma_m$ ) is ineffective in yielding it follows that plastic deformation depends only upon the deviatoric stress tensor ( $\sigma'_{ij}$ ) and its invariants ( $J_1'$ ,  $J_2'$  and  $J_3'$ ). Since the invariant is independent of transformation of the chosen coordinate system then obviously so are the principal deviatoric stresses ( $\sigma'_1, \sigma'_2, \sigma'_3$ ). It follows that  $J_1', J_2'$  and  $J_3'$  are the coefficients in the principal deviatoric stress cubic (1)\*. That is,

$$\sigma'^3 + J_1' \sigma'^2 - J_2' \sigma' - J_3' = 0$$

where

$$\begin{aligned}
 J_1' &= \sigma'_{ii} = 0 \\
 J_2' &= \frac{1}{2} \sigma'_{ij} \sigma'_{ij} \\
 J_3' &= \frac{1}{3} \sigma'_{ij} \sigma'_{jk} \sigma'_{ki}
 \end{aligned} \tag{2}$$

Thus a yield criterion may be reduced to a function ( $f$ ) of the two non-zero symmetrical invariants  $J_2'$  and  $J_3'$  as

\* References are given at the end of this Appendix.

$$f(J_2', J_3') = c \tag{3}$$

Symmetry here implies that all the principal stresses play the same role in yielding. A further restriction may be imposed for an ideal plastic body to make the yield stresses in tension and compression the same. Now since  $J_3'$  changes sign when the stresses are reversed ( $-\sigma_{ij}'$ ,  $-\sigma_{jk}'$ ,  $-\sigma_{ki}'$ ) in equation (2) it follows then that 'f' must be an even function (g) of  $J_2'$ . Lastly during subsequent plastic flow the ideal plastic body assumes isotropic hardening. This implies that the function 'g' remains unchanged whilst the c term in equation (3) accounts for it. We therefore have,

$$g(J_2') = c \tag{4}$$

The most commonly used yield criterion, that attributed to von Mises, is obtained by taking the simplest form of this equation. That is,

$$J_2' = k^2 \tag{5}$$

where k may be identified as the yield stress in shear.

Another yield criterion in common use is that due to Tresca. This may be obtained from equation (3) by writing it as

$$4J_2'^3 - 27J_3'^2 - 36k^2J_2' + 96k^4J_3' = 64k^2 \tag{6}$$

but this form of equation is complicated and not very useful. It does show however that the Tresca yield criterion contains only those assumptions which were made in the development of equation (3).

A physical meaning of the von Mises criterion is that yielding depends upon the shear strain energy or the octahedral shear stress reaching a critical value whilst the Tresca criterion depends upon the maximum shear stress (k) reaching a critical value.

### 1.2 Flow Rules

The assumptions made in the derivation of a flow rule are that

- (1) the volume of material remains constant during plastic flow. This may be written as an equation, in the progression of plastic deformation, where the sum of the instantaneous plastic strain increments associated with a stress change is zero. That is,

$$d\epsilon_{ii}^p = 0 \tag{7}$$

(2) the principal axes of stress and plastic strain increment remain coincident throughout plastic deformation.

The increments of deformation  $d\epsilon_{ij}^p$  that occur during plastic flow are best obtained from a yield criterion  $f(\sigma_{ij}) = c$  in applying the concept of a plastic potential (1). That is

$$d\epsilon_{ij}^p = \frac{\partial [f(\sigma_{ij})]}{\partial \sigma_{ij}} \delta\lambda \quad (8)$$

where  $\delta\lambda$ , a constant for a point in the deformation, is described in more detail in paragraph 1.4.

If we take  $f(\sigma_{ij})$  as the von Mises criterion we have from equations (2) and (5) that  $f(\sigma_{ij}) = J_2' = \frac{1}{2} \sigma_{ij}'^2$ . Then equation (8) becomes

$$d\epsilon_{ij}^p = \frac{1}{2} \frac{\partial (\sigma_{ij}'^2)}{\partial \sigma_{ij}} \delta\lambda = \sigma_{ij}' \frac{\partial \sigma_{ij}'}{\partial \sigma_{ij}} \delta\lambda$$

which, from equation (1) can be written as

$$d\epsilon_{ij}^p = \sigma_{ij}' \frac{\partial (\sigma_{ij} - \delta_{ij} \sigma_m)}{\partial \sigma_{ij}} \delta\lambda$$

Since  $\sigma_m$  is ineffective in yielding then  $\partial \sigma_m / \partial \sigma_{ij} = 0$  and this equation then becomes

$$d\epsilon_{ij}^p = \delta\lambda \sigma_{ij}' \quad (9)$$

which is known as the Levy-Mises flow rule.

A flow rule associated with the Tresca yield criterion is most simply obtained by applying equation (8) to the yield criterion  $f(\sigma_{ij}) = c$  for  $f(\sigma_{ij})$  as the maximum shear stress  $k$  in this case. Then for a principal stress system  $(\sigma_1, \sigma_2, \sigma_3)$  and  $\sigma_1 > \sigma_2 > \sigma_3$  we have that

$$f(\sigma_{ij}) = k = \frac{1}{2} (\sigma_1 - \sigma_3) \quad (10)$$

and principal strain increments, from equation (8) as

$$\begin{aligned} d\epsilon_1^p &= \frac{1}{2} \frac{\partial (\sigma_1 - \sigma_3)}{\partial \sigma_1} \delta\lambda = \frac{\delta\lambda}{2} \\ d\epsilon_2^p &= \frac{1}{2} \frac{\partial (\sigma_1 - \sigma_3)}{\partial \sigma_2} \delta\lambda = 0 \\ d\epsilon_3^p &= \frac{1}{2} \frac{\partial (\sigma_1 - \sigma_3)}{\partial \sigma_3} \delta\lambda = -\frac{\delta\lambda}{2} \end{aligned} \quad (11)$$

Unlike the Levy-Mises equation(9) it is seen that these equations are incorrect when applied to the simple tension system  $(\sigma_1, 0, 0)$  where, from equation(7),  $d\epsilon_2^p = d\epsilon_3^p = -d\epsilon_1^p/2$ . The flow rule as derived from the Tresca yield criterion is therefore rarely used for the prediction of multiaxial strain increments and the Levy-Mises flow rule is now almost universally used for this purpose.

### 1.3 Equivalent Stress and Strain

It is often desirable to write the stresses and plastic strain increments of a multiaxial system in terms of a stress ( $\bar{\sigma}$ ) and a strain increment ( $d\bar{\epsilon}^p$ ) equivalent to that of a uniaxial system. If for the latter system the yield stress is  $Y$  then the yield criteria of paragraph 1.1 may be employed for this purpose.

Then for the von Mises criterion, equation(5),  $k = \frac{Y}{\sqrt{3}}$  so that,

$$Y = \sqrt{\frac{3}{2}} (\sigma'_{ij} \sigma'_{ij})^{1/2} \quad (12)$$

and for the Tresca criterion, equation(10),  $k = \frac{Y}{2}$  which gives for a principal stress system,

$$Y = \sigma_1 - \sigma_3 \quad (13)$$

Both equations(12) and (13) then have right-hand sides which reduce to  $\sigma_1$  for simple tension.

For a multiaxial system it is more usual to write the right-hand side in these equations as a function  $\bar{\sigma}$  that increases with progressive plastic deformation and so accounts for work hardening. Then the von Mises equivalent stress is

$$\bar{\sigma} = \sqrt{\frac{3}{2}} (\sigma'_{ij} \sigma'_{ij})^{1/2} \quad (14)$$

which, for a principal multiaxial stress system  $(\sigma_1, \sigma_2, \sigma_3)$ , appears in its more usual form as

$$\bar{\sigma} = \frac{1}{\sqrt{2}} \left\{ (\sigma_1 - \sigma_2)^2 + (\sigma_2 - \sigma_3)^2 + (\sigma_1 - \sigma_3)^2 \right\}^{1/2} \quad (15)$$

and the Tresca equivalent stress for the system is

$$\bar{\sigma} = (\sigma_1 - \sigma_3) \quad (16)$$

If either equation (15) or (16) successfully correlate the stress strain behaviour of a multiaxial test with that of a uniaxial test then for any specified equivalent strain  $\bar{\epsilon} = Y$  and the use of equation (12) or (13) is justified. Obviously both equations must give  $\bar{\sigma} = \sigma_1$  for simple tension or compression  $(\sigma_1, 0, 0)$ .

The equivalent plastic strain increment is best derived from the work hypothesis (2). The increment of plastic work ( $dW^p$ ) associated with an equivalent stress ( $\bar{\sigma}$ ) and its corresponding plastic strain increment ( $d\bar{\epsilon}^p$ ) is written as

$$dW^p = \bar{\sigma} d\bar{\epsilon}^p \quad (17)$$

or, in terms of tensors  $\sigma'_{ij}$  and  $d\epsilon'_{ij}$  as,

$$dW^p = \sigma'_{ij} d\epsilon'_{ij}$$

Equation (17) is more conveniently written in terms of the deviatoric stress tensor  $\sigma'_{ij}$  here. Thus from equation (1)

$$\begin{aligned} dW^p &= (\sigma'_{ij} + \delta_{ij} \sigma_m) d\epsilon'_{ij} \\ &= \sigma'_{ij} d\epsilon'_{ij} + \delta_{ij} \sigma_m d\epsilon'_{ij} \\ &= \sigma'_{ij} d\epsilon'_{ij} + \sigma_m d\epsilon'_{ii} \text{ since } \delta_{ij} = 1 \text{ for } i = j \text{ and } 0 \text{ for } i \neq j \end{aligned}$$

and from equation (7) we then have,

$$dW^p = \sigma'_{ij} d\epsilon'_{ij} \quad (18)$$

which must be so because, for an ideal plastic solid, no deformation work is done by the hydrostatic component ( $\sigma_m$ ) of the stress tensor  $\sigma'_{ij}$ .

Equating equations (17) and (18) we have,

$$\bar{\sigma} d\bar{\epsilon}^p = \sigma'_{ij} d\epsilon'_{ij} = (\sigma'_{ij} d\epsilon'_{ij})^{1/2} (\sigma'_{ij} d\epsilon'_{ij})^{1/2}$$

Then substituting from equation (9)

$$\begin{aligned} \bar{\sigma} d\bar{\epsilon}^p &= (\sigma'_{ij} \delta \lambda \sigma'_{ij})^{1/2} \left( \frac{d\epsilon'_{ij} \cdot d\epsilon'_{ij}}{\delta \lambda} \right)^{1/2} \\ &= \left( \frac{3}{2} \sigma'_{ij} \sigma'_{ij} \right)^{1/2} \left( \frac{2}{3} d\epsilon'_{ij} d\epsilon'_{ij} \right)^{1/2} \end{aligned}$$

which, from equation (14), can be simplified to,

$$\bar{\sigma} d\bar{\epsilon}^p = \bar{\sigma} \left( \frac{2}{3} d\epsilon'_{ij} d\epsilon'_{ij} \right)^{1/2}$$

so that,

$$d\bar{\epsilon}^p = \sqrt{\frac{2}{3}} (d\epsilon'_{ij} d\epsilon'_{ij})^{1/2} \quad (19)$$

For a principal multiaxial system with strain increments of  $d\epsilon_1^p$ ,  $d\epsilon_2^p$  and  $d\epsilon_3^p$  equation (19) appears in its more usual form as

$$d\bar{\epsilon}^p = \frac{\sqrt{2}}{3} \left\{ (d\epsilon_1^p - d\epsilon_2^p)^2 + (d\epsilon_2^p - d\epsilon_3^p)^2 + (d\epsilon_1^p - d\epsilon_3^p)^2 \right\}^{1/2} \quad (20)$$

and since equation (7) would appear here as  $d\epsilon_1^p + d\epsilon_2^p + d\epsilon_3^p = 0$  an alternative form of this equation is,

$$d\bar{\epsilon}^p = \sqrt{\frac{2}{3}} \left\{ (d\epsilon_1^p)^2 + (d\epsilon_2^p)^2 + (d\epsilon_3^p)^2 \right\}^{1/2} \quad (21)$$

The Tresca equivalent strain is formulated from two stand points:

(1) To correspond to the absence of intermediate stress  $\bar{\sigma}_2$  in the yield criterion of equation (10) the intermediate plastic strain  $d\epsilon_2^p$  is not included.

(2) The expression in  $d\bar{\epsilon}^p$  is made to agree with the major principal plastic strain ( $d\epsilon_1^p$ ) of a simple tension test where  $d\epsilon_2^p = d\epsilon_3^p = -d\epsilon_1^p/2$

We therefore have,

$$d\bar{\epsilon}^p = \frac{2}{3} (d\epsilon_1^p - d\epsilon_3^p) \quad (22)$$

Although the Tresca  $\bar{\sigma}$ ,  $d\bar{\epsilon}^p$  expressions of equations (16) and (22) agree with von Mises expressions of equations (15) and (20) for the case of simple tension this is not so for other stress systems. For example, in the case of pure shear  $(\sigma_1, -\sigma_1, 0)$  and  $(d\epsilon_1^p, -d\epsilon_1^p, 0)$  substitution in these equations would show a ratio between the von Mises and Tresca equivalent stresses and plastic strains of  $\sqrt{3}/2$ . A consideration of the corresponding plastic work increments from equation (17) would show only the von Mises definitions to yield the correct result  $(2\sigma_1 d\epsilon_1^p)$ . In general, experimental work performed on ductile metals has shown the definitions associated with the von Mises criterion to be the more correct. In view of its mathematical simplicity however the Tresca criterion and its associated definitions are occasionally employed.

#### 1.4 The $\delta\lambda$ Term

The  $\delta\lambda$  term in the von Mises and Tresca flow rules of equations (9) and (11) may be regarded as a constant for any given increment of plastic deformation but varying with successive increments as deformation proceeds. Since both the equivalent stress  $\bar{\sigma}$  and the equivalent strain increment  $d\bar{\epsilon}^p$  also vary in this way then  $\delta\lambda$  is shown to relate them in the following treatment.

Upon substituting equation(9) into equation(19) we have for the von Mises definitions,

$$d\bar{\epsilon}^p = \sqrt{\frac{2}{3}} (d\epsilon_{ij}^p d\epsilon_{ij}^p)^{1/2} = \sqrt{\frac{2}{3}} \delta\lambda (\sigma'_{ij} \tau'_{ij})^{1/2}$$

and identifying the right-hand side of this equation with equation(14) leads to

$$d\bar{\epsilon}^p = \frac{2}{3} \delta\lambda \bar{\sigma}$$

from which,

$$\delta\lambda = \frac{3}{2} \frac{d\bar{\epsilon}^p}{\bar{\sigma}} \quad (23)$$

Substituting equation(23) into equation(9) we have the most frequently used form of the Levy-Mises flow rule. That is,

$$d\epsilon_{ij}^p = \left( \frac{3 d\bar{\epsilon}^p}{2 \bar{\sigma}} \right) \tau'_{ij} \quad (24)$$

This equation allows the path of plastic deformation to be traced through  $d\bar{\epsilon}^p$  and  $\bar{\sigma}$ —which in turn are referred to a simple uniaxial system.

The Tresca definitions of equivalent stress and strain, equations (16) and (22), would be equated to  $\delta\lambda$  in the same way as equation(23) if they are related through the Levy-Mises flow rule in this way. Thus in substituting equation(9) into equation(22) we have

$$\begin{aligned} d\bar{\epsilon}^p &= \frac{2}{3} (d\epsilon_1^p - d\epsilon_3^p) = \frac{2}{3} \delta\lambda (\sigma'_1 - \sigma'_3) \\ &= \frac{2}{3} \delta\lambda (\sigma_1 - \sigma_3) = \frac{2}{3} \delta\lambda \bar{\sigma} \end{aligned}$$

which is in agreement with equation(23).

Equation(24) is then used with either the von Mises or Tresca definitions of equivalent stress and strain. It should be noted however that only the former definitions are strictly in accordance with plasticity theory. This may be seen through the plastic potential  $f'$  of equation(8) when it is written in terms of equivalent stress and strain. Thus for the von Mises yield criterion we have from equations(2) and(14) that

$$f'(\sigma_{ij}) = J_2' = \frac{\bar{\sigma}^2}{3} \quad (25)$$

Then upon substituting equations(23) and(25) in equation(8) we have

$$\begin{aligned} d\epsilon_{ij}^p &= \frac{1}{2} \frac{\partial(\bar{\sigma}^2)}{\partial\tau'_{ij}} \frac{d\bar{\epsilon}^p}{\bar{\sigma}} \\ &= \left( \frac{\partial\bar{\sigma}}{\partial\tau'_{ij}} \right) d\bar{\epsilon}^p \end{aligned} \quad (26)$$

Equation (26) can be shown\* to agree with equation (24) only for the case where  $\bar{\sigma}$  and  $d\bar{\epsilon}^p$  are von Mises definitions. The plastic potential form of equation (8), in strict accordance with plasticity theory, only gives plastic strain increment relations for a yield criterion with its derived flow rule, equivalent stress and strain.

The  $\delta\lambda$  term in the Tresca flow rule of equation (11) should therefore only strictly be identified with its associated equivalent stress and strain. Then substituting equation (11) into equation (22) we have,

$$d\bar{\epsilon}^p = \frac{2}{3} (d\epsilon_1^p - d\epsilon_3^p) = \frac{2}{3} (\delta\lambda - (-\frac{\delta\lambda}{2}))$$

from which

$$\delta\lambda = \frac{3}{2} d\bar{\epsilon}^p \quad (27)$$

and substituting equation (27) into equation (11) we have the following principal plastic strain increments for the Tresca flow rule,

$$\begin{aligned} d\epsilon_1^p &= \frac{3}{4} d\bar{\epsilon}^p \\ d\epsilon_2^p &= 0 \\ d\epsilon_3^p &= -\frac{3}{4} d\bar{\epsilon}^p \end{aligned} \quad (28)$$

Lastly if the von Mises equivalent strain is related through the Tresca flow rule in a similar way the resulting  $\delta\lambda$  expression does not agree with equation (27). Thus on substituting equation (11) into equation (21) we have,

$$d\bar{\epsilon}^p = \sqrt{\frac{2}{3}} \left\{ (d\epsilon_1^p)^2 + (d\epsilon_2^p)^2 + (d\epsilon_3^p)^2 \right\}^{1/2} = \sqrt{\frac{2}{3}} \left\{ \left(\frac{\delta\lambda}{2}\right)^2 + 0 + \left(-\frac{\delta\lambda}{2}\right)^2 \right\}^{1/2}$$

from which,

$$\delta\lambda = \sqrt{3} d\bar{\epsilon}^p \quad (29)$$

\* If these equations are to agree then,

$$\frac{3}{2} \sigma'_{ij} / \bar{\sigma} = \partial \bar{\sigma} / \partial \sigma'_{ij} = \partial \bar{\sigma} / \partial \sigma'_{ij}$$

then,

$$\frac{3}{2} \sigma'_{ij} \partial \sigma'_{ij} = \bar{\sigma} \partial \bar{\sigma}$$

which upon integration gives,

$$\frac{3}{4} \sigma'_{ij}{}^2 = \bar{\sigma}^2$$

and,

$$\bar{\sigma} = \sqrt{\frac{3}{2}} (\sigma'_{ij}{}^2)^{1/2}$$

which of course is the von Mises equivalent stress definition of equation (14).

Then on substituting equation (29) into equation (11) the Tresca flow rule with a von Mises equivalent strain yields the following principal plastic strain increments,

$$\begin{aligned} d\epsilon_1^p &= \frac{\sqrt{3}}{2} d\bar{\epsilon}^p \\ d\epsilon_2^p &= 0 \\ d\epsilon_3^p &= -\frac{\sqrt{3}}{2} d\bar{\epsilon}^p \end{aligned} \quad (30)$$

It will be noted that although equations (28) and (30) do not contain any equivalent stress definition the current state of stress is required however in order to determine  $d\bar{\epsilon}^p$  for a multiaxial system.

Of the three flow rule equations (24), (28) and (30) derived here, equation (24) with either von Mises or Tresca definitions of equivalent stress and strain, has found the most common use.

## 2. MULTIAXIAL CREEP FOR AN ISOTROPIC MATERIAL

The prediction of creep rates for the multiaxial stress case have simply been developed by writing the plastic strain increments of the foregoing section as time derivatives. Thus the time independent plastic strain increment tensor  $d\epsilon_{ij}^p$  is replaced by a creep strain rate tensor  $\dot{\epsilon}_{ij}$  from the equation,

$$\dot{\epsilon}_{ij} = \frac{d\epsilon_{ij}^p}{dt} \quad (31)$$

The Levy-Mises flow rule of equation (24) would then appear as,

$$\dot{\epsilon}_{ij} = \frac{3\dot{\bar{\epsilon}}}{2\bar{\sigma}} \sigma'_{ij} \quad (32)$$

The assumptions made in the derivation of equation (24) (see paragraph 1.2) for time independent plasticity have also had satisfactory experimental support by Johnson (3) for secondary creep (constant  $\dot{\epsilon}_{ij}$ ) and to a lesser extent, primary creep (decreasing  $\dot{\epsilon}_{ij}$ ).

### 2.1 Relationships between $\bar{\sigma}$ and $\dot{\bar{\epsilon}}$

Many multiaxial creep tests have been done in order to establish the functional relationship that might exist between the equivalent stress and the equivalent strain rate. The latter has been both primary and secondary creep based. Such experiments have shown that for most

engineering materials a unique relationship exists between them for all stress systems that operate at identical temperatures.

This has considerably simplified the multiaxial creep problem since it means that the creep rates for a multiaxial system may be predicted from equation (32) along with the  $\dot{\epsilon}$ ,  $\bar{\sigma}$  functional relationship as obtained from a simpler laboratory test, e.g. tension or torsion.

In general,

$$\dot{\epsilon} = f(\bar{\sigma}) \quad (33)$$

and the most commonly used functions for secondary creep in engineering are power, exponential and hyperbolic types,

$$\begin{aligned} \dot{\epsilon} &= A \bar{\sigma}^n \\ \dot{\epsilon} &= B \exp(\bar{\sigma}/C) \\ \dot{\epsilon} &= D \sinh(\bar{\sigma}/E) \end{aligned} \quad (34)$$

where A, B, C, D, E and n are experimentally determined constants.

The choice of function depends upon the best fit to experimental data but usually each function is more applicable to a specific stress range (see Appendix III). Thus if a power law is chosen for use in the Levy-Mises flow rule of equation (32) we have

$$\dot{\epsilon}_{ij} = \frac{3}{2} \cdot \frac{A \bar{\sigma}^n}{\bar{\sigma}} \sigma'_{ij} = \frac{3}{2} A \bar{\sigma}^{n-1} \sigma'_{ij} \quad (35)$$

which, for a principal multiaxial stress system ( $\sigma_1, \sigma_2, \sigma_3$ ), predicts secondary creep rates as,

$$\begin{aligned} \dot{\epsilon}_1 &= \frac{3}{2} A \bar{\sigma}^{n-1} \left[ \sigma_1 - \frac{1}{3} (\sigma_1 + \sigma_2 + \sigma_3) \right] \\ &= A \bar{\sigma}^{n-1} \left[ \sigma_1 - \frac{1}{2} (\sigma_2 + \sigma_3) \right] \end{aligned}$$

similarly

$$\dot{\epsilon}_2 = A \bar{\sigma}^{n-1} \left[ \sigma_2 - \frac{1}{2} (\sigma_1 + \sigma_3) \right] \quad (36)$$

and

$$\dot{\epsilon}_3 = A \bar{\sigma}^{n-1} \left[ \sigma_3 - \frac{1}{2} (\sigma_1 + \sigma_2) \right]$$

where  $\bar{\sigma}$  has been written either as the von Mises or Tresca equivalent stresses of equations (15) and (16) respectively.

If alternatively a hyperbolic sinh law is preferred in the Levy-Mises flow rule we have,

$$\dot{\epsilon}_{ij} = \frac{3}{2} \frac{D \sinh(\bar{\sigma}/E)}{\bar{\sigma}} \sigma'_{ij} \quad (37)$$

Lastly if the power law is chosen for use in the Tresca flow rule we have from the time derivatives of equation (28) principal secondary creep rates of the form,

$$\begin{aligned}\dot{\epsilon}_1 &= \frac{3}{4} \dot{\bar{\epsilon}} = \frac{3}{4} A \bar{\sigma}^n \\ \dot{\epsilon}_2 &= 0 \\ \dot{\epsilon}_3 &= -\dot{\epsilon}_1\end{aligned}\quad (38)$$

for a Tresca equivalent stress, or from equation (30),

$$\begin{aligned}\dot{\epsilon}_1 &= \frac{\sqrt{3}}{2} \dot{\bar{\epsilon}} = \frac{\sqrt{3}}{2} A \bar{\sigma}^n \\ \dot{\epsilon}_2 &= 0 \\ \dot{\epsilon}_3 &= -\dot{\epsilon}_1\end{aligned}\quad (39)$$

for a von Mises equivalent stress.

While equation (38) has had some specific applications (but not to uniaxial tests where it is normally assumed that  $\dot{\epsilon}_2 = \dot{\epsilon}_3 = -\dot{\epsilon}_1/2$ ) equation (39) has never appeared in the literature. On the basis that in some instances the Tresca equivalent stress has been used in the Levy-Mises flow rule to provide the best correlation with experimental data there is no reason why the von Mises equivalent stress should not be used with the Tresca flow rule if this combination were to provide the best correlation in other instances.

Multiaxial creep rate equations may be applied to primary creep provided a time function  $\phi(t)$  is introduced that describes it. Then combining equations (32) and (33) and adding the time function we have for the Levy-Mises flow rule,

$$\dot{\epsilon}_{ij} = \frac{3}{2} f\left(\frac{\bar{\sigma}}{\bar{\sigma}}\right) \sigma'_{ij} \phi(t) \quad (40)$$

A time function may be added in this way provided that it is separable from stress and provided it is the same function for each component creep curve of the multiaxial state.

Equation (40) is often written in terms of  $J_2'$  through equation (25) and appears in the form

$$\dot{\epsilon}_{ij} = A' F(J_2') \sigma'_{ij} \phi(t) \quad (41)$$

where  $A'$  is a constant. Comparison with equation (35) further shows that

$$A' = \frac{3}{2} (3)^{\frac{n-1}{2}} A$$

$$\text{and } f(J_2') = J_2'^P = J_2'^{\frac{n-1}{2}} = \left(\frac{\bar{\sigma}}{\sqrt{3}}\right)^{n-1} \quad (42)$$

for the power law of equation (34).

### 3. OTHER MULTIAXIAL CREEP RATE EQUATIONS

The equations initially proposed by Bailey (4) on the tension-torsion creep of carbon steels at 480°C and the combined internal pressure-axial load creep of lead at room-temperature have often found favour when the equations of paragraph 2.1 have been inadequate to represent experimental data.

In terms of a principal stress system ( $\sigma_1, \sigma_2, \sigma_3$ ) the secondary creep rates are expressed here as,

$$\begin{aligned}\dot{\epsilon}_1 &= \frac{A}{2} \bar{\sigma}^{2m} \left\{ (\sigma_1 - \sigma_2)^{n-2m} + (\sigma_1 - \sigma_3)^{n-2m} \right\} \\ \dot{\epsilon}_2 &= \frac{A}{2} \bar{\sigma}^{2m} \left\{ (\sigma_2 - \sigma_1)^{n-2m} + (\sigma_2 - \sigma_3)^{n-2m} \right\} \\ \dot{\epsilon}_3 &= \frac{A}{2} \bar{\sigma}^{2m} \left\{ (\sigma_3 - \sigma_1)^{n-2m} + (\sigma_3 - \sigma_2)^{n-2m} \right\}\end{aligned}\quad (43)$$

where it is seen that the extra experimental constant  $m$  in these equations affords greater flexibility in application. It should be noted however that equations of this type violate assumption (2) of paragraph 1.2 except for the case where  $2m = n - 1$  when equations (43) are then identical to the Marin-Soderberg type for  $\bar{\sigma}$  defined as the von Mises equivalent stress of equation (15) in equation (36).

To make the Bailey equations (43) consistent with the concept of a plastic potential Davis (5) suggested the following redefinition of equivalent stress,

$$\sigma^* = \left\{ \frac{(\sigma_1 - \sigma_2)^{n-2m+1} + (\sigma_2 - \sigma_3)^{n-2m+1} + (\sigma_3 - \sigma_1)^{n-2m+1}}{2} \right\}^{\frac{1}{n-2m+1}} \quad (44)$$

Thus when equation (44) is used as a plastic potential in an equation similar in form to the time derivative of equation (26), we have,

$$\dot{\epsilon}_{ij} = \frac{\partial \sigma^*}{\partial \sigma_{ij}} \dot{\epsilon} \quad (45)$$

which leads to the Bailey equations (43) with  $\bar{\sigma} = \sigma^*$  and provided a power function relationship exists between  $\sigma^*$  and  $\dot{\epsilon}$  of the form,

$$\dot{\epsilon} = A \sigma^{*n} \quad (46)$$

with  $\dot{\epsilon}$  presumably defined as,

$$\dot{\epsilon} = \left[ \frac{2}{9} \left\{ (\dot{\epsilon}_1 - \dot{\epsilon}_2)^{n-2m+1} + (\dot{\epsilon}_2 - \dot{\epsilon}_3)^{n-2m+1} + (\dot{\epsilon}_3 - \dot{\epsilon}_1)^{n-2m+1} \right\} \right]^{\frac{1}{n-2m+1}} \quad (47)$$

Bailey obtained the constant  $m$  in his equation (4.3) from a torsional creep test and  $n$  in a manner identical to that described in paragraph 2.1 relating  $\dot{\bar{\epsilon}}$  to  $\bar{\sigma}$ . The problem here of finding the  $n$  value contained in the expressions (4.4) and (4.7) and as the power index relating them (equation (4.6)) would be more complicated. This approach however has been shown by Wahl (6) to yield a better correlation between the equivalent secondary creep rate and stress for many of the multiaxial creep tests quoted in the literature. It will further be noted that the von Mises definitions of stress and equivalent strain rate, on which the correlations were originally based, is contained in equations (4.4) and (4.7) as a special case for  $n - 2m = 1$ .

Further creep rate equations may be obtained from a modified concept of the plastic potential as suggested by Berman and Pai (7). They expressed secondary creep rates in the more general form of equation (4.5). That is,

$$\dot{\epsilon}_{ij} = KM^n \frac{\partial D}{\partial \sigma_{ij}} \quad (4.8)$$

where, contrary to the statement made in paragraph 1.4, they allowed the equivalent stress (through  $D$ ) and the equivalent strain rate (through  $KM^n$ ) to be separated from the one yield criterion. Thus the equivalent stress functions  $M$  and  $D$  may be different and the equations employed by Berman and Pai, in their reanalysis of some published data, were obtained by replacing  $M$  and  $D$  with the Tresca ( $\bar{\sigma}_T$ ) and the von Mises ( $\bar{\sigma}_M$ ) equivalent stresses respectively such that equation (4.8) became

$$\dot{\epsilon}_{ij} = k(\bar{\sigma}_T)^n \frac{\partial \bar{\sigma}_M}{\partial \sigma_{ij}} \quad (4.9)$$

which gives principal secondary creep rates of the form,

$$\begin{aligned} \dot{\epsilon}_1 &= \frac{k(\bar{\sigma}_T)^n}{\bar{\sigma}_M} \left[ \sigma_1 - \frac{1}{2}(\sigma_2 + \sigma_3) \right] \\ \dot{\epsilon}_2 &= \frac{k(\bar{\sigma}_T)^n}{\bar{\sigma}_M} \left[ \sigma_2 - \frac{1}{2}(\sigma_1 + \sigma_3) \right] \\ \dot{\epsilon}_3 &= \frac{k(\bar{\sigma}_T)^n}{\bar{\sigma}_M} \left[ \sigma_3 - \frac{1}{2}(\sigma_1 + \sigma_2) \right] \end{aligned} \quad (50)$$

The use of equation (50) was shown to correct the discrepancies, attributed to anisotropy, between experiment and isotropic calculations.

A second set of equations, not used by Berman and Pai, may be obtained from equation (4.8) in replacing  $M$  and  $D$  by the von Mises ( $\bar{\sigma}_M$ ) and Tresca ( $\bar{\sigma}_T$ ) equivalent stresses respectively. That is,

$$\dot{\epsilon}_{ij} = K(\bar{\sigma}_M)^n \frac{\partial \bar{\sigma}_T}{\partial \sigma_{ij}} \quad (51)$$

which gives principal secondary creep rates of the form,

$$\begin{aligned} \dot{\epsilon}_1 &= K(\bar{\sigma}_M)^n \\ \dot{\epsilon}_2 &= 0 \\ \dot{\epsilon}_3 &= -\dot{\epsilon}_1 \end{aligned} \quad (52)$$

These equations are of course identical to those of equation (39) for  $K = \sqrt{3}/2 A$ .

Lastly when M and D are the same function in equation (48) and equal to the von Mises equivalent stress it gives the Marin-Soderberg equations (36) for  $K = A$  whilst a Tresca definition for both M and D gives the principal creep rates of equation (38) for  $K = 3A/4$ .

It would appear through the application of equation (48) with this choice of equivalent stress that the secondary creep rates of any multiaxial creep test may be satisfactorily described. The difficulty however lies in the correct choice of equivalent stress expression(s) if the more accepted forms are unsatisfactory.

#### 4. ANISOTROPIC PLASTIC FLOW

The equations developed in Section 2 are consistent with classical plasticity theory in that the assumption is made that engineering materials are initially isotropic and remain so during subsequent creep deformation. Experimental work, however, mainly on the verification of yield surfaces (8-12) has shown that insufficient attention has been paid to the question of anisotropy. The data collected in these studies has shown that anisotropy develops with deformation irrespective of whether the material is initially isotropic or not.

Anisotropic creep behaviour is much less understood. There is however a set of creep rate equations consistent with a yield criterion and suitable for a material exhibiting a certain type of anisotropy. Their development and usage is described in this and the following sections.

##### 4.1 Forms of Anisotropy

A rolled or drawn section is initially anisotropic since it exhibits

crystallographic orientation. The texture in the crystal structure is normally associated with greater strength and the flow properties then vary depending upon the relative orientation of the stress system and the rolled direction.

Alternatively, a preferred grain orientation may develop during the flow process itself. In more complex alloys plastic flow may cause a directional arrangement of certain phases, inclusions, porosities and cracks in a structure that was initially isotropic. Voids and crack growth are normally associated with breakdown of the structure such as the tertiary stage of creep or local necking.

A cold working process that introduces residual stress may render a material anisotropic. The residual stress pattern interacts with an applied stress system and so modifies it to produce behaviour quite different from isotropic. Depending upon the nature of the residual strain and the applied stress the material may be either stronger or weaker for it. A prestraining operation, like a preferred structure, can therefore be used to advantage.

It is possible that both types of anisotropy may be present due to the manufacturing process itself. In certain circumstances an annealing treatment may make the metal isotropic but it is more likely that the anneal results in a partial retention of the initial anisotropy or in the development of a new type of anisotropy associated with the annealing process itself.

#### 4.2 The Deviatoric Plane

Anisotropic plastic flow is best examined from a knowledge of changes in shape of yield surfaces as plastic flow progresses. For a general stress system such surfaces may conveniently be represented as a two-dimensional locus on a deviatoric or  $\pi$  plane (Fig. 1A)\*. The deviatoric plane is constructed from the deviatoric components ( $\sigma'_{ij}$ ) of every possible stress state. For simplicity the principal stress space ( $\sigma_1, \sigma_2, \sigma_3$ ) is shown in Fig. 1A and the deviatoric components ( $\sigma'_1, \sigma'_2, \sigma'_3$ ) are obtained from equation (1) as

$$\begin{aligned}\sigma'_1 &= \sigma_1 - \sigma_m \\ \sigma'_2 &= \sigma_2 - \sigma_m \\ \sigma'_3 &= \sigma_3 - \sigma_m\end{aligned}$$

\* Figures are given at the end of this Appendix.

In Fig. 1A if vector  $OP$  represents the stress state  $(\sigma_1, \sigma_2, \sigma_3)$ ,  $O'P$  the deviatoric stress state  $(\sigma'_1, \sigma'_2, \sigma'_3)$  and  $OO'$  the hydrostatic stress  $(\sigma_m)$  then the vector representation of these equations is

$$(OP)^2 = (OO')^2 + (O'P)^2$$

The hydrostatic vector  $(OO')$  of magnitude  $\frac{1}{3}(\sigma_1 + \sigma_2 + \sigma_3)$  and equally inclined to the stress axes 1, 2 and 3 has no effect on yielding and cannot therefore cut the yield surface. The deviatoric vector  $(O'P)$  is seen to lie in a plane perpendicular to the hydrostatic vector. Since  $(O'P)$  contains the components of stress that are responsible for yielding then  $O'$  is the origin of possible yield surfaces containing  $O'P$  and lying in this plane. The magnitude of vector  $O'P$  in this deviatoric plane determines the yield characteristics of the material. When  $O'P$  reaches a certain limiting magnitude, represented by a yield locus that forms the intersection of the deviatoric plane and a yield surface, then yielding is said to occur. To include every possible principal stress state the yield surface is therefore a prism of constant cross-section with the hydrostatic vector as its axis.

A chosen yield criterion defines the cross-section of this prism. It can be shown (2) that the von Mises criterion of equation (5) is a circle of radius  $Y$  on this plane whilst the Tresca criterion of equation (10) appears as a regular hexagon inscribed in the von Mises circle (Fig. 1B). Since the deviatoric plane makes equal angles with the deviatoric axes then they are shown projected on the plane as three lines  $120^\circ$  apart. Actually they project as  $\sqrt{\frac{2}{3}} \sigma'_1$  etc. but it is more usual to multiply these projections by  $\sqrt{\frac{3}{2}}$  so that they appear as actual deviatoric stresses.

In tension-torsion stress space  $(\sigma_{11}, \sigma_{12})$  the von Mises and Tresca prisms cut the plane of this space as ellipses  $\sigma_{11}^2 + 3\sigma_{12}^2 = \bar{\sigma}^2$  and  $\sigma_{11}^2 + 4\sigma_{12}^2 = \bar{\sigma}^2$  respectively—these being the forms more usually referred to for this stress system (Fig. 1C). For the following discussion, however, we consider in Fig. 1B a general stress system represented in yielding by a von Mises circle on the deviatoric plane of initial radius  $Y$  and current state  $\bar{\sigma}$  and the effect of straining in tension ( $\theta = 30^\circ$ ) followed by compression ( $\theta = 210^\circ$ ).

#### 4.3 Effect of Plastic Flow on the Yield Surface

A number of hypotheses have been suggested to depict the nature of changes in shape of the yield surface for various types of prestrain history. Once a state of stress is reached outside that defined by the initial yield surface (radius  $Y$ ) a new yield surface is then required to

define yielding for the strained state (defined by  $\bar{\sigma}$ ). Conceivably there are four ways by which the yield surface may change from its initial shape to some other shape.

#### 4.3.1 Isotropic Hardening (Fig. 2A)

This predicts that the yield surface grows in size as a uniform expansion of the initial yield surface. This is shown here as a succession of concentric circles of initial radius  $Y$  and current radius  $\bar{\sigma}$ . Isotropic hardening is easiest to handle mathematically but implies the following assumptions:

(1) an isotropic material remains isotropic and an anisotropic material remains anisotropic.

(2) a negative Bauschinger effect. This means that tensile loading to  $\bar{\sigma}$  on a material of initial yield stress  $Y$  (path  $O'QP$ ) followed by reverse loading (path  $PFG$ ) produces a yield point  $F$  in compression greater than the initial yield point  $Q$ . As actual experiments indicate the reverse effect then this assumption is not valid. The effect of this on the yield surface is to reduce the size on one side as that on the other side is increased.

Thus the surface changes shape as deformation proceeds.

#### 4.3.2 Minimum Surface (Fig. 2B)

This surface contains part of the initial yield locus of radius  $Y$  and a modification to embrace the new stress state  $\bar{\sigma}$  (point  $P$ ). The new yield surface is then the minimum surface enclosing the two. The resulting surface contains a yield corner at  $P$ , shows no cross-effect and again implies no Bauschinger effect. In tension-torsion stress space cross-effects would be apparent as an increase in the tensile yield stress after plastic deformation in torsion and vice versa. This however appears to depend upon the definition employed to define yielding since experiment has shown this effect for a proof strain or a back extrapolation definition (8, 9) but none for the departure from linearity definition (10, 11). Further experimental work on the existence of corners as carried by the stress vector (12) showed more of a local distortion in this region. The minimum surface model is therefore incorrect in shape although it correctly predicts that for some directions an isotropic material becomes anisotropic, and an anisotropic material attains a higher degree of anisotropy but both retain their original state in other directions.

#### 4.3.3 Rigid Translation - Prager's Kinematic Model (13)

In this model (Fig. 2C) no change in shape of the initial yield locus is assumed but a rigid translation occurs as the locus is carried by the stress vector  $\bar{\sigma}$  and contains the current stress state  $P$ . The model is consistent with a Bauschinger effect but the predictions from the model are too severe in this respect. An absence of cross-effect is implied with this model and like the minimum surface model (4.3.2) it correctly predicts that an isotropic material becomes anisotropic and an anisotropic material becomes more anisotropic. The accompanying changes in properties are seen to bear a definite geometrical relationship to the loading path with greatest hardening in this direction.

#### 4.3.4 Combined Model

It is conceivable that a new yield locus may be accurately represented by combinations of these three models. For example Hodge (14) suggested the combination of kinematic and isotropic hardening of Fig. 2D which successfully displays a Bauschinger effect, a cross-effect and a closeness of subsequent loci at points on the opposite side to the stress vector. The model does not however display the experimentally observed (15) flattening of the yield locus in this region and an associated rounded corner at the loading point. Like the kinematic model (4.3.3) the development of anisotropy with progressive straining is shown here but to a lesser extent and with a more even spread of hardening.

#### 4.4 Anisotropic Plastic Flow Equations

Equations describing the plastic flow behaviour of materials that possess anisotropy due to preferred orientation were originally proposed by Hill (16). By writing  $f(\sigma_{ij})$  as the anisotropic stress invariant function

$$6f(\sigma_{ij}) = 2\bar{\sigma}_a^2 = F(\sigma_{11} - \sigma_{22})^2 + G(\sigma_{22} - \sigma_{33})^2 + H(\sigma_{11} - \sigma_{33})^2 + 3[L(\sigma_{12}^2 + \sigma_{21}^2) + M(\sigma_{23}^2 + \sigma_{32}^2) + N(\sigma_{13}^2 + \sigma_{31}^2)] \quad (53)$$

and applying this as a plastic potential in equation (8) the plastic strain increments are then,

$$d\epsilon_{11}^p = \delta\lambda/3 [F(\sigma_{11} - \sigma_{22}) - H(\sigma_{33} - \sigma_{11})]$$

$$d\epsilon_{22}^p = \delta\lambda/3 [G(\sigma_{22} - \sigma_{33}) - F(\sigma_{11} - \sigma_{22})]$$

$$d\epsilon_{33}^p = \delta\lambda/3 [H(\sigma_{33} - \sigma_{11}) - G(\sigma_{22} - \sigma_{33})]$$

and

$$d\epsilon_{12}^p = d\epsilon_{21}^p = L \delta\lambda \sigma_{12}$$

$$d\epsilon_{23}^p = d\epsilon_{32}^p = M \delta\lambda \sigma_{23}$$

$$d\epsilon_{13}^p = d\epsilon_{31}^p = N \delta\lambda \sigma_{13}$$

(54)

where subscripts 1, 2 and 3 refer to the principal axes of anisotropy.

Now  $\delta\lambda$  may be expressed (17) in terms of an anisotropic equivalent stress ( $\bar{\sigma}_a$ ) and plastic strain increment ( $d\bar{\epsilon}_a^p$ ) in a similar way to that outlined in paragraph 1.4 for the isotropic case to give

$$\delta\lambda = \frac{3}{2} \left( \frac{\lambda \bar{\epsilon}_a^p}{\bar{\sigma}_a} \right) \quad (55)$$

Then equation (54) may be written

$$d\epsilon_{11}^p = \frac{\lambda \bar{\epsilon}_a^p}{2\bar{\sigma}_a} [F(\sigma_{11} - \sigma_{22}) - H(\sigma_{33} - \sigma_{11})] \quad \text{etc.} \quad (56)$$

$$d\epsilon_{12}^p = \frac{3L}{2} \frac{\lambda \bar{\epsilon}_a^p}{\bar{\sigma}_a} \tau_{12} \quad \text{etc.}$$

where  $\bar{\sigma}_a$  is defined from equation (53) as

$$\bar{\sigma}_a = \frac{1}{\sqrt{2}} \left[ F(\sigma_{11} - \sigma_{22})^2 + G(\sigma_{22} - \sigma_{33})^2 + H(\sigma_{11} - \sigma_{33})^2 + 6(L\tau_{12}^2 + M\tau_{23}^2 + N\tau_{31}^2) \right]^{1/2} \quad (57)$$

and  $\lambda \bar{\epsilon}_a^p$ , obtained from the solution to equations (54) and (57), is defined as

$$\lambda \bar{\epsilon}_a^p = \frac{\sqrt{2}}{3} \left[ \frac{9}{(GH + FG + HF)^2} \left\{ F(Gd\epsilon_{11}^p - Hd\epsilon_{22}^p)^2 + G(Hd\epsilon_{22}^p - Fd\epsilon_{33}^p)^2 + H(Gd\epsilon_{11}^p - Fd\epsilon_{33}^p)^2 \right\} + 6 \left\{ \frac{(d\epsilon_{12}^p)^2}{L} + \frac{(d\epsilon_{23}^p)^2}{M} + \frac{(d\epsilon_{31}^p)^2}{N} \right\} \right]^{1/2} \quad (58)$$

The constants F, G, H, L, M and N in these equations describe the current state of anisotropy and may therefore be functions of stress and plastic deformation. The theory is more readily applied however for constants that are independent as have been observed (18 - 20) in sheet metals. For this case the theory assumes permanent initial anisotropy and a hardening function similar to that of Fig. 2A for an isotropic material ( $F = G = H = L = M = N = 1$ )

## 5. MULTIAXIAL CREEP FOR AN ANISOTROPIC MATERIAL

Equations (56) may be applied to creep in the usual way (Section 2) to yield principal secondary creep rates for an anisotropic material as

$$\begin{aligned} \dot{\epsilon}_1 &= \frac{\dot{\bar{\epsilon}}_a}{2\bar{\sigma}_a} [F(\sigma_1 - \sigma_2) - H(\sigma_3 - \sigma_1)] \\ \dot{\epsilon}_2 &= \frac{\dot{\bar{\epsilon}}_a}{2\bar{\sigma}_a} [G(\sigma_2 - \sigma_3) - F(\sigma_1 - \sigma_2)] \\ \dot{\epsilon}_3 &= \frac{\dot{\bar{\epsilon}}_a}{2\bar{\sigma}_a} [H(\sigma_3 - \sigma_1) - G(\sigma_2 - \sigma_3)] \end{aligned} \quad (59)$$

This form of equation is similar to that employed by Johnson (3) in describing his anisotropic redistribution of creep rates that was observed to occur for higher stresses and temperatures.

### 5.1 Relationship between $\bar{\sigma}_a$ and $\dot{\epsilon}_a$

The correlation of the many tests performed by Johnson was always made on the basis of isotropic definitions of equivalent stress and strain. (Actually Johnson used octrahedral shear stress and strain for this correlation but these are made equal to  $\bar{\sigma}$  and  $\dot{\epsilon}$  in multiplying by  $\sqrt{2}/3$  and  $\sqrt{2}$  respectively). Since the function  $F(J_2')$  of equation (41), used to represent this correlation, was of the complex form,

$$F(J_2') = A_1(J_2')^{p_1} + A_2(J_2')^{p_2} = A_1\left(\frac{\bar{\sigma}^2}{3}\right)^{p_1} + A_2\left(\frac{\bar{\sigma}^2}{3}\right)^{p_2}$$

it would be interesting to know if the function representing the anisotropic correlation for equations (57) and (58) would be of the same simple power function form as for isotropic behaviour. That is,

$$\dot{\epsilon}_a = A \bar{\sigma}_a^n \quad (60)$$

If this were the case then this would imply that the constants A and n in this equation should not depart from those in the isotropic equation (34) since equation (60) reduces to equation (34) for isotropic behaviour ( $F = G = H = 1$ ). The one function would then suffice to correlate all tests for both isotropic and anisotropic creep behaviour. The problem however lies in knowing the point in the deformation at which anisotropy begins through the introduction of these constants and the form they might take for different stress systems.

Equation (59) is probably more usefully employed in a situation where the constants are independent of the creep process. Thus like the use of equation (56) for a material whose initial anisotropy is not affected by subsequent plastic strain (paragraph 4.4) then the use of equation (59) is implied here to a material whose initial anisotropy is not changed by subsequent creep deformation. Although there has been little experimental work done on the effects of anisotropy in the study of creep the validity of this statement remains uncertain. However the tensile and torsional creep tests of Sneddon (21) on the primary creep of anisotropic RR58 at 180°C do add some support to this.

## APPENDIX

## References

- (1) HILL, R. 'Mathematical Theory of Plasticity' 1950. (Oxford University Press, London).
- (2) FORD, H. and ALEXANDER, J. M. 'Advanced Mechanics of Materials' 1963. (Longmans, London).
- (3) JOHNSON, A. E. 'Creep under complex stress systems at elevated temperatures'. Proc. Instn. Mech. Engrs. 1951, 164(4), 432-447.
- (4) BAILEY, R. W. 'The utilization of creep test data in engineering design'. Proc. Instn. Mech. Engrs. 1935, 131(11), 131-349.
- (5) DAVIS, E. A. 'The Bailey flow rule and its associated yield surface'. J. Appl. Mech. 1961, 28E, 310.
- (6) WAHL, A. M. 'Application of the modified Bailey equations under biaxial tension stress'. Proc. 4th U.S. Nat. Conf. Appl. Mech., A.S.M.E. 1962, Berkeley, New York.
- (7) BERMAN, I. and PAI, D. H. 'A theory of anisotropic steady-state creep'. Int. J. Mech. Sci. 1966, 8, 341-352.
- (8) PUGH, H. Ll. D., MAIR, W. M. and RAPIER, A. C. 'The plastic yielding of metals under combined stress'. NEL Rpt. No. 43, 1962, East Kilbride, Glasgow.
- (9) MAIR, W. M. and PUGH, H. Ll. D. 'The effect of torsional prestrain on the yield surface in copper'. NEL Rpt. No. 90, 1963, East Kilbride, Glasgow.
- (10) IVEY, H. J. 'Plastic stress-strain relations and yield surfaces for aluminium alloys'. J. Mech. Engng. Sci. 1961, 3(1), 15-31.
- (11) NAGHDI, P. M. ESSENBURG, F. and KOFF, W. 'An experimental study of initial and subsequent yield surfaces in plasticity'. J. Appl. Mech. 1958, 25(2), 201-209.
- (12) MAIR, W. M. 'The yield surface in metals'. NEL Rpt. No. 215, 1966, East Kilbride, Glasgow.

- (13) PRAGER, W. 'A new method of analysing stresses and strains in work hardening plastic solids'. J. Appl. Mech. 1956, 23(4), 493-496.
- (14) HODGE, P. G. "Discussion on Prager's paper 'A new method of analysing stresses and strains in work hardening plastic solids'." J. Appl. Mech. 1957, 24(3), 482-483.
- (15) WILLIAMS, J. F. and SVENSSON, N. L. 'Effect of tensile prestrain on the yield locus of 1100-F aluminium'. J. Strain Analysis 1970, 5(2), 128-139.
- (16) HILL, R. 'A theory of yielding and plastic flow of anisotropic metals'. Proc. Roy. Soc. Lond. 1948, 193A, 281.
- (17) HU, L. W. 'Studies on plastic flow of anisotropic metals'. Trans. A.S.M.E. 1955, 55-A-79, 1-7.
- (18) KLINGLER, L. J. and SACHS, G. 'Plastic flow characteristics of aluminium alloy plate'. J. Aeronaut. Sci. 1948, 15, 499-604.
- (19) HAZLETT, T. H., ROBINSON, A. T. and DORN, J. E. 'An evaluation of a theory of plastic flow in anisotropic sheet metals'. Trans. ASM 1950, 42, 1326-1356.
- (20) MEHAN, R. L. 'Effect of combined stress on yield and fracture behaviour of zircaloy-2'. Trans ASM, J. Basic Eng. 1961, 499-512.
- (21) SNEDDON, J. D. 'Primary creep of anisotropic RR58 Aluminium alloy at 180°C. NEL Rpt. No. 531, 1972. East Kilbride, Glasgow.

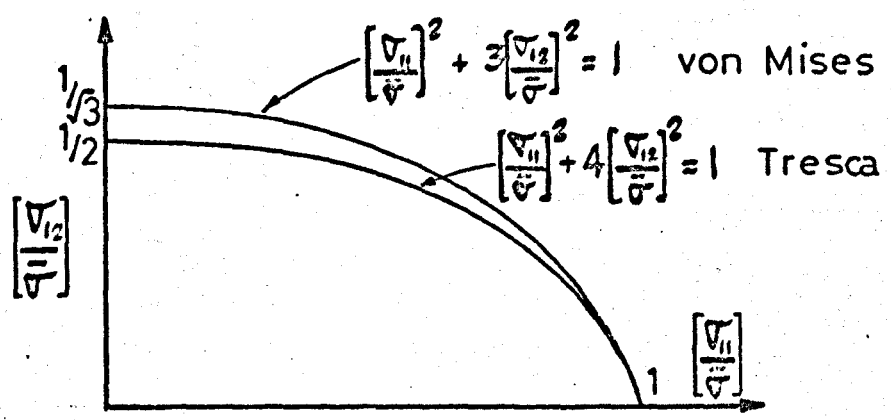
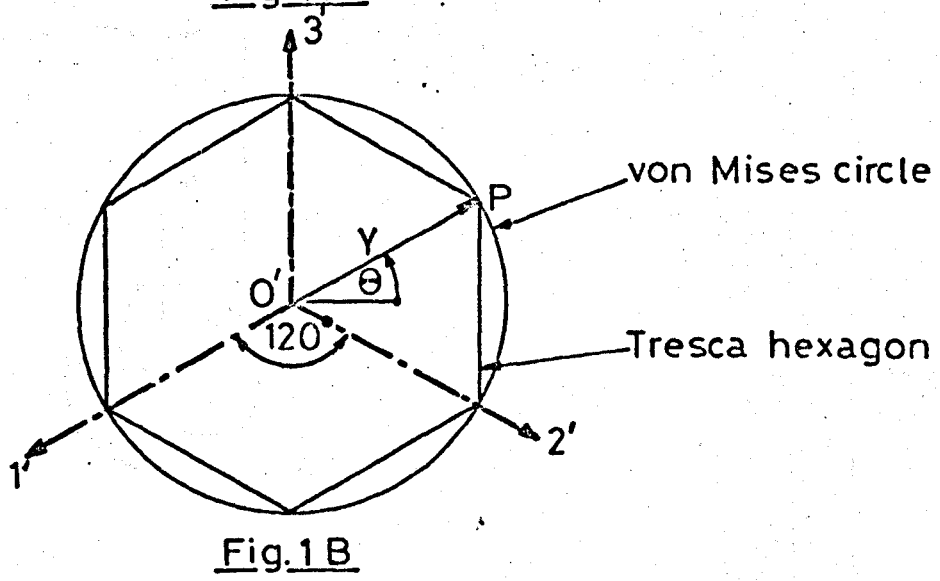
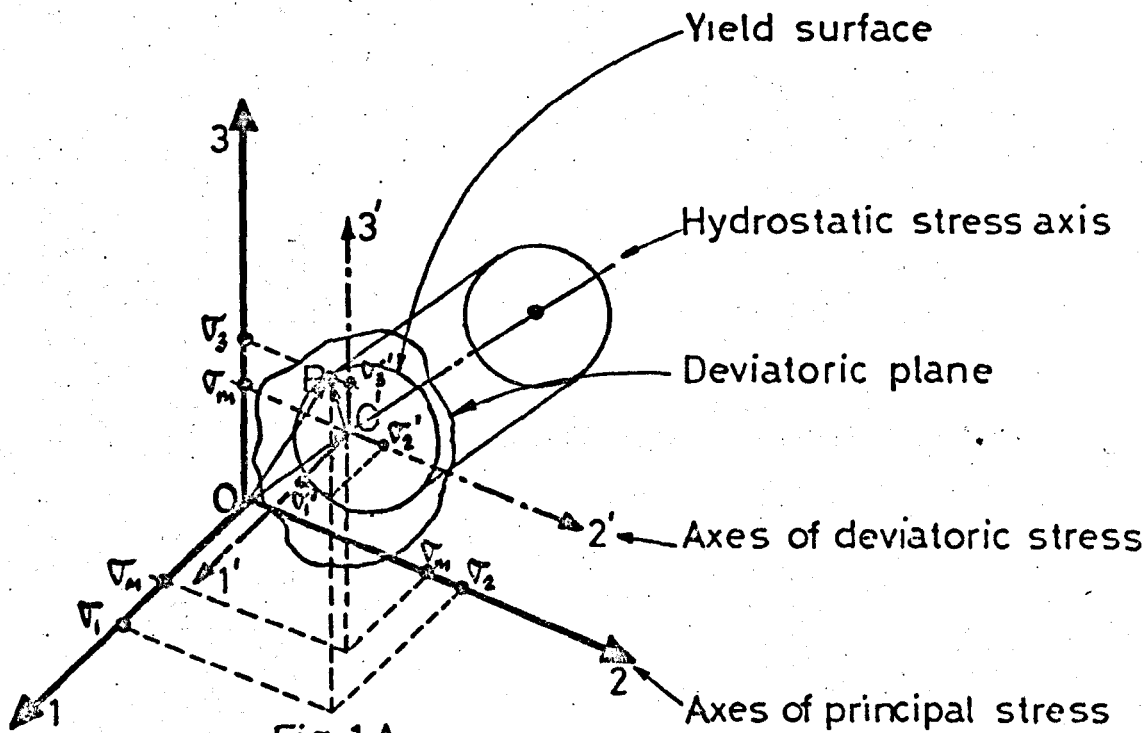


Fig. 1 Yield Loci

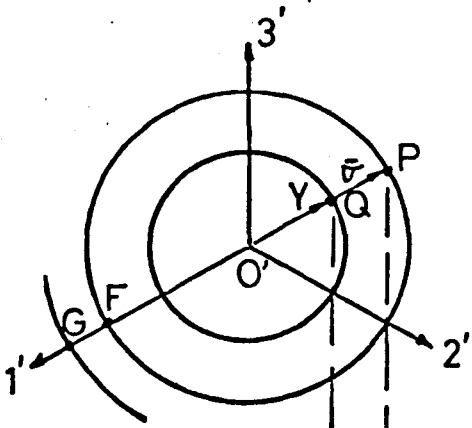


Fig.2A

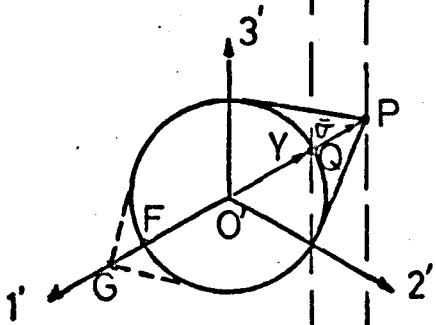
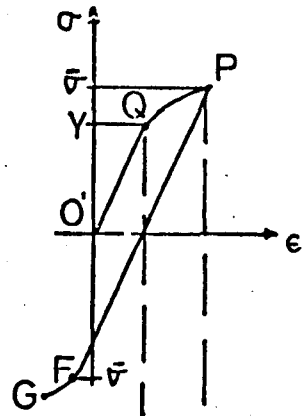


Fig.2B

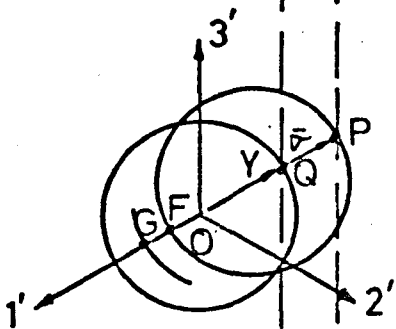
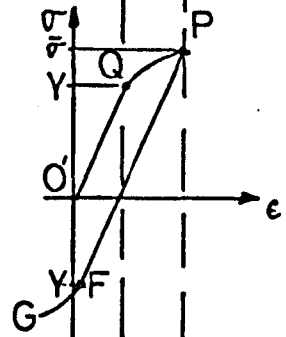


Fig.2C

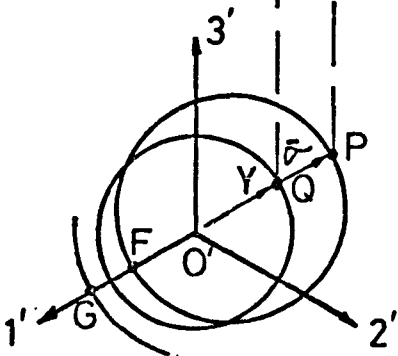
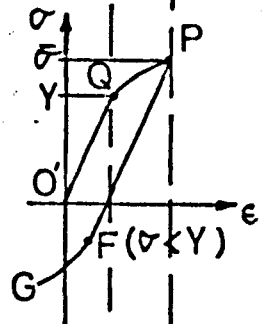


Fig.2D

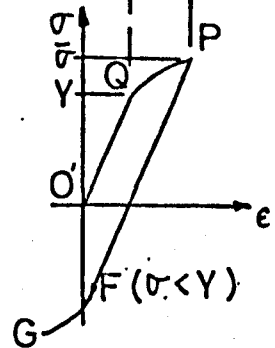


Fig.2 Hardening Models

# APPENDIX II

A P P E N D I X II

CALIBRATIONS

1. TENSILE CELLS - LEVER MAGNIFICATION

The two load cells were first calibrated on a Denison 12500 lbf machine (Fig. 1).<sup>\*</sup> The slopes of these lines gave the tensile force per unit of bridge output. By repeating the calibration for the two cells in parallel in the tension-torsion machine (Fig. 2), and comparing with Fig. 1, the ratio of each cell force per unit of applied force was established. The tensile magnification was then the sum of these two as follows:

$$\begin{aligned}
\text{Tensile Magnification} &= \text{Mag. for Cell 1} + \text{Mag. for Cell 2} \\
&= \frac{11.72}{4.747} + \frac{12.05}{4.903} \quad \begin{matrix} (N/0.01\Delta V) \\ (N/0.01\Delta V) \end{matrix} \\
&= 2.469 + 2.458 \\
&= 4.927 \quad N/N
\end{aligned}$$

The effect of various fixed torsional loads on this magnification figure was further examined. The addition of the beam for this purpose increased the tensile dead weight which was seen as a shift in the two curves in Fig. 2 but the magnification remained unaltered since the calibrations for each cell were parallel. The same pair of lines in Fig. 2 represented the calibration for all the chosen torsional loads. Extrapolation of these showed the tensile dead weight for the beam in position to be equivalent to a tensile force on the specimen of 350 N or a tensile stress of 2.76 N/mm<sup>2</sup>.

2. TORSION CELLS - PULLEY MAGNIFICATION

The two solid Duralumin torque cells were calibrated initially on an Avery 15000 kg cm torsion machine (Fig. 3). A further calibration for each cell assembled in series with a test specimen (Fig. 4) enabled the torsion magnification to be obtained as follows:

\* Figures are given at the end of this Appendix.

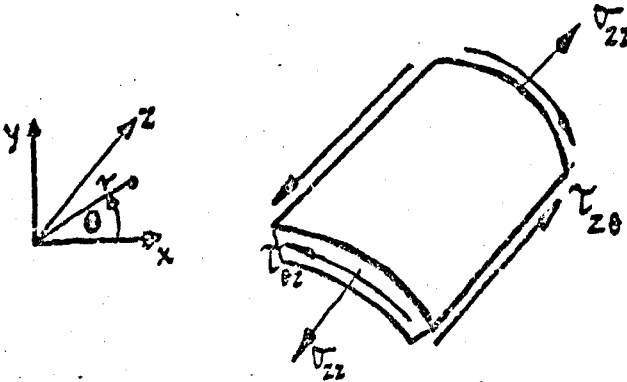
$$\begin{aligned} \text{Torsion magnification (Cell 1)} &= \frac{254.2}{4079} \frac{(\text{Nm}/0.01\Delta v)}{(\text{N}/0.01\Delta v)} \\ &= 0.0623 \text{ Nm/N} \end{aligned}$$

$$\begin{aligned} \text{Torsion magnification (Cell 2)} &= \frac{247.6}{3987.2} \frac{(\text{Nm}/0.01\Delta v)}{(\text{N}/0.01\Delta v)} \\ &= 0.0621 \text{ Nm/N} \end{aligned}$$

This showed that an equal and opposite torque was applied to the specimen. The effect of various fixed tensile loads was seen from Fig. 4 to have no effect on this calibration and extrapolation here showed the dead weight of beam, pulleys and cables to be equivalent to a specimen torque of 2.55 Nm or a shear stress of 3 N/mm<sup>2</sup>.

Both the tensile and torsional magnifications were later checked by tensile and torsional creep tests in the main test programme. Agreement was seen to be within 1% of the calibrated values.

### 3. STRESS RATIO FOR COMBINED TENSION AND TORSION



Element of cylinder in combined tension-torsion

The beam was calibrated for its eighth and third length positions. At each position weights were increasingly added and the outputs from the tension and torsion cells recorded. These were then used to obtain the ratio of the shear and tensile stresses for that position as follows:

The stress ratio  $\lambda = \frac{\tau_{\theta z}}{\sigma_{zz}}$  can be written in terms of a specimen torque  $T$ , (Nm) and tensile force  $W$ , (N) as:

$$\lambda = \frac{T r_m \times A}{J W} \quad (1)$$

and substituting for the specimen polar moment of area  $J$ , the cross-sectional area  $A$ , and the mean radius  $r_m$  with dimensions  $d_1 = 28.4$  mm o.d. and  $d_2 = 25.4$  mm i.d. then,

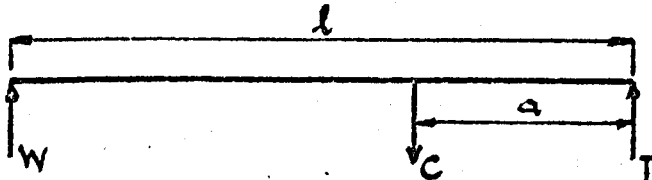
$$\lambda = 74.11 \frac{T}{W} \quad (2)$$

For a combined load the outputs from the tension cells were designated  $1_1$  and  $1_2$  and the output from one torsion cell (cell 1) was designated  $2_1$ . Then equation (2) may be written in terms of the calibrations in Figs. 1 and 3 as:

$$\begin{aligned} \lambda &= \frac{74.11 (2_1 \times 254.2)}{10^3 [(1_1 \times 11.72) + (1_2 \times 12.05)]} \\ &= \frac{18.84 \times (2_1 / 1_1)}{11.72 + 12.05 (1_2 / 1_1)} \quad (3) \end{aligned}$$

For each beam position the bridge outputs were plotted to give slopes of  $(2_1 / 1_1)$  and  $(1_2 / 1_1)$ . These were then substituted in equation (3) to give the stress ratio  $\lambda$  for that position. For all beam positions constancy of  $\lambda$  for each position was observed through the linearity of these plots. The  $\lambda$  values obtained are shown in the table of Fig. 5.

A check on the  $\lambda$  values obtained in this way may be made by the following theoretical solution: Here a combined force  $C$  (N) is applied at a point  $a$  (m) from the torsion support. Let the beam length be  $l$  (m) and the tensile and torsional reactions be  $W$  and  $T$  respectively:



Then by moments:  $W = Ca/l$   
 $T = C(1 - a/l)$  (4)

and from the tension and torsion magnifications (paragraphs 1 and 2)

$$\begin{aligned} W_1 &= 4.927W = 4.927 Ca/l \\ T_1 &= 0.0622T = 0.0622 C(1-a/l) \end{aligned} \quad (5)$$

Then substituting for  $W_1$  and  $T_1$  from (5) into equation (2),

$$\begin{aligned} \lambda &= \frac{74.11 \times 0.0622 C(1-a/l)}{4927 Ca/l} \\ &= 0.936 \left[ \left( \frac{l}{a} \right) - 1 \right] \end{aligned} \quad (6)$$

Equation (6) was used as a theoretical solution for the stress ratio  $\lambda$  in terms of any beam position ( $a/l$ ). Agreement between this solution and the 1/8 and 1/3 calibrated points is seen in Fig. 5.

A further check on the tensile beam reaction  $W$  for an applied combined load  $C$  was made from equation (4) for which  $W/C = a/l$ . The  $W/C$  ratio can be written in terms of the calibration for cell 1 in Fig. 2 as

$$W/C = \frac{4.747 \times l_1}{C} \quad (7)$$

For each position on the beam the slope of a  $l_1$  vs  $C$  plot was used in equation (7) to yield the  $W/C$  ratio. These are shown plotted in Fig. 5 about a theoretical  $45^\circ$  line. These points actually represent the true  $a/l$  beam positions corresponding to the calibrated stress ratios.

The theoretical check, equation (6), has been shown here to confirm it for elastic deformation. The modification made to equation (3) during loading in a creep test is to account for the plastic deformation following the application of a load. Then from equilibrium,

$$\begin{aligned} \delta T_1 &= 2\pi r^2 \delta r \tau_{\theta z} \\ \therefore T_1 &= 2\pi \tau_{\theta z} \int_{d_2/2}^{d_1/2} r^2 dr \end{aligned} \quad (8)$$

from which the mean shear stress,

$$\tau_{\theta z} = \frac{12 T_1}{\pi (d_1^3 - d_2^3)} \quad (9)$$

and as before,

$$\sigma_{zz} = \frac{W_1}{A} = \frac{4W_1}{\pi(d_1^2 - d_2^2)} \quad (10)$$

then,

$$\lambda = \frac{\tau_{\theta z}}{\sigma_{zz}} = \frac{3T_1(a_1 + a_2)}{W_1(d_1^2 + d_1a_2 + d_2^2)} = 74.27 \frac{T_1}{W_1} \quad (11)$$

which, in terms of the calibrations Figs. 1 and 3, can be written as,

$$\lambda = \frac{18.88 \times (2_1/1_1)}{11.72 + 12.05(1_2/1_1)} \quad (12)$$

If the stresses were to be separated in this equation then the axial stress was calculated from the bridge outputs  $l_1$  and  $l_2$  and the calibrations of Fig. 1 as follows:

For a combined load  $C$  applied at any beam position,

$$\frac{W_1}{C} = \left[ 11.72 \left( \frac{l_1}{C} \right) + 12.05 \left( \frac{l_2}{C} \right) \right] 10^3$$

where  $(l_1/C)$  and  $(l_2/C)$  were the slopes of a  $l_1$  v  $C$  and  $l_2$  v  $C$  loading plot.

Then substitution in equation (10) yields,

$$\begin{aligned} \sigma_{zz} &= \frac{4C \left[ 11.72 \left( \frac{l_1}{C} \right) + 12.05 \left( \frac{l_2}{C} \right) \right] 10^3}{\pi(d_1^2 - d_2^2)} \\ &= \frac{C}{12676} \left[ 11.72 \left( \frac{l_1}{C} \right) + 12.05 \left( \frac{l_2}{C} \right) \right] 10^3 \end{aligned} \quad (13)$$

It is important to make some assessment of how  $\lambda$  and  $\sigma_{zz}$  of equations (12) and (13) change with the development of plastic strain. A true stress ratio ( $\lambda'$ ) is based on current specimen dimensions and since, during loading, these are changing then so is the stress ratio. An estimation of the stress ratio based on the current value of axial strain ( $e_{zz}$ ) may be made by defining  $\lambda'$  as the ratio of the true shear and axial stresses. Thus

$$\lambda' = \frac{\tau'_{\theta z}}{\sigma'_{zz}} \quad (14)$$

where the true shear stress ( $\tau'_{\theta z}$ ) is obtainable from equilibrium conditions. In terms of the current specimen diameters  $d'_1$  and  $d'_2$  equation (8) may then be written as

$$T_1 = 2\pi\tau'_{\theta z} \int_{d'_{1/2}}^{d'_{2/2}} r^2 dr$$

from which

$$\tau'_{\theta z} = \frac{12T_1}{\pi(d_1^3 - d_2^3)} \quad (15)$$

The current diameters in this equation can be written in terms of the original diameters by making the usual assumption of constancy of volume during plastic deformation. Then for a current specimen area ( $A'$ ) and gauge length ( $l'$ ) this is written as

$$\begin{aligned} A'l' &= Al \\ \text{or } d_1'^2 l' &= d_1^2 l \end{aligned} \quad (16)$$

$$\text{from which } \left(\frac{d'}{d}\right)^2 = \frac{l}{l'} \quad (17)$$

If  $z$  is the axial extension on an original length  $l$  then the engineer's axial strain is

$$e_{zz} = \frac{z}{l}$$

and

$$\frac{l}{l'} = \frac{l}{l+z} = \frac{1}{1+e_{zz}} \quad (18)$$

which from equation (17) gives

$$\left(\frac{d'}{d}\right)^2 = \frac{1}{1+e_{zz}}$$

Substitution in equation (15) yields

$$\tau'_{\theta z} = \frac{12T_1 (1+e_{zz})^{3/2}}{\pi(d_1^3 - d_2^3)}$$

which in terms of the nominal shear stress of equation (9) is

$$\tau'_{\theta z} = \tau_{\theta z} (1+e_{zz})^{3/2} \quad (19)$$

The true tensile stress is given by

$$\sigma'_{22} = \frac{W_1}{A'}$$

which from equation (16) may be written as

$$\sigma'_{22} = \frac{W_1 l'}{A l}$$

Writing  $W_1/A$  as the nominal stress  $\sigma_{22}$  and substituting from equation (18) we have that

$$\sigma'_{22} = \sigma_{22} (1 + e_{22}) \quad (20)$$

Substitution of equations (19) and (20) in equation (14) for the current stress ratio gives

$$\lambda' = \lambda (1 + e_{22})^{1/2}$$

or

$$\frac{\lambda'}{\lambda} = (1 + e_{22})^{1/2} \quad (21)$$

From equation (21) it can be seen that  $\lambda$  varies by  $\frac{1}{2}\%$  for each 1% of longitudinal strain up to 10% for all values of the ratio and thereafter the variation is smaller. Thus the stress ratio values obtained for plastic loading are not expected to be the same as the calibrated elastic values. Although equation (21) predicts greater stress ratios for a plastically deforming specimen, the effect of changing magnifications in the rig itself have not been considered. Generally, this has the effect of lowering both the tensile and torsional loads on the specimen. Since the degree to which each is lowered depends upon the position on the beam at which the combined load is placed, the overall effect on the stress ratio is difficult to estimate. The stress ratio values quoted in this text were therefore those calculated from the bridge outputs obtained at the time of testing. Equations (12) and (13) were applied to the bridge outputs for this purpose from which the overall accuracy of stress measurement was probably better than  $\pm 1\%$ .

#### 4. AXIALITY OF LOADING

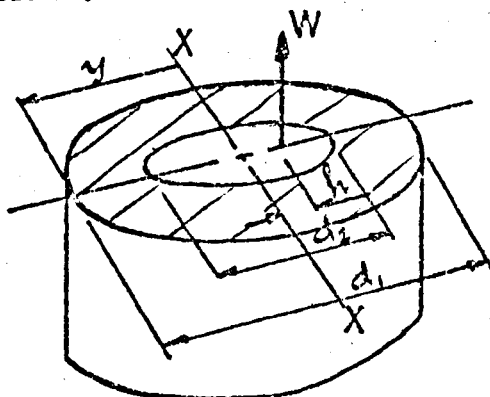
Unwanted bending could occur if either the tensile load or the applied torque were not axial. To examine this a Duralumin cylinder was longitudinally strain gauged at four 90° positions around the tube and loaded incrementally to 75% of its yield load for each of the following:

- (a) pure tension
- (b) pure torsion
- (c) combined loading

Axiality of tensile loading would mean that the load vs strain gauge reading plot for each gauge should be parallel. In fact, it was found to be necessary to adjust the position of the table (component (22) in Fig. 2.2) slightly to observe the best set of parallel lines. The variation in their slopes was then never greater than  $\pm 1.5\%$  of the mean value and even less for the combined loading calibrations of Section (3).

Axiality of torsional loading would mean that the normal strain for all longitudinal directions is zero. Thus for this to be so there should be no output from the four longitudinal gauges during a pure torsion calibration. Since this was in fact always observed it may be concluded that the torque loading system was axial.

The effect of an eccentricity  $h$  in the line of load application and its effect on the axial stress may be examined from the following theoretical solution.



$$\frac{\delta \sigma_{22}}{\sigma_{22}} \% = \pm 100 \left( \frac{W h y}{I_x} \right) / \left( \frac{W}{A} \right) = \pm \frac{100 h y A}{I_x}$$

$$= \frac{800 h d_1}{(d_1^2 + d_2^2)} \% = 15.65 h \% \quad (22)$$

The variation was actually  $\pm 1.5\%$  which means that the eccentricity was of the order of 0.1 mm.

## 5. SPECIMEN GEOMETRY

Holloway\* made an assessment of the effect of variations in wall thickness, ovality and straightness on axial, circumferential and shear stress for his OFHC cylinders and concluded that the effect of geometrical errors were more serious than deviations from axial loading in this respect. The same conclusions are not drawn for the specimens of these tests however in following Holloway's assessment.

### 5.1 Wall Thickness Variation

Assuming a variation of  $\pm \delta t$  from the mean wall thickness  $t$  the variation in axial stress for a tensile load applied concentric with the outer diameter ( $d_1$ ) is,

$$\frac{\delta \sigma_{zz}}{\sigma_{zz}} \% = \pm \frac{800 k^2 \delta t}{d_1 (k^4 - 1)} \quad \text{where } k = \frac{d_1}{d_2}$$

$$= \pm 62.56 \delta t$$

and for the load applied concentric with the inner diameter ( $d_2$ ),

$$\frac{\delta \sigma_{zz}}{\sigma_{zz}} \% = \pm \frac{800 k^4 \delta t}{d_1 (k^4 - 1)} = \pm 78.21 \delta t$$

Taking  $\pm \delta t = \pm 0.005$  mm and  $t = 1.501$  mm from the wall thickness measurements recorded in paragraph 2.3.5 the variation in axial stress for the worst case of loading is seen to be not in excess of  $\pm 0.4\%$ .

The effect of this variation on the circumferential stress of pressure loading† is,

$$\frac{\delta \sigma_{\theta\theta}}{\sigma_{\theta\theta}} \% = \pm \frac{200 k \delta t}{(k+1)t} \approx \pm 0.35$$

and the shear stress of torsional loading,

$$\frac{\delta \tau_{\theta z}}{\tau_{\theta z}} \% = \pm 100 \frac{\delta t}{t} \approx \pm 0.33$$

\* Ph.D. Thesis 1972, University of London

† Not performed

## 5.2 Ovality

The effect of ovality is to cause a variation in the circumferential stress. If the deviation of either diameter is  $\pm \delta d$  on an average diameter of  $d$  then,

$$\frac{\delta \sigma_{\theta\theta}}{\sigma_{\theta\theta}} \% = \pm 100 \frac{\delta d}{d}$$

By far the greater variation occurred in the bore. Taking  $\pm \delta d = \pm 0.012$  mm and  $d = 25.404$  mm from the bore measurements recorded in paragraph 2.3.5 the variation in hoop stress is seen to be not in excess of 0.05%.

The through-thickness variation on the mean circumferential stress is,

$$\frac{\delta \sigma_{\theta\theta}}{\sigma_{\theta\theta}} \% = \pm 150 \frac{\delta d_i}{t}$$

is negligible here since the variation of the outer diameter was of insignificant amount. Such variations are only applicable to the circumferential stress of internal pressure and are therefore not applicable here.

## 5.3 Straightness Variation

The effect of variation in specimen straightness on the axial stress is assessed in a manner identical to that for non axiarity of loading. Thus equation (22) applies here where  $h$  in this case is the relative lateral displacement between the centre and ends of the test specimen. Since the method of specimen manufacture (Table 2.3) was devised to eliminate errors of this kind then any variation in axial stress due to a lack of straightness is thought to be slight only.

Whilst all these variations may be regarded as tolerable it should be noted that they diminish as the stresses increase. Lastly the worst variation is that caused by load eccentricity on the axial stress.

## 6. CHOICE OF GAUGE LENGTH

For an overall parallel length of 75 mm, 50 mm of it was chosen as the extensometer mounting length. Uniformity of strain over this length was checked from the outputs of in-line strain gauges affixed longitudinally and circumferentially to an axially loaded Duralumin cylinder. Elastic loading showed that the strains were uniform over this length. This is not however representative of the situation in an

aluminium test specimen when plastic strains and creep strains are the dominant components in the deformation. If the aluminium cylinder deforms in an isotropic manner (Appendix I) it means that the flow strengths of all directions are the same and that the strains at all points in those directions are the same (homogenous deformation). However the results reported in the main text shows deformation by combined tension-torsion to be anisotropic. The anisotropy of deformation was not severe in cylinders of annealed aluminium (Chapter 4) where the grain size was approximately uniform. The anisotropy of deformation in cylinders of extruded (Chapter 5) and prestrained aluminium (Chapter 6) was severe. It was associated with a non uniform preferred grain structure and the Bauschinger and cross-effects of a prior strain history. To eliminate the effect of variation in gauge length strain during anisotropic deformation axial ( $\epsilon_{zz}$ ) and shear ( $\delta_{\theta z}$ ) strain components were always calculated from displacements measured on the 50 mm gauge length.

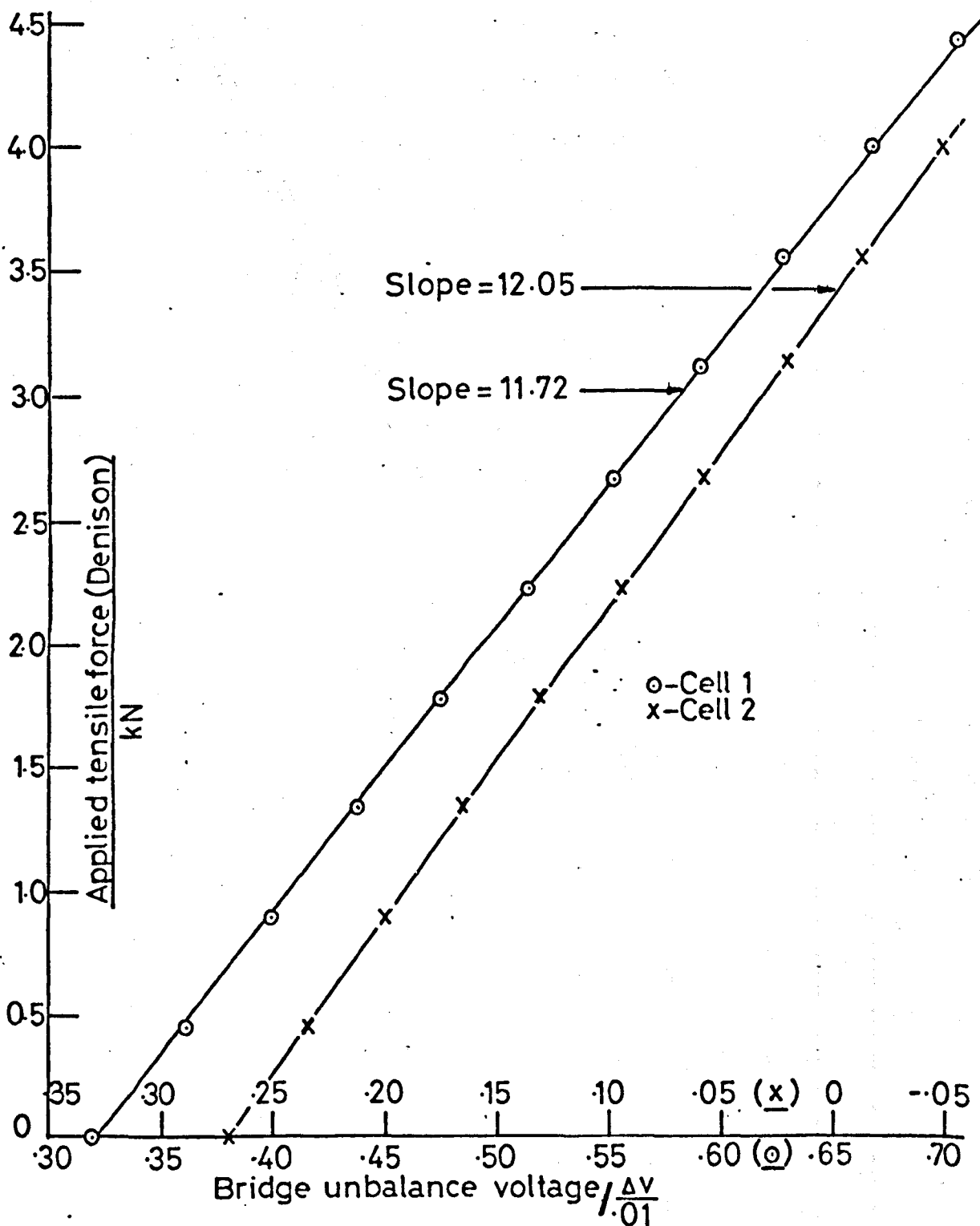


Fig. 1 Tension Cell Calibration (Denison)

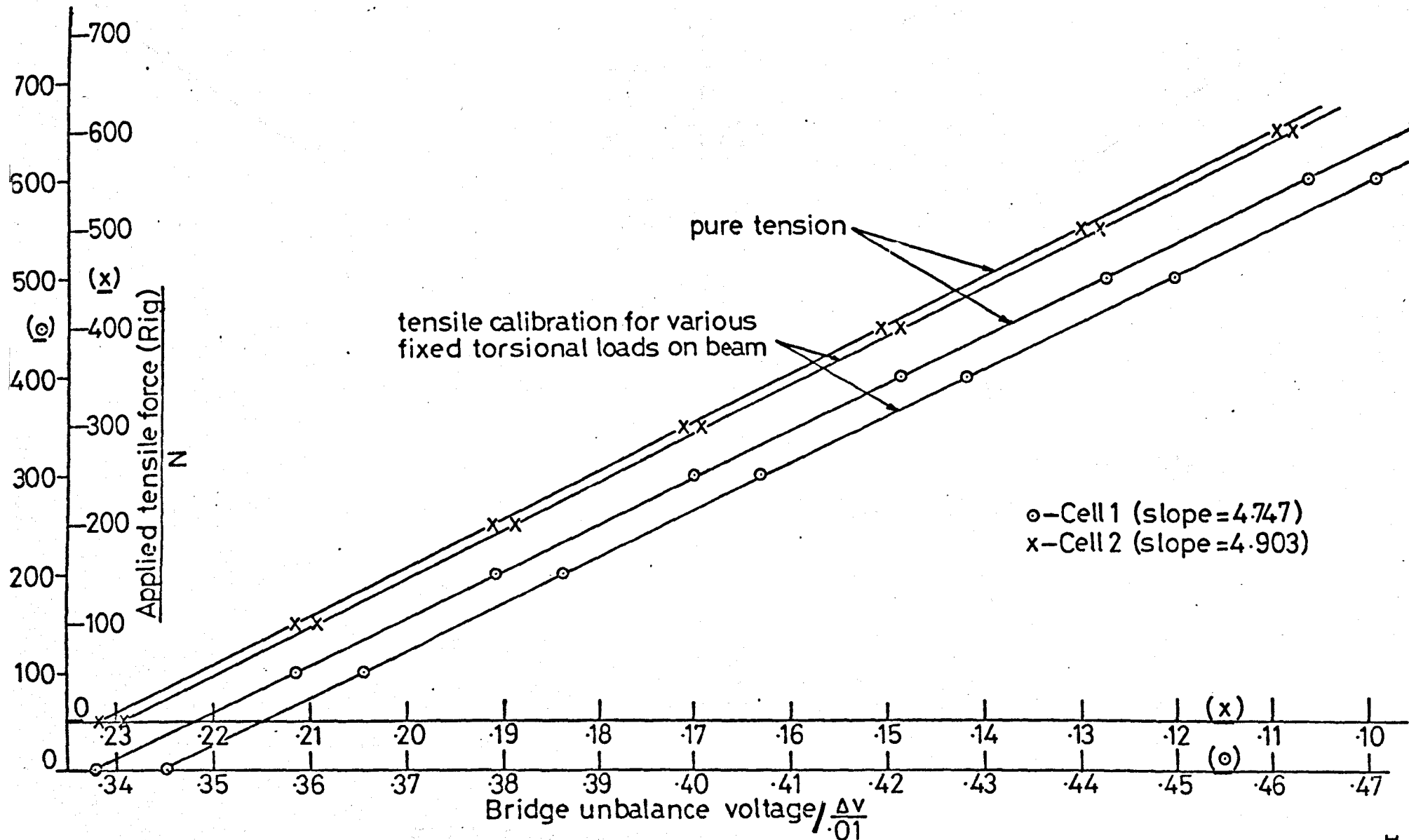


Fig.2 Tension Cell Calibration (Rig)

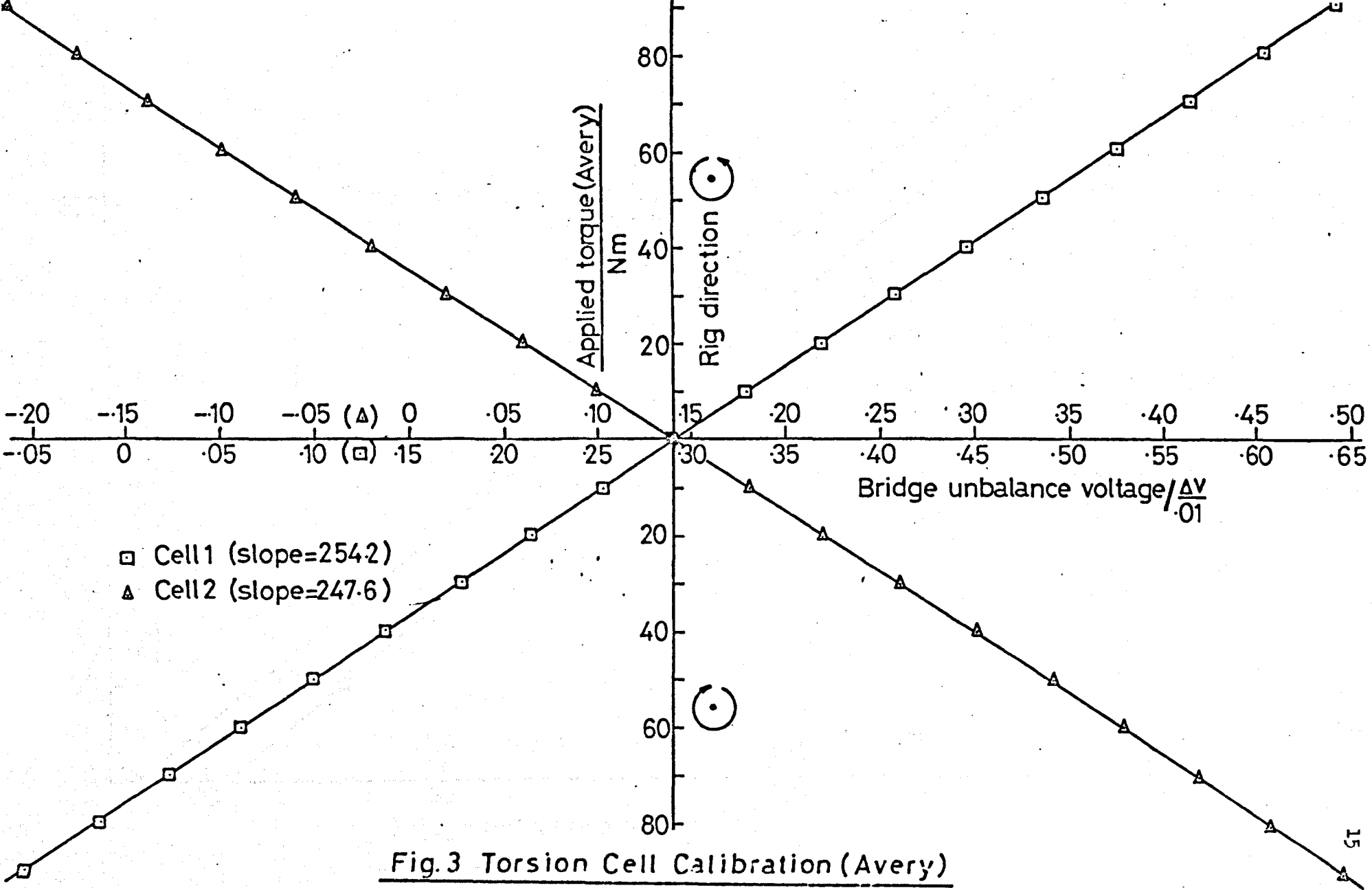


Fig.3 Torsion Cell Calibration (Avery)

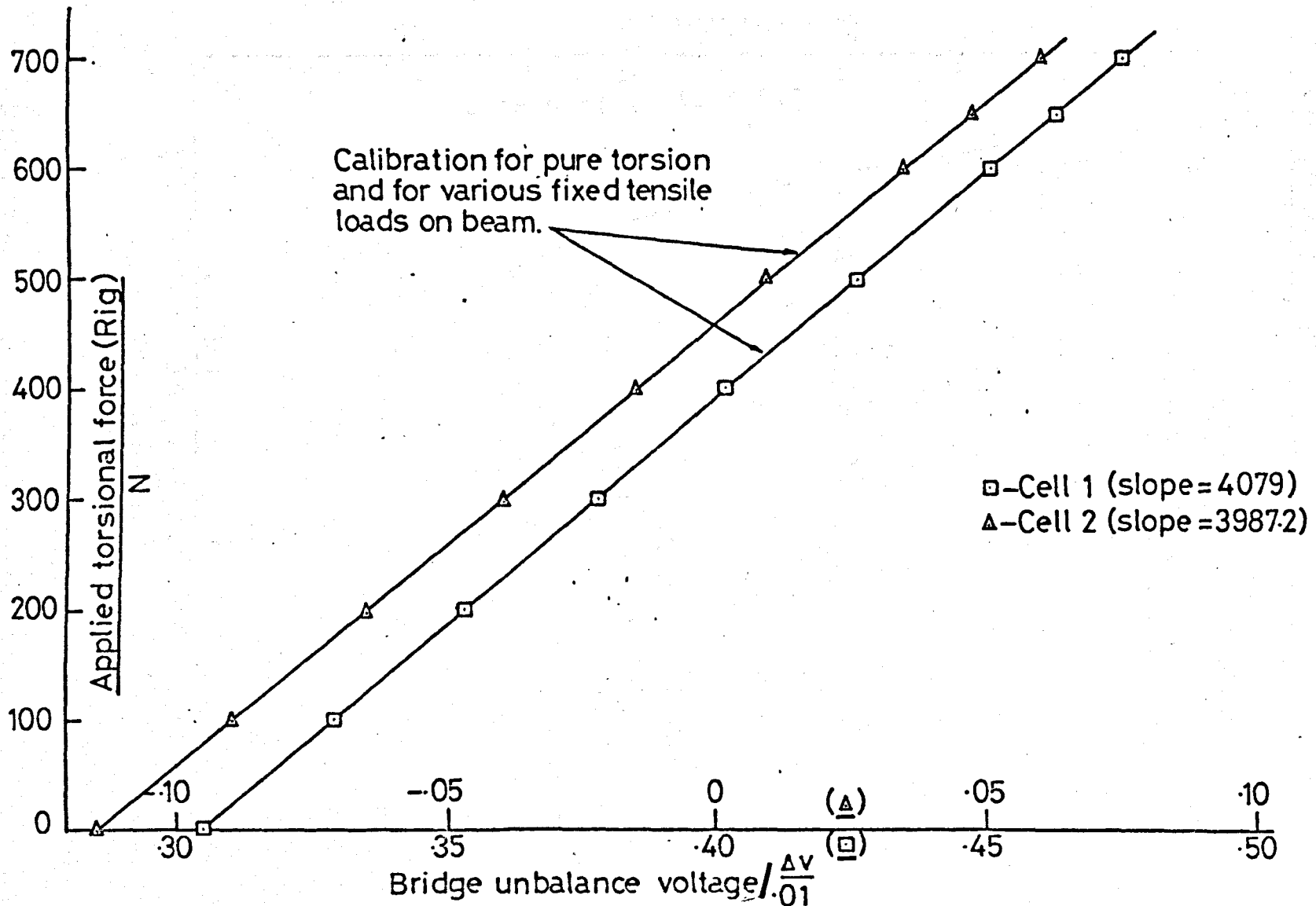


Fig.4 Torsion Cell Calibration (Rig)

$a/l$	1	7/8	3/4	2/3	5/8	1/2	3/8	1/3	1/4	1/8	0
$\lambda$	0	.143	.316	.469	.578	.651	.716	.773	.823	6.979	$\infty$
$W/C$	1.0	.855	.746	.658	.586	.523	.470	.427	.392	.367	0

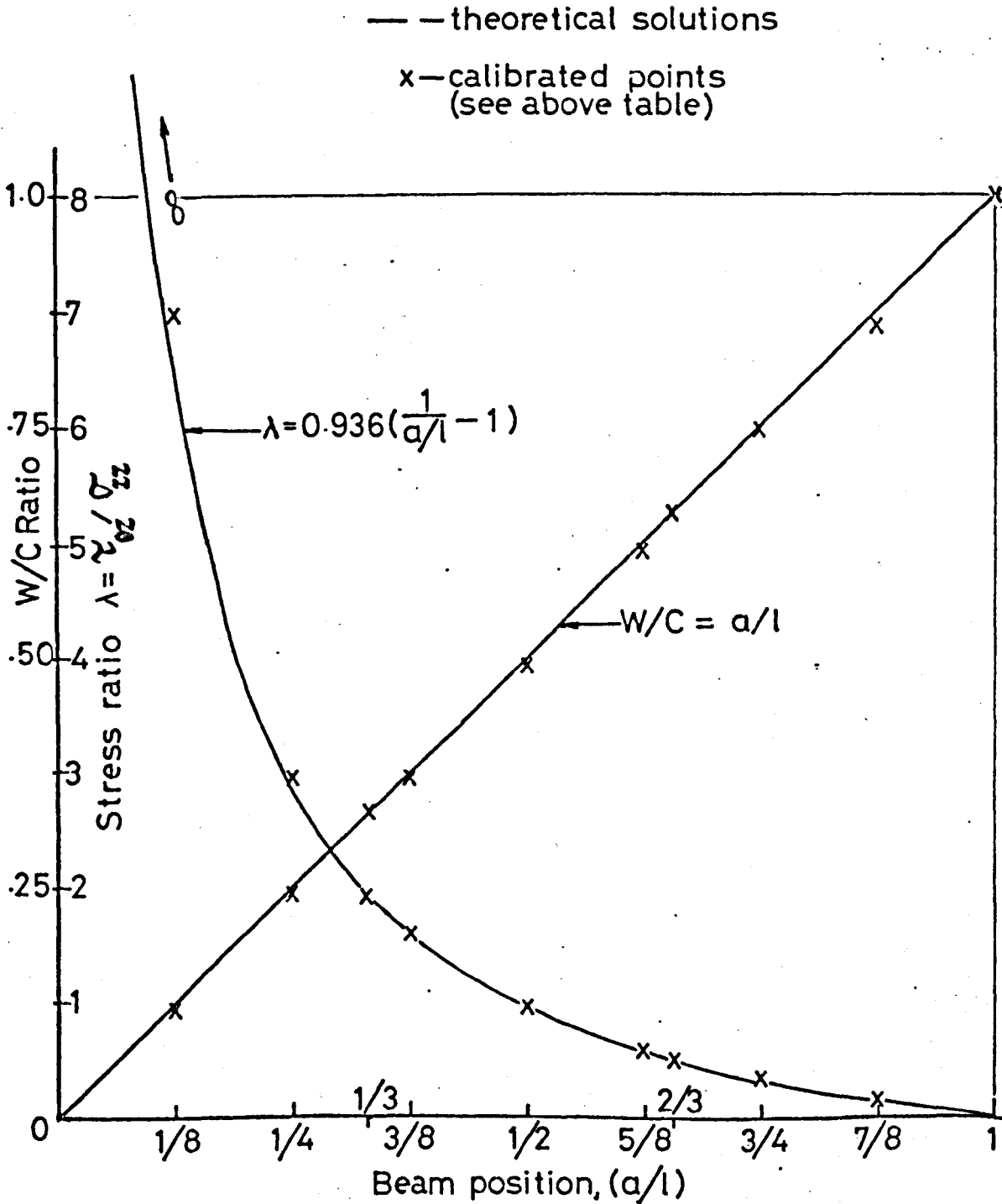


Fig.5 Tension-Torsion Calibration

# APPENDIX III

## APPENDIX III

## CREEP AND PLASTIC FLOW OF ALUMINIUM DURING INCREMENTAL LOADING

by D. W. A. Rees

A paper presented at a research seminar held in the School of Mechanical, Aeronautical and Production Engineering, Kingston Polytechnic on 28th May 1975.

1. SUMMARY

The transient creep of a commercial grade of pure aluminium (B.S. 1476, E1A) has been studied for short-time incremental loading. These tests show that in the temperature range of  $0.3 T_m - 0.6 T_m$  the creep occurring between loads is adequately described by a simple parabolic law  $\epsilon = \epsilon_0 + at^m$  and in no case was logarithmic creep observed ( $\epsilon = \epsilon_0 + a \ln t$ ).

Test conditions were varied to examine the effect on the parabolic constants  $m$ ,  $a$  and  $\epsilon_0$ . In general the time exponent  $m$  was found to increase with test temperature and decrease with load increment and in only a few cases did Andrade's equation hold ( $m = \frac{1}{3}$ ). The constant  $a$ , is shown to be a complex function of stress level, stress increment and temperature of the form,  $S \exp(\Delta\sigma) \exp\left(\frac{Q}{T}\right) \sigma^p$  while  $\epsilon_0$  represents the instantaneous strain on loading. To eliminate the errors in  $a$  and  $m$  due to an incorrect selection of  $\epsilon_0$ , a derivative analysis was employed in the analysis of each test.

2. NOTATION

$A, n$	Constants in the tensile stress-strain law.
$a, b, k, l, p, q, r, s$	Constants in the transient creep equations.
$\epsilon$	Total strain.
$\epsilon^e, \dot{\epsilon}^e$	Creep strain, creep strain rate.
$\epsilon_0, \epsilon^e, \epsilon^p$	Instantaneous, elastic and plastic strains.
$\Delta H_c$	Apparent activation energy for creep.
$i, n$	Points on a transient creep curve.

m	Time exponent.
$\sigma$	Total applied nominal stress level.
$\Delta\sigma$	Applied stress increment.
R	Universal gas constant.
T	Absolute temperature.
$T_m$	Absolute melt temperature
t	Time

### 3. INTRODUCTION

In the study of the plastic deformation of metals engineering plasticity theory assumes that the total instantaneous strain resulting from the application of a load consists of an elastic and plastic component. Thus

$$\epsilon_0 = \epsilon^e + \epsilon^p \quad (1)$$

Whilst this may be acceptable for certain test conditions higher test stresses and temperatures with incremental loading give rise to additional transient creep strains. The instantaneous strain is followed by a time dependent strain which may well be of the same or higher order if intervals are allowed between successive increments. It is, therefore, necessary to add such strains to equation (1) for a full understanding of the deformation associated with this type of forward loading.

A great number of investigators have examined the nature of creep shortly after the application of a load. The early work of Andrade (1)\* showed this to be a transient phenomenon where the rate of creep decreased with time. This is generally displayed by many different materials for various conditions of temperature and stress. Considerable interest has therefore been shown in its mathematical representation and empirical expressions of one type or another are usually employed.

The number of these expressions from which to choose are numerous (2) although the choice ultimately depends upon the accuracy required. Generally the equations which can be made to describe transient creep most accurately are those requiring the greatest computational time.

The two most commonly used expressions are those describing logarithmic creep and those describing parabolic creep. Logarithmic creep is typical of exhaustion theories for transient creep and is often successfully employed to describe transient creep in steel at lower stresses and temperatures (3). In its simplest form it is represented

\* References are given in the Appendix.

by the equation:

$$\epsilon = \epsilon_0 + a \ln t \quad (2)$$

The objection here is that the equation predicts a creep strain of minus infinity for time  $t = 0$ , but this is easily corrected by either realistically defining  $\epsilon_0$  as the instantaneous loading strain after a very short time and therefore  $t > 0$  in this equation or modifying it to,

$$\epsilon = \epsilon_0 + a \ln(1+t) \quad (3)$$

Parabolic creep is represented by the equation:

$$\epsilon = \epsilon_0 + at^m \quad (4)$$

When  $m = \frac{1}{3}$  in this equation this leads to Andrade's law for transient creep:

$$\epsilon = \epsilon_0 + at^{1/3} \quad (5)$$

Crussard (4) shows that by allowing  $m$  to take any value equation (4) can be made to represent the transient creep of many materials over a wide range of temperature and stress. Furthermore, Conway (5) shows in a comparison of the degree of representation of the many transient expressions to an experimental curve that equation (4) was almost as good as a third degree polynomial in  $t^{1/3}$ . It should also be noted that the time exponent of the logarithmic equation (2) is a particular case of equation (4) for  $m = 0$  when they are expressed as creep rates. The disadvantage is that equation (4) with a varying  $m$  value does not have the metallurgical backing that logarithmic creep has (6) though it is generally identified as a work hardening theory.

Very much less work has been done on the nature of creep occurring between successive increments of load. Wyatt (7) in his studies on copper and fine grained aluminium showed this to be of a transient nature and employed equations (2) and (5) to describe it after having shown their applicability to a certain range of constant stress tests. Rogan and Alexander (8) showed that the logarithmic equation (2) could successfully be used for copper and mild steel at room-temperature for moderate stress levels but when higher stresses were reached in an incremental fashion logarithmic creep was no longer observed. They also showed the constant  $a$  in equation (2), when applicable, to be a function of the sinh of the applied stress at this temperature.

In this paper both the logarithmic equation (2) and the parabolic equation (4) are applied to the transient creep occurring between increments of load. Since the parabolic equation has been used to describe the transient creep of aluminium at constant stress (9) it is expected therefore that this equation would be more applicable over the range of test variables to be investigated here. The effect of temperature, stress level and stress increment on the constants  $m$ ,  $a$  and  $\epsilon_0$  are also examined.

#### 4. ANALYSIS

The procedure employed in fitting equations (2) and (3) to transient creep curves is to replot the curve on a logarithmic time scale. Logarithmic creep is then said to be observed if the result is linear. The constants  $a$  and  $\epsilon_0$  are then the slope and intercept respectively. Often equation (2) is preferred as a time can be selected to make the intercept on it compatible with the experimentally observed instantaneous strain.

The parabolic equation (4) presents some difficulties when applied to curves. Commonly an estimate is made of the instantaneous strain  $\epsilon_0$ . This is subtracted from the total strain  $\epsilon$  and the resulting creep strain  $\epsilon^c = \epsilon - \epsilon_0$  is plotted against time on logarithmic axes. Then the slope is  $m$  and the intercept is the logarithm of  $a$ . Analysed in this way Crussard (4) shows that a small change in the value of  $\epsilon_0$  causes a larger change in the value of  $m$ .

Clearly, in an investigation of this kind, where the dependence of  $m$  on various test variables is sought, this method should be avoided. Crussard shows that a derivative analysis eliminates this problem. This derivative method has been employed in the following way for analysis of transient creep curves in this paper:

Expressing equation (4) in terms of creep rates

$$\dot{\epsilon}^c = \frac{d\epsilon^c}{dt} = ma t^{m-1} \quad (6)$$

It will be seen that this equation does not contain  $\epsilon_0$ . Then taking logarithms:

$$\ln\left(\frac{d\epsilon^c}{dt}\right) = (m-1) \ln t + \ln(ma) \quad (7)$$

A plot of  $\ln\left(\frac{d\epsilon^c}{dt}\right)$  vs  $\ln t$  yields a line whose slope is  $(m-1)$  and whose intercept is  $\ln(ma)$ .

The creep rate  $\left(\frac{d\epsilon^c}{dt}\right)$  is numerically evaluated for a time  $t_i$  in a central difference form:

$$\frac{d\epsilon^c}{dt} = \frac{\epsilon_{i+1} - \epsilon_{i-1}}{t_{i+1} - t_{i-1}} \quad (8)$$

where  $i = 2, 3, \dots, n-1$ , and represents any point along the equally divided curve while  $n$  represents the last.

Hence equation (7) becomes:

$$\ln\left(\frac{\epsilon_{i+1} - \epsilon_{i-1}}{t_{i+1} - t_{i-1}}\right) = (m-1) \ln t_i + \ln(ma) \quad (9)$$

This equation was solved for  $a$  and  $m$  using a least squares fit on input data  $(\epsilon_i, t_i)$ . The constant  $a$  was further checked as the slope of a  $\epsilon_i$  v  $t_i^m$  plot in equation (4).

## 5. EXPERIMENTAL

### 5.1 Material and Specimens

A commercial grade of pure aluminium BS.1476 EIA was supplied in the form of an extruded bar 44.5 mm diameter. The composition was: Mg < 0.005, Cu < 0.005, Si < 0.04; Fe = 0.04, Mn < 0.01, Zn = 0.02, Ni < 0.015, Ti < 0.015% and Al (the balance). Specimens were machined from this in the longitudinal and oblique directions in the form of blanks initially. These were then annealed to give an average grain size of 0.23 mm and finally light finished machined to a B.S.3500 size (5.64 mm dia.). At the extremes of the 28 mm gauge length two 0.9 mm ridges were machined to allow an extensometer to be mounted. Consistency of specimen manufacture was obtained by using an identical machining procedure with a copy lathe and template.

### 5.2 Apparatus

All tests were carried out on a standard type tensile creep machine with a three zone furnace and controller. Displacements were measured at room temperature by attaching two  $\pm 2.5$  mm inductance

transducers in parallel with and either side of the specimen gauge length. The attachment was made by two rings each making three-point contact with a gauge length ridge. To take up the changes in diameter of the ridge under load and to ensure good contact between ring and ridge at all times a portion of each ring was made as a sprung loaded insert. At higher temperature testing the same arrangement was used but with a dogleg between each ring and transducer. This allowed each transducer to be mounted in parallel with and either side of the lower pull rod and sited well clear of the furnace bottom.

In measuring displacements the output from each transducer was averaged before driving a 0.3s response time potentiometric recorder. This enabled a continuous displacement-time record for the intervals between loads and a matched transducer trimming arrangement allowed each record to start from the one datum.

### 5.3 Test Temperatures

Experiments were carried out at test temperatures of 21, 100, 200 and 300°C. In terms of the homologous temperature  $T/T_m$ , these are 0.315, 0.40, 0.507 and 0.615 respectively. In no case did a complete test exceed 12 hours and during this time the temperatures were always maintained to within  $\pm 1^\circ\text{C}$ . Three chromel-alumel thermocouples were used as the temperature sensing elements and these were positioned at equal intervals along the gauge length and as near as possible to it.

### 5.4 Procedure

For a particular test temperature incremental loading was performed for load increments of 2, 5 and 7N. At room temperature (21°C) an additional load increment of 9N was used. For a 10 : 1 lever ratio and a specimen cross-sectional area of 25 mm<sup>2</sup> these loads correspond to nominal applied stress increments ( $\Delta\sigma$ ) of 0.8, 2, 2.8 and 3.6 N/mm<sup>2</sup> respectively.

The test method was as follows:

A temperature and load increment was first decided upon and, where applicable, the specimen was then left overnight in the furnace to attain the steady test temperature. The load increment was then applied, allowing 15 minutes of recording time before the application of the next increment. Loading was continued in this way until such a time as either the specimen had fractured or the displacement was too large for

the maximum chart range. Those specimens that had not fractured were tested for recovery by unloading and allowing 15 minutes of recording time on the more sensitive chart ranges before the removal of the next decrement.

Two further tests were made involving variable load increments and one with a prestrained specimen. In almost all cases at least two specimens were tested for each load increment - temperature combination.

## 6. EXPERIMENTAL RESULTS

### 6.1 Material Isotropy

The tensile stress-strain isotropy was checked from Hounsfield tests on a series of annealed longitudinal, transverse and oblique specimens. The results of these tests showed near coincidence of these curves and confirms isotropic behaviour. More important here, however, is the strain-time isotropy. This was checked in the main test programme by observations on longitudinal and oblique specimen behaviour under identical test conditions. Since the deviation here was no more than that for repeat tests between longitudinal specimens (Fig. 5)\* it is concluded that the material exhibited tensile creep isotropy.

### 6.2 Transient Creep Analysis

It was first assumed that the material crept logarithmically between load increments. Equation (2) was therefore applied as outlined in the analysis. A typical plot is shown in Fig. 1 for the test conditions and stress levels indicated. In this plot the time is reckoned as zero at the instant the increment is applied and the stress levels are the total applied nominal stresses for the duration of creep period. It is seen that in no case is the plot linear and the non linearity increases with applied stress level. At higher stress levels on copper and steel Rogan and Alexander (8) observed increasing non linearity although at lower stress levels logarithmic creep was observed. Aluminium like copper has been shown (7) to obey a logarithmic law at similar homologous test temperatures in the range  $0 < \frac{T}{T_m} < 0.25$ . Thus while copper at room-temperature falls within this range aluminium at room temperature does not ( $T/T_m = 0.315$ ). In general, therefore, logarithmic creep is only observed for low stress levels and temperatures.

\* Figures are given at the end of this Appendix.

Parabolic creep was then investigated by the derivative equation (9). This equation is shown graphically in Fig. 2 with each creep period presented in the same way as Fig. 1 and for the same test. It is seen here the plots for each stress level are all linear over each creep period. With the exception of the higher stress levels at a test temperature of 300°C, where some secondary creep occurred, this observation applied to all other tests and Fig. 3 shows a similar plot for a different set of test conditions with  $\Delta\sigma = 2 \frac{N}{mm^2}$  and a temperature of 21°C. The parabolic equation (4) was, therefore, seen to apply for short time deformations between successive load increments.

### 6.3 Parabolic Constants

A further important observation here is that the plots in each of Figs. 2 and 3 are sensibly parallel. This would indicate that the time exponent ( $m$ ) for each interval is independent of the stress level and total prior strain in each test. Table 1† shows the very small variation in  $m$  for the applied stress levels in Fig. 2. All tests considered, where  $m$  did vary it was usually found to do so at the lower stress levels but this was attributed to the difficulty of computing strain rates accurately here rather than it being any function of stress. The effect of a continuously decreasing lever ratio was eliminated as far as possible in this respect by maintaining the same beam geometry at the start of each test and increment.

#### 6.3.1. Effect on $m$

Although for a particular test  $m$  was seen to be constant it did vary from test to test. The effect of stress increment value and test temperature on the average  $m$  value for each test is shown in Table 2. At a glance this shows that  $m$  increases with temperature of testing but decreases with stress increment value. The effect of temperature is hardly surprising since at the lower end of the temperature scale, where logarithmic creep is observed (7) a parabolic equation could equally well be employed with a small  $m$  value (4) and for higher temperatures it is possible to observe only secondary creep ( $m = 1$ ) after the application of a load.

The effect of an increasing stress increment value is seen from Table 2 to lower the value of  $m$ . There is evidence here, however, that a steady  $m$  value is approached since the differences in  $m$  are smaller between the higher stress increments. Furthermore, an additional test at

† Tables are given at the end of this Appendix.

room temperature for  $\Delta\sigma = 3.6 \text{ N/mm}^2$  yielded an  $m$  value almost equal to the value for the  $\Delta\sigma = 2.8 \text{ N/mm}^2$  test.

Lastly, it will be observed from Table 2 that for only two test combinations of stress increment and temperature did the material creep approximately according to Andrade's  $t^{1/3}$  law in this type of test.

### 6.3.2. Effect on $a$

The fact that  $m$  is constant for a particular test allows the analysis to be taken a stage further. The value of the second parabolic constant ( $a$ ) for each applied stress level of a test can then conveniently be observed as the slope of an  $\epsilon$  vs  $t^m$  plot. Typically Fig. 4 follows from Fig. 2 and shows that  $a$  increases with the level of stress. Various plots were tried in the search for the functional relationship between these two. It was found for all tests that when plotted on logarithmic coordinates they were linearly related. Figs. 5, 6 and 7 show these logarithmic plots for all the tests. Fig. 7 also shows the relationship to be slightly affected at higher stresses when current specimen dimensions were employed for the computation of  $a$ . Qualitatively these show that the constant  $a$  increases with stress level, stress increment value and test temperature. For conventional constant stress transient creep analysis  $a$  is also known to increase with both stress and temperature (10) though the precise forms of dependence apply only to limited stress ranges.

A knowledge of the dependence here can be attempted from the important observation that the logarithmic plots in Figs. 5, 6 and 7 are all remarkably parallel. Linearity on a logarithmic plot firstly implies a power function dependence on stress and secondly parallelism implies a constant power index for all the test conditions. Thus, in general, the stress dependence is expressed by:

$$a = k\sigma^p \quad (10)$$

where  $p$  is the slope of the  $\log a$  vs  $\log \sigma$  plot and  $k$  is the intercept. The average value of  $p$  from Figs. 5, 6 and 7 was 6.2 with extremes of 5.96 and 6.43.

An indication of the dependence of  $a$  on temperature could next be examined from the  $k$  intercept values. Since creep is a thermally activated process then the temperature dependence must appear through the Arrhenius expression:

$$k = l \exp(q/T) \quad (11)$$

The  $k$  intercepts are therefore shown plotted logarithmically against

the reciprocal of the absolute test temperature (T) for the three stress increment values in Fig. 8. Then  $q$ , obtained from the average slope here, was found to be -5950. A check on the validity of this value, made later, shows it to be in accordance with accepted values for aluminium.

Lastly, the intercepts  $l$  in Fig. 8 were used to examine the stress increment dependence. It was found that these were best plotted logarithmically against their corresponding stress increment values ( $\Delta\sigma$ ) in Fig. 9 to yield a dependence of the form:

$$l = s \exp(r[\Delta\sigma]) \quad (12)$$

where  $r$ , obtained from the slope of Fig. 9, was 1 and  $s$ , the intercept, equalled  $177.8 \times 10^{-8}$ . Although there are too few points in Fig. 9 to make equation (12) conclusive it was felt to be worthwhile completing it so that a possible equation of  $a$ 's dependence upon all the test variables could be formulated.

Thus combining equations (10), (11) and (12) in the general form:

$$a = s \exp(r[\Delta\sigma]) \exp(q/T) \sigma^p \quad (13)$$

This then allows for the prediction of transient creep rates here when used with equation (6) as:

$$\dot{\epsilon} = m s \exp(r[\Delta\sigma]) \exp(q/T) \sigma^p t^{m-1} \quad (14)$$

and substituting the constants  $p, q, r$ , and  $s$  for the range of test variables here we have:

$$\dot{\epsilon} = 177.8 \times 10^{-8} m \exp(\Delta\sigma) \exp\left(\frac{-5950}{T}\right) \sigma^{6.2} t^{m-1} \quad (15)$$

where  $m$  varies as in Table 2.

### 6.3.3. Effect on $\epsilon_0$

The instantaneous strain immediately following the application of a single stress increment was obtained in these tests as the intercept values in Fig. 4. In general, this was observed to increase in the following ways:

- (1) as the stress increment increased for a given temperature and total stress.
- (2) as the total stress increased for a given temperature and stress increment.
- (3) as the temperature increased for a given total stress and stress increment.

When the total instantaneous strain ( $\Sigma \epsilon_o$ ) was computed at each stress and plotted against it, no apparent load increment effect was observed (Fig. 10) as the three curves for each temperature were almost coincident. Mean curves were then calculated for each temperature and plotted in Fig. 10 to show the growth of instantaneous strain with stress level. This shows that an increased test temperature decreases the stress level to reach a specified strain and also decreases the total amount of instantaneous strain. The fact that creep strain is predominant at higher temperatures and stresses is shown in Fig. 11 where the mean curves of Fig. 10 were used to compute the ratio of total creep strain ( $\Sigma \epsilon^c$ ) to total instantaneous strain ( $\Sigma \epsilon_o$ ) and plotted against stress for the four test temperatures. These curves also show the stress levels at each temperature for which the total creep strain (15 minutes after the application of a load) equalled the total instantaneous strain. Beyond this relatively small increases in stress increase the ratio considerably. For the higher test temperatures the total creep strain reached as much as eight times the total instantaneous strain. For all test temperatures the stress-strain characteristics based on  $\epsilon_o$  from equation (4) agreed with observed behaviour and this in turn compared with separate tensile tests. A double logarithmic plot in each case yielded a law of the form:

$$\sigma = A (\Sigma \epsilon_o)^n \quad (16)$$

where  $n$  was typically 0.3 for aluminium and  $A$  decreased with temperature.

A plot of  $\Sigma \epsilon_o$  vs  $\frac{\Sigma \epsilon^c}{\Sigma \epsilon_o}$  in Fig. 11 shows the relative amounts of total creep and instantaneous strain at the end of any stage during an incremental test (defined by  $\sigma$ ). These curves also confirm the 10-25% total strain at the end of all tests as obtained by measurement.

#### 6.4 Recovery

Upon unloading from higher stress levels only elastic strain was recovered. This increased linearly with decreasing stress until very low stress levels were reached where some time dependent recovery was observed. However, this was always small compared to the elastic recovery and in total never exceeded 5% of the overall recovered strain. Further independent gauge length measurements at 150 hours subsequent to unloading showed no further recovery. This is interesting in view of work (11) that has shown a significant part of the forward creep strain as recoverable. An explanation is attempted in the following section.

## 7. DISCUSSION

Since the time exponent ( $m$ ) and the instantaneous loading strain ( $\epsilon_o$ ) have been shown to be dependent upon both stress increment ( $\Delta\sigma$ ) and test temperature it is not unreasonable to assume that  $m$  is possibly dependent upon  $\epsilon_o$ . Another possibility is that  $m$  is dependent upon the magnitude of the total prior strain or on the creep curve immediately preceding it.

To investigate these possibilities further specimens were tested at room-temperature under the following conditions:

- (1) A changing incremental test  $\Delta\sigma = 2.8 \text{ N/mm}^2$  for the first series of steps and then changed to  $0.8 \text{ N/mm}^2$  for the remainder (Fig. 12).
- (2) A 2% prestrained specimen tested under identical conditions as the annealed specimen (Fig. 3).

It is apparent from Fig. 12 that the change in  $m$  on lowering the stress increment value is dependent either upon the change in instantaneous strain associated with it or on the prior creep curve. The relatively small increase in  $\epsilon_o$  with each step, in Fig. 2 due to non-linear stress-strain behaviour, does not appear to affect  $m$  noticeably nor does the total amount of prior strain otherwise parallelism would not have been observed. Comparison of the slopes in Fig. 3 showed a 2% prior plastic prestrain not to affect  $m$  significantly but only to increase the stress at which creep first started. This is seen as non linear behaviour in Fig. 6 where the parabolic constant  $a$  is lowered by the prestrain. After this the dependence upon stress is seen to be identical to that of the annealed specimen. It appears, therefore, that the prior creep curve controls the subsequent curve more than the instantaneous strain does. This is further substantiated from Fig. 12 where it is seen that upon changing to the smaller stress increments the value of  $m$  remains unsettled until the sum of these exceeded the last larger increment. Thereafter  $m$  settled at a constant value. The degree of dependence between subsequent and prior creep curves is seen from Table 2 to be less when the stress increment values are large. Here  $m$  approaches a constant value to indicate that the creep curves occurring between increments of larger loads are approximately of the same shape. This would seem to confirm Wyatt's observation that for large stress increments the less the resulting creep curve depended upon the prior one. Mention should also be made to the experiments of Davis and Thompson (12) who showed that a prior creep curve also controlled the degree of instantaneous strain associated with the next increment. Indeed a critical

stress increment was determined for which increments less than this produced no instantaneous strain whereas those greater did. It is not thought here that this interdependence occurs over a very large range of stress increments since the stress - total instantaneous strain plots in Fig. 10 show no consistent stress increment effect.

Equation (15) has been developed here for the prediction of creep rates within the range of experimental variables employed in these tests. While it is felt that it would do this with reasonable accuracy some mention should be made to the form of the equation. The stress index of 6.2 appears from the parallelism in Figs. 5, 6 and 7 to be the correct power in this type of incremental test. Experiments by Dorn (13) on the secondary creep rate - stress dependence of conventional creep tests also yielded a power function relationship for this material but with a stress index typically of 4, though the value does decrease with temperature. For the transient creep it is generally accepted (10) that the stress - creep rate dependence does change over a wide range of stress and temperature. Linear, power, hyperbolic sinh and exponential laws have all been employed at some time to describe this dependence with each function applicable only to a small range of applied stress. Linear dependence is observed for low stresses and is believed to be a process of stress directed diffusion (6). For increased stress, where the controlling mechanism is dislocation climb, the dependence may be expressed as either power or hyperbolic sinh functions for the intermediate range and an exponential function for the higher range. Over a wider range one function has been employed but it is usually a complex one. Henderson and Sneddon (11) combined the low and high stress range with a function of the form  $a\sigma^p + b\sigma$  to describe the primary creep in copper while Garofalo (10) combined the intermediate and high stress ranges with a function of the form  $A(\sinh B\sigma)^n$  to describe the secondary creep rate in both metals and alloys.

A power function dependence here is consistent with other work on transient parabolic creep at low stress, though the power of stress has only been made insensitive to temperature when a constant structure has been maintained (10). Since this is unlikely here it can only be concluded that the constant power observed over the whole range of stress and temperature is a consequence of this type of incremental test.

The constant in the exponential temperature function may be expressed in terms of an apparent activation energy for creep ( $\Delta H_c$ ) if equation (11) is written in the form:

$$k = k_0 \exp(-\Delta H_c/RT) \quad (17)$$

For transient creep it is usual to apply a formula of the Dorn type, in which the time and temperature dependence are contained in one function. Since the time dependence has been shown to be parabolic then:

$$k = \ell [t \exp(-\Delta H_c/RT)]^m \quad (18)$$

and taking an average value of  $m$  here as 0.4, over the temperatures where only transient creep was observed, we have that:

$$k = \ell [t^{0.4} \exp(-0.4 \Delta H_c/RT)] \quad (19)$$

On comparing this with the exponential temperature term of equation (15) for  $R = 1.98$  cal/mole, then  $\Delta H_c = 29.5$  kcal/mole which, for aluminium, is in fair agreement with accepted values.

Approached in this way the activation energy for transient and secondary creep is made constant. This may be taken to mean that the two processes have the same energy and this has been proved from another standpoint (14) where for polycrystalline aluminium  $\Delta H_c$  was found to be independent of creep strain. Other than tests on constant structures  $\Delta H_c$  is known to vary with temperature (14). Since  $m$  and  $\Delta H_c$  increase with temperature it is possible that the  $m$  values of Table 2 have a physical significance in this respect when used with equation (18). The average value of 29.5 kcal/mole for this series of tests was calculated here to check the validity of the constant  $q$  in equation (11).

The validity of the stress increment function in equation (12) is less certain since no other work of this type exists. It is interesting to note that the constant  $r$  in this equation was unity. This means that the dependence of strain rate on stress increment is a simple exponential one. Clearly this is an area for further investigation since it is of direct concern in all creep tests that are loaded incrementally to some test stress.

An explanation of the almost complete absence of recovery in these tests may be attempted from a consideration of the structural mechanisms involved in each strain component. The permanent component of the instantaneous strain exhibited the characteristics of plastic strain which involves the production, movement, interaction and multiplication of dislocations. Since the application of a load and the production of this strain are simultaneous the dislocation movement is therefore extremely rapid. This movement slows and becomes time dependent when the entangled dislocation structure so formed acts in itself as a block to further rapid movement. In plastic deformation the barriers which pin the entangled dislocations are already present within the crystal in the form of impurity atoms, grain boundaries, sessile dislocations and screw dislocations that cut across the active slip plane of the lattice.

The mechanism that accounts for low-temperature plastic deformation in a face-centred cubic lattice is essentially slip with dislocations as the source for it. Cross slip and pencil glide are typical slip processes associated with screw dislocations. At higher temperatures an additional mechanism may predominate when vacancies and interstitials diffuse from deformed regions to the sites of edge dislocations causing them to climb out of their original slipplanes.

The magnitude of instantaneous strain produced with each increment was observed to increase parabolically with stress in a manner consistent with usual tensile stress-strain behaviour. Thus the process by which dislocations move to produce plastic deformation for one increment is repeated for each successive increment. The net effect is a work hardened structure which requires increased stress in order to move existing dislocations past barriers and to generate the new ones necessary for the slip processes of further plastic deformation.

The time dependent strain occurring between increments of load is generally attributable to the motion of dislocations as discussed above for plastic deformation together with grain boundary shearing. The rate determining factor here is thermal activation under the action of an applied stress. Thus the creep rate is initially quite high when the links in the dislocation network are able to break free due to small fluctuations but slows thereafter as only the stronger links escape.

Parabolic creep of the type observed here is the result of both work hardening and recovery acting simultaneously but with creep rates in opposition. Work hardening, produced by the same mechanisms of plastic deformation, would produce a structure increasingly resistant to an applied stress. If this were the only effect then creep would always occur at a decreasing rate. However, as the dislocation density increases so does the stored energy of the tangled structure. This acts as the driving force in the recovery process where, provided the temperature is high enough, dislocations are thermally activated to climb over barriers where they may mutually annihilate or form stable walls (polygonize). The net effect is a decreased dislocation density, a softer metal and an accelerating creep rate. Recovery is therefore the controlling process in creep because if it is sufficient to compensate for work hardening the constant strain rate of secondary creep would be observed but if it is not the decreasing rate of primary creep would result.

Recovery is observed in a different way when the load is removed from the specimen and the internal stress field developed during forward creep may cause a similar rearrangement of the dislocations.

Macroscopically this is observed as an inverted primary creep curve. In this light the creep recovery curve has been identified with anelastic strain and the total forward creep curve regarded as the sum of two different kinds of time dependent strain, anelastic and plastic occurring together but following independent laws (15). Where no recovery occurred this was attributed to the stress levels being in excess of the "plastic creep limit". Below this limit, however, the recovered strain was important to consider since the plastic strain was shown to be negligible in comparison with the anelastic strain. Microscopically the amount of strain recoverable would seem to depend upon whether the work hardened structure contains sufficient stored energy at the test temperature to thermally diffuse vacancies to dislocation sites and so make possible their climb over barriers.

In the type of test performed here the instantaneous strain was followed by 15 minutes of creep strain for each increment. In general this was continued until total strains of the order of 20% were reached. Of this strain Fig. 11 shows that at lower temperatures the instantaneous strain component was dominant, whilst at higher temperatures the short-time creep strain component accounted for most of it. Irrespective of temperature, however, the strain recovered from unloading was mostly the elastic component of the instantaneous strain and to a very much lesser extent, and then only at loads approaching the fully unloaded state, the anelastic component of the creep strain. It is possible that the plastic strain caused by the addition of an increment interacted with the internal stress field developed during prior creep in such a way as to prevent the rearrangement of dislocations associated with recovery. This implies that the work hardening mechanisms of creep and plastic deformation, although basically equivalent, act on the structure in different ways. There appears from the literature to be some evidence that this is the case.

During creep inhomogenous deformation within individual grains and across grain boundaries is caused by the non uniform complex internal stress field that operates by interaction between the differently orientated neighbouring grains. Wood and Wilms (16) observed that this has the effect of fragmenting the individual grains into a large number of closely spaced subgrains bounded by dense arrays of low angle boundary networks. Each subgrain contained within it isolated jogs, kinked dislocations and dipoles that form an overall structure common to metals and solid solutions of high stacking fault energy. The stability of such a structure depends upon the recovery and recrystallisation characteristics of which the test temperature plays an important part. Anker, Hazlett

and Parker (17) in their studies on high purity nickel concluded that this type of structure was unique to creep and different from that associated with plastic deformation where subgrains form as a result of dislocations piling up at barriers already present within the crystal. Furthermore the subgrain formation of plastic deformation was observed to be generally larger and free from the multitude of small angle boundaries of creep deformation. Lagneborg (18), reviewing dislocation mechanisms in creep observed that the subgrain boundaries of high temperature creep were more distinct and well defined than the tangled dislocation structure forming the cell walls of low-temperature plastic deformation though at similar temperatures the two processes were regarded as equivalent. Sherby, Goldberg and Dorn (19), in a study on subgrain formation, compared the crept structures of initially annealed and prestrained/annealed pure aluminium. A comparison of creep and tensile properties made on the degree of polygonization of each subgrain structure following various degrees of creep showed the properties to improve in the annealed metal as the polygonization increased. The correlation did not hold, however, for the increased polygonization structure of the prestrained metal where the least polygonized structure of the highest prestrain exhibited the best creep resistance. Subgrain formation is not now associated with polygonization and in this light Lagneborg suggested that the factor controlling creep strength is the subgrain walls and the rate at which dislocations drain from the grain interior to strengthen them. Thus the subgrain size and perfection would appear to control creep strength. This has shown to be the case for nickel by Coldren and Freeman (20) and for aluminium by Hazlett and Hansen (21) provided the subgrains were stable. On the other hand Yim and Grant (22) have cast doubt on this postulate for nickel as have Grant et al (23) for aluminium. Based on the knowledge that subgrain boundaries have a high degree of mobility during creep at temperatures where recovery is effective it is likely that the structures formed as a result of plastic deformation coalesce with those formed during creep so as to yield a net structure little different from that of an originally annealed structure. The test temperature may, therefore, be accountable for some of these discrepancies.

At test temperatures exceeding  $0.3 T_m$  the contribution to creep deformation in grain boundary sliding must be considered. The grain boundary seems to reverse its role in providing strength at low temperatures to one of weakness at higher temperatures. Grain boundary sliding is observed as a rotation or translation of one grain with respect to its neighbours and occurs in addition to the intercrystalline modes of low-temperature deformation. The question arises as to whether the two

processes independently contribute to the total creep strain or whether grain boundary sliding is dependent upon the intercrystalline mode in that it serves to accommodate it. In a review on the stress and temperature dependence of grain boundary sliding along with observations on appropriate crept structures Garofalo (10) concluded that there was strong evidence to indicate that grain boundary sliding was controlled by intercrystalline deformation for certain conditions of stress, temperature and structural properties. Over the whole range of possible combinations, however, the literature indicates that grain boundary sliding may contribute anything between 1 and 90% of the total observed creep strain.

With regard to the tests performed here in view of the test temperatures ( $T/T_m > 0.315$ ) it is thought that the creep strain was largely composed of grain boundary deformation. This would also explain the absence of the anelastic component of creep strain associated with intergranular deformation. Microstructural studies showed grains elongated in the direction of the applied stress and sliding along their boundaries which adds support to this (Fig. 13).

## 8. CONCLUSIONS

(1) For EIA aluminium the short-time creep occurring between successive increments of load over a wide range of temperature ( $0.3 < T/T_m < 0.6$ ) and stress is transient in nature and describable by a parabolic equation of the form  $\epsilon^c = at^m$ .

(2) The time exponent  $m$  is dependent upon the test temperature and the magnitude and sequence of load increments but not on the test stress level. In general its value was increased by:

- (a) an increase in temperature;
- (b) loading with smaller increments;
- (c) a change in the value of the stress increment from high to low during a test.

Possible physical significance of  $m$  has been shown in the degree to which a subsequent creep curve is affected by a prior one, to the magnitude of the instantaneous loading strain and to an activation energy which increases with temperature.

(3) The parameter  $a$  in the parabolic law is dependent upon temperature, stress level and stress increment value. The functions containing these variables are separable into the form:

$$a = s \exp(\Delta\sigma) \exp(q/T) \sigma^p$$

to show that the creep rate ( $\dot{\epsilon}^c = \text{mat}^{m-1}$ ),  $t$  seconds after the application of an increment ( $\Delta\sigma$ ) making a total applied stress ( $\sigma$ ) at a temperature ( $T$ ), increases:

- (a) exponentially with the test temperature;
- (b) as a power function of the total stress level.

(4) The magnitude of the creep rate at a particular stress, time and temperature for incremental loading is also dependent:

- (a) exponentially upon the stress increment used to reach that stress;
- (b) upon the prior creep curve when the increments are small and, to a lesser extent, the instantaneous loading strain when the increments are large;

but not on the total amount of prior strain aggregated from the previous loads.

This shows that it would not be possible to formulate a mechanical equation of state

$$\dot{\epsilon}^c = f(\sigma, T, t, \epsilon^c)$$

for which the creep rate at any time depends on the state of the system at that time and is independent of how or by what path the system reached this state. There is conclusive evidence now that this cannot generally be true but it would be approximately correct if in tests of this kind the loading were always restricted to a fixed increment value and the time exponent  $m$  were assumed constant at some average value acceptable over a specific temperature range.

(5) Over the range of temperature and stress employed in these tests the mechanism responsible for creep deformation is predominantly grain boundary sliding. A consistent feature in this type of test was the insignificant order of recovered strain associated with unloading. It is more likely that the predominance of grain boundary sliding accounts for this rather than any interaction between the dislocation fields of the instantaneous strain and the prior creep strain.

## APPENDIX

## References

- (1) ANDRADE, E.N.D.A.C. 'The viscous flow in metals and allied phenomena'. Proc. Roy. Soc. Lond. 1910. 84A,1., 1914 90A, 329.
- (2) KENNEDY, A. J. Processes of creep and fatigue in metals 1962. (Oliver and Boyd, Edinburgh).
- (3) JOSEFSSON, A. and LAGERBERG, G. 'Creep tests on mild steel at room temperature'. Jerkontorets Annaler 1958, 142, 570.
- (4) CRUSSARD, C. 'Transient creep of materials'. Joint International Conference on Creep, Instn. Mech. Engrs. London 1963, 2, 123.
- (5) CONWAY, J. B. Numerical methods for creep and rupture analysis. (Gordon and Breach, London).
- (6) MOTT, N. F. and NABARRO, F. R. N. 'Report on the strength of solids'. Phys. Soc. London 1948, 1.
- (7) WYATT, O. H. 'Transient creep in pure metals'. Proc. Phys. Soc. 1953, 66B, 459.
- (8) ROGAN, J. and ALEXANDER, J. M. 'An investigation into the room temperature creep of steels and copper'. J. Inst. Metals 1966, 94, 61.
- (9) BHATTACHARYA, S., CONGREVE, W. K. A. and THOMPSON, F. C. 'The creep time relationship under constant tensile stress'. J. Inst. Metals 1952-53, 81, 83.
- (10) GAROFALO, F. Fundamentals of creep and creep-rupture in metals 1965. (Collier-Macmillan, London).
- (11) HENDERSON, J. and SNEDDEN, J. D. 'Creep recovery of commercially pure copper'. J. Mech. Engng. Sci. 1968, 10 (1), 24.

- (12) DAVIS, M. and THOMPSON, N. 'Creep in a precipitation hardened alloy'. Proc. Phys. Soc. 1950, 638, 847.
- (13) DORN, J. E. 'Some fundamental experiments on high temperature creep'. J. Mech. Phys. Solids 1955, 3, 85.
- (14) SHERBY, O. D., LYTTON, J. L. and DORN, J. E. Acta metall. 1957, 5, 219.
- (15) LUBAHN, J. D. 'The role of anelasticity in creep, tension and relaxation behaviour'. Trans. Amer. Soc. Metals 1953, 45, 787.
- (16) WOOD, W. A. and WILMS, G. R. 'Mechanism of creep of metals'. J. Inst. Metals 1949, 75, 693.
- (17) ANKER, B., HAZLETT, T. H. and PARKER, E. R. 'Relationship between small angle dislocation boundaries and creep'. J. Appl. Phys. 1956, 27(4), 333.
- (18) LAGNEBORG, R. 'Dislocation mechanisms in creep'. Inter. Met. Rev. 1972, 17(165), 130.
- (19) SHERBY, O. D., GOLDBERG, A. and DORN, J. E. 'Effect of prestrain histories on the creep and tensile properties of aluminium'. Trans. Amer. Soc. Metals 1954, 46, 681.
- (20) COLDREN, A. P. and FREEMAN, J. W. Unpublished data given in ASD Tech. Rpt. 1961, 61, 440.
- (21) HAZLETT, T. H. and HANSEN, R.D. 'Influence of substructure on the shape of the creep curve'. Trans. Amer. Soc. Metals 1955, 47, 508.
- (22) YIM, W. M. and GRANT, N. J. 'The effect of prior strain and polygonization on the creep rupture properties of nickel'. Trans. AIME. 1963, 227, 868.
- (23) GRANT, N. J., CHAUDHURI, A.R., SILVER, I. R. and GANOW, D. C. 'Effect of prestrain on the creep rupture properties of high purity aluminium and an Al-2% Mg alloy'. Trans. AIME. 1959, 215, 540.

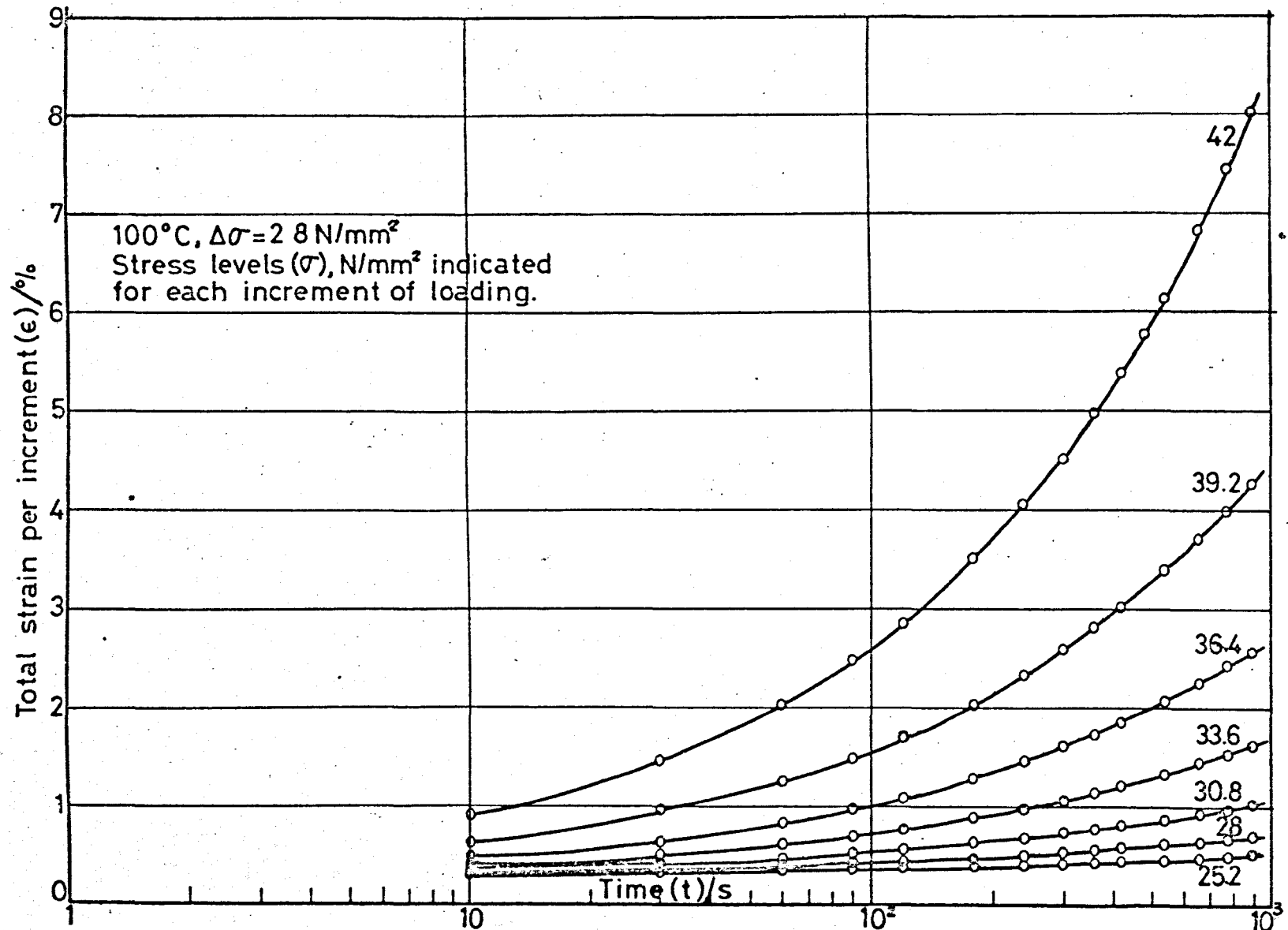


Fig.1. Logarithmic plot based on the law,  $\epsilon = \epsilon_0 + a \ln t$

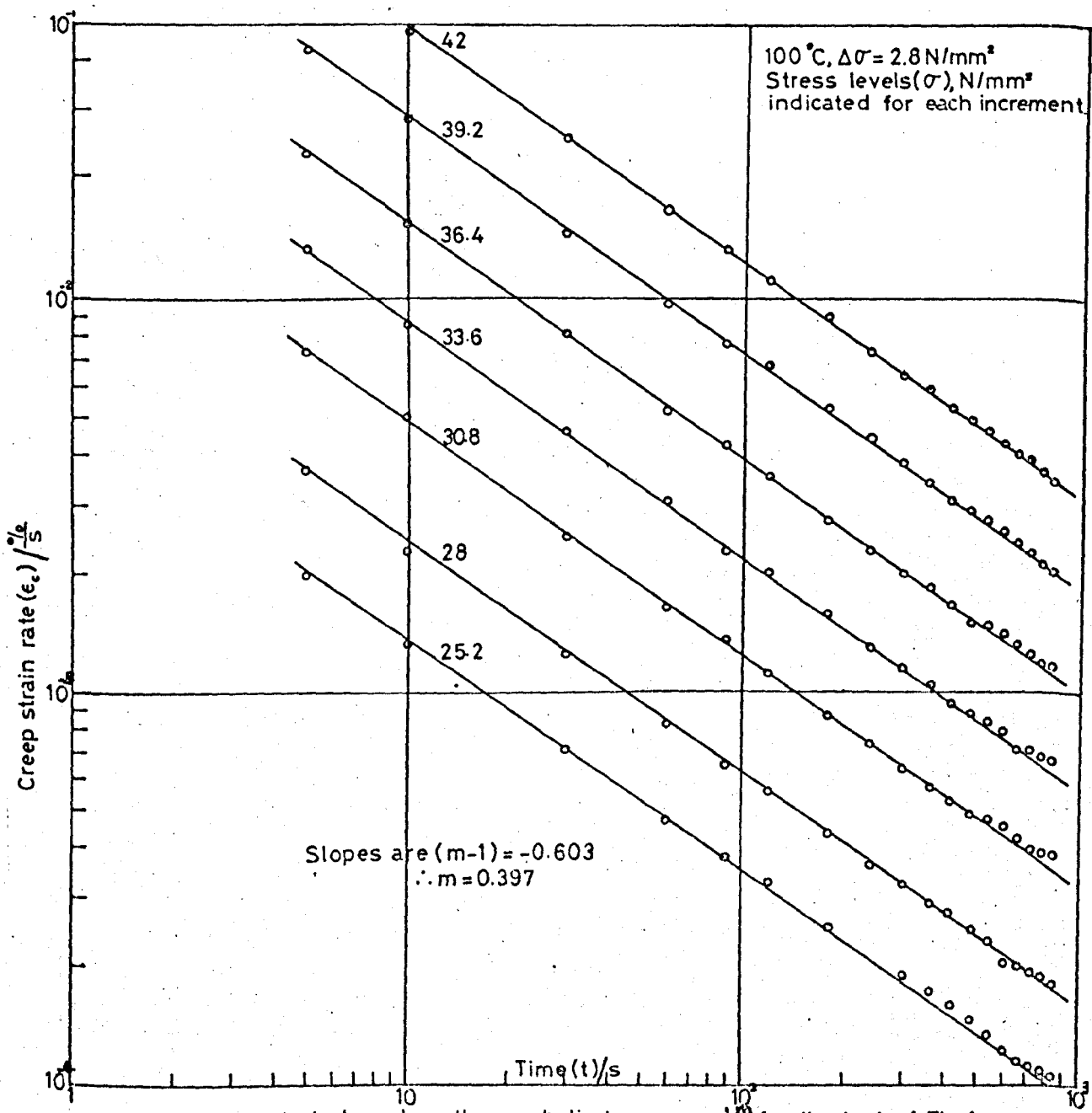


Fig.2. Derivative analysis based on the parabolic law  $\epsilon_c = \epsilon_0 + \sigma t^m$  for the test of Fig.1.

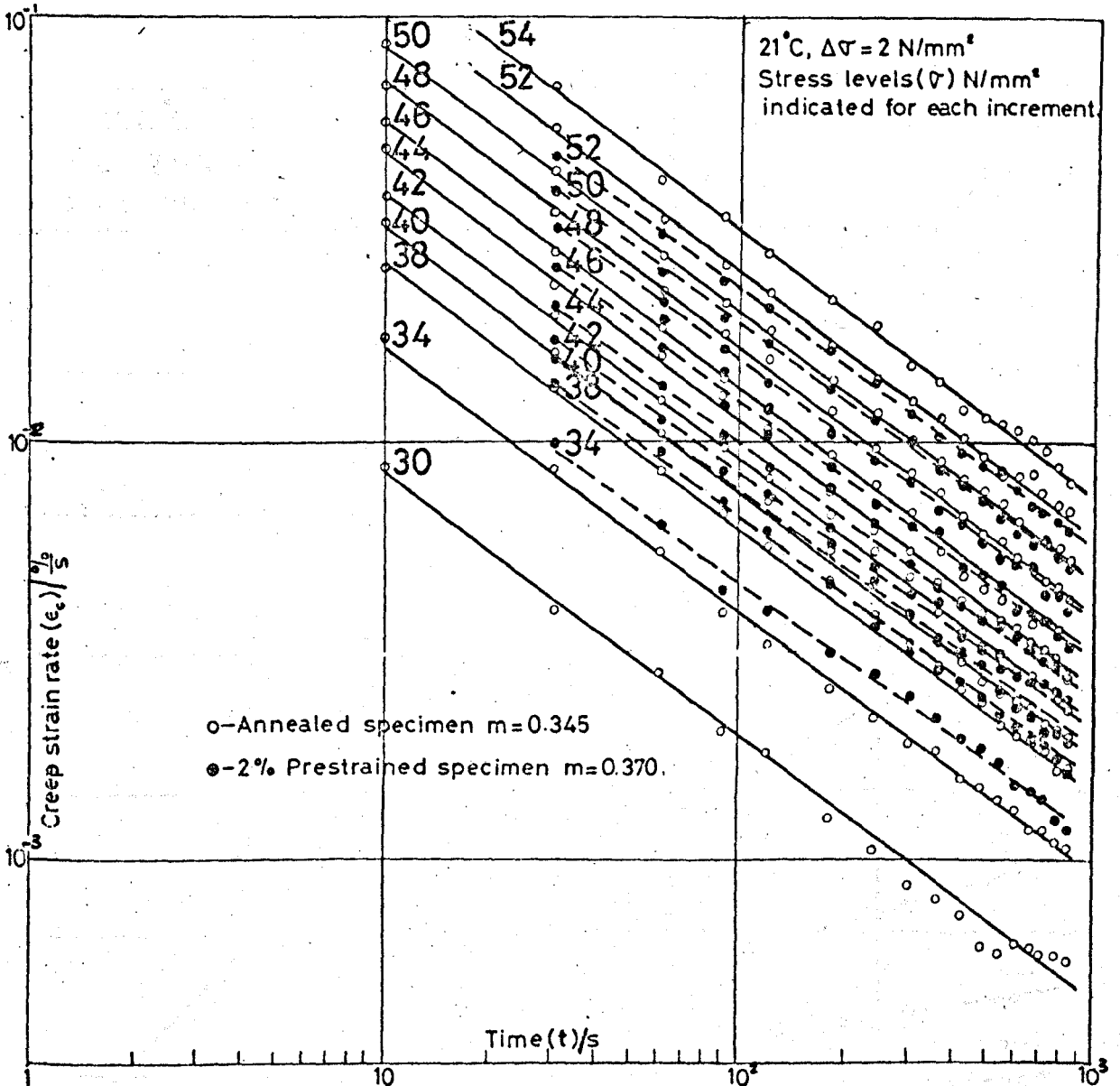


Fig.3. Derivative analysis showing the effect of a 2% prior plastic prestrain on the parabolic time exponent  $m$ .

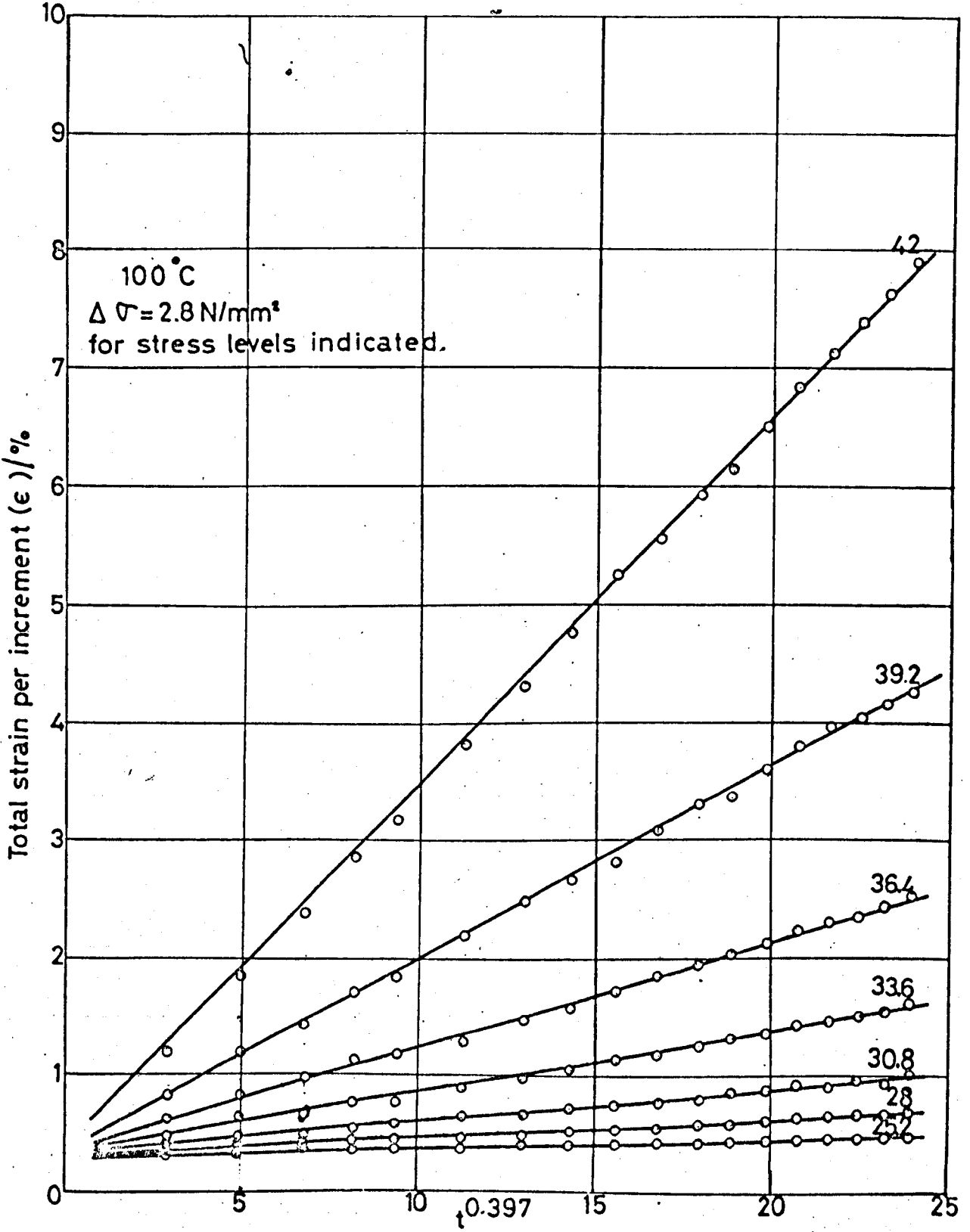


Fig. 4 Evaluation of parabolic constants  $a$  &  $e_0$  for the test in Fig. 2  
 Intercept is  $e_0$ , slope is  $a$  for the stress levels indicated.

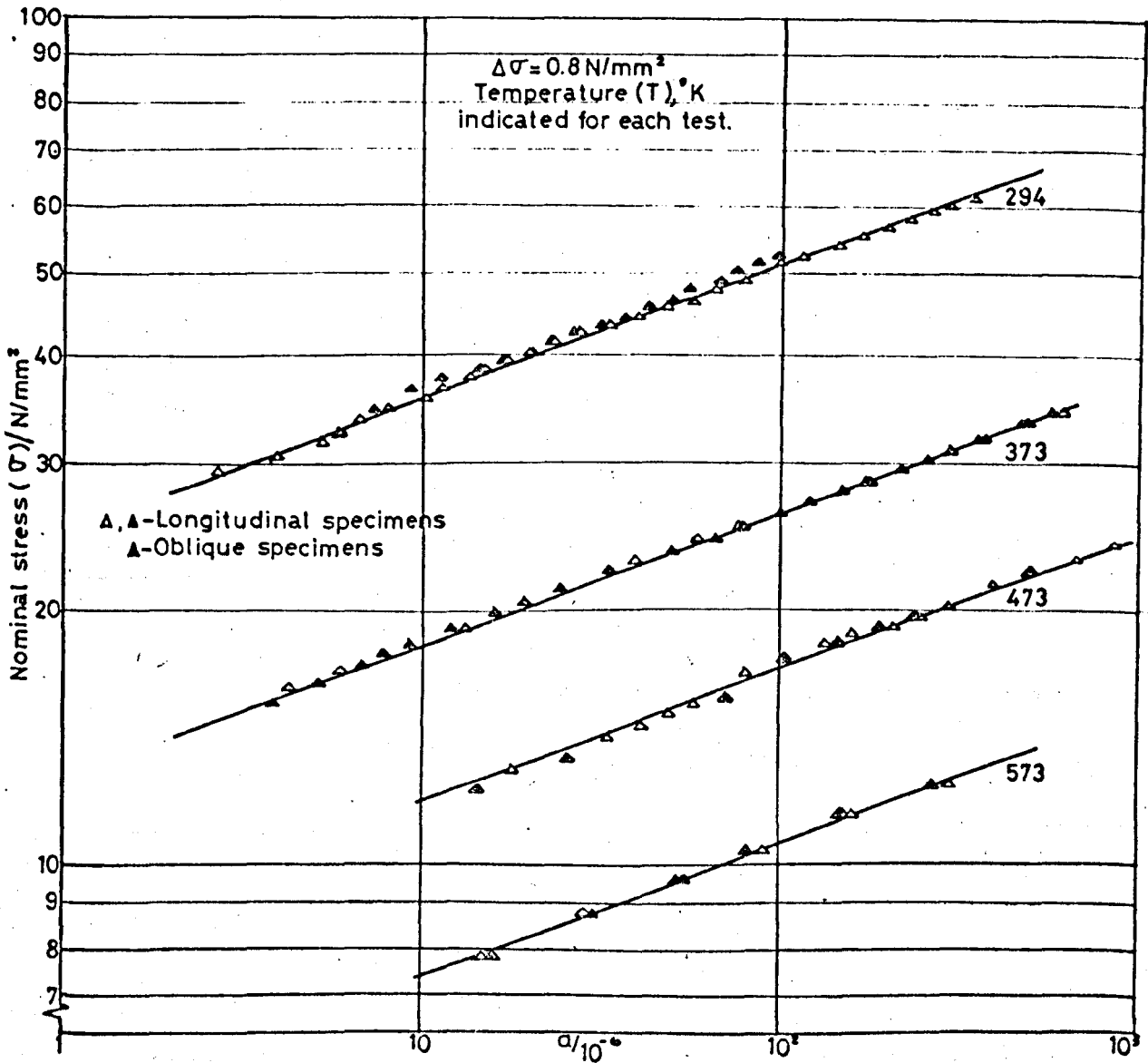


Fig.5 Stress dependence of 'a' for  $\Delta\sigma = 0.8 \text{ N/mm}^2$  at all test temperatures ( $a = k\sigma^{-p}$ )

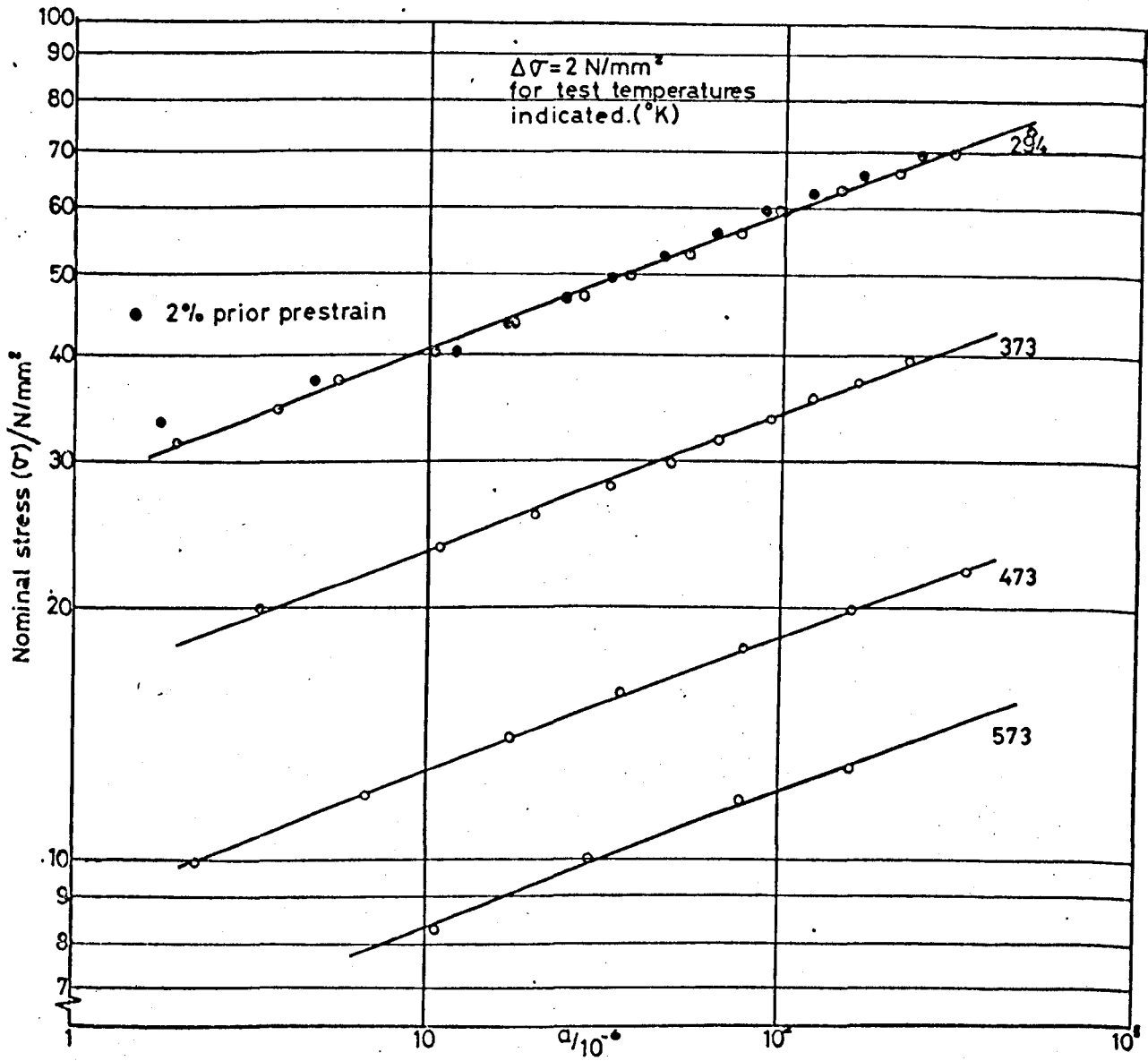


Fig.6 Stress dependence of 'α' for  $\Delta\sigma = 2 \text{ N/mm}^2$  at all test temperatures ( $a = k\sigma^P$ )

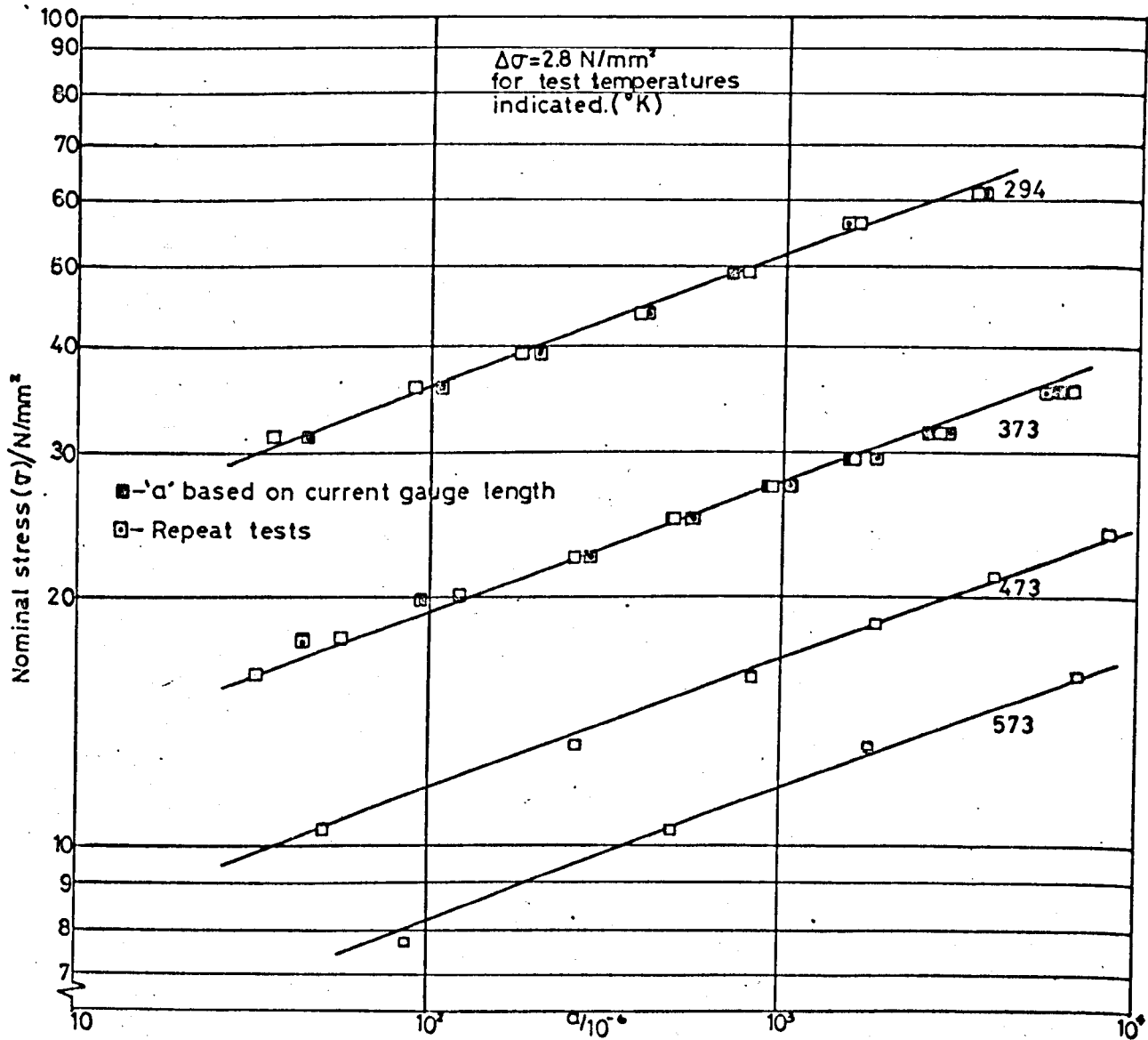


Fig.7 Stress dependence of 'a' for  $\Delta\sigma = 2.8 \text{ N/mm}^2$  at all test temperatures ( $a = k\sigma^P$ )

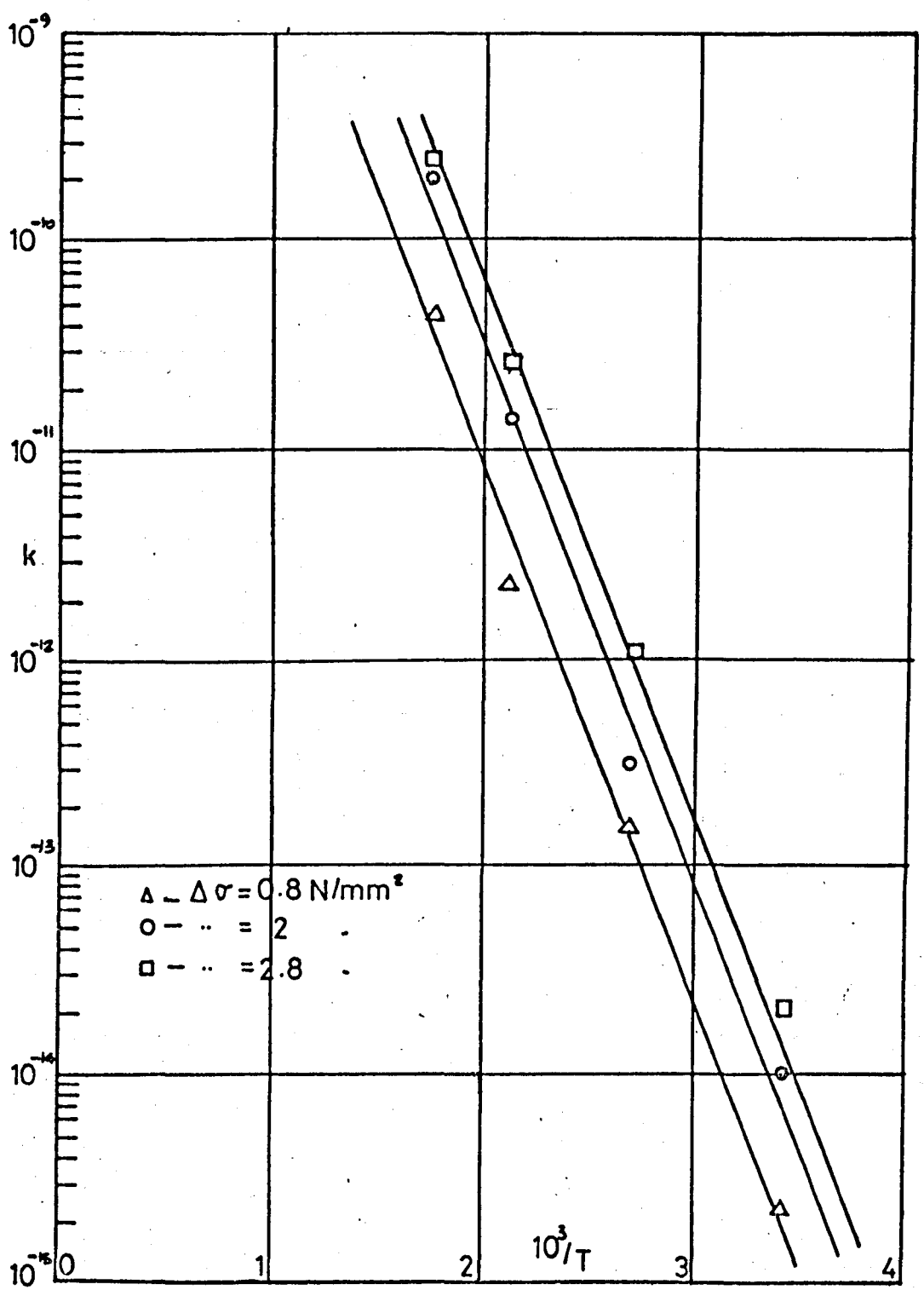


Fig.8 Temperature dependence of 'k' for  $\Delta\sigma = 0.8, 2 \text{ \& } 2.8$  [ $k = \exp(\frac{q}{T})$ ]

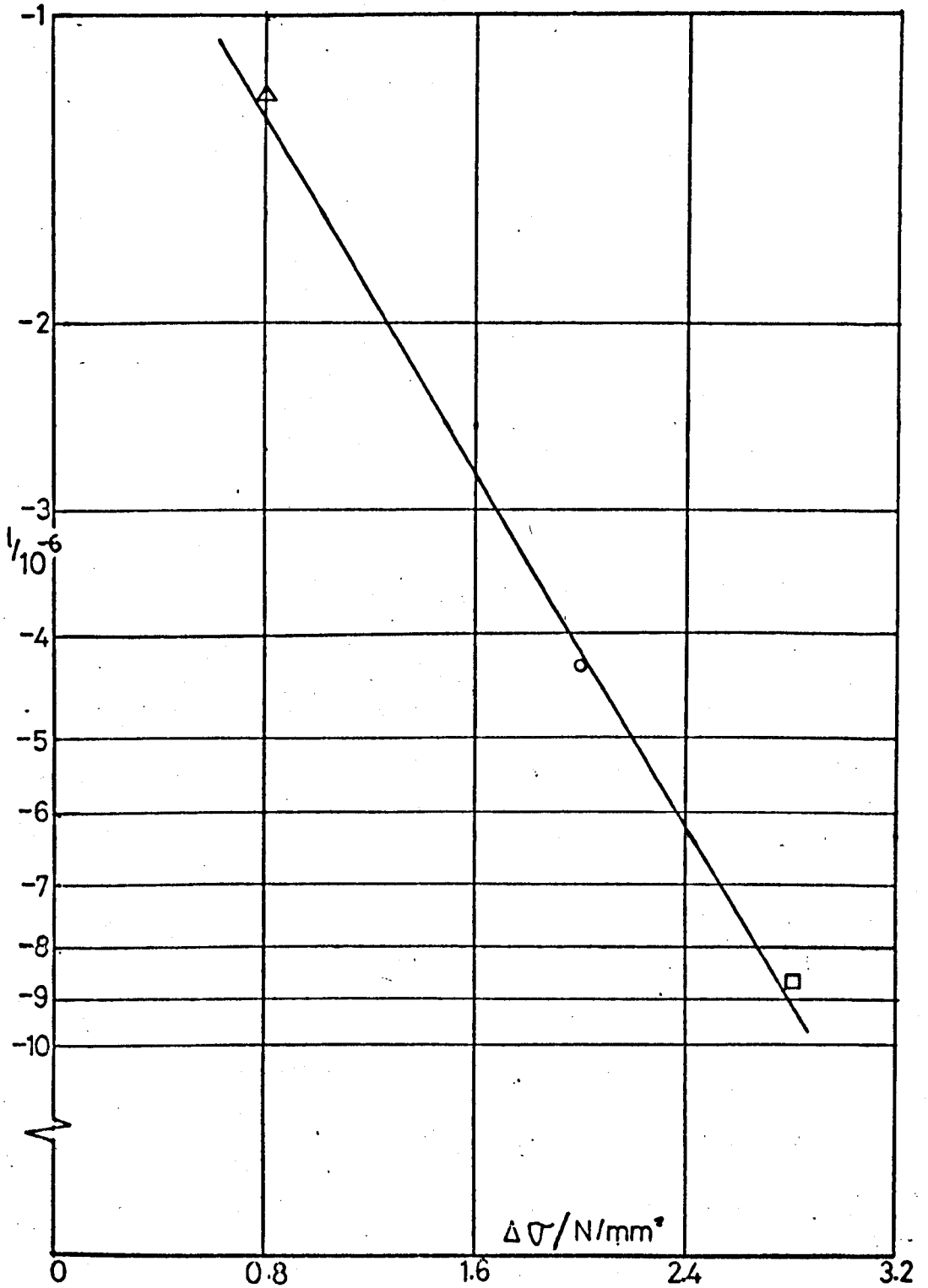


Fig.9 Stress increment dependence of  $l' \{l = s \exp(r[\Delta\sigma])\}$

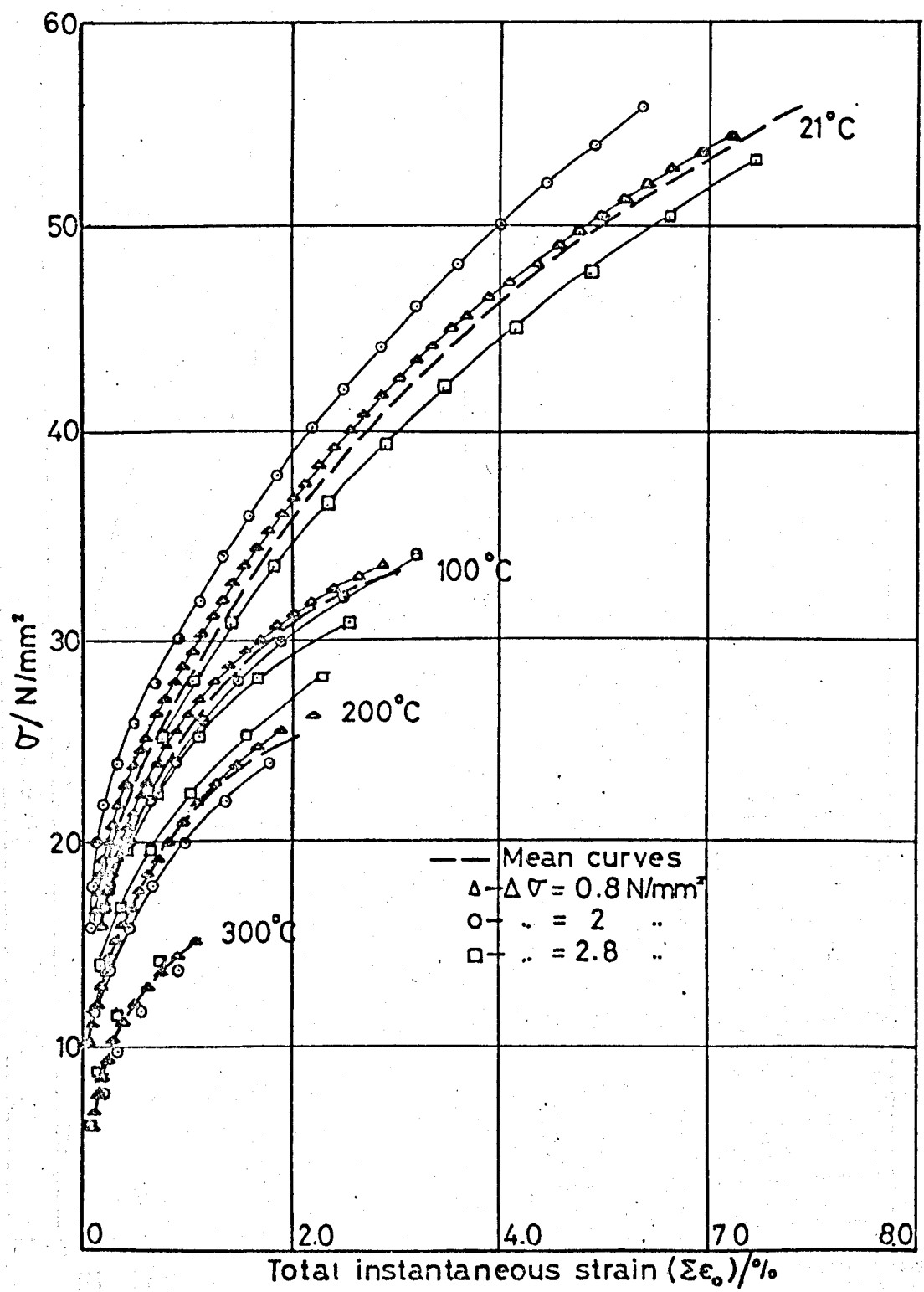


Fig.10 Growth of  $\epsilon_0$  with stress ( $\sigma$ ) for all tests.

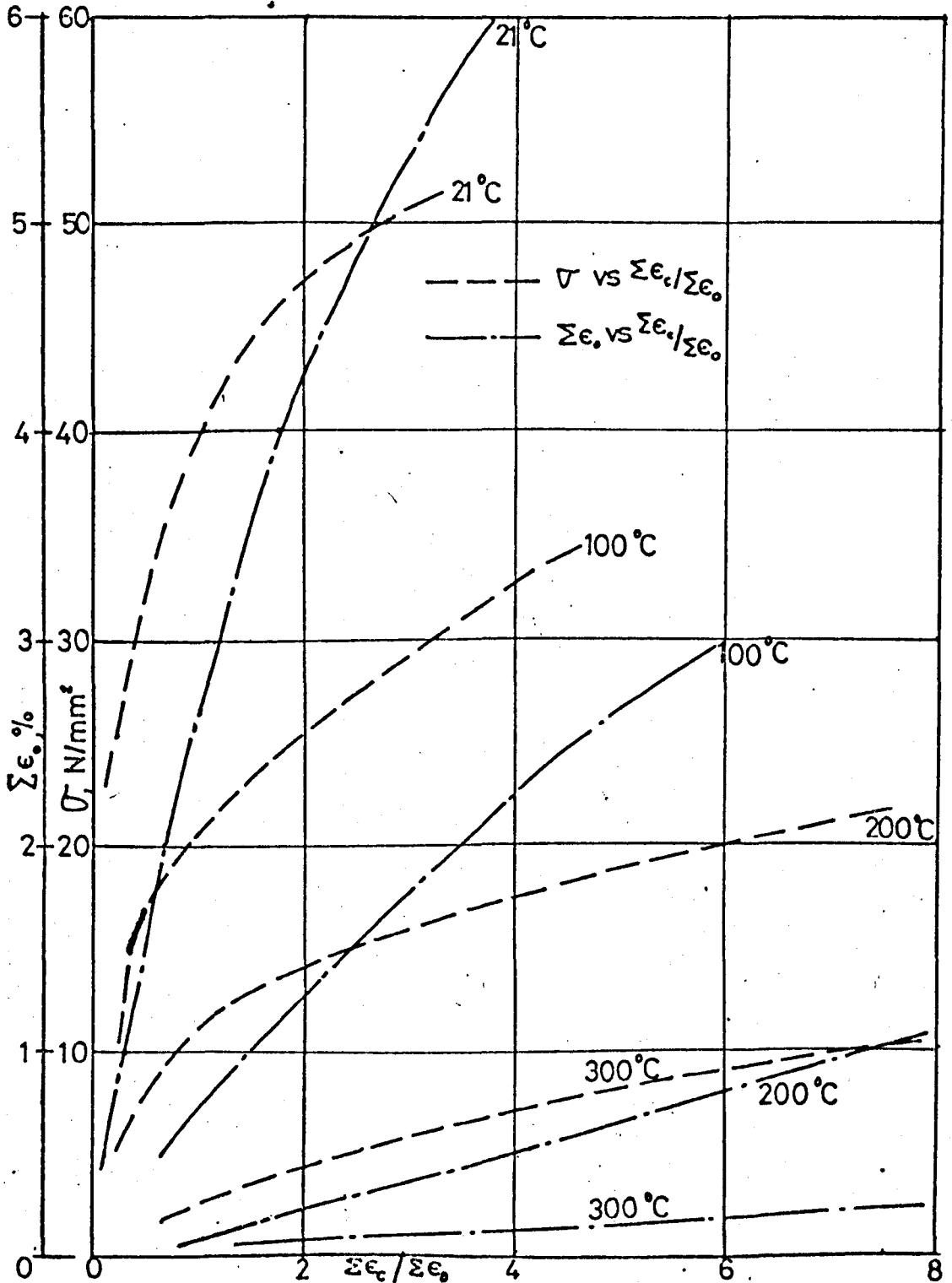


Fig.11 Mean curves showing relative amounts of total creep strain ( $\Sigma \epsilon_c$ ) and total instantaneous strain ( $\Sigma \epsilon_i$ ) with  $\sigma$  & temperature.

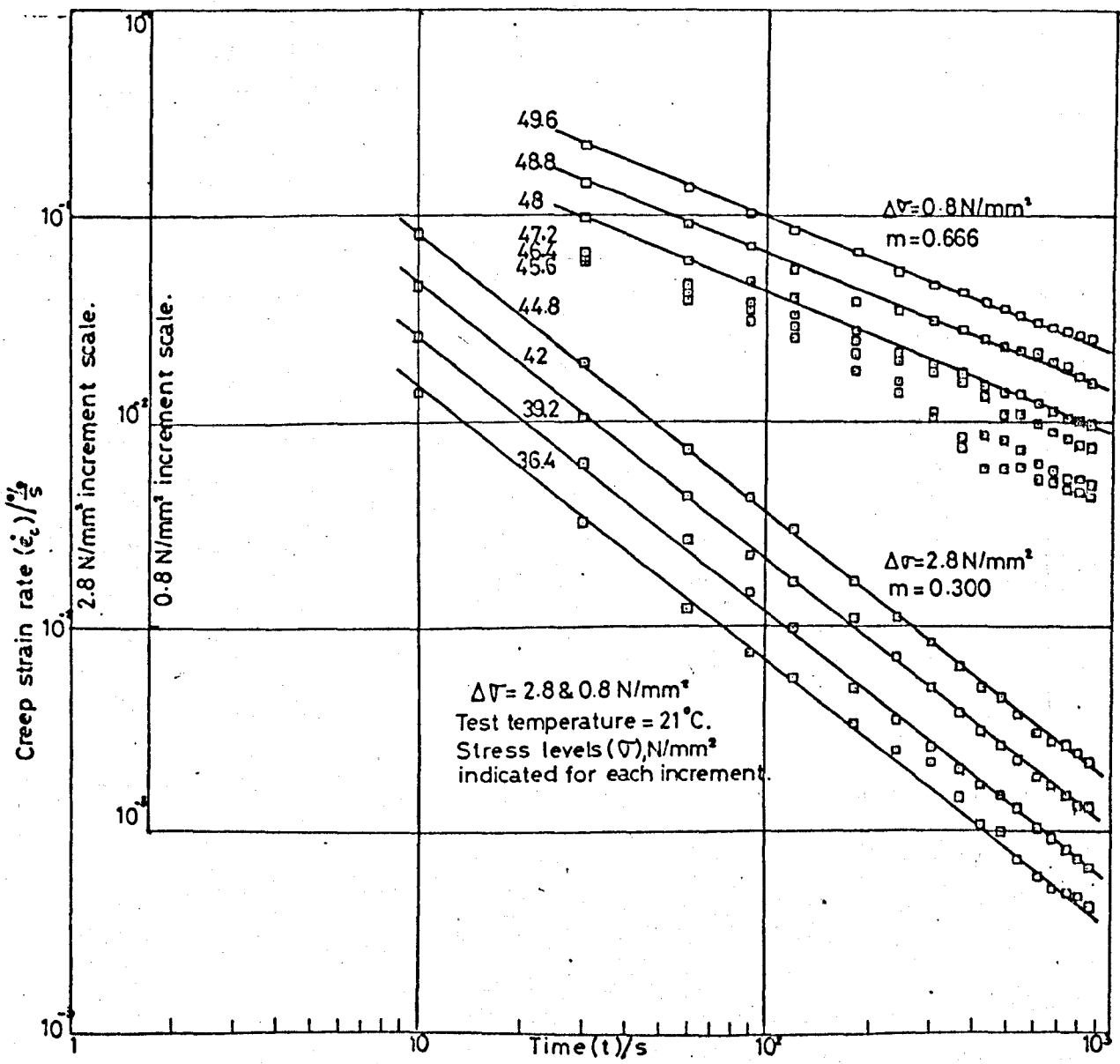


Fig.12 Derivative analysis showing the effect on the constant 'm' when  $\Delta\sigma$  is changed from 2.8 to 0.8 N/mm<sup>2</sup> during test.

TABLE 1

Test temperature = 100°C

Variation of time exponent  $m$  with stress level  $\sigma$ .

$\sigma \frac{N}{mm^2}$	25.2	28	30.8	33.6	36.4	30.2	42
$m$	0.3916	0.3996	0.3856	0.3996	0.3986	0.4051	0.4049
Average $m = 0.397$							

TABLE 2

Variation of time exponent  $m$  with temperature  $T$   
and stress increment value  $\Delta\sigma$ .

$T$ °K	294	373	473	573
$\Delta\sigma \frac{N}{mm^2}$	0.315	0.400	0.507	0.615
0.8	0.500	0.526	0.575	0.880
2	0.345	0.385	0.429	0.726
2.8	0.282	0.397	0.353	0.639
3.6	0.271	-	-	-

Fig.13 Grain boundary sliding  
(Electropolished x250)

TO MY PARENTS